

Final Report for


NASA Grant NAG 3-729


Computer Simulation of a Pilot in V/STOL Aircraft Control Loops

Funded By:
NASA Lewis Research Center
21000 Brookpark Road
Cleveland, OH 44135

Performed By
Department of Electrical Engineering
University of Pittsburgh
Pittsburgh, PA 15261
January 31, 1989

PRINCIPAL INVESTIGATORS:


William G. Vogt
Professor of Electrical Engineering
University of Pittsburgh
Pittsburgh, PA 15261
(412) 624-9686


Marlin H. Mickle
Professor of Electrical Engineering
University of Pittsburgh
Pittsburgh, PA 15261
(412) 624-9682

PARTICIPANTS:

Mark E. Zipf, Research Assistant
Department of Electrical Engineering
University of Pittsburgh
Pittsburgh, PA 15261

Senol Kucuk, Research Assistant
Department of Electrical Engineering
University of Pittsburgh
Pittsburgh, PA 15261

(NASA-CR-184815) COMPUTER SIMULATION OF A
PILOT IN V/STOL AIRCRAFT CONTROL LOOPS Final
Report (Pittsburgh Univ.) 447 p CSCI 05H

N89-21479

Unclas
G3/54 0194220

TABLE OF CONTENTS

TABLE OF CONTENTS	2
ABSTRACT	3
TECHNICAL DESCRIPTION	3
Previous Research	3
Current Results.....	4
The Optimal Control Model (OCM) in a Vertical Tracking Maneuver.....	5
The Adaptive Control Model (ACM) in a Lateral Tracking Maneuver.....	12
Unsettled Research Problems.....	19
REFERENCES	19
APPENDIX I	21

"A Computer Simulation of Low Order Pilot Models Flying a Thrust Vectored V/STOL Research Aircraft", M. E. Zipf, W. G. Vogt, M. H. Mickle, S. Kucuk, J. R. Mihalow, Proceedings of the Nineteenth Modeling and Simulation Conference, University of Pittsburgh, May 5-6, 1988, (Instrument Society of America, Durham, NC., 1988), Vol. 19, pp. 733-764.

APPENDIX II(Separately Bound)

The Optimal Control Model of a Pilot in V/STOL Aircraft Control Loops of "Computer Simulation of a Pilot in V/STOL Aircraft Control Loops: Final Report for NASA Grant NAG 3-729", William G. Vogt, Marlin H. Mickle, Mark E. Zipf and Senol Kucuk, Department of Electrical Engineering, University of Pittsburgh, January 31, 1989. This is a copy of the Final Report, THE INSERTION OF HUMAN DYNAMICS MODELS IN THE FLIGHT CONTROL LOOPS OF V/STOL RESEARCH AIRCRAFT, by Mark E. Zipf, Department of Electrical Engineering, University of Pittsburgh, 1989.

APPENDIX III(Separately Bound)

The Adaptive Control Model of a Pilot in V/STOL Aircraft Control Loops of "Computer Simulation of a Pilot in V/STOL Aircraft Control Loops: Final Report for NASA Grant NAG 3-729", William G. Vogt, Marlin H. Mickle, Mark E. Zipf and Senol Kucuk, Department of Electrical Engineering, University of Pittsburgh, January 31, 1989. This is a version of the thesis for a Master of Science Degree by Senol Kucuk, "AN ADAPTIVE HUMAN RESPONSE MECHANISM CONTROLLING THE V/STOL AIRCRAFT," Department of Electrical Engineering, University of Pittsburgh, 1988.

Computer Simulation of a Pilot in V/STOL Aircraft Control Loops

ABSTRACT

The objective of the research described herein was to develop a computerized adaptive pilot model for the computer model of the research aircraft, the Harrier II AV-8B V/STOL with special emphasis on propulsion control. In fact, the research reported herein gives two versions of the adaptive pilot, the first, simply called the Adaptive Control Model (ACM) of a pilot which includes a parameter estimation algorithm for the parameters of the aircraft and an adaption scheme based on the root locus of the poles of the pilot controlled aircraft. The second, called the Optimal Control Model of the pilot (OCM), which includes an adaption algorithm and an optimal control algorithm. These computer simulations were developed as a part of the ongoing research program in pilot model simulation supported by NASA Lewis from April 1, 1985 to August 30, 1986 under NASA Grant NAG 3-606 and from September 1, 1986 through November 30, 1988 under NASA Grant NAG 3-729.

Once installed, these pilot models permitted the computer simulation of the pilot model to close all of the control loops normally closed by a pilot actually manipulating the control variables. The current version of this has permitted a baseline comparison of various qualitative and quantitative performance indices for propulsion control, the control loops and the work load on the pilot. Actual data for an aircraft flown by a human pilot furnished by NASA has been compared to the outputs furnished by the computerized pilot and found to be favorable.

TECHNICAL DESCRIPTION

Previous Research

Previous research efforts have been directed toward the establishment of computer simulations of pilots for a modern helicopter model [1,2,3,4], and the extension of this model to a modern V/STOL aircraft, Appendix I, of this report [5]. Both of these models depended on the off-line identification of the low-order, small-signal parameters of the aircraft under a particular flight regime and then an off-line synthesis-by-hand of the pilot characteristics required for control of the aircraft in that particular flight regime. This meant that the low-order, small-signal parameters of the aircraft had to be identified off-line and then, the pilot also had to be designed off-line so that it could be installed into the model of the aircraft for that particular flight regime.

This technique led to very good pilot models for these particular flight regimes, but for flight scenarios which include large deviations from trim conditions, the computer simulation pilots can no longer be used because of the change in aircraft parameters. Clearly, a human pilot can adapt to the change in aircraft parameters for maneuvers which include those in which large deviations from trim conditions occur.

Current Results

Previous research efforts have been directed toward the establishment of computer simulations of pilots for a modern helicopter model [1,2,3,4], and the extension of this model to a modern V/STOL aircraft.[5]. Both of these models depended on the off-line identification of the low-order, small-signal parameters of the aircraft under a particular flight regime and then an off-line synthesis-by-hand of the pilot characteristics required for control of the aircraft in that particular flight regime. This meant that the low-order, small-signal parameters of the aircraft had to be identified off-line and then, the pilot also had to be designed off-line so that it could be installed into the model of the aircraft for that particular flight regime.

This technique led to very good pilot models for these particular flight regimes, but for flight scenarios which include large deviations from trim conditions, the computer simulation pilots can no longer be used because of the change in aircraft parameters. Clearly, a human pilot can adapt to the change in aircraft parameters for maneuvers which include those in which large deviations from trim conditions occur. Thus, in order for a pilot model to control an aircraft in a way similar to an actual human pilot, the computer model of the pilot would be required to:

- (1) identify on-line and in real time the values of the changing parameters of the aircraft; and
- (2) adapt to the changing parameters of the aircraft as the small signal parameters of the aircraft change during large excursions from trim conditions.

In a later stage of the research conducted under this grant, the objective of having an adaptive pilot was achieved in two different ways:

- (a) an adaptive pilot called the OCM model using a Kalman filter and an on-line optimal controller [6,7,8,9] which has been modified for use in a V/STOL type aircraft.
- (b) an adaptive pilot called the ACM model using the McRuer-Krendal model [10,11] with parameters adapting to changes in the aircraft parameters in order to maintain a desired region of closed-loop operation of the aircraft in the parameter plane of damping-ratio vs undamped-natural-frequency.

Both of these pilot models were successfully installed in the computer simulation model of the Harrier II AV-8B aircraft residing on the University of Pittsburgh computer system and utilized to control a restricted range of maneuvers similar to real manned maneuvers provided the University of Pittsburgh by NASA Lewis Research Center with flight variables recorded on the tape labelled "PITT".

From this tape, data was extracted and corresponding scenarios were set up on both the OCM and the ACM pilot controlled simulation models of the Harrier II AV-8B installed on the University of Pittsburgh computer system. A

graphical comparison of data recorded from the simulated model with simulated pilot and the actual data taken from piloted aircraft as recorded on the NASA tape is shown in the next few figures. Some editing of the actual data was required in order to achieve the proper initialization of the simulation models.

The Optimal Control Model (OCM) in a Vertical Tracking Maneuver

The Optimal Control Model (OCM) pilot's dynamic response characteristics were evaluated by confronting the OCM with various multi-axis control objectives while actively participating within the flight control loops of the Harrier II AV-8B [6]. The control objectives were based on classical precision hovering maneuvers performed outside of the ground effects region. To illustrate the OCM pilot performance, consider a flight control maneuver that is complex in nature and exploits various aspects of the pilot's control characteristics, the vertical tracking maneuver. The vertical tracking maneuver consists of traversing between and positioning/aligning the vehicle at two vertically spaced targets, as shown in Figure 1. The targets are placed at 40 feet and 80 feet above the runway surface, and thus are outside of the vehicle's ground effects region. The control objective is to approach, align, and hold at one target for a period of time, traverse to the other target at a constant rate, hold at that target for a period of time and then return to the initial target. Alignment with the targets is considered to be a positioning/disturbance regulation operation, while motion between the target is considered to be a rate control/tracking maneuver. The multi-axis complexity and basic control structure requires that the pilot maintain a fixed nozzle angle, thus forward velocity and longitudinal positioning control are indirectly handled through pitch angle control. The displays monitored by the pilot are assumed to be the targets (external visual cues). A detailed description of the pilot configuration and control objectives of this and other maneuvers are presented in [6].

The following graphical comparisons relate the simulated OCM pilot's flight control operations (solid line) to those of the human piloted flight data (dashed line), provided by NASA-Lewis. The approach to and alignment with the target, by the OCM, is simulated by an initial yawing rotation (to simulate the final stages of the pilot's alignment with the targets). Plot 1 shows a heading angle comparison of the OCM (solid line) and the piloted flight data (dashed line). Transients associated with the target alignment phases are limited for times greater than 35 seconds ($\text{TIME} > 35 \text{ seconds}$). Regulation activities during the later stages of the maneuver show similar closed loop behavior. Plots 2 and 3 compare the altitude and vertical rate responses, respectively. These plots show similar trends in command trajectory following. Target alignment operations, of the human pilot, can be seen during the initial phases of the run ($\text{TIME} < 35 \text{ seconds}$). The vertical rate responses of Plot 3 show that the OCM has similar behavior during the execution of the vertical maneuvers ($\text{TIME} > 35 \text{ seconds}$), but does not completely capture the higher frequency content of the pilot data. This has been attributed to the low order altitude component representation of the OCM's internal reference model [6], and possibly the lack of engine auditory feedback. Plot 4 shows a comparison of the engine speeds. During the execution of the vertical maneuvers ($\text{TIME} > 35 \text{ seconds}$), the engine speeds show strikingly similar response characteristics in the OCM and human pilot. Plot 5 compares the pitch angle responses. This plot shows very similar vehicle orientations during the vertical maneuvering. This is an important

response characteristic due to the fixed nozzle angle which couples the pitch angle to the forward velocity and position. Plot 6 shows a comparison of the airspeed responses. The OCM pilot shows very similar characteristics in both magnitude and frequency content during the vertical maneuvers (TIME>35 seconds). Plot 7 compares the longitudinal position. This plot shows similar but out-of-phase positioning response. This has been attributed to the difference in initial conditions due to the human pilot's approach to the target. The position offset is also due to the initial target approach operations by the pilot. Report [6] provides additional insight into the OCM's operations and its application to other flight control maneuvers.

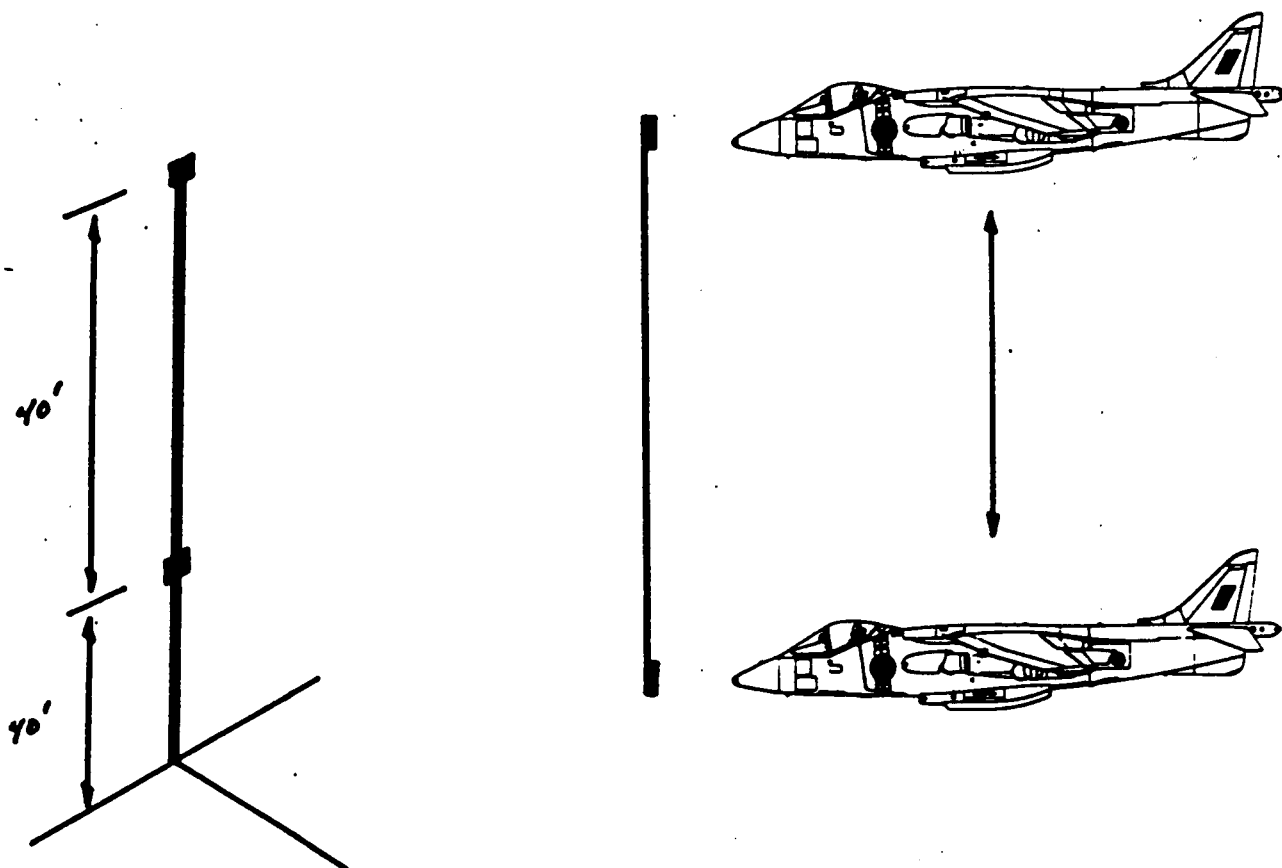
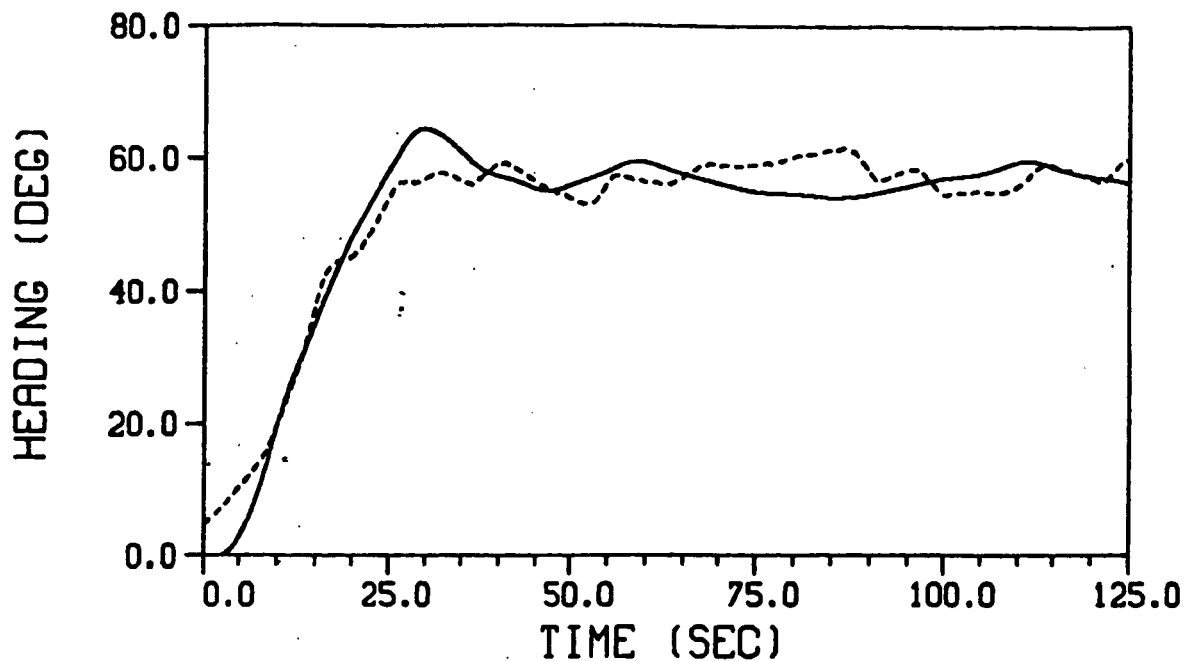
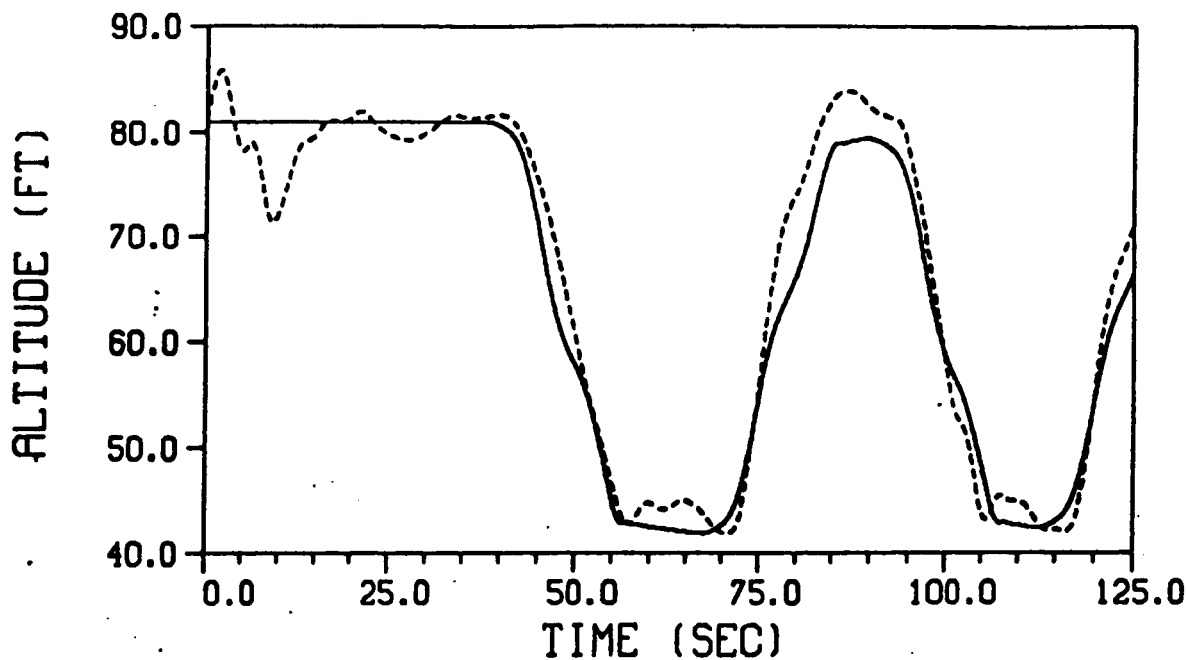


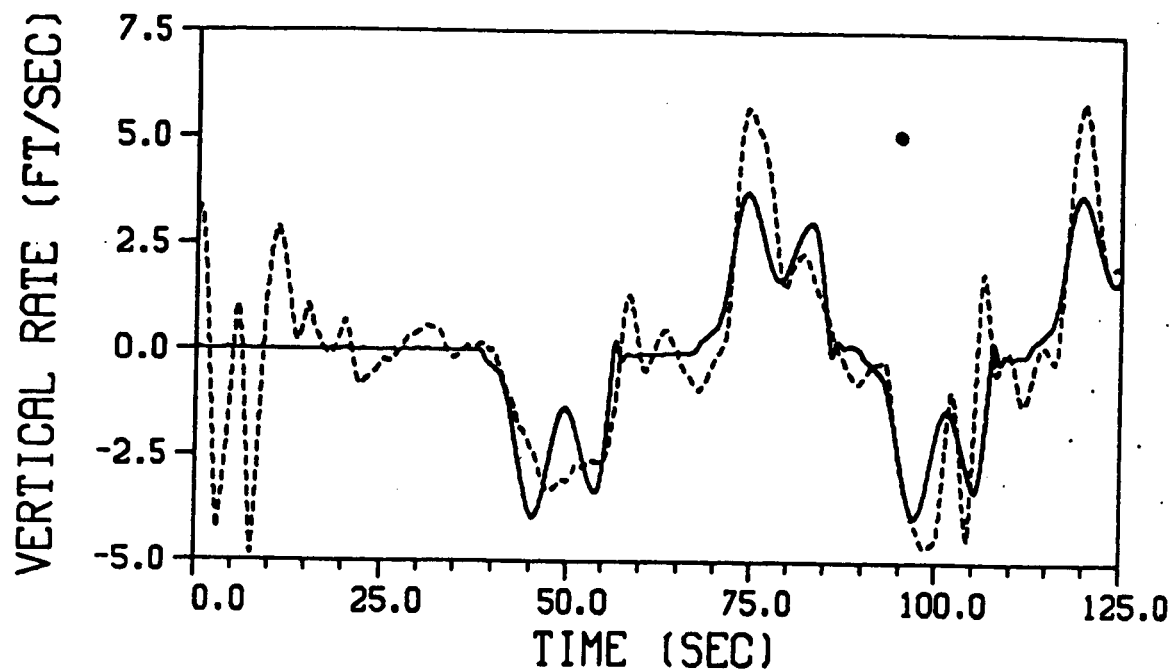
Figure 1. - Illustration of the target orientation and vehicle motion during the Vertical Tracking maneuver



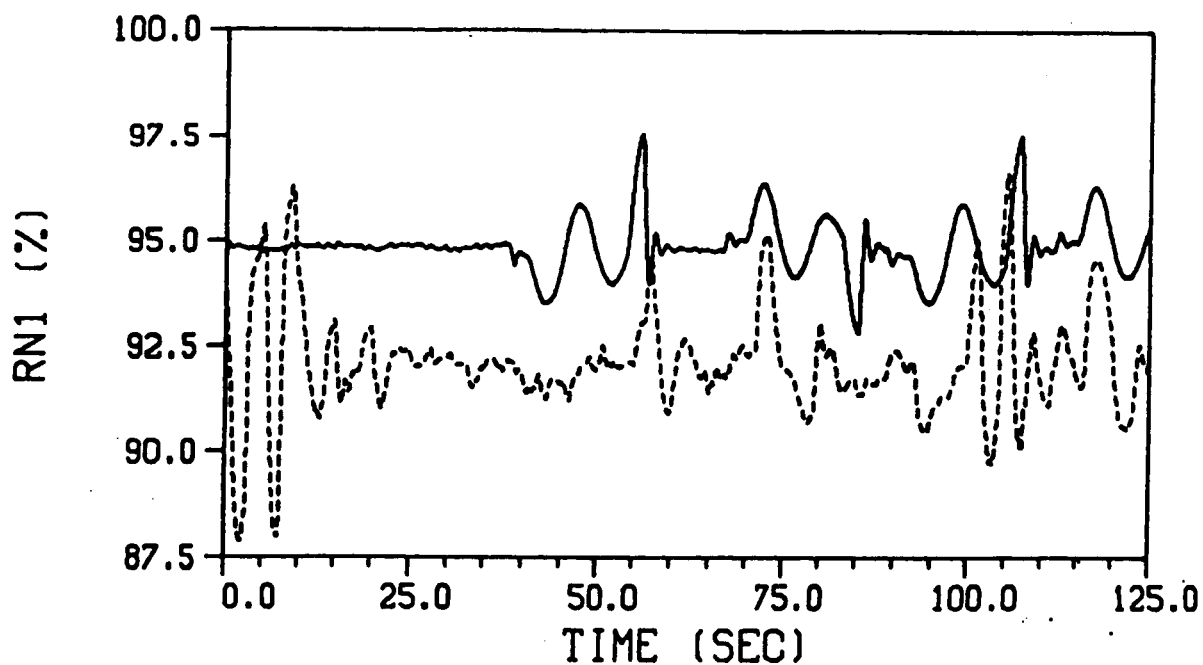
Plot 1. - Heading response comparison of the OCM pilot and piloted flight data during the vertical tracking maneuver.



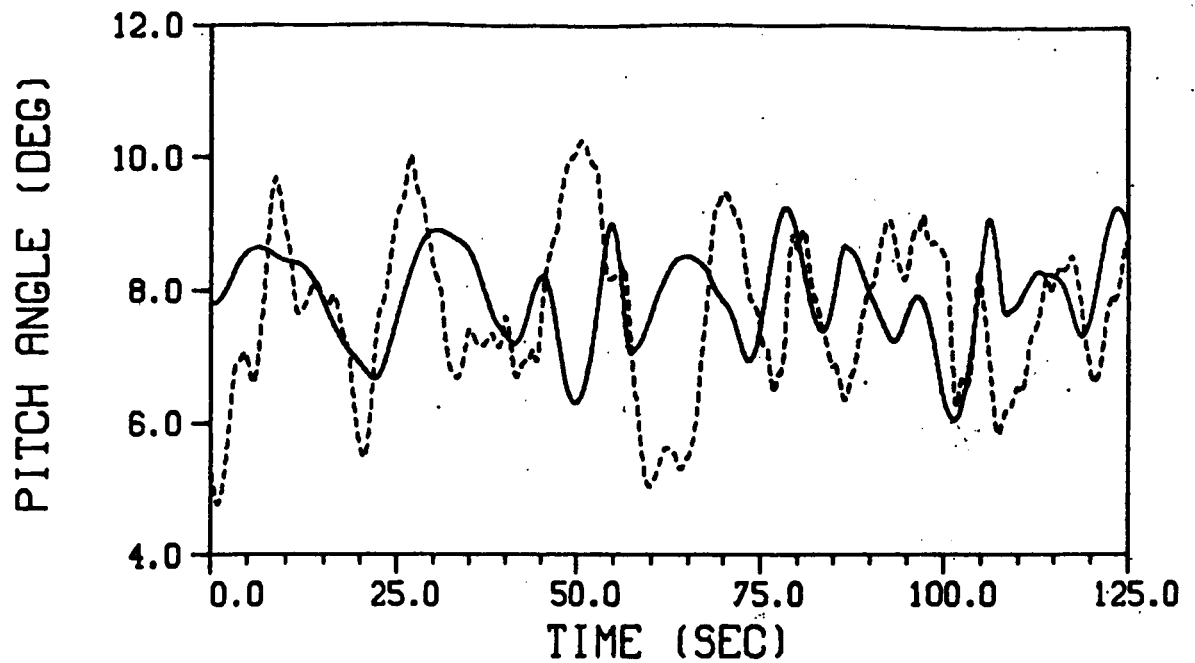
Plot 2. - Altitude response comparison of the OCM pilot and piloted flight data during the vertical tracking maneuver.



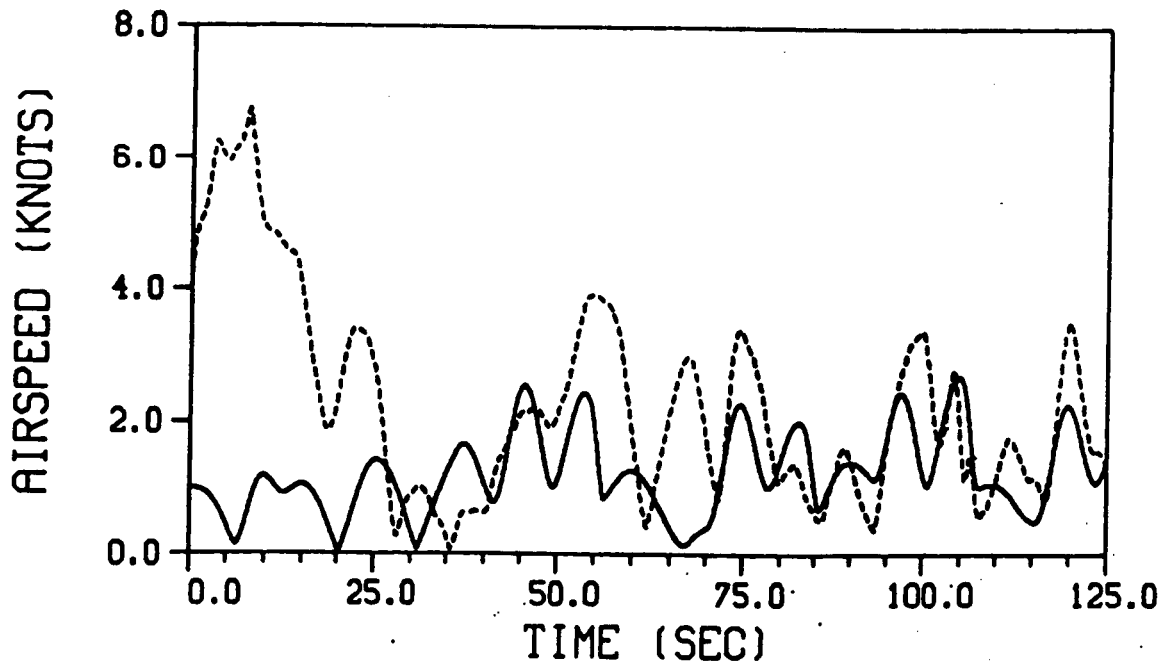
Plot 3. - Vertical rate response comparison of the OCM pilot and piloted flight data during the vertical tracking maneuver.



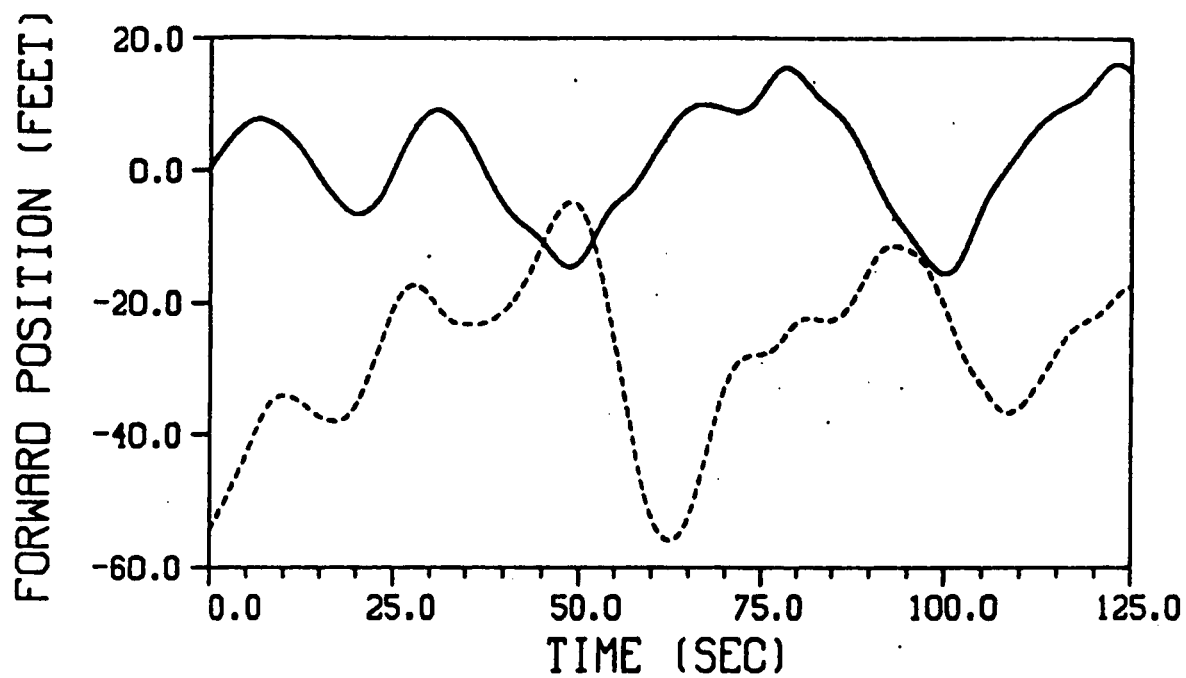
Plot 4. - Engine speed comparison of the OCM pilot and piloted flight data during the vertical tracking maneuver.



Plot 5. - Pitch angle response comparison of the OCM pilot and piloted flight data during the vertical tracking maneuver.



Plot 6. - Airspeed response comparison of the OCM pilot and piloted flight data during the vertical tracking maneuver.



Plot 7. - Longitudinal position comparison of the OCM pilot and piloted flight data during the vertical tracking maneuver.

The Adaptive Control Model (ACM) in a Lateral Tracking Maneuver

Figure 2 represents a schematic of the lateral tracking maneuver. Just as in the case of the Vertical Tracking Maneuver previously shown, Plots 8-17 show the aircraft and pilot responses (dotted line) using data taken from the NASA tape to the aircraft and pilot responses (solid line) using the Adaptive Control Model (ACM) for the simulated pilot. Once again, it is seen that these responses are very similar.

Note that, in both cases, there is a high frequency component in the actual data as compared to the simulated data. This is attributed to the actual pilot scanning the instruments and delay in his perception of the need for control action, which is often modeled by inserting residuals in human models. In the simulated pilots, there was no attempt to put this pilot residual into the pilot model versions since we do not have enough data to accurately model these residuals.

ORIGINAL PAGE IS
OF POOR QUALITY

LATERAL TRACKING MANEUVER

Target configuration and vehicle motion

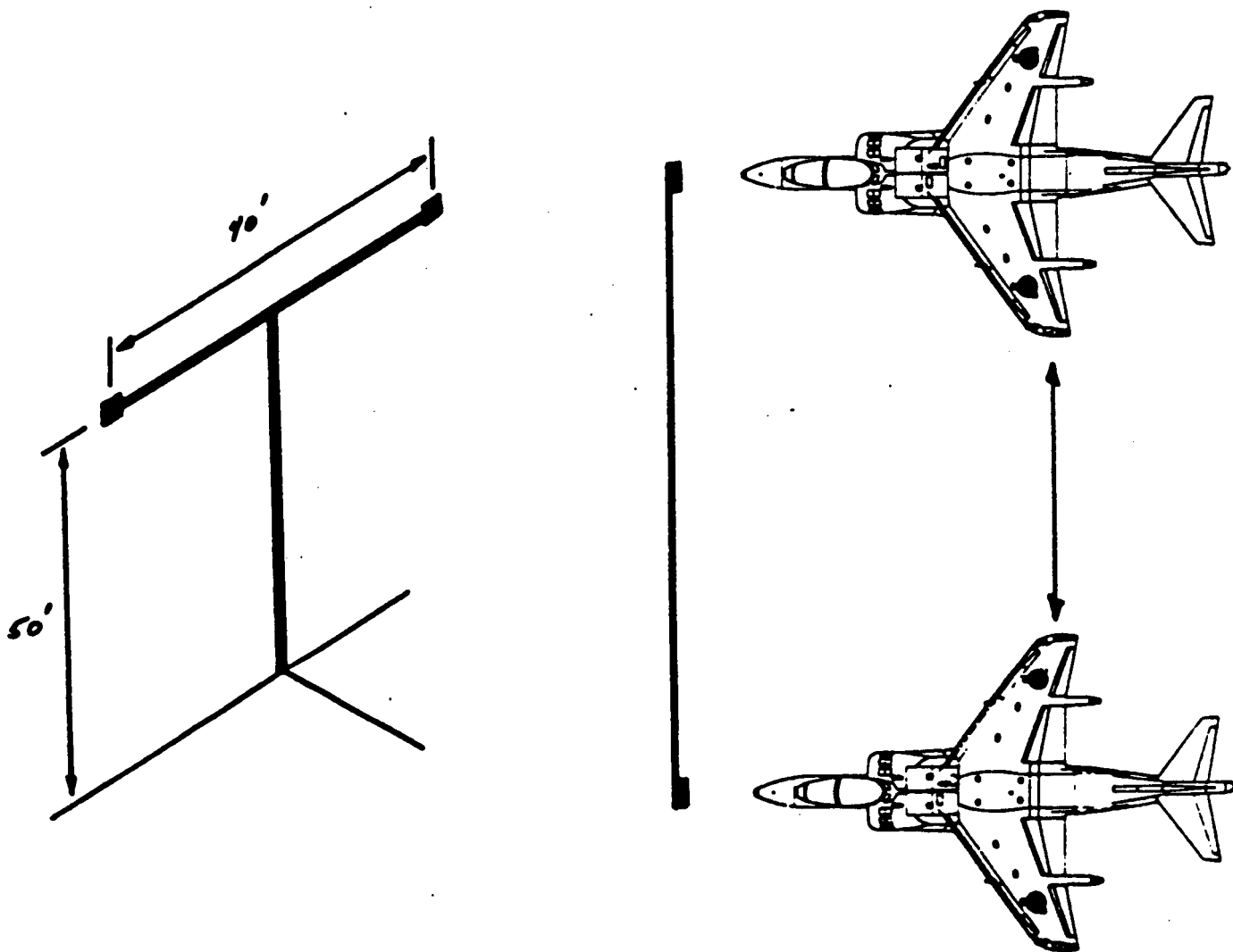
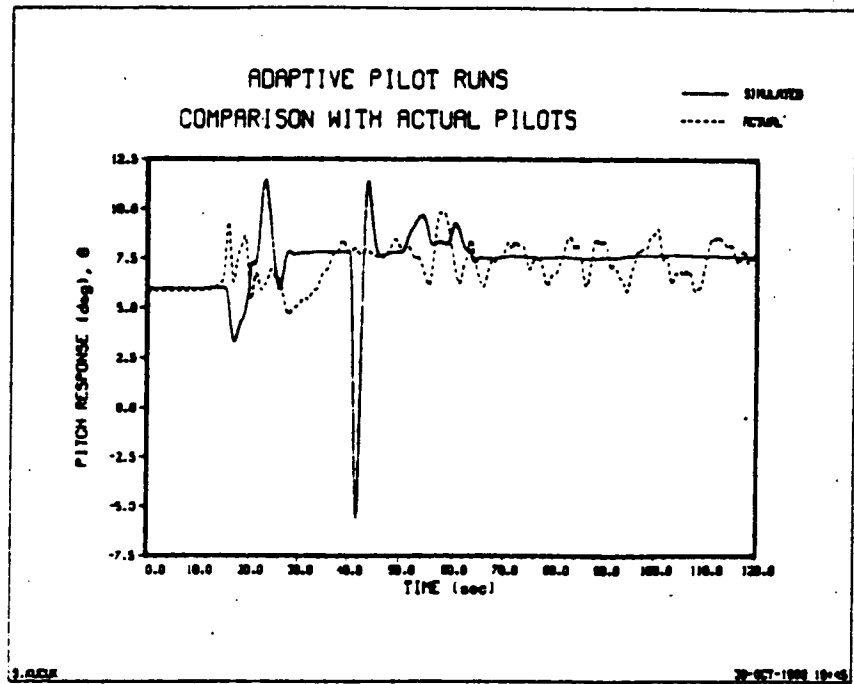
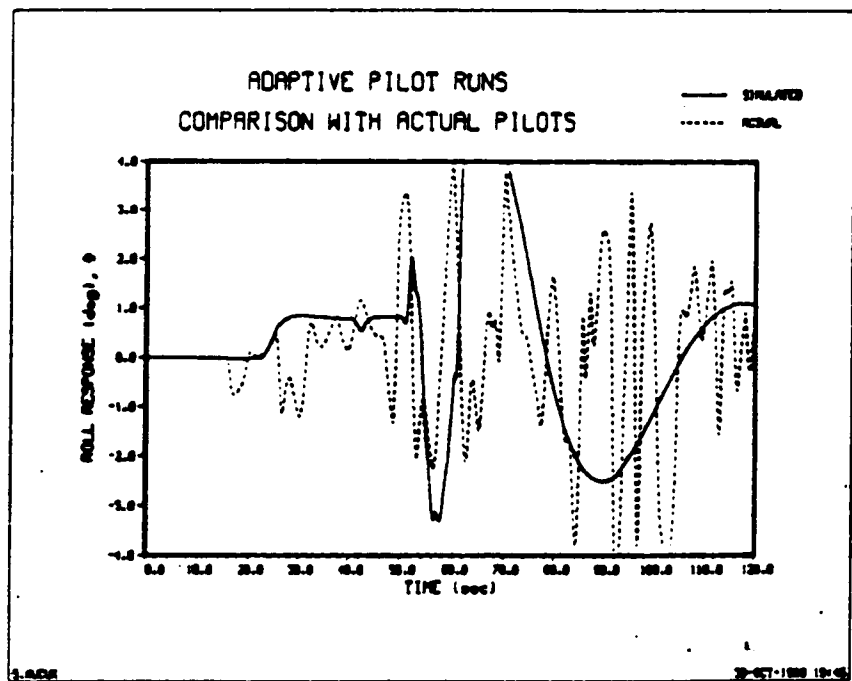


Figure 2. Lateral Tracking Maneuver - Target Configuration and Vehicle Motion

ORIGINAL PAGE IS
OF POOR QUALITY

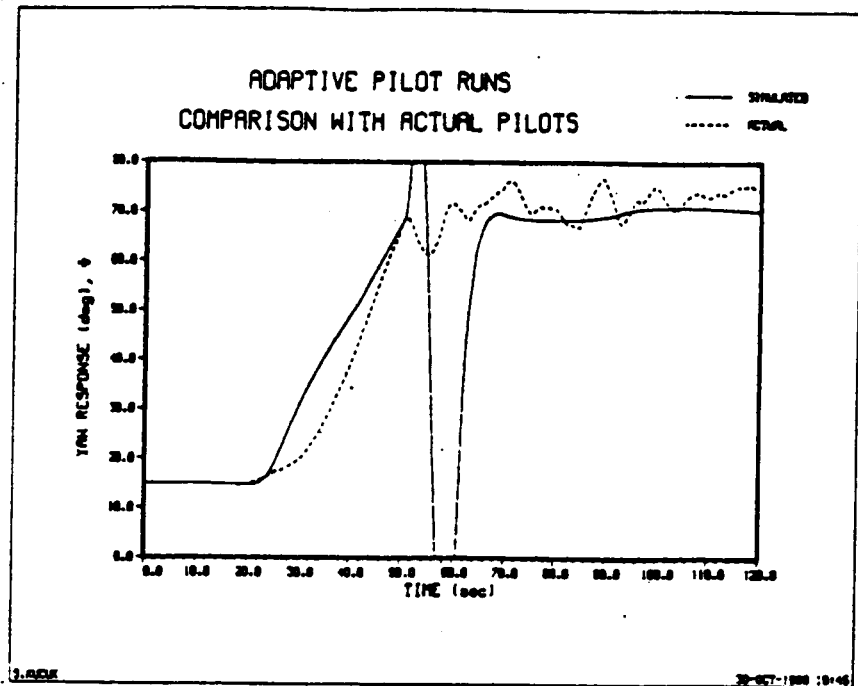


Plot 8. Actual vs. simulated pitch response (from NASA data)

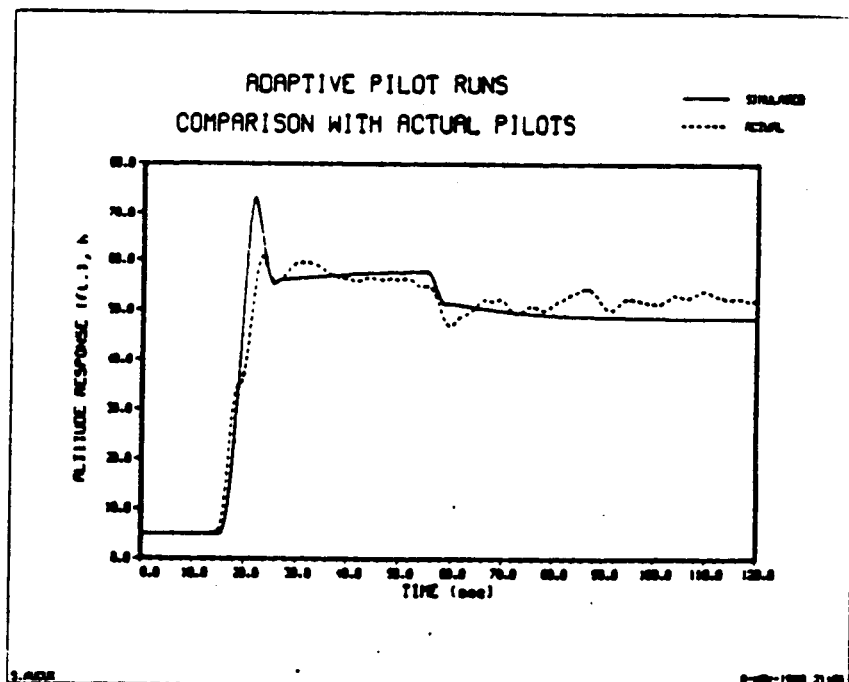


Plot 9. Actual vs. simulated roll response (from NASA data)

ORIGINAL PAGE IS
OF POOR QUALITY

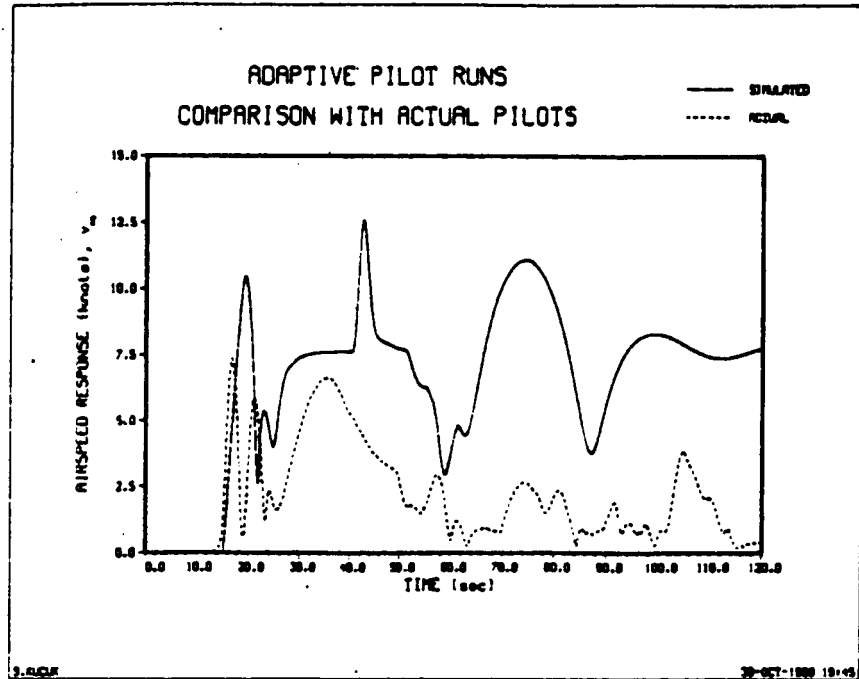


Plot 10. Actual vs. simulated yaw response (from NASA data)

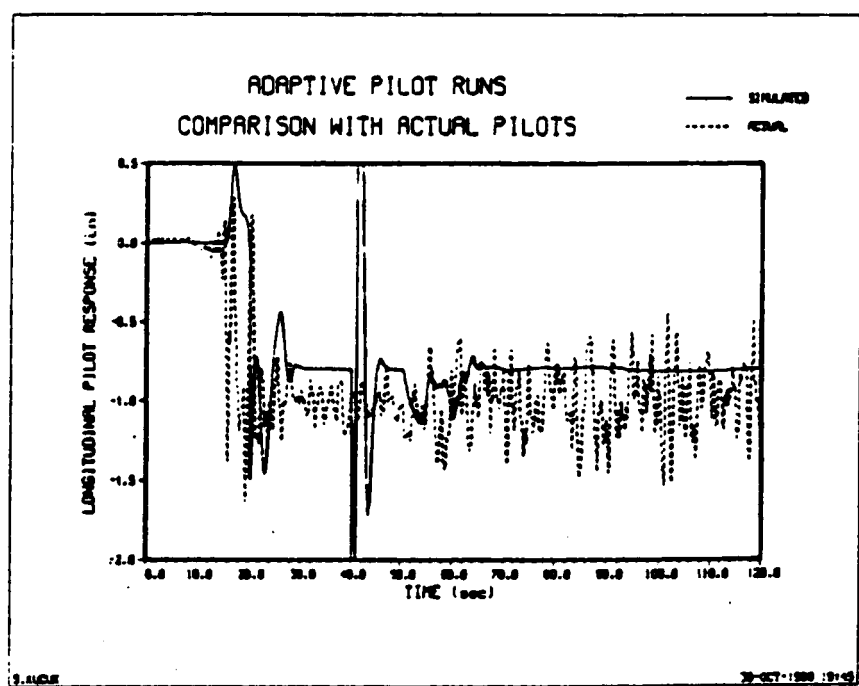


Plot 11. Actual vs. simulated altitude response (from NASA data)

ORIGINAL PAGE IS
OF POOR QUALITY

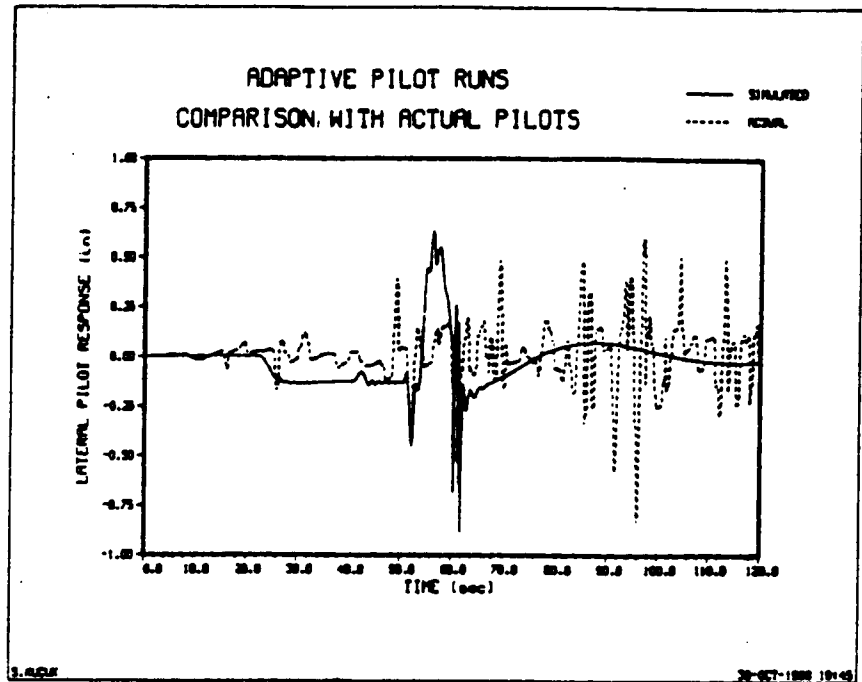


Plot 12. Actual vs. simulated speed response (from NASA data)

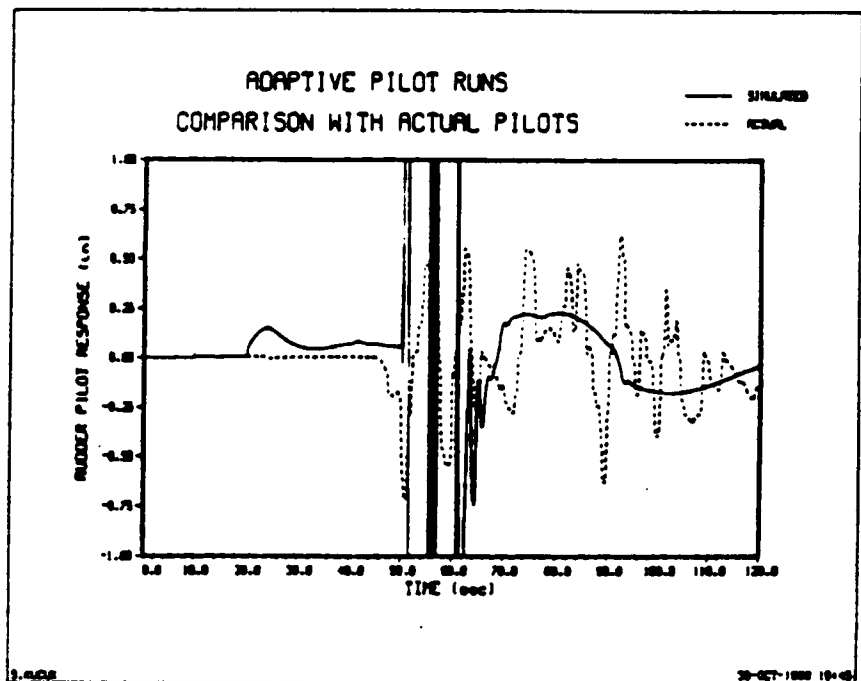


Plot 13. Actual vs. simulated longitudinal stick input (from NASA data)

ORIGINAL PAGE IS
OF POOR QUALITY

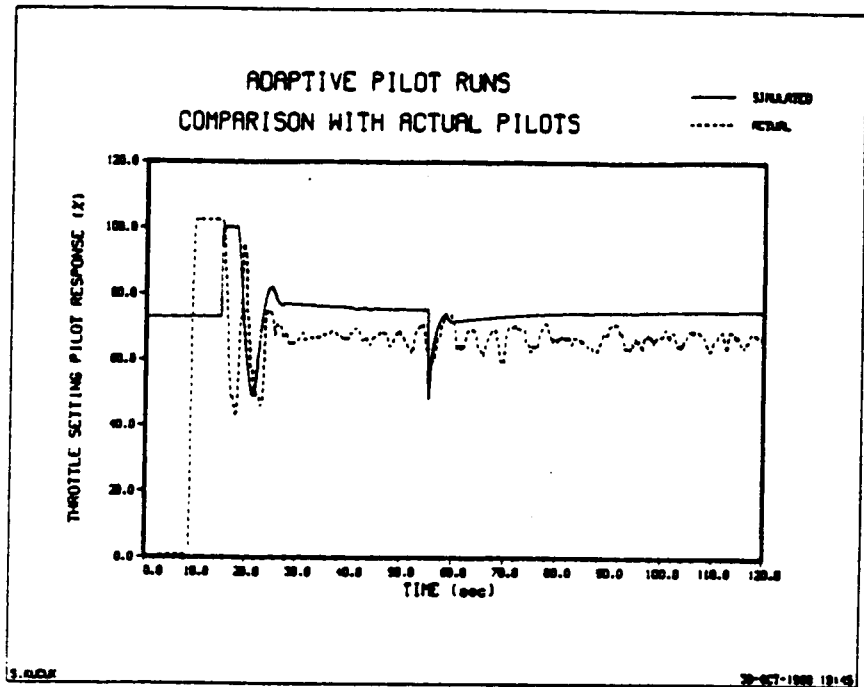


Plot 14. Actual vs. simulated lateral stick input (from NASA data)

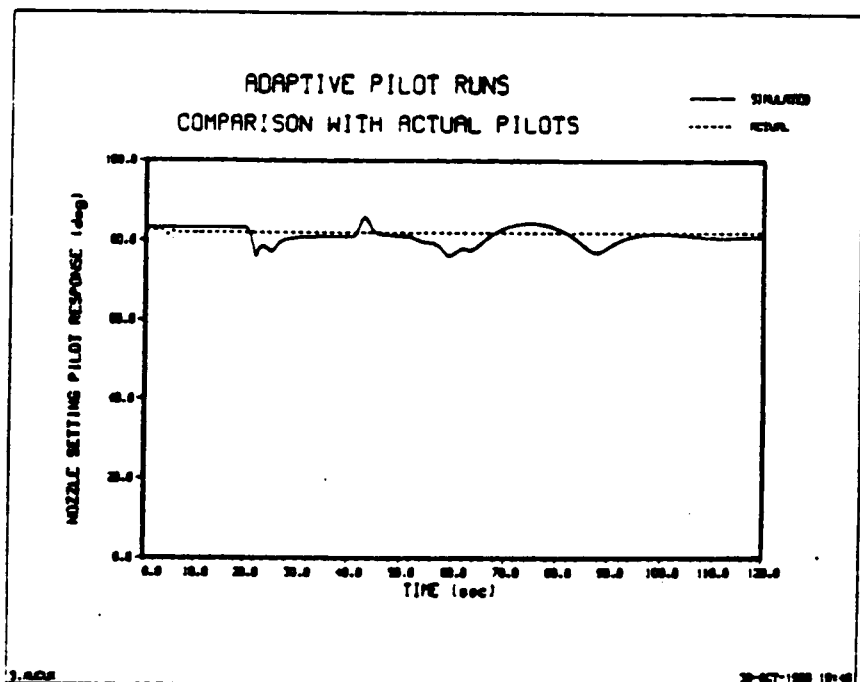


Plot 15. Actual vs. simulated rudder pedal input (from NASA data)

ORIGINAL PAGE IS
OF POOR QUALITY



Plot 16. Actual vs. simulated throttle setting input (from NASA data)



Plot 17. Actual vs. simulated nozzle setting input (from NASA data)

Unsettled Research Problems

As is often the case, new problems deserving additional attention arose during the course of this research. Those problems particularly related to the research proposed herein are listed below:

- (1) Further investigate the dynamics of the adaptive pilot model to minimize large initial control excursions
- (2) Investigate the occurrence of the negative real pole inside the unit circle in the NASA data -- and account for it in the discrete McRuer - Krendal Model
- (3) Refine both (a) the Optimal Control Pilot and (b) the Adaptive Control Pilot with additional data and scenarios from NASA
- (4) Provide and investigate full mission envelope capability
- (5) Hover / Transition / High Speed / Transition / Hover
- (6) Analyze additional scenarios to evaluate and refine the models for other uses
- (7) Evaluate human pilot to human pilot variations (differences) for the same maneuver from actual data
- (8) Evaluate high frequency differences in actual vs. simulated scenarios
- (9) Repeat the study for an Advanced STOVL aircraft.

REFERENCES

A complete list of references can be found in Appendix I [5], Appendix II [6] and Appendix III [10].

1. "Computer Simulation of a Single Pilot Flying a Modern High Performance Helicopter", M. E. Zipf, W. G. Vogt, M. H. Mickle, R. G. Hoelzeman, Fei Kai, J. R. Mihalow, Proceedings of the Eighteenth Modeling and Simulation Conference, University of Pittsburgh, April 23-24, 1987, (Instrument Society of America, Durham, NC., 1987), Vol. 18, pp. 1279-1294.
2. "Computer Simulation of Multiple Pilots Flying a Modern High Performance Helicopter", M. E. Zipf, W. G. Vogt, M. H. Mickle, R. G. Hoelzeman, Fei Kai, J. R. Mihalow, Proceedings of the Eighteenth Modeling and Simulation Conference, University of Pittsburgh, April 23-24, 1987, (Instrument Society of America, Durham, NC., 1987), Vol. 18, pp. 1295-1314.
3. Computer Simulation of a Single Pilot Flying a Modern High Performance Helicopter", M. E. Zipf, W. G. Vogt, M. H. Mickle, R. G. Hoelzeman, Fei Kai, J. R. Mihalow, NASA Technical Memorandum TM-100182, July 1988.

4. "Computer Simulation of Multiple Pilots Flying a Modern High Performance Helicopter", M. E. Zipf, W. G. Vogt, M. H. Mickle, R. G. Hoelzeman, Fei Kai, J. R. Mihaloew, NASA Technical Memorandum TM-100183, July 1988.
5. "A Computer Simulation of Low Order Pilot Models Flying a Thrust Vectored V/STOL Research Aircraft", M. E. Zipf, W. G. Vogt, M. H. Mickle, S. Kucuk, J. R. Mihaloew, Proceedings of the Nineteenth Modeling and Simulation Conference, University of Pittsburgh, May 5-6, 1988, (Instrument Society of America, Durham, NC., 1988), Vol. 19, pp. 733-764; Also, Appendix I, A Computer Simulation of Low Order Pilot Models Flying a Thrust Vectored V/STOL Research Aircraft of "Computer Simulation of a Pilot in V/STOL Aircraft Control Loops: Final Report for NASA Grant NAG 3-729", William G. Vogt, Marlin H. Mickle, Mark E. Zipf and Senol Kucuk, Department of Electrical Engineering, University of Pittsburgh, January 31, 1989.
6. Appendix II, The Optimal Control Model of a Pilot in V/STOL Aircraft Control Loops of "Computer Simulation of a Pilot in V/STOL Aircraft Control Loops: Final Report for NASA Grant NAG 3-729", William G. Vogt, Marlin H. Mickle, Mark E. Zipf and Senol Kucuk, Department of Electrical Engineering, University of Pittsburgh, January 31, 1989. This is a copy of the Final Report, THE INSERTION OF HUMAN DYNAMICS MODELS IN THE FLIGHT CONTROL LOOPS OF V/STOL RESEARCH AIRCRAFT, by Mark E. Zipf, Department of Electrical Engineering, University of Pittsburgh, 1989.
7. "An Optimal Control Model of Human Response, Part I: Theory and Validation", D.L. Kleinman, S. Baron, and W.H. Levison, Automatica, Vol. 6, pp. 357-369, 1970.
8. "An Optimal Control Model of Human Response, Part II: Prediction of Human Performance in a Complex Task", S. Baron, D.L. Kleinman, and W.H. Levison, Automatica, Vol. 6, pp. 371-383, 1970.
9. "A Model of Human Controller Remnant", William H. Levison, Sheldon Baron, David L. Kleinman, IEEE Transactions on Man-Machine Systems, Vol. MMS-10, No. 4, December 1969.
10. Appendix III, The Adaptive Control Model of a Pilot in V/STOL Aircraft Control Loops of "Computer Simulation of a Pilot in V/STOL Aircraft Control Loops: Final Report for NASA Grant NAG 3-729", William G. Vogt, Marlin H. Mickle, Mark E. Zipf and Senol Kucuk, Department of Electrical Engineering, University of Pittsburgh, January 31, 1989. This is a version of the thesis for a Master of Science Degree by Senol Kucuk, "AN ADAPTIVE HUMAN RESPONSE MECHANISM CONTROLLING THE V/STOL AIRCRAFT," Department of Electrical Engineering, University of Pittsburgh, 1988.
11. "Dynamic Response of Human Operators", D.T. McRuer and E.S. Krendal, Wright Air Development Center, WDAC TR-56-524, October 1957.

APPENDIX I

A Computer Simulation of Low Order Pilot Models Flying a Thrust Vectored V/STOL Research Aircraft

by

M. E. Zipf, W. G. Vogt, M. H. Mickle, S. Kucuk
Department of Electrical Engineering, University of Pittsburgh
and
J. R. Mihalow
NASA Lewis Research Center

Proceedings of the Nineteenth Modeling and Simulation Conference
University of Pittsburgh, May 5-6, 1988, (Instrument Society of America,
Durham, NC., 1988), Vol. 19, pp. 733-764

Final Report for NASA Grant NAG 3-729

Computer Simulation of a Pilot in V/STOL Aircraft Control Loops

Funded By:
NASA Lewis Research Center
21000 Brookpark Road
Cleveland, OH 44135

PRINCIPAL INVESTIGATORS:

William G. Vogt
Professor of Electrical Engineering
University of Pittsburgh
Pittsburgh, PA 15261
(412) 624-9686

Marlin H. Mickle
Professor of Electrical Engineering
University of Pittsburgh
Pittsburgh, PA 15261
(412) 624-9682

PARTICIPANTS:

Mark E. Zipf, Research Assistant
Department of Electrical Engineering
University of Pittsburgh
Pittsburgh, PA 15261

Senol Kucuk, Research Assistant
Department of Electrical Engineering
University of Pittsburgh
Pittsburgh, PA 15261

ORIGINAL PAGE IS
OF POOR QUALITY

**A COMPUTER SIMULATION OF LOW ORDER PILOT MODELS
FLYING A THRUST VECTORED V/STOL RESEARCH AIRCRAFT ***

Mark E. Zipf, William G. Vogt, Marlin H. Mickle, Senol Kucuk
Department of Electrical Engineering
University of Pittsburgh
Pittsburgh, Pennsylvania

James R. Mihaloew
NASA Lewis Research Center
Cleveland, Ohio

ABSTRACT

A computer simulation of low order human response pilot mechanisms actively participating within the flight control loops of a full thrust vectoring V/STOL research aircraft is presented. The emphasis is placed on the low speed, powered-lift region of the V/STOL flight envelope. A set of low order, linear transfer function models of the V/STOL research aircraft are created from time and frequency domain analysis of the dominant responses of a nonlinear, total force simulation model program provided by NASA. A low order transfer function is utilized to model the activities and intrinsic limitations of a human pilot. Human response pilot mechanisms are selected via root locus techniques and inserted into the flight control loops. The responses of the inserted pilot mechanisms to test maneuvers are presented and discussed.

INTRODUCTION

The interesting region of the V/STOL flight envelope occurs during low speed powered-lift activities. In this region, the aerodynamic properties of the aircraft significantly differ from those of high speed conventional flight. A case in point, is the V/STOL research aircraft that has been used in this study - a thrust vectored jet fighter (Harrier II AV-8B). During low speed flight the components of lift produced by aerodynamic means are small. The vehicle relies primarily on lift components supplied by the propulsion system. In addition, the aircraft's aerodynamic control surfaces (e.g. rudder, ailerons, etc.) no longer function as the primary control mechanisms. The Harrier relies on its reaction control system (RCS) to provide the additional control components that are needed to maneuver the aircraft.

When operating in this region of the flight envelope, the thrust vector is directed upward (nozzles downward). The propulsion system supplies the primary vehicle lift and the forward thrust in a manner similar to that of a helicopter main rotor. The magnitude of the thrust vector (controlled via the throttle) is used primarily to control the vehicle altitude and the longitudinal direction of the thrust vector (controlled via the nozzle angle) is used to control the vehicle speed. These controls are of course coupled to some degree, but can be used in various decoupled orientations.

Computer simulation has been used to better understand the activities of human pilots within the control loops of thrust vectored V/STOL aircraft. Similar research has been conducted on a high performance helicopter [1,2]. Powered-lift V/STOL aircraft pose unique problems in propulsion control design since the propulsion controls are an integral part of the overall flight control system. The pilot supplies inputs to both flight and propulsion control systems and pilot opinion is the major criterion for deciding whether control system performance is satisfactory. The pilot must therefore be considered throughout the design and evaluation process. The current approach is to use piloted simulators for

* Partially supported by National Aeronautics and Space Administration Grant Number NAG 3-729.

evaluating the overall integrated control system after it has been designed. This is an effective and necessary step, but it is a process that requires development and evaluation at a remote site within a simulator system structure and schedule. Analytic pilot models provide an alternative to the use of manned simulators. The ability to analyze and evaluate integrated flight-propulsion controls for V/STOL aircraft, before they are introduced to a remote simulator facility, provides a powerful design tool. The remainder of this introduction will provide a brief summary of the techniques that have been used to develop and analyze piloted flight control.

Control Structure

Pilot activities during low speed operations are primarily directed toward achieving stabilized control over the vehicle. A control structure for piloted flight simulation is described by the command based, cascaded control configuration shown in Figure 1.

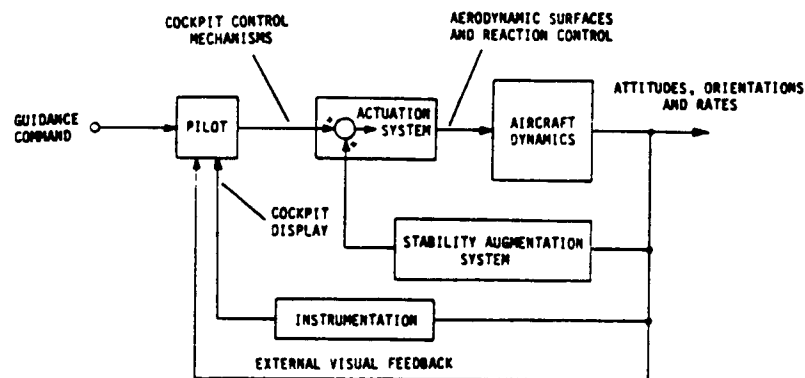


Figure 1. - Cascaded Structure for Piloted Flight Control Simulation

Within this structure, the pilot appears as a cascaded compensator that is driven by command based vehicle attitudes and orientations from some type of guidance or navigation process. The pilot attempts to orient the vehicle in the manner specified by the command by manipulating the cockpit control mechanisms. The control configuration shown in Figure 1 assumes that the pilot feedback is based on visual assessments of cockpit instrumentation and external visual cues. The use of visual feedback will however, reduce the effectiveness of the pilot because of the inherent limitations of human visual system information processing capabilities. In addition, the pilot's physical make-up tends to limit his ability to supply the desired cockpit control mechanism deflections because of muscular systems restrictions in bandwidth and range. For the purpose of simulation, the pilot is modeled by a low order transfer function that has been developed by McRuer and Krendal [3]. The parameters of the transfer function are selected from an analysis of aircraft dynamics and control function requirements in a manner similar to those in [1.2]. Simulation of aircraft dynamics are supplied by a nonlinear model program [5.6], provided by NASA-Lewis. In this simulation model the stability augmentation system (SAS) provides damping of aircraft angular rates. The SAS is engaged during all aircraft dynamic tests and pilot insertion studies.

Pilot Dynamics

The linear transfer function model for the pilot as used in this research was developed by [3] and is illustrated in Figure 2.

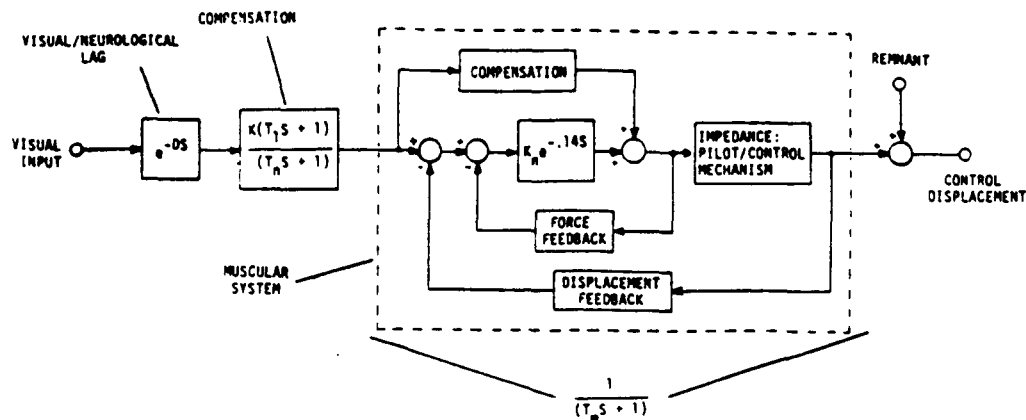


Figure 2. - Block Diagram of a Human Response Model

The pilot model transfer function is given by

$$G_{\text{pilot}}(S) = \frac{K (T_1 S + 1) e^{-DS}}{(T_m S + 1) (T_n S + 1)} \quad (1)$$

The model uses assessments of visually-based information to produce compensative control mechanism displacements. Human activities are represented by physiological and equalization sections. Physiologic attributes simulate the limitations and abilities of human physical mechanisms. The inherent lags associated with the human visual, information processing, and signal transmission systems are modeled by the pure delay, D . The bandwidth of the muscular system is represented by a first order lag network with a time constant, T_m . The physiologic parameters are constrained in the following manner:

$$0.15 \leq D \leq 0.23 \text{ sec}$$

$$T_m = 0.1 \pm 20\% \text{ sec}$$

The equalization attributes simulate the control strategies employed by the human to achieve the required closed loop responses. The time constants of this lead-lag network, T_1 , T_n , are adjusted to close the control loop at approximately 0.5 Hz. The equalization network is constrained in the following manner:

$$T_1 \leq 2.5 \text{ sec}$$

$$T_n \leq 20 \text{ sec}$$

The inherent randomness of human behavior is simulated by the remnant. The remnant is the simulation of the nonlinear, random actions that are inherent to human behavior. The primary focus of this research has been directed toward the fundamental control activities of the pilot during various maneuvers. A zero remnant is therefore used during the development of the pilot control strategies. Remnant selection for these types of piloted flight configurations have been determined in [4].

Aircraft Model Identification

The principal simulation tool used in the study was time simulation program described in [5] and provided by NASA-Lewis. This program implements a total force, large angle, nonlinear mathematical model developed in [6]. Low order linear models of the aircraft dynamics were obtained by an analysis of the time and frequency responses of the simulation program to test deflections of the cockpit control mechanisms. The models that have been developed indicate the dominant vehicle behavior and are based primarily on short period dynamics in the pilot frequencies [1.3.8]. Phugoid modes and cross couplings

are neglected and considered secondary to the dominant responses. Figure 3 illustrates this type of separation.

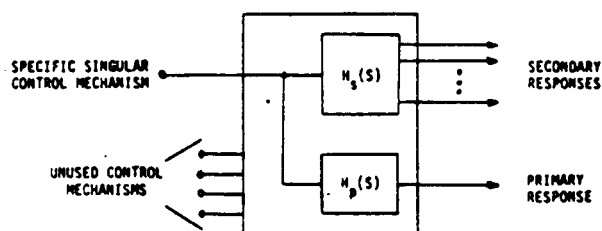


Figure 3. - Block Diagram of the Primary and Secondary Vehicle Responses

Techniques of Pilot Selection

The determination of the pilot's equalization parameters is based on the single variable control configuration shown in Figure 4.

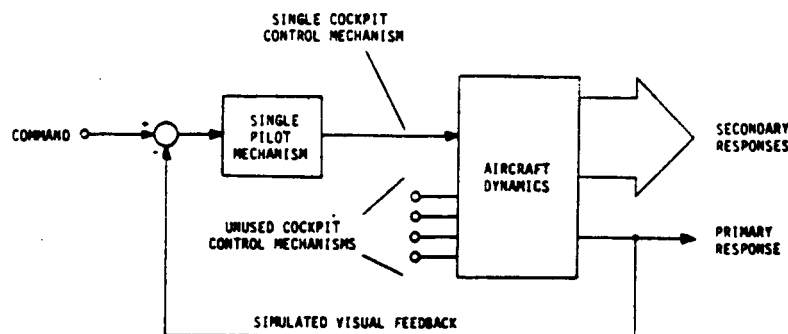


Figure 4. - Single Variable Flight Control Configuration

The configuration is organized in such a way that the manipulation of each specific cockpit control mechanism is based on the assessment of the visual feedback obtained from the observation of a specific cockpit instrument or external visual cue. This allows control of only the dominant variable for that control mechanism. Secondary variable reactions are treated as disturbances.

The pilot's equalization parameters are selected via root locus techniques [1]. One factor that tends to complicate this type of developmental analysis is the lag associated with human visual and information processing systems. This time delay tends to produce a destabilizing distortion of root loci asymptotic behavior. The delay is approximated by placing a large number of poles (20), at a comparatively large distance from the origin on the negative real axis (-100). The physical limitations of the human response are given by the time constant of the muscular system ($T_m = 0.1$ sec) and the lag of the visual/neurological system ($D = 0.2$ sec). The modified transfer function of the single variable pilot mechanism, shown in equation (1), that is used for design purposes is given by:

$$G_{\text{pilot}}^{\text{design}}(s) = \frac{K(s+a)}{(s+b)} \cdot \frac{(100)^{20}}{(s+10)(s+100)^{20}} \quad (2)$$

where

$$a \geq 0.8$$

$$b \geq 0.0$$

During pilot insertion studies a zero order hold discrete time representation of equation (1) was used.

Pilot Insertion Strategies

When a participating human pilot is introduced into the control loops, he uses all cockpit control mechanisms to provide an operational control by employing visual, audio, and other forms of feedback cues. For the purpose of simulation, a comprehensive human response pilot model is constructed by integrating various single variable pilot mechanisms into a multivariable structure, as shown in Figure 5.

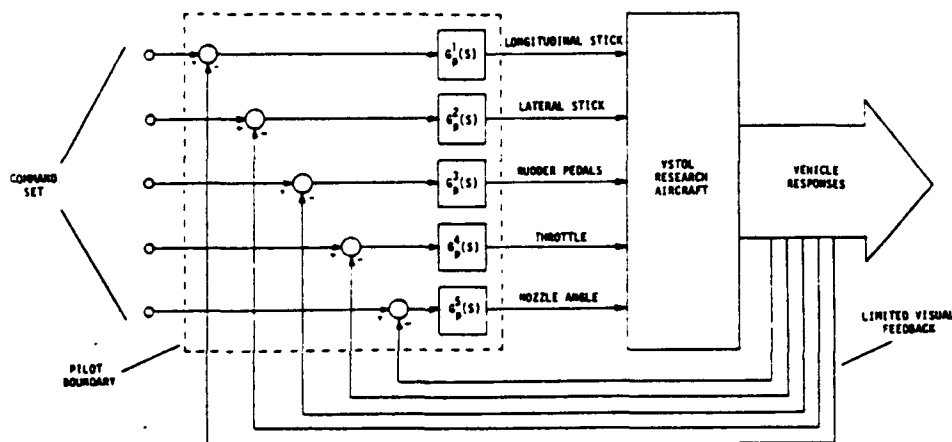


Figure 5. - Multivariable Pilot Structure

The multivariable pilot structural configuration is defined by the manner in which visual feedback is interpreted and applied to the cockpit control mechanisms via a specific set of single variable pilot mechanisms. The intrinsic limitations of each configuration make it applicable to only a specific set of flight control maneuvers. Each type of flight maneuver or command sequence is therefore associated with a specific multivariable pilot configuration. In general, a command maneuver will be described by a set of vehicle attitudes and/or rates that define the new orientation that the vehicle is required to attain. The pilot's task is to manipulate the cockpit control mechanisms in such a way as to reorient the vehicle. The intricacy of the maneuver defines the number of attitudes and/or rates that are simultaneously involved in the operation.

The flight control objectives associated with simple maneuvers require the control of only one primary vehicle attitude or rate. The remaining secondary variables are monitored and regulated to preserve the stabilized aspects of the vehicle orientation (e.g. level flight). This type of operation can be performed by the configuration shown in Figure 6.

The remainder of this paper consists of three primary parts:

1. An analysis of test responses of the nonlinear simulation model. Here, test deflections are injected into the cockpit control mechanisms and vehicle reactions are analyzed. Low order transfer function models of the aircraft's responses are generated for use in the selection of pilot characteristics.
2. Discussion and construction of a set of single variable control mechanisms. The low order aircraft models, obtained in part 1, are used to construct a group of single variable pilots. These pilots will provide the control of single aircraft variables, by visually assessing the aircraft variable and closing the control loop through a specific cockpit control mechanism. Each pilot will be designed with a specific control objective in mind.

3. Discussion and construction of a single multivariable pilot mechanism. The set of single variable pilot mechanisms will be organized into a single, multivariable pilot. This pilot will provide a comprehensive control of the aircraft by closing multiple control loops through all available cockpit control mechanisms. The pilot's control organization/configuration will depend on the control objectives that are required. A group of pilot configurations will be obtained for a set of standard aircraft control maneuvers.

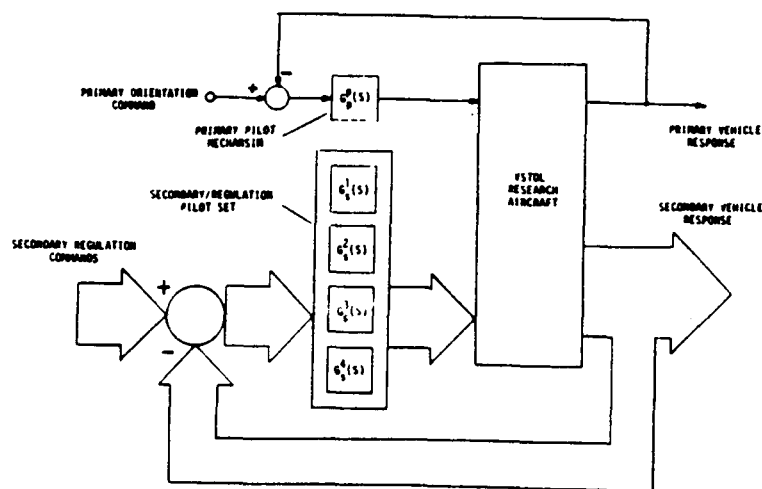


Figure 6. - A Primary / Regulation Control Configuration

ANALYSIS OF AIRCRAFT DYNAMICS

This section presents the development of a set of low order transfer function models that are based on an investigation of the fundamental behavior of the nonlinear aircraft simulation model. The low order models describe primary, short period vehicle reactions that are induced by deflections of specific cockpit control mechanisms. These models are primarily intended to identify the strongest operational modes of the specific control mechanisms. For the context of this and the remaining discussions, the dynamics and overall accuracies and distortions of the cockpit instrumentation will not be considered.

Flight Envelopes

The flight envelope of the VSTOL research aircraft that has been used in this study can be defined by the direction of the thrust vector [7]. Figure 7 shows three basic flight configurations. The high speed configuration, shown in Figure 7a, is characterized by the thrust vector being directed forward (i.e. nozzle jet vectors aft). In this mode, the propulsion system supplies the forward thrust component in a manner that is common to conventional aircraft. The lift and control components are supplied by the aerodynamic surfaces as they are forced through the atmosphere. The magnitude of the thrust vector supplied by the propulsion system is used to control vehicle speed. The stabilator is used to control the angle of attack and altitude.

The transition mode, shown in Figure 7b, is described by a general loss of aerodynamic responsiveness. As forward speed decreases, aerodynamic surfaces lose their ability to provide necessary lift and control functions. As the name implies, the vehicle control actions are in a transition between atmospheric flight and powered-lift activities. In general, sustained flight in this region is avoided by typical maneuvers associated with acceleration to and deceleration from the high speed envelope [7].

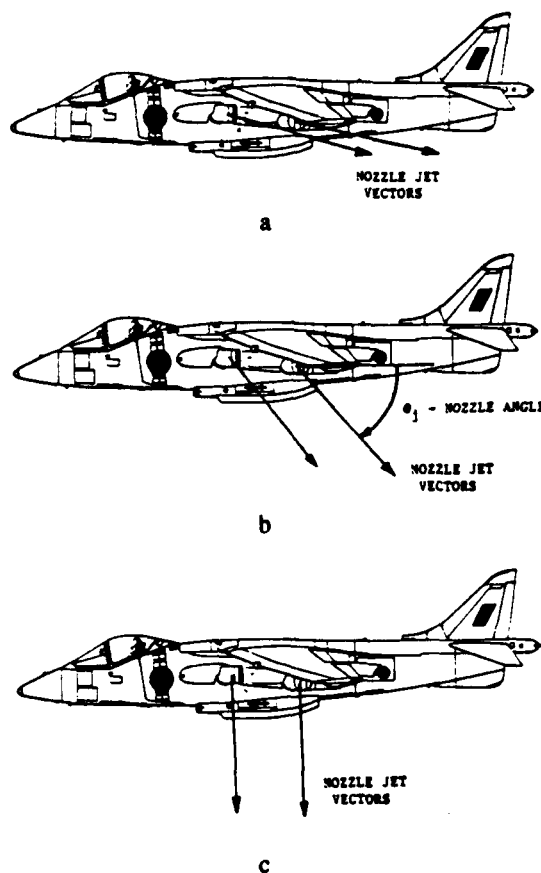


Figure 7. - Thrust Vectored Flight Envelopes

The low speed configuration, shown in Figure 7c, is characterized by the thrust vector being directed upward (i.e. nozzle jet vectors downward). The lack of sufficient forward velocity requires that the propulsion system provide the lift components (powered-lift). A closer examination reveals that the propulsion system supplies the forward thrust and the primary lift component in a manner similar to a helicopter's main rotor. The magnitude of the thrust vector is primarily utilized to control the altitude and its direction is used to adjust forward speed. The aircraft relies on its reaction control system (RCS) to supply control and maneuver thrusting.

As mentioned previously, the primary focus of the research has been directed toward the low speed - powered-lift flight envelope. Dynamic response tests were conducted while in trimmed forward flight at speeds ranging from hover to 35 knots. The vehicle was configured with the landing gear down, flaps extended to 60 degrees, and the lift enhancement devices fully extended. The SAS was enabled and provided damping of angular rates. To simplify and structure the investigation, an initial decoupling was achieved by separating the control and response characteristics of the aircraft into the longitudinal and lateral-directional control sets. These sets are of course coupled to some degree, but many of their operational modes can be separated [8].

Longitudinal Control Set

The longitudinal control set specifies the control mechanisms and their associated reactions that primarily exist in the X-Z body plane. The three cockpit control mechanisms that operate within this region are: 1) nozzle angle, 2) throttle, 3) longitudinal stick.

Nozzle Angle

The nozzle angle controls the direction of the propulsion system thrust vector. A typical low speed - powered-lift thrust diagram of a decrease in nozzle angle is shown in Figure 8.

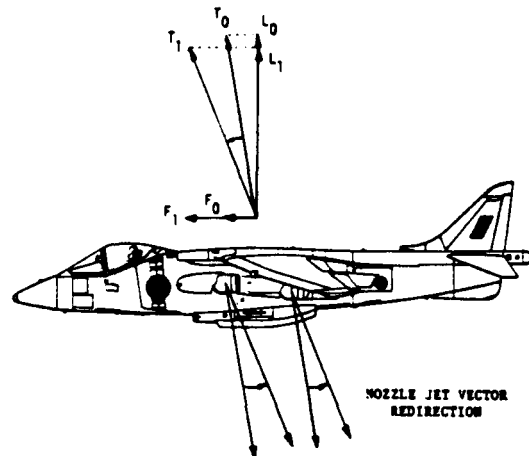


Figure 8. - Thrust diagram of a reduction of nozzle angle during power lift activities

The nozzle angle for this flight envelope is large. The control structure is very similar to that of the longitudinal cyclic of a helicopter. Minor changes in the direction of the thrust vector will tend to dominate the forward component. This suggests that the nozzle angle will primarily control the vehicle speed. Variations of the nozzle angle in the low speed flight envelope will not have a significant impact on the primary lift components.

Throttle

The throttle controls the magnitude of the propulsion system thrust vector. A thrust diagram of an increase in engine speed is shown in Figure 9.

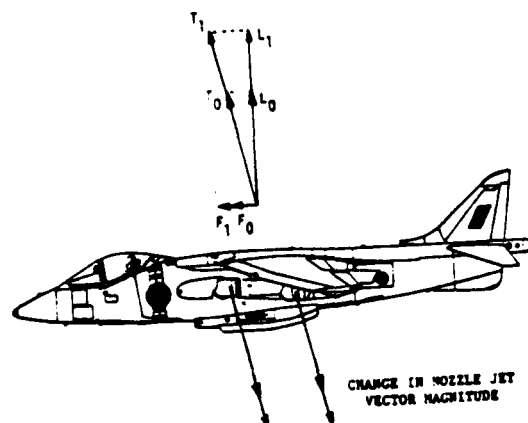


Figure 9. - Thrust diagram of an increase in engine speed during powered-lift activities

This control behavior is similar to the main rotor collective of a helicopter. Changes in the magnitude of the thrust vector will tend to dominate the lift component. Vehicle altitude components will therefore be controlled with the throttle. Minor changes in the thrust vector magnitude will not have a significant impact on the velocity components.

Longitudinal Stick

The longitudinal stick is the first of the control mechanisms that use the auxiliary thrust components of the RCS jets to perform pitching maneuvers. Figure 10 illustrates the auxiliary thrust components produced by deflecting the longitudinal stick.

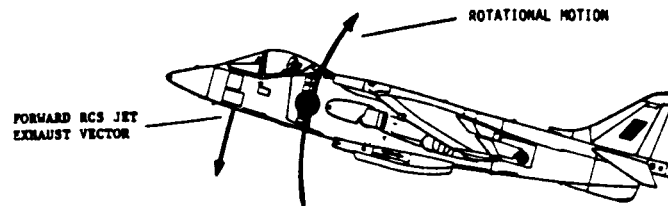


Figure 10. - Thrust diagram of the backward deflection of the longitudinal stick

Effects of RCS on the propulsion system due to engine air bleed have been ignored. The RCS thrust vectors produce rotational movements about the y-body axis. The aircraft longitudinal inertial components tend to induce sluggish responses. During low speed flight the longitudinal stick is used primarily to preserve longitudinal orientations (e.g. angle of attack, pitch angle). Level flight at low speeds is accomplished by delicately balancing the aircraft about its center of gravity. It is important to note that the primary thrust vector of the propulsion system will be redirected during pitching maneuvers if the nozzle angle is fixed.

Lateral - Directional Control Set

The lateral - directional control set specifies the control mechanisms and their associated reactions that exist primarily in the Y-Z body plane (lateral) and the X-Y body plane (directional). The two cockpit control mechanisms that operate within these planes are: 1) lateral stick, 2) Rudder Pedals.

Lateral Stick

The lateral stick uses the auxiliary thrust components of the wing tip RCS jets to perform rolling maneuvers. Figure 11 illustrates the auxiliary thrust components produced by deflection of the lateral stick.

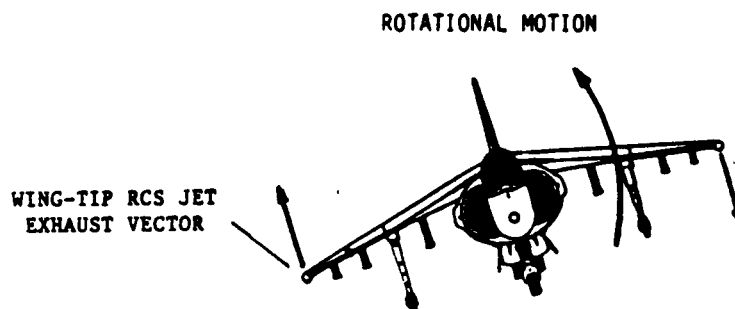


Figure 11. - Thrust diagram for a right deflection of the lateral stick

Again, the effects of the RCS bleed on the propulsion system are ignored. The lateral inertial components and the RCS wing tip geometry create a highly responsive rotational moment about the X body axis. The rolling motion redirects the lateral components of the thrust vector. This redirection will tend to dominate the lateral velocity components. In addition, the preservation of level flight (roll angle) characteristics is performed with the lateral stick. It is important to note that the responsiveness of the roll components can lead to situations that are unrecoverable [7].

Rudder Pedals

The rudder pedals use the tail end RCS jets to perform yawing and lateral maneuvers. Figure 12 illustrates the auxiliary thrust components produced by deflection of the rudder pedals.

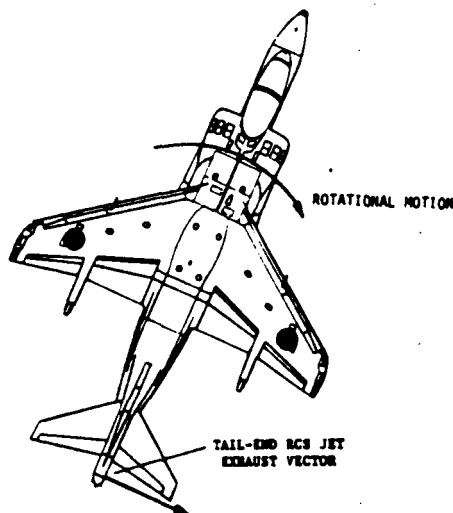


Figure 12. - Thrust diagram for a counter-clockwise rotation of the rudder pedals

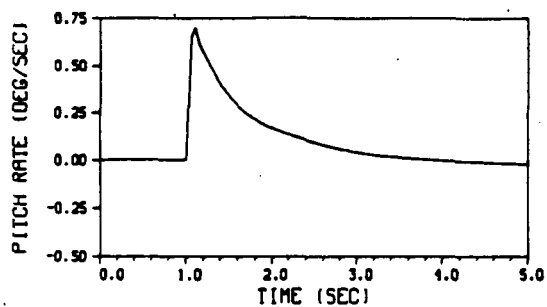
The RCS thrust vectors induce rotations about the Z body axis. This allows rudder pedal control of the lateral velocity during turn coordination tasks (sideslip reduction). In addition, heading regulation can be provided via the rudder pedals.

Longitudinal Models

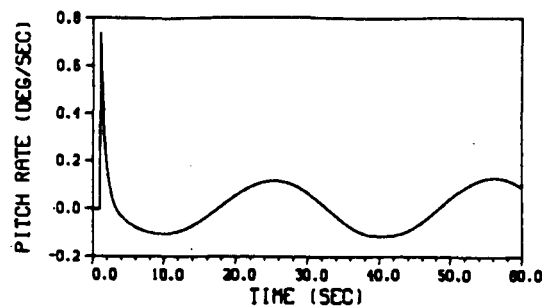
This section presents the low order models of the longitudinal dynamics of the V/STOL research aircraft. The primary responses that will be investigated are: 1) pitch angle components, 2) altitude components, 3) forward velocity components.

Pitch Angle Model

This model considers the fundamental response characteristics of the pitch angle components due to operation of the longitudinal stick. The time based body pitch rate response at 10 knots and hover, due to a 1 inch impulse deflection of the longitudinal stick can be seen in Plots 1,2, respectively. Plot 1 shows the initial phase of the time response and tends to indicate simple pole behavior in pitch rate. The time constant reveals a relatively sluggish response that is characteristic of the auxiliary thrust component of the forward RCS jet when matched against the longitudinal inertial components. Plot 2 shows the longer term response characteristics. Signs of the parasitic phugoid mode are present in the later phases of the response. This indicates a long term "teetering" behavior in the pitch response. Changes in forward speed tend to increase the period of the phugoid mode. No significant variations in the short period response characteristics due to changes in forward speed are apparent. This type of characteristic is expected because there is little change in the aerodynamic behavior in the low speed envelope.



Plot 1.



Plot 2.

A low order transfer function model that describes the short period response in the pilot frequencies over the low speed flight envelope is given by:

$$G_{\text{THETDT}}(S) = \frac{\text{THETADT}(S)}{\text{LONG}(S)} \approx \frac{K_{\text{THETDT}}}{S + a_{\text{THETA}}} \quad (3)$$

where

$$K_{\text{THETDT}} = 0.71 \text{ deg}/(\text{inch-sec}^2)$$

$$a_{\text{THETA}} = 1.56 \text{ sec}^{-1}$$

The parameters vary only slightly over the entire low speed envelope. The pitch angle model is the direct integration of the pitch rate model and is given by:

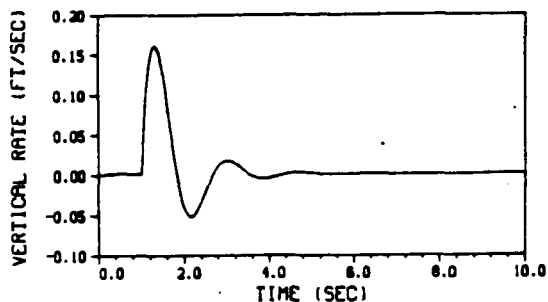
$$G_{\text{THETA}}(S) = \frac{\text{THETA}(S)}{\text{LONG}(S)} \approx \frac{K_{\text{THETA}}}{S(S + a_{\text{THETA}})} \quad (4)$$

where

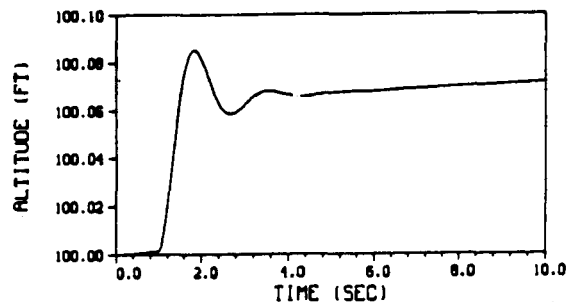
$$K_{\text{THETA}} = 0.71 \text{ deg}/(\text{inch-sec})$$

Altitude Models

These models are based on the vertical rate and relative altitude position responses due to the operation of the throttle. Plots 3,4 show the time based responses of the vertical rate and the altitude at 25 knots due to a 10% impulse deflection of the throttle.



Plot 3.



Plot 4.

Plot 3 shows a damped sinusoidal response of aircraft vertical rate. The sinusoidal response is due to the thrust development time constant of the engine control system and vehicle mass interactions. The vertical rate response shows no direct signs of any long term phugoid modes. The vertical rate response in the pilot frequencies is described by the low order transfer function shown below:

$$G_{ALTDT}(S) = \frac{ALTDT(S)}{THTL(S)} \approx \frac{K_{ALTDT}}{S^2 + 2\xi_{ALT}\omega_{ALT}S + \omega_{ALT}^2} \quad (5)$$

where

$$K_{ALTDT} = 0.086 \text{ feet}/(\%-\text{sec}^3)$$

$$\omega_{ALT} = 3.7 \text{ rads/sec}$$

$$\xi_{ALT} = 0.45$$

The parameters of this transfer function vary only slightly with changes in the nozzle angle and velocity. The time based response of the relative altitude position of Plot 4 shows a pure integration of the vertical rate response. The relative altitude transfer function model is given by:

$$G_{ALT}(S) = \frac{ALT(S)}{THTL(S)} \approx \frac{K_{ALT}}{S(S^2 + 2\xi_{ALT}\omega_{ALT}S + \omega_{ALT}^2)} \quad (6)$$

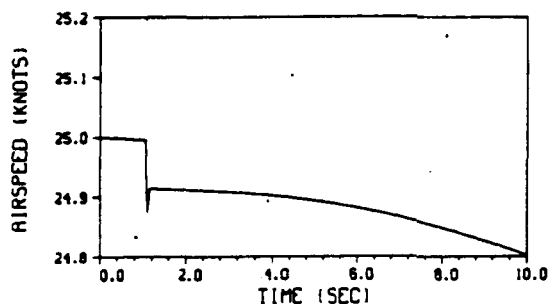
where

$$K_{ALT} = 0.086 \text{ feet}/(\%-\text{sec}^2)$$

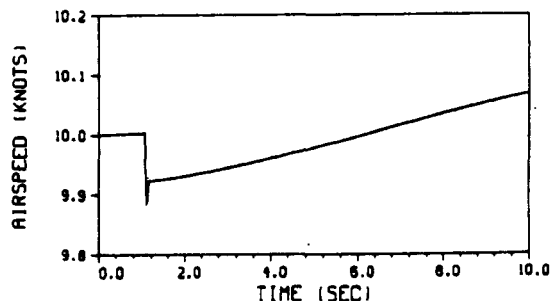
Many guidance applications will require only a vertical rate model. The relative altitude model will be used primarily in the design of altitude regulation pilots.

Forward Velocity Model

This model considers the variations in forward velocity due to operation of the nozzle angle control. Plots 5,6 show the time-based responses of the forward velocity at 25 and 10 knots, due to 5 degree impulse test deflections of the nozzle angle.



Plot 5.



Plot 6.

Plots 5,6 show a rapid step in forward velocity to an impulse deflection in the nozzle angle. This tends to support the thrust vector realization of Figure 8. The high speed transient is due to the nozzle positioning actuating system during nozzle redirection. The long term phugoid mode of the response can be seen in the later phases of Plots 5,6 which show slow changes in the forward velocity. This is due to the relatively small rotational moment that is provided by the instantaneous redirection of the primary thrust vector and a general response to the atmospheric drag. The slow "teetering" reaction illustrates the balancing of the vehicle on the thrust vector. A general short period model of the velocity reaction can be described by the transfer function shown below.

$$G_{VEL}(S) = \frac{VEL(S)}{NOZZLE(S)} \approx \frac{K_{VEL}}{S} \quad (7)$$

where

$$K_{VEL} = 0.017 \text{ knots}/(\text{deg-sec})$$

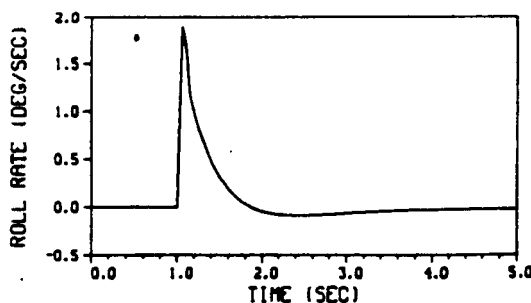
The overall accuracy of this model is not important because it will be utilized for a general regulation of the vehicle velocity and not as a specific velocity control.

Lateral-Directional Models

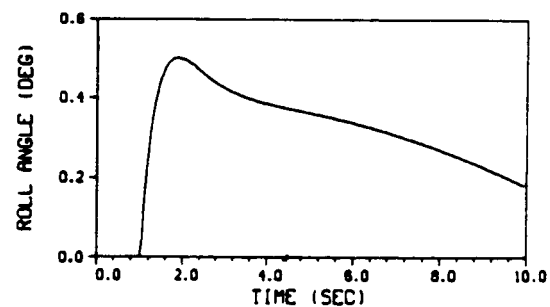
This section will present the low order models of the lateral dynamics of the V/STOL research aircraft. The primary responses that will be investigated are: 1) roll angle components, 2) heading / directional components, 3) lateral velocity and sideslip components.

Roll Angle Models

This model considers the response characteristics of the roll angle components due to the operation of the lateral stick. The time-based impulse responses of the body roll rate and the roll angle, for a 1 inch deflection of the lateral stick at 25 knots can be seen in Plots 7,8, respectively.



Plot 7.



Plot 8.

Plot 7 shows simple pole behavior similar to that of the pitch components, but with a much greater and faster dynamics. This indicates a relatively lively response characteristic in the roll axis. This is primarily due to the increased auxiliary thrust components in the wing tip RCS vents and the inertial components in the roll axes. No apparent long term phugoid distortions are observable. The response characteristics of the roll rate can be described by:

$$G_{PHIDT}(S) = \frac{PHIDT(S)}{LAT(S)} \approx \frac{K_{PHIDT}}{S + a_{PHI}} \quad (8)$$

where

$$K_{PHIDT} = 1.89 \text{ deg}/(\text{inch-sec}^2)$$

$$a_{PHI} = 3.45 \text{ sec}^{-1}$$

This transfer function varies little with changes in forward velocity. Plot 8 illustrates the pure integration of the roll rate, but shows a strong return to level flight. This response characteristic is expected because of the limited thrusting of the wing tip RCS vents. The roll angle response in the pilot frequencies can be described by:

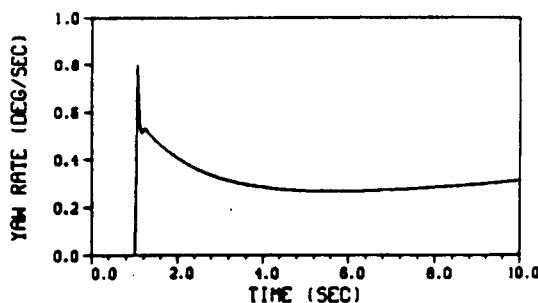
$$G_{PHI}(S) = \frac{PHI(S)}{LAT(S)} \approx \frac{K_{PHI}}{S(S + a_{PHI})} \quad (9)$$

where

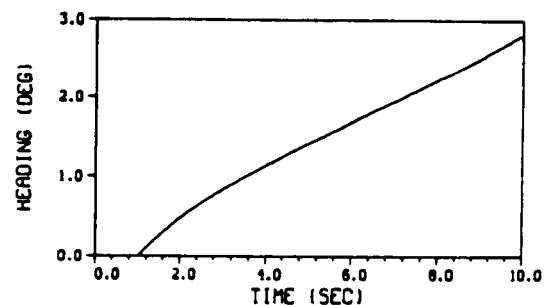
$$K_{PHI} = 1.89 \text{ deg}/(\text{inch-sec})$$

Heading / Directional Models

This model considers the response characteristics of the yaw rate and heading components due to the operation of the rudder pedals. Plots 9,10 show the responses of the yaw rate and yaw angle due to 1 inch impulse deflections of the rudder pedals at 10 knots.



Plot 9.



Plot 10.

The yaw rate response of Plot 9 shows an initial highly responsive response followed by a sluggish continued rotation about the vertical axis. The lack of aerodynamic forces and the size of the inertial components contribute to this continued rotation. The yaw rate can be described by:

$$G_{PSIDT}(S) = \frac{PSIDT(S)}{PED(S)} \approx \frac{K_{PSIDT}(S + b_{PSI})}{S(S + a_{PSI})} \quad (10)$$

where

$$K_{PSIDT} = 0.56 \text{ deg}/(\text{inch-sec}^2)$$

$$a_{PSI} = 0.83 \text{ sec}^{-1}$$

$$b_{PSI} = 0.38 \text{ sec}^{-1}$$

Plot 10 shows the expected double integration characteristics which can be described by:

$$G_{PSI}(S) = \frac{PSI(S)}{PED(S)} \approx \frac{K_{PSI}(S + b_{PSI})}{S^2(S + a_{PSI})} \quad (11)$$

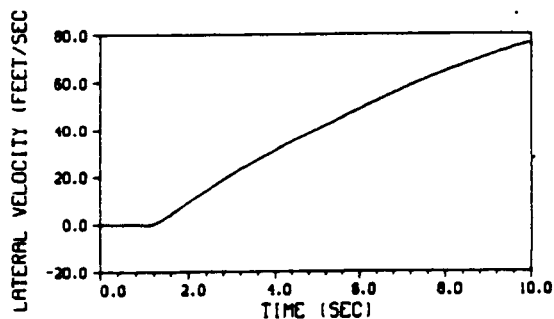
where

$$K_{PSI} = 0.56 \text{ deg}/(\text{inch-sec})$$

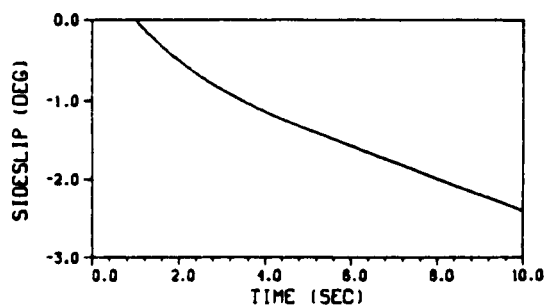
The yaw models will primarily be used for heading regulation and small scale changes in direction. The yaw rate model can be utilized in flat turning applications where low speed/high sideslip characteristics are permitted.

Lateral Velocity Models

These models consider the responses of the lateral velocity and the vehicle sideslip due to operation of the rudder pedals and the lateral stick. Plot 11 shows the response of the lateral velocity due to a 1 inch impulse of the lateral stick while hovering. Plot 12 shows the sideslip reaction from a 1 inch impulse in the rudder pedals at 25 knots.



Plot 11.



Plot 12.

The lateral velocity response of Plot 11 shows a rapid sideways acceleration due to the sustained roll angle of Plot 8. This indicates a strong "crabbing" reaction to the lateral redirection of the thrust vector, which supports the thrust diagram of Figure 11. The large degree of asymmetric flight associated with this type of maneuver will require cautious pilot reactions. The response characteristic of the lateral velocity can be described by:

$$G_{LATVEL}(S) = \frac{LATVEL(S)}{LAT(S)} \approx \frac{K_{LATVEL}}{S^2} \quad (12)$$

where

$$K_{LATVEL} = 10.5 \text{ feet}/(\text{inch-sec}^3)$$

The lateral velocity did not show any significant variations to changes in speed. This is important because this type of control is utilized to maneuver laterally during vertical landing approaches. Plot 12 shows the reactions of the vehicle sideslip. This type of reaction indicates that the aircraft is rotating into the wind in a asymmetric/broadsided flight characteristic. This type of response can be described by:

$$G_{SIDESLIP}(S) = \frac{SIDESLIP(S)}{PED(S)} \approx \frac{K_{SIDESLIP}}{S^2} \quad (13)$$

where

$$K_{SIDESLIP} = 0.37 \text{ deg}/(\text{inch-sec})$$

This type of control reaction will be used to correct asymmetric flight characteristics primarily during coordinated turn maneuvers.

PILOT SELECTION

This section presents the design strategies and implementations of the individual single variable pilots. These pilots are selected to perform specific control functions. It is important to remember that the aircraft dynamic models have been chosen to simplify pilot selection. The responses of the long term phugoid modes have not been strictly considered because they tend to be very much slower than the control objectives. The ability to achieve the desired closed loop response characteristics was at times hampered by the control mechanism deflection restriction. Gain limitations and reduced closed loop bandwidths were required in some cases to keep the pilot from banging into the control stops. This of course is not the case when actual human pilots are actively participating in the aircraft control loops. Many times the control mechanism limits are overlooked by the pilot during attempts to provide quick/wide ranging maneuvers. Conversations with Harrier pilots tended to suggest that this type of control behavior is typical in the low speed flight envelope (e.g. "pegged throttle") [7.9].

Longitudinal Pilots

Pitch Control Pilot

This pilot provides the position control of the pitch angle by assessing the pitch angle and operating the longitudinal stick. Typically a human pilot would rely on visual feedback of the artificial horizon or some form of horizontal external cue. This pilot mechanism will be used primarily to provide a level flight characteristic in the longitudinal plane. In addition, this pilot can also be used to provide specific pitch angle positioning and to augment nozzle angle controls during acceleration and deceleration maneuvers. The integration pole of the pitch response provides an intrinsic Type I system characteristic. Attempts at introducing the pilot's compensating pole as a secondary integrator to achieve a Type II response characteristic did not provide an adequate closed loop behavior because of the positioning restrictions ($a \geq 0.8$) of the compensating zero in the human response limitations and the destabilization of the root locus due to the pure delay. Figure 13 shows a root locus of the closed loop system.

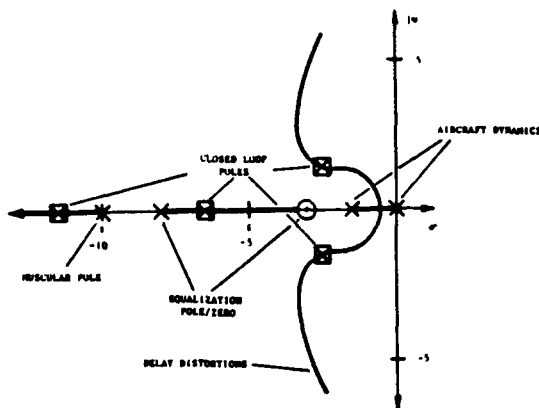


Figure 13. - Root locus of the closed loop pitch control system

The pilot equalization profile was configured as a lead network to improve the low frequency response characteristics. The pilot compensating zero has been placed in such a way as to force the dominant poles to reside in the desired locations ($\omega_n = 3.1$ rads/sec, $\xi = 0.74$). The pitch control pilot transfer function is given by:

$$G_{\text{PILOT THETA}}(S) = \frac{4.3(S + 3) e^{-0.2S}}{(S + 8)(S + 10)} \quad (14)$$

Vertical Rate Pilot

This pilot provides the control of the vertical rate by assessing the vertical rate and operating the engine throttle control. Typically a human pilot would acquire the feedback from the vertical rate indicator. This pilot will be used to control ascent and descent rates or can be used as an indirect altitude controller. The second order response characteristics of the vertical rate requires that the pilot supply the integrating pole to create a Type I system. This type of equalization configuration produces a lag network which tends to create a sluggish closed loop response. The pilot transfer function is described by:

$$G_{\text{PILOT ALTD}}(S) = \frac{36(S + 0.8) e^{-0.2S}}{S(S + 10)} \quad (15)$$

During the pilot design it was feared that the complex poles of the vertical rate response would migrate into the right half plane before an acceptable closed loop response characteristic was achieved. This however was not the case. Initially the closed loop bandwidth was set at ($\omega_n = 3.1$ rads/sec, $\xi = 0.81$), but this caused overzealous pilot responses which tended to drive the throttle to it's limit. The intrinsic characteristics of the low speed flight envelope require that the engine throttle be maintained near it's upper limit to supply adequate lifting thrust. To overcome this type of noncontinuous behavior in pilot control operations, the bandwidth was reduced to ($\omega_n = 1.7$ rads/sec, $\xi = 0.43$), which created a poor response characteristic.

Altitude Position Pilot

This pilot provides the control of the relative altitude position by assessing the vehicle altitude and operating the engine throttle. Pilot feedback is provided through the altimeter. This pilot mechanism will be used in situations where altitude regulation is required. The inherent integrating pole of the altitude response was initially augmented by a pilot integrator profile to produce a Type II system. The integrating poles were strongly influenced by the presence of the complex poles and the asymptotics of the pure delay. The gain required to provide an adequate closed loop response characteristic, produced a pilot that suffered from the throttle operations too near the upper limit. This however appears to be an acceptable activity during this type of maneuvering [7.9]. To provide a response characteristic that is appropriate to the human response model, the pilot equalization was reconfigured to the lead network form shown below.

$$G_{ALT}^{PILOT}(S) = \frac{52(S + 0.8) e^{-0.2s}}{(S + 3)(S + 10)} \quad (16)$$

This type of pilot configuration produced a sluggish response characteristic but did not suffer from throttle overdrive. The closed loop response was dominated by the real axis poles and provided a closed loop bandwidth ($\omega_n = 2.15$ rads/sec). This type of response was considered reasonable because of the large mass/inertial interactions with the main engine thrust components.

Forward Velocity Pilot

The forward velocity pilot controls forward velocity by assessing the airspeed and operating the nozzle angle. Pilot feedback is supplied by the airspeed indicator or by external visual cues. Although the response characteristics of the vehicle velocity show a simple integrating reaction, the large inertial components of the vehicle and the nozzle angle limitations tend to insist on sluggish closed loop responses. The velocity control pilot was configured to provide a Type II system by using the pilot's compensation pole as an integrator. The pilot's compensating zero was placed at its limiting position ($a = 0.8$) to provide the most rapid migration to a low damping ratio as possible. The closed loop poles were placed at $\omega_n = 2.4$ rads/sec, $\xi = 0.82$. This placement produced pilot control deflections that consistently overdrove the nozzle control mechanism. The pilot gain was reduced to limit the control mechanism operation and resulted in the pilot model shown below.

$$G_{VEL}^{PILOT}(S) = \frac{-14(S + 0.8) e^{-0.2s}}{S(S + 10)} \quad (17)$$

The resulting closed loop poles were situated at $\omega_n = 1.4$ rads/sec, $\xi = 0.6$. This produced a very sluggish closed loop response, but maintained valid pilot control mechanism deflections. The problem with the velocity control orientation in this flight envelope is that the vehicle is basically balancing on its thrust vector. Perturbation of the thrust vector direction cause reactions in the longitudinal axes, primarily in the pitch group. This tends to complicate the overall control objectives in the longitudinal axes.

Lateral - Directional Control Pilots

Roll Control Pilot

This pilot provides the control of the roll angle components by assessing the roll angle and manipulating the lateral stick. The pilot feedback is provided by the lateral components of the artificial horizon or external visual cues. This pilot is used to provide a level flight characteristic in the lateral plane and to provide bank angle control during coordinated turn maneuvers. The design of the roll control pilot is very similar to that of the pitch control pilot. Roll components are, however, much more responsive. The responsiveness has been described as being similar to "straddling a greased log" [7]. Initial attempts at obtaining a Type II configuration suffered from the high gain asymptotic distortions of the pilot's pure delay. A Type I system was utilized and the pilot's equalization was configured as a lead network. The lack of large inertial components in the axis permitted dominant pole placement in a highly desirable location ($\omega_n = 3.1$ rads/sec, $\xi = 0.65$). The resulting pilot transfer function is given by:

$$G_{PHI}^{PILOT}(S) = \frac{2.9(S + 3.6) e^{-0.2S}}{(S + 8)(S + 10)} \quad (18)$$

This pilot configuration required no gain adjustments to limit the control mechanism operations.

Heading Control Pilot

This pilot controls the relative vehicle heading by assessing the yaw angle and operating the rudder pedals. Typically the pilot would receive this feedback through the compass. This type of pilot will be used to provide small scale heading changes and heading regulation. The large mass/inertial components of this control plane tend to create slow response characteristics. The inherent Type II profile of the heading response model will provide good regulation and rejection of off-heading disturbances. The presence of the real pole will, however, limit the closed loop dynamics. The pilot compensation zero was placed at its limit ($a = 0.8$) to force the integrating poles to migrate to the desired locations with minimum gain, but this tended to reduce the bandwidth set by the real pole ($\omega_n = 2.1$ rads/sec). The resulting pilot transfer function is given by:

$$G_{PSI}^{PILOT}(S) = \frac{26(S + 0.8) e^{-0.2S}}{(S + 20)(S + 10)} \quad (19)$$

The pilot responses showed some signs of rudder pedal overdrive, but these were not considered significant enough to warrant further pilot gain reductions.

Yaw Rate Pilot

This pilot configuration provides control of the flat turning rate by assessing the yaw rate and operating the rudder pedals. Feedback is supplied by the compass. This pilot will be utilized to provide flat turns that are controlled through the yaw rate. A Type II system is formed by utilizing the pilot's compensation pole as an integrator. The compensation zero is placed at its limit to provide a quick migration of the integrating poles. The presence of the real pole in the yaw rate response will again reduced the closed loop bandwidth. The pilot transfer function is given by:

$$G_{PSIDT}^{PILOT}(S) = \frac{58(S + 0.8) e^{-0.2S}}{S(S + 10)} \quad (20)$$

The pilot's control mechanism operations required a gain reduction to maintain proper operation. This placed the dominant closed loop poles near $\omega_n = 2.21$ rads/sec, $\xi = 0.65$, which created a rather sluggish response characteristic.

Sideslip Regulation Pilot

During coordinated turn maneuvers it will be necessary to minimize the vehicle sideslip. This pilot will regulate the sideslip by assessing the weather vane and operating the rudder pedals. The pilot equalization will be configured as a lead network to utilize the Type II characteristics of the sideslip response. The Type II profile will provide adequate regulation of the sideslip disturbances that are expected. The pilot transfer function is described by:

$$G_{SIDESLIP}^{PILOT}(S) = \frac{-32(S + 0.8) e^{-0.2S}}{(S + 20)(S + 10)} \quad (21)$$

The closed loop poles were placed at $\omega_n = 2.45$, $\xi = 0.6$. This type of response did not cause control mechanism limiting but did tend to create a wobbling behavior.

Lateral Velocity Pilot

In the low speed envelope, non-rotational lateral motion can be utilized to maneuver the vehicle. This type of maneuver is characterized by a "crabbing" motion that has a large sideslip. Many vertical landing operations will require this type of maneuverability to land on target. The lateral velocity will be controlled by assessing external visual cues and operating the lateral stick. The pilot transfer function is given by:

$$G_{LATVEL}^{PILOT}(S) = \frac{1.1(S + 0.8) e^{-0.2S}}{(S + 6)(S + 10)} \quad (22)$$

Care must be taken when utilizing this type of maneuver, because a nonrecoverable situation may result if large forward speed or nonlevel flight characteristics are present.

PILOT INSERTION

The manner in which a pilot model is inserted into the control loops of the V/STOL research aircraft is dependent upon the maneuvering characteristics that are required. The maneuvering characteristics will define the configuration of single variable pilot mechanisms within the control structure of Figure 5. Each type of maneuver will require a specific pilot configuration. This section will illustrate the insertion of various pilot configurations and maneuvering characteristics.

Static Pilot Mechanisms

Static pilot mechanisms are the single variable piloted control loops that have only one maneuvering characteristic. These are:

1. Pitch Control via Longitudinal Stick
2. Velocity Control via Nozzle Angle

These pilot mechanisms are the only pilots that use their respective cockpit control mechanism. The static pilot mechanisms will therefore reside in every comprehensive pilot configuration.

Dynamic Pilot Mechanisms

Dynamic pilot mechanisms are the single variable piloted control loops that have more than one maneuvering characteristic. These are:

1. Altitude Control via Throttle
2. Vertical Rate via Throttle
3. Roll Control via Lateral Stick
4. Lateral Velocity via Lateral Stick
5. Heading Control via Rudder Pedals
6. Yaw Rate Control via Rudder Pedals
7. Sideslip Regulation via Rudder Pedals

The pilot model used to manipulate a specific cockpit control mechanism is chosen by the maneuver that is desired. Thus each maneuver will require the use of a specific set of dynamic pilot mechanisms. Translation between maneuvers will at times require a modification of pilot feedback and equalization parameters [2]. This type of behavior will not be considered in this discussion.

Pilot Insertion and Maneuvering Configurations

As previously mentioned, each flight control maneuver will require a specific comprehensive pilot profile. This section will present some typical pilot configurations and analyze their behavior within the cockpit of the V/STOL research aircraft. Before considering the various pilot structures, an important point should be made. During conversations with Harrier pilots [7.9], it became obvious that certain flight control situations known as "Death Angles" exist in the low speed - powered-lift flight regime. Death angles are vehicle orientations that can produce nonrecoverable flight characteristics in the V/STOL research aircraft. These situations occur when either velocity, angle of attack, or sideslip reach large values simultaneously. If more than one of these flight control variables grow too large the pilot risks a complete loss of control. This behavior stems from the balancing of the vehicle on its thrust vector during powered-lift activities. An example of this phenomena can be seen in low speed high angle of attack maneuvers like the execution of an altitude control operation. Here the vehicle forward velocity is relatively low and the high angle of attack is generated by the altitude translation. If a small sideslip angle is not maintained, the lateral rotational forces can create very large rolling motions that can not be compensated by the wing tip RCS auxiliary thrust components. This type of behavior can be suppressed if conservative pilot configurations are used and the pilot is not subjected to outlandish command sequences. The flight control maneuvers that will be presented are shown below.

1. Pitch Reorientation
2. Velocity Translation
3. Altitude Translation
4. Small Scale Heading Translation
5. Altitude Rate Maneuver
6. Flat Turn Maneuver
7. Coordinated Turn

Maneuvers 1 - 4 use an identical pilot configuration. The maneuvers are defined by the variations of a single flight control variable in the command sequence. This pilot configuration will be considered fundamental and is shown in Figure 14.

$$G_p^1(S) = G_{\text{PILOT}}^{\text{THETA}}(S) \quad [\text{EQ 14}]$$

$$G_p^2(S) = G_{\text{PILOT}}^{\text{PHI}}(S) \quad [\text{EQ 18}]$$

$$G_p^3(S) = G_{\text{PILOT}}^{\text{PSI}}(S) \quad [\text{EQ 19}]$$

$$G_p^4(S) = G_{\text{PILOT}}^{\text{ALT}}(S) \quad [\text{EQ 16}]$$

$$G_p^5(S) = G_{\text{PILOT}}^{\text{VEL}}(S) \quad [\text{EQ 15}]$$

Figure 14. - The Fundamental Pilot configuration

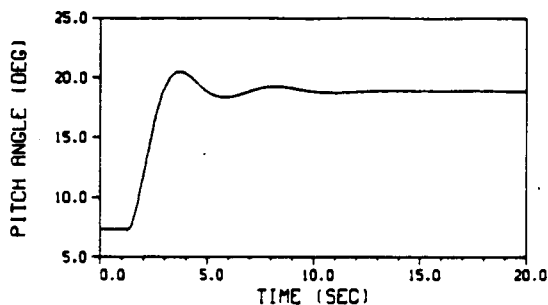
This pilot configuration is based in the control structure of Figure 5. The remaining maneuvers will require specific pilot configurations, feedback paths, and command sequences.

Pitch Reorientation

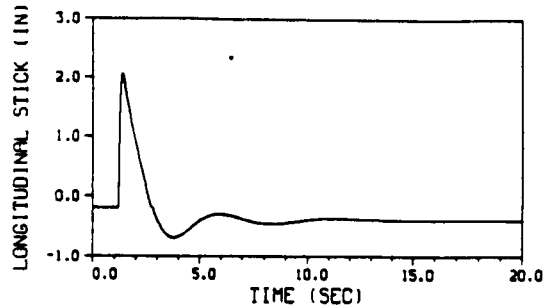
The pitch reorientation maneuver is designed to provide pitch angle translation while maintaining level flight characteristics in the lateral, altitude, and velocity components. The pitch angle rotation will cause a redirection in the primary thrust vector which will directly influence the altitude and velocity components. The altitude and velocity pilot mechanisms will be forced to compensate the disturbances associated with the pitch pilot's activities. The fundamental pilot configuration is used to perform this maneuver. The command sequence will provide that only the pitch angle be modified, the other variables will remain at their precommand trimmed values. This type of command sequence will implement the control structure shown in Figure 6. A 10 degree step maneuver in pitch from a 10 knot trimmed flight at 100 feet is commanded by the following sequence.

TRIMMED	COMMAND
THETA = 7.3 degrees	THETA = 17.3 degrees
PHI = 0.0 degrees	PHI = 0.0 degrees
PSI = 0.0 degrees	PSI = 0.0 degrees
ALT = 100 feet	ALT = 100 feet
VEL = 10 knots	VEL = 10 knots

The command sequence was injected at 1 second into the simulation run. Plot 13 shows the 10 degree step in vehicle pitch angle. Plot 14 shows the pilot's manipulation of the longitudinal stick.

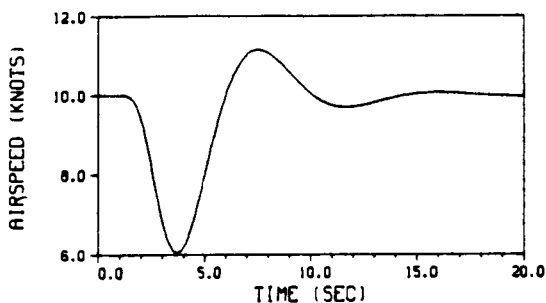


Plot 13.

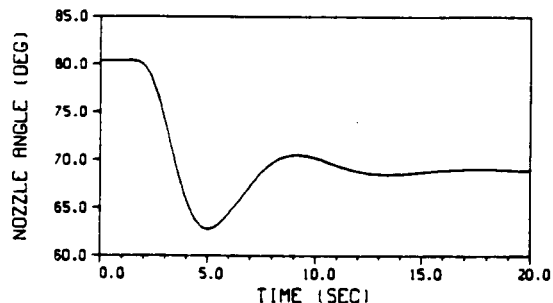


Plot 14.

The reorientation of the thrust vector created decelerating disturbances in the velocity component. Plot 15 shows the velocity response due to the pitch maneuver. Plot 16 shows the pilot's compensating deflection of the engine nozzles.



Plot 15.



Plot 16.

Altitude and lateral/directional disturbances were not significant and required only small scale compensation by the pilot mechanisms.

Velocity Translation

The velocity translation maneuver is designed to provide modification of the vehicle forward velocity, while maintaining level flight at a constant altitude. This maneuver uses the redirection of the primary thrust vector to modify the forward thrust. The reoriented thrust vector will disturb the flight characteristics of the pitch and altitude components. This maneuver will utilize the fundamental pilot configuration of Figure 14. A 5 knot reduction in forward velocity from a 25 knot trimmed flight at 100 feet is commanded by the following sequence.

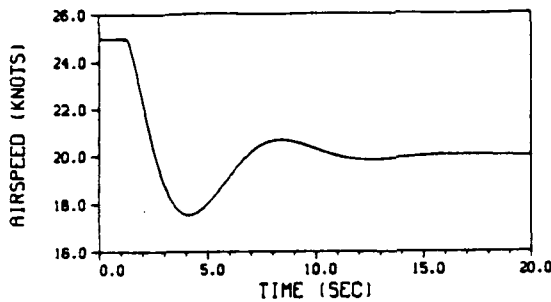
TRIMMED

THETA = 6.5 degrees
PHI = 0.0 degrees
PSI = 0.0 degrees
ALT = 100 feet
VEL = 25 knots

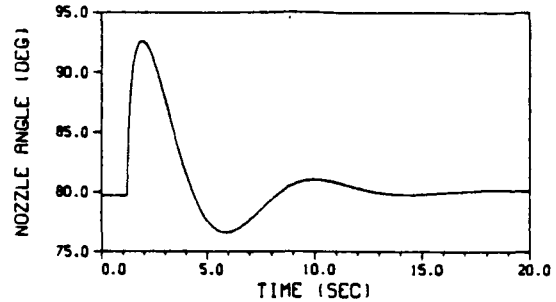
COMMAND

THETA = 6.5 degrees
PHI = 0.0 degrees
PSI = 0.0 degrees
ALT = 100 feet
VEL = 20 knots

This command sequence was injected 1 second into the simulation run. Plot 17 shows a sluggish velocity response which is a characteristic of the interaction of the rotated thrust vector and the vehicle's longitudinal mass/inertial components. Plot 18 shows the pilot's control deflection of the engine nozzles. Note that the pilot's deflection of the nozzle angle control is near it's upper limit (98 degrees).

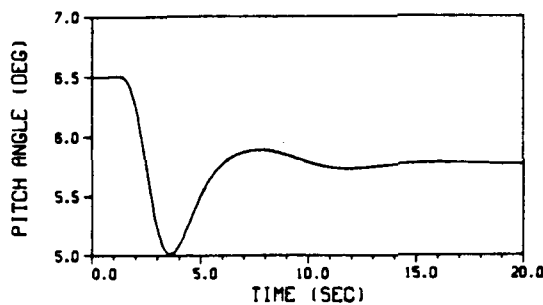


Plot 17.

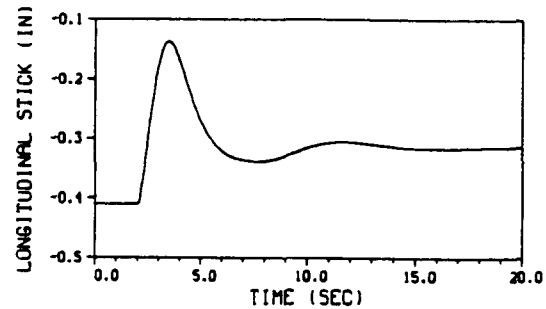


Plot 18.

Plot 19 shows the pitch angle reaction to the thrust vector rotation during the velocity control maneuver. Plot 20 shows the associated compensatory manipulation of the longitudinal stick by the pitch pilot to maintain level flight.

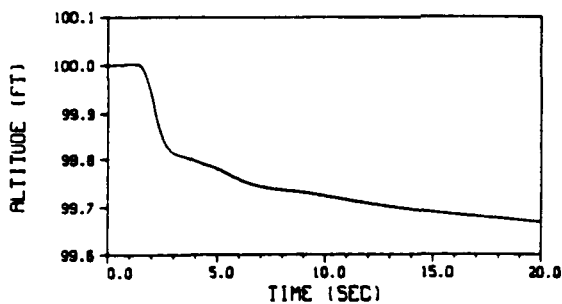


Plot 19.

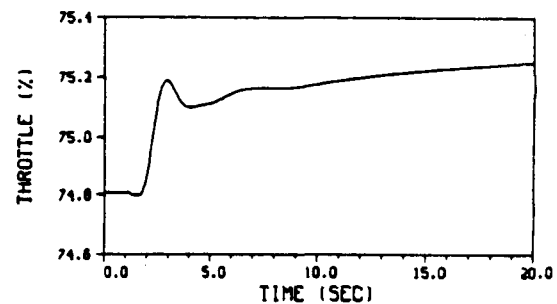


Plot 20.

Plot 21 shows the altitude disturbance associated with the thrust vector rotation. The small magnitude of the disturbance supports the thrust diagram of Figure 8. Plot 22 shows the pilot's deflection of the throttle to compensate for the reduction of lift associated with the change in forward velocity.



Plot 21.



Plot 22.

Altitude Translation

The altitude translation maneuver provides changes in vehicle altitude while maintaining level flight characteristics and constant velocity. This maneuver will require modification in the magnitude of the primary thrust vector which will directly influence the forward velocity components. Again the fundamental pilot configuration is utilized. A 10 foot increase in altitude from a 10 knot trimmed flight at 100 feet is commanded by the following sequence.

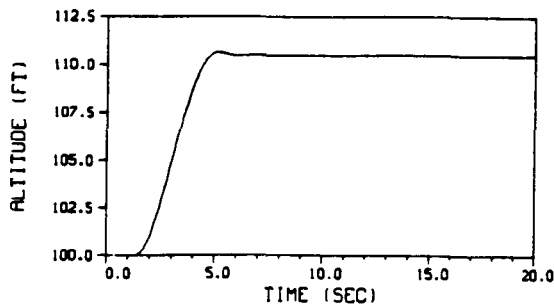
TRIMMED

THETA = 7.3 degrees
 PHI = 0.0 degrees
 PSI = 0.0 degrees
 ALT = 100 feet
 VEL = 10 knots

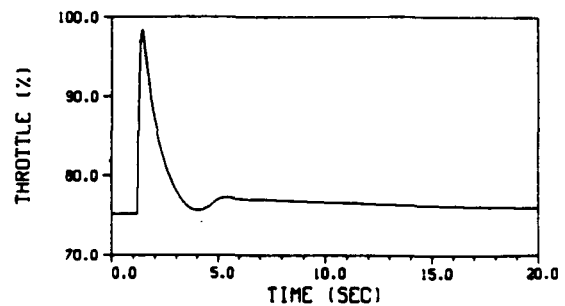
COMMAND

THETA = 7.3 degrees
 PHI = 0.0 degrees
 PSI = 0.0 degrees
 ALT = 110 feet
 VEL = 10 knots

Plot 23 shows the altitude step which tends to be dominated by the lagging dipole on the real axis. Plot 24 shows the pilot's manipulation of the throttle. Note that the pilot's throttle deflection is close to the upper limit (100 %).

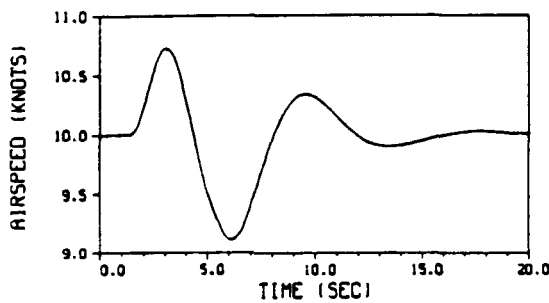


Plot 23.

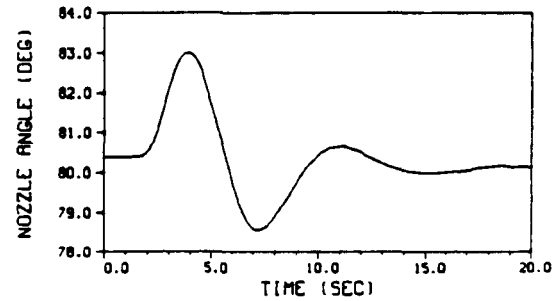


Plot 24.

Plot 25 shows the velocity reaction due to the increase in primary thrust. As was expected, the large angle associated with the thrust vector's direction induces only small disturbances in the forward velocity. Plot 26 shows the pilot's redirection of the thrust vector to maintain the forward velocity.

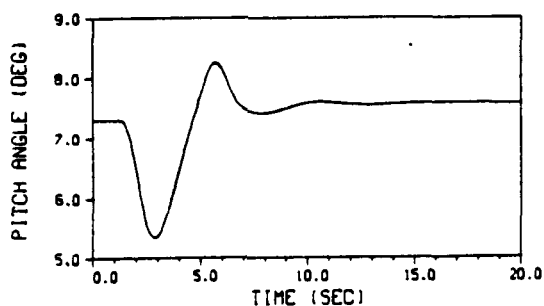


Plot 25.

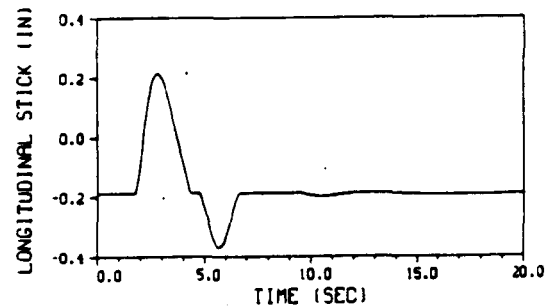


Plot 26.

Plot 27 shows the pitch angle disturbance of the altitude translation. Plot 28 shows the pilot's compensating operation of the longitudinal stick.



Plot 27.



Plot 28.

Heading Change

Low speed heading changes are performed by direct directional rotation of the vehicle while maintaining level flight at a constant altitude. This type of flight maneuver is generally used only for small scale direction changes or for heading regulation. Vehicle rotation is provided by the thrust components of the tail-end RCS jets. The direct vehicle yawing rotation induces pitching and rolling disturbances due to the asymmetric flight characteristics. The rotation of the directional components of the thrust vector caused only small disturbances in the altitude and velocity. Care must be taken during the execution of this maneuver to not allow a large sideslip angle to develop. Large asymmetric behavior may excite "Death Angle" responses. The fundamental pilot configuration is used to perform this maneuver. A 10 degree step in vehicle heading from a 25 knot trimmed flight at 100 feet is commanded by the following sequence.

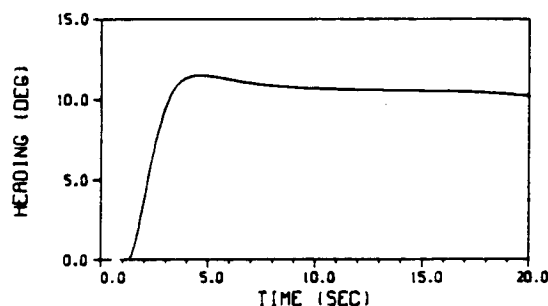
TRIMMED

THETA = 6.5 degrees
PHI = 0.0 degrees
PSI = 0.0 degrees
ALT = 100 feet
VEL = 25 knots

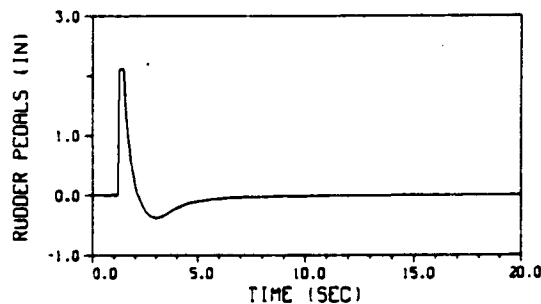
COMMAND

THETA = 6.5 degrees
PHI = 0.0 degrees
PSI = 10.0 degrees
ALT = 100 feet
VEL = 25 knots

Plot 29 shows the step response in heading. This response shows evidence of the lagging dipole introduced by the pilot's compensating zero. Plot 30 shows the pilot's deflection of the rudder pedals. The pilot response shows a small degree of noncontinuous behavior due to the pilot's driving the rudder pedals to their upper limit. This noncontinuous behavior is however, not significant.

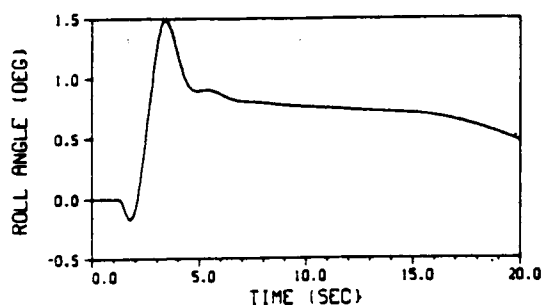


Plot 29.

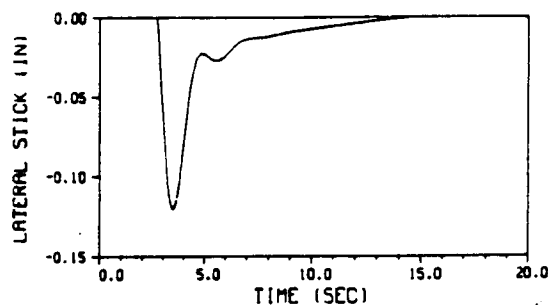


Plot 30.

Plot 31 shows the roll angle reaction to the directional rotation of the vehicle. This type of response shows the inherent roll/yaw coupling of the lateral-directional control set. Plot 32 shows the lateral stick deflection to compensate for the roll disturbance.

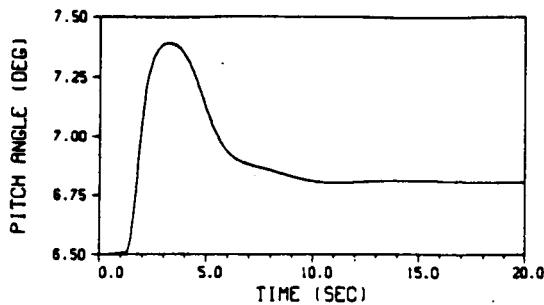


Plot 31.

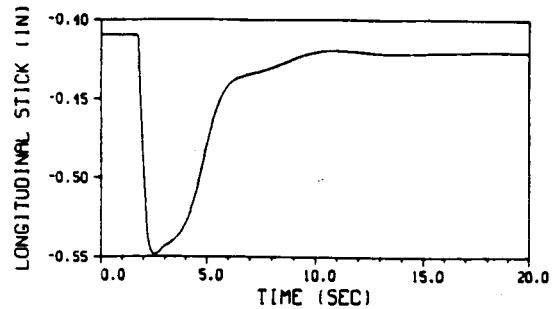


Plot 32.

Plot 33 shows the pitch angle disturbances due to the asymmetric flight characteristics. This disturbed longitudinal reaction is quite small but does show a characteristic nose up reaction to the yaw transition. Plot 34 shows the longitudinal stick reaction.



Plot 33.



Plot 34.

Altitude Rate Maneuver

The altitude rate maneuver provides ascent and descent rate control while maintaining level flight characteristics. This maneuver uses thrust magnitude control which will tend to disturb the velocity and pitch angle components. The altitude rate maneuver uses a modified fundamental pilot. The single variable modification to Figure 14 is shown below:

$$G_p^4(S) = G_{ALTD}^{PILOT}(S) \quad [EQ 15]$$

This configuration differs from the fundamental pilot by utilizing vertical rate feedback and modifying the throttle control to the altitude rate pilot parameters. A 5 ft/sec step in vertical rate from a 25 knot trimmed flight at 100 feet is commanded by the sequence shown below.

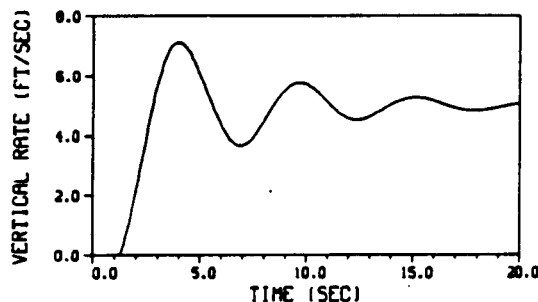
TRIMMED

THETA = 6.5 degrees
 PHI = 0.0 degrees
 PSI = 0.0 degrees
 ALTD = 0.0 feet/sec
 VEL = 25 knots

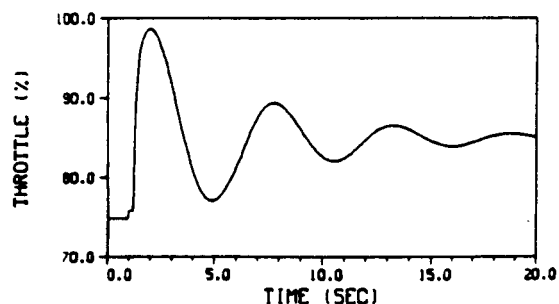
COMMAND

THETA = 6.5 degrees
 PHI = 0.0 degrees
 PSI = 0.0 degrees
 ALTD = 5.0 feet/sec
 VEL = 25 knots

Plot 35 shows a sluggish step in vertical rate. Plot 36 shows the pilot's control operation of the throttle. The poor quality of the vertical rate response is due to the reduction of pilot gain needed to supply limited throttle deflections.

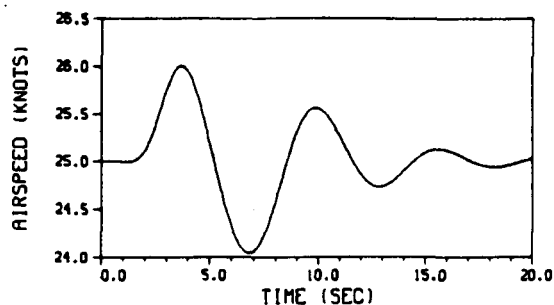


Plot 35.

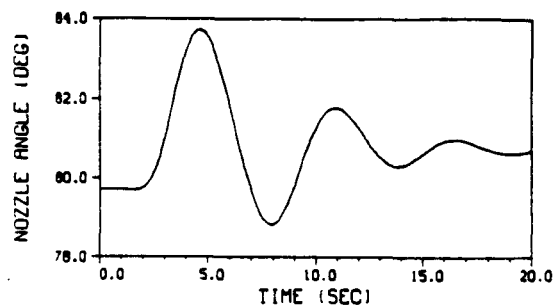


Plot 36.

Plot 37 shows the velocity disturbance due to the increase in thrust of the throttle operation. Plot 38 show the pilot's adjustment of the thrust direction to compensate for the velocity response.

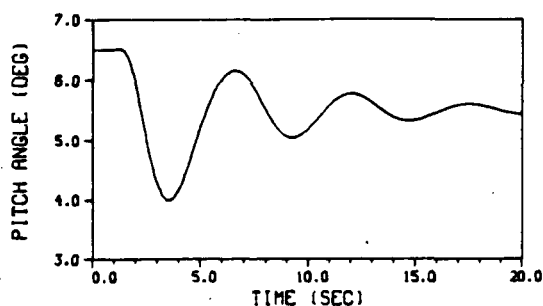


Plot 37.

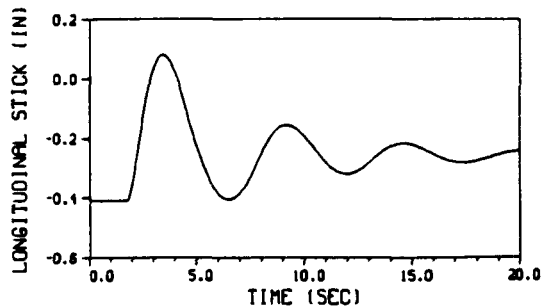


Plot 38.

Plot 39 shows the pitch angle reaction to the step in vertical rate. This type of response characteristic is primarily due to the large change in the angle of attack associated with this type of maneuver. Plot 40 shows the pilot's compensatory operation of the longitudinal stick.



Plot 39.



Plot 40.

Yaw Rate / Flat Turn Maneuver

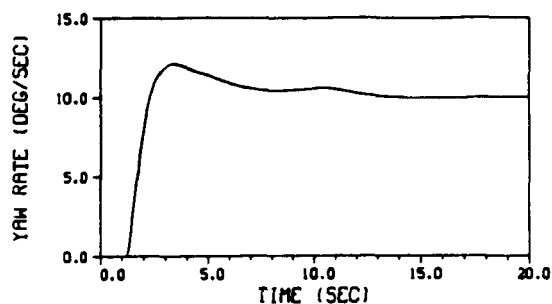
The yaw rate/flat turn maneuver provides non-coordinated turning capabilities when large sideslip maneuvers are permitted. This type of maneuver is reserved only for the low speed envelope. This maneuver utilizes a single variable modification to the fundamental pilot configuration shown below:

$$G_p^1(S) = G_{PSIDT}^{PILOT}(S) \text{ [EQ 20]}$$

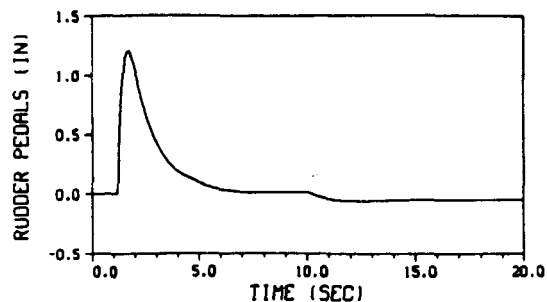
A 10 degree/sec step in yaw rate from a 25 knot trimmed flight at 100 feet is commanded by the sequence shown below:

TRIMMED	COMMAND
THETA = 6.5 degrees	THETA = 6.5 degrees
PHI = 0.0 degrees	PHI = 0.0 degrees
PSIDT = 0.0 degrees/sec	PSIDT = 10.0 degrees/sec
ALT = 100 feet	ALT = 100 feet
VEL = 25 knots	VEL = 25 knots

Plot 41 shows the 10 degree/sec step in yaw rate. The response shows signs of a lagging dipole on the real axis. Plot 42 shows the pilot's controlling deflection of the rudder pedals.

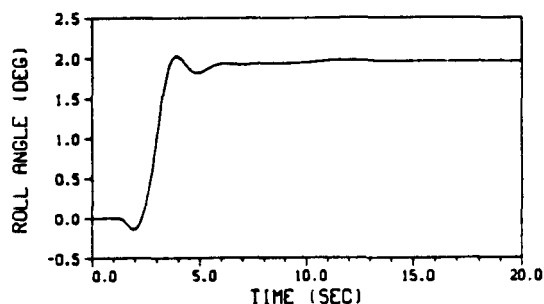


Plot 41.

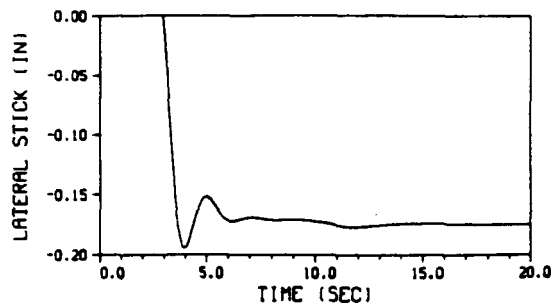


Plot 42.

Plot 43 shows the roll angle disturbance of the roll/yaw coupling in the lateral-directional control set. Plot 44 shows the pilot's compensatory operation of the lateral stick. The pilot's compensation produces a step in roll which tends to induce additional yaw rate components. Without compensative pilot actions the roll angle would have parabolically increased to a nonrecoverable point.

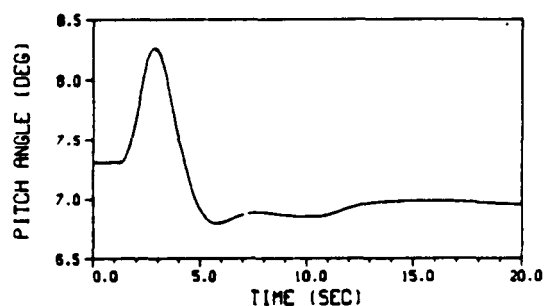


Plot 43.

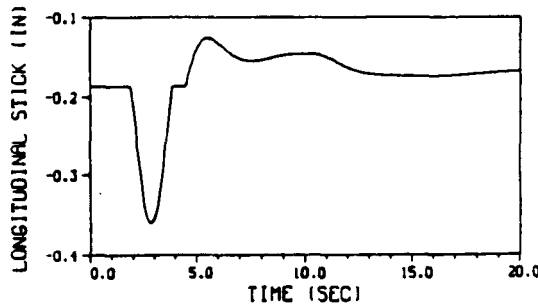


Plot 44.

Plot 45 shows the disruption of the pitch angle due to the yaw rate maneuver. This type of disturbance is characteristic of the nose up type response during yawing maneuvers. Plot 46 shows the pilot's deflection of the longitudinal stick to maintain level flight.



Plot 45.



Plot 46.

Coordinated Turn Maneuver

The coordinated turn maneuver provides heading changes via banked turns. Turn coordination is achieved by suppressing sideslip via the rudder pedals. A higher level guidance process is assumed to control the heading transition through the roll angle. In an ideally decoupled longitudinal and lateral system the turn rate is given by [8]:

$$PSIDT(r_b) = \frac{K g}{V} \sin(\phi) \quad (23)$$

Symmetric (i.e. zero sideslip) flight is assumed. This representation indicates that the turn rate can be controlled through the bank angle. Although the V/STOL research aircraft is not completely turn decoupled, this is a very good approximation. The fundamental pilot configuration is modified to provide sideslip suppression in the following manner:

$$G_p^3(S) = G_{SIDESLIP}^{PILOT}(S) \quad [EQ 21]$$

A 10 degree bank turn from a 25 knot trimmed flight at 100 feet is commanded by the following sequence:

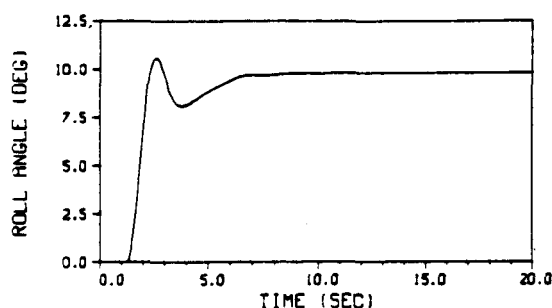
TRIMMED

THETA = 6.5 degrees
PHI = 0.0 degrees
BETA = 0.0 degrees
ALT = 100 feet
VEL = 25 knots

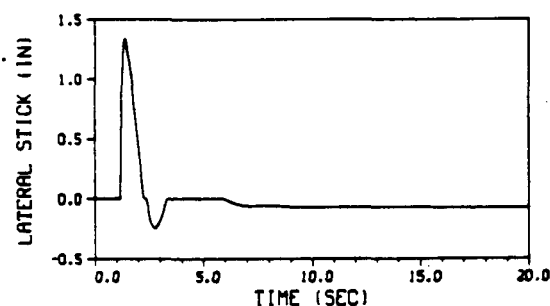
COMMAND

THETA = 6.5 degrees
PHI = 10.0 degrees
BETA = 0.0 degrees
ALT = 100 feet
VEL = 25 knots

Plot 47 shows the commanded 10 degree step in roll angle. The disturbed transient is due to the sideslip correction. Plot 48 shows the lateral stick deflection by the pilot.

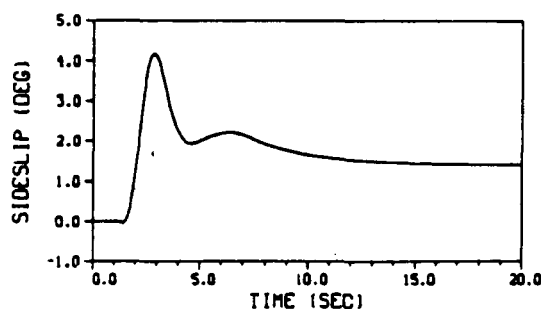


Plot 47.

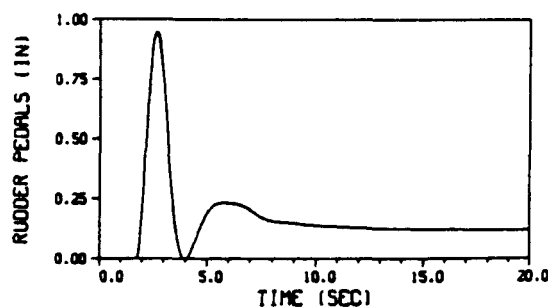


Plot 48.

Plot 49 shows the sideslip suppression. Plot 50 shows the pilot's operation of the rudder pedals to minimize the sideslip.

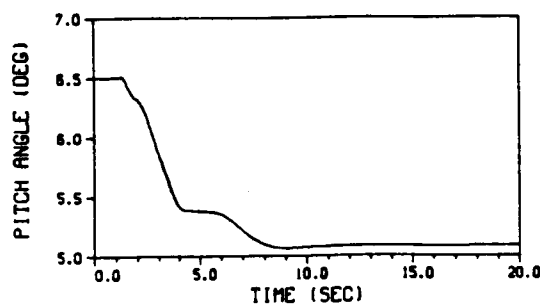


Plot 49.

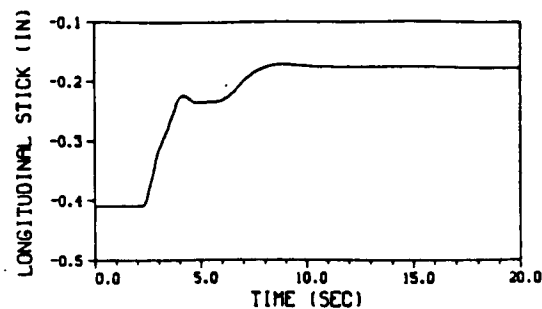


Plot 50.

Plot 51 shows the pitch angle reaction to the execution of the coordinated turn. Note the nose down behavior that is in direct conflict with the flat turn maneuver responses shown in Plots 33 and 45. This is due to the primary use of roll components versus the use of purely yaw components. Plot 52 shows the pilot's compensatory operation of the longitudinal stick.



Plot 51.



Plot 52.

CONCLUSION

The development of a set of low order human pilot models and their insertion into the flight control loops of a thrust vectored V/STOL research aircraft has been presented. The response characteristics of the pilot configurations when actively participating in the aircraft flight control has shown an adequate following of the vehicle trajectory commands. Although simple in approach, the multivariable pilot model appears to represent typical flight control maneuvers. Results presented in this paper have yet to be correlated with actual piloted flight simulation.

Present research is focussed on the use of parameter identification, adaptive, and optimal control techniques to improve pilot modeling. These approaches provide many advantages ranging from adapting to changes in aircraft dynamics to variations of control structure. The eventual goal is to develop a generic pilot model that can be inserted into a wide variety of aircraft and will learn/adapt to the control structure of the vehicle.

REFERENCES

1. "Computer Simulation of Multiple Pilots Flying a Modern High Performance Helicopter," Mark E. Zipf, William G. Vogt, Marlin H. Mickle, Ronald G. Hoelzeman, Fei Kai and James R. Mihaleow. Proceedings of the Eighteenth Modeling and Simulation Conference, pages 1295-1314. University of Pittsburgh, April 23-24, 1987.
2. "Computer Simulation of a Single Pilot Flying a Modern High Performance Helicopter," Mark E. Zipf, William G. Vogt, Marlin H. Mickle, Ronald G. Hoelzeman, Fei Kai and James R. Mihaleow. Proceedings of the Eighteenth Modeling and Simulation Conference, pages 1279-1294. University of Pittsburgh, April 23-24, 1987.
3. "Dynamic Response of Human Operators," D.T. McRuer and E.S. Krendal, Wright Air Development Center, WADC TR-56-524, October, 1957.
4. "A Model for Human Controller Remnant," William H. Levison, Sheldon Baron, David L. Kleinman, IEEE Transactions on Man-Machine Systems, Vol. MMS-10, No. 4, December 1969.
5. "AV-8B Simulation Software," John W. Bunnell, Laurence C. Anderson, Naval Air Test Center, N00421-8-R-0289, May 1985.
6. "AV-8B Simulation Model," John W. Bunnell, Laurence C. Anderson, Naval Air Test Center, N00421-81-C-0289, November 1985.
7. Capt. Charles M. Reif, USMC-VMAT 335, Cherry Point, NC., Personal Communications.
8. "Dynamics of Atmospheric Flight," Bernard Etkin, John Wiley and Sons, Inc., 1972.
9. Lt. Patrick T. Madden, USMC-VMA 331, Cherry Point, NC., Personal Communications.

APPENDIX II

The Optimal Control Model of a Pilot in V/STOL Aircraft Control Loops

This is a copy of the Final Report

THE INSERTION OF HUMAN DYNAMICS MODELS IN THE FLIGHT CONTROL LOOPS OF V/STOL RESEARCH AIRCRAFT

by

Mark E. Zipf

Department of Electrical Engineering
University of Pittsburgh, 1989.

Final Report for NASA Grant NAG 3-729

Computer Simulation of a Pilot in V/STOL Aircraft Control Loops

Funded By:

**NASA Lewis Research Center
21000 Brookpark Road
Cleveland, OH 44135**

PRINCIPAL INVESTIGATORS:

William G. Vogt
Professor of Electrical Engineering
University of Pittsburgh
Pittsburgh, PA 15261
(412) 624-9686

Marlin H. Mickle
Professor of Electrical Engineering
University of Pittsburgh
Pittsburgh, PA 15261
(412) 624-9682

PARTICIPANTS:

Mark E. Zipf, Research Assistant
Department of Electrical Engineering
University of Pittsburgh
Pittsburgh, PA 15261

Senol Kucuk, Research Assistant
Department of Electrical Engineering
University of Pittsburgh
Pittsburgh, PA 15261

SEPARATELY BOUND

APPENDIX III

The Adaptive Control Model of a Pilot in V/STOL Aircraft Control Loops

This is a version of the Thesis for a Master of Science Degree

by Senol Kucuk

AN ADAPTIVE HUMAN RESPONSE MECHANISM CONTROLLING THE V/STOL AIRCRAFT

Department of Electrical Engineering
University of Pittsburgh, 1988.

Final Report for NASA Grant NAG 3-729

Computer Simulation of a Pilot in V/STOL Aircraft Control Loops

Funded By:
NASA Lewis Research Center
21000 Brookpark Road
Cleveland, OH 44135

PRINCIPAL INVESTIGATORS:

William G. Vogt
Professor of Electrical Engineering
University of Pittsburgh
Pittsburgh, PA 15261
(412) 624-9686

Marlin H. Mickle
Professor of Electrical Engineering
University of Pittsburgh
Pittsburgh, PA 15261
(412) 624-9682

PARTICIPANTS:

Mark E. Zipf, Research Assistant
Department of Electrical Engineering
University of Pittsburgh
Pittsburgh, PA 15261

Senol Kucuk, Research Assistant
Department of Electrical Engineering
University of Pittsburgh
Pittsburgh, PA 15261

SEPARATELY BOUND

APPENDIX II

The Optimal Control Model of a Pilot in V/STOL Aircraft Control Loops

This is a copy of the Final Report

THE INSERTION OF HUMAN DYNAMICS MODELS IN THE FLIGHT CONTROL LOOPS OF V/STOL RESEARCH AIRCRAFT

by

Mark E. Zipf

Department of Electrical Engineering
University of Pittsburgh, 1989.

Final Report for NASA Grant NAG 3-729

Computer Simulation of a Pilot in V/STOL Aircraft Control Loops

Funded By:

**NASA Lewis Research Center
21000 Brookpark Road
Cleveland, OH 44135**

PRINCIPAL INVESTIGATORS:

William G. Vogt
Professor of Electrical Engineering
University of Pittsburgh
Pittsburgh, PA 15261
(412) 624-9686

Marlin H. Mickle
Professor of Electrical Engineering
University of Pittsburgh
Pittsburgh, PA 15261
(412) 624-9682

PARTICIPANTS:

Mark E. Zipf, Research Assistant
Department of Electrical Engineering
University of Pittsburgh
Pittsburgh, PA 15261

Senol Kucuk, Research Assistant
Department of Electrical Engineering
University of Pittsburgh
Pittsburgh, PA 15261

**THE INSERTION OF HUMAN DYNAMICS MODELS IN THE FLIGHT
CONTROL LOOPS OF V/STOL RESEARCH AIRCRAFT**

A FINAL REPORT FOR NASA GRANT NAG-729

Mark E. Zipf

Department of Electrical Engineering

University of Pittsburgh

Pittsburgh, PA.

ABSTRACT

This report presents an overview of research work focussed on the design and insertion of classical models of human pilot dynamics within the flight control loops of V/STOL aircraft. The pilots have been designed and configured for use in integrated control system research and design. The models of human behavior that have been considered are: 1) McRuer-Krendel - a single variable transfer function model, 2) Optimal Control Model - a multi-variable approach based on optimal control and stochastic estimation theory. These models attempt to predict human control response characteristics when confronted with compensatory tracking and state regulation tasks.

An overview, mathematical description, and discussion of predictive limitations of the pilot models is presented. Design strategies and closed loop insertion configurations are introduced and considered for various flight control scenarios. Models of aircraft dynamics (both transfer function and state space based) are developed and discussed for their use in pilot design and application. Pilot design and insertion are illustrated for various flight control objectives. Results of pilot insertion within the control loops of two V/STOL research aircraft (1) Sikorski Black Hawk UH-60A, 2) McDonnell Douglas Harrier II AV-8B) are presented and compared against actual pilot flight data. Conclusions are reached on the ability of the pilot models the adequately predict human behavior when confronted with similar control objectives.

TABLE OF CONTENTS

Abstract	i
Table of Contents	iii
Figure Listing	vi
Table Listing	viii
Plot Listing	x
Nomenclature	xv
I. - Introduction	1
I.A. - A Piloted Control Simulation Structure	3
II. - Models of Human Pilot Behavior	7
II.A. - McRuer-Krendel Model of Human Dynamics	8
II.B. - The Optimal Control Model	11
III. - Strategies of Pilot Model Application	15
III.A. - Aircraft Simulation Environments	15
III.B. - McRuer-Krendel Pilot Models with Static Parameters	16
III.B.1. - Structure of Aircraft Dynamics Models	16
III.B.2. - Development of SVPM Equalization Parameters	18
III.B.3. - Multi-variable McRuer-Krendel Pilot Insertion Techniques	19
III.C. - Optimal Control Model	21
III.C.1. - Control Task Description	21
III.C.2. - Pilot Description	22
III.C.3. - Difficulties in Applying the OCM	23
IV. - Models of V/STOL Research Aircraft	25
IV.A. - Harrier II AV-8B : A Thrust Vectored Jet Fighter	25
	iii

TABLE OF CONTENTS - continued

IV.A.1. - Harrier Control Structure	27
IV.A.2. - Low Order Transfer Function Models of Harrier Dynamics	30
IV.A.3. - High Order State Space Models of Harrier Dynamics	33
IV.B. Black Hawk UH-60A : A High Performance Helicopter	39
IV.B.1. - Control Structure and Low Order Transfer Function Models	40
V. - Pilot Development and Insertion	44
V.A. Static McRuer-Krendel Pilots	44
V.A.1. - Design of the Single Variable Pilot Mechanisms	45
V.A.2. - Selection of Multi-variable Configurations	48
V.A.3. - Results of Static Pilot Insertion	49
V.A.4. - Conclusions on the McRuer-Krendel Models	52
V.B. Optimal Control Model Pilots	53
V.B.1. - Description of the Control Tasks and Display Configurations	53
V.B.2. - Overview of Piloted Flight Data and Analysis	54
V.B.3. - Description of Pilot and Task Parameter Selection	55
V.B.4. - Results and Comparisons of OCM Pilot Insertions	56
V.B.5. - Conclusions on the OCM pilots	59
VI. - Summary and Conclusions	62
Appendix A - Description of the OCM	66
A.1. - Mathematical Overview of the OCM	66
A.2. - Discrete Time Representation of the OCM	73
Appendix B - A Linear State Space Model	81
B.1. - Harrier AV-8B Model Development	81

TABLE OF CONTENTS - continued

B.2. - Identification of Model Parameters	93
Appendix C - User's Guide for the OCM Software	101
C.1. - Overview of the OCM software	101
C.2. - Installing the OCM	103
C.3. - Configuring the OCM	105
C.4. - Executing the OCM within the VSRA environment	107
C.5. - Output generated by the OCM	109
C.6. - Examples of VSRA/OCM execution	112
C.7. - List of variables of the OCM	116
References	119
Figure Group	123
Table Group	138
Plot Group	156

FIGURE LISTINGS

Figure I.A.-1 - Block Diagram of the closed loop piloted control structure	124
Figure II.-1. - Block diagram of the basic human controller characteristics	124
Figure II.A.-1. - Block diagram of the internal structure of the McRuer-Krendel model	125
Figure II.B.-1. - Simple block diagram of the OCM within a control environment.	125
Figure III.B.1.-1. - A block diagram of the separation of the primary and secondary response characteristics associated with the decoupled transfer function models.	126
Figure III.B.2.-1. - Control loop closing strategy for the design of single variable pilot mechanisms	126
Figure III.B.2.-2. - Illustration of the destabilizing distortions associated with a delay Root-Locus	127
Figure III.B.2.-3. - Illustration of a delay approximation using a large pole set	127
Figure III.B.3.-1. - Multi-variable control structure for the insertion of the McRuer-Krendel pilot models	128
Figure III.B.3.-2. - Multi-variable control structure for executing simple flight control maneuvers.	128
Figure IV.A.-1. - Flight envelope of the Harrier II AV-8B.	129
Figure IV.A.1.-1. - Illustration of the modification of the engine thrust vector due to a reduction in nozzle angle during low speed/powered-lift activities	130
Figure IV.A.1.-2. - Illustration of the modification of the engine thrust vector due to an increase in engine speed during low speed/powered-lift activities	130
Figure IV.A.1.-3 - Illustration of the rotational motion due to the operation of the forward RCS jet from the backward deflection of the longitudinal stick during low speed/powered-lift activities.	131
Figure IV.A.1.-4. - Illustration of the rotational motion due to the operation of the wing-tip RCS jets from the deflection of the lateral stick during low speed/powered-lift activities	131

FIGURE LISTINGS - continued

Figure IV.A.1.-5. - Illustration of the rotational motion due to the operation of the tail-end RCS jet from the deflection of the rudder pedals during low speed/powered-lift activities	132
Figure V.A.1.-1. - Root-Locus of the pitch control pilot mechanism	132
Figure V.B.1.-1. - Illustration of the target orientation and vehicle motion during the Vertical Tracking Hover maneuver	133
Figure V.B.1.-2. - Illustration of the target orientation and vehicle motion during the Lateral Tracking Hover maneuver	133
Figure V.B.4.-1. - Diagram of a trajectory reference generator for the pitch angle components driven by a pitch rate command sequence.	134
Figure V.B.4.-2. - Vertical rate and yaw rate command sequence for the vertical tracking maneuver.	134
Figure V.B.4.-3. - Lateral velocity command sequence for the lateral tracking maneuver	135
Figure A.1. -1. - Block diagram of the internal structure of the OCM	135
Figure B.2.-1. - Full rank linear state space model of the Harrier AV-8B flight dynamics from trimmed forward flight while in the low speed/powered-lift region of the flight envelope.	136
Figure C.1. - 1. - Block diagram of the software modules and configuration files of the OCM simulation environment.	137

TABLE LISTINGS

Table IV.A.3.-1 - List of the state vector variables for the high order Harrier model.	139
Table IV.A.3.-2. - List of the control vector variables for the high order Harrier model.	140
Table IV.B.1.-1. - Transfer function parameters for the pitch response of the Black Hawk.	140
Table IV.B.1.-2. - Transfer function parameters for the altitude response components of the Black Hawk.	141
Table V.A.1.-1. - Parameter list of the additional Harrier pilot mechanisms.	142
Table V.A.1.-2. - Parameters of the pitch control pilot of the Black Hawk	143
Table V.A.1.-3. - Parameters of the altitude control pilot for the Black Hawk	144
Table V.A.1.-4. - Parameters of the altitude rate control pilot for the Black Hawk	145
Table V.A.1.-5. - Parameters of the roll angle control pilot for the Black Hawk	146
Table V.A.1.-6. - Parameters of the heading control pilot for the Black Hawk	147
Table V.A.1.-7. - Parameters of the Sideslip regulation pilot of the Black Hawk	148
Table V.A.2.-1. - Table of various flight control maneuvers and their associated configurations of Harrier SVPs.	149
Table V.A.2.-2. - Table of various flight control maneuvers and their associated configurations of Black Hawk SVPs.	150
Table V.A.3.-1. - Pitch reorientation command sequence for the multi-variable Harrier pilot.	151
Table V.A.3.-2. - Velocity translation command sequence for the multi-variable Harrier pilot.	152
Table V.A.3.-3. - Coordinated turn command sequence for the multi-variable Black Hawk pilot	153
Table V.B.3.-1. - Cost function weights of the OCM for the vertical tracking maneuver	153
Table V.B.3.-2. - Cost function weights of the OCM for the lateral tracking maneuver	154

TABLE LISTINGS - continued

Table V.B.3.-3. - Magnitudes of the OCM motor noise sources applied to each cockpit control mechanism	154
Table V.B.4.-1. - Trimmed values of the Harrier simulation environment for the vertical tracking precision hover maneuver.	155
Table V.B.4.-2. - Trimmed values of the Harrier simulation environment for the lateral tracking precision hover maneuver.	155

PLOT LISTINGS

Plot IV.A.2.-1. - Pitch rate response of the Harrier AV-8B due to a unit impulse deflection of the longitudinal stick in a near hover	157
Plot IV.A.2.-2. - Roll rate response of the Harrier AV-8B due to a unit impulse deflection of the lateral stick in a near hover	157
Plot IV.A.2.-3. - Forward velocity response of the Harrier AV-8B due to a 5 degree impulse deflection of the nozzle angle at 10 knots	158
Plot IV.A.3.-1. - Long term pitch rate response of the Harrier AV-8B due to a unit impulse deflection of the longitudinal stick at 10 knots	158
Plot IV.B.1.-1. - Pitch rate response of the Black Hawk UH-60A due to an impulse of the longitudinal cyclic stick at 60 knots.	159
Plot IV.B.1.-2. - Pitch rate response of the Black Hawk UH-60A due to an impulse of the longitudinal cyclic stick at 100 knots.	159
Plot IV.B.1.-3. - Roll rate frequency response of the Black Hawk UH-60A due to the operation of the lateral cyclic stick at 80 knots.	160
Plot IV.B.1.-4. - Altitude rate response of the Black Hawk UH-60A due to a step of the main rotor collective stick at 60 knots.	160
Plot V.A.3.-1. - Pitch angle response during a pitch reorientation maneuver by a multi-variable McRuer-Krendel pilot inserted in the Harrier AV-8B	161
Plot V.A.3.-2. - Longitudinal stick response of a multi-variable McRuer-Krendel pilot during a pitch reorientation maneuver in the Harrier AV-8B	161
Plot V.A.3.-3. - Forward velocity response during a pitch reorientation maneuver by a multi-variable McRuer-Krendel pilot inserted in the Harrier AV-8B	162
Plot V.A.3.-4. - Nozzle angle response of a multi-variable McRuer-Krendel pilot during a pitch reorientation maneuver in the Harrier AV-8B	162
Plot V.A.3.-5. - Altitude response during a pitch reorientation maneuver by a multi-variable McRuer-Krendel pilot inserted in the Harrier AV-8B	163
Plot V.A.3.-6. - Throttle response of a multi-variable McRuer-Krendel pilot during a pitch reorientation maneuver in the Harrier AV-8B	163
Plot V.A.3.-7. - Forward velocity response during a velocity translation maneuver by a multi-variable McRuer-Krendel pilot inserted in the Harrier AV-8B	164

PLOT LISTINGS - continued

Plot V.A.3.-8. - Nozzle angle response of a multi-variable McRuer-Krendel pilot during a velocity translation maneuver in the Harrier AV-8B	164
Plot V.A.3.-9. - Pitch angle response during a velocity translation maneuver by a multi-variable McRuer-Krendel pilot inserted in the Harrier AV-8B	165
Plot V.A.3.-10. - Longitudinal stick response of a multi-variable McRuer-Krendel pilot during a velocity translation maneuver in the Harrier AV-8B	165
Plot V.A.3.-11. - Altitude response during a velocity translation maneuver by a multi-variable McRuer-Krendel pilot inserted in the Harrier AV-8B	166
Plot V.A.3.-12. - Throttle response of a multi-variable McRuer-Krendel pilot during a velocity translation maneuver in the Harrier AV-8B	166
Plot V.A.3.-13. - Roll angle response during a coordinated turn maneuver by a multi-variable McRuer-Krendel pilot inserted in the Black Hawk UH-60A	167
Plot V.A.3.-14. - Yaw angle response during a coordinated turn maneuver by a multi-variable McRuer-Krendel pilot inserted in the Black Hawk UH-60A	167
Plot V.A.3.-15. - Sideslip angle response during a coordinated turn maneuver by a multi-variable McRuer-Krendel pilot inserted in the Black Hawk UH-60A	168
Plot V.A.3.-16. - Altitude response during a coordinated turn maneuver by a multi-variable McRuer-Krendel pilot inserted in the Black Hawk UH-60A	168
Plot V.A.3.-17. - Pitch angle response during a coordinated turn maneuver by a multi-variable McRuer-Krendel pilot inserted in the Black Hawk UH-60A	169
Plot V.B.4.-1. - Heading response comparison of the OCM pilot and piloted flight data during the vertical tracking maneuver.	169
Plot V.B.4.-2. - Rudder pedal deflection response comparison of the OCM pilot and piloted flight data during the vertical tracking maneuver.	170
Plot V.B.4.-3. - Altitude response comparison of the OCM pilot and piloted flight data during the vertical tracking maneuver.	170
Plot V.B.4.-4. - Vertical rate response comparison of the OCM pilot and piloted flight data during the vertical tracking maneuver.	171
Plot V.B.4.-5. - Throttle deflection response comparison of the OCM pilot and piloted flight data during the vertical tracking maneuver.	171

PLOT LISTINGS - continued

Plot V.B.4.-6. - Engine speed comparison of the OCM pilot and piloted flight data during the vertical tracking maneuver.	172
Plot V.B.4.-7. - Pitch angle response comparison of the OCM pilot and piloted flight data during the vertical tracking maneuver.	172
Plot V.B.4.-8. - Longitudinal stick operation comparison of the OCM pilot and piloted flight data during the vertical tracking maneuver.	173
Plot V.B.4.-9. - Airspeed response comparison of the OCM pilot and piloted flight data during the vertical tracking maneuver.	173
Plot V.B.4.-10. - Longitudinal position comparison of the OCM pilot and piloted flight data during the vertical tracking maneuver.	174
Plot V.B.4.-11. - Roll angle response comparison of the OCM pilot and piloted flight data during the vertical tracking maneuver.	174
Plot V.B.4.-12. - Lateral stick operation comparison of the OCM pilot and piloted flight data during the vertical tracking maneuver.	175
Plot V.B.4.-13. - Lateral position response comparison of the OCM pilot and piloted flight data during the lateral tracking maneuver.	175
Plot V.B.4.-14. - Lateral velocity response comparison of the OCM pilot and piloted flight data during the lateral tracking maneuver.	176
Plot V.B.4.-15. - Roll angle response comparison of the OCM pilot and piloted flight data during the lateral tracking maneuver.	176
Plot V.B.4.-16. - Lateral stick operation comparison of the OCM pilot and piloted flight data during the lateral tracking maneuver.	177
Plot V.B.4.-17. - Heading angle response comparison of the OCM pilot and piloted flight data during the lateral tracking maneuver.	177
Plot V.B.4.-18. - Rudder pedal operation comparison of the OCM pilot and piloted flight data during the lateral tracking maneuver.	178
Plot V.B.4.-19. - Pitch angle response comparison of the OCM pilot and piloted flight data during the lateral tracking maneuver.	178
Plot V.B.4.-20. - Longitudinal stick operation comparison of the OCM pilot and piloted flight data during the lateral tracking maneuver.	179

PLOT LISTINGS - continued

Plot B.1.-1. - Forward velocity response of the Harrier AV-8B due to a 10 percent positive impulse of the throttle.	179
Plot B.1.-2. - Forward velocity response of the Harrier AV-8B due to a 1 inch impulse on the longitudinal stick while in a near hover.	180
Plot B.1.-3. - Short period response of the Harrier AV-8B forward velocity due to an impulse of the lateral stick.	180
Plot B.1.-4. - Short period response of the Harrier AV-8B forward velocity due to an impulse of the rudder pedals.	181
Plot B.1.-5. - Simulation model pitch rate response of the Harrier AV-8B due to a 10 percent impulse of the throttle.	181
Plot B.1.-6. - Simulation model pitch rate response of the Harrier AV-8B due to a 5 degree impulse of the nozzle angle.	182
Plot B.1.-7. - Short period response of the Harrier AV-8B pitch rate due to an impulse of the lateral stick.	182
Plot B.1.-8. - Short period response of the Harrier AV-8B pitch rate due to an impulse of the rudder pedals.	183
Plot B.1.-9. - Simulation model vertical rate response of the Harrier AV-8B due to a 1 inch impulse of the longitudinal stick.	183
Plot B.1.-10. - Simulation model vertical rate response of the Harrier AV-8B due to a 5 degree impulse of the nozzle angle.	184
Plot B.1.-11. - Short period response of the Harrier AV-8B vertical rate due to an impulse of the lateral stick.	184
Plot B.1.-12. - Short period response of the Harrier AV-8B vertical rate due to an impulse of the rudder pedals.	185
Plot B.1.-13. - Pitch rate response of the Harrier AV-8B due to an impulse of the longitudinal stick at a near hover.	185
Plot B.1.-14. - Pitch rate response of the Harrier AV-8B due to an impulse of the longitudinal stick at 10 knots.	186
Plot B.1.-15. - Lateral acceleration of the Harrier AV-8B simulation model program due to the roll angle of Plot B.1.-16.	186

PLOT LISTINGS - continued

Plot B.1.-16. - Roll angle perturbation of the Harrier AV-8B due to an impulse of the lateral stick	187
Plot B.1.-17. - Lateral acceleration of the Harrier AV-8B due to an impulse of the rudder pedals.	187
Plot B.1.-18. - Yaw rate response of the Harrier AV-8B due to an impulse of the rudder pedals.in a near hover.	188
Plot B.2.-1. - Short period dynamics of the Harrier AV-8B pitch rate response due to an impulse of the longitudinal stick in a near hover.	188
Plot B.2.-2. - Short period dynamics of the Harrier AV-8B forward velocity due to a 5 degree impulse of the nozzle angle at a near hover.	189
Plot B.2.-3. - Short period response of the Harrier AV-8B vertical rate due to an impulse of the throttle at a near hover.	189
Plot B.2.-4. - Short period response of the Harrier AV-8B engine speed due to an impulse of the throttle.	190
Plot B.2.-5. - Short period dynamics of the Harrier AV-8B roll rate due to an impulse of the lateral stick at a near hover.	190
Plot B.2.-6. - Short period dynamics of the Harrier AV-8B yaw rate due to an impulse of the lateral stick at a near hover.	191
Plot B.2.-7. - Short period response of the Harrier AV-8B yaw rate due to an impulse of the rudder pedals at a near hover.	191
Plot B.2.-8. - Short period response of the Harrier AV-8B roll rate due to an impulse of the rudder pedals at a near hover.	192

NOMENCLATURE

t	\triangleq Time variable.
S	\triangleq Laplacian complex variable.
$H_n()$	\triangleq Transfer function model of the human's muscular system.
T_n	\triangleq Time constant of the human's muscular system.
$H_p()$	\triangleq Transfer function model of human response dynamics.
K_p	\triangleq Forward path gain of the human response model.
T_D	\triangleq Time delay of the human response model.
T_L, T_L	\triangleq Lead/Lag time constants of the McRuer_Krendel pilot equalization network.
T_K, T_K'	\triangleq Time constants of the general form McRuer_Krendel muscular system.
w_n	\triangleq Undamped natural frequency
ζ, ζ_n	\triangleq Damping ratio
A, F	\triangleq System matrix of a state space representation.
B, G	\triangleq Input distribution matrix of a state space representation.
C, H	\triangleq Measurement matrix of a state space representation.
\bar{x}	\triangleq State vector of a state space representation.
\bar{u}	\triangleq Input vector of a state space representation.
\bar{y}, \bar{y}_p	\triangleq Precieved system output vector of a state space representation.

NOMENCLATURE - continued

\bar{w} \triangleq Disturbance vector of a state space representation.

V_{uu}, Q_u \triangleq Remnant motor noise model.

V_{yy}, R_y \triangleq Remnant observation noise model.

$J()$ \triangleq Cost function associated with the control objectives.

Q, Q_{opt} \triangleq State weighting matrix of the cost function.

R, R_{opt} \triangleq Input weighting matrix of the cost function.

S, G_{opt} \triangleq Control rate weighting matrix of the cost function.

q, p, r \triangleq Vehicle pitch, roll, and yaw rates.

θ, ϕ, ψ \triangleq Vehicle pitch, roll and yaw(heading) Euler angles.

V_u, V_v, V_w \triangleq Forward, lateral, and vertical vehicle velocities.

XX_u, YY_y, ZZ_w \triangleq Longitudinal, lateral and vertical positions.

$ALT, ALTDT$ \triangleq Altitude and vertical rate, respectively.

$X_{(u, \theta, q, w, e, j, T)}$ \triangleq Parameters of the X-directed force components of the longitudinal dynamics.

$M_{(u, \theta, q, w, e, j, T)}$ \triangleq Parameters of the pitch rotational moment components of the longitudinal dynamics.

$Z_{(u, \theta, q, w, e, j, T)}$ \triangleq Parameters of the Z-directed force components of the longitudinal dynamics.

NOMENCLATURE - continued

$L_{(p,v,r,a,r)}$	\triangleq Parameters of the roll rotational moment components of the lateral dynamics.
$N_{(p,v,r,a,r)}$	\triangleq Parameters of the yaw rotational moment components of the lateral dynamics.
$Y_{(\phi,p,v,r,a,r)}$	\triangleq Parameters of the Y-directed force components of the lateral dynamics.
δ_e	\triangleq Longitudinal stick cockpit control mechanism for the Harrier AV-8B.
δ_a	\triangleq Lateral stick cockpit control mechanism for the Harrier AV-8B.
δ_r	\triangleq Rudder pedal cockpit control mechanism for the Harrier AV-8B.
δ_j	\triangleq Nozzle angle lever cockpit control mechanism for the Harrier AV-8B.
δ_T	\triangleq Throttle lever cockpit control mechanism for the Harrier AV-8B.
δ_{mr_c}	\triangleq Main rotor collective stick cockpit control mechanism for the Black Hawk.
δ_{tr_c}	\triangleq Tail rotor collective pedal cockpit control mechanism for the Black Hawk.
δ_{lo_c}	\triangleq Longitudinal cyclic stick cockpit control mechanism for the Black Hawk.
δ_{la_c}	\triangleq Lateral cyclic stick cockpit control mechanism for the Black Hawk.

I. INTRODUCTION

The practical problems associated with aircraft flight control system design and evaluation are complex and wide ranging. During the design phase, control system designers are faced with the selection of the control parameters that will best fit the system performance and control objectives, the vehicle configuration, and the particular situation. Powered-lift V/STOL aircraft pose unique problems in controls design since the propulsion controls are an integral part of the overall flight control system. Control system response characteristics and thus the control parameters are typically chosen from analytic evaluations and iterative design methods. Mathematical models of the vehicle and control system are developed. Control parameters are selected by various techniques to achieve the desired response characteristics. Evaluations of the control system performance are carried out in computer simulation environments or by a closed form approaches. Test input deflections (i.e. steps, ramps, disturbances, etc.) are injected into the various control mechanisms to directly excite specific closed loop dynamics. Measurement and subsequent evaluation of the closed loop vehicle and control system responses determine if the desired characteristics have been achieved.

The analysis of the control system and aircraft dynamics, in this typical design approach, provides the designer with valuable insight to the system's general/functional operation, but with only a limited basis to gauge the final selection of the control parameters. These limitations are associated with the lack of the total system response (i.e. the summation of the aircraft, control system, and the human pilot's dynamics). When an actively participating human is introduced to the flight control environment, he brings with him a complex array of control responses, that serve as inputs to the vehicle and control system. These inputs differ significantly from the test inputs used during the initial design

process. Thus the pilot's dynamic behavior must be carefully considered throughout the design and evaluation process.

When actively involved and participating in a flight control environment, the pilot acts as a controls integrator by performing a variety of control tasks via the manipulation of the multiple cockpit control mechanisms (e.g. longitudinal and lateral stick, rudder pedals, throttle, etc.). In addition, some flight scenarios require the pilot to perform tasks other than the control commitments (e.g. communications, navigation, weaponry system, etc.). Because the pilot is such an integral component of the overall flight control structure, pilot opinion tends to be the major criterion for deciding whether control system performance is satisfactory.

Current approaches to incorporating human response characteristics during the control system design involve the use of fixed-base piloted simulators. This phase is a necessary step in the overall system design process and provides the ultimate source of human response characteristics for evaluation purposes. In addition, the pilot's opinion can be directly incorporated as the final gauge of the overall system performance. The direct incorporation of fixed-base human piloted simulation within the design phases provides a safe and effective environment for controls design, but suffers from problems of cost, scheduling, and inconvenience. These stem from the necessity that the development take place at remote sites within the simulator structure and schedule. To further complicate matters, one must also take into account the acquisition of qualified pilots.

An alternative approach, to the direct incorporation of actual human pilots, is the use of analytic models of human behavior within a computer simulation environment. These

"paper pilots" attempt to simulate various aspects of a human's dynamic response characteristics when confronted with certain classes of closed loop control objectives. Analytic pilot models provide the ability to analyze and evaluate the fully integrated, total system response characteristics, before the control system is introduced to a remote manned simulator facility. This approach represents a significant advantage in cost, time, and convenience by allowing the base line control system design to be completed at the home institution and then to be thoroughly tested and adjusted at a remote, manned simulator site.

Human pilot behavior is, however, very complex. Analytic models tend to be limited in their abilities to precisely predictor human behavior in a given situation. These limitations stem from the model's inability to fully simulate the human's methods of deriving information from a variety of sources (e.g. visual, auditory, etc.), the human's complex information processing activities, and his physical methods of applying the control commands. In addition, individual human pilots perform/act differently when confronted with identical control objectives. Thus, human pilot models can only attempt to represent human behavior in a very general sense.

I.A. A Piloted Control Simulation Structure

Pilot activities within a flight control environment are directed at a wide variety of operations and objectives. The pilot must provide the necessary control, stabilization, guidance, and navigation, along with any additional tasks associated with a specific mission. The pilot supplies the controls needed to achieve the mission objective by actively analyzing his environment and instituting the appropriate control commands. The pilot

therefore functions as a control integrator, by acting as the center piece of the entire control structure and actively participating in the closed loop control efforts.

A human pilot flies an airplane by a feedback method. He senses by sight or feels by "the seat of the pants", the motion of the aircraft, and manipulates various cockpit control mechanisms to minimize the error between the actual and some desired motion. In other words, the motion of the aircraft is perceived, both directly and indirectly through the visual inspection of cockpit flight instrumentation (e.g. altimeter, artificial horizon, etc), external visual cues, auditory (the manner by which a car driver can shift gears by the sound of the engine), and by physical means. Through his computational mechanisms and thought processes, the pilot assesses the perceived vehicle attitudes/orientations, and determines the necessary compensative corrections. The pilot applies the corrections to the cockpit control mechanisms, through the physical movement of his muscular system. This is a form of negative feedback control, where the controller (pilot), must close the loop to achieve some desired, overall control objective.

To simulate active pilot participation within a closed loop control environment, the control structure illustrated in Figure I.A.-1. has been considered. Within this structure, the pilot appears as a cascaded compensator that is driven by command based vehicle attitudes and orientations from some type of guidance or navigation process. The pilot attempts to orient the vehicle in the manner specified by the command via the manipulation of the appropriate cockpit control mechanisms. The control configuration shown in Figure I.A.-1 assumes that the pilot feedback is based on visual assessments of cockpit instrumentation and external visual cues. The assumption of visual feedback reduces the effectiveness of

the simulated pilot because of the inherent limitations due to the lack of other forms of feedback (i.e. auditory, physical, etc.).

The research work that is presented in this report is focussed on the development of analytic human pilot models, "Paper Pilots", to serve as design tools for controls systems research. The models are tailored for use in computer simulation environments involving V/STOL research aircraft. The control structure of Figure I.A.-1 is used as the basis for the design, analysis, and insertion of the pilot model within the control loops of the V/STOL aircraft that are considered. This report will present an overview of the human models, simulated aircraft environments, and inserted pilot results of the research that has been conducted. Chapter II presents a description of the models of human dynamic behavior that have been utilized. The inherent limitations in their abilities of predicting human behavior are discussed. Chapter III discusses the techniques utilized in the design and insertion of the pilot models. Aircraft simulation environments and some simplified models of vehicle dynamics are introduced for use in the design of the pilot models. Pilot design is demonstrated and control objective considerations are discussed. Finally, configurations for pilot insertion to the control environment are discussed. Chapter IV introduces the concepts involved in the development of the vehicle dynamics models that have been used in the design of the pilots. Model structure and parameter identification are discussed and considered for their compatibility with the specific pilot configuration. Models of specific V/STOL vehicles and regions of the flight envelope are presented. Chapter V illustrates the pilot design and control loop insertion strategies for the specific V/STOL vehicles. Pilot parameters are presented for the various vehicles and flight scenarios. Results of pilot insertion are presented and discussed. Comparisons are made between the pilot models and the flight data of actual human pilots performing similar flight control operations. Chapter

VI presents a discussion of the results and an overall conclusion of the research that has been conducted and poses questions to be considered for future research efforts. Appendix A discusses the general mathematical characteristics of the Optimal Control Model of human behavior. The continuous time OCM is discussed and a discrete time representation is derived. Appendix B presents the derivation of a high order state space model of the V/STOL research aircraft (Harrier II AV-8B) for use with the OCM. Appendix C is a users guide for the OCM software. The general structure of the OCM code is introduced and procedures for installation and application of the OCM are presented and discussed.

II. MODELS OF HUMAN PILOT BEHAVIOR

The human pilot models that have been considered in this research are based on quasi-linear models of human behavior in closed loop compensatory tracking and state regulation tasks. The predicted/simulated human compensative control responses are generated from visual assessments of some displayed error or external visual cue. The models do not consider the other techniques that actual humans utilize to obtain information (i.e. auditory, physical (seat of the pants)). A human's control characteristics can be simulated by a cascade of three linear operators[1,2,3,4,5,6,7], as shown in Figure II.-1, and enumerated below:

1. Neuro-Muscular/Motor Dynamics - This operator describes the lags/bandwidth constraints imposed by the human's muscular system and is approximated by an adjustable, linear, first-order lag given by:

$$H_n(S) = \frac{1}{T_n S + 1} \quad (\text{II.-1})$$

where T_n is the time constant of the neuro-motor response. It is important to note that the human's muscular bandwidth is often restricted by the rate limitations of the cockpit control mechanism. The time constant of this lag can be selected to accommodate these effects on the bandwidth at which the human can exert control operations.

2. Pure Time Delays - These operators describe various internal time delays associated with visual information processing and neuro-motor signal pathways.

3. Equalization Network - This operator describes the control strategy implemented by the human to close the loop in a manner that best fits a given situation. Typically, the human

will select the equalization network to provide the dominant closed loop control response with a damping ratio (ξ) in the range, 0.5-0.8, and a natural frequency (ω_n) in the range, 3-4 rad/sec.

The inherent unpredictability of the human's response is simulated by a random component called the controller remnant.

In this research, two types of human dynamics models have been considered: 1) McRuer-Krendel - a single variable linear transfer function description, 2) An Optimal Control Model - a multi-variable state space approach based on optimal control and stochastic estimation theory. Each model is based on differing implementations of the three cascaded operator description. This section presents a general overview of the two models, their mathematical foundations and their inherent limitations of simulating/predicting human dynamic behavior.

II.A. - McRuer-Krendel Model of Human Dynamics

The McRuer-Krendel model (MKM) is a single-degree of freedom quasi-linear model based on a best fit analysis of experimental human response data [1,2,3,6,7]. The model uses assessments of visually-based information to produce compensative control mechanism displacements. The general form is given by:

$$H_p(s) = K_p e^{-T_D s} \frac{(T_L s + 1)}{(T_I s + 1)} \left\{ \frac{(T_K s + 1)}{(T_K s + 1)} \frac{1}{[(s/\omega_N)^2 + 2(\xi_N/\omega_N)s + 1]} \right\} \quad (\text{II.A.-1})$$

where $H_p(s)$ is the transfer function of the human response, often referred to as the describing function, s is the complex Laplace transform variable, the input is the visually based error signal, while the output is the corresponding control displacement. McRuer and Krendel discuss typical values of the precision model in [1,2,3].

Within this model, human activities are represented by physiological and equalization sections. Physiologic attributes simulate the limitations and abilities of the human's physical mechanisms. The inherent lags associated with the human's visual, information processing, and signal transmission systems are modeled by a pure delay. The restrictions associated with the muscular system are represented by the system within the brackets. The equalization attributes simulate the control strategies employed by the human to achieve the required closed loop responses in the form of a lead-lag network. The primary focus of the research using this type of human pilot model has been directed toward the fundamental control activities of the pilot during various flight control maneuvers. A zero remnant is therefore used during the development of the McRuer/Krendel pilot control strategies. Remnant selection for these types of piloted flight configurations is described in [8].

The model of EQ(II.A.-1) can be simplified to obtain the transfer function,

$$H_p(s) = \frac{K_p e^{-TDs} (T_L s + 1)}{(T_N s + 1)(T_I s + 1)} \quad (\text{II.A.-2})$$

where very low and very high frequency accuracy is not necessary. This transfer function model is illustrated in the simplified block diagram of Figure II.A.-1. The rejection of the very low and high frequency content is a reasonable assumption for the human pilot since, as discussed before, the bandwidth of the closed loop is 3-4 rad/sec (or 0.48-0.64 Hz).

The pure transmission time delay parameter T_D is estimated to be between 0.13-0.23 seconds [1,2,3,6,7]. Although the changes in the time delay can be significant depending on the particular control task, the parameter selected at $T_D=0.20$ was considered reasonable for the purposes of this research. The term $1/(T_Ns+1)$ is an approximation of the neuromuscular lag of the arm meaning that the pilot can not move his arm faster than the rate of this pole. The value of T_N is assumed to be constant and approximately 0.10 seconds. The remaining term, $K_p(T_Ls+1)/(T_Is+1)$, is the equalization part of the model (a time dependent variable gain and a lead-lag compensator) whose parameters are altered by the pilot to the particular flight configuration and control objective. The constraints on the model parameters are as follows:

$$0.0 \leq T_L \leq 2.50 \quad (T_L \neq T_N) \quad (\text{II.A.-3a})$$

$$0.0 \leq T_I \leq 20.0 \quad (\text{II.A.-3b})$$

$$T_N = 0.10 \quad (\text{II.A.-3c})$$

$$T_D = 0.20 \quad (\text{II.A.-3d})$$

The lead-lag compensator/equalizer is based on the assumption that the human is required to furnish at least one differentiation and one integration to obtain the desired performance, and the constraints on the parameters, T_L and T_I determine how efficiently the integration and differentiation processes are performed by the human. Even though there are only a few parameters to be adjusted, the analysis is still not trivial because of the time delay, time-varying pilot parameters and time-varying aircraft dynamics.

II.B. - The Optimal Control Model

The Optimal Control Model (OCM) [4,5,6,7] is a multi-variable approach to the modeling of human behavior. The OCM is based on the use of modern control and estimation theory to simulate/predict human behavior in closed loop control operations. The OCM is capable of treating multi-variable systems by incorporating a single conceptual framework based on state space techniques. The primary assumption involved in the OCM is that a well trained human pilot/operator behaves in a near optimal manner subject to his inherent limitations, constraints, and control tasks [4]. This optimal behavior is simulated by an analogous optimal control system. The optimal control system operates to minimize a quadratic performance index in the presence of various system inputs, noises, and disturbances.

The system under control consists of the control element and displays which are modeled by a linear state equation and output equation.

$$\dot{\bar{x}}(t) = A \bar{x}(t) + B \bar{u}(t) + \bar{w}(t) \quad (\text{II.B.-1})$$

$$\bar{y}(t) = C \bar{x}(t) \quad (\text{II.B.-2})$$

The "n" dimensional state vector is defined by:

$$\bar{x} = [x_1, x_2, \dots, x_n]^T \quad (\text{II.B.-3})$$

The human manipulates "m" controls:

$$\bar{u} = [u_1, u_2, \dots, u_m]^T \quad (\text{II.B.-4})$$

and observes "I" system displays (output variables):

$$\bar{y} = [y_1, y_2, \dots, y_l]^T \quad (\text{II.B.-5})$$

It is assumed, from remnant and psychophysical studies of human perception [9] that the human can extract position and rate from a single display or external visual cue, but can not extract higher derivatives. Thus the output "y(t)" contains those quantities explicitly displayed as well as those implicitly derived by the human. This is an important concept because it will be directly incorporated in the organization of the vehicle model and the strategies associated with displayed information. The disturbance, $\bar{w}(t)$, is a vector of zero mean, white gaussian noise processes and is generally associated with atmospheric turbulence when considering aircraft applications.

The OCM models human behavior in two categories: 1) intrinsic human limitations, 2) human control/equalization efforts. Simulation of human limitations is provided by a time delay, a neuro-muscular dynamics model, and a controller remnant. The time delays associated with visual information processing, neuro-muscular signal propagation, and other operations are combined into a lumped equivalent perceptual time delay, T_D . It is assumed that all outputs are delayed by the same amount. Typically, this delay is on the order of 0.2 seconds [4,5,6,7,10,11,12]. Neuro-muscular/motor dynamics are represented by an adjustable lag matrix, T_N . This lag is not directly modeled as an inherent limitation, but is indirectly incorporated by weighting the control rate terms in the cost function of the optimal control strategy. The inclusion of a control rate term results in a first-order lag being introduced in the optimal controller. This term is utilized to indirectly model the physiological limitations of the rate at which a human can perform a control action due to

the neuro-muscular/motor dynamics. Controller remnant is modeled by an observation noise vector, $V_{yy}(t)$, and a motor noise vector, $V_{uu}(t)$, where

$$E\{\bar{V}_{yy}(t), \bar{V}_{yy}^T(\sigma)\} = R_y \delta(t-\sigma) \quad (\text{II.B.-6})$$

$$E\{\bar{V}_{uu}(t), \bar{V}_{uu}^T(\sigma)\} = Q_u \delta(t-\sigma) \quad (\text{II.B.-7})$$

The observation noise models the inherent uncertainty of the human's visual assessments of the displayed information. A separate noise source is associated with each displayed output. The noise processes are modeled as an independent, zero mean, white, gaussian noise sources. The spectral density is proportional to the mean-squared value of the displayed variable, which is basically a signal-to-noise ratio that is on the order of -20dB [5,6,7,8,10]. The motor noise models the inherent uncertainty of the human's control execution. Like the observation noise, the motor noise is assumed to be independent, zero-mean, white, and gaussian. The spectral density is proportional to the mean-squared operator output. The motor signal-to-noise ratio is typically chosen near -25dB [5,6,7,8,10].

The human's equalization network describes the manner in which the human attempts to optimize his control strategy to match a given situation. As shown in Figure II.B.-1, the human perceives a delayed noisy replica of the system output, $y_p(t)$, where:

$$y_p(t) = y(t-d) + V_{yy}(t-d) \quad (\text{II.B.-8})$$

Estimation of the delayed state vector, $\hat{X}(t-T_D)$, is accomplished via a Kalman filter. The Kalman filter models the human's deduction of the system states from the displayed information. A least mean-squared predictor generates a present time state estimate, $\hat{X}(t)$,

from the delayed estimate, $\hat{X}(t-T_D)$. The predictor models the human's compensation for his inherent time delay. The optimal gain matrix, K^* , is generated by the solution, in steady state, of the optimal regulator problem [13] for the cost function of the form:

$$J(u) = \lim_{T \rightarrow \infty} E \left\{ \frac{1}{T} \int_0^T [\bar{x}(t)^T Q \bar{x}(t) + \bar{u}(t)^T R \bar{u}(t) + \dot{\bar{u}}(t)^T S \dot{\bar{u}}(t)] dt \right\}_{y_p(\sigma)} \quad (\text{II.B.-9})$$

where

$$\sigma \leq t$$

Q and R are positive semi-definite

S is positive definite

The application of the optimal control, Kalman filter, and predictor require the use of an internal reference model (i.e. the model of the vehicle as perceived by the operator) to generate their appropriate gains and parameters. Thus the model of the system under control plays an important role in the response actions of the OCM. Appendix A.1 presents a mathematical overview of the OCM in a continuous time representation. For use in the simulation model program, the continuous time model is converted to a discrete time representation. The concepts involved and the resulting discrete time OCM are presented in Appendix A.2.

III. STRATEGIES OF PILOT MODEL APPLICATION

The inherently different structures of the McRuer-Krendel model (MKM) and the Optimal Control Model (OCM) require different approaches in parameter selection and control loop insertion. The MKMs are specifically designed for each control objective and region of the flight envelope. The equalization parameters are selected off-line, by Root-Locus techniques and arranged in a gain table format. The multi-variable aspects of the OCM are directly incorporated in high order control configurations. Cost function weightings are selected according to parameters extracted from actual piloted flight data and arranged for the specific control situation. This section will discuss the techniques utilized to select the pilot's control parameters and the configurations used to insert the pilots within the simulated control environment.

III.A. Aircraft Simulation Environments

Before introducing the techniques utilized to select and insert the pilot models, it is important to discuss the computer-based aircraft simulation environments that were used in this research. The principle tools utilized to examine the V/STOL vehicles and evaluate the performance of the pilot models were two computer simulation programs [14,15,16,17] provided by NASA Lewis. These programs implement nonlinear, total force, large angle representations, in six degrees of freedom. These programs provide full flight envelope operation and incorporate all on-board stability augmentations systems.

III.B. McRuer-Krendel Pilot Models with Static Parameters

The static MKM pilots are based on the selection of the equalization parameters, for specific regions of the flight envelope, through the use of off-line application of Root-Locus techniques. In this approach, low order transfer function models of the aircraft dynamics are developed for regions of the flight envelope that are of interest. The regions of the flight envelope are designated by the vehicle's forward velocity. Pilot equalization parameters are selected from the use of a delayed Root-Locus and the direct incorporation of the pilot's physically limiting factors. Pilot parameters are then arranged in gain tables according to the flight envelope region. This design process is carried out for all cockpit control mechanisms (e.g. Lateral and Longitudinal Stick, Rudder Pedals, etc.) and for the vehicle attitudes and orientations that are relevant to the flight control objectives. This creates a set of Single Variable Pilot Mechanisms (SVPM). The insertion of a static MKM pilot is achieved by selecting an appropriate group of SVPMs for the objectives associated with the flight scenario. The insertion group has a SVPM defined for each cockpit control mechanism and thus has a unique feedback structure. The insertion group is therefore valid for only a limited number of flight control objectives.

III.B.1. - Structure of Aircraft Dynamics Models

The models of aircraft dynamics for use in the design of the MKM pilots, are based on single variable low order, linear transfer functions. The transfer function models are derived from the dominant response characteristics of the vehicle dynamics due to the injection of test inputs (e.g. impulses, steps, etc.) to the cockpit controls. The dominant responses refer to the most pronounced (primary) vehicle attitude reaction due to the deflection of a single cockpit control mechanism. The remaining vehicle reactions (i.e. the

coupled responses occurring in the other attitudes due to the operation of the cockpit control mechanism), are considered secondary. This definition of primary and secondary vehicle responses is illustrated in Figure III.B.1.-1. During SVPM development, the secondary reactions are ignored and considered as disturbances. The secondary reactions are, however, considered in the selection of an insertion group.

The dominant aircraft dynamics responses were identified by the direct evaluation of the time and frequency domain responses of the simulation model programs due to the test input deflections of the cockpit control mechanisms. Time based responses were utilized to match simplified low order responses. The frequency responses were obtained by Fast Fourier Transforms of the time responses. Attempts at the determination of ultra-low frequency response characteristics were hampered by the presence of parasitic low frequency response modes (Phugoid Modes) and distortions associated with the cross-couplings of the secondary variables. Solutions to these problems are considered in [19,20].

Along with the initial decoupling of the primary and secondary responses, the control and response characteristics of each vehicle were separated into two groups: 1) Longitudinal Control Set, and 2) Lateral-Directional Control Set. These sets consider the effects of the control mechanisms on the overall orientations of the vehicle to the primary orthogonal planes [18,19,20]. These sets simplify the selection of the SVPM when constructing an insertion group.

III.B.2. - Development of SVPM Equalization Parameters

The development of the Single Variable Pilot Mechanisms are based on the single loop control structure shown in Figure III.B.2.-1. This single variable control configuration is organized in such a way that the manipulation of a specific cockpit control mechanism is based on the assessment of visual feedback obtained from the observation of a single cockpit instrument or external visual cue. The relationship of aircraft dynamics to the specific cockpit control is obtained from the analysis of the aircraft dynamics discussed previously, and the desired control variable.

The MKM equalization parameters are selected via Root-Locus techniques. A problem that complicates this approach is the pure time delay associated with the human's visual, computational, and signal conduction delay model. In the continuous time domain, a pure time delay corresponds to an infinite number of poles positioned at $S = -\infty$ on the real axis. These poles introduce an infinite number of asymptotes that are parallel to the real axis. The presence of these asymptotes (specifically the primary asymptote) create significantly destabilizing distortions of the asymptotic behavior of the Root-Locus, as shown in Figure III.B.2.-2. An additional problem that is presented by the delayed Root-Locus is that many of the non-delayed assumptions are no longer valid.

To overcome the complications associated with the delayed Root-Locus, an approximation to the infinite pole set was applied in a non-delayed format. The pure delay approximation is given by:

$$e^{-T_D S} \sim \frac{1}{(1 + \frac{T_D}{N} S)^N} \quad (\text{III.B.2.-1})$$

where $T_D = 0.2$ seconds for this application.

This approximation not only simulates asymptotic behavior, but also permits all non delayed assumptions. To remain within computational limits (Quad Precision), 20 poles were placed at $S = -100$ on the real axis, as shown in Figure III.B.2.-3. The primary asymptote of this pole set has a 9° angle of incidence and has an imaginary axis intercept at 15.84 rads/sec (15.71 rads/sec for the ideal pure delay). This pole set serves as a reasonable approximation to the pure delay when considering the closed loop natural frequency of the piloted control ($W_N \sim 3.5$ rads/sec).

Incorporating the delay approximation and the muscular system limitation pole, a modified transfer function for design purposes only) can be given by:

$$G_{\text{PILOT}}^{\text{DESIGN}}(s) = \frac{K(S + a)}{(S + b)} \left\{ \frac{(100)^{20}}{(S + 10)(S + 100)^{20}} \right\} \quad (\text{III.B.2.-2})$$

where $a \geq 0.8$

$b \geq 0.0$

III.B.3. Multi-variable McRuer-Krendel Pilot Insertion Techniques

When a participating human pilot is introduced into the control loops, he uses all cockpit control mechanisms to provide an operational control by employing visual, audio, and other forms of feedback cues. For the purpose of simulation, a comprehensive human

response pilot model is constructed by integrating various single variable pilot mechanisms (SVPM) into a multi-variable structure (an insertion group), as shown in Figure III.B.3.-1.

The multi-variable pilot structural configuration is defined by the manner in which visual feedback is interpreted and applied to the cockpit control mechanisms via a specific set of Single Variable Pilot Mechanisms (SVPM). The intrinsic limitations of each configuration (insertion set) make it applicable to only a specific set of flight control maneuvers. This is primarily due to the limited number of feedback paths that are available (i.e. the number of feedback paths equals the number of cockpit control mechanisms). Each type of flight maneuver or command sequence is therefore associated with a specific multi-variable pilot configuration. In general, a command maneuver will be described by a set of vehicle attitudes and/or rates that define the new orientation that the vehicle is required to attain. The intricacy of the maneuver defines the number of attitudes and/or rates that are simultaneously involved in the operation.

The flight control objectives associated with simple maneuvers require the control of only one primary vehicle attitude or rate. The remaining secondary variables are monitored and regulated (regulation set) to preserve the stabilized aspects of the vehicle orientation (e.g. level flight). This type of operation can be performed by the configuration shown in Figure III.B.3.-2. A regulation set is defined by the single variable pilot mechanisms that are associated with the flight control variables needed to maintain a stabilized operation in a specific maneuver. The selection of the regulation set is based on the primary command attitude and the general operations involved in the execution of the maneuver. Large scale secondary responses must be compensated, proper feedback paths must be allocated, and the appropriate SVPMs must be utilized. This is similar to the manner in which a well

trained pilot reconfigures his feedback for a given situation. An additional concern in the selection of an insertion set is the use of multi-function cockpit control mechanisms. These controls are utilized differently depending on the control objectives. A good example of a multi-function control mechanism is the rudder pedals. During level forward flight, the pedals are used to make minor heading corrections, while during coordinated turns, they are used to minimize sideslip. This type of control mechanism is handled through the assignment of the feedback path and equalization network.

III.C. - Optimal Control Model

The multi-variable structure of the OCM makes its insertion to the control loop relatively simple. The application of the OCM is based on parameter selection in two basic categories: 1) Control task related, 2) Pilot model related. This section will provide an overview of the general construction of the OCM.

III.C.1. - Control Task Description

The first concern is the description of the control task. The control task must be described analytically, this includes the specifications of the system under control (vehicle) and the objective of the control activity (trajectory). As indicated previously, the vehicle is represented by a state space model. Care must be taken in selecting the vehicle model due to its implicit use in the formulation of the optimal control gains, Kalman filter and predictor. The state and output vectors must be chosen in such a way as to not limit the manner in which the OCM will extract estimates of vehicle orientation from the visually displayed

information. Control objectives are reflected in the cost function parameters. The controller's specific task is to choose a control input, on the basis of observing the displays, so as to minimize a weighted sum of the averaged state and control variables.

Once the vehicle and the control task have been specified, determination of the displayed variables is relatively straight forward. The control task, can at times, indicate the variables that are considered, or the displayed variables can be concluded from the available cockpit instrumentation. In certain control tasks a marked target, in the form of an external visual cue, is used. The variables available from the target are therefore related to it's markings and are thus described by the display vector associated with the target. As mentioned previously, the displayed variables include the quantities explicitly displayed plus their first derivatives.

III.C.2. - Pilot Description

The OCM pilot is described by four parameters: 1) Time delay, 2) Observation noise, 3) Motor noise, 4) Neuromuscular lag. The overall structure of the OCM is based on optimal control theory, but the theory does not provide the parameter selection. This information is typically obtained from human performance data.

The time delay in simple compensatory tracking and state regulation tasks is generally on the order of 0.1 to 0.3 seconds [4,5,6,7,10,11,12]. In complex tasks, the time delay is difficult to determine. Values near 0.2 seconds have shown to be reasonable choices from human performance data [7,10,12].

Observation noise plays an important role in the estimation problem, because it tends to be the dominant source of controller remnant. Various experiments have been performed [8] to obtain reasonable estimates of the observation noise spectral density. Typical values, for simple tracking tasks are on the order of -20dB while for complex operations -10dB has shown good results [10].

Motor noise is a difficult quantity to extract from human performance information. Typically, model matching techniques are incorporated to determine reasonable values. Spectral density signal-to-noise ratios on the order of -25dB have been indicated for relatively simple tasks [5,6,7] and near -10dB for complex tasks [10]. The effects of motor noise, however, do not appear to be great and have even been neglected in some cases [5].

The muscular system model of the OCM is based on the subjective weighting of the control rate terms of the cost function. The values of the lag matrix, T_N , must be chosen for the specific muscular activity and cockpit control dynamics. Classical values of $T_N=0.1$ do not appear to be valid when considering complex control tasks or stiff control mechanisms. Time constants on the order of $T_N=1.4 - 0.2$ have been shown to more closely agree with pilot data [6,7,10,11,12]. In addition, the muscular system involved with the use of the legs (for executing control manipulation of the rudder pedals) must take into consideration the inherent reduction in bandwidth.

III.C.3. - Difficulties in applying the OCM

The OCM provides a great many algorithmic and computational advantages in the quantitative estimation of a human operator's dynamics. There are, however, some difficulties that arise during the application of the OCM. The first relates to the explicit

requirement that the human pilot description be based on an internal model of the human's inherent characteristics, the dynamics of the system under control, and external disturbances. To provide a present time state estimate, $\hat{X}(t)$, the system matrices (A,B,C), system disturbances, the human time delay, observation and motor noises must all be known. To generate the controller's optimal state variable feedback gains the A and B matrices along with the control objective weights of the cost function are required. Essentially, this amounts to a complete knowledge of the pilot from man-machine system concepts. The OCM requires a very accurate internal model if it is to adequately function in a manner consistent with human behavior within the control environment.

The second difficulty stems from the fundamentally difficult problems associated with identifying the pilot's internal model parameters from experimental data. In addition, the optimal control strategy suffers from a degree of over parameterization. From an identification viewpoint, observation and motor noises are unresolvable and optimal control and state estimation gains can only be determined from the matching of experimental data or through the similarity transformation of the model [6].

The final problem is associated with the specification of the control objective cost function. The cost function parameters must be selected in accordance with the control task and thus the OCM designer must speculate on the parameters that will be of importance to the actual human pilot.

IV. MODELS OF V/STOL RESEARCH AIRCRAFT

Two types of V/STOL research aircraft have been used in this study: 1) Sikorski Black Hawk UH-60A - a modern high performance helicopter and 2) McDonnell Douglas Harrier II AV-8B - a thrust vectored jet fighter. Aircraft dynamics were simulated by nonlinear computer program models [14,15,16,17], provided by NASA-Lewis. Both programs implement total force, large angle, nonlinear representations of the individual aircraft dynamics in time based computer simulation environments. These vehicle definitions provide full flight envelope operation and support the onboard flight stabilization and control systems.

The vehicle models that have been developed in this study are designed to complement the structures of the individual pilot models. The McRuer/Krendel pilots require the use of low order/decoupled transfer function vehicle models, while the OCM model relies on high order/coupled state space representations. Linearized models of the aircraft dynamics (for use in the design of the pilot models) were developed by a mix of analytic models of vehicle motion and direct analysis of the time and frequency responses of the simulation program to test deflections of the cockpit control mechanisms. The following sections provide an overview of the vehicle, the model structures, parameter identification techniques, and the resulting vehicle models.

IV.A. Harrier II AV-8B : A Thrust Vectored Jet Fighter

The Harrier AV-8B's thrust vectoring capabilities make it a truly unique aircraft. The regions of the Harrier's flight envelope can be defined by the direction of the thrust vector, and consists of the three basic flight configurations shown in Figure IV.A.-1. The high

speed configuration, shown in Figure IV.A.-1.a, is characterized by the thrust vector being directed forward (i.e. nozzle jet vectors aft). In this mode, the propulsion system supplies the forward thrust component in a manner that is common to conventional aircraft. The lift and control components are supplied by the aerodynamic surfaces as they are forced through the atmosphere. The magnitude of the thrust vector supplied by the propulsion system is used to control vehicle speed. The stabilator is used to control the angle of attack and altitude.

The transition mode, shown in Figure IV.A.-1.b, is described by a general loss of aerodynamic responsiveness. As forward speed decreases, aerodynamic surfaces lose their ability to provide necessary lift and control functions. As the name implies, the vehicle control actions are in a transition between atmospheric flight and powered-lift activities. In general, sustained flight in this region is avoided by the typical maneuvers associated with acceleration to and deceleration from the high speed envelope.

The low speed configuration, shown in Figure IV.A.-1.c, is characterized by the thrust vector being directed upward (i.e. nozzle jet vectors downward). The lack of sufficient forward velocity requires that the propulsion system provide the lift components (powered-lift). A closer examination reveals that the propulsion system supplies the forward thrust and the primary lift component in a manner similar to a helicopter's main rotor. The magnitude of the thrust vector is primarily utilized to control the altitude and its direction is used to adjust forward speed.

The interesting region of the Harrier's flight envelope occurs during low speed powered-lift activities. In this region, the aerodynamic properties of the aircraft

significantly differ from those of high speed conventional flight. During low speed flight the components of lift produced by aerodynamic means are small. The vehicle relies primarily on lift components supplied by the propulsion system. In addition, the aircraft's aerodynamic control surfaces (e.g. rudder, ailerons, etc.) no longer function as the primary control mechanisms. The Harrier relies on the Reaction Control System (RCS) to provide the additional control components that are needed to maneuver the aircraft.

The primary focus of the research on pilot models for the Harrier II AV-8B has been directed toward the low speed - powered-lift region of the flight envelope. Dynamic response tests and general use of the simulation model programs were conducted while in trimmed forward flight at speeds ranging from hover to 35 knots. The vehicle was configured with the landing gear down, flaps extended to 60 degrees, and the lift enhancement devices fully extended. The SAS was enabled to provide damping of angular rates.

IV.A.1. - Harrier Control Structure

When operating in the low speed region of the flight envelope, the Harrier's control structure shows signs of a modest decoupling of the longitudinal and lateral dynamics. Longitudinal and lateral control sets are defined by the control strategies that are associated with the cockpit control mechanisms. The longitudinal control set specifies the control mechanisms and their associated reactions that primarily influence vehicle responses in the longitudinal plane (X-Z body plane). The three cockpit control mechanisms that operate within this region are: 1) nozzle angle control, 2) throttle, 3) longitudinal stick.

Nozzle Angle Control

The nozzle angle controls the direction of the propulsion system thrust vector. A typical low speed - powered-lift thrust diagram of a decrease in nozzle angle is shown in Figure IV.A.1.-1. The nozzle angle for this region of the flight envelope is large. The control structure is very similar to that of the longitudinal cyclic of a helicopter. Minor changes in the direction of the thrust vector will tend to dominate the forward thrust component. This indicates that the nozzle angle will dominate the control of the vehicle's forward speed. Small variations of the nozzle angle in low speed flight will have only a small effect on the primary lift components. The moment arm associated with the thrust vector displacement from the vehicle's center of gravity will induce a relatively small pitching torque in the longitudinal plane.

Throttle

The throttle controls the magnitude of the propulsion system's thrust vector. A thrust diagram of an increase in engine speed is shown in Figure IV.A.1.-2. This control behavior is similar to the main rotor collective of a helicopter. Changes in the magnitude of the thrust vector will tend to dominate the lift component and thus the vehicle altitude. Minor changes in the thrust vector magnitude will have only a small impact on the velocity components and the thrust vector displacement from the vehicle center of gravity will induce a relatively small pitching torque in the longitudinal plane.

Longitudinal Stick

The longitudinal stick controls the stabilator angle of attack and the vents of the RCS's forward and aft jets. During powered-lift activities the auxiliary thrust components and the associated moment arms (due to their physical configurations) of the forward and aft RCS jets to induce pitching torque responses about the Y body axis in the longitudinal plane. Figure IV.A.1.-3 illustrates the auxiliary thrust components produced by deflecting the longitudinal stick. Engine air bleed of the RCS will tend to effect the propulsion system performance. The aircraft longitudinal inertial components tend to induce sluggish responses. During low speed flight, the longitudinal stick is primarily used to control longitudinal orientations (e.g. angle of attack, pitch angle). It is important to note that the primary thrust vector of the propulsion system will be redirected during pitching maneuvers if the nozzle angle is fixed. This can result in changes in forward speed and altitude.

The lateral - directional control set specifies the control mechanisms and their associated reactions that influence vehicle responses in the lateral plane (Y-Z body plane) and in the directional plane (X-Y body plane). The two cockpit control mechanisms that operate in this set are: 1) lateral stick, 2) rudder pedals.

Lateral Stick

The lateral stick controls the ailerons and the vents of the wing-tip RCS jets. When operating in the low speed region of the flight envelope the auxiliary thrust components and the moment arms of the wing tip RCS jets are used to induce rolling torques about the X body axis. Figure IV.A.1.-4 illustrates the auxiliary thrust components produced by deflection of the lateral stick. Again, the air bleed of the RCS jets will effect engine

performance. The lateral inertial components and the RCS wing tip geometry create a highly responsive rotational moment about the X body axis. The rolling motion redirects the lateral components of the thrust vector and will therefore tend to dominate the lateral velocity components. The lateral plane components tend to be coupled to reactions in the directional plane.

Rudder Pedals

The rudder pedals control the rudder angle and the vents of the tail-end RCS jets. During powered-lift operations, the thrust components and moment arm of the tail-end RCS jets are used to execute yawing and lateral control maneuvers. Figure IV.A.1.-5 illustrates the auxiliary thrust components produced by deflection of the rudder pedals. Again, RCS air bleed will effect engine performance. The RCS thrust vectors induce rotations about the Z body axis. This allows rudder pedal control of the lateral velocity during turn coordination tasks (sideslip reduction) and heading regulation.

IV.A.2. - Low Order Transfer Function Models of Harrier Dynamics

This section presents the development of a set of low order linear transfer function models (for use in the design of the McRuer/Krendel pilot models) that are based on an investigation of the fundamental behavior of the nonlinear aircraft simulation model. The low order models describe dominant, decoupled, short period vehicle dynamics that are induced by deflections of specific cockpit control mechanisms [20]. These models do not attempt to account for the inherent couplings of the vehicle dynamics or any long term response characteristics (e.g. longitudinal phugoid modes, lateral spiral or dutch roll

modes). Long term dynamic modes and cross couplings are neglected and considered secondary to the dominant responses.

The low order linear transfer function models of the aircraft dynamics were obtained by an analysis of the time and frequency responses of the simulation program to test deflections of the cockpit control mechanisms. To simplify and limit this discussion, several examples of low order model identification will be presented. A comprehensive analysis and evaluation of the transfer function models can be seen in [20].

Pitch Angle/Longitudinal Stick Model

As shown in Figure IV.A.1.-3, the longitudinal stick dominates the pitching motions. The time based, short period pitch rate response while in a near hover, due a 1 inch impulse deflection of the longitudinal stick can be seen in Plot IV.A.2.-1. This type of time response can be modeled by a simple pole residing on the negative real axis of the Laplacian complex plane. A low order transfer function model that describes this type of time response is given by:

$$\frac{q(s)}{\delta_e(s)} \sim \frac{K_{THETDT}}{s + a_{THETA}} \quad (IV.A.2.-1)$$

where

$$K_{THETDT} = 0.71 \frac{\text{deg}}{\text{inch-sec}^2} \quad (IV.A.2.-2a)$$

$$a_{THETA} = 1.56 \text{ sec}^{-1} \quad (IV.A.2.-2b)$$

The pitch angle model is the direct integral of the pitch rate model and is given by:

$$\frac{\theta(S)}{\delta_e(S)} \sim \frac{K_{THET}}{S(S + a_{THETA})} \quad (IV.A.2.-3)$$

The parameters of these equations vary only slightly, due to the relatively small changes in aerodynamic effects within the low speed region of the flight envelope.

Roll Angle/Lateral Stick Model

The lateral stick's dominant effect on rolling motions can be seen in Figure IV.A.1.-4 tends to dominate the rolling motions. The time based response of the roll rate due to a 1 inch impulse on the lateral stick is shown in Plot IV.A.2.-2. The roll rate response is similar to the pitch rate response, but has a much shorter time constant. The transfer function model is given by:

$$\frac{p(S)}{\delta_a(S)} \sim \frac{K_{PHIDT}}{S + a_{PHI}} \quad (IV.A.2.-4)$$

where

$$K_{PHIDT} = 1.89 \frac{\text{deg}}{\text{inch-sec}^2} \quad (IV.A.2.-5a)$$

$$a_{PHI} = 3.45 \text{ sec}^{-1} \quad (IV.A.2.-5b)$$

The roll angle model is the direct integration of the roll rate model and is given by:

$$\frac{\phi(S)}{\delta_a(S)} \sim \frac{K_{PHIDT}}{S(S + a_{PHI})} \quad (IV.A.2.-6)$$

Parameter variations are insignificant within the low speed environment.

Forward Velocity/Nozzle Angle Model

As a final example of the low order transfer function models, consider the response characteristics of the nozzle angles effect on forward velocity. The time based response of the forward velocity due to a 5 degree impulse of the nozzle angle is shown in Plot IV.A.2.-3. The short period response can be modeled as a step function (i.e. integral of the impulse input). The ramping response appearing in the later phases of Plot IV.A.2.-3 is due to the long term phugoid effects. The transfer function model of an integrator is a simple pole residing at the origin of the complex Laplace plane, and is represented by:

$$\frac{V_u(S)}{\delta_T(S)} \sim \frac{K_{VEL}}{S} \quad (IV.A.2.-7)$$

where

$$K_{VEL} = -0.017 \frac{\text{knots}}{\text{deg-sec}} \quad (IV.A.2.-8)$$

IV.A.3. - High Order State Space Models of Harrier Dynamics

The high order, coupled state space vehicle models that have been developed for use in the design of the OCM pilot's internal reference model, are based on a set of generalized linear, first-order differential equations [21,22], that describe the vehicle motion. The equations of motion are of the form:

$$\dot{\bar{x}}(t) = A \bar{x}(t) + B \bar{u}(t) \quad (IV.A.3.-1)$$

The state vector, $\bar{x}(t)$, represents the perturbations from trim of the vehicle's pseudo-body axis variables. To maximize the overall usefulness of the internal reference model and to apply the control tasks (described in later sections), the state vector of Table IV.A.3.-1 was used. Utilizing this large order state vector provides for a flexible internal reference model. The use of pseudo-body axis variables results from the manner in which the human pilot model will interpret the flight control environment via a mix of external visual cues and instrumental feedback. A close examination of the state vector variable selection and organization shows that the state vector is made up of a set of vehicle body angles and positions, along with their first derivatives (i.e. angular rates and body velocities).

The control vector, $\bar{u}(t)$, represents the deviations from the trim positions of the cockpit control mechanisms and is defined in Table IV.A.3.-2. The use of the cockpit control mechanisms is due to the manner in which the human will institute his control actions upon the vehicle.

The output or measurement equation is of the form:

$$\bar{y}(t) = C \bar{x}(t) \quad (\text{IV.A.3.-2})$$

This equation provides the relationship of the variables that are displayed to the pilot from a linear combination of states. The structure and organization of the state vector permits the displays to primarily include vehicle positions and body angles. This is indeed a good structure because many of the cockpit displays and information available from external visual cues are in the form of a position indication. It is assumed that the pilot will therefore derive the first derivative information from the displays, and thus the entire state vector can be estimated given the proper display organization.

In the most general aircraft model, the elements of the system matrix A, and the control distribution matrix B, consist of two basic types. The first consists of inertial and gravitational components that are obtained analytically from the equations of motion. The second consists of partial derivatives associated with aerodynamic forces and moments. Due to the use of the low speed region of the flight envelope, many of the aerodynamic terms can be neglected. In addition, no attempt will be made to incorporate the SAS, instrumental, actuation, or cockpit control mechanism dynamics as components external to the state model. Instead, these dynamics will be incorporated directly within the state model.

The total linearized vehicle dynamics can be described by a completely coupled state model given by:

$$\dot{\bar{x}}(t) = \begin{bmatrix} A_{\text{long}} & A_{\text{lat-long}} \\ A_{\text{long-lat}} & A_{\text{lat}} \end{bmatrix} \bar{x}(t) + \begin{bmatrix} B_{\text{long}} & B_{\text{lat-long}} \\ B_{\text{long-lat}} & B_{\text{lat}} \end{bmatrix} \bar{u}(t) \quad (\text{IV.A.3.-3})$$

In general, the cross coupling terms, $A_{\text{long-lat}}$, $A_{\text{lat-long}}$, $B_{\text{long-lat}}$, and $B_{\text{lat-long}}$, can be ignored because of their limited secondary response characteristics and the low speed assumption [21,22,23]. Extensive testing of the simulation model program showed this to be true (see Appendix B). It is interesting to note that the lateral system did not show any signs of response excitation due to longitudinal activities, which results in:

$$A_{\text{long-lat}} \equiv B_{\text{long-lat}} \equiv 0 \quad (\text{IV.A.3.-4})$$

It is believed that this response characteristic is due to the absolute symmetry of the computer simulation model. The lateral system components did, however, induce relatively small reactions within the longitudinal system, thus:

$$A_{\text{lat-long}} \sim B_{\text{lat-long}} \sim 0 \quad (\text{IV.A.3.-5})$$

The effects of the lateral components will be discussed in the development of the longitudinal model in Appendix B.

Longitudinal Dynamics Model

A generalized linear representation of the core longitudinal dynamics is given by:

$$\begin{bmatrix} \dot{V}_u \\ \dot{\theta} \\ \dot{q} \\ \dot{V}_w \end{bmatrix} = \begin{bmatrix} X_u & X_\theta & X_q & X_w \\ 0 & 0 & 1 & 0 \\ M_u & 0 & M_q & M_w \\ Z_u & Z_\theta & Z_q & Z_w \end{bmatrix} \begin{bmatrix} V_u \\ \theta \\ q \\ V_w \end{bmatrix} + \begin{bmatrix} X_e & X_j & X_T \\ 0 & 0 & 0 \\ M_e & M_j & M_T \\ Z_e & Z_j & Z_T \end{bmatrix} \begin{bmatrix} \delta_e \\ \delta_j \\ \delta_T \end{bmatrix} \quad (\text{IV.A.3.-6})$$

The core dynamics are those variables which are the principle components involved in the description of the motions and responses. The remaining variables are the direct integration of the core dynamics. Using various low speed assumptions (see Appendix B), a variety of simplifications were made and verified by an analysis of the responses of the simulation model program. The longitudinal system of EQ(IV.A.3.-6) was simplified to:

$$\begin{bmatrix} \dot{V}_u \\ \dot{\theta} \\ \dot{q} \\ \dot{V}_w \end{bmatrix} = \begin{bmatrix} X_u & X_\theta & 0 & 0 \\ 0 & 0 & 1 & 0 \\ M_u & 0 & M_q & 0 \\ 0 & 0 & 0 & Z_w \end{bmatrix} \begin{bmatrix} V_u \\ \theta \\ q \\ V_w \end{bmatrix} + \begin{bmatrix} 0 & X_j & 0 \\ 0 & 0 & 0 \\ M_e & 0 & 0 \\ 0 & 0 & Z_T \end{bmatrix} \begin{bmatrix} \delta_e \\ \delta_j \\ \delta_T \end{bmatrix}$$

(IV.A.3.-7)

This model describes the generalized low speed dynamics of a thrust vectored aircraft. The response characteristics of this state model were examined and compared against the classical V/STOL responses [21,22] and those of the Harrier simulation program [15,16,17] (see Appendix B). The comparisons showed and explained many interesting response modes associated with the Harrier simulation programs operations. An example of this, can be seen in the long term pitch rate response due to an impulse on the longitudinal stick while operating outside the ground effects region, as shown in Plot IV.A.3.-1. The low frequency oscillatory response characteristics (noticeable in the latter phases of the response) can be attributed to the Phugoid mode [21,22] (see appendix B). The Phugoid response characteristic rarely troubles pilot activities because of it's ultra-low frequency content. This is similar to driving a car that is "out-of-alignment". The car driver simply compensates by providing an offset at the steering wheel that is necessary to overcome the misalignment. A closer examination of the system parameters that introduce the Phugoid response characteristics revealed that certain parameters could be neglected when operations are primarily directed at the pilot frequencies (i.e. pilot operations are directed at the short period dynamics). Applying these additional simplifications to the model of EQ(IV.A.3.-7) resulted in the low speed/powered-lift longitudinal model for pilot frequencies as given by:

$$\begin{bmatrix} \dot{V}_u \\ \dot{\theta} \\ \dot{q} \\ \dot{V}_w \end{bmatrix} = \begin{bmatrix} 0 & X_\theta & 0 & 0 \\ 0 & 0 & 1 & 0 \\ 0 & 0 & M_q & 0 \\ 0 & 0 & 0 & Z_w \end{bmatrix} \begin{bmatrix} V_u \\ \theta \\ q \\ V_w \end{bmatrix} + \begin{bmatrix} 0 & X_j & 0 \\ 0 & 0 & 0 \\ M_e & 0 & 0 \\ 0 & 0 & Z_T \end{bmatrix} \begin{bmatrix} \delta_e \\ \delta_j \\ \delta_T \end{bmatrix} \quad (\text{IV.A.3.-8})$$

This model represents the core longitudinal dynamics that were incorporated in the OCM's internal reference model.

Lateral-Directional Dynamics Model

A generalized linear representation of the core lateral-directional dynamics is given by:

$$\begin{bmatrix} \dot{\phi} \\ \dot{p} \\ \dot{r} \\ \dot{V}_v \end{bmatrix} = \begin{bmatrix} 0 & 1 & 0 & 0 \\ 0 & L_p & L_r & L_v \\ 0 & N_p & N_r & N_v \\ Y_\phi & Y_p & Y_r & Y_v \end{bmatrix} \begin{bmatrix} \phi \\ p \\ r \\ V_v \end{bmatrix} + \begin{bmatrix} 0 & 0 \\ L_a & L_{\pi} \\ N_a & N_{\pi} \\ Y_a & Y_{\pi} \end{bmatrix} \begin{bmatrix} \delta_a \\ \delta_r \end{bmatrix} \quad (\text{IV.A.3.-9})$$

Applying the low speed assumptions of Appendix B, a variety of simplifications were obtained, which resulted in the following low speed/powered-lift lateral-directional model.

$$\begin{bmatrix} \dot{\phi} \\ \dot{p} \\ \dot{r} \\ \dot{V}_v \end{bmatrix} = \begin{bmatrix} 0 & 1 & 0 & 0 \\ 0 & L_p & L_r & 0 \\ 0 & N_p & N_r & 0 \\ Y_\phi & 0 & 0 & Y_v \end{bmatrix} \begin{bmatrix} \phi \\ p \\ r \\ V_v \end{bmatrix} + \begin{bmatrix} 0 & 0 \\ L_a & L_{\pi} \\ N_a & N_{\pi} \\ 0 & Y_{\pi} \end{bmatrix} \begin{bmatrix} \delta_a \\ \delta_r \end{bmatrix} \quad (\text{IV.A.3.-10})$$

The response characteristics of this model were examined and compared against the non-linear simulation program and the classical V/STOL responses (see Appendix B). As in the longitudinal case, many of the low frequency lateral modes could be neglected (e.g. spiral and dutch roll modes). Applying these further simplifications to the model of EQ(IV.A.3.-10), a low speed/powered-lift lateral-directional model for pilot frequencies is given by:

$$\begin{bmatrix} \dot{\phi} \\ \dot{p} \\ \dot{r} \\ \dot{V}_v \end{bmatrix} = \begin{bmatrix} 0 & 1 & 0 & 0 \\ 0 & L_p & 0 & 0 \\ 0 & 0 & N_r & 0 \\ Y_\phi & 0 & 0 & 0 \end{bmatrix} \begin{bmatrix} \phi \\ p \\ r \\ V_v \end{bmatrix} + \begin{bmatrix} 0 & 0 \\ L_a & L_r \\ N_a & N_r \\ 0 & 0 \end{bmatrix} \begin{bmatrix} \delta_a \\ \delta_r \end{bmatrix} \quad (\text{IV.A.3.-11})$$

This model represents the core longitudinal dynamics that were incorporated in the OCM's internal reference model.

IV.B. Black Hawk UH-60A: A High Performance Helicopter

The primary focus of the research on pilot models for the Black Hawk helicopter was directed at developing a group of McRuer-Krendel pilots that spanned the flight envelope. This section discusses the development of a set of low order linear transfer function models that were obtained by an analysis of the nonlinear simulation model responses due to cockpit control mechanism operations. To simplify and limit this discussion, only a few transfer function models will be examined. The full set of vehicle models obtained are presented in [19].

During the initial stages of the pilot model development a linear point mass, small perturbation, state space model [24] of Black Hawk dynamics was utilized. This model was linearized about trimmed flight conditions and considered only the pure body dynamics. Augmenting this model with actuation and automated systems created a model whose complexity approached that of the nonlinear simulation model. The high order of this model created significant difficulties in the design and evaluation of the low order pilot models. For this reason, low order transfer functions were utilized to create more understandable vehicle models. As suggested above, these transfer function models were developed and used in a manner similar to the low order Harrier models.

Simulation model response tests were conducted while in trimmed flight at forward velocities of 20, 40, 60, 80, and 100 knots. The initial test scenarios were carried out with all onboard automatic control systems disabled and showed low frequency divergence. To improve the overall response characteristics, the pitch bias actuator, automatic tail stabilator control, and stability augmentation systems (both digital and analog) were enabled. The results showed substantial improvement.

IV.B.1. - Control Structure and Low Order Transfer Function Models

The cockpit control mechanisms and their associated vehicle responses were decoupled into the longitudinal control set (Longitudinal cyclic stick (δ_{lo_c}), Main rotor collective stick (δ_{mr_c}) and the lateral control set (Lateral cyclic stick (δ_{la_c}), Tail rotor collective pedals (δ_{tr_c})). A more detailed analysis of the control sets and their associated response characteristics is presented in [19]. The following model identification examples illustrate the fundamental approach utilized.

Pitch Angle/Longitudinal Cyclic Stick

Consider the pitch angle dynamics associated with the manipulation of the longitudinal cyclic stick. Plot IV.B.1-1 and Plot IV.B.1-2 show the pitch rate responses due to an impulse on the longitudinal cyclic stick while flying at 60 and 100 knots, respectively. Both plots show a damped sinusoidal response characteristic whose damping ratio decreases with increasing forward velocity. This type of response can be approximated by the transfer function shown below.

$$\frac{q}{\delta_{lo_c}} \sim \frac{K_{TD}}{S^2 + 2\delta_\theta w_\theta S + w_\theta^2} \quad (IV.B.1.-1)$$

The pitch angle response is given by:

$$\frac{\theta}{\delta_{lo_c}} \sim \frac{K_T}{S(S^2 + 2\delta_\theta w_\theta S + w_\theta^2)} \quad (IV.B.1.-2)$$

Where the pitch rate is measured in radians/second and the pitch angle is measured in degrees. Evaluating the pitch rate response throughout the flight envelope resulted in the parameter values listed in Table IV.B.1.-1.

Roll Angle/Lateral Cyclic Stick

Helicopter roll dynamics are dominated by the operation of the lateral cyclic stick. An analysis of the response characteristics of the simulation model program indicated slightly different roll reactions, one for low speeds (20 to 40 kn) and one for high speeds (60 to

100 kn). This type of behavior has been attributed to the low/high speed mode switching of the on-board yaw SAS near 60 kn. The low speed model is given by the transfer function:

$$\frac{\phi}{\delta_{la_c}} (20,40) \sim \frac{820}{S(S^2 + 2\delta_p w_p S + w_p^2)^2} \quad (IV.B.1.-3)$$

where $\delta_p \sim 0.15$ and $w_p \sim 9.0$ rads/sec.

The high speed model is given by:

$$\frac{\phi}{\delta_{la_c}} (60,80,100) \sim \frac{210(S + 3)}{S(S^2 + 2\delta_p w_p S + w_p^2)^2} \quad (IV.B.1.-4)$$

These models do not indicate the resonant behavior that can be seen in the time and frequency responses. Figure IV.B.1.-3 shows the frequency response of the roll rate at 80 kn. A relatively large peak-notch type characteristic can be seen near 2 and 22 rads/sec. The high frequency resonance is attributed to the main rotor. The low frequency resonance is associated with aerodynamic phenomena. The low frequency peak is, however, troublesome because the pilot will attempt to close the control loop near this frequency.

Altitude/Main Rotor Collective

The altitude components of the helicopter's flight dynamics are dominated by the main rotor collective. Figure IV.B.1.-4 shows the altitude rate response due to the injection of a 1 inch step on the main rotor collective stick while at a traveling at 60 kn. This type of first order response suggests the transfer function model given by:

$$\frac{ALTDT}{\delta_{mr_c}} \sim \frac{K_{ALT}}{S+a_{ALT}} \quad (IV.B.1.-5)$$

The altitude response is therefore given by:

$$\frac{ALT}{\delta_{mr_c}} \sim \frac{K_{ALT}}{S(S+a_{ALT})} \quad (IV.B.1.-6)$$

Evaluating the altitude rate response throughout the flight envelope resulted in the parameter values listed in Table IV.B.1.-2.

V. PILOT DEVELOPMENT AND INSERTION

This chapter will illustrate the development and insertion of a variety of pilot models within the control loop of the non-linear simulation programs. First, a set of McRuer-Krendel pilot mechanisms will be developed for the Harrier and the Black Hawk. A group of flight control maneuvers is defined and insertion set configurations are organized. Results of multi-variable pilot insertions are illustrated by examining several examples of Harrier and Black Hawk flight control maneuvers. Finally, the OCM is developed for use in the Harrier. Control tasks and display configurations are discussed. Task and pilot parameters are chosen. Results of OCM insertion are examined and compared to actual human pilot flight data.

V.A. - Static McRuer-Krendel Pilots

The concepts involved in the selection and insertion of the McRuer-Krendel model are based on the selection of a set of single variable pilot mechanisms (SVPM), to provide a variety of control functions associated with each of the cockpit control mechanisms. From this set/pool of SVPMs, a group (insertion set) is chosen, one SVPM for each cockpit control mechanism. The insertion set is chosen from an analysis of the control functions associated with the expected flight maneuvers. This section will illustrate the design of some example single variable pilot mechanisms and the selection of various insertion sets based on the flight control objectives. Examples of insertion set operation within the simulation environment of the non-linear program are presented and discussed.

V.A.1. - Design of the Single Variable Pilot Mechanisms

This section presents some examples of the design of the single variable pilot mechanisms (SVPM). The objective is to develop a set of SVPMs, where each pilot mechanism is selected to perform a specific control function. The elements of the multi-variable configurations will ultimately be chosen from this pool of SVPMs.

During the design of the individual pilot's, attempts were made to maximize the system TYPE. This simulates the pilot's ability to choose the control parameters that will tend to improve his error tracking ability. The ability to obtain the desired closed loop response characteristics was at times hampered by control mechanism restrictions and difficult vehicle response modes (e.g. high frequency complex poles near the right half plane, resonant behavior near the closed loop frequencies). Gain limitation and reduced closed loop bandwidths were required, in some cases, to keep pilot responses within limits.

Harrier Pitch Control Pilot

This pilot provides the position control of the pitch angle by considering visual assessment of the pitch angle and manipulating the longitudinal stick. Typically the human pilot would derive this feedback from the artificial horizon or from some type of external target. This individual SVPM will be used to maintain level flight or to perform specific pitch angle positioning. In addition, the pitch angle control can be applied to velocity control when performing fixed nozzle angle maneuvers.

Returning to the pitch angle response model of EQ(IV.A.2.-3), one can see that the integrating pole of the pitch angle response provides an intrinsic TYPE I system

characteristic. Attempts at introducing the pilot's equalization pole as a second integrating pole (to achieve a TYPE II system characteristic) did not provide adequate response characteristics due to the positioning restrictions of the equalization zero ($a \geq 0.8$). The pilot's equalization profile was relaxed and the equalization pole was removed to $S = 8$. The equalization zero was placed at $S = 3$ to maximize the Root-Locus dominant pole placement characteristics and provide the necessary phase considerations. This configured the equalization as a lead network which in-turn improved the low frequency response characteristics and oriented the pilot to be error rate sensitive. The resulting pilot transfer function is given by:

$$G_{\text{THETA}}^{\text{HARRIER}}(s) = \frac{4.3 (S + 3) e^{-0.2S}}{(S + 8)(S + 10)} \quad (\text{V.A.1.-1})$$

The Root-Locus for this configuration is shown in Figure V.A.1.-1. The dominant poles were placed near the desired locations ($w_n = 3.1$ rads/sec, $\zeta = 0.74$).

Additional Pilot Mechanisms for the Harrier

Table V.A.1.-1 lists the remaining single variable pilot mechanisms for the Harrier, that were developed in [20]. The models are based on the form:

$$G_{\text{PILOTS}}^{\text{HARRIER}}(s) = \frac{K (S + A) e^{-0.2S}}{(S + B)(S + 10)} \quad (\text{V.A.1.-2})$$

Black Hawk Pitch Control Pilot

As in the Harrier pitch control pilot, this pilot also controls the pitch angle position by visually assessing the pitch angle and operating the longitudinal cyclic stick. The different response characteristics of the Black Hawk required a significantly different pilot configuration. The transfer function model of the Black Hawk's pitch dynamics, EQ(IV.B.1.-2), permits the construction of a TYPE II system. The problems associated with the pitch control pilot development stemmed from the presence of the high frequency complex poles (see EQ(IV.B.1.-2). These poles are quite close to the imaginary axis and due to the destabilizing distortions of the delay Root-Locus, can be easily shifted into unstable conditions. Closing the loop near $w_n = 3$ rads/sec introduced large resonant reactions in the vehicle's lateral-directional body plane (X-Y body plane), due to torque reactive disturbances. To reduce this type of behavior, the closed loop dominant poles were placed near $w_n = 1.8$ rads/sec and $\zeta = 0.65$. The pitch control pilot transfer function was given by:

$$G_{\text{THETA}}^{\text{PILOT}}(s) = \frac{K_{\text{PT}} (S + 0.8) e^{-0.2S}}{S(S + 10)} \quad (\text{V.A.1.-3})$$

The gain profile is listed in Table V.A.1.-2.

Additional Pilot Mechanisms for the Black Hawk

Tables V.A.1.-3 through V.A.1.-7 list the remaining single variable pilot mechanisms for the Black Hawk, that were developed in [18,19]. The models are based on the form:

$$G_{PILOTS}^{BHAWK}(s) = \frac{K (S + A) e^{-0.2S}}{(S + B)(S + 10)} \quad (V.A.1.-4)$$

V.A.2. - Selection of Multi-Variable Configurations

The maneuvering characteristics associated with flight control objectives will determine the configuration of the insertion set. The insertion set configuration is based on the multi-variable control structure shown in Figure III.B.3.-1 (for the Harrier, the Black Hawk provides only four cockpit control mechanisms [18]). Some typical flight control maneuvers that are considered in [18,20] are listed below.

1. Pitch Reorientation
2. Velocity Translation
3. Altitude Translation
4. Small Scale Heading Modification
5. Altitude Rate Maneuver
6. Flat Turn
7. Coordinated Turn

These maneuvers can be executed by the control configuration shown in Figure III.B.3.-2. The application of this method to this class of control maneuvers is straight forward. The insertion sets and their associated configurations for the above maneuvers are discussed in [18,20], and are summarized in Tables V.A.2.-1 and V.A.2.-2.

V.A.3. - Results of Static Pilot Insertion

The results of pilot insertion can be best illustrated by considering several examples of multi-variable McRuer-Krendel pilot configurations actively participating in the control structure of the non-linear simulation program. Further results of static pilot insertion can be seen in [18,19,20].

Harrier : Pitch Reorientation

The pitch reorientation maneuver is designed to provide pitch angle translation while maintaining level flight characteristics in the lateral, altitude, and velocity components. The multi-variable pilot configuration, for this maneuver, is given in Table V.A.2.-1. The pitch angle rotation will cause a redirection of the primary thrust vector, which will directly influence the altitude and velocity components. The velocity and altitude component pilot mechanisms will therefore be called upon to provide the necessary compensation. The command sequence issued to the pilot is of the form of a step in pitch angle while the remaining variables are held at their trimmed values. A 10 degree step maneuver in pitch from a 10 knot trimmed flight at 100 feet is driven by the control sequence shown in Table V.A.3.-1.

The command sequence was injected at 1 second into the simulation run. Plot V.A.3.-1 shows the execution of the 10 degree set in vehicle pitch angle. This closed loop pitch angle response indicates a reasonably close match to the closed loop poles placed in the Root-Locus design. Plot V.A.3.-2 shows the pitch control pilots manipulation of the longitudinal stick. The change in pitch angle causes the primary thrust vector to be reoriented, creating a decelerating disturbance in the forward velocity. Plot V.A.3.-3 shows the forward velocity

response due to the pitch maneuver. Plot V.A.3.-4 shows the velocity pilot's compensative reactions to the velocity disturbance. Plot V.A.3.-3 shows that the pilot successfully reoriented the thrust vector and restored the commanded forward velocity. It is interesting to note that the final, steady state nozzle redirection is approximately 10 degrees (the commanded pitch angle). Plot V.A.3.-5 shows the altitude reaction due to the pitch maneuver. Plot V.A.3.-6 shows the pilot's manipulation of the throttle to handle the altitude disturbance. These plots indicate that the velocity pilot's reactions were fast enough to maintain proper thrust vector orientation with respect to the inertial frame (i.e. the velocity pilot was able to keep the thrust vector pointed towards the ground and therefore suffered little lift component degradation). The symmetry associated with this maneuver created insignificant disturbances in the lateral-direction modes.

Harrier : Velocity Translation

The velocity translations maneuver is designed to modify the forward velocity while maintaining level flight at a constant altitude. The multi-variable pilot configuration, for this maneuver, is given in Table V.A.2.-1. This maneuver uses the redirection of the primary thrust vector to modify the forward thrust. Reorienting the primary thrust vector tends to disturb the flight characteristics of the pitch and lift components. The command sequence issued to the pilot is of the form of a step in forward velocity while the remaining variables are held at their trimmed values. A 5 knot step reduction in forward velocity from a 25 knot trimmed flight at 100 feet is commanded by the control sequence shown in Table V.A.3.-2.

This command sequence was injected at 1 second into the simulation run. Plot V.A.3.-7 shows the execution of the 5 knot reduction in velocity. Plot V.A.3.-8 shows the velocity control pilot's reaction to the application of the command. Plot V.A.3.-7 's response

characteristic is very sluggish. This is due to the reduction in closed loop bandwidth via forward path gain reduction to reduce the pilot's control deflection. The initial pilot parameter selection created a response characteristics that tended to overdrive the nozzle angle ($\theta_j > 98.5^\circ$) during decelerating maneuvers. The velocity pilot parameters were adjusted to prevent the control mechanism overdrive, see Plot V.A.3.-8. Plot V.A.3.-9 shows the pitch angle reaction to the thrust vector redirection during the execution of the velocity control maneuver. Plot V.A.3.-10 shows the pitch control pilot's compensative response due to the "nose down" effects of the velocity translation. The steady state error of Plot V.A.3.-9 is typical for the TYPE I system characteristic of the piloted pitch control loop. Plot V.A.3.-11 shows a very small altitude response due to the velocity change. Plot V.A.3.-12 shows the small scale adjustments to the throttle by the pilot mechanism.

Black Hawk : Coordinated Turn

The coordinated turn maneuver provides a heading change through the execution of roll operations. The coordinated turn is executed by performing a roll maneuver while minimizing sideslip and maintaining level flight (pitch angle only) and constant altitude. The multi-variable pilot configuration, for this maneuver, is given in Table V.A.2.-2. It is interesting to note that the tail rotor collective pedal pilot mechanism has had its visual feedback redirected from the heading to the sideslip indicator (slip ball). Heading control must therefore be supplied by the commanding process (i.e. the navigation/guidance process that is issuing the command). The roll angle modification will tend to cause a loss of the lift components due to the redirection of the main rotor thrust vector. The command sequence issued to the pilot is of the form of a step in roll angle, while the remaining variables are held at their trimmed values. A 20 degree bank turn from an 80 knot trimmed flight at 200 feet is driven by the control sequence shown in Table V.A.3.-3.

The command sequence was injected at the initiation of the simulation run. Plot V.A.3.-13 shows a smooth roll angle response to the command. The heading response, shown in Plot V.A.3.-14, indicates the execution of the turn. The transient heading response is due to the settling of the roll angle and the turn coordination operations. Plot V.A.3.-15 shows the suppression of the sideslip angle and indicates that turn coordination has been achieved. Plot V.A.3.-16 shows the altitude response during the bank turn and shows the compensatory effects of the altitude control pilot. Plot V.A.3.-17 shows the compensatory effects of the pilot mechanism on the pitch angle.

V.A.4. - Conclusions on the McRuer-Krendel Models

The McRuer-Krendel pilot models have shown their ability to operate the V/STOL aircraft over a wide range of flight control maneuvers. Control and regulation activities have been shown to adequately achieve the control objectives. The multi-variable configurations provide for a wide range of possible flight scenarios. The fixed structure of the multi-variable configurations does, however, create certain difficulties when the flight control objectives require the use of multiple configurations. The switch between configurations has been examined in [19]. Finally, the sluggish response characteristics due to the reduction of closed loop bandwidths to accommodate various vehicle constraints tends to limit successful prediction of human behavior.

V.B. - Optimal Control Model Pilots

The concepts involved in the insertion of the OCM are based on the selection of two parameter sets: 1) Control task related, 2) Pilot related. The control task parameters describe the vehicle under control and the control objectives associated with the flight maneuvers that the pilot is required to perform. The pilot parameters describe the basic human response characteristics and inherent limitations. This section will illustrate the design and insertion of the OCM within the control loops of the Harrier and will present the results of various flight control tasks along with a comparison of the response characteristics of the OCM to some actual pilot flight data.

V.B.1. - Description of the Control Tasks and Display Configurations

The flight control tasks that have been considered for the testing of the OCM are classical precision hovering maneuvers that are performed outside of the ground effects region. Two primary maneuvers have been utilized to analyze the OCM: 1) Vertical tracking maneuver, 2) Lateral tracking maneuver. Each maneuver is complex in nature and exploits various aspects of the pilots control characteristics. The vertical hover maneuver consists of traversing between and positioning/aligning the vehicle at two vertically spaced targets, as shown in Figure V.B.1.-1. The targets, described in [25], are placed at 40 feet and 80 feet above the runway surface, and thus are outside of the vehicles ground effects region. The control objective is to hold at one target for a period of time, traverse to the other target at a constant rate, hold at that target for a period of time and then return to the initial target. Alignment with the targets is considered to be a positioning/disturbance regulation operation, while motion between the target is considered to be a rate control/tracking maneuver [25]. The Lateral tracking maneuver is similar to the Vertical task with the

exception that the targets are separated horizontally, as shown in Figure V.B.1.-2. The targets are placed 40 feet apart at an altitude of 50 feet.

The vehicle that is used in this study is the Harrier II AV-8B. The cockpit controls available to the pilot, for the maneuvers in question, are: 1) Longitudinal stick (right hand), 2) Lateral stick (right hand), 3) Throttle (left hand), 4) Rudder pedals (feet). The complexity of the maneuvers and their basic control structure, requires that the pilot maintain a fixed nozzle angle, thus forward velocity and longitudinal positioning control are indirectly handled through pitch angle control.

The displays that the pilot monitors are assumed to be the targets (external visual cues). The targets have been designed [25] to supply the pilot with the following information: Pitch, Roll, and Yaw angles, Longitudinal, Lateral, and Vertical positions. The pilot can therefore derive the output vector shown in Table IV.A.3.-1. The state space model and the above output vector, derived in Appendix B, are based on this display assumption.

V.B.2. - Overview of the Piloted Flight Data and Analysis

The precision hover maneuvers, described above, were used in a simulation fidelity study by [25]. The time domain flight test data of the actual pilot activities and the vehicle responses from this study were supplied by NASA-Lewis. This information provided a valuable tool in the design and insertion of the OCM pilot. The flight data was reviewed and the basic flight maneuver trajectories were extracted. This trajectory information is the basis of the command sequences that are injected into the OCM.

V.B.3. - Description of Pilot and Task Parameter Selection

The OCM task parameters were selected from an analysis of the fundamental structure of the control tasks in the piloted flight data. The limited information available from the flight data required that most task parameters were selected subjectively. Thus, a simplified performance index was chosen to represent the task of minimizing the hover attitude and position errors indicated by the external target.

$$J = J_{\text{long}} + J_{\text{lat}}$$

$$J_{\text{long}} = \lim_{T \rightarrow \infty} \left\{ \frac{1}{T} \int_0^T \left[\left(\frac{XX_u}{XX_M} \right)^2 + \left(\frac{V_u}{V_M^u} \right)^2 + \left(\frac{\theta}{\theta_M} \right)^2 + \left(\frac{ZZ_w}{ZZ_M} \right)^2 + \left(\frac{\delta_e}{\delta_M^e} \right)^2 + \left(\frac{\delta_T}{\delta_M^T} \right)^2 \right] dt \right\} \quad (\text{V.B.3.-1})$$

$$J_{\text{lat}} = \lim_{T \rightarrow \infty} \left\{ \frac{1}{T} \int_0^T \left[\left(\frac{YY_y}{YY_M} \right)^2 + \left(\frac{V_y}{V_M^y} \right)^2 + \left(\frac{\phi}{\phi_M} \right)^2 + \left(\frac{\psi}{\psi_M} \right)^2 + \left(\frac{\delta_a}{\delta_M^a} \right)^2 + \left(\frac{\delta_r}{\delta_M^r} \right)^2 \right] dt \right\} \quad (\text{V.B.3.-2})$$

The maximum desirable values of the position errors (XX_M , YY_M , ZZ_M), were chosen to correspond to the relative target size and reflects the specifications associated with precision hovering. The values of the attitude angle cost parameters were chosen subjectively by considering a 10 degree deviation as being large. The maximum values of the cockpit control mechanisms were selected to be approximately 0.25 of the total control travel, as suggested in [26]. Table V.B.3.-1 and V.B.3.-2 list the values of the cost function weights associated with the vertical and lateral flight maneuvers, respectively.

The vertical maneuver parameters were originally designed for all maneuvers. During tests (discussed later sections), the lateral operations showed unstable response characteristics in the pitch and yaw (heading) components when using the values of Table V.B.3.-1. Tightening the allowable deviations in pitch and yaw (compare Tables V.B.3.-2 to V.B.3.-1), improved these response modes. The response characteristics in the yaw angle are expected because of the inherent couplings in the lateral-directional components. The responses of the pitch angle were more pronounced than were expected. These problems appear to stem from the limitations of the OCM's internal reference model, since the optimal control gains are based on the internal reference model (it's knowledge of the system under control). Another possible reason for the differences of Tables V.B.3.-1 and V.B.3.-2 can be reflection of the OCM's sensitivity to the inherent differences between the two maneuvers. This may be due to a reconfiguration of the manner in which the pilot must obtain information during the maneuvers.

The pilot parameters were chosen according to some typical values. The weightings of the control rates were selected to provide a neuro-muscular lag time constant, T_N , near 0.15 seconds for each control mechanism. The magnitude of the motor noise sources for each control is shown in Table V.B.3.-3. These correspond to an approximate -15dB signal to noise ratio (S/N). The magnitude of the observation noise was chosen to correspond to an approximate -10dB (S/N). These values create a remnant that is considered reasonable for a multi-axis hovering control task [10]. The pure time delay was selected to be 0.2 seconds.

V.C.4. - Results and Comparisons of OCM Pilot Insertion

The OCM pilot was inserted into the nonlinear simulation environment of the Harrier. The structure of the OCM required that the vehicle trajectory associated with the control

task be specified in position/attitude and velocity/rate. This type of trajectory is generated by the velocity/rate driven system shown in Figure V.B.4.-1, for the pitch angle components. This generator is replicated for the other state variables. The low pass filter provides bandwidth limiting of the forcing function as described in [2]. The time constant of this filter was selected to be 2.5 seconds.

An analysis of the vertical and lateral flight data showed a variety of pre-test procedures used by the pilot to approach and align the vehicle with the target. In both cases, the vehicle was at rest on the ground away from the targets. The approach and alignment operations consisted of a vertical takeoff, followed by a ground translation and a flat rotation (yawing maneuver). During initial attempts at constructing the command sequence for these maneuvers for the OCM, trim discrepancies in the non-linear simulation program created problems. These primarily stemmed from problems associated with simulating the vehicle on the ground. To overcome these problems, the OCM tests were initialized near the targets with the vehicle already airborne. This allowed closer matches of trimmed values and simplified the test command sequences.

Vertical Tracking Maneuver

The vertical tracking maneuver consisted of an initial yawing rotation (to simulate the final stages of the pilot's alignment with the targets), followed by a holding period and then by the cyclic execution of the vertical operations. The cost function weightings of Table V.B.3.-1 were used to select the control aspects of the OCM. The vehicle was trimmed to the values shown in Table V.B.4.-1. The vertical rate and yaw rate command sequences of Figure V.B.4.-2 were applied to the OCM pilot during a 125 second simulation run. This command sequence requires the pilot to rotate the vehicle (flat turn - approximately 60°) to

acquire the upper target. The pilot holds at the target (for approximately 10 seconds) then proceeds to the lower target at a constant rate (2.5 feet/sec). The pilot is then repeatedly commanded to proceed back and forth between targets.

Plot V.B.4.-1 shows a heading angle comparison of the OCM (solid line) and the piloted flight data (dashed line). This type of comparison strategy will be used throughout the following discussion. Transients associated with the target alignment phases are not present for times greater than 35 seconds ($\text{TIME} > 35$ seconds). Plot V.B.4.-2 shows a comparison of the rudder pedal activity. The "fuzziness" of the OCM response is due to the noise model of the controller remnant. Rudder pedal operations differ significantly. This has been attributed to the limitations in the lateral dynamics of the OCM's internal reference model. The flight data tends to suggest that the heading angle regulation is not particularly critical to this maneuver. It appears that this type of activity may stem from a threshold regulation process where no corrective actions are taken until the error crests a certain level. The present version of the OCM does not account for this type of behavior.

Plots V.B.4.-3 and V.B.4.-4 compare the altitude and vertical rate responses, respectively. These plots show similar trends in command trajectory following. Target alignment operations can be seen during the initial phases of the run ($\text{TIME} < 35$ sec). The vertical rate responses of Plot V.B.4.-4 show that the OCM has similar behavior during the execution of the vertical maneuvers ($\text{TIME} > 35$ sec), but does not capture the higher frequency content of the pilot data. This has been attributed to the low order altitude component representation of the of OCM's internal reference model, and possibly the lack of auditory feedback.

Plot V.B.4.-5 shows a very dissimilar comparison of throttle operations. Plot V.B.4.-6 shows a comparison of the engine speeds. During the execution of the vertical maneuvers (TIME>35 sec), the engine speeds show strikingly similar response characteristics from very dissimilar throttle operations. This discrepancy may be due to infidelities in the simulation environment, particularly in the throttle linkages and servo-systems.

Plot V.B.4.-7 compares the pitch angle responses. This plot shows very similar vehicle orientations during the vertical maneuvering. This is an important response characteristic due to the fixed nozzle angle which couples the pitch angle to the forward velocity and position. Plot V.B.4.-8 shows the comparison of the longitudinal stick activity. The offset in stick operations is due to the trimmed value of the piloted data being ~ -1.35 inches. As in the case of the rudder pedal, the OCM does not predict the higher frequency operations of the pilot.

Plot V.B.4.-9 shows a comparison of the airspeed responses. The OCM pilot shows very similar characteristics in both magnitude and frequency content during the vertical maneuvers (TIME>35 sec). Plot V.B.4.-10 compares the longitudinal position. The offset is due to the initial target approach operations by the pilot. This plot shows similar but out-of-phase positioning response.

Plots V.B.4.-11 and V.B.4.-12 show comparisons of the roll angle responses and lateral stick deflections, respectively. In both plots, the OCM fails to match the frequency content of the actual pilot.

Lateral Tracking Maneuver

The lateral tracking maneuver was simplified by not including the initial yawing operations of the target alignment. The vehicle was trimmed to the values shown in Table V.B.4.-2. The lateral velocity command sequence of Figure V.B.4.-3 was applied to the OCM pilot during a 100 second simulation run.

Plot V.B.4.-13 shows a comparison of the lateral position responses. This plot indicates a good trajectory following by the OCM. Plot V.B.4.-14 compares the lateral velocity responses. As in the vertical maneuvers, the OCM's response characteristics do not capture the higher frequency content of the pilot data. This is illustrated in the regulatory operations shown in Plots V.B.4.-15 - V.B.4.-20.

V.C.5. - Conclusions on the OCM pilots

The OCM pilots have shown their abilities of providing adequate multi-variable flight control of the V/STOL research aircraft. The OCM is not structurally limited in its maneuvering characteristics and can therefore be applied to a wide range of flight control objectives. Differences between the cost function weightings of the vertical and lateral tracking maneuvers illustrate the pilot's alteration of his approach to the individual control problems (possible modification of feedback to handle the characteristics of a specific maneuver). The OCM showed an excellent match in the longitudinal components of the vertical maneuver. This appears to stem from a reasonable model of the aircraft's longitudinal dynamics (since lateral excitation is minimal) and subjective assumptions in the cost function weight selection.

The reasons behind the OCM's inability to predict the higher frequency components of the pilot data are not clear. A possible reason stems from the manner in which the pilot obtains information. The limited information available on the targets and actual flight control objectives of the piloted flight data required the use of an intuitive selection of displays. A close examination of the pilot's control activities showed a higher degree of sensitivity to the angular rates than to the angular position. Attempts at configuring the OCM to be more sensitive to angular rates did not resolve this issue. The addition of a display scanning algorithm induced a cyclic feature in the OCM's responses that was similar to that of the pilot data. The presence of scanning behavior in the pilot flight data can not be substantiated and thus the OCM scanning model is only marginally permissible. Another possible reason is the OCM's remnant models. In some regulation operations [10], the pilot tends to "battle" his own remnant more than the external disturbance. Modifying the OCM's remnant models did not significantly alter the frequency content. Finally, it is possible that the OCM's reliance on the internal reference model of the vehicle dynamics creates this phenomena. Limitations in the model may restrict the manner in which the OCM applies its control efforts. The lack of deadband considerations in the model (i.e. the 0.1 inch deadband in the servo-channels of the longitudinal and lateral stick linkages) leads to the suppression of OCM control mechanism deflections that are based on small errors. Possible over-accuracy in the model may provide the OCM with such a good understanding of the vehicle under control that all compensative actions are near optimal. This would account for the OCM's limited control deflection activities in the regulation modes.

The OCM is very sensitive to changes in cost function weightings and muscular system time constants. In some cases (pitch and roll components), maximum deviation values of

20-30% larger produced unstable results. This may be due to the nonlinearities in the simulation environment. This tends to complicate the subjective selection of cost functions.

VI. - SUMMARY AND CONCLUSIONS

This report has illustrated the application of "Paper Pilots" within the flight control loops of V/STOL research aircraft. Two types of human dynamics models have been considered: 1) McRuer-Krendel - single variable transfer function, 2) Optimal Control Model - multi-variable approach based on optimal control and stochastic estimation theory. Descriptions of the models and discussions of their inherent limitations in predicting human behavior have been provided. Design strategies and methods of inserting the pilots within the control loops have been discussed and illustrated for two V/STOL research aircraft: 1) Sikorski Black Hawk UH-60A - a high performance helicopter, 2) McDonnell Douglas Harrier II AV-8B - a thrust vectored jet fighter. Results of simulated pilot insertion have been analyzed and compared to the control activities of actual human pilots performing similar control objectives.

The "Paper Pilots" have shown their abilities to successfully "fly" the V/STOL aircraft that have been considered in this research. The simulated pilots provide a stabilized control over the vehicle and respond to control objectives in a manner similar to human pilots. The response characteristics of the pilot models are, however, very general in nature. This appears to stem from the "Paper Pilots" inability to completely simulate the human's complex manner of obtaining and processing information, and applying the controls to the vehicle. In addition, it may be possible that the pilots have an over-detailed description of the vehicle under control and thus exert a nearly ideal control response.

Of the two human dynamics models that have been considered, the OCM appears to provide the better simulation of human activities. Its multi-variable structure and state variable framework provide a simple yet effective method for describing the pilot's abilities and the control objectives that the pilot is confronted with. The maneuvers that have been considered for the OCM are in the low speed/powered-lift region of the flight envelope. To maneuver in other regions of the flight envelope, the control objectives (i.e. the vehicle model and control strategies) must be altered because of the changes in vehicle dynamics. The use of envelope based gain tables provides a possible solution but the tables must be constructed in an off-line approach (not a simple task) and do not allow for alternative flight configurations. In addition, transition/interpolation between flight regions must be well defined to avoid control transients.

Improvements are needed to provide the OCM with a more complete description of pilot activities and to simplify the OCM pilot design process. Adaptive procedures have been successfully applied to the single variable McRuer-Krendel model. This strategy appears to have a good prospects for use in the OCM based pilots. The OCM is, however, a much more detailed and complex system. Adaptive procedures for the OCM will require a different parameter estimation scheme (because of its high order) and will also need a different optimization scheme if muscular system time constants are to remain the same. Initial research on this subject (not discussed in this report) indicated favorable results. Due to time constraints, this work was not fully established. A further investigation in these areas is suggested as the focus of future research efforts.

In conclusion, the "paper pilot" provides a safe, convenient, and seemingly effective method for introducing human pilot response characteristics during the design process

without resorting to the use of manned, fixed-base simulators. Construction and application of the pilot models are relatively straight forward and the pilots can be configured to achieve a large number of flight configurations and control objectives.

APPENDIX A

DESCRIPTION OF THE OCM

This appendix presents a mathematical overview of the Optimal Control Model of Human Dynamics that is developed in [4]. A continuous time description of the OCM is discussed, and a discrete time representation is then developed for use in the computer simulation environment.

A.1. Mathematical Overview of the OCM

This section provides a general overview of the mathematical concepts involved with the OCM. Figure A.1.-1 shows a block diagram of the internal structure of the OCM. For the purpose of definition, the dynamics of the system under control will include the dynamics of the actuation, sensory subsystem, SAS, and any other on-board control systems. The overall system under control will be represented by a set of linearized equations of motion.

$$\dot{\bar{x}}(t) = A \bar{x}(t) + B \bar{u}(t) + \bar{w}(t) \quad (\text{A.1.-1})$$

$$\bar{y}(t) = C \bar{x}(t) \quad (\text{A.1.-2})$$

The system dimension is assumed to be "n", the number of inputs (i.e. cockpit control mechanisms) is assumed to be "m" and the number of outputs (i.e. visually and extracted displays) is assumed to be "l". The variables and parameters are defined as follows:

$\bar{x}(t)$ = "n" dimensional system state vector

$\bar{u}(t)$ = vector of "m" control inputs (in this case, the cockpit control mechanisms)

$\bar{y}(t)$ = vector of "l" system outputs (linear combination of the system states as perceived and deduced by the human from the displayed information)

$\bar{w}(t)$ = vector of "n" external disturbances that are independent, zero mean, white, gaussian noise sources, where:

$$E\{\bar{w}(t), \bar{w}^T(\sigma)\} = Q_w \delta(t-\sigma) \quad (A.1.-3)$$

A = (n,n) system matrix

B = (n,m) input distribution matrix

C = (l,n) output measurement matrix

It is assumed that the human pilot/operator maintains an internal model of the system under control to base his control and estimates on.

$$\dot{\bar{x}}(t) = F \bar{x}(t) + G \bar{u}(t) \quad (A.1.-4)$$

$$\bar{y}(t) = H \bar{x}(t) \quad (A.1.-5)$$

The parameters are defined as follows:

F = Human's perception of the system matrix

G = Human's perception of the input distribution matrix

H = C

It is assumed that the control task is adequately reflected in the human's choice of the best control input, " $u^*(t)$ ". In addition, the human's choice is also based on his inherent knowledge of his neuro-muscular limitations. The optimal control input " $u^*(t)$ " minimizes, in steady state, the cost function given by:

$$J(u) = \lim_{T \rightarrow \infty} E \left\{ \frac{1}{T} \int_0^T [\bar{x}(t)^T Q \bar{x}(t) + \bar{u}(t)^T R \bar{u}(t) + \dot{\bar{u}}(t)^T S \dot{\bar{u}}(t)] dt \right\}_{y_p(\sigma)} \quad (A.1.-6)$$

where

$$\sigma \leq t$$

Q and R are positive semi-definite

S is positive definite

The formulation of EQ(A.1.-6) does not directly include the neuro-muscular dynamics of EQ(II.-1), but instead provides a cost on the control rate in $J(u)$. The inclusion of a control rate term results in a first-order lag being introduced in the optimal controller. This term is utilized to indirectly model the physiological limitations of the rate at which a human can perform a control action due to the neuro-muscular/motor dynamics.

The solution to this optimization problem is obtained by defining an augmented system.

$$\dot{\bar{X}}_0(t) = F_0 \bar{X}_0(t) + G_0 \dot{\bar{u}}(t) + W_0 \quad (A.1.-7)$$

where

$$\bar{X}_0(t) = \begin{bmatrix} \bar{x}(t) \\ \bar{u}(t) \end{bmatrix} \quad (\text{A.1.-8a})$$

$$F_0 = \begin{bmatrix} F & G \\ 0 & 0 \end{bmatrix} \quad G_0 = \begin{bmatrix} 0 \\ I \end{bmatrix} \quad W_0 = \begin{bmatrix} \bar{w}(t) \\ 0 \end{bmatrix} \quad (\text{A.1.-8b})$$

An optimal control rate is generated by the linear feedback law:

$$\dot{\bar{u}}^*(t) = -K_0 \bar{X}_0(t) = - \begin{bmatrix} K_0^0 & K_0^1 \end{bmatrix} \begin{bmatrix} \bar{x}(t) \\ \bar{u}(t) \end{bmatrix} \quad (\text{A.1.-9})$$

From EQ(II.A.2.A.-3) and Figure II.A.2.A.-2 we have:

$$T_n \dot{\bar{u}}^*(t) + \bar{u}^*(t) = \bar{u}_c(t) + V_{uu}(t) \quad (\text{A.1.-10a})$$

$$\bar{u}_c(t) = -K^* \bar{x}(t) \quad (\text{A.1.-10b})$$

thus

$$\dot{\bar{u}}^*(t) = -T_n^{-1} \bar{u}^*(t) + T_n^{-1} \bar{u}_c(t) + T_n^{-1} V_{uu}(t) \quad (\text{A.1.-10c})$$

or

$$\dot{\bar{u}}^*(t) = -T_n^{-1} \bar{u}^*(t) - T_n^{-1} K^* \bar{x}(t) + T_n^{-1} V_{uu}(t) \quad (\text{A.1.-10d})$$

which results in

$$\dot{\bar{u}}^*(t) = -K_0 \bar{X}_0(t) = - \begin{bmatrix} K_0^0 & K_0^1 \end{bmatrix} \begin{bmatrix} \bar{x}(t) \\ \bar{u}^*(t) \end{bmatrix} + K_0^1 V_{un}(t) \quad (A.1.-10e)$$

where

$$K_0^0 = T_n^{-1} K^* \quad (A.1.-10f)$$

$$K_0^1 = T_n^{-1} \quad (A.1.-10g)$$

The feedback gain matrix, K_0 , is obtained from:

$$K_0 = G_0^T S^{-1} P_0 \quad (A.1.-11)$$

P_0 is the unique positive definite solution of the "n+m" dimensional matrix Ricatti Equation.

$$F_0^T P_0 + P_0 F_0 + Q_0 - P_0 G_0 S^{-1} G_0^T P_0 = 0 \quad (A.1.-12)$$

where

$$Q_0 = \begin{bmatrix} Q & 0 \\ 0 & R \end{bmatrix} \quad (A.1.-13)$$

The key to implementing this control strategy is in the selection of the control rate cost weightings, S , to obtain:

$$K_0 = \begin{bmatrix} K_0^0 & T_n^{-1} \end{bmatrix} \quad (A.1.-14)$$

The Kalman Filter estimates the delayed system state from the observation of the delayed, noisy system outputs and an inherent knowledge of the delayed "command" control, $\bar{u}_c(t-d)$. The Kalman Filter uses an alternate augmented system to derive its estimates.

$$\dot{\bar{X}}_1(t) = F_1 \bar{X}_1(t) + G_1 \bar{u}_c(t-d) + G_{11} W_1 \quad (\text{A.1.-15})$$

where

$$\bar{X}_1(t-d) = \begin{bmatrix} \bar{x}(t-d) \\ \bar{u}(t-d) \end{bmatrix} \quad \bar{W}_1 = \begin{bmatrix} \bar{w}(t-d) \\ \bar{V}_w(t-d) \end{bmatrix} \quad (\text{A.1.-16a})$$

$$F_1 = \begin{bmatrix} F & G \\ 0 & -T_n^{-1} \end{bmatrix} \quad G_1 = \begin{bmatrix} 0 \\ T_n^{-1} \end{bmatrix} \quad G_{11} = \begin{bmatrix} I & 0 \\ 0 & T_n^{-1} \end{bmatrix} \quad (\text{A.1.-16b})$$

$$H_1 = [H \quad 0] \quad (\text{A.1.-16c})$$

It is important to note that the estimated state of EQ(A.1.-15) utilizes the delayed desired control input, $\bar{u}_c(t-d)$, as the driven deterministic input. The Kalman Filter generates the delayed estimate of the delayed state via:

$$\hat{\bar{X}}_1(t-d) = F_1 \hat{\bar{X}}_1(t-d) + G_1 \bar{u}_c(t-d) + K_1 [\bar{y}_p(t) - H_1 \hat{\bar{X}}_1(t-d)] \quad (\text{A.1.-17})$$

The output error is weighted by the Kalman gains, K_1 , that are generated by:

$$K_1 = P_1 H_1^T R_y^{-1} \quad (\text{A.1.-18})$$

where the error covariance matrix, P_1 , satisfies

$$F_1^T P_1 + P_1 F_1 + Q_1 - P_1 H_1 R_y^{-1} H_1^T P_1 = 0 \quad (\text{A.1.-19})$$

$$Q_1 = \begin{bmatrix} Q_w & 0 \\ 0 & \hat{Q}_u \end{bmatrix} \quad (\text{A.1.-20a})$$

where

$$\hat{Q}_u = E \{ T_n^{-1} V_{uu}(t), V_{uu}(t)^T T_n^{-1T} \} = T_n^{-1} Q_u T_n^{-1T} \quad (\text{A.1.-20b})$$

The least-squared error predictor generates a time advanced estimate of the present time state from the delayed estimated state of EQ(A.1.-17). The prediction is based on the internal reference model:

$$\dot{\bar{\zeta}}(t) = F_1 \bar{\zeta}(t) + G_1 \bar{u}_c(t) \quad (\text{A.1.-21})$$

where

$$\bar{\zeta}(t) = \begin{bmatrix} \hat{\bar{x}}(t) \\ \bar{u}_c(t) \end{bmatrix} \quad (\text{A.1.-22})$$

The time update of the predicted state is generated by:

$$\hat{\bar{X}}_1(t) = \hat{\bar{\zeta}}(t) + K_2 [\hat{\bar{X}}_1(t-d) - \hat{\bar{\zeta}}(t-d)] \quad (\text{A.1.-23})$$

The delayed state error weighting, K_2 , is given by:

$$K_2 = e^{F_1 d} \quad (A.1.-24)$$

which is the state transition matrix for the time advancement.

The fundamental modules of the OCM, that have been defined above, are summarized by Figure II.B.-2.

A.2. Discrete Time Representation of the OCM

The continuous time OCM described above was transformed to a discrete time equivalence for insertion into the simulation environment. The following sections describe the transformation technique and the resulting discrete time model. It is important to note that the Kalman Filter and the Optimal Control gain calculations will be based on time varying solutions.

Discrete Time System Model

The discrete time representation of the system's involved in the OCM are based on the Zero-Order-Hold equivalence transform (ZOH) described in [27]. The difference equation representation of the perceived system's state equation, EQ(A.1.-4), is given by

$$\bar{x}_{k+1} = \Phi \bar{x}_k + \Gamma \bar{u}_k + \Gamma_w \bar{w}_k \quad (A.2.-1)$$

and the measurement equation, EQ(A.1.-5), is given by

$$\bar{y}_k = H \bar{x}_k + H_y V_k^y \quad (\text{A.2.-2})$$

The discrete time "n" system states, "m" system inputs, and "l" system outputs are represented by

$$\bar{x}_k = [x_k^1, x_k^2, \dots, x_k^n]^T \quad (\text{A.2.-3})$$

$$\bar{u}_k = [u_k^1, u_k^2, \dots, u_k^m]^T \quad (\text{A.2.-4})$$

$$\bar{y}_k = [y_k^1, y_k^2, \dots, y_k^l]^T \quad (\text{A.2.-5})$$

The discrete time process noise model and covariance matrix are given by

$$\bar{w}_k = [w_k^1, w_k^2, \dots, w_k^n]^T \quad (\text{A.2.-6})$$

$$Q_k^w = E [\bar{w}_k, \bar{w}_k^T] = \Gamma_w Q_w \Gamma_w^T \quad (\text{A.2.-7})$$

The discrete time observation noise model and covariance matrix are given by

$$V_k^y = [v_y^1, v_y^2, \dots, v_y^m]^T \quad (\text{A.2.-8})$$

$$R_k^y = E [V_k^y, V_k^{yT}] = R_y \quad (\text{A.2.-9})$$

The ZOH discrete time equivalence transformations are given by

$$\Phi = e^{F T_s} \quad (\text{A.2.-10a})$$

$$\Gamma = \int_0^{T_s} e^{F T_s} d\sigma \quad G \quad (A.2.-10b)$$

$$\Gamma_w = \int_0^{T_s} e^{F T_s} d\sigma \quad (A.2.-10c)$$

where

T_s = Sampling period

Pure Delay Model

Information processing and neuro-motor signal delays are represented by the pure delays shown in Figure A.1.-1. The delays are implemented by a sliding window FIFO buffer of length D.

$$D = \text{MOD}\left(\frac{d}{T_s}\right) \quad (A.2.-11)$$

where

D = Number of sampling periods

d = Continuous time delay

T_s = Sampling period

The FIFO buffer is driven by

DO I = D, 1, -1

$$\bar{X}_{K-I} = \bar{X}_{K-I+1} \quad (A.2.-12)$$

ENDDO

Neuro-muscular and Optimal Control Generator

A recursive time varying solution of the discretized optimal control/gain generator described in [27] is utilized. The optimal control rate is defined by EQ(A.1.-10e) and its discrete time representation is given by

$$\bar{u}_{k+1}^* = \Phi_{K_0^1} \bar{u}_k^* + \Gamma_{K_0^0} \bar{x}_k + \Gamma_{K_0^1} \bar{V}_k^u \quad (\text{A.2.-13})$$

where the motor noise and its covariance matrix are given by

$$\bar{V}_k^u = [\bar{v}_k^{u_1}, \bar{v}_k^{u_2}, \dots, \bar{v}_k^{u_m}] \quad (\text{A.2.-14a})$$

$$Q_k^u = E[\bar{V}_k^u, \bar{V}_k^{uT}] = \Gamma_{K_0^1} Q_u \Gamma_{K_0^1}^T \quad (\text{A.2.-14b})$$

The optimal state feedback gains can be rewritten into the form of the recursive solution

$$\bar{u}_{k+1}^* = -K_k^0 \begin{bmatrix} \bar{x}_k \\ \bar{u}_k^* \end{bmatrix} + \Gamma_{K_0^1} \bar{V}_k^u \quad (\text{A.2.-15a})$$

where

$$K_k^0 = \begin{bmatrix} K_{0k}^0 & \Phi_{K_0^1} \end{bmatrix} \quad (\text{A.2.-15b})$$

The feedback gain matrix is obtained from the recursive relations in terms of the augmented system

$$\Phi_0 = \begin{bmatrix} \Phi & \Gamma \\ 0 & 0 \end{bmatrix} \quad \Gamma_0 = \begin{bmatrix} 0 \\ I \end{bmatrix} \quad (\text{A.2.-16})$$

The recursive solution of the optimal control gains is given by:

$$K_k^0 = (S_k + \Gamma_0^T \bar{P}_k^0 \Gamma_0)^{-1} \Gamma_0^T \bar{P}_k^0 \Phi_0 \quad (\text{A.2.-17a})$$

$$P_k^0 = \bar{P}_k^0 - \bar{P}_k^0 \Gamma_0 (S_k + \Gamma_0^T \bar{P}_k^0 \Gamma_0)^{-1} \Gamma_0^T \bar{P}_k^0 \quad (\text{A.2.-17b})$$

$$\bar{P}_k^0 = \Phi_0^T P_k^0 \Phi_0 + Q_k^0 \quad (\text{A.2.-17c})$$

The cost weightings on the states, controls, and control rates (Q,R,S) respectively, are introduced in the manner used in the continuous problem

$$Q_k^0 = \begin{bmatrix} Q & 0 \\ 0 & R \end{bmatrix} \quad S_k = S \quad (\text{A.2.-18})$$

The control rate weightings, S_k , are chosen such that, in steady state, the set of equations EQ(A.1.-17) result in

$$\Phi_{K_0^1} = e^{-K_0^1 T_s} = e^{-T_s T_n^{-1}} = \begin{bmatrix} e^{-\frac{T_s}{T_n^1}} & & & \\ & e^{-\frac{T_s}{T_n^2}} & & \\ & & \ddots & \\ & & & e^{-\frac{T_s}{T_n^m}} \end{bmatrix} \quad (\text{A.2.-19})$$

The state feedback matrix directly results from the solutions of EQ(A.1.-17). The diagonal elements represent the time constants of the individual neuro-muscular systems associated

with the separated cockpit control mechanisms. The motor noise gain matrix is obtained from

$$\Gamma_{K_0^1} = I - \Phi_{K_0^1} \quad (\text{A.2.-20})$$

The finalized state feedback matrix results from

$$\Gamma_{K_0^0} = \Gamma_{K_0^1} K_{0k}^0 \quad (\text{A.2.-21a})$$

Discrete Time Kalman Filter

A recursive time varying solution of the discrete time Kalman Filter described in [28] is utilized. The Kalman Filter is used to estimate the delayed system state from the observation of the delayed noisy system outputs

$$y_k^p = \bar{y}_{k-D} + V_{k-D}^y \quad (\text{A.2.-22})$$

from a knowledge of the desired delayed control command

$$\bar{u}_{k-D}^c = [u_1^c, u_2^c, \dots, u_m^c]_{k-D}^T = -K_0^{0*} \hat{\bar{x}}_k = -\Phi_{K_0^1} \Gamma_{K_0^0} \hat{\bar{x}}_k \quad (\text{A.2.-23})$$

and an understanding of the motor and process noises and their respective covariences. The Kalman Filter bases it's estimates on the augmented system given by

$$\hat{\bar{X}}_{k-D}^1 = \begin{bmatrix} \hat{\bar{x}}_{k-D} \\ \hat{\bar{u}}_{k-D} \end{bmatrix} \quad \hat{\bar{W}}_{k-D}^1 = \begin{bmatrix} \hat{\bar{w}}_{k-D} \\ \hat{\bar{V}}_{k-D}^u \end{bmatrix} \quad (\text{A.2.-24a})$$

$$\Phi_1 = \begin{bmatrix} \Phi & \Gamma \\ 0 & \Phi_{K_0}^1 \end{bmatrix} \quad \Gamma_1 = \begin{bmatrix} 0 \\ \Phi_{K_0}^{1-1} \end{bmatrix} \quad (\text{A.2.-24b})$$

The measurement update equations are

$$\hat{\bar{X}}_{k-D}^1 = \hat{\bar{X}}_{k-D}^1 + K_k^1 [y_k^p - H \hat{\bar{X}}_{k-D}^1] \quad (\text{A.2.-25a})$$

$$P_k^1 = \bar{P}_k^1 - K_k^1 H \bar{P}_k^1 \quad (\text{A.2.-25b})$$

and the time updates are given by

$$\hat{\bar{X}}_{k-D}^1 = \Phi_1 \hat{\bar{X}}_{k-D}^1 + \Gamma_1 \bar{u}_{k-D}^c \quad (\text{A.2.-26a})$$

$$\bar{P}_k^1 = \Phi_1 P_k^1 \Phi_1^T + Q_k^1 \quad (\text{A.2.-26b})$$

where

$$Q_k^1 = \begin{bmatrix} Q_k^w & 0 \\ 0 & \hat{Q}_k^u \end{bmatrix} \quad \hat{Q}_k^u = \Gamma_{K_0}^1 Q_k^u \Gamma_{K_0}^{1T} \quad (\text{A.2.-26c})$$

The time varying Kalman gains are generated by

$$K_k^1 = \bar{P}_k^1 H^T (H \bar{P}_k^1 H^T + R_k^y)^{-1} \quad (\text{A.2.-27})$$

with the initial conditions

$$\bar{P}_k^1 = 0 \quad (\text{A.2.-28a})$$

$$\hat{\bar{X}}_{k-D}^1 = \bar{x}_k \quad (\text{A.2.-29b})$$

Discrete Time Predictor

The discrete time, time advance predictor uses the internal reference model given by

$$\bar{\zeta}_{k+1} = \Phi_1 \bar{\zeta}_k + \Gamma_1 \bar{u}_k^c \quad (\text{A.2.-30a})$$

$$\bar{\zeta}_k = \begin{bmatrix} \hat{\bar{x}}_{k-D} \\ \hat{\bar{u}}_{k-D} \end{bmatrix} \quad (\text{A.2.-30b})$$

The prediction matrix is given by

$$\hat{\bar{X}}_k^1 = \bar{\zeta}_k + K_k^2 \left[\hat{\bar{X}}_{k-D}^1 - \bar{\zeta}_{k-D} \right] \quad (\text{A.2.-31})$$

where the state projection matrix is given by

$$K_k^2 = e^{F_1 D} \quad (\text{A.2.-32})$$

APPENDIX B

A LINEAR STATE SPACE MODEL

This appendix presents a linear state space model of the Harrier AV-8B dynamics from trim, while operating in the low speed/powered lift region of the flight envelope. This model is directly utilized as the internal reference model in the OCM implementations. This appendix is separated into two sections: 1) Assumptions, simplifications and general derivation of the model, 2) Identification of model parameters from an analysis of the response characteristics of the non-linear simulation program.

B.1. - Harrier AV-8B Model Development

A generalized linear representation of the core longitudinal dynamics is given by:

$$\begin{bmatrix} \dot{V}_u \\ \dot{\theta} \\ \dot{q} \\ \dot{V}_w \end{bmatrix} = \begin{bmatrix} X_u & X_\theta & X_q & X_w \\ 0 & 0 & 1 & 0 \\ M_u & 0 & M_q & M_w \\ Z_u & Z_\theta & Z_q & Z_w \end{bmatrix} \begin{bmatrix} V_u \\ \theta \\ q \\ V_w \end{bmatrix} + \begin{bmatrix} X_e & X_j & X_T \\ 0 & 0 & 0 \\ M_e & M_j & M_T \\ Z_e & Z_j & Z_T \end{bmatrix} \begin{bmatrix} \delta_e \\ \delta_j \\ \delta_T \end{bmatrix} \quad (\text{B.1.-6})$$

Due to the low speed assumption, a variety of simplifications can be made and verified by an analysis of the responses of the simulation model program. The first series of assumptions are directed at the forward velocity components. A very general assumption that can be made is: $X_q \sim 0$. This assumption is based on the relative unimportance of the angular rate on the forward velocity through the entire flight envelope [21,22]. The next simplification is: $X_w \sim 0$. This assumption is based on aerodynamic symmetry and an analysis of the vehicle's forward velocity response characteristic due to an positive impulse

of the throttle while in a near hover as shown in Plot B.1.-1. An additional simplification of $X_T \sim 0$, can be derived from Plot B.1.-1 and an intuitive analysis of the low speed/powered-lift thrust vector's effect on the forward velocity as shown in Figure IV.A.1.-2. The final forward velocity component assumption is: $X_e \sim 0$. This simplification is based on the longitudinal stick's dominant effect on vehicle pitching motions, shown in Figure IV.A.1.-3. Plot B.1.-2 backs-up this assumption by illustrating that the longitudinal stick's effect on forward velocity is coupled to the redirection of the thrust vector associated with the pitching motion and is therefore not direct. Thus as shown in the thrust diagram of Figure IV.A.1.-1, the nozzle angle control, X_j , will dominate the control of the vehicle's forward velocity. It is important to note that this model does take into account the pitch angle's effect on the forward velocity, where typically, $X_\theta = g$, the gravitational acceleration.

The effects of the lateral system components on the response characteristics of the forward velocity were considered insignificant from an analysis of the responses of the simulation model program. Plot B.1.-3 shows the forward velocity response due to an impulse on the lateral stick. Plot B.1.-4 shows the response of the same state variable due to an impulse on the rudder pedals. The forward velocity reactions to the lateral stick and rudder pedal operations are similar in magnitude to those of the longitudinal stick and throttle. For this reason, the lateral components of the forward velocity are ignored.

The next series of assumptions are directed at the rotational modes of the longitudinal dynamics. The first assumption is based on aerodynamic symmetry and the negligible pitching reactions due to vertical motion, thus $M_w \sim 0$. Plot B.1.-5 illustrates the relatively small pitch rate response due to an impulse of the throttle. Although M_w does have a small

effect on the pitching rate, it will not effect the hovering characteristics. An additional assumption that can be derived from Plot B.1.-5 is $M_T \sim 0$. This term primarily describes the moment arm of the thrust vector on the vehicle's center of gravity. A final rotational component assumption is $M_j \sim 0$. This term describes the rotational effects of the nozzle angle due to the thrust vector's moment arm on the vehicle center of gravity. Plot B.1.-6 shows pitch rate reaction due to an impulse of the nozzle angle. Again, this response characteristic will not have a significant effect on the low speed flight dynamics. The control mechanism assumptions of $M_T \sim M_j \sim 0$, indicate that the longitudinal stick will dominate the control of the rotational dynamics due to the relatively large moment arm associated with the physical locations of the forward and aft RCS jet vents, as shown in Figure IV.A.1.-3. The term M_u is retained to provide a coupling between the forward velocity and longitudinal rotations. Although, low speeds are assumed, it will be shown later that this term and the forward velocity terms, X_θ and X_u , provide the couplings that tend to generate the long term Phugoid responses.

The pitch rate responses due to impulses of the lateral stick and rudder pedals are shown in Plot B.1.-7 and Plot B.1.-8, respectively. These reactions are similar in magnitude to those of the throttle component, M_T , and are therefore neglected.

The final series of assumptions in the longitudinal dynamics are directed at the vertical velocity components. The first assumption is based on the relatively small contribution of the pitch rate on the vertical components [21,22], thus, $Z_q \sim 0$. Plot B.1.-9 illustrates the vertical rate response due to an impulse on the longitudinal stick. This response characteristics reveals that the longitudinal stick's component, $Z_\epsilon \sim 0$, is also a realistic assumption. The pitch angle component is small due to the small angle and low speed

assumptions, thus, $Z_\theta \sim 0$. Another simplification due to the low speed assumption is $Z_u \sim 0$. This assumption would not hold true if the Harrier was a tilt-wing V/STOL aircraft. For those types of vehicles, Z_u approaches Z_w . The final simplification is directed at the relation between the nozzle angle and the vertical components. Plot B.1.-10 shows the response of the vertical rate due to an impulse of the nozzle angle. An examination of Plot B.1.-10 and Figure IV.A.1.-1 shows that perturbations about the large nozzle angle has only a small effect on the lift components, thus $Z_j \sim 0$. The control mechanism assumptions of $Z_j \sim Z_e \sim 0$, indicate that the throttle control will tend to dominate the vertical dynamics due to the large nozzle angle associated with low speed/powered-lift flight.

The vertical rate reactions due to operations of the lateral stick and rudder pedals can be seen in Plot B.1.-11 and Plot B.1.-12, respectively. These responses are on the order of those associated with the longitudinal stick and nozzle angle. This suggests that the lateral components can be neglected.

Incorporating the above assumptions within the longitudinal system model of EQ(B.1.-6) results in the following low speed/powered-lift longitudinal model.

$$\begin{bmatrix} \dot{V}_u \\ \dot{\theta} \\ \dot{q} \\ \dot{V}_w \end{bmatrix} = \begin{bmatrix} X_u & X_\theta & 0 & 0 \\ 0 & 0 & 1 & 0 \\ M_u & 0 & M_q & 0 \\ 0 & 0 & 0 & Z_w \end{bmatrix} \begin{bmatrix} V_u \\ \theta \\ q \\ V_w \end{bmatrix} + \begin{bmatrix} 0 & X_j & 0 \\ 0 & 0 & 0 \\ M_e & 0 & 0 \\ 0 & 0 & Z_T \end{bmatrix} \begin{bmatrix} \delta_e \\ \delta_j \\ \delta_T \end{bmatrix} \quad (\text{B.1.-7})$$

To better understand the longitudinal responses of the low speed/powered-lift region of the flight envelope and the correspondence of the vehicle model that has been developed, an

analysis of the vehicle's longitudinal dynamics will now be conducted. This analysis is based on the Laplacian approach used in [22]. An additional objective of this analysis is to obtain an understanding of the transfer function relationships to the above system model. This will be helpful in implementing parameter identification techniques. Before initiating the analysis it should be observed that the vertical components are strongly decoupled from the translational and rotational components. This is primarily due to the dominance of the powered-lift assumptions associated with the vertical components and Z_u being negligibly small while in low speed flight.

The rotational and translational components of the longitudinal dynamics can be approximated by the following system.

$$\begin{bmatrix} \dot{V}_u \\ \dot{\theta} \\ \dot{q} \end{bmatrix} = \begin{bmatrix} X_u & X_\theta & 0 \\ 0 & 0 & 1 \\ M_u & 0 & M_q \end{bmatrix} \begin{bmatrix} V_u \\ \theta \\ q \end{bmatrix} + \begin{bmatrix} 0 & X_j \\ 0 & 0 \\ M_e & 0 \end{bmatrix} \begin{bmatrix} \delta_e \\ \delta_j \end{bmatrix} \quad (\text{B.1.-8})$$

The characteristic equation of this reduced system is given by:

$$\Delta_{\text{LONG}} = \det(SI - A) = \det \begin{bmatrix} S - X_u & -X_\theta & 0 \\ 0 & S & -1 \\ -M_u & 0 & S - M_q \end{bmatrix} \quad (\text{B.1.-9})$$

which results in

$$\Delta_{\text{LONG}} = S(S - M_q)(S - X_u) - X_\theta M_u \quad (\text{B.1.-10a})$$

or

$$\Delta_{\text{LONG}} = S^3 - (X_u + M_q)S^2 + M_q X_u S - X_\theta M_u \quad (\text{B.1.-10b})$$

EQ(B.1.-10b) is the classical longitudinal hovering cubic [22]. From Plot B.1.-13, one can observe both the short period and long period dynamics of the pitch rate's response. This type of response supports a characteristic equation of the form:

$$\Delta_{\text{LONG}} \sim (S + T_{\text{sp}})(S^2 + 2w_{\text{lp}}\delta_{\text{lp}}S + w_{\text{lp}}^2) \quad (\text{B.1.-11})$$

where the parameters are given by:

T_{sp} = The pole associated with the time constant of the short period response

w_{lp} = The natural frequency of the long period response

δ_{lp} = The damping ratio of the long period response

Expanding EQ(B.1.-11) to the form of EQ(B.1.-10b) results in:

$$S^3 + S^2(2w_{\text{lp}}\delta_{\text{lp}} + T_{\text{sp}}) + S(w_{\text{lp}}^2 + 2w_{\text{lp}}\delta_{\text{lp}}T_{\text{sp}}) + T_{\text{sp}}w_{\text{lp}}^2 \quad (\text{B.1.-12})$$

Relating the terms of EQ(B.1.-10b) and EQ(B.1.-12) we have:

$$-(X_u + M_q) = 2w_{\text{lp}}\delta_{\text{lp}} + T_{\text{sp}} \quad (\text{B.1.-13a})$$

$$M_q X_u = w_{\text{lp}}^2 + 2w_{\text{lp}}\delta_{\text{lp}}T_{\text{sp}} \quad (\text{B.1.-13b})$$

$$-X_\theta M_u = T_{\text{sp}}w_{\text{lp}}^2 \quad (\text{B.1.-13c})$$

From [16,17,19], we can assume:

$$T_{sp} \gg w_{lp} \quad (B.1.-14a)$$

$$w_{lp}^2 \text{ is small} \quad (B.1.-14b)$$

Applying these assumptions to EQ(B.1.-13) results in:

$$M_q \sim -T_{sp} \quad (B.1.-15a)$$

$$X_u \sim -2w_{lp}\delta_{lp} \quad (B.1.-15b)$$

Thus we can see that the long period modes are due to the coupling between the translational and rotational components. The short period modes are purely due to the rotation of the vehicle about it's center of gravity. X_θ transmits the short and long period rotational perturbations to the translational motion. M_u primarily couples the long term translational perturbations to the rotational dynamics. It can be shown, through a more detailed analysis [23], that $M_u < 0$ causes divergence in the phugoid modes. This may be the case for the Harrier configuration that is used in this study. Plot B.1.-14 shows a diverging phugoid mode in the pitch rate. This type of unstable phugoid oscillation appears to be typical for hovering vehicles when out of ground effect [22].

The resulting low speed/powered-lift longitudinal model for pilot frequencies is given by:

$$\begin{bmatrix} \dot{V}_u \\ \dot{\theta} \\ \dot{q} \\ \dot{V}_w \end{bmatrix} = \begin{bmatrix} 0 & X_\theta & 0 & 0 \\ 0 & 0 & 1 & 0 \\ 0 & 0 & M_q & 0 \\ 0 & 0 & 0 & Z_w \end{bmatrix} \begin{bmatrix} V_u \\ \theta \\ q \\ V_w \end{bmatrix} + \begin{bmatrix} 0 & X_j & 0 \\ 0 & 0 & 0 \\ M_e & 0 & 0 \\ 0 & 0 & Z_T \end{bmatrix} \begin{bmatrix} \delta_e \\ \delta_j \\ \delta_T \end{bmatrix} \quad (B.1.-16)$$

The characteristic equation of this system is given by:

$$\Delta'_{\text{LONG}} = S^2(S - M_q)(S - Z_w) \quad (\text{B.1.-17a})$$

or

$$\Delta'_{\text{LONG}} = S^4 - S^3(M_q + Z_w) + S^2 M_q Z_w \quad (\text{B.1.-17b})$$

A generalized representation of the lateral-directional dynamics is given by:

$$\begin{bmatrix} \dot{\phi} \\ \dot{p} \\ \dot{r} \\ \dot{V}_v \end{bmatrix} = \begin{bmatrix} 0 & 1 & 0 & 0 \\ 0 & L_p & L_r & L_v \\ 0 & N_p & N_r & N_v \\ Y_\phi & Y_p & Y_r & Y_v \end{bmatrix} \begin{bmatrix} \phi \\ p \\ r \\ V_v \end{bmatrix} + \begin{bmatrix} 0 & 0 \\ L_a & L_\pi \\ N_a & N_\pi \\ Y_a & Y_\pi \end{bmatrix} \begin{bmatrix} \delta_a \\ \delta_r \end{bmatrix} \quad (\text{B.1.-18})$$

In a manner similar to the longitudinal model, a variety of simplifications can be made and verified by an analysis of the simulation model responses. The first series of assumptions are directed at the lateral velocity components. The coupling of the roll rate to the lateral velocity, Y_p , can be neglected due to its general unimportance throughout the flight envelope [21,22]. The primary coupling of the roll rotational dynamics is provided by the roll angle component, Y_ϕ . This is because of the thrust vector redirection due to roll angle perturbations, as shown in Figure IV.A.1.-4. A comparison of Plots B.1.-15, B.1.-16 shows the direct relationship of roll angle to the lateral acceleration. In the low speed region of the flight envelope, the yaw rate component, $Y_r \sim 0$, due to the lack of forward velocity. This component tends to translate the forward velocity into the lateral velocity. As the

forward velocity increases this term directly increases in the form $Y_r \sim -V_u$. The geometry of the wing-tip RCS jets, as shown in Figure IV.A.1.-4, relates the operations of the lateral stick to purely rolling motions. Assuming symmetry and the wing-tip RCS jet's lack of a direct effect on the lateral velocity, results in $Y_a \sim 0$. The primary coupling of the yaw rotational motions to the lateral translations is provided by the tail-end RCS jets via rudder pedal control, Y_{rr} . Plot B.1.-17 shows the direct relation of the rudder pedals to the lateral acceleration. This is due to the relatively large moment arm of the tail-end jet's physical configuration.

The next group of simplifications are directed at the yaw/directional components. Using the geometry and symmetry arguments of above, the low speed characteristics of the couplings of the roll rate to the yaw rate is through N_p . The lateral velocity effects on the yaw rate are primarily due to the non-symmetric vehicle body configuration along the x axis (i.e. cross sectional area of the vertical stabilizer/rudder when compared to that of the forward/nose section). During low speed flight the yaw rate is not very sensitive to lateral translations and thus $N_v \sim 0$. It is interesting to note that this term is important when dealing with a single main rotor helicopter with a tail rotor. This is due to the tail rotor's sensitivity to local sideslip and it's generally high main rotor disk loading [22].

The final area of simplification is directed at the roll dynamics. During low speed flight, the effects of small perturbations in lateral velocity on the roll rate, L_v , can be neglected. This, however, is not the case for larger lateral velocities due to the size and orientation of the Harrier II AV-8B's critical wing.

Incorporating the above assumptions within the lateral-directional model of EQ(B.1.-18) results in the following low speed/powered-lift lateral model.

$$\begin{bmatrix} \dot{\phi} \\ \dot{p} \\ \dot{r} \\ \dot{V}_v \end{bmatrix} = \begin{bmatrix} 0 & 1 & 0 & 0 \\ 0 & L_p & L_r & 0 \\ 0 & N_p & N_r & 0 \\ Y_\phi & 0 & 0 & Y_v \end{bmatrix} \begin{bmatrix} \phi \\ p \\ r \\ V_v \end{bmatrix} + \begin{bmatrix} 0 & 0 \\ L_a & L_{ar} \\ N_a & N_{ar} \\ 0 & Y_{ar} \end{bmatrix} \begin{bmatrix} \delta_a \\ \delta_r \end{bmatrix} \quad (\text{B.1.-19})$$

An analysis will now be conducted to better understand the lateral responses of the low speed region of the flight envelope. This analysis will also provide some insight to further simplifications of the system model. The characteristic equation of the simplified system of EQ(B.1.-19) is given by:

$$\Delta_{LAT} = \det \begin{bmatrix} S(S - L_p) & -L_r & 0 \\ -SN_p & S - N_r & 0 \\ -Y_\phi & 0 & S - Y_v \end{bmatrix} \quad (\text{B.1.-20})$$

which results in

$$\Delta_{LAT} = S(S - L_p)(S - N_r)(S - Y_v) - SL_r N_p (S - Y_v) \quad (\text{B.1.-21a})$$

or

$$\Delta_{LAT} = S^4 - (L_p + N_r + Y_v)S^3 + (L_p N_r + Y_v L_p + Y_v N_r - L_r N_p)S^2 + Y_v (L_r N_p - L_p N_r)S \quad (\text{B.1.-21b})$$

The classical lateral dynamics can be described by the characteristics equation:

$$\Delta_{LAT} = (S + T_s)(S + T_r)(S^2 + 2w_d\delta_d S + w_d^2) \quad (B.1.-22)$$

where

T_s = The pole associated with the time constant of the spiral mode

T_r = The pole associated with the time constant of the roll subsidence mode

w_d = Natural frequency of the dutch roll mode

δ_d = Damping ratio of the dutch roll mode

In general the time constant of the spiral mode is very long. For this reason and the fact that only the pilot frequencies are considered, the spiral mode can be reduced to an integrator model, thus:

$$\Delta'_{LAT} = S(S + T_r)(S^2 + 2w_d\delta_d S + w_d^2) \quad (B.1.-23a)$$

or

$$\Delta'_{LAT} = S^4 + S^3(T_r + 2w_d\delta_d) + S^2(2w_d\delta_d T_r + w_d^2) + S T_r w_d^2 \quad (B.1.-23b)$$

The terms of EQ(B.1.-23b) can be related to those of EQ(IV.a.1.b.-21b) as follows:

$$-L_p - N_r - Y_v = T_r + 2w_d\delta_d \quad (B.1.-24a)$$

$$L_p N_r + Y_v L_p + Y_v N_r - L_r N_p = 2w_d \delta_d T_r + w_d^2 \quad (\text{B.1.-24b})$$

$$Y_v (L_r N_p - L_p N_r) = T_r w_d^2 \quad (\text{B.1.-24c})$$

Plot B.1.-18 shows both the long and short period modes of the yaw rate response due to an impulse on the rudder pedals. This plot shows a divergent dutch roll mode that maintains a relatively long period. From this, one can assume:

$$w_d^2 \text{ is small} \quad (\text{B.1.-25})$$

Including this assumption within EQ(B.1.-24c) we have:

$$Y_v \sim 0 \quad (\text{B.1.-26a})$$

$$L_r N_p \sim 0 \quad (\text{B.1.-26b})$$

The resulting low speed/powered-lift lateral dynamics model for pilot frequencies is given by:

$$\begin{bmatrix} \dot{\phi} \\ \dot{p} \\ \dot{r} \\ \dot{V}_v \end{bmatrix} = \begin{bmatrix} 0 & 1 & 0 & 0 \\ 0 & L_p & 0 & 0 \\ 0 & 0 & N_r & 0 \\ Y_\phi & 0 & 0 & 0 \end{bmatrix} \begin{bmatrix} \phi \\ p \\ r \\ V_v \end{bmatrix} + \begin{bmatrix} 0 & 0 \\ L_a & L_\pi \\ N_a & N_\pi \\ 0 & Y_\pi \end{bmatrix} \begin{bmatrix} \delta_a \\ \delta_r \end{bmatrix} \quad (\text{B.1.-27})$$

The characteristic equation of this system is given by:

$$\Delta''_{LAT} = S^4 - S^3(L_p + N_r) + S^2 L_p N_r \quad (\text{B.1.-28})$$

B.2. - Identification of Vehicle Model

The high order state space models have been developed to facilitate direct parameter identification techniques. This section will derive the relationships that are used to identify the model parameters and finally obtain a parameter set from an analysis of the responses of the simulation program. The parameter identification techniques that are considered, rely on transfer function representations. To interface with these identification approaches, a set of transfer functions will be derived from the system models developed above. The transfer function representations are obtained by applying the Laplacian techniques used in the previous sections. The key to this approach is the development of a set of coupling numerators. These numerators will provide the transmission path characteristics from the cockpit control mechanisms to a specific state variable. The transfer function of a specific control function is obtained by introducing the appropriate characteristic equation as the denominator. To simplify this analysis, the longitudinal and lateral dynamics will again be decoupled to the forms of EQ(B.1.-16) and EQ(B.1.-27).

The longitudinal transfer functions are based on the state system of EQ(B.1.-16) and the characteristics equation of EQ(B.1.-17a). The parameters that require identification within the longitudinal model are: M_e , M_q , X_θ , X_j , Z_T , and Z_w . The coupling numerator of the longitudinal stick to the pitch angle is given by:

$$\frac{\theta(S)}{\delta_e(S)} \Delta'_{\text{LONG}}(S) = \det \begin{bmatrix} S & 0 & 0 \\ 0 & M_e & 0 \\ 0 & 0 & S - Z_w \end{bmatrix} = M_e S(S - Z_w) \quad (\text{B.2.-1})$$

The resulting transfer function is:

$$\frac{\theta(S)}{\delta_e(S)} = \frac{M_e S}{\Delta'_{LONG}(S)} = \frac{M_e}{S(S - M_q)} \quad (B.2.-2)$$

The pitch rate transfer function is therefore:

$$\frac{p(S)}{\delta_e(S)} = \frac{M_e}{(S - M_q)} \quad (B.2.-3)$$

This transfer function is a reasonably accurate model of the short period response characteristics of the pitch rate in Plot B.2.-1. The parameters M_e and M_q are directly identifiable from EQ(B.2.-3) and Plot B.2.-1.

$$M_e \sim 0.71 \quad (B.2.-4a)$$

$$M_q \sim -1.56 \quad (B.2.-4b)$$

The coupling numerator of the nozzle angle to the forward velocity is given by:

$$\frac{V_x(S)}{\delta_j(S)} \Delta'_{LONG}(S) = \det \begin{bmatrix} X_j & 0 & 0 \\ 0 & S(S-M_q) & 0 \\ 0 & 0 & S-Z_w \end{bmatrix} = X_j S(S-M_q)(S-Z_w) \quad (B.2.-5)$$

The resulting transfer function is given by:

$$\frac{V_x(S)}{\delta_j(S)} = \frac{X_j S(S-M_q)(S-Z_w)}{\Delta'_{LONG}(S)} = \frac{X_j}{S} \quad (B.2.-6)$$

This provides a fairly accurate approximation to the initial time response of Plot B.2.-2. The parameter X_j is obtained from the step height and is given by:

$$X_j \sim -0.017 \quad (\text{B.2.-7})$$

The pitch angle coupling term, X_θ , can be directly obtained from gravitational components. Due to the low speed assumption, the pitching component will tend to follow the response characteristics of the nozzle angle, which results in:

$$X_\theta = -0.017 \quad (\text{B.2.-8})$$

This is a good assumption if fixed nozzle angles are considered.

The coupling numerator for the throttle to the vertical rate is given by:

$$\frac{V_z(S)}{\delta_T(S)} \Delta'_{\text{LONG}}(S) = \det \begin{bmatrix} S & 0 & 0 \\ 0 & S(S-M_q) & 0 \\ 0 & 0 & Z_T \end{bmatrix} = Z_T S^2 (S-M_q) \quad (\text{B.2.-10})$$

The resulting transfer function is given by:

$$\frac{V_z(S)}{\delta_T(S)} = \frac{Z_T S^2 (S-M_q)}{\Delta'_{\text{LONG}}(S)} = \frac{Z_T}{(S - Z_w)} \quad (\text{B.2.-11})$$

Plot B.2.-3 shows a damped sinusoidal response instead of the first order response. This is due to the engine response characteristics as shown in Plot B.2.-4. Comparing these plots, the terms Z_T and Z_w can be extracted and result in:

$$Z_T \sim 0.024 \quad (\text{B.2.-12a})$$

$$Z_w \sim -0.83 \quad (\text{B.2.-12b})$$

The lateral transfer functions are based on the state system of EQ(B.1.-27) and the characteristics equation of EQ(B.1.-28). The parameters that require identification in the lateral-directional model are: L_p , N_p , N_r , Y_ϕ , L_a , L_r , N_{π} , and Y_{π} . The coupling numerator of the lateral stick to the pitch angle is given by:

$$\frac{\phi(S)}{\delta_a(S)} \Delta'_{LAT}(S) = \det \begin{bmatrix} L_a & 0 & 0 \\ 0 & (S-N_r) & 0 \\ 0 & 0 & S \end{bmatrix} = L_a S(S-N_r) \quad (B.2.-13)$$

The resulting transfer function is given by:

$$\frac{\phi(S)}{\delta_a(S)} = \frac{L_a S(S-N_r)}{\Delta_{LAT}(S)} = \frac{L_a}{S(S-L_p)} \quad (B.2.-14)$$

The roll rate transfer function is therefore:

$$\frac{p(S)}{\delta_a(S)} = \frac{L_a}{(S-L_p)} \quad (B.2.-15)$$

This transfer function is a reasonable approximation to the short period response of Plot B.2.-5. The parameters L_a and L_p can be directly obtained from Plot B.2.-5 and EQ(B.2.-15):

$$L_a \sim 1.89 \quad (B.2.-16a)$$

$$L_p \sim -3.45 \quad (B.2.-16b)$$

The coupling numerator for the lateral stick to the yaw rate is given by:

$$\frac{r(S)}{\delta_a(S)} \Delta'_{LAT}(S) = \det \begin{bmatrix} S(S - L_p) & L_a & 0 \\ 0 & N_a & 0 \\ -Y_\phi & 0 & S \end{bmatrix} = N_a S^2 (S - L_p) \quad (B.2.-17)$$

The resulting transfer function is given by:

$$\frac{r(S)}{\delta_a(S)} = \frac{N_a S^2 (S - L_p)}{\Delta'_{LAT}(S)} = \frac{N_a}{(S - N_r)} \quad (B.2.-18)$$

The parameter N_a can be obtained by comparing the short term response of Plot B.2.-6 to EQ(B.2.-18).

$$N_a \sim 0.2 \quad (B.2.-19)$$

The term N_r is not easily derived from the relation of EQ(B.2.-18) or Plot B.2.-7. Plot B.2.-7 will be utilized to determine N_r in a later examination.

The coupling numerator for the lateral stick to the lateral velocity is given by:

$$\frac{V_y(S)}{\delta_a(S)} \Delta'_{LAT}(S) = \det \begin{bmatrix} S(S - L_p) & 0 & L_a \\ 0 & (S - N_r) & 0 \\ -Y_\phi & 0 & 0 \end{bmatrix} = L_a Y_\phi (S - N_r) \quad (B.2.-21)$$

The resulting transfer function is given by:

$$\frac{V_y(S)}{\delta_a(S)} = \frac{L_a Y_\phi}{\Delta'_{LAT}(S)} = \frac{L_a Y_\phi}{S^2 (S - L_p)} \quad (B.2.-22)$$

The above transfer function provides a manner in which the pitch coupling term, Y_ϕ , can be obtained. The difficulty with this approach is the presence of the double integrator. A more straight forward approach is to directly obtain Y_ϕ from a comparison of Plots B.1.-15 and B.1.-16 which yields:

$$Y_\phi \sim 0.56 \quad (B.2.-23)$$

The coupling numerator of rudder pedals to the yaw rate is given by:

$$\frac{r(S)}{\delta_r(S)} \Delta'_{LAT}(S) = \det \begin{bmatrix} S(S - L_p) & L_\pi & 0 \\ 0 & N_\pi & 0 \\ -Y_\phi & Y_\pi & S \end{bmatrix} = N_\pi S^2(S - L_p) \quad (B.2.-24)$$

The resulting transfer function is given by:

$$\frac{r(S)}{\delta_r(S)} = \frac{N_\pi S^2(S - L_p)}{\Delta'_{LAT}(S)} = \frac{N_\pi}{(S - N_r)} \quad (B.2.-25)$$

A comparison of EQ(B.2.-25) and Plot B.2.-7 shows a much more direct access to the parameter N_r . The parameters, N_r and N_π are given by:

$$N_r \sim -0.83 \quad (B.2.-26a)$$

$$N_\pi \sim 0.5 \quad (B.2.-26b)$$

The coupling numerator for the rudder pedals to the roll angle is given by:

$$\frac{\phi(S)}{\delta_r(S)} \Delta'_{LAT}(S) = \det \begin{bmatrix} L_\pi & 0 & 0 \\ N_\pi & (S-N_r) & 0 \\ Y_\pi & 0 & S \end{bmatrix} = L_\pi S(S-N_r) \quad (B.2.-27)$$

The resulting transfer function is given by:

$$\frac{\phi(S)}{\delta_r(S)} = \frac{L_\pi S(S-N_r)}{\Delta'_{LAT}(S)} = \frac{L_\pi}{S(S-L_p)} \quad (B.2.-28)$$

The roll rate transfer function is therefore:

$$\frac{p(S)}{\delta_r(S)} = \frac{L_\pi}{(S-L_p)} \quad (B.2.-29)$$

The parameter L_π can be obtained from Plot B.2.-8 and the use of the result of EQ(B.2.-29).

$$L_\pi \sim -0.25 \quad (B.2.-30)$$

The full rank linearized state model used in the development of the OCM pilot can be seen in Figure B.2.-1. The identified parameters are listed below.

$$M_e = 0.71$$

$$M_q = -1.56$$

$$X_j = -0.017$$

$$X_\theta = -0.017$$

$$Z_T = 0.024$$

$$Z_w = -0.83$$

$$L_a = 1.89$$

$$L_p = -3.45$$

$$L_r = -0.25$$

$$N_r = -0.83$$

$$N_p = 0.21$$

$$N_\pi = 0.5$$

$$Y_\phi = 0.56$$

$$Y_\pi = 0.0$$

(B.2.-31)

APPENDIX C

A USERS GUIDE TO THE OCM SOFTWARE

This appendix serves as a user's guide for the OCM pilot software. An overview of the OCM software implementation is presented. The algorithm for configuring the OCM is illustrated. The procedure for operating the OCM within the VSRA environment is illustrated and examples are provided.

C.1. - Overview of the OCM Software

The OCM software is designed to be utilized as an active element of the NASA-VSRA simulation environment. The OCM software system consists of four software modules and a configuration file, as shown in the block diagram of Figure C.1.-1. The modules and file are defined as follows:

1. OCM_LIST.NML - This file serves as the configuration file for the OCM. The continuous time internal reference model (F,G,H matrices), pilot delay (T_D), noise parameters (Q_u , R_y), system initial conditions, forcing function time constant, and OCM cost function weightings (Q,R,S) are contained in this file. The file is arranged in a "namelist" format.

2. OCM_SETUP - This module initializes and configures the OCM environment. OCM initial condition, internal reference model, pilot data, and cost function weights are read from the OCM_LIST file. A discrete time representation of the internal reference model is generated. Optimal control gains are calculated by solving the steady state matrix Ricatti equation. Steady state Kalman gains are computed and covariance matrices are

initialized. The state transition matrix of the predictor is generated. All necessary information is loaded into specific COMMON regions for use by other OCM functions.

3. OCM_TRAJ - This module generates the time based trajectory that the OCM_PILOT is to follow. The time referenced command sequence is integrated and bandlimited to provide a full rank command. The command sequence is independent of the sampling rate of the simulation environment. The integration computations require sample period information.

4. OCM_PILOT - This module performs the active computations involved in the closed loop participation of the OCM within the VSRA simulation environment. These include measurements of the VSRA state, obtaining the command trajectory from the OCM_TRAJ module, noise model generation (via Box-Meuller approach), delay progression, measurement and update of the Kalman filter estimates, time advance predictions, and control input calculations. The control inputs are then applied to the VSRA through the cockpit control mechanism variables.

5. OCM_SUBS - This module contains a pool of utilities that simplify the organization and implementation of the other OCM modules. Some of the utility functions include: matrix and linear algebra operations, Kalman filter gain and covariance progression generators, optimal control solver and gain generator, and a continuous time to discrete time converter.

To interface the OCM software to the VSRA simulation environment, the main VSRA driver program (VSRA_DRIVER) was modified to accommodate the OCM system. The

modifications involved that allocation of various common areas to support OCM operations, and the implantation of the OCM_SETUP and OCM_PILOT modules at specific points within the simulation initialization and primary execution loops. In addition, two new VSRA commands were introduced to handle the OCM initialization phases and the flight simulation operations involving the participating OCM. The use of these commands will be explained in greater detail in later sections. To accommodate the output of the OCM, the file writing code of the PLOTDATA.FOR subroutine was modified to include OCM variables within the unformatted output data file VSRA_POLY.PLT.

C.2. - Installing the OCM

The OCM software is contained on a VAX Files-11 formatted tape labeled "PITT". The following files must be recovered from the tape:

- | | |
|------------------|------------------|
| 1) OCM_SETUP.FOR | 11) NAMELIST.NML |
| 2) OCM_PILOT.FOR | 12) OCM_LIST.VRT |
| 3) OCM_SUBS.FOR | 13) OCM_LIST.LAT |
| 4) OCM_TRAJ.FOR | 14) P00A.VRT |
| 5) PLOTDATA.FOR | 15) P00A.LAT |
| 6) VSRA_OCM.FOR | 16) OCM_PLT.VRT |
| 7) OCM_PLOT.FOR | 17) OCM_PLT.LAT |
| 8) VSRA_OCM.OPT | 18) PITT151.DAT |
| 9) FTP.OLB | 19) PITT210.DAT |
| 10) *.OBJ | |

Files 1-6 correspond to the primary OCM software modules. File 7 is the modified plotting routine for the OCM. File 8 is the special linking configuration for the OCM. File 9 is the

VSRA library supplied by NASA-LEWIS. The file set *.OBJ (10) corresponds to the pool of pre-compiled VSRA modules used during the linking procedures by VSRA_OCM.OPT. File 11 is the VSRA configuration file. Files 12 and 13 are the OCM configuration files for vertical and lateral maneuvers, respectively. Files 14 and 15 are the VSRA setup command files for vertical and lateral maneuvers, respectively. Files 16 and 17 are the plotting configuration files for the vertical and lateral maneuvers, respectively. Files 18 and 19 are the unformatted data files of the pilot flight operations for the lateral and vertical maneuvers, respectively.

Files 1-6 should be compiled with the VAX Debug function enabled (to be consistent with the VSRA format). The VMS command string for compiling is as follows:

```
$ FORTRAN/DEBUG/NOOPT/CROSS_REF/CONT=99 filename.FOR
```

where "filename.FOR" is the appropriate Fortran file from the above list. Linking operations are controlled by a modified version of VSRA_DRIVER.OPT (VSRA_OCM.OPT). The modifications incorporate the OCM software modules during the link process. The linking command string is given by:

```
$ LINK/DEBUG VSRA_OCM/OPT,LIB:FTP/LIB
```

where the device LIB: contains the library FTP.OLB.

A previous version of the OCM software utilized three external libraries: 1) SLATECH, 2) IMSL, 3) DISPLA. These libraries offer many routines (particularly the SLATECH routine RICSOL, that solves various versions of the matrix Ricatti equation) that simplify the generation of the optimal control gains, muscular system time constants, Kalman filter gains and covariance matrices. To comply with the requirements that the software generated

in this research be completely self-supporting, the IMSL and SLATECH libraries were removed and the OCM was fitted with comparable algorithms. The algorithms utilized by the present version of the OCM are based primarily on iterative/time-varying solutions and are therefore rather sluggish. The DISPLA library was, however, retained because the plotting packages supplied by NASA-LEWIS were supported by DISPLA.

C.3. - Configuring the OCM

The configuration of the OCM defines the vehicle under control, control objectives, and the pilot description. The principle operations involved in the configuration of the OCM pilot are summarized in the following:

1. - Develop and insert the continuous time internal reference model of the vehicle under control into the OCM configuration file, OCM_LIST.NML. Appendix B illustrates the construction of the Harrier II AV-8B low speed/powered-lift, pilot frequency model that is supplied. Within the OCM_LIST.NML, the two dimensional arrays (FM,GM,HM) correspond to the state space representation matrices (A,B,C) or (F,G,H). Section C.7 of this appendix provides a listing of the primary variables used in the OCM. The model is dimensioned by the variables (NOCM,MOCM,LOCM) which correspond to the system order, number of inputs and outputs, respectively. The arrays, FM and GM, describe the vehicle dynamics while the measurement array, HM, is primarily dependent on the display configuration. The two dimensional array, WM, corresponds to the disturbance distribution matrix. The sampling period of the OCM execution (typically the sampling period of the simulation program) is selected and specified by the variable T1. This variable is primarily

for use in OCM applications that require execution at rates other than the fundamental frequency of the simulation environment.

2. - Determine and code the time based command sequence of the desired trajectory. The trajectory generating code resides in OCM_TRAJ. The version of OCM_TRAJ that has been supplied provides a simple implementation of the rate driven command sequencer and the rate integrating/bandlimiting full rank command generator. To use this strategy, a rate driven trajectory must be defined in the form of pulse trains on the appropriate rate commands. The pulse trains, in this case, are implemented by a sequence of "IF" statements creating a string of step functions that are overridden by the step occupying the present interval. With the trajectory specified, the time constant of the forcing function bandlimiting filter is selected and specified by the variable AFORCE in the configuration file OCM_LIST.NML. This time constant typically ranges between 1.5 and 4.5 seconds [2]. A value of 2.5 seconds has been utilized in the implementation supplied. The user may wish to insert his own trajectory defining code or route the trajectory information to the OCM from some external process via this routine. It is important to note that modifications to the OCM_TRAJ routine will require that the OCM_TRAJ.FOR file be re-compiled and the total software system be re-linked.

3. - The control objectives of the pilot's task is defined in the form of cost function weightings. The values utilized reflect the manner in which the pilot will respond to the given situation. The values will typically vary from task-to-task and from vehicle-to-vehicle. The cost function weights are loaded into the two dimensional arrays QOPT, ROPT, GOPT within OCM_LIST.NML. The array QOPT corresponds to the definition of the acceptable maximum deviations of the errors in vehicle attitude and orientation from that

of the trajectory. ROPT defines the maximum deflection of the cockpit control mechanisms and is usually a function of the vehicle (see section V.B.3.). The array GOPT is adjusted to obtain the desired muscular system time constants. This typically requires a degree of iterative adjustment. The values supplied in this version reflect a subjective analysis of the piloted flight data and a limited knowledge of the target configuration and control objectives.

4. - The final step is the selection of the pilot's inherent parameters. The discrete nature of the OCM and the VSRA simulation environment requires that the pilot delay be implemented as a chain of sample delay periods arranged in a FIFO buffer. The length of the buffer is determined by the number of sample periods needed to achieve the delay. The variable NDEL of the OCM_LIST.NML file, specifies the number of sample periods/elements of the buffer, that the pilot delay occupies. The remnant model noise sources, observation and motor, are selected according to the control objectives, vehicle under control, and the display configurations. The arrays STVU and STVY correspond to the noise model variances, Q_u and R_y , of the motor and observation noises respectively.

C.4. - Executing the OCM within the VSRA Simulation Environment

Executing the OCM software within the VSRA is relatively simple. The OCM operations are broken into two separate functions: 1) Initialization and preparation of the OCM environment, 2) Execution of the VSRA with the OCM actively participating in the flight control loops. These operations are provided by two VSRA commands:

/SOCM - This command executes the software module OCM_SETUP. The OCM environment is configured and loaded into specific common regions. This operation is typically performed after the vehicle has been trimmed with the TRIM command. The user may wish to modify the OCM_SETUP routine to create an external file of the pilot configurations instead of loading the common regions. The user will, however, have to provide the necessary file reading and common region loading facilities (possibly by an additional VSRA command). Upon the completion of this command, the pilot's parameters are displayed to the user. Again, the user may wish to modify the OCM_SETUP to have the pilot's parameters loaded into an external file.

/ROCM - This command executes the primary simulation of the VSRA and enables the OCM operations. This command is tailored after the DYNC command with the exception that it utilizes the cockpit control mechanism deflections of the OCM instead of the dynamic check tests. This command can only be executed after the use of the TRIM and SOCM commands. It is important to note that the OCM is designed to operate with ONLY the AV-8B aircraft dynamics and not those of the YAV-8B.

As mentioned previously, the algorithms utilized by the present version of the OCM software are based on iterative/time-varying solutions of the matrix Ricatti equation [27,28] (instead of the SLATECH RICSOL routine). This causes some complications in the techniques utilized to generate the optimal control gains, muscular system time constants. These are typically in the form of trial-and-error iterations of the OCM_SETUP operations

by using the command SOCM until the desired muscular system time constants are obtained.

The overall operation of the OCM within the VSRA can be summarized as follows:

1. - Configure the OCM environment by preparing the OCM_LIST file according to procedures of section C.3 of this appendix. The VSRA simulation environment is configured by preparing the NAMELIST.NML file.

2. - Enter the VSRA simulation environment and issue the command SOCM. This will generate the OCM control and estimation gains and loads the specific common areas. The values of the pilot parameters are displayed upon completion. The user should examine the pilot parameters to determine if a satisfactory pilot profile has been obtained. If so, proceed to step 3, if not, exit the VSRA and modify the OCM_LIST file, then repeat step 2.

3. - With the proper pilot parameters resident within the VSRA environment, the flight simulation may begin. The user issues the command ROCM and the VSRA proceeds to execute the simulation according to the NAMELIST.NML file. The output of the VSRA is deposited in the unformatted data file VSRA_POLY.PLT.

C.5. - Output Generated by the OCM

The time based output sequence of the VSRA simulation is deposited in the unformatted data file VSRA_POLY.PLY. This file is generated by a modified version of the subroutine PLOTDATA.FOR. The modifications were made to accommodate the output of the OCM.

In addition to the OCM software that has been provided, a pair of unformatted data files containing the human piloted flight data (PITT151.DAT [lateral tracking maneuver] and PITT210.DAT [vertical tracking maneuver]) are also included.

The data of the unformatted files can be plotted with the routine OCM_PLT.FOR. This routine is a modified version of the plotting package supplied by NASA-LEWIS and is based on the DISPLA library. This routine relies on the configuration file OCM_PLT.SRC to provide the necessary default plotting information. OCM_PLT.FOR permits the user to: 1) plot the OCM output, 2) plot the piloted flight data (either lateral or vertical maneuvers), or 3) plot a comparison of both (as shown in OCM comparison plots). This routine can also be utilized to plot data from strictly DYNC runs.

The plotting activities are arranged according to the cockpit control mechanisms and the dominant aircraft responses of those controls. These break-downs are given below:

1) <u>Longitudinal Stick</u>	Pitch angle	Pitch rate	Longitudinal stick
2) <u>Lateral Stick</u>	Roll angle	Roll rate	Lateral stick
	Lateral position	Lateral velocity	
3) <u>Rudder Pedals</u>	Yaw angle	Yaw rate	Rudder pedals
	Sideslip		

4) Throttle Altitude Vertical rate Throttle

Engine speed

5) Nozzle Angle Forward velocity Nozzle angle

Forward position

To execute the OCM plotting routine issue the following VMS commands:

```
$ FOR OCM_PLT.FOR
```

```
$ LINK OCM_PLT,LIB:DISPLA/LIB
```

```
$ RUN OCM_PLT
```

The term LIB:DISPLA/LIB corresponds to the link search of the DISPLA library residing on device LIB:. This command will depend on the VMS configuration and file structure being used. The routine will respond with the following question:

```
PLOTS?? (Flight:0, OCM:1, Both:2) >
```

The user should select the appropriate data set to plot and give a numerical answer. If the user selects either 0 or 2, the routine will request the desired flight maneuver.

```
Task??(Vert:0, Lat:1)>
```

The routine will then request the control mechanism group to be plotted by:

What kind of control input?

1 = Longitudinal Stick

2 = Lateral Stick

3 = Rudder Pedals

4 = Throttle

5 = Nozzle

Enter the appropriate number : >

The routine will then read in the VSRA_POLY.PLT, PITT151.DAT, or PITT210.DAT files and proceed to generate the appropriate plots. The plotted output of this routine will be a set of plot files that are in the Tektronix 4010 graphics format.

C.6. - Examples of VSRA/OCM Execution

As a conclusion to this overview of the OCM software, an example will now be presented. This example illustrates the configuration and execution of the OCM within the VSRA environment. The listings of the this interactive session was captured via terminal monitoring facilities. The maneuver in question is the vertical tracking maneuver.

Vertical Tracking Maneuver Example

The OCM_LIST.NML file for this maneuver is provided in the file OCM_LIST.VRT. The VSRA setup file is P00A.VRT. Both of these files must be copied to their operational names of OCM_LIST.NML and P00A.COM, respectively.

\$ COPY OCM_LIST.VRT OCM_LIST.NML

Copying USR5:[02350.MZVSTOL.HARRIER.SPOOL]OCM_LIST.VRT;6 to USR5:[02350.MZVSTOL.HARRIER.SPOOL]OCM_LIST.NML;131 3 blocks

\$ COPY POOA.VRT POOA.COM

Copying USR5:[02350.MZVSTOL.HARRIER.SPOOL]POOA.VRT;3 to USR5:[02350.MZVSTOL.HARRIER.SPOOL]POOA.COM;25 2 blocks

\$ RUN VSRA_OCM

VAX DEBUG Version V5.0-00 MP

DEBUG-I-INITIAL, language is FORTRAN, module set to VSRA_OCM

DBG> @POOA

WELCOME TO THE VSRA VAX SIMULATION PROGRAM

Which aerodynamics would you like to use ?

1 = AV-8B aerodynamics

2 = YAV-8B aerodynamics

Enter the appropriate number: 1

ENTER ?? FOR COMMAND LIST

VSRA> ??

VSRA SIMULATION INTERACTIVE COMMAND LIST:

/TRIM	RUN TRIM PROGRAM
/TRIM XX	RUN TRIM PROGRAM FOR XX CYCLES
/PRNT X	TO PRINT COMMON BLOCKS: X=2 FOR XFLOAT COMMON BLOCK X=3 FOR USER COMMON BLOCKS X=4 FOR IFIXED COMMON BLOCK
/DATA	INPUT DATA TO XFLOAT AND IFLOAT FROM DATA FILE
/UDAT	INPUT DATA TO USER COMMON BLOCKS FROM DATA FILE
/ICRN XX	EXECUTE I.C. RUN FOR XX CYCLES
/DYN X	RUN DYNAMIC CHECK - X>0 PRINT HEADER AND DATA FOR X SECS
/OPRN XX	TO EXECUTE RUN FOR XX SECONDS
/MESS	SEND MESSAGE TO PRINT OUTPUT FILE
/CHNG	TO CHANGE COMMON BLOCK VARIABLE INTERACTIVELY
/STAB	TO COMPUTE STABILITY DERIVATIVES
/FGTB	TO WRITE F & G MATRICES
/SAVT	TO SAVE TRIM VALUES
/REST	TO RESTORE TRIM VALUES
/CHGC	TO CHANGE CONFIGURATION ID
/SOCM	TO INITIALIZE AND SETUP THE OCM
/ROCM	TO EXECUTE THE OCM WITHIN THE VSRA
/END	TO TERMINATE THE PROGRAM
??	TO PRINT THIS LIST

VSRA> /SOCM

```
*****
*                                     *
*               OCM SETUP             *
*                                     *
*****
```

DISCRETE TIME REPRESENTATION COMPLETED
OPTIMAL CONTROL GENERATED
KALMAN FILTER GENERATED
TIME ADVANCE PREDICTOR GENERATED

OCM SETUP COMPLETED

PILOT PARAMETERS

PILOT DELAY 0.20

FORCING FUNCTION TIME CONSTANT 2.500

MUSCULAR SYSTEM TIME CONSTANTS

CONTROL MECHANISM	1	0.15929
CONTROL MECHANISM	2	0.00000
CONTROL MECHANISM	3	0.15389
CONTROL MECHANISM	4	0.15397
CONTROL MECHANISM	5	0.13471

MOTOR NOISE VARIANCES

CONTROL MECHANISM	1	1.00000
CONTROL MECHANISM	2	1.00000
CONTROL MECHANISM	3	20.00000
CONTROL MECHANISM	4	0.50000
CONTROL MECHANISM	5	0.50000

OBSERVATION NOISE VARIANCES

DISPLAYED VARIABLE	1	0.85000
DISPLAYED VARIABLE	2	0.60000
DISPLAYED VARIABLE	3	1.00000
DISPLAYED VARIABLE	4	0.71000
DISPLAYED VARIABLE	5	0.85000
DISPLAYED VARIABLE	6	0.60000
DISPLAYED VARIABLE	7	1.00000
DISPLAYED VARIABLE	8	0.71000
DISPLAYED VARIABLE	9	1.00000
DISPLAYED VARIABLE	10	0.71000
DISPLAYED VARIABLE	11	0.85000
DISPLAYED VARIABLE	12	0.60000

VSRA> /TRIM

```
*****
*                                     *
*               TRIM MODE           *
*                                     *
*****
```

TRIM IS SUCCESSFUL AFTER 205 CYCLES
VSRA> /ROCM

```
*****
*                                     *
*               OCM EXECUTION       *
*                                     *
*****
```

VSRA> /END
VSRA SIMULATION COMPLETED SUCCESSFULLY
%DEBUG-I-EXITSTATUS, is '%SYSTEM-S-NORMAL, normal successful completion'
DBG> EXIT
\$ DIR *.PLT
Directory USR5:[02350.MZVSTOL.HARRIER.SPOOL]

SMARTHIS.PLT;1 TRIMHIS.PLT;1 VSRA_POLY.PLT;1

Total of 3 files.
\$

C.7. - Listing of the OCM variables

The OCM data structure has been implemented with the user in mind. No high performance array declaration or common area structures have been constructed. This will allow the user to best tailor the OCM environment to his application. The following list defines the primary variables utilized within the OCM.

INTEGERS

- NOCM - Dimension of the OCM's internal reference model of the system under control.
- MOCM - Number of cockpit control mechanisms (inputs).
- LOCM - Number of displayed variables (system displays).
- NDEL - Number of simulation sample periods per pilot delay

REAL*8

- T1 - Sampling period of the OCM execution in seconds.
- X(*) - System state vector.
- U(*) - Vector of cockpit control mechanisms
- FM(*,*) - System matrix of the internal reference model.
- GM(*,*) - Input distribution matrix of the internal reference model.
- HM(*,*) - Measurement matrix of the internal reference model
- WM(*,*) - Disturbance distribution matrix
- PHIM(*,*) - Discrete time system matrix
- GMA(*,*) - Discrete time input distribution matrix
- U0(*) - Initial conditions of the cockpit control mechanisms.
- UC(*) - Desired control vector.
- UCKDZ(*,*) - FIFO buffer for the control input delay.

YKDZ(*,*) - FIFO buffer for the system output delay.
 QOPT(*,*) - Cost function weights for the system states
 ROPT(*,*) - Cost function weights for the control inputs
 GOPT(*,*) - Cost function weights for the control rates.
 KOPT(*,*) - Optimal control gain state feedback matrix
 POPT(*,*) - Update matrix of the optimal control gain generator
 PMOPT(*,*) - Measurement update matrix of the optimal control gain generator
 PHI0(*,*) - Augmented system matrix for the solution of the optimal control gains.
 GMA0(*,*) - Augmented input distribution matrix for the solution of the optimal control gains.
 Q1OPT(*,*) - Augmented cost function state weighting matrix for the solution of the optimal control gains.
 STVU(*) - Variances of the motor noise sources.
 STVY(*) - Variances of the observation noise sources.
 VUM(*,*) - Covariance matrix of the motor noises.
 VYM(*,*) - Covariance matrix of the motor noises.
 PKAL(*,*) - Covariance matrix of the time-varying Kalman filter solution
 PMKAL(*,*) - Measurement covariance matrix of the time-varying Kalman filter solution
 PHIK10(*,*) - Full rank optimal control gain matrix
 GMAK00(*,*) - State feedback optimal control gains
 GMAK10(*,*) - Muscular system optimal control gains (time constants)
 K1(*,*) - Kalman filter output error correction gain matrix
 H1(*,*) - Augmented measurement matrix for the solution of the Kalman filter gains.
 PHI1(*,*) - Augmented system matrix for the solution of the Kalman filter gains.
 GMA1(*,*) - Augmented input distribution matrix for the solution of the Kalman filter gains.

Q1(*,*)	- Augmented noise model covariance matrix for the solution of the Kalman filter gains.
X1(*)	- Augmented estimate of the state vector from the Kalman filter.
X1MINUS(*)	- Update estimate of the augmented state vector of the Kalman filter.
FM1(*,*)	- Augmented continuous time system matrix for the generation of the state transition matrix of the least-squared predictor.
K2(*,*)	- State transition matrix of the least-squared predictor.
ZKDZ(*,*)	- FIFO buffer for the state estimate delay.
X2(*)	- Time advanced prediction of the system augmented state
ZETA(*)	- Predicted state estimate
XR(*)	- Trajectory reference state vector.
XRKD(*)	- Delayed trajectory reference state vector
XR1(*)	- State vector of the bandlimiting filters of the trajectory generators
AR1(*,*)	- System matrix of the bandlimiting filters
BR1(*,*)	- Input distribution matrix of the bandlimiting filters
AFORCE	- Time constant of the forcing function bandlimiting filter
XR2(*,*)	- State vector of the integrated and distributed command sequence
AR2(*,*)	- System matrix of the command sequence integrator
BR2(*,*)	- Input distribution matrix of the command sequence integrator
XR3(*,*)	- State vector of the rate command sequence
IDNT(*,*)	- Utility identity matrix
NULL(*,*)	- Utility zero matrix.
W(*,*)	- Working array
W1(*,*)	- Working array
W2(*,*)	- Working array
WINV(*,*)	- Working inversion array

REFERENCES

1. - "Dynamic Response of Human Operators", D.T. McRuer and E.S. Krendel, Wright Air Development Center, WDAC TR-56-524, October 1957.
2. - "Human Dynamics in Compensatory Systems", D.T. McRuer, D. Graham, E. Krendel, and W. Reisner, Jr., Air Force Dynamics Laboratory, AFFDL-TR-65-15, 1965.
3. - "Human Operator as a Servo System Element", D.T. McRuer and E.S. Krendel, Journal of the Franklin Institute, Vol. 267, pp 381-403, May 1959.
4. - "An Optimal Control Model of Human Response, Part I: Theory and Validation", D.L. Kleinman, S. Baron, and W.H. Levison, Automatica, Vol. 6, pp. 357-369, 1970.
5. - "An Optimal Control Model of Human Response, Part II: Prediction of Human Performance in a Complex Task", S. Baron, D.L. Kleinman, and W.H. Levison, Automatica, Vol. 6, pp. 371-383, 1970.
6. - "Human Dynamics in Man-Machine Systems", D.T. McRuer, presented at the 7th IFAC World Congress on a Link between Science and Applications of Automatic Control, Helsinki, Finland, June 1978.
7. - "Handbook of Human Factors", Salvendy Gavriel (editor), pp 1216, John Wiley and Sons, New York, 1977.
8. - "A Model of Human Controller Remnant", William H. Levison, Sheldon Baron, David L. Kleinman, IEEE Transactions on Man-Machine Systems, Vol. MMS-10, No. 4, December 1969.

9. - "The Relationship Between Saccadic and Smooth Tracking Eye Movements", C. Rashbass, Journal of Physiology, Vol. 159, pp. 326-388, 1961.
10. - "Model-Based Analysis of Control/Display Interaction in the Hover Task", Sanjay Garg and David K. Schmidt, presented at the AIAA Atmospheric Flight Mechanics Conference, Monterey, CA., August 1987.
11. - "Model-Based Evaluation of Display-Dynamics Effects in Pursuit Tracking", Sanjay Garg and David K. Schmidt, presented at the 22nd Annual Conference on Manual Control, Dayton, OH., July 1986.
12. - "An Analysis of Pilot Adaption on a Simulated Multiloop VTOL Hovering Task", E.W. Vinje, IEEE Transactions on Man-Machine Systems, MMS-9, No. 4, December 1968.
13. - "Optimum Systems Control", A.P. Sage and C.C. White, Prentice-Hall Inc., Englewood Cliffs, NJ., 1977.
14. - "UH-60A Black Hawk Engineering Simulation Program, Vol. 1, Mathematical Model.", (ISER-70452, Sikorsky Aircraft; NASA Contract NAS2-10626), NASA CR-166309, 1981.
15. - "AV-8B Simulation Software", John W. Bunnell, Laurence C. Anderson, Naval Air Test Center, N00421-8-R-0289, May 1985.
16. - "AV-8B Simulation Model", John W. Bunnell, Laurence C. Anderson, Naval Air Test Center, N00421-81-C-0289, November 1985.

17. - "AV-8B Model Identification Results: Low and High Speed Longitudinal Model", Laurence C. Anderson, (SCT Report No. 5504-2), Systems Control Technology Inc., Palo Alto, CA., 1984.
18. - "Computer Simulation of Multiple Pilots Flying a Modern High Performance Helicopter", M.E. Zipf, W.G. Vogt, M.H. Mickle, R.G. Hoelzeman, Fei Kai, J.R. Mihalow, NASA Technical Memorandum TM-100182, July 1988.
19. - "Computer Simulation of a Single Pilots Flying a Modern High Performance Helicopter", M.E. Zipf, W.G. Vogt, M.H. Mickle, R.G. Hoelzeman, Fei Kai, J.R. Mihalow, NASA Technical Memorandum TM-100183, July 1988.
20. - "A Computer Simulation of Low Order Pilot Models Flying a Thrust Vectored V/STOL Research Aircraft", M.E. Zipf, W.G. Vogt, M.H. Mickle, S. Kucuk, J.R. Mihalow, To be published in the Proceedings of the Nineteenth Modeling and Simulation Conference, (Instrument Society of America, Durham, NC., 1988), Vol. 19.
21. - "Dynamics of Atmospheric Flight", Bernard Etkin, John Wiley and Sons, Inc. 1972.
22. - "Aircraft Dynamics and Automatic Control", Duane T. McRuer, Irving Ashkenas, Dunstan Graham, Princeton University Press, Princeton, New Jersey, 1973.
23. - "Flight Control of Manned Booster", F.D. Hauser and J.H. Bigelow, (T-70-48901-004), Martin Marietta Co., Denver, CO., 1971.
24. - "Multivariable Digital Control Laws For The UH-60A Black Hawk Helicopter", B.H. Mayhew, M.S. Thesis, Air Force Institute of Technology, 1984. (Available as NTIS AD-A141046)

25. - "Simulation Evaluation of the Control System Command Monitoring Concept for the NASA V/STOL Research Aircraft (VSRA)", J.A. Schroeder, AIAA Guidance, Navigation and Control Conference, AIAA-87-2255-CP, Monterey, CA., August 1987.
26. - "Prediction of Pilot Opinion Ratings Using an Optimal Pilot Model", R.A. Hess, Human Factors, Vol 19, No. 5, 1977, pp 459-475.
27. - "Digital Control of Dynamic Systems", G.F. Franklin and J.D. Powell, Addison-Wesley Publishing Co., Reading, MA., 1980.
28. - "Introduction to Random Signal Analysis and Kalman Filtering", R.G. Brown, John Wiley and Sons, New York, NY., 1983.

FIGURE GROUP

ORIGINAL PAGE IS
OF POOR QUALITY

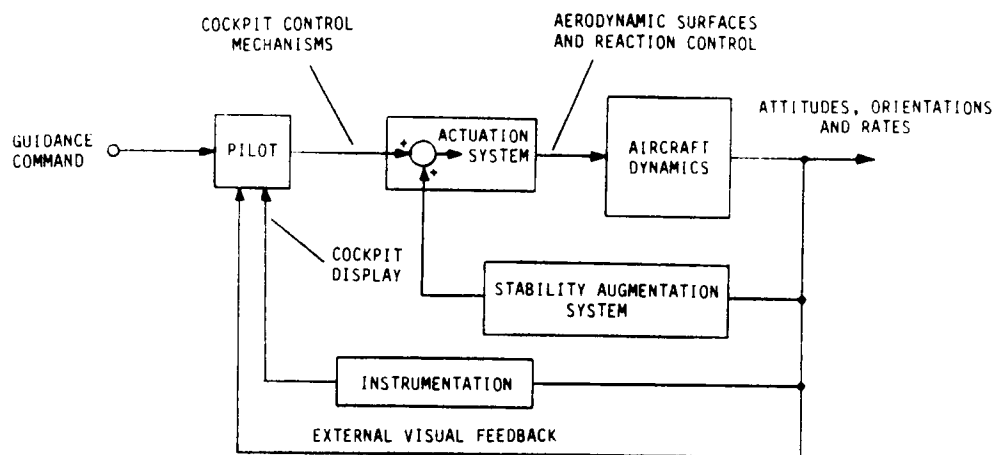


Figure I.A.-1 - Block Diagram of the closed loop piloted control structure

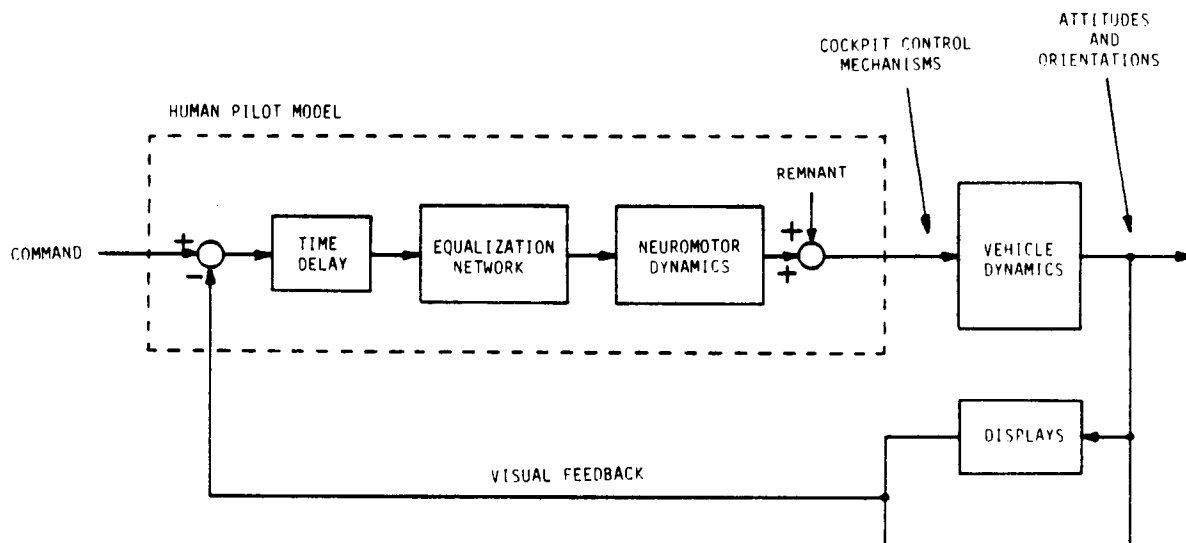


Figure II.-1. - Block diagram of the basic human controller characteristics

ORIGINAL PAGE IS
OF POOR QUALITY

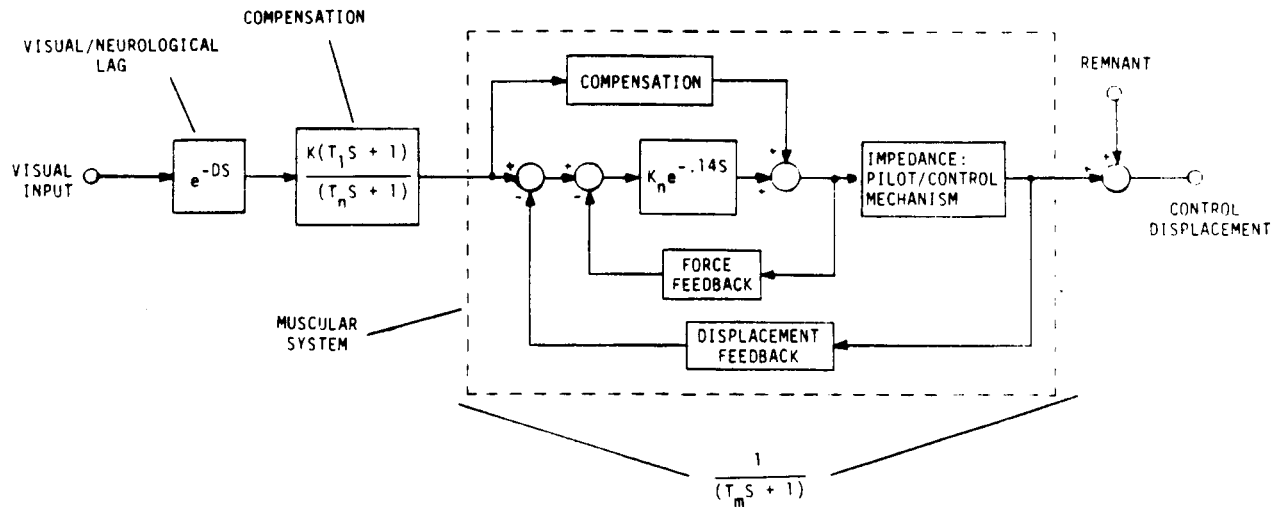


Figure II.A.-1. - Block diagram of the internal structure of the McRuer-Krendel model

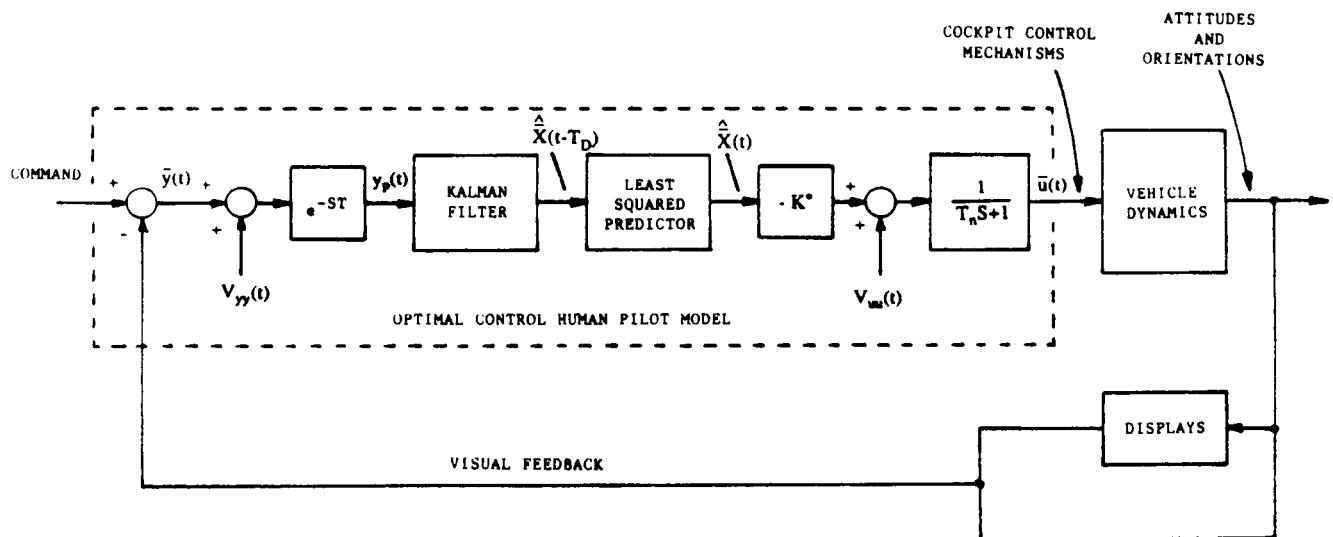


Figure II.B.-1. - Simple block diagram of the OCM within a control environment.

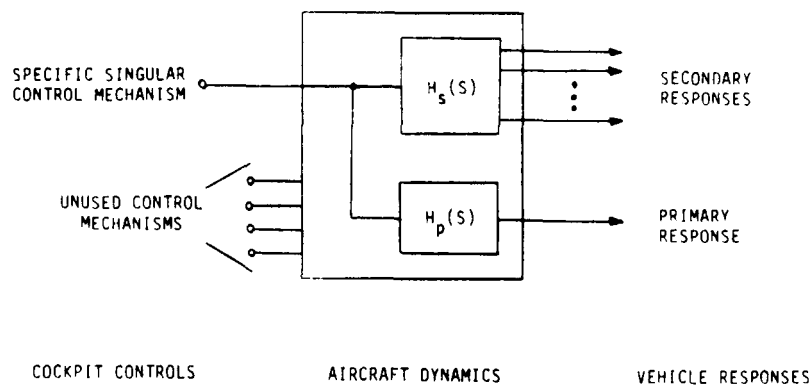


Figure III.B.1.-1. - A block diagram of the separation of the primary and secondary response characteristics associated with the decoupled transfer function models.

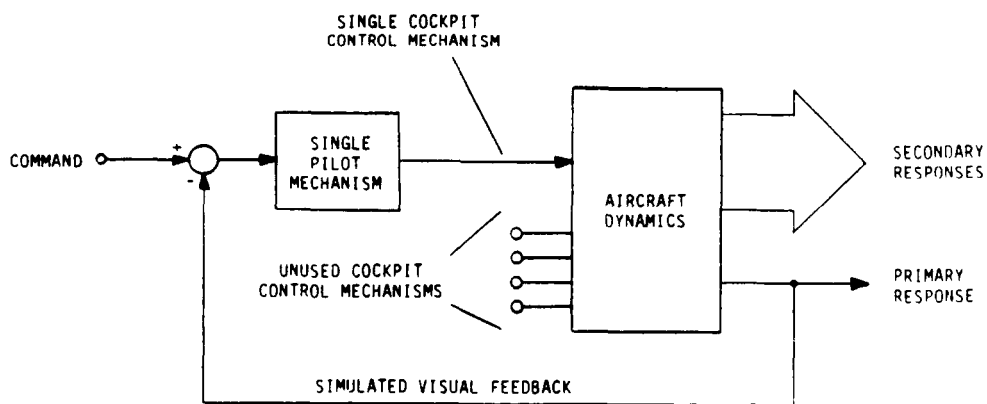


Figure III.B.2.-1. - Control loop closing strategy for the design of single variable pilot mechanisms

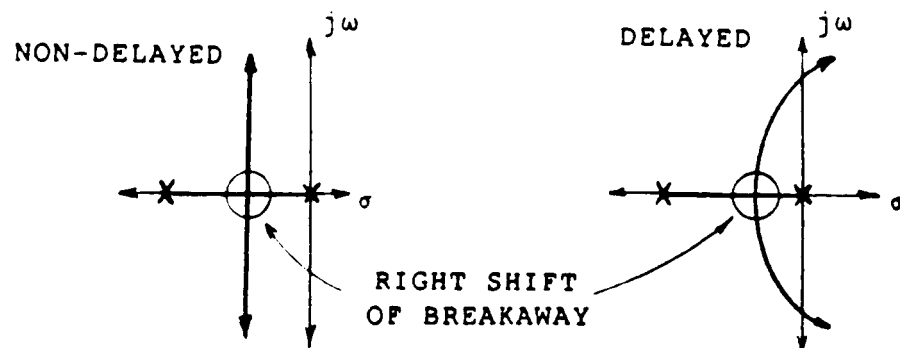


Figure III.B.2.-2. - Illustration of the destabilizing distortions associated with a delay
Root-Locus

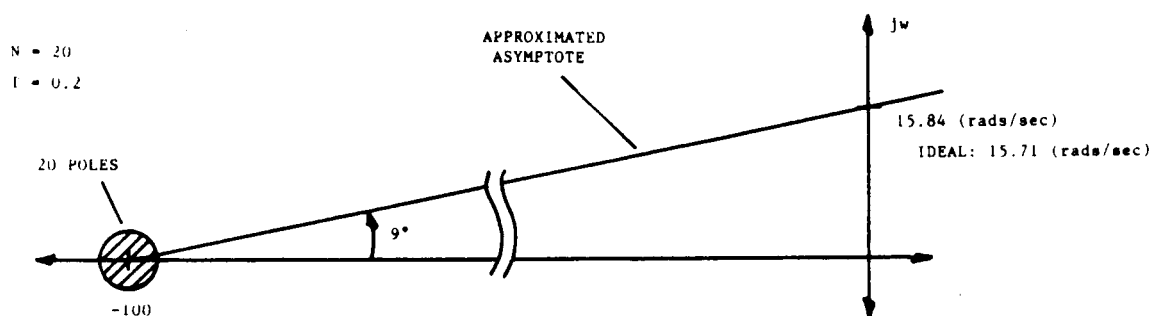


Figure III.B.2.-3. - Illustration of a delay approximation using a large pole set

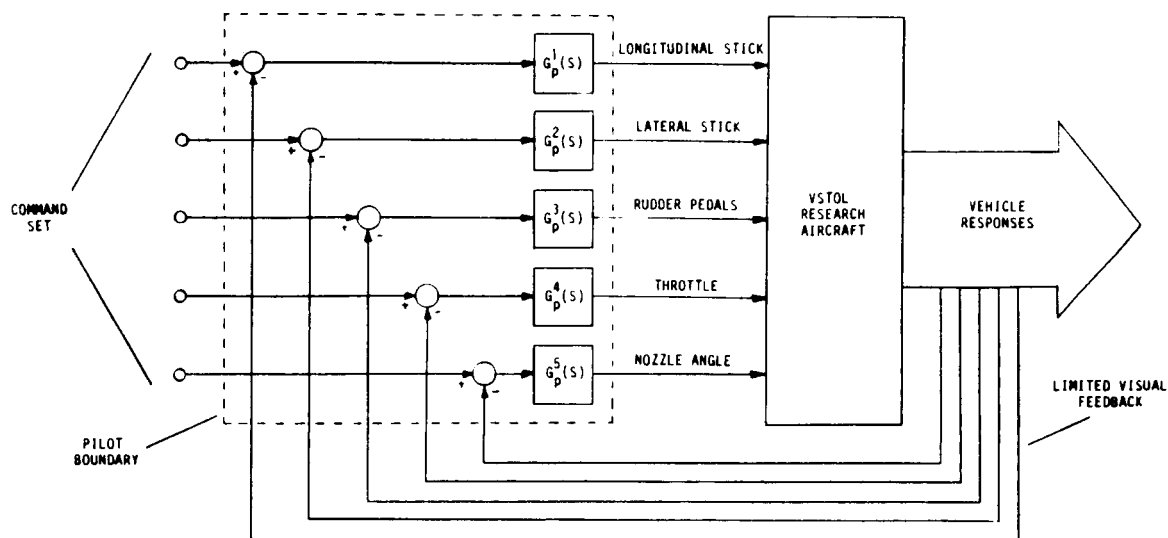


Figure III.B.3.-1. - Multi-variable control structure for the insertion of the McRuer-Krendel pilot models

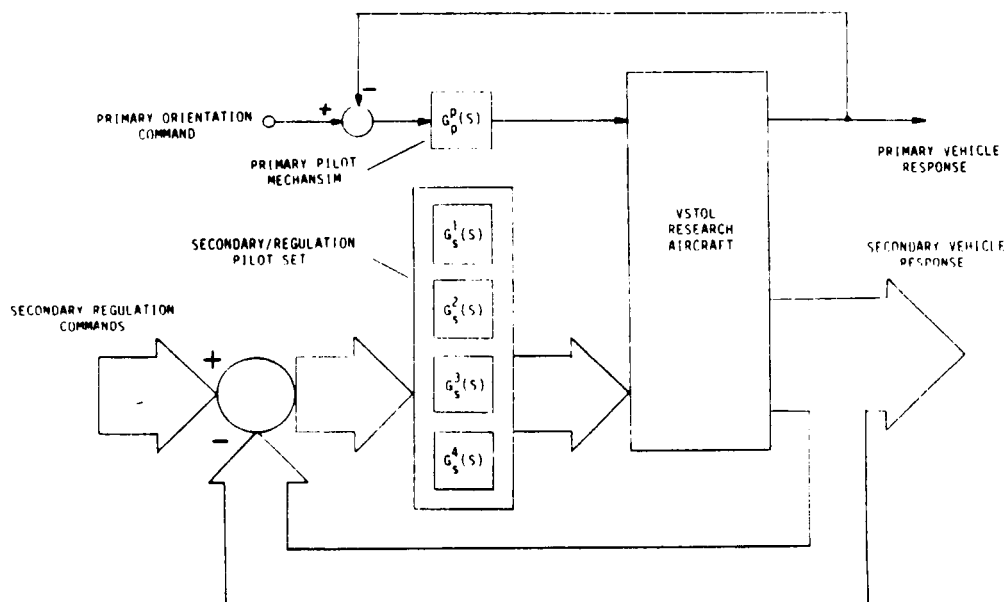


Figure III.B.3.-2. - Multi-variable control structure for executing simple flight control maneuvers.

ORIGINAL PAGE IS
OF POOR QUALITY

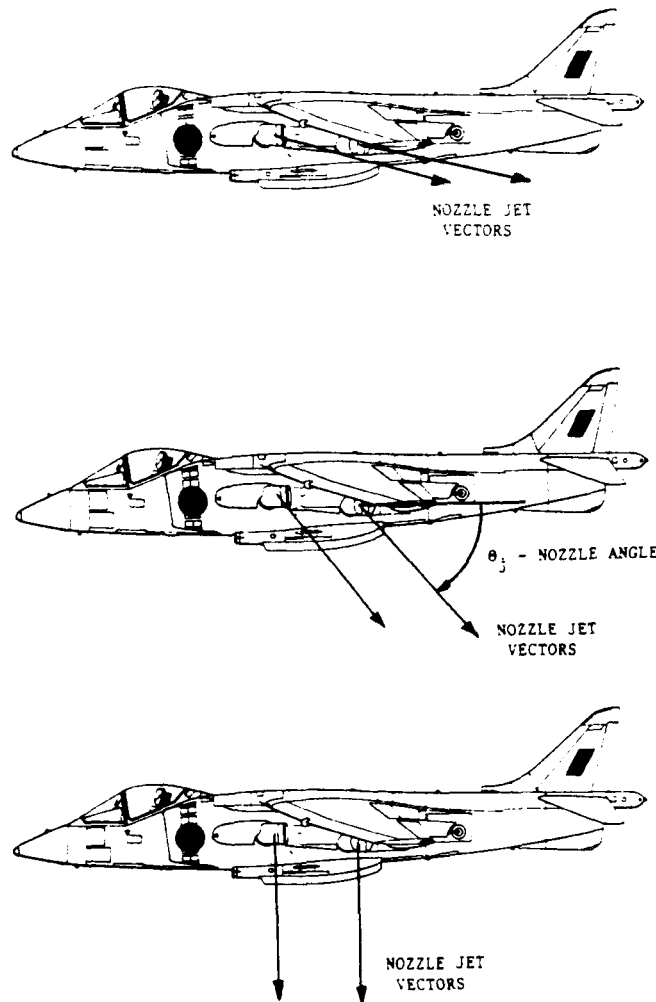


Figure IV.A.-1. - Flight envelope of the Harrier II AV-8B.

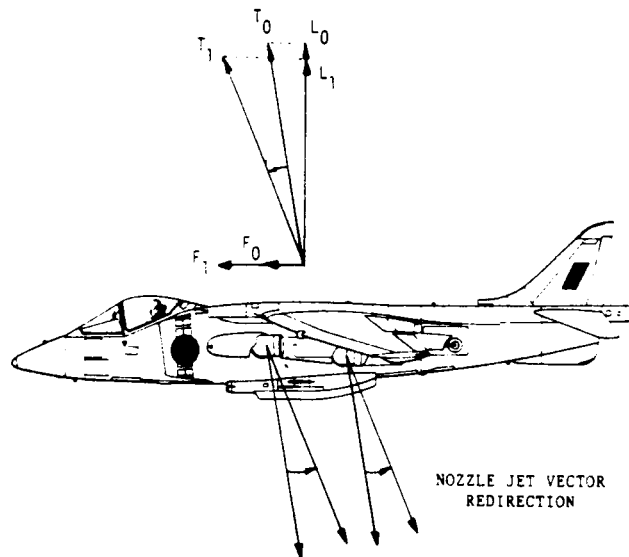


Figure IV.A.1.-1. - Illustration of the modification of the engine thrust vector due to a reduction in nozzle angle during low speed/powered-lift activities

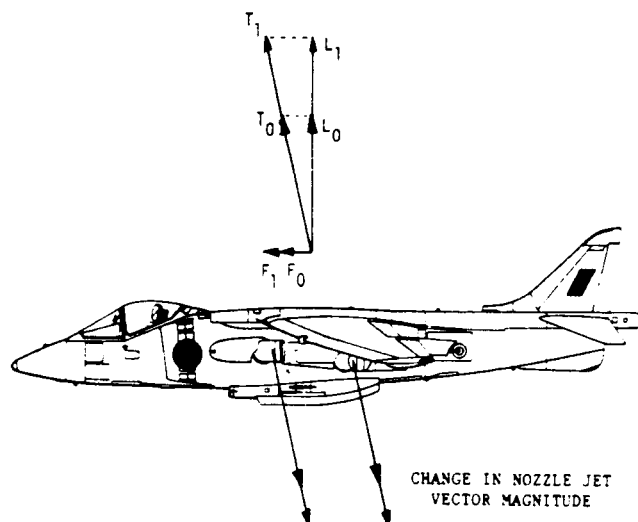


Figure IV.A.1.-2. - Illustration of the modification of the engine thrust vector due to an increase in engine speed during low speed/powered-lift activities

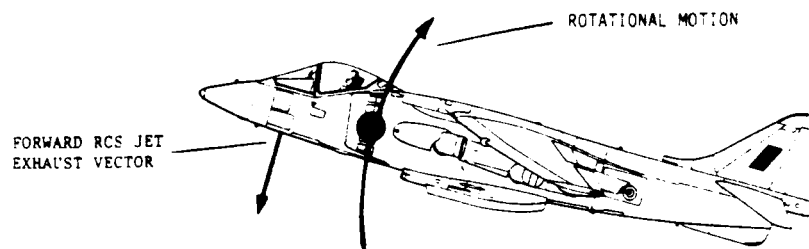


Figure IV.A.1.-3 - Illustration of the rotational motion due to the operation of the forward RCS jet from the backward deflection of the longitudinal stick during low speed/powered-lift activities.

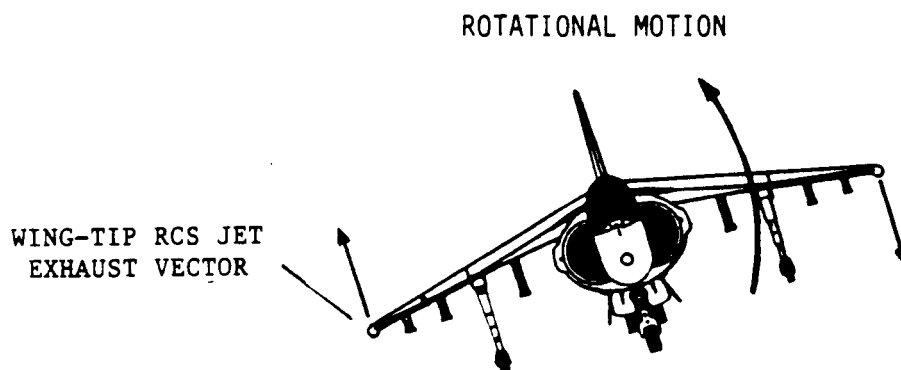


Figure IV.A.1.-4. - Illustration of the rotational motion due to the operation of the wing-tip RCS jets from the deflection of the lateral stick during low speed/powered-lift activities

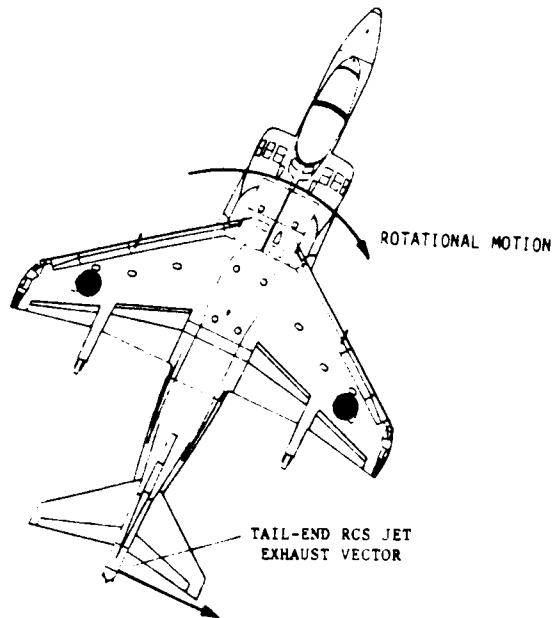


Figure IV.A.1.-5. - Illustration of the rotational motion due to the operation of the tail-end RCS jet from the deflection of the rudder pedals during low speed/powered-lift activities

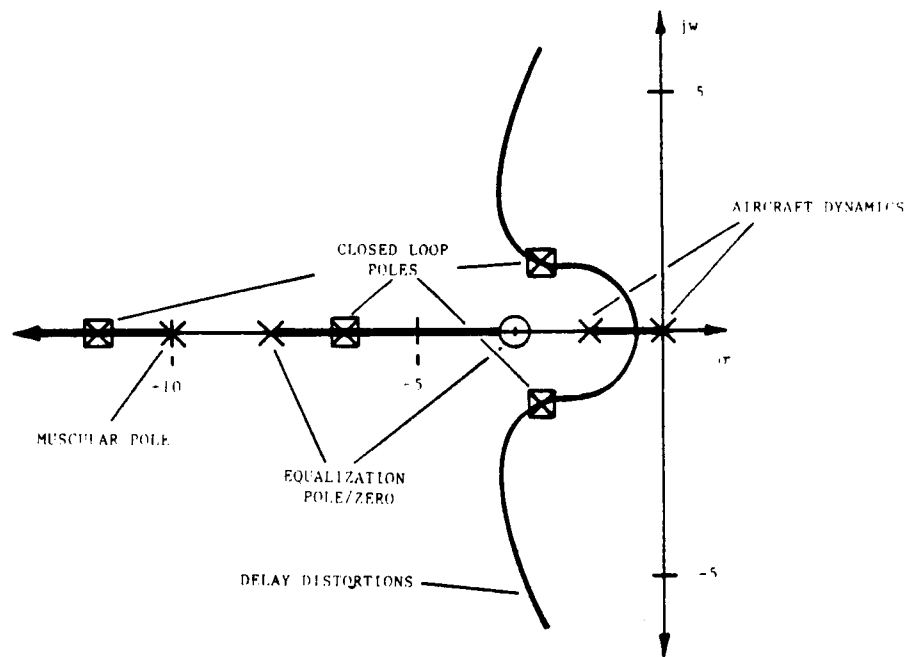


Figure V.A.1.-1. - Root-Locus of the pitch control pilot mechanism

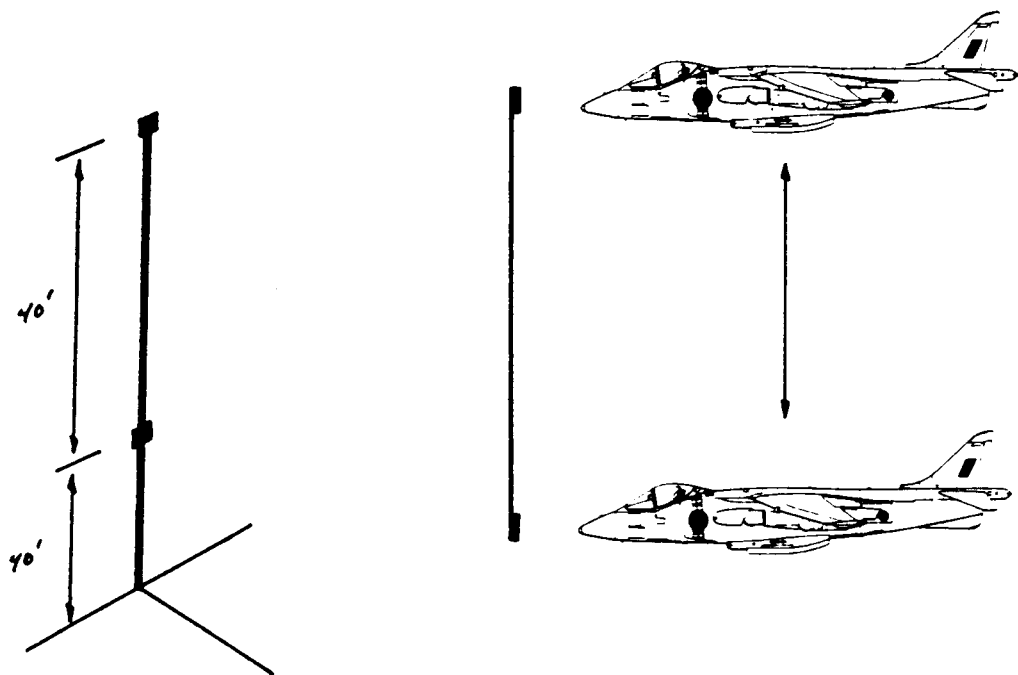


Figure V.B.1.-1. - Illustration of the target orientation and vehicle motion during the Vertical Tracking Hover maneuver

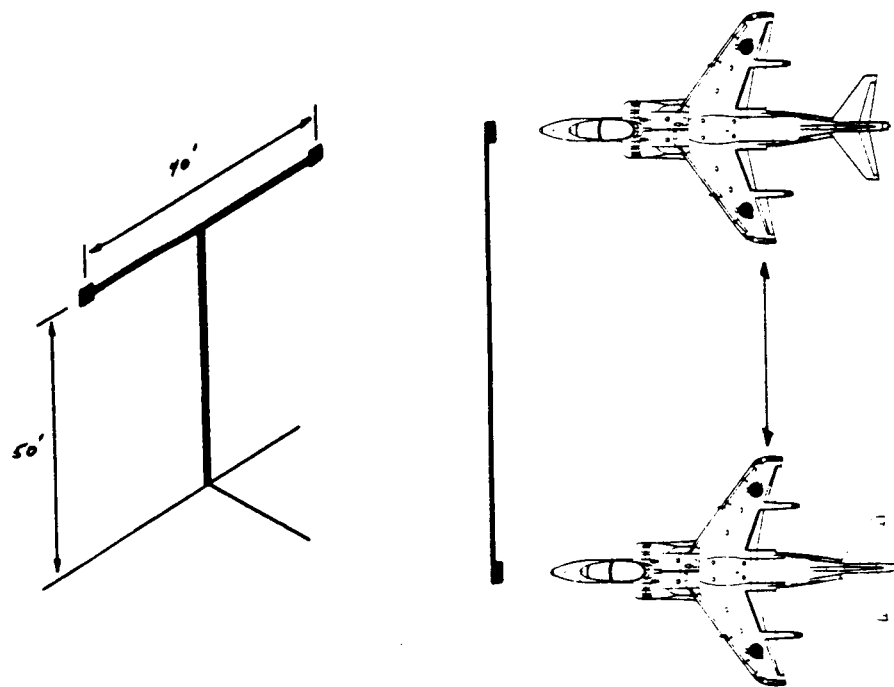


Figure V.B.1.-2. - Illustration of the target orientation and vehicle motion during the Lateral Tracking Hover maneuver

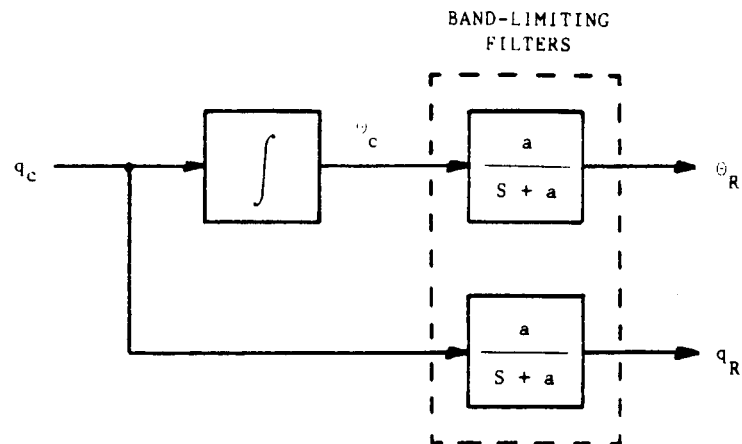


Figure V.B.4.-1. - Diagram of a trajectory reference generator for the pitch angle components driven by a pitch rate command sequence.

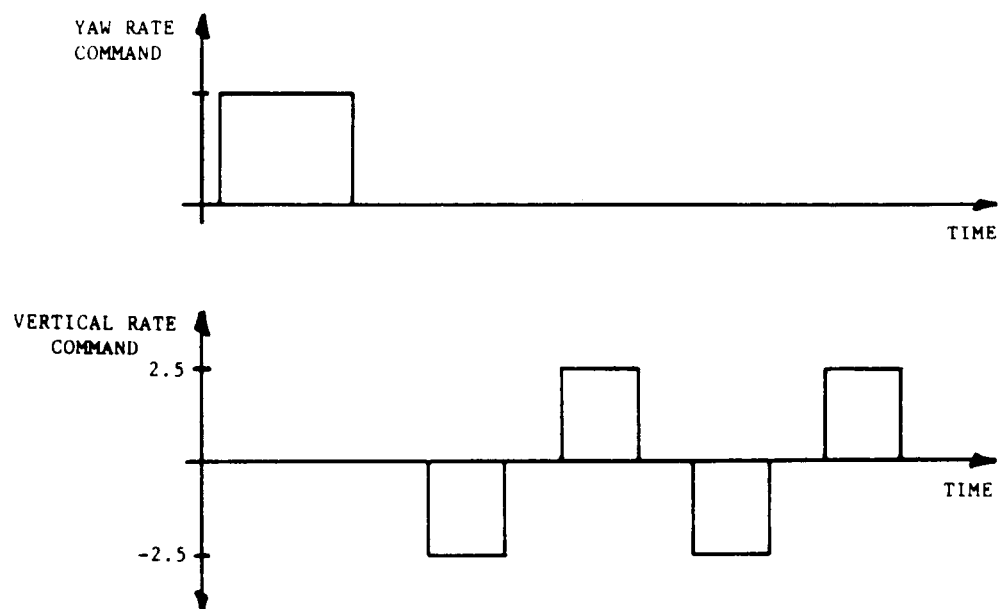


Figure V.B.4.-2. - Vertical rate and yaw rate command sequence for the vertical tracking maneuver.

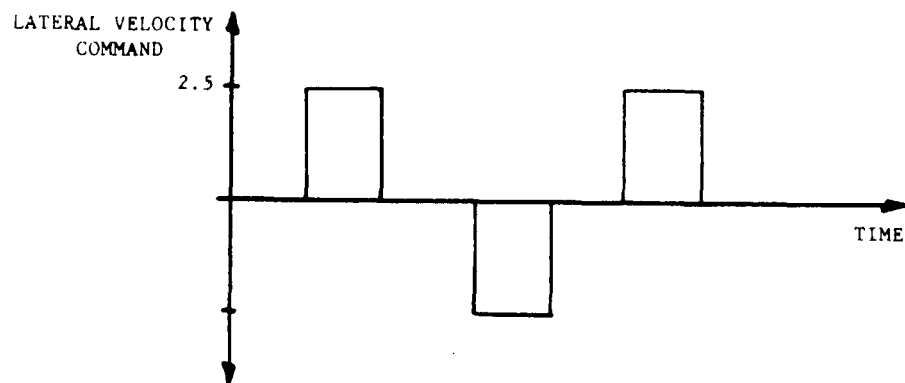


Figure V.B.4.-3. - Lateral velocity command sequence for the lateral tracking maneuver

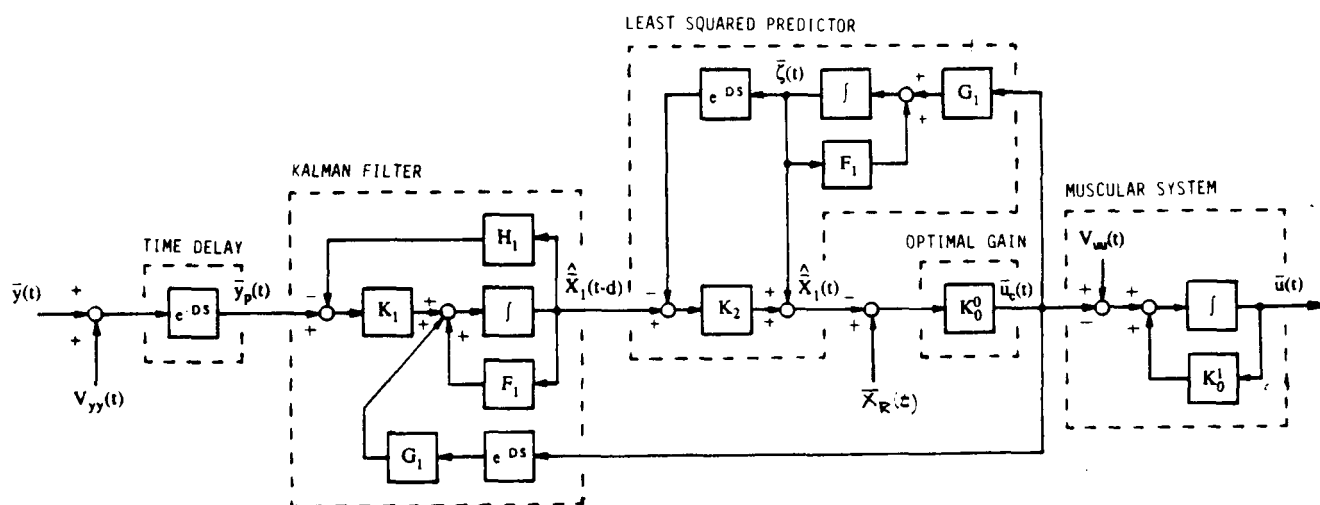


Figure A.1.-1. - Block diagram of the internal structure of the OCM

$$\begin{bmatrix} \dot{x}_{L_n} \\ \dot{V}_n \\ \dot{\theta} \\ \dot{\phi} \\ \dot{z}_w \\ \dot{V}_w \\ \dot{\psi} \\ \dot{p} \\ \dot{q} \\ \dot{r} \\ \dot{\gamma}_c \\ \dot{V}_c \end{bmatrix} = \begin{bmatrix} 0 & 1 & 0 & 0 & 0 & 0 & 0 & 0 & 0 & 0 & 0 & 0 \\ 0 & 0 & X_b & 0 & 0 & 0 & 0 & 0 & 0 & 0 & 0 & 0 \\ 0 & 0 & 0 & 0 & 1 & 0 & 0 & 0 & 0 & 0 & 0 & 0 \\ 0 & 0 & 0 & 0 & 0 & m_y & 0 & 0 & 0 & 0 & 0 & 0 \\ 0 & 0 & 0 & 0 & 0 & 0 & 0 & 1 & 0 & 0 & 0 & 0 \\ 0 & 0 & 0 & 0 & 0 & 0 & 0 & 0 & 0 & 0 & z_w & 0 \end{bmatrix} + \begin{bmatrix} x_{L_n} \\ V_n \\ \theta \\ \phi \\ z_w \\ V_w \\ \phi \\ p \\ q \\ r \\ \gamma_c \\ V_c \end{bmatrix} + \begin{bmatrix} 0 & 0 & 0 & 0 & 0 & 0 & 0 & 0 & 0 & 0 & 0 & 0 \\ 0 & X_j & 0 & 0 & 0 & 0 & 0 & 0 & 0 & 0 & 0 & 0 \\ 0 & 0 & 0 & 0 & 0 & 0 & 0 & 0 & 0 & 0 & 0 & 0 \\ m_c & 0 & 0 & 0 & 0 & 0 & 0 & 0 & 0 & 0 & 0 & 0 \\ 0 & 0 & 0 & 0 & 0 & 0 & 0 & 0 & 0 & 0 & 0 & 0 \\ 0 & 0 & 0 & 0 & 0 & 0 & 0 & 0 & 0 & 0 & 0 & 0 \end{bmatrix} + \begin{bmatrix} 0 & 0 & 0 & 0 & 0 & 0 & 0 & 0 & 0 & 0 & 0 & 0 \\ 0 & 0 & 0 & 0 & 0 & 0 & 0 & 0 & 0 & 0 & 0 & 0 \\ 0 & 0 & 0 & 0 & 0 & 0 & 0 & 0 & 0 & 0 & 0 & 0 \\ 0 & 0 & 0 & 0 & 0 & 0 & 0 & 0 & 0 & 0 & 0 & 0 \\ 0 & 0 & 0 & 0 & 0 & 0 & 0 & 0 & 0 & 0 & 0 & 0 \\ 0 & 0 & 0 & 0 & 0 & 0 & 0 & 0 & 0 & 0 & 0 & 0 \\ 0 & 0 & 0 & 0 & 0 & 0 & 0 & 0 & 0 & 0 & 0 & 0 \\ 0 & 0 & 0 & 0 & 0 & 0 & 0 & 0 & 0 & 0 & 0 & 0 \\ 0 & 0 & 0 & 0 & 0 & 0 & 0 & 0 & 0 & 0 & 0 & 0 \\ 0 & 0 & 0 & 0 & 0 & 0 & 0 & 0 & 0 & 0 & 0 & 0 \\ 0 & 0 & 0 & 0 & 0 & 0 & 0 & 0 & 0 & 0 & 0 & 0 \\ 0 & 0 & 0 & 0 & 0 & 0 & 0 & 0 & 0 & 0 & 0 & 0 \end{bmatrix} + \begin{bmatrix} 0 & 0 & 0 & 0 & 0 & 0 & 0 & 0 & 0 & 0 & 0 & 0 \\ 0 & 0 & 0 & 0 & 0 & 0 & 0 & 0 & 0 & 0 & 0 & 0 \\ 0 & 0 & 0 & 0 & 0 & 0 & 0 & 0 & 0 & 0 & 0 & 0 \\ 0 & 0 & 0 & 0 & 0 & 0 & 0 & 0 & 0 & 0 & 0 & 0 \\ 0 & 0 & 0 & 0 & 0 & 0 & 0 & 0 & 0 & 0 & 0 & 0 \\ 0 & 0 & 0 & 0 & 0 & 0 & 0 & 0 & 0 & 0 & 0 & 0 \\ 0 & 0 & 0 & 0 & 0 & 0 & 0 & 0 & 0 & 0 & 0 & 0 \\ 0 & 0 & 0 & 0 & 0 & 0 & 0 & 0 & 0 & 0 & 0 & 0 \\ 0 & 0 & 0 & 0 & 0 & 0 & 0 & 0 & 0 & 0 & 0 & 0 \\ 0 & 0 & 0 & 0 & 0 & 0 & 0 & 0 & 0 & 0 & 0 & 0 \\ 0 & 0 & 0 & 0 & 0 & 0 & 0 & 0 & 0 & 0 & 0 & 0 \\ 0 & 0 & 0 & 0 & 0 & 0 & 0 & 0 & 0 & 0 & 0 & 0 \end{bmatrix} + \begin{bmatrix} \delta_c \\ \delta_j \\ \delta_r \\ \delta_a \\ \delta_r \end{bmatrix}$$

Figure B.2.-1. - Full rank linear state space model of the Harrier AV-8B flight dynamics from trimmed forward flight while in the low speed/powered-lift region of the flight envelope.

ORIGINAL PAGE IS
OF POOR QUALITY

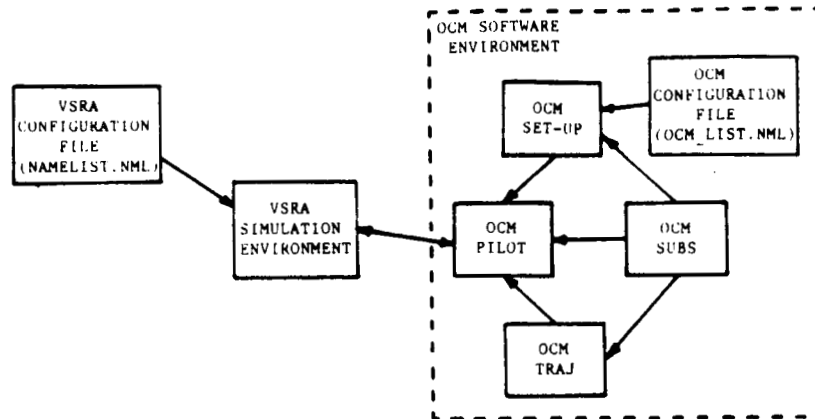


Figure C.1. - 1. - Block diagram of the software modules and configuration files of the OCM simulation environment.

TABLE GROUP

TABLE LISTING

XX_u		Longitudinal position
V_u		Forward velocity
θ		Pitch angle
q		Pitch rate
ZZ_w		Altitude
V_w		Vertical rate
ϕ	=	Roll angle
p		Roll rate
ψ		Yaw angle
r		Yaw rate
YY_v		Lateral position
V_v		Lateral velocity

Table IV.A.3.-1 - List of the state vector variables for the high order Harrier model.

$$\begin{bmatrix} \delta_e \\ \delta_j \\ \delta_T \\ \delta_a \\ \delta_r \end{bmatrix} = \begin{bmatrix} \text{Longitudinal stick position (inches)} \\ \text{Nozzle angle control position (degrees)} \\ \text{Power level/throttle position (percent)} \\ \text{Lateral stick position (inches)} \\ \text{Rudder pedal position (inches)} \end{bmatrix}$$

Table IV.A.3.-2. - List of the control vector variables for the high order Harrier model.

V (knots)	w_θ (rads/sec)	δ_θ	K_{TD} (in-sec ³) ⁻¹	K_T (in-sec ²) ⁻¹
20	4.7	0.28	0.041	2.32
40	4.9	0.19	0.045	2.59
60	5.1	0.14	0.051	2.91
80	5.4	0.10	0.049	2.83
100	5.7	0.07	0.048	2.77

Table IV.B.1.-1. - Transfer function parameters for the pitch response of the Black Hawk.

V (knots)	K _{ALT} $\left(\frac{\text{feet}}{\text{in-sec}^2}\right)$	a _{ALT} (sec) ⁻¹
20	6.6	0.30
40	7.0	0.45
60	7.0	0.50
80	7.3	0.50
100	7.5	0.50

Table IV.B.1.-2. - Transfer function parameters for the altitude response components of the Black Hawk.

Pilot Mechanism	K	A (sec) ⁻¹	B (sec) ⁻¹
Altitude Control	52. ($\frac{\text{in}}{\text{feet-sec}}$)	0.8	3.0
Vertical Rate Control	36. ($\frac{\text{in}}{\text{feet}}$)	0.8	0.0
Velocity Control	-14. ($\frac{\text{deg}}{\text{knot-sec}}$)	0.0	0.0
Roll Control	2.9 ($\frac{\text{in}}{\text{deg-sec}}$)	3.6	8.0
Lateral Velocity Control	1.1 ($\frac{\text{in}}{\text{feet}}$)	0.8	6.0
Heading Control	26. ($\frac{\text{in}}{\text{deg-sec}}$)	0.8	20.
Yaw Rate Control	58. ($\frac{\text{in}}{\text{deg}}$)	0.8	0.0
Sideslip Regulation	-32. ($\frac{\text{in}}{\text{deg-sec}}$)	0.8	20.

Table V.A.1.-1. - Parameter list of the additional Harrier pilot mechanisms.

ORIGINAL PAGE IS
OF POOR QUALITY

V (knots)	K_{PT} $(\frac{\text{in}}{\text{deg-sec}})$
20	1.31
40	1.48
60	1.53
80	2.07
100	1.82

Table V.A.1.-2. - Parameters of the pitch control pilot of the Black Hawk

V	K
(knots)	($\frac{\text{in}}{\text{foot-sec}}$)
20	5.77
40	5.68
60	4.97
80	5.07
100	5.19

$$A = 0.8 \text{ (sec)}^{-1}$$

$$B = 5.5 \text{ (sec)}^{-1}$$

Table V.A.1.-3. - Parameters of the altitude control pilot for the Black Hawk

V (knots)	K ($\frac{\text{in}}{\text{feet}}$)
20	1.82
40	1.74
60	1.43
80	1.51
100	1.57

$$A = 0.8 \text{ (sec)}^{-1}$$

$$B = 0.0 \text{ (sec)}^{-1}$$

Table V.A.1.-4. - Parameters of the altitude rate control pilot for the Black Hawk

V (knots)	K ($\frac{\text{in}}{\text{deg-sec}}$)
20	0.57
40	0.57
60	0.68
80	0.68
100	0.68

$$A = 0.8 \text{ (sec)}^{-1}$$

$$B = 0.0 \text{ (sec)}^{-1}$$

Table V.A.1.-5. - Parameters of the roll angle control pilot for the Black Hawk

V (knots)	K $(\frac{\text{in}}{\text{deg-sec}})$	A (sec) ⁻¹	B (sec) ⁻¹
20	0.63	2.0	1.5
40	0.60	1.4	0.75
60	0.43	0.8	0.0
80	0.51	0.8	0.0
100	0.65	0.8	0.0

Table V.A.1.-6. - Parameters of the heading control pilot for the Black Hawk

V (knots)	K ($\frac{\text{in}}{\text{deg-sec}}$)
20	-0.25
40	-0.45
60	-0.55
80	-0.55
100	-0.55

$$A = 0.8 \text{ (sec)}^{-1}$$

$$B = 0.0 \text{ (sec)}^{-1}$$

Table V.A.1.-7. - Parameters of the Sideslip regulation pilot of the Black Hawk

cockpit control mechanism maneuver	Longitudinal Stick	Lateral Stick	Rudder Pedals	Throttle	Nozzle Angle
Pitch Reorientation	Pitch Control Pilot	Roll Control Pilot	Heading Control Pilot	Altitude Control Pilot	Velocity Control Pilot
Velocity Translation	Pitch Control Pilot	Roll Control Pilot	Heading Control Pilot	Altitude Control Pilot	Velocity Control Pilot
Altitude Translation	Pitch Control Pilot	Roll Control Pilot	Heading Control Pilot	Altitude Control Pilot	Velocity Control Pilot
Heading Modification	Pitch Control Pilot	Roll Control Pilot	Heading Control Pilot	Altitude Control Pilot	Velocity Control Pilot
Altitude Rate Translation	Pitch Control Pilot	Roll Control Pilot	Heading Control Pilot	Altitude Rate Pilot	Velocity Control Pilot
Flat Turn	Pitch Control Pilot	Roll Control Pilot	Yaw Rate Control Pilot	Altitude Control Pilot	Velocity Control Pilot
Coordinated Turn	Pitch Control Pilot	Roll Control Pilot	Sideslip Regulation Pilot	Altitude Control Pilot	Velocity Control Pilot

Table V.A.2.-1. - Table of various flight control maneuvers
and their associated configurations of
Harrier SVPMs.

cockpit control mechanism maneuver	Longitudinal Cyclic Stick	Lateral Cyclic Stick	Rudder Pedals	Collective Stick
Pitch Reorientation	Pitch Control Pilot	Roll Control Pilot	Heading Control Pilot	Altitude Control Pilot
Altitude Translation	Pitch Control Pilot	Roll Control Pilot	Heading Control Pilot	Altitude Control Pilot
Heading Modification	Pitch Control Pilot	Roll Control Pilot	Heading Control Pilot	Altitude Control Pilot
Altitude Rate Translation	Pitch Control Pilot	Roll Control Pilot	Heading Control Pilot	Altitude Rate Pilot
Coordinated Turn	Pitch Control Pilot	Roll Control Pilot	Sideslip Regulation Pilot	Altitude Control Pilot

Table V.A.2.-2. - Table of various flight control maneuvers and their associated configurations of Black Hawk SVPs.

VARIABLE	TRIMMED	COMMAND
Pitch (θ_c)	7.3 degrees	17.3 degrees
Roll (ϕ_c)	0.0 degrees	0.0 degrees
Heading (ψ_c)	0.0 degrees	0.0 degrees
Altitude	100 feet	100 feet
Velocity	10 knots	10 knots

Table V.A.3.-1. - Pitch reorientation command sequence for the multi-variable Harrier pilot.

VARIABLE	TRIMMED	COMMAND
Pitch (θ_C)	6.5 degrees	6.5 degrees
Roll (ϕ_C)	0.0 degrees	0.0 degrees
Heading (ψ_C)	0.0 degrees	0.0 degrees
Altitude	100 feet	100 feet
Velocity	25 knots	20 knots

Table V.A.3.-2. - Velocity translation command sequence for the multi-variable Harrier pilot.

VARIABLE	TRIMMED	COMMAND
Pitch (θ_C)	2.8 degrees	2.8 degrees
Roll (ϕ_C)	0.0 degrees	20.0 degrees
Sideslip (β_C)	0.0 degrees	0.0 degrees
Altitude	200 feet	200 feet

Table V.A.3.-3. - Coordinated turn command sequence for the multi-variable Black Hawk pilot

XX_M	V_M^u	θ_M	ZZ_M	δ_M^e	δ_M^T
3.15	3.15	10.	5.	3.5	3.5

YY_M	V_M^y	ϕ_M	ψ_M	δ_M^a	δ_M^r
3.15	3.15	10.	7.0	3.5	1.25

Table V.B.3.-1. - Cost function weights of the OCM for the vertical tracking maneuver

XX_M	V_M^u	θ_M	ZZ_M	δ_M^e	δ_M^T
3.15	3.15	7.0	5.	3.5	3.5

YY_M	V_M^y	ϕ_M	ψ_M	δ_M^a	δ_M^r
3.15	3.15	10.	6.0	3.5	1.25

Table V.B.3.-2. - Cost function weights of the OCM for the lateral tracking maneuver

δ_e	δ_j	δ_T	δ_a	δ_r
1.0	1.0	0.22	1.4	1.4

Table V.B.3.-3. - Magnitudes of the OCM motor noise sources applied to each cockpit control mechanism

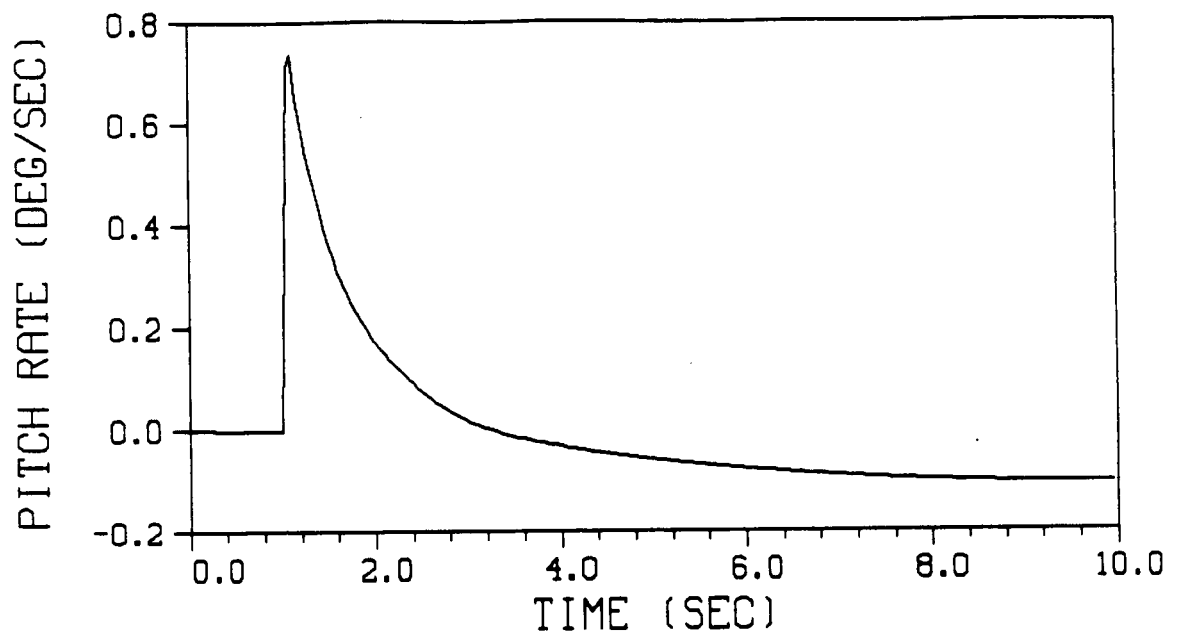
θ (degrees)	ϕ (degrees)	ψ (degrees)	ALT (feet)	Airspeed (knots)
6.5	0.0	0.0	80	1.0

Table V.B.4.-1. - Trimmed values of the Harrier simulation environment for the vertical tracking precision hover maneuver.

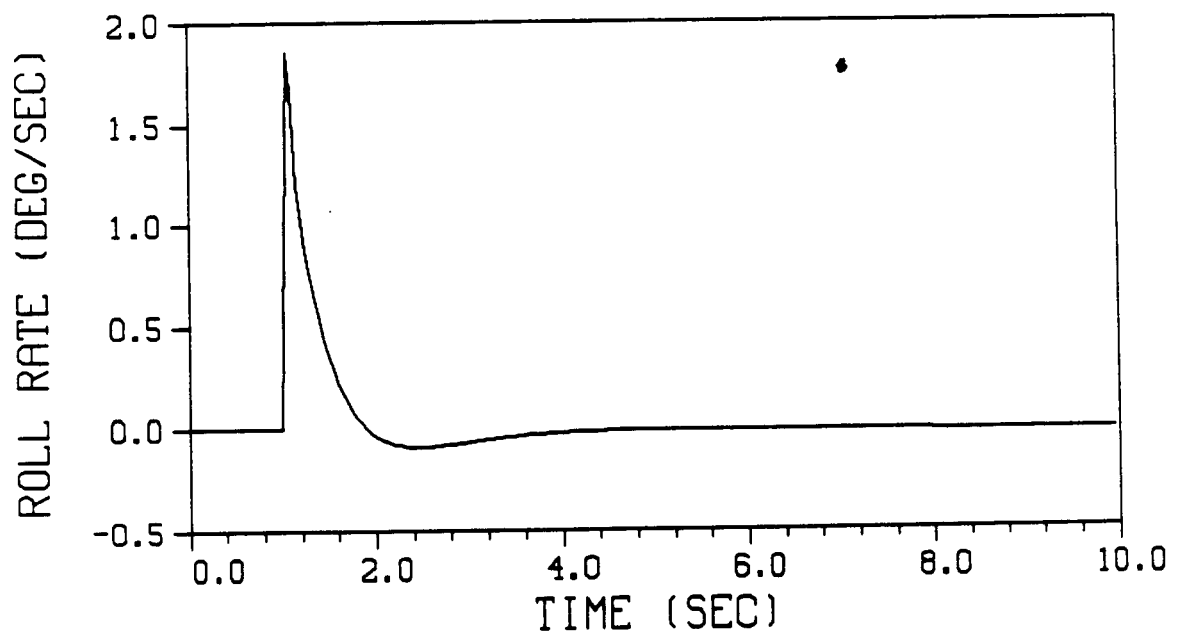
θ (degrees)	ϕ (degrees)	ψ (degrees)	ALT (feet)	Airspeed (knots)
6.5	0.0	0.0	55	1.0

Table V.B.4.-2. - Trimmed values of the Harrier simulation environment for the lateral tracking precision hover maneuver.

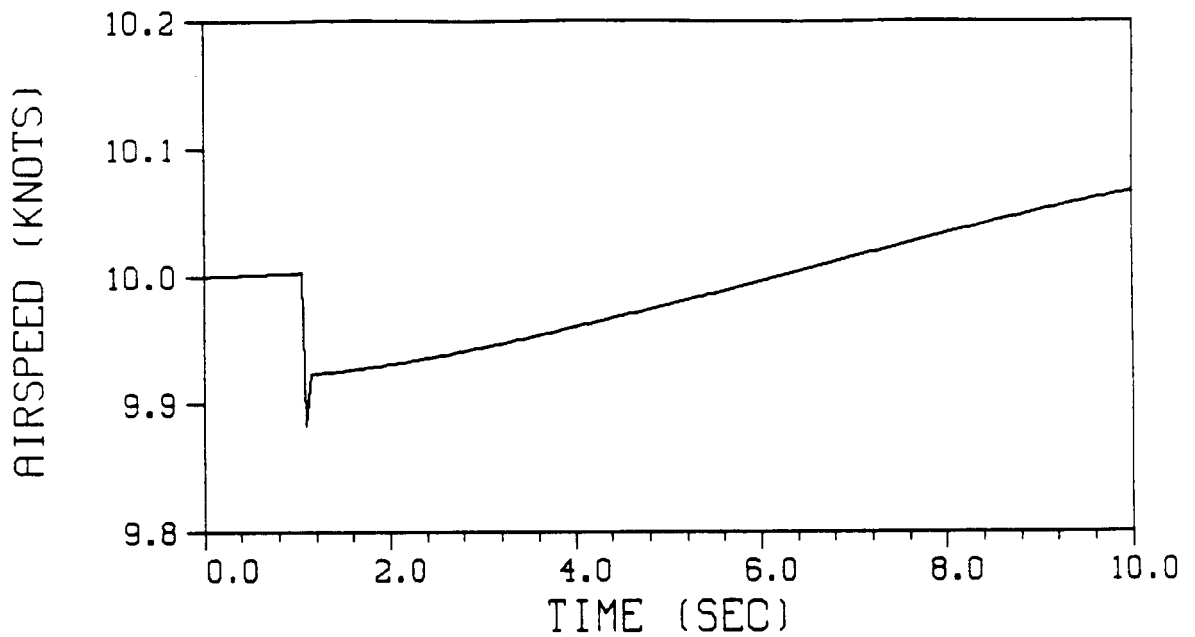
PLOT GROUP



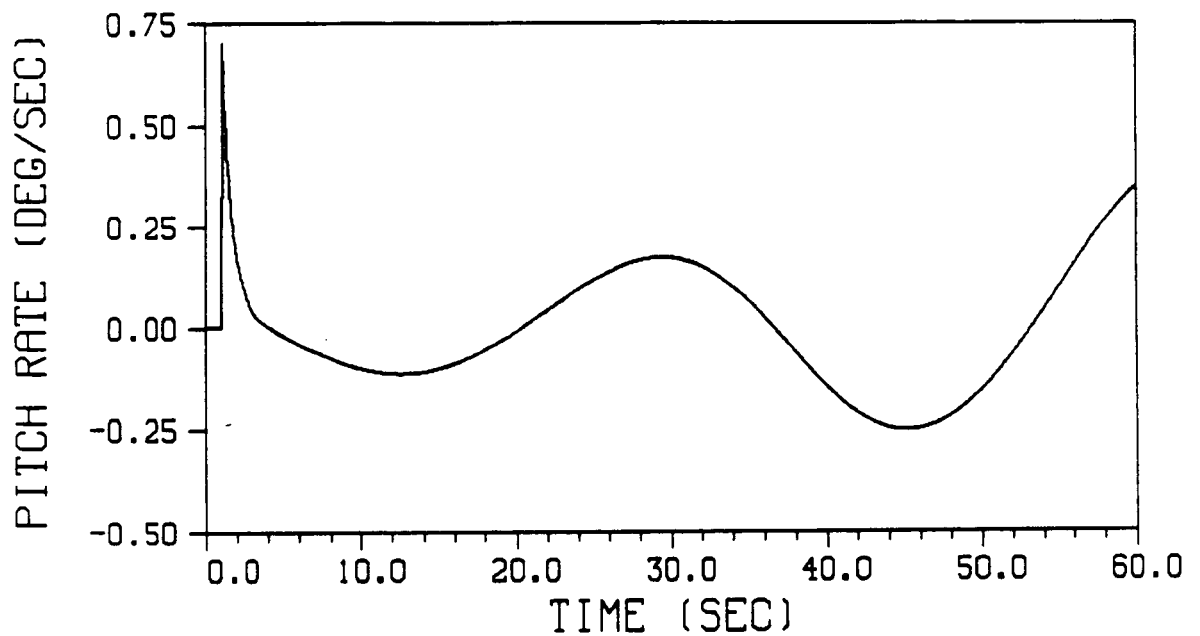
Plot IV.A.2.-1. - Pitch rate response of the Harrier AV-8B due to a unit impulse deflection of the longitudinal stick in a near hover



Plot IV.A.2.-2. - Roll rate response of the Harrier AV-8B due to a unit impulse deflection of the lateral stick in a near hover

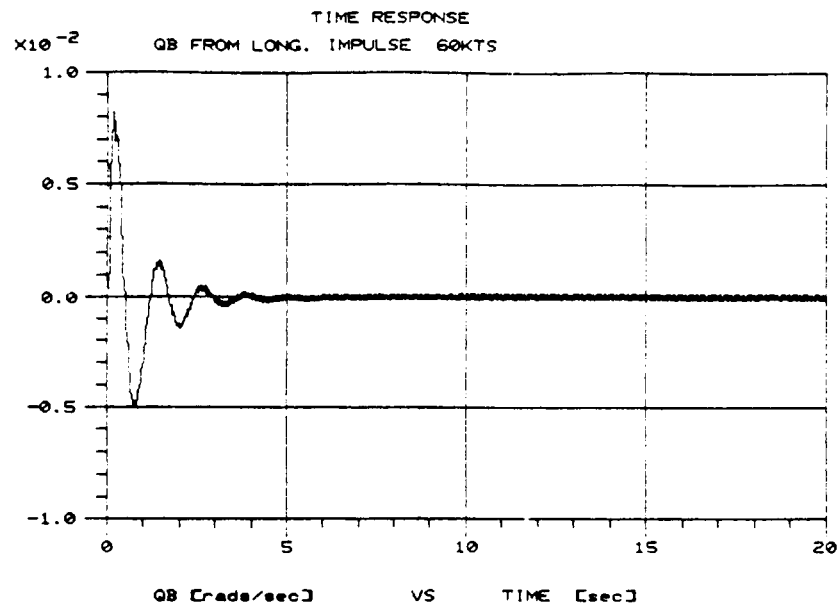


Plot IV.A.2.-3. - Forward velocity response of the Harrier AV-8B due to a 5 degree impulse deflection of the nozzle angle at 10 knots

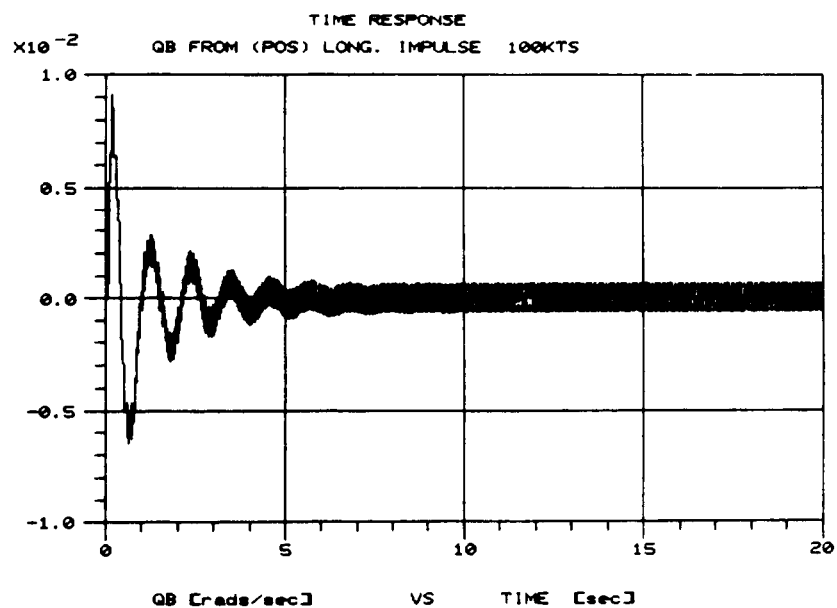


Plot IV.A.3.-1. - Long term pitch rate response of the Harrier AV-8B due to a unit impulse deflection of the longitudinal stick at 10 knots

ORIGINAL PAGE IS
OF POOR QUALITY

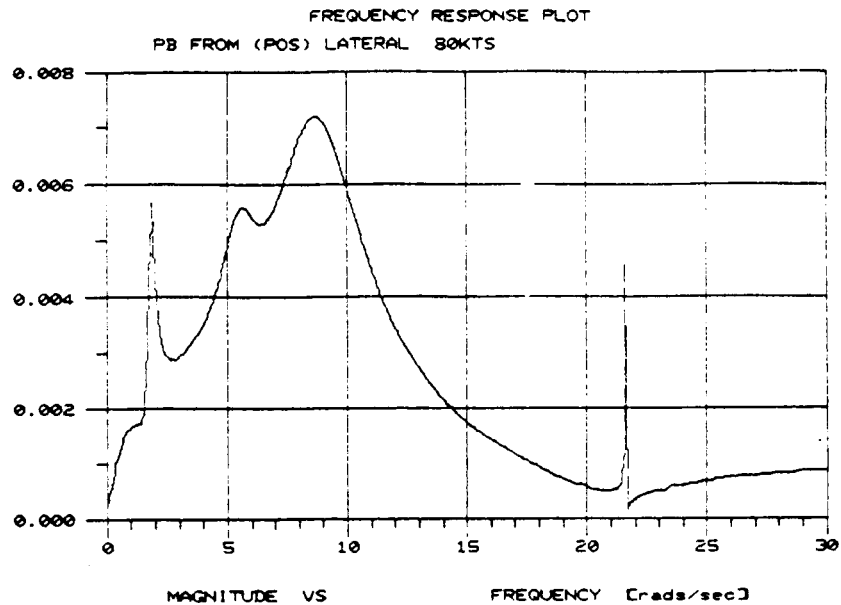


Plot IV.B.1.-1. - Pitch rate response of the Black Hawk UH-60A due to an impulse of the longitudinal cyclic stick at 60 knots.

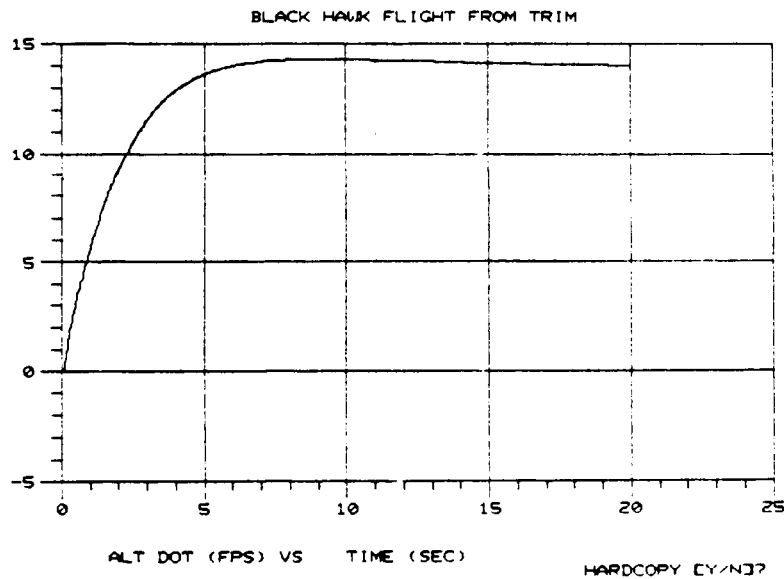


Plot IV.B.1.-2. - Pitch rate response of the Black Hawk UH-60A due to an impulse of the longitudinal cyclic stick at 100 knots.

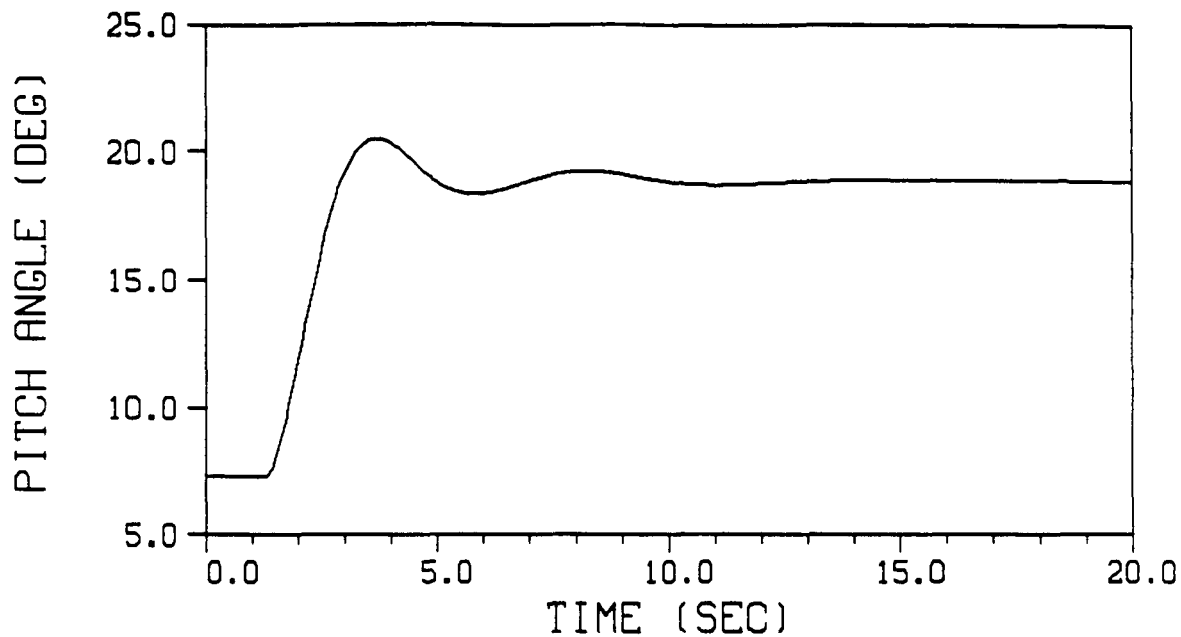
ORIGINAL PAGE IS
OF POOR QUALITY



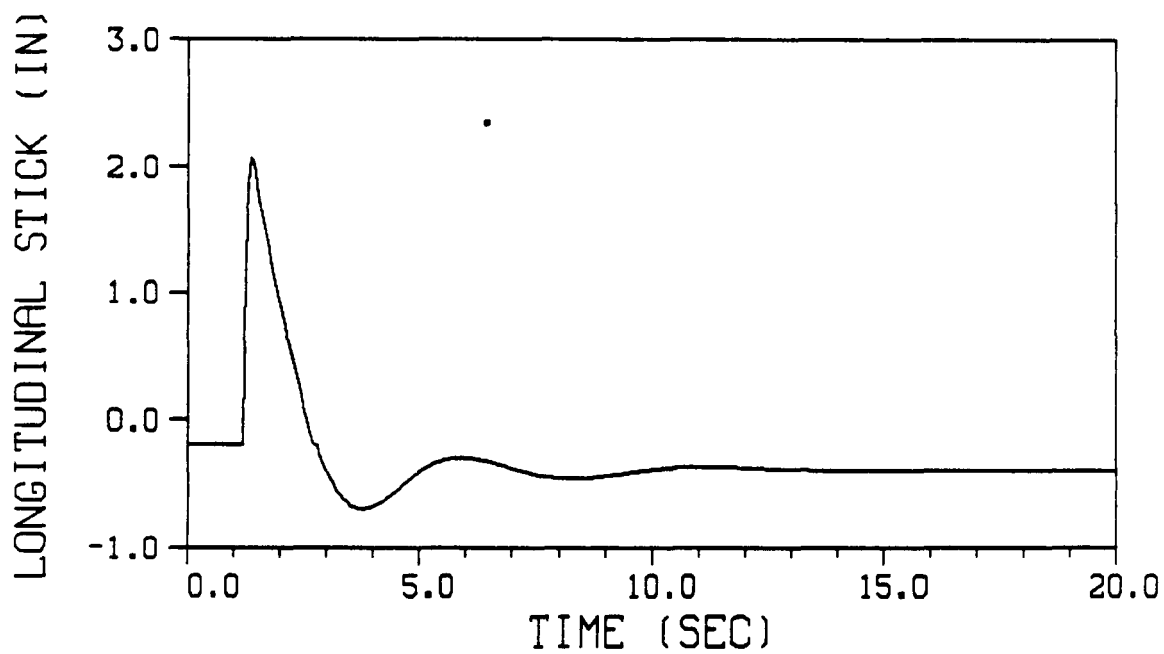
Plot IV.B.1.-3. - Roll rate frequency response of the Black Hawk UH-60A due to the operation of the lateral cyclic stick at 80 knots.



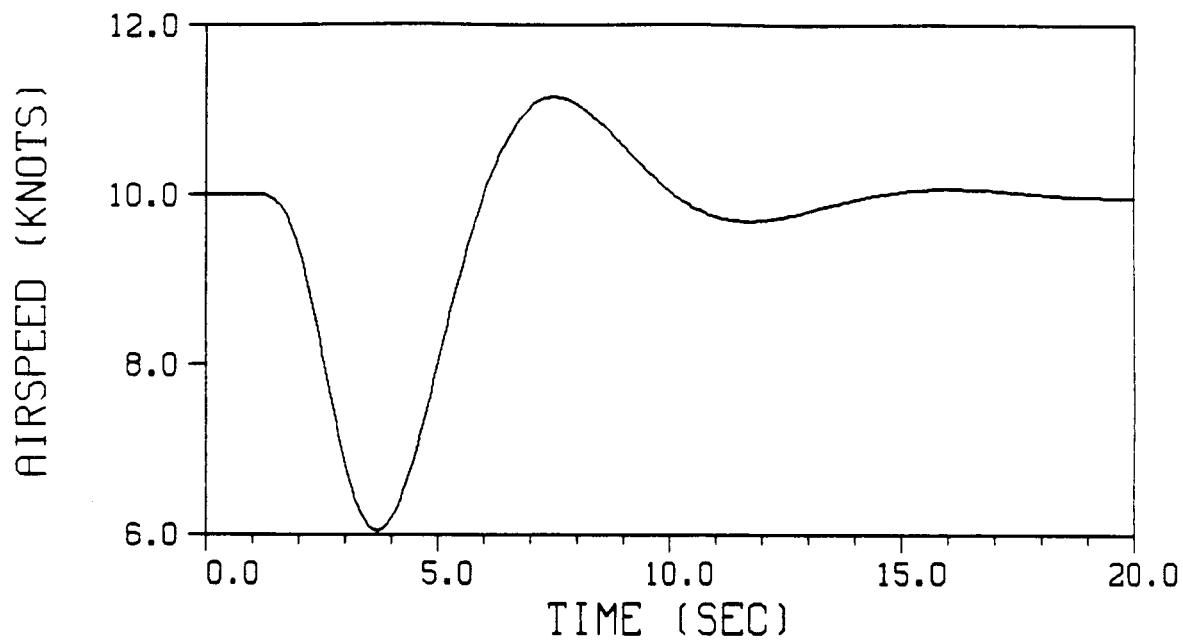
Plot IV.B.1.-4. - Altitude rate response of the Black Hawk UH-60A due to a step of the main rotor collective stick at 60 knots.



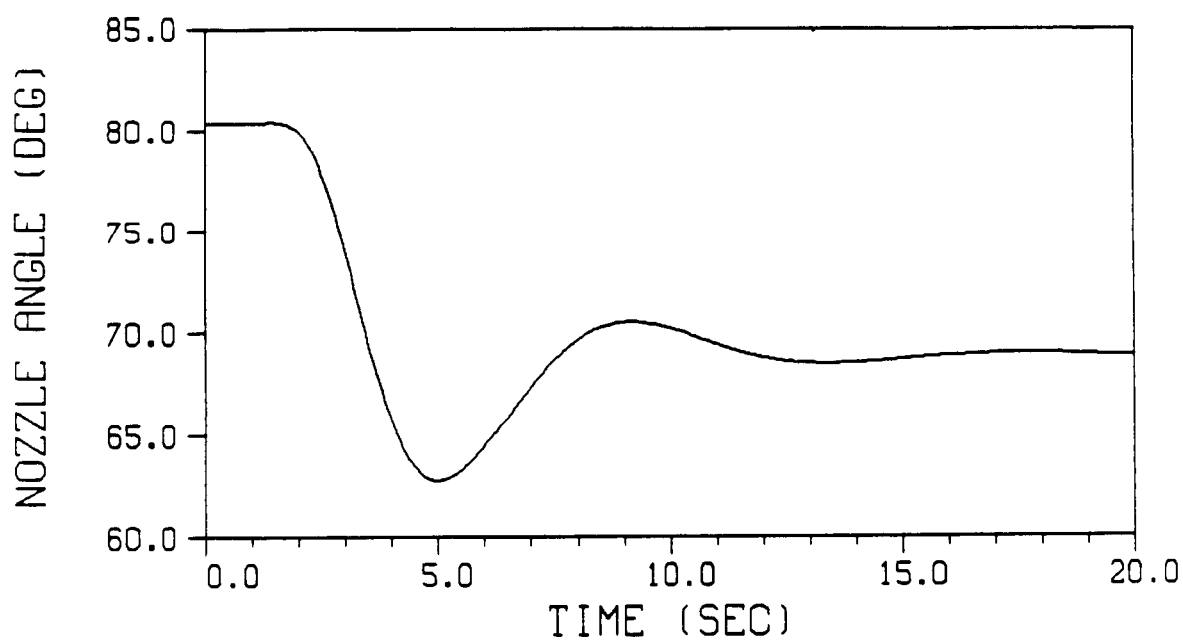
Plot V.A.3.-1. - Pitch angle response during a pitch reorientation maneuver by a multi-variable McRuer-Krendel pilot inserted in the Harrier AV-8B



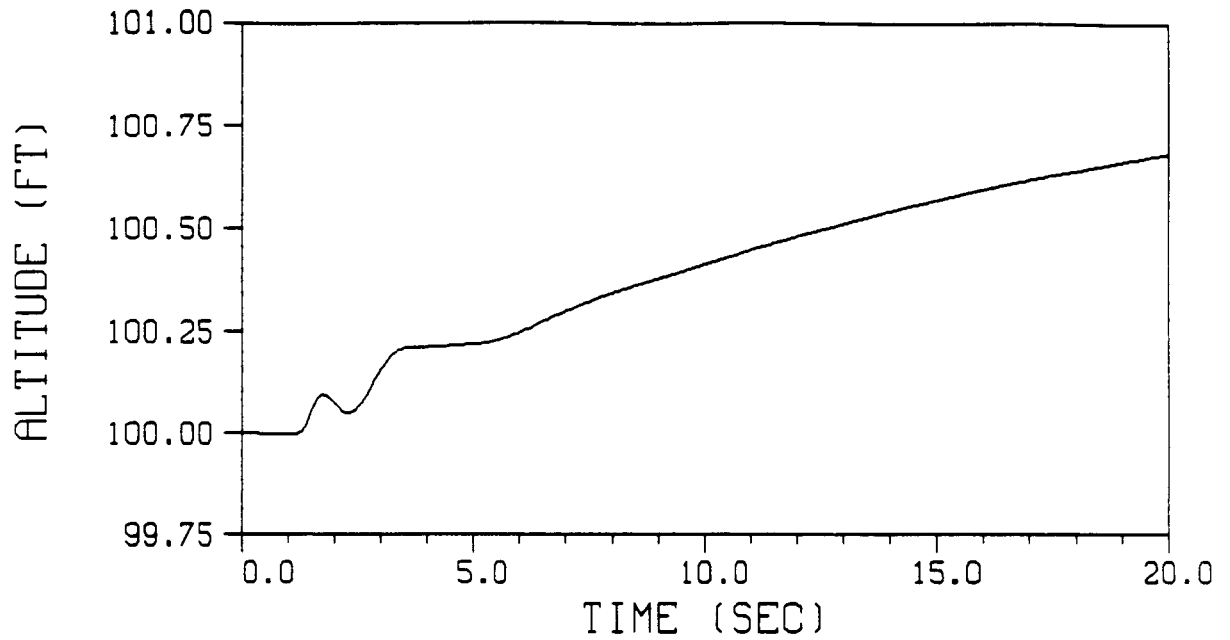
Plot V.A.3.-2. - Longitudinal stick response of a multi-variable McRuer-Krendel pilot during a pitch reorientation maneuver in the Harrier AV-8B



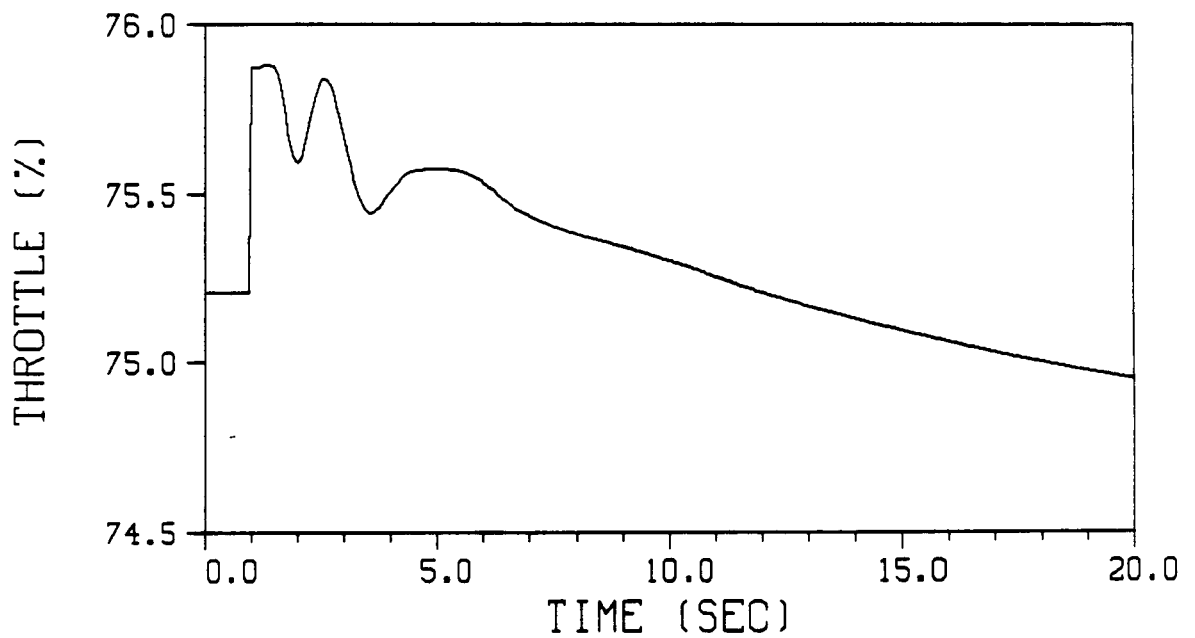
Plot V.A.3.-3. - Forward velocity response during a pitch reorientation maneuver by a multi-variable McRuer-Krendel pilot inserted in the Harrier AV-8B



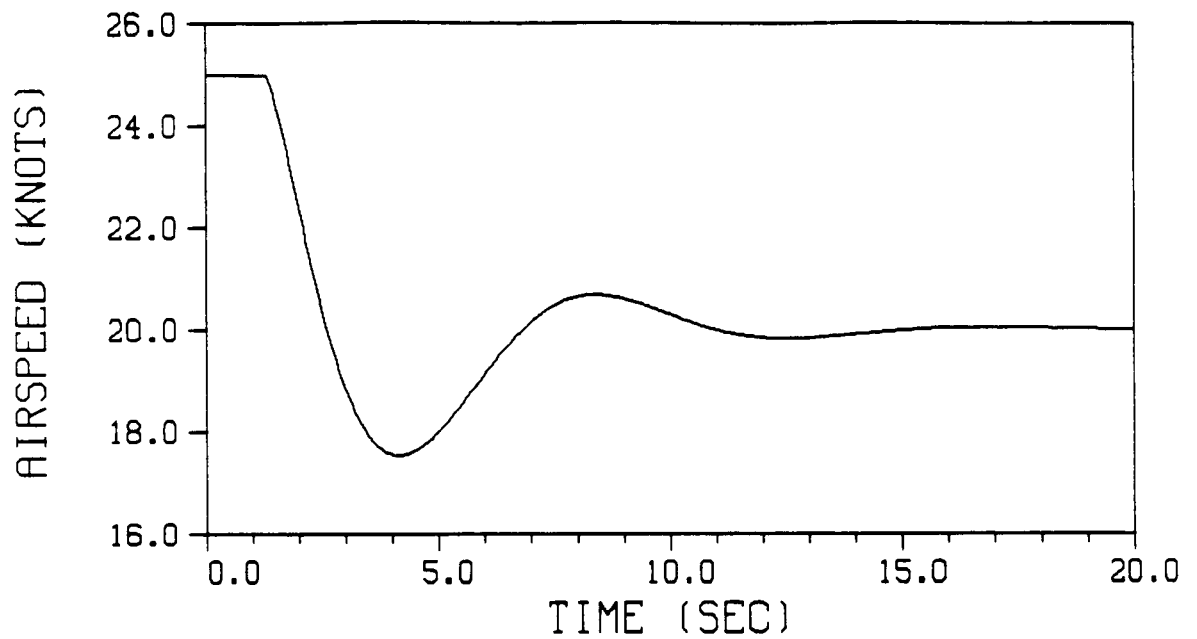
Plot V.A.3.-4. - Nozzle angle response of a multi-variable McRuer-Krendel pilot during a pitch reorientation maneuver in the Harrier AV-8B



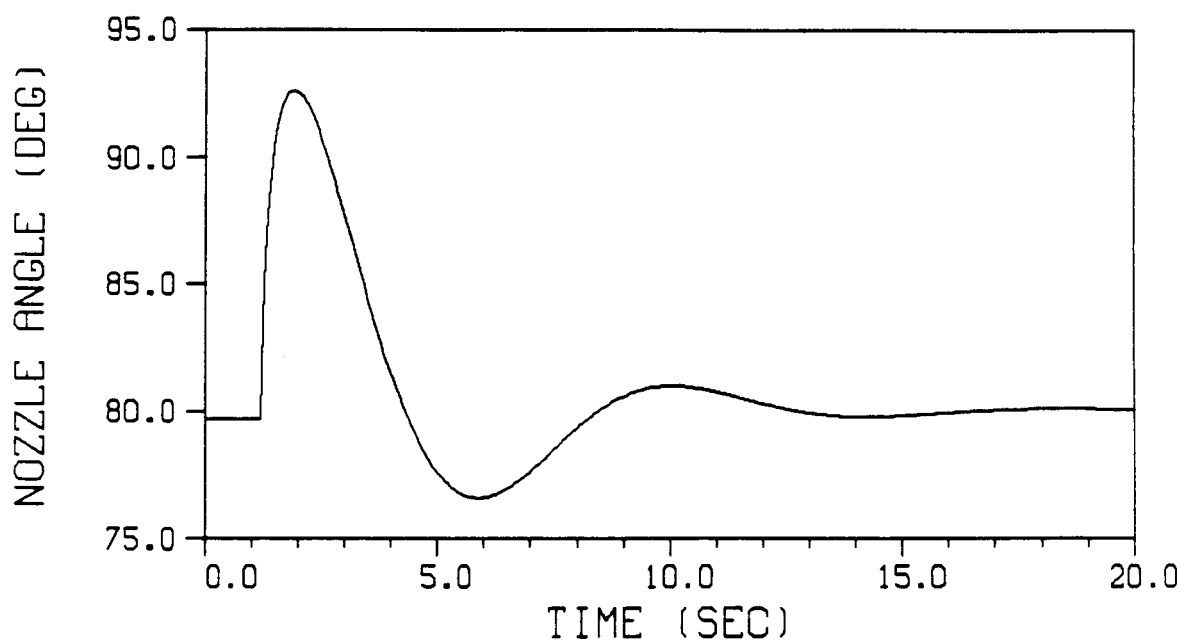
Plot V.A.3.-5. - Altitude response during a pitch reorientation maneuver by a multi-variable McRuer-Krendel pilot inserted in the Harrier AV-8B



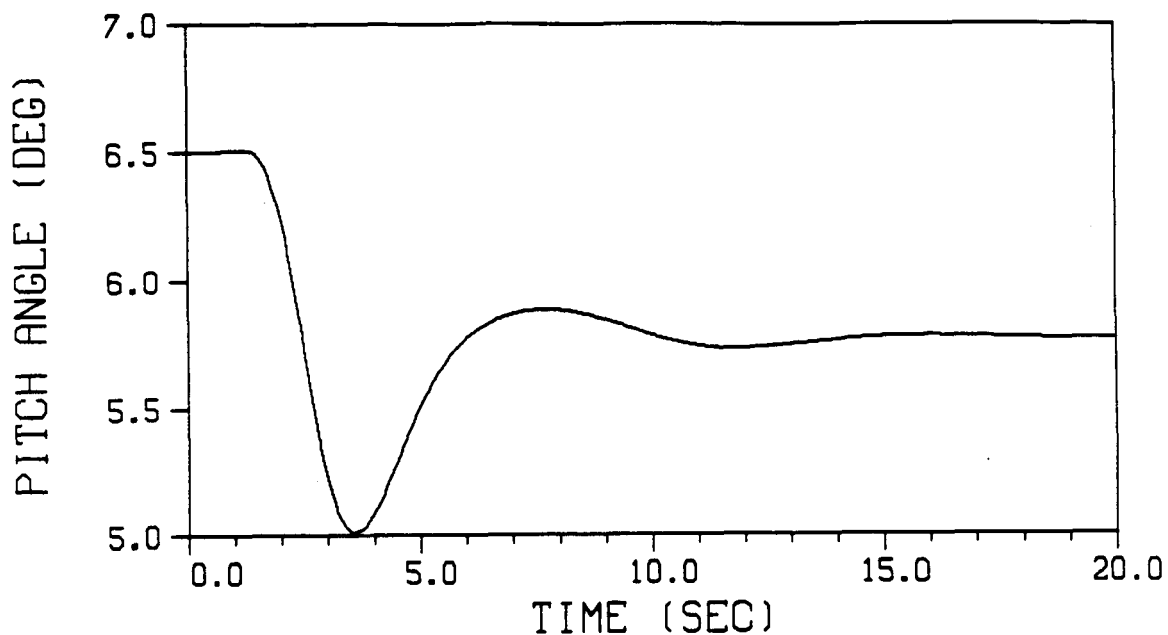
Plot V.A.3.-6. - Throttle response of a multi-variable McRuer-Krendel pilot during a pitch reorientation maneuver in the Harrier AV-8B



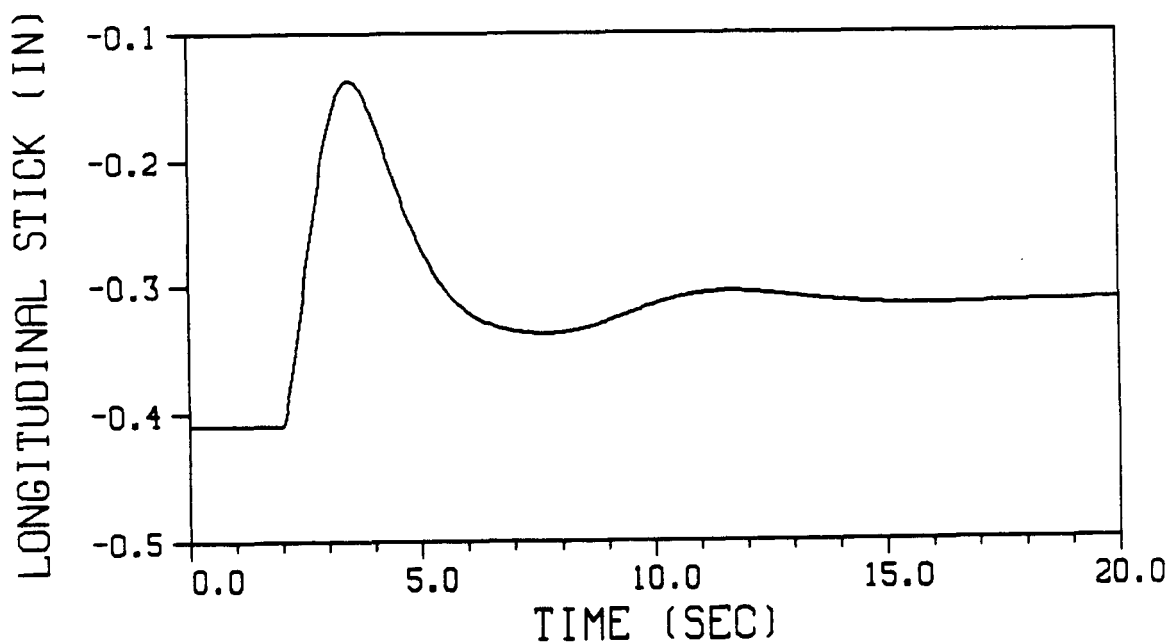
Plot V.A.3.-7. - Forward velocity response during a velocity translation maneuver by a multi-variable McRuer-Krendel pilot inserted in the Harrier AV-8B



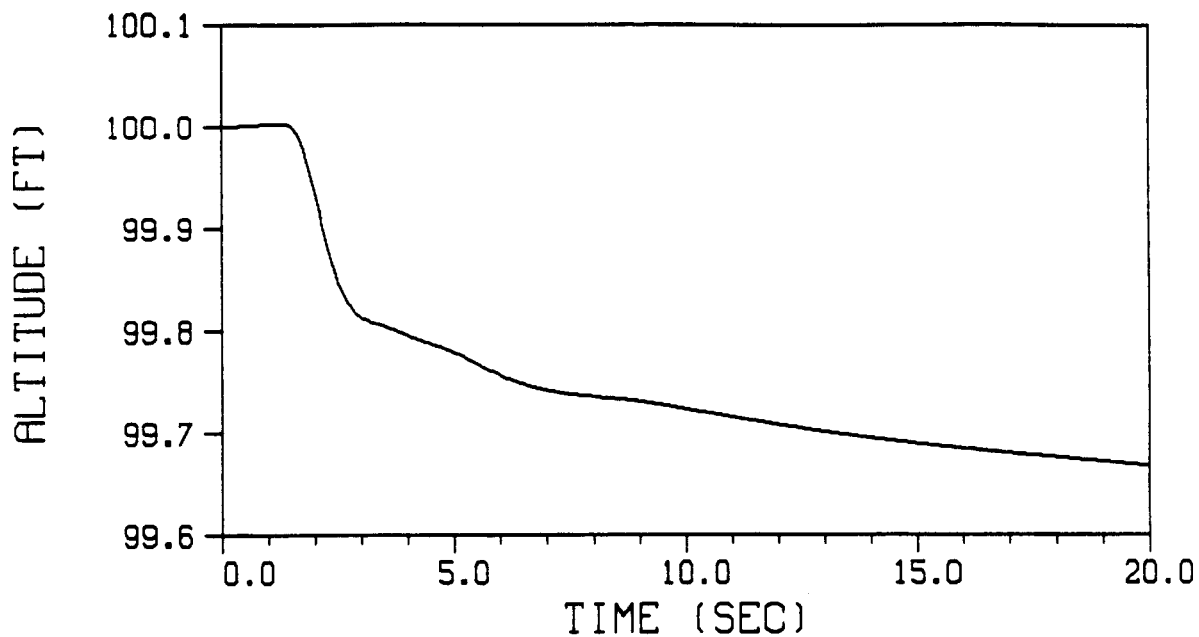
Plot V.A.3.-8. - Nozzle angle response of a multi-variable McRuer-Krendel pilot during a velocity translation maneuver in the Harrier AV-8B



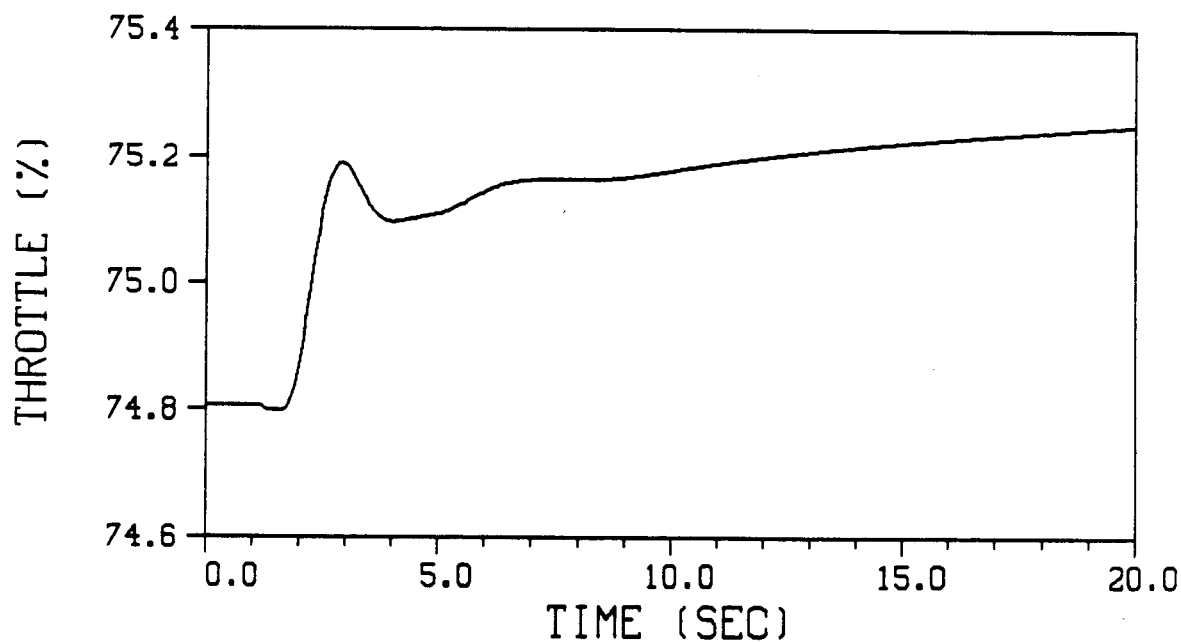
Plot V.A.3.-9. - Pitch angle response during a velocity translation maneuver by a multi-variable McRuer-Krendel pilot inserted in the Harrier AV-8B



Plot V.A.3.-10. - Longitudinal stick response of a multi-variable McRuer-Krendel pilot during a velocity translation maneuver in the Harrier AV-8B

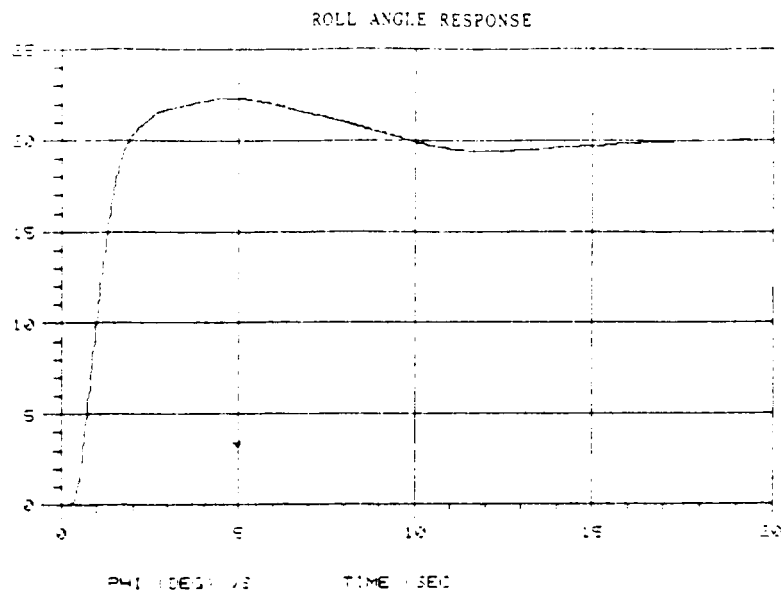


Plot V.A.3.-11. - Altitude response during a velocity translation maneuver by a multi-variable McRuer-Krendel pilot inserted in the Harrier AV-8B

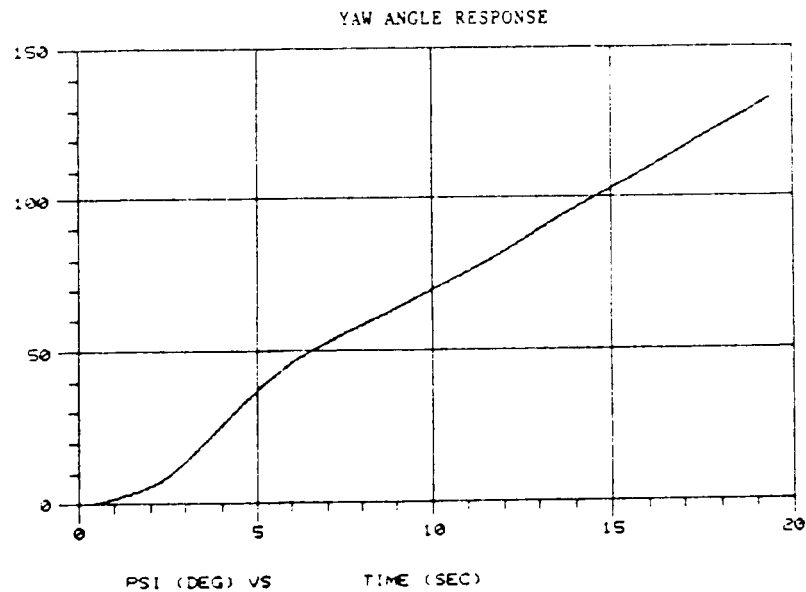


Plot V.A.3.-12. - Throttle response of a multi-variable McRuer-Krendel pilot during a velocity translation maneuver in the Harrier AV-8B

ORIGINAL PAGE IS
OF POOR QUALITY

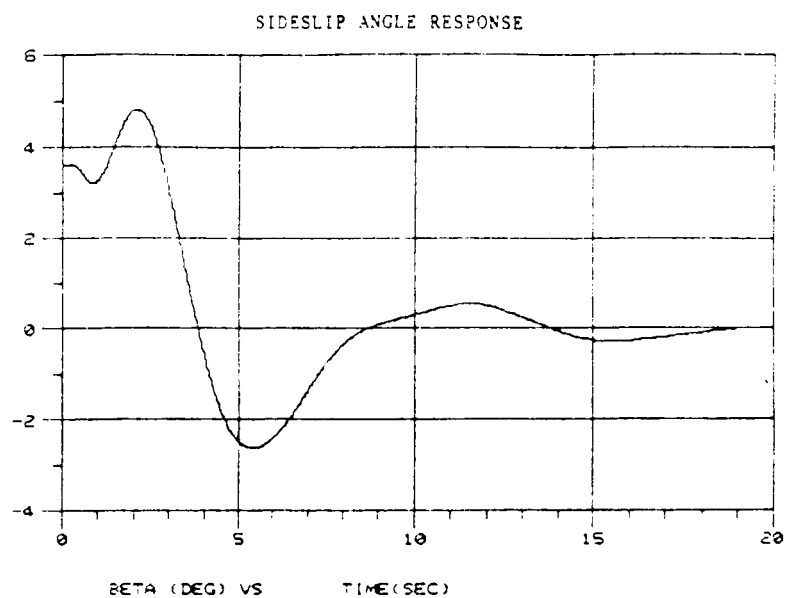


Plot V.A.3.-13. - Roll angle response during a coordinated turn maneuver by a multi-variable McRuer-Krendel pilot inserted in the Black Hawk UH-60A

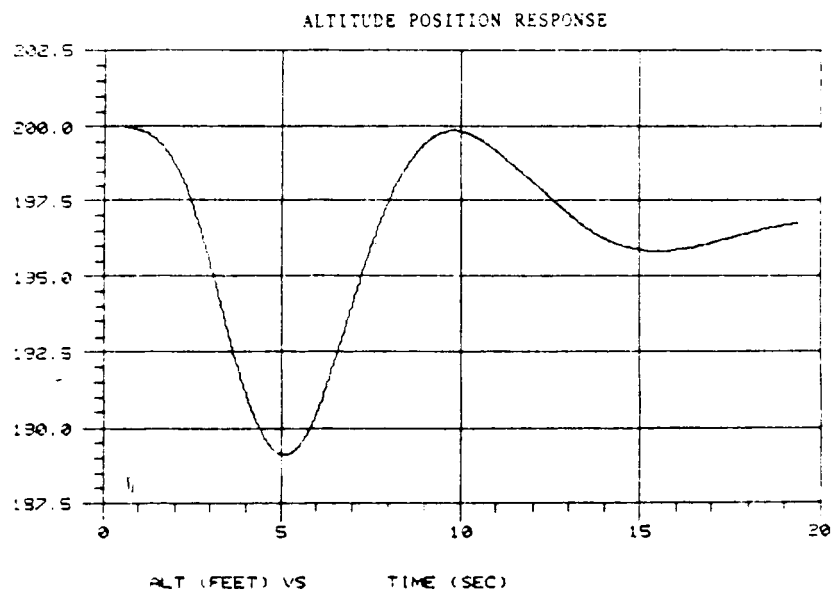


Plot V.A.3.-14. - Yaw angle response during a coordinated turn maneuver by a multi-variable McRuer-Krendel pilot inserted in the Black Hawk UH-60A

ORIGINAL PAGE IS
OF POOR QUALITY

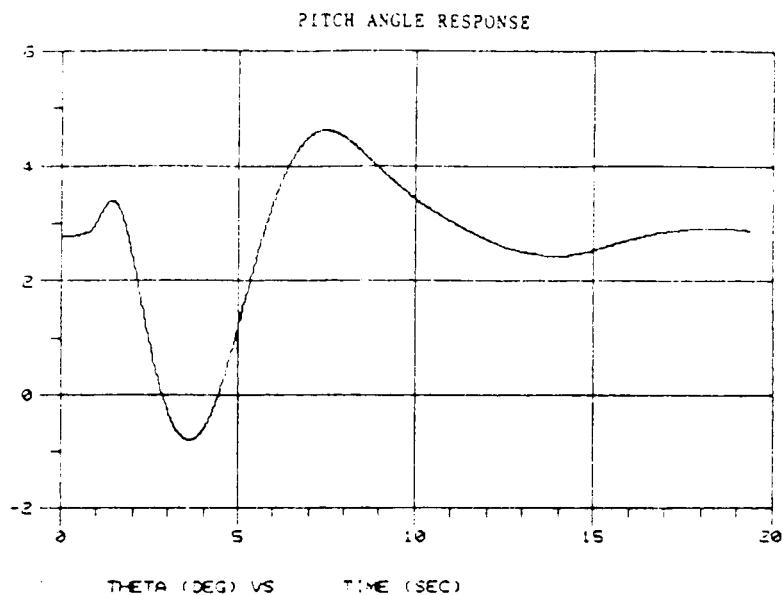


Plot V.A.3.-15. - Sideslip angle response during a coordinated turn maneuver by a multi-variable McRuer-Krendel pilot inserted in the Black Hawk UH-60A

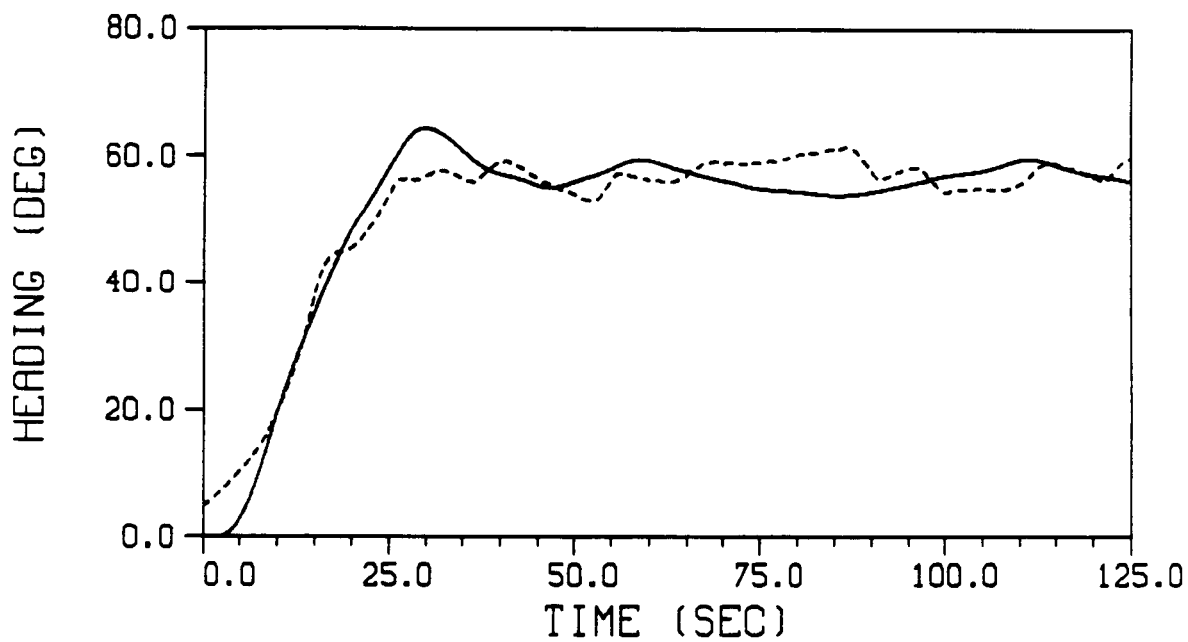


Plot V.A.3.-16. - Altitude response during a coordinated turn maneuver by a multi-variable McRuer-Krendel pilot inserted in the Black Hawk UH-60A

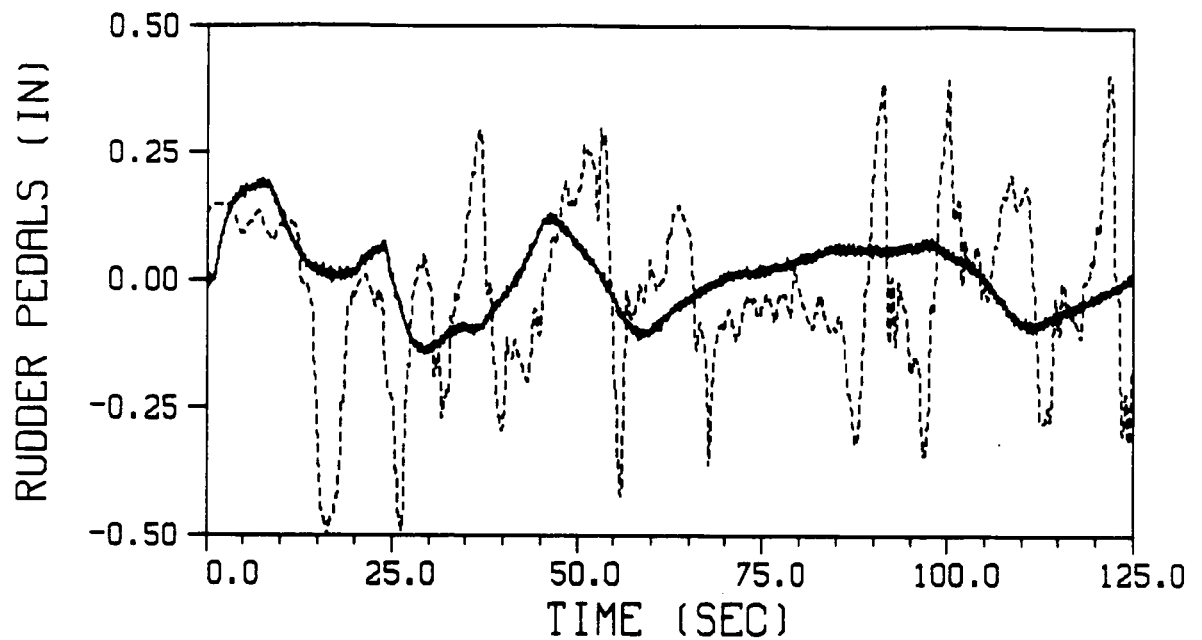
ORIGINAL PAGE IS
OF POOR QUALITY



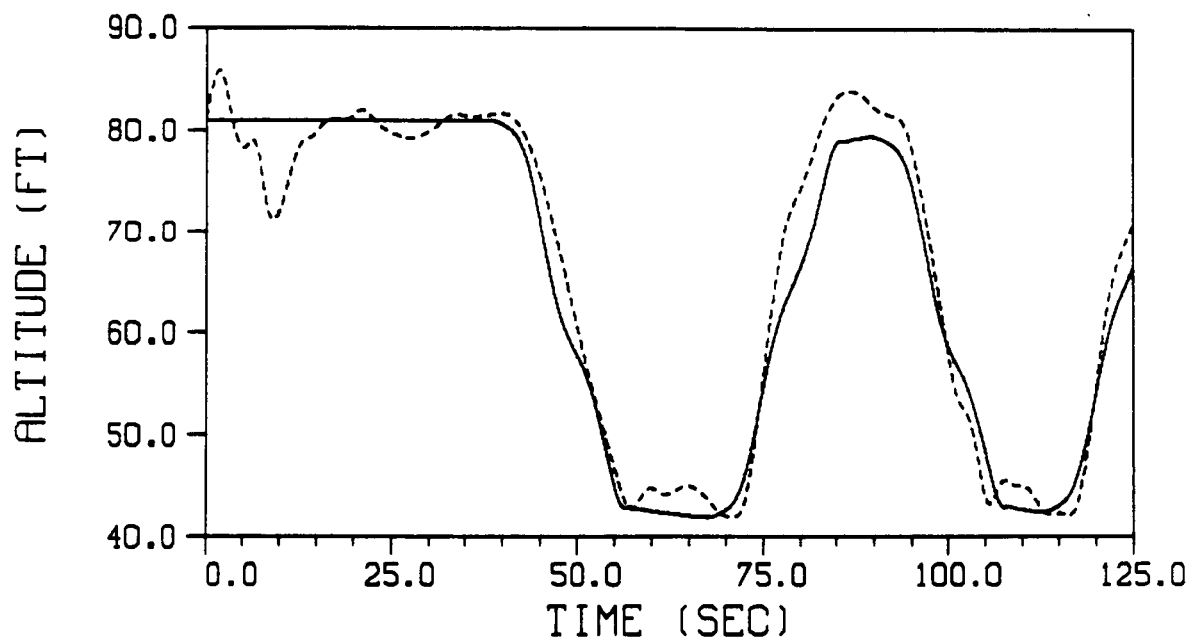
Plot V.A.3.-17. - Pitch angle response during a coordinated turn maneuver by a multi-variable McRuer-Krendel pilot inserted in the Black Hawk UH-60A



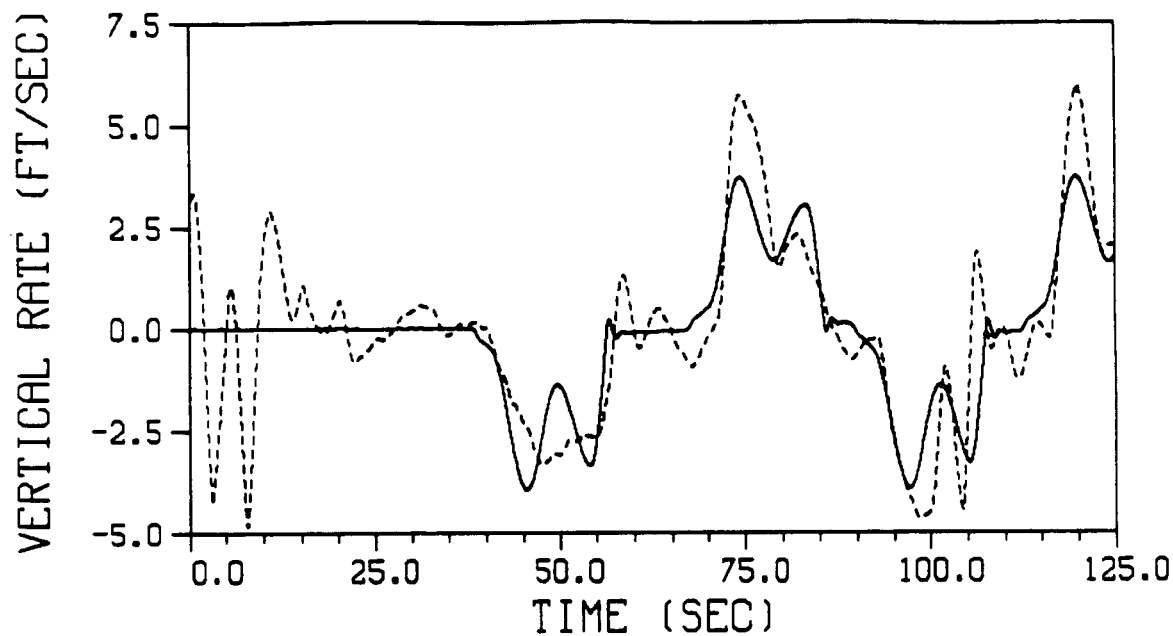
Plot V.B.4.-1. - Heading response comparison of the OCM pilot and piloted flight data during the vertical tracking maneuver.



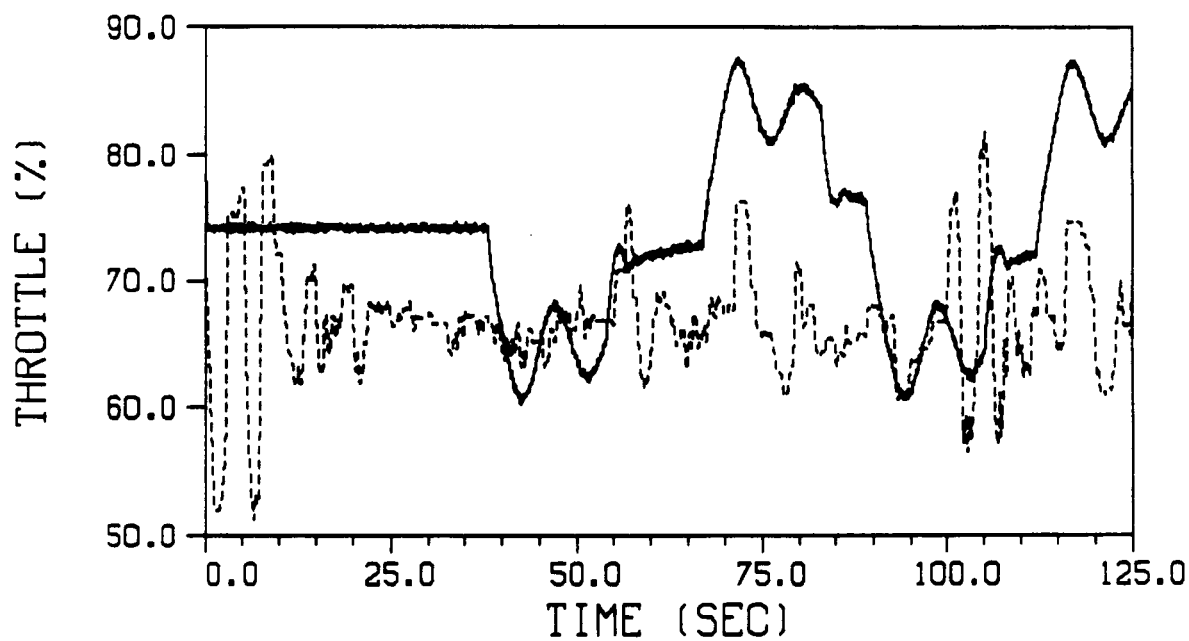
Plot V.B.4.-2. - Rudder pedal deflection response comparison of the OCM pilot and piloted flight data during the vertical tracking maneuver.



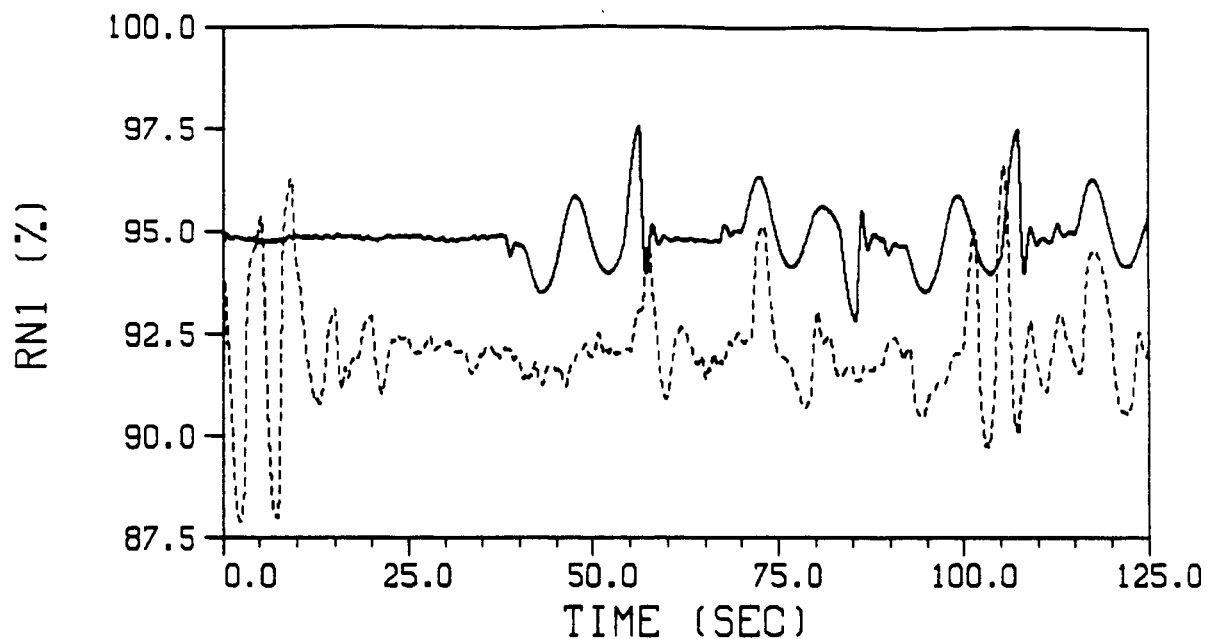
Plot V.B.4.-3. - Altitude response comparison of the OCM pilot and piloted flight data during the vertical tracking maneuver.



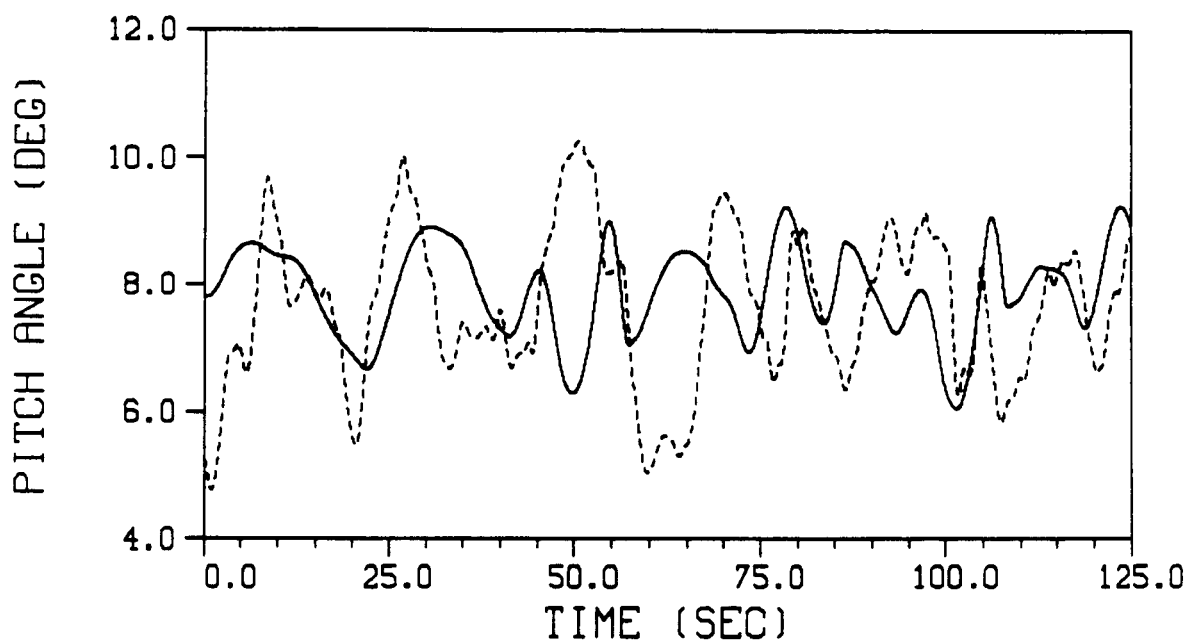
Plot V.B.4.-4. - Vertical rate response comparison of the OCM pilot and piloted flight data during the vertical tracking maneuver.



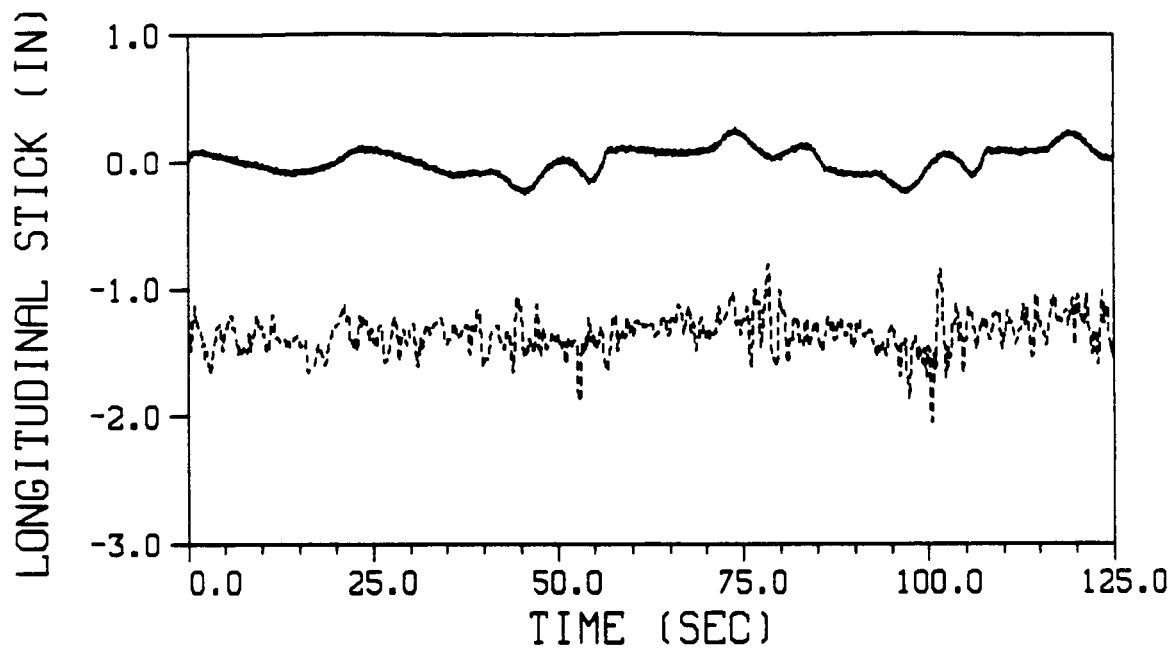
Plot V.B.4.-5. - Throttle deflection response comparison of the OCM pilot and piloted flight data during the vertical tracking maneuver.



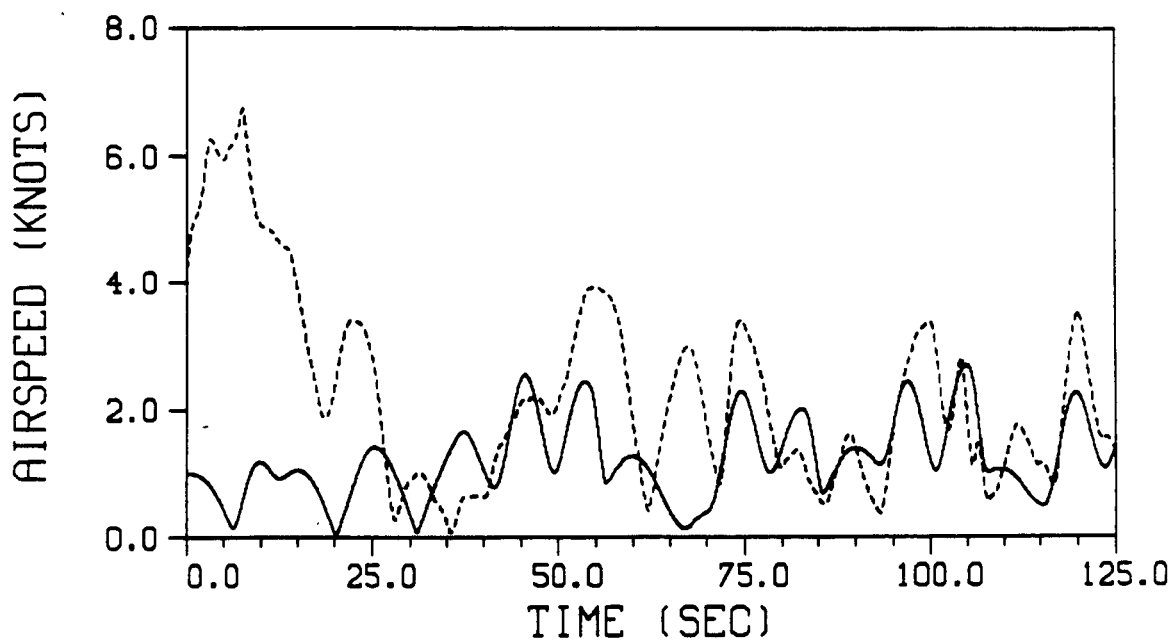
Plot V.B.4.-6. - Engine speed comparison of the OCM pilot and piloted flight data during the vertical tracking maneuver.



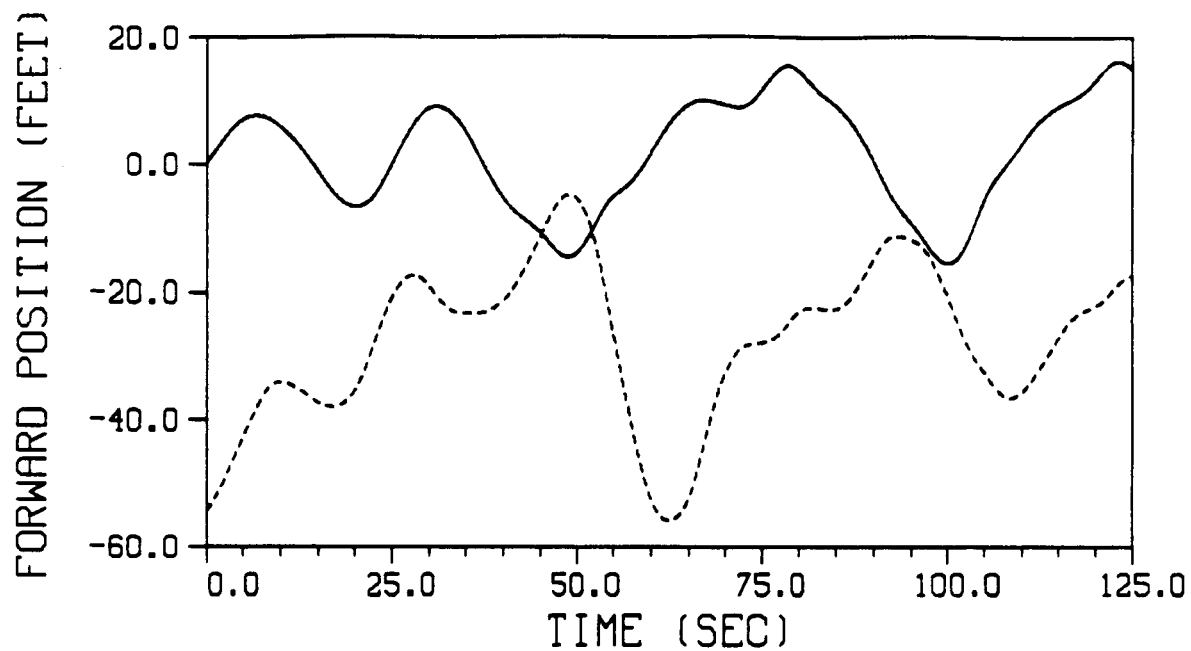
Plot V.B.4.-7. - Pitch angle response comparison of the OCM pilot and piloted flight data during the vertical tracking maneuver.



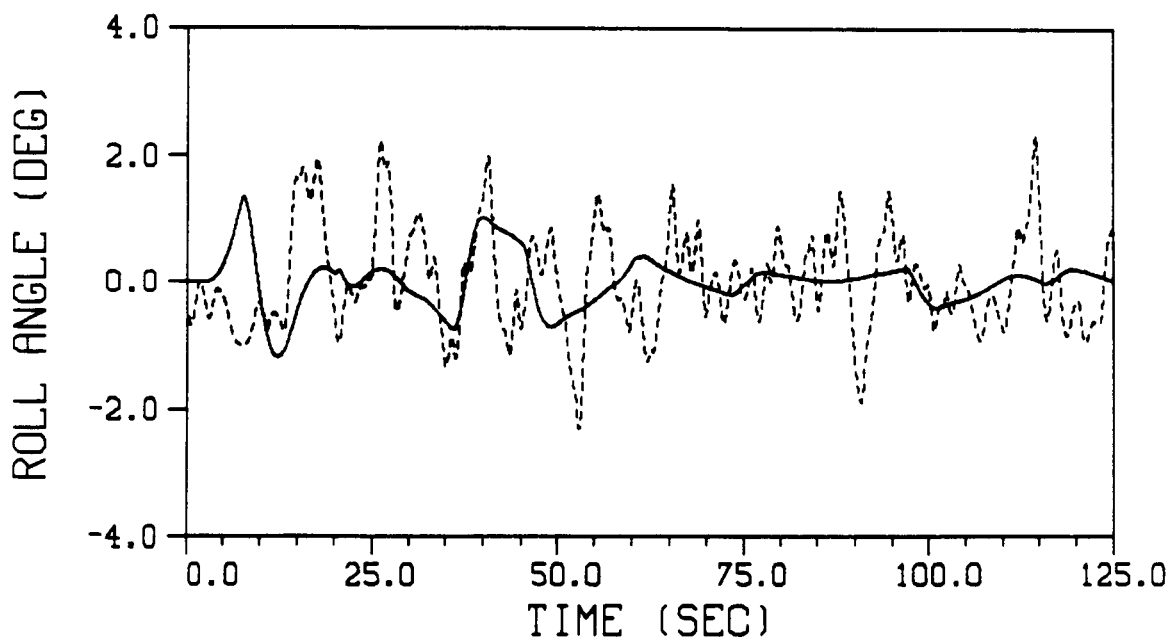
Plot V.B.4.-8. - Longitudinal stick operation comparison of the OCM pilot and piloted flight data during the vertical tracking maneuver.



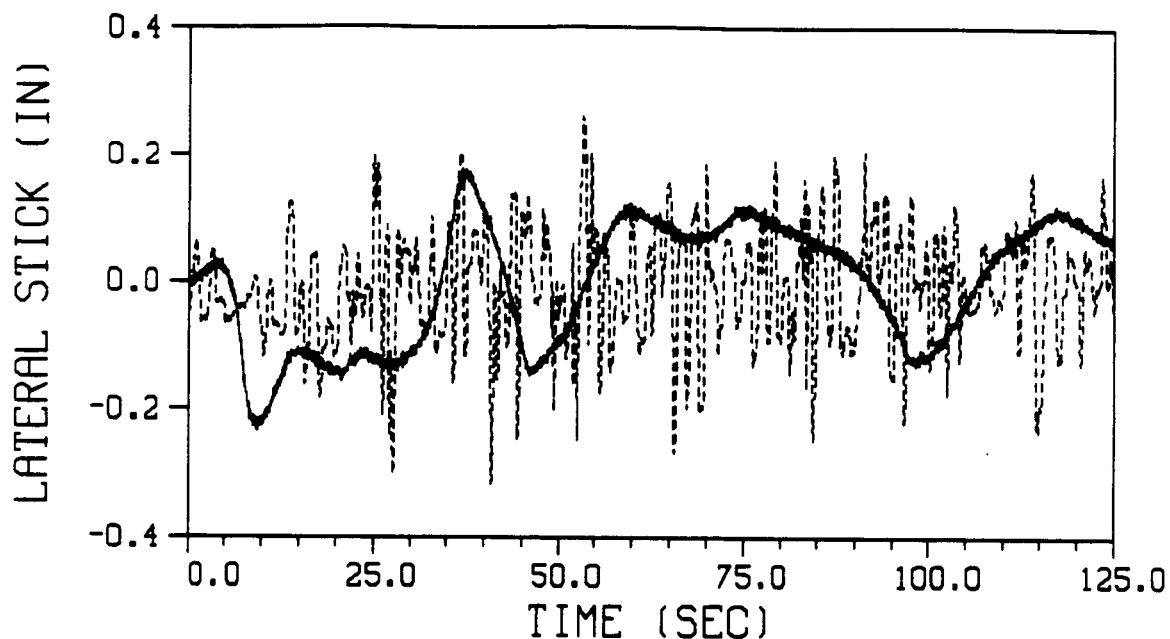
Plot V.B.4.-9. - Airspeed response comparison of the OCM pilot and piloted flight data during the vertical tracking maneuver.



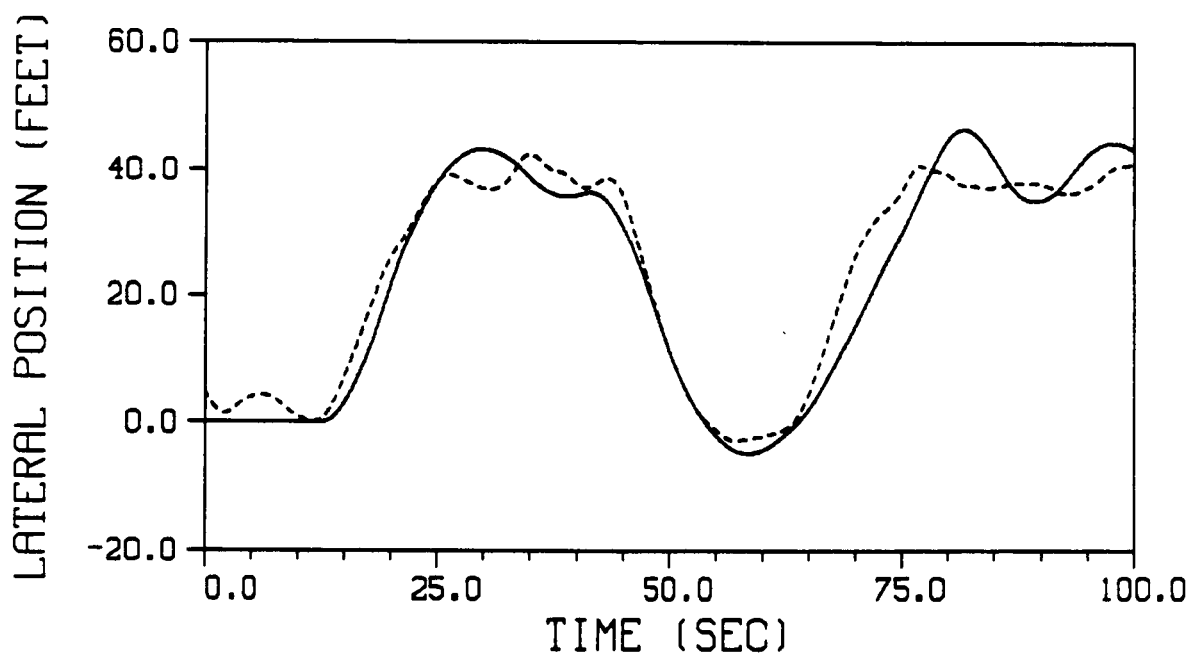
Plot V.B.4.-10. - Longitudinal position comparison of the OCM pilot and piloted flight data during the vertical tracking maneuver.



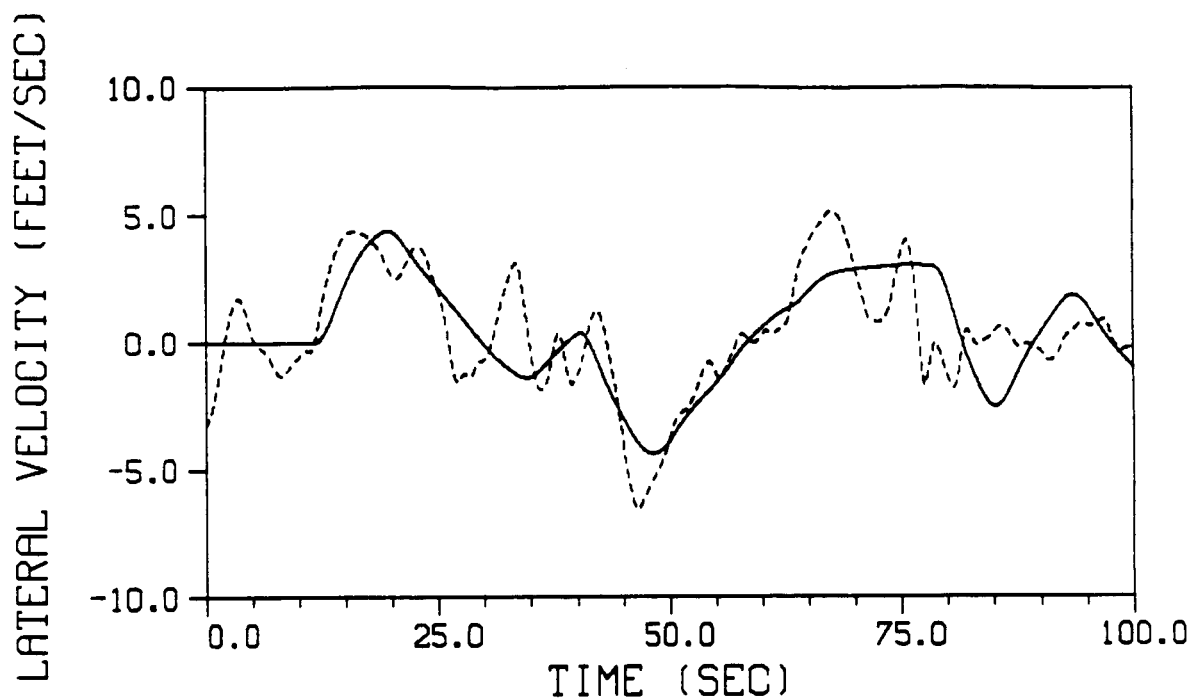
Plot V.B.4.-11. - Roll angle response comparison of the OCM pilot and piloted flight data during the vertical tracking maneuver.



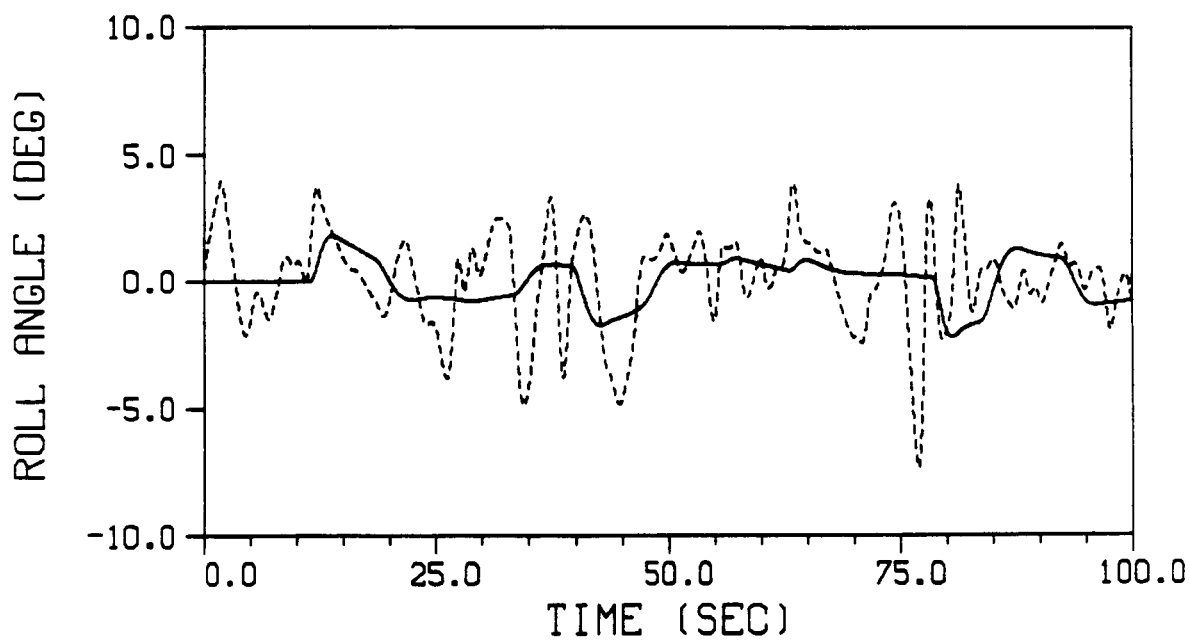
Plot V.B.4.-12. - Lateral stick operation comparison of the OCM pilot and piloted flight data during the vertical tracking maneuver.



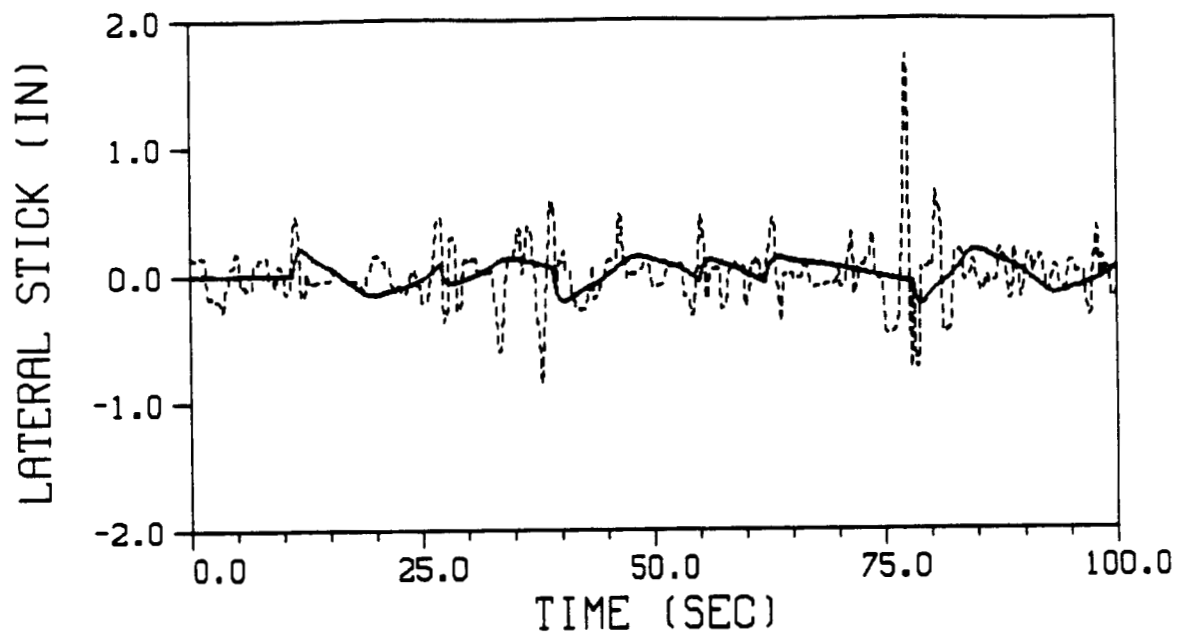
Plot V.B.4.-13. - Lateral position response comparison of the OCM pilot and piloted flight data during the lateral tracking maneuver.



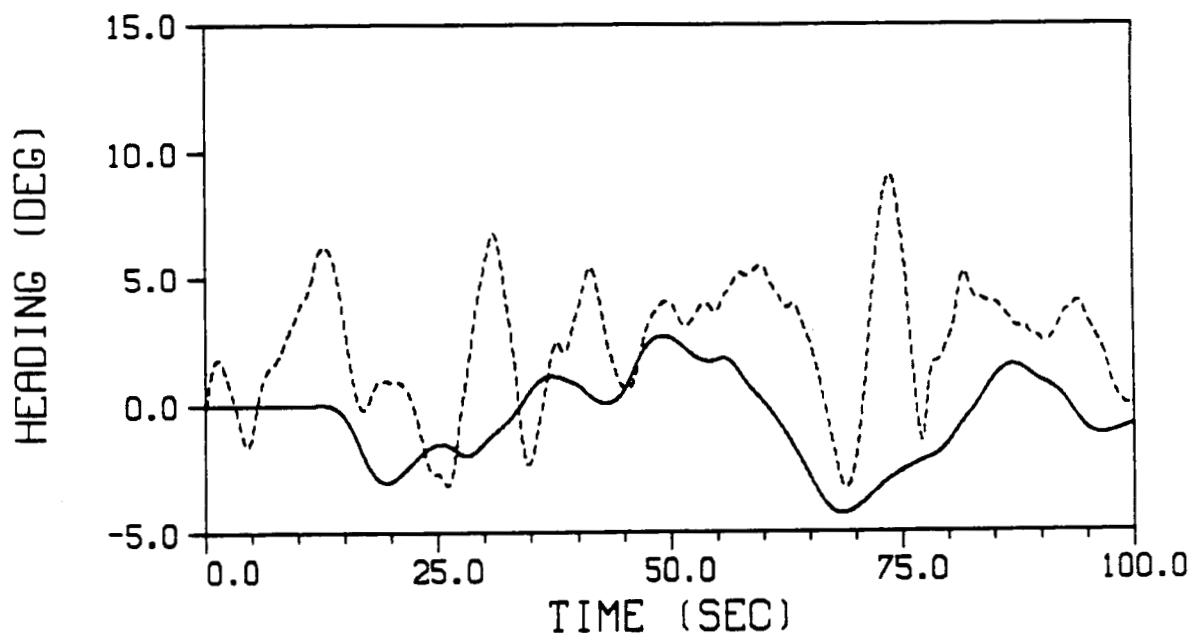
Plot V.B.4.-14. - Lateral velocity response comparison of the OCM pilot and piloted flight data during the lateral tracking maneuver.



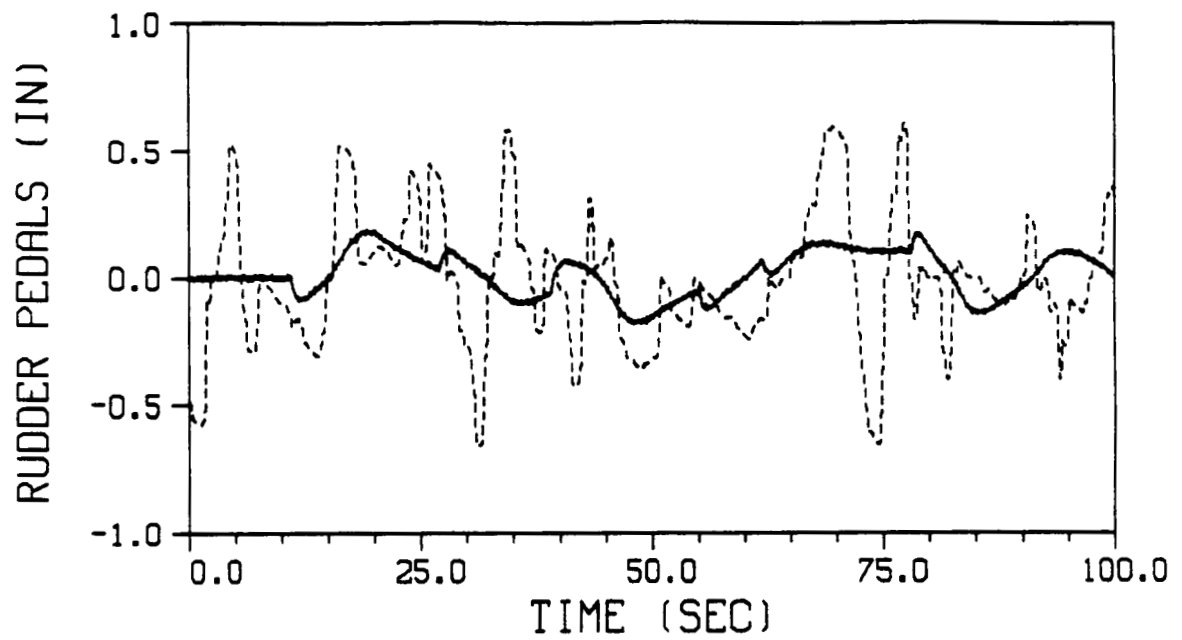
Plot V.B.4.-15. - Roll angle response comparison of the OCM pilot and piloted flight data during the lateral tracking maneuver.



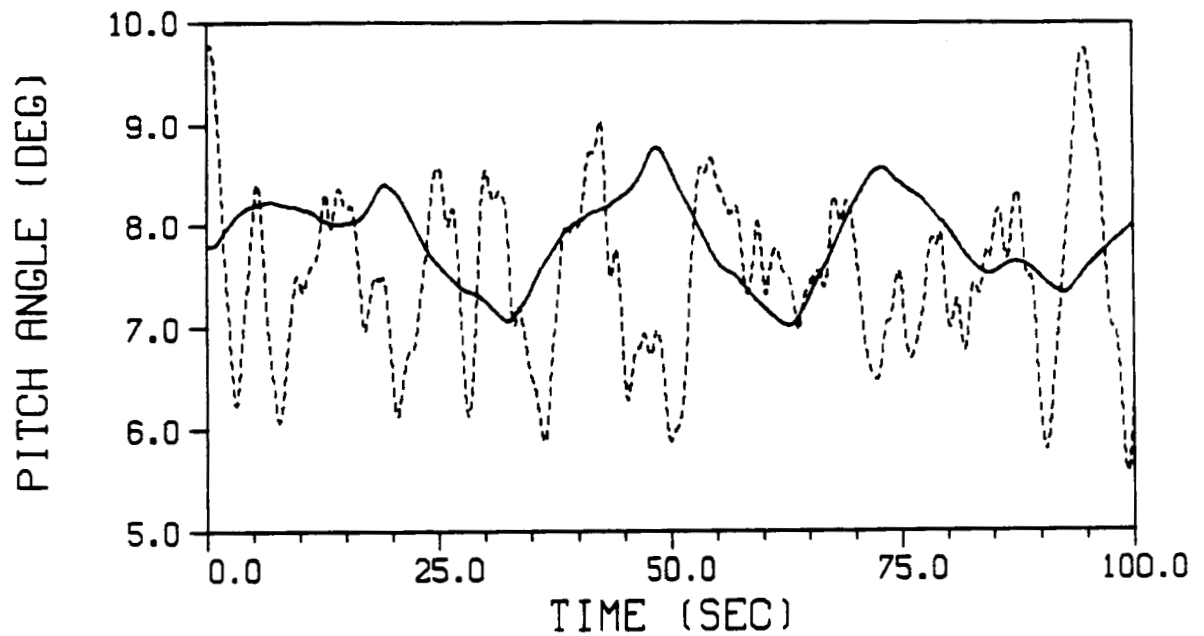
Plot V.B.4.-16. - Lateral stick operation comparison of the OCM pilot and piloted flight data during the lateral tracking maneuver.



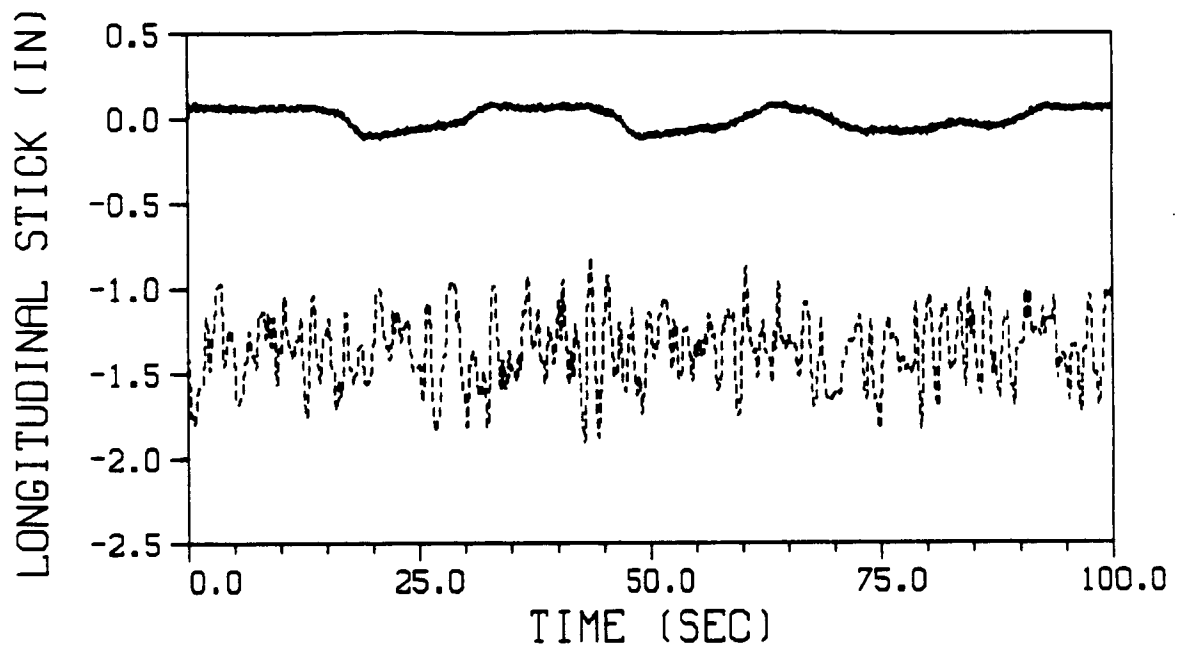
Plot V.B.4.-17. - Heading angle response comparison of the OCM pilot and piloted flight data during the lateral tracking maneuver.



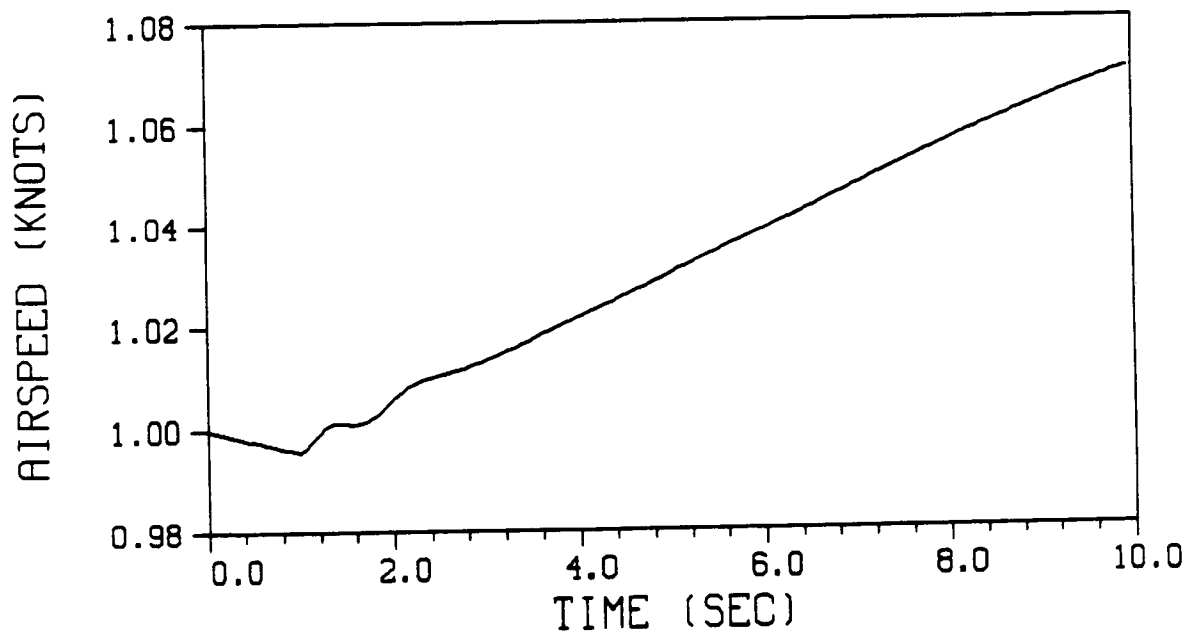
Plot V.B.4.-18. - Rudder pedal operation comparison of the OCM pilot and piloted flight data during the lateral tracking maneuver.



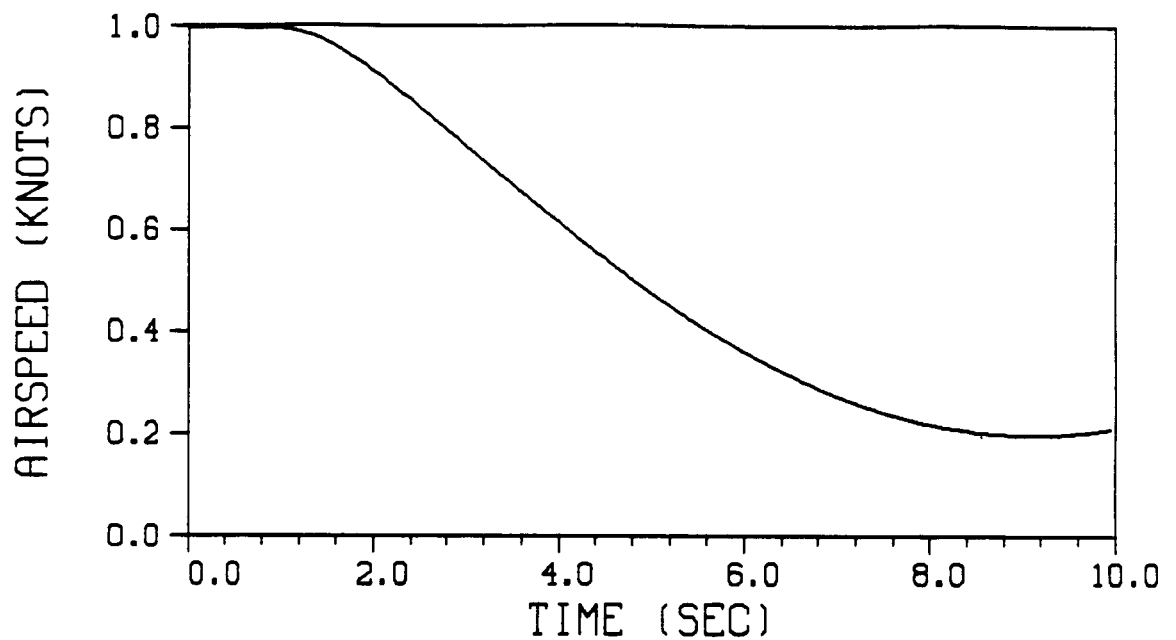
Plot V.B.4.-19. - Pitch angle response comparison of the OCM pilot and piloted flight data during the lateral tracking maneuver.



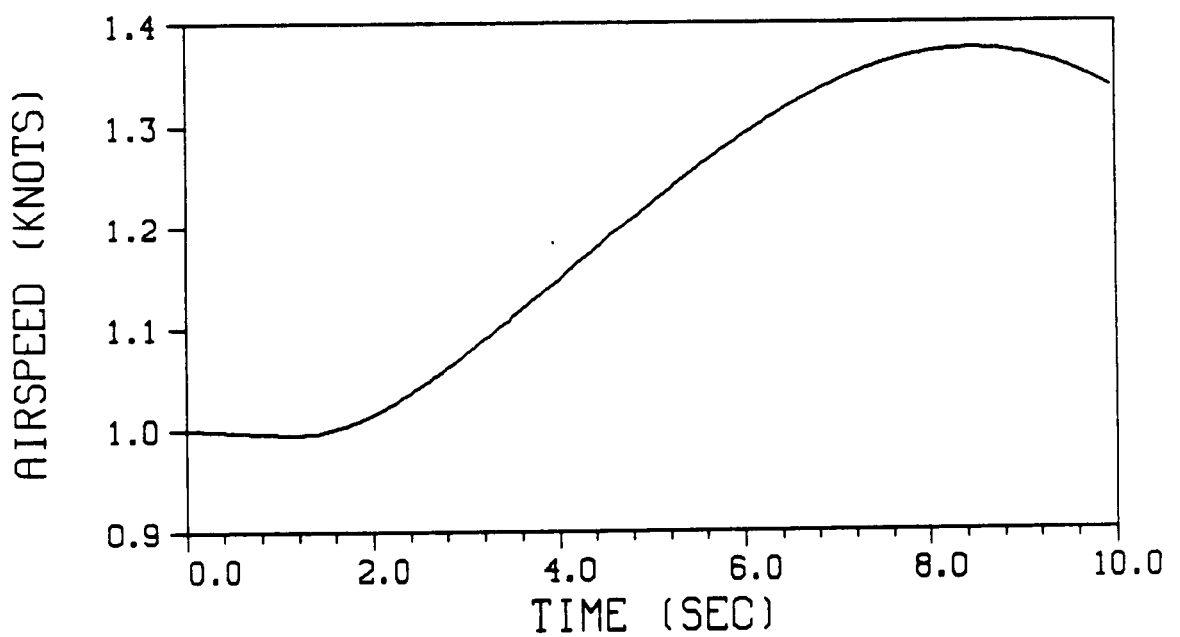
Plot V.B.4.-20. - Longitudinal stick operation comparison of the OCM pilot and piloted flight data during the lateral tracking maneuver.



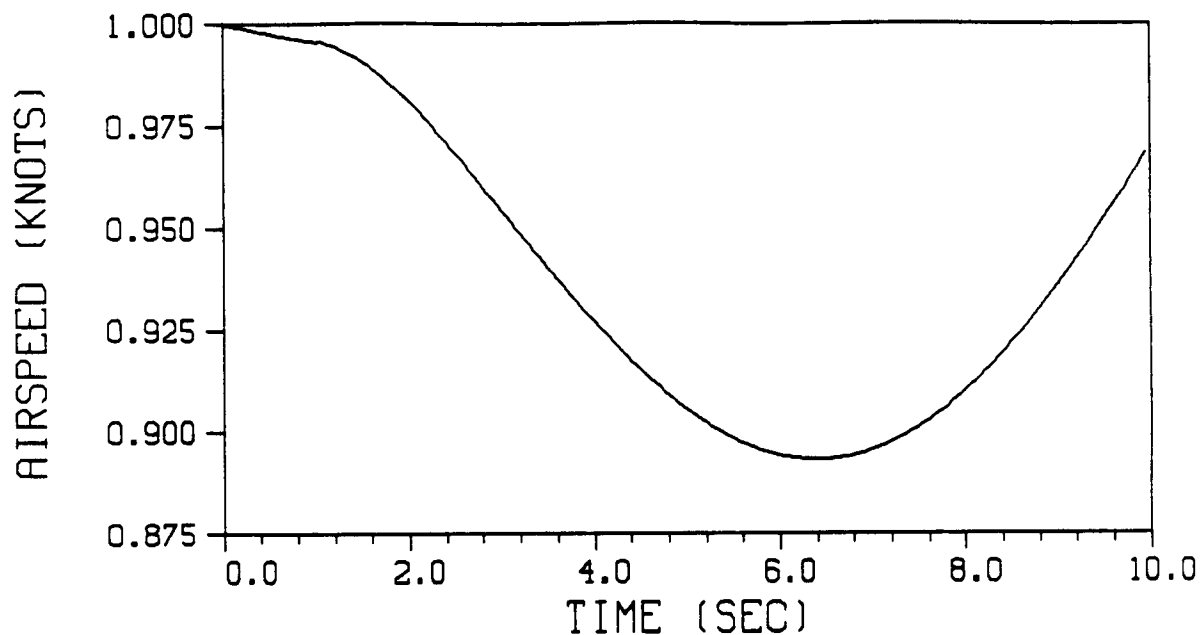
Plot B.1.-1. - Forward velocity response of the Harrier AV-8B due to a 10 percent positive impulse of the throttle.



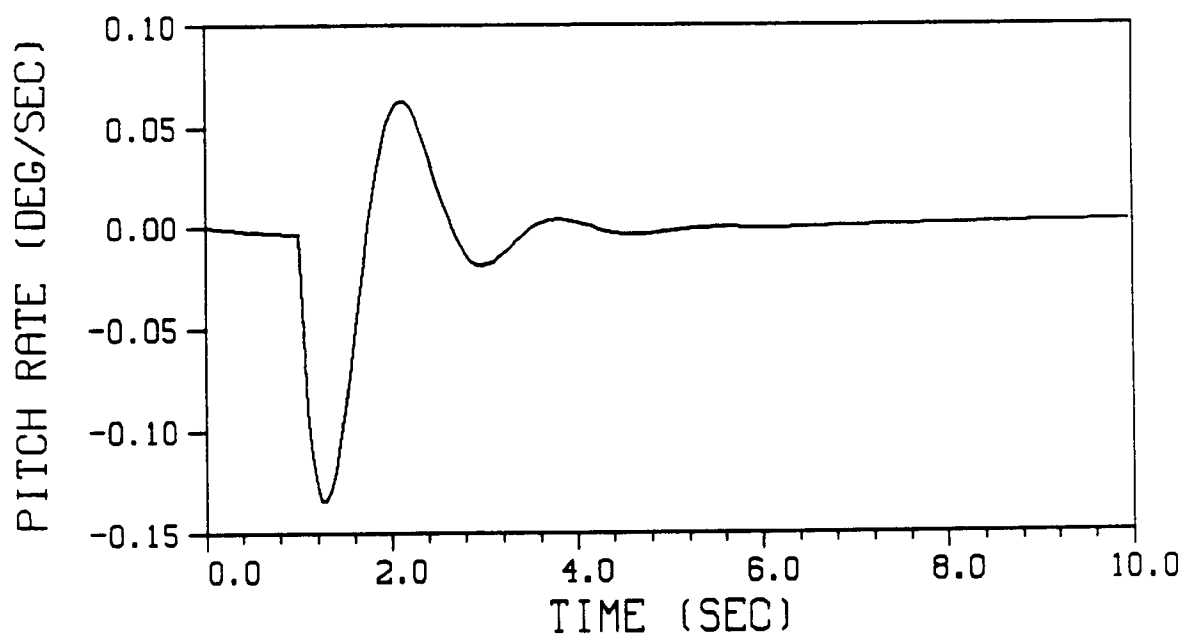
Plot B.1.-2. - Forward velocity response of the Harrier AV-8B due to a 1 inch impulse on the longitudinal stick while in a near hover.



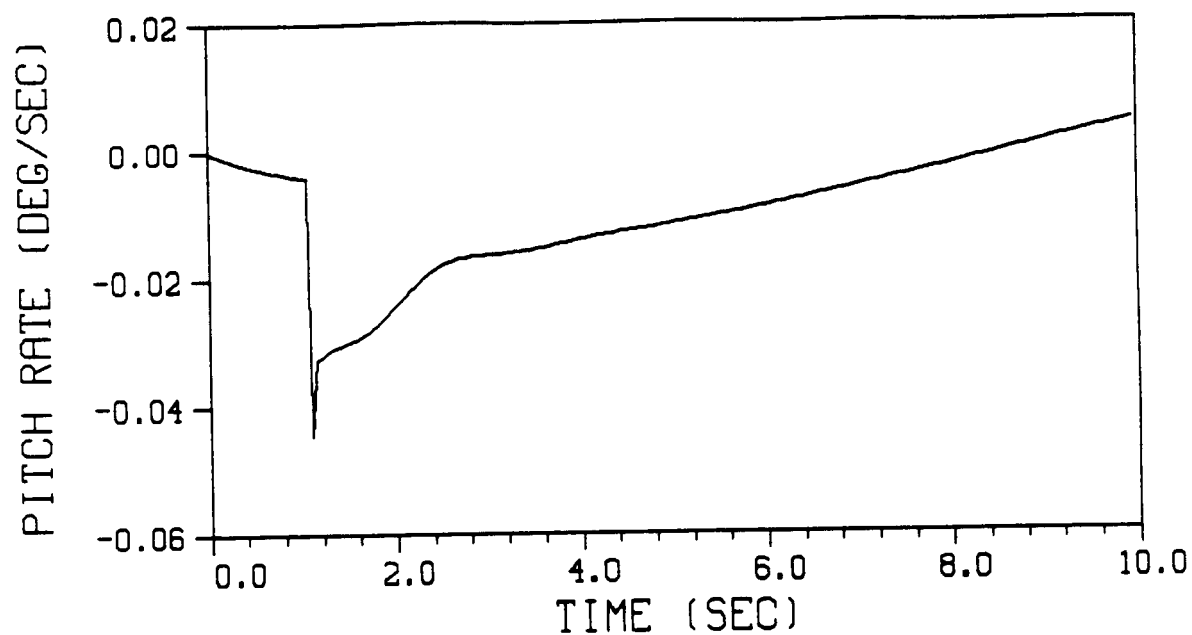
Plot B.1.-3. - Short period response of the Harrier AV-8B forward velocity due to an impulse of the lateral stick.



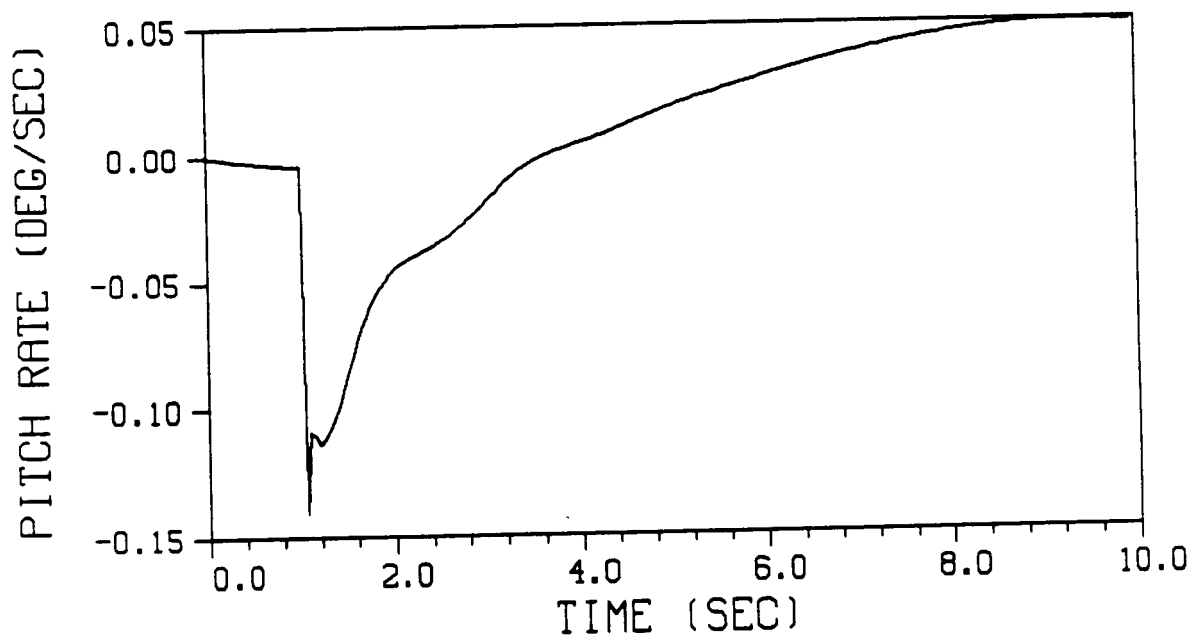
Plot B.1.-4. - Short period response of the Harrier AV-8B forward velocity due to an impulse of the rudder pedals.



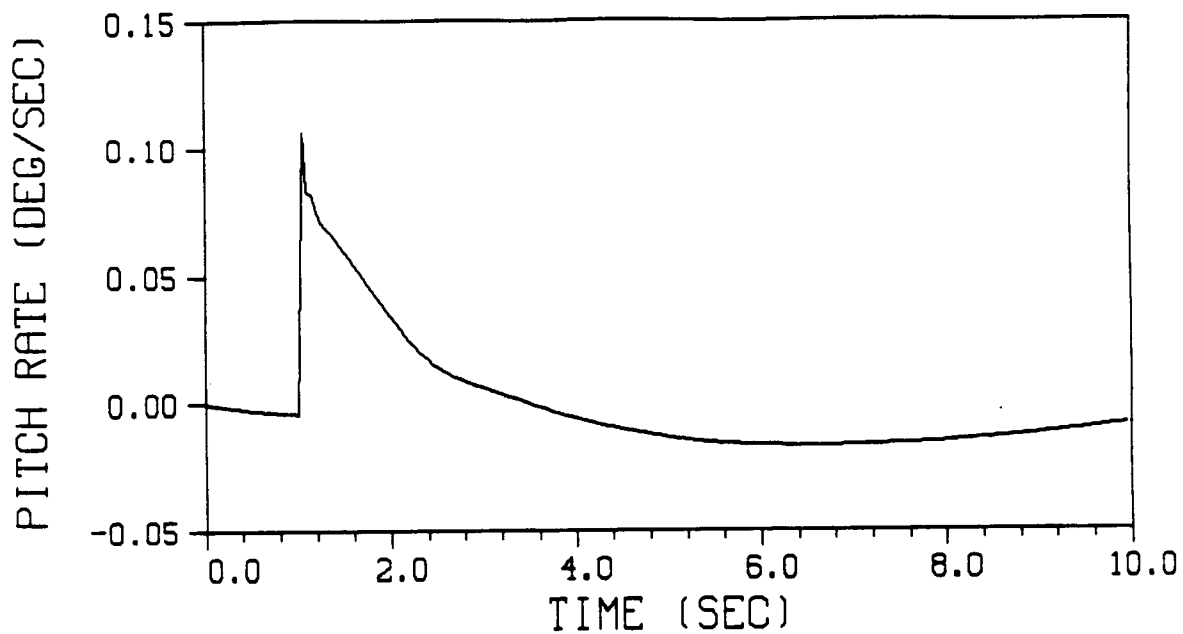
Plot B.1.-5. - Simulation model pitch rate response of the Harrier AV-8B due to a 10 percent impulse of the throttle.



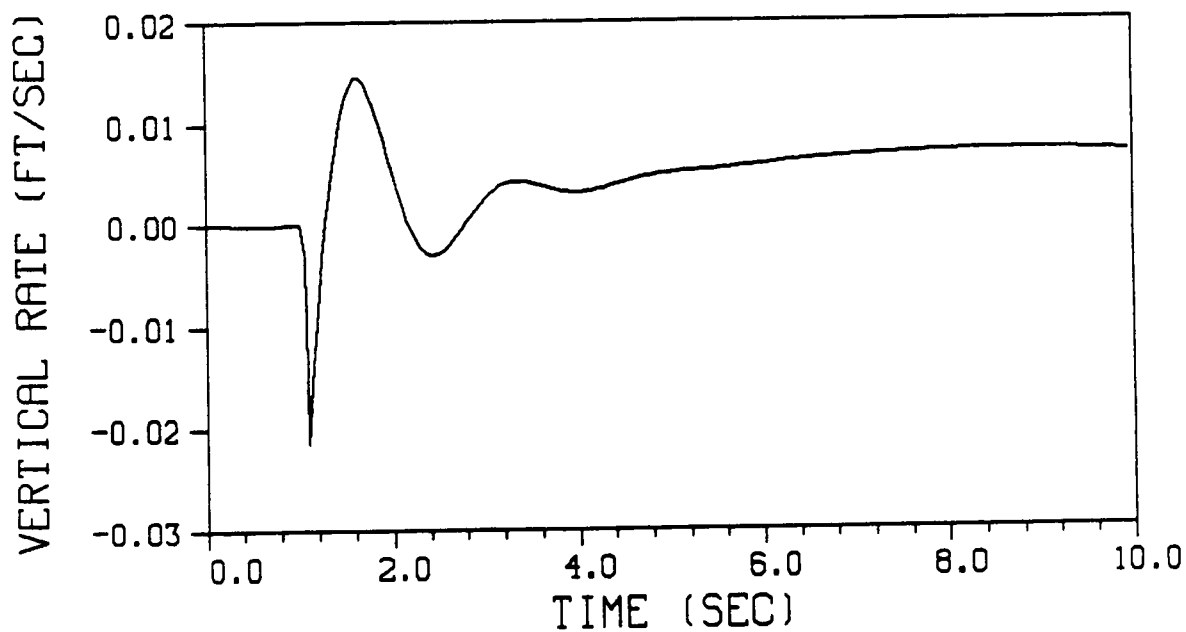
Plot B.1.-6. - Simulation model pitch rate response of the Harrier AV-8B due to a 5 degree impulse of the nozzle angle.



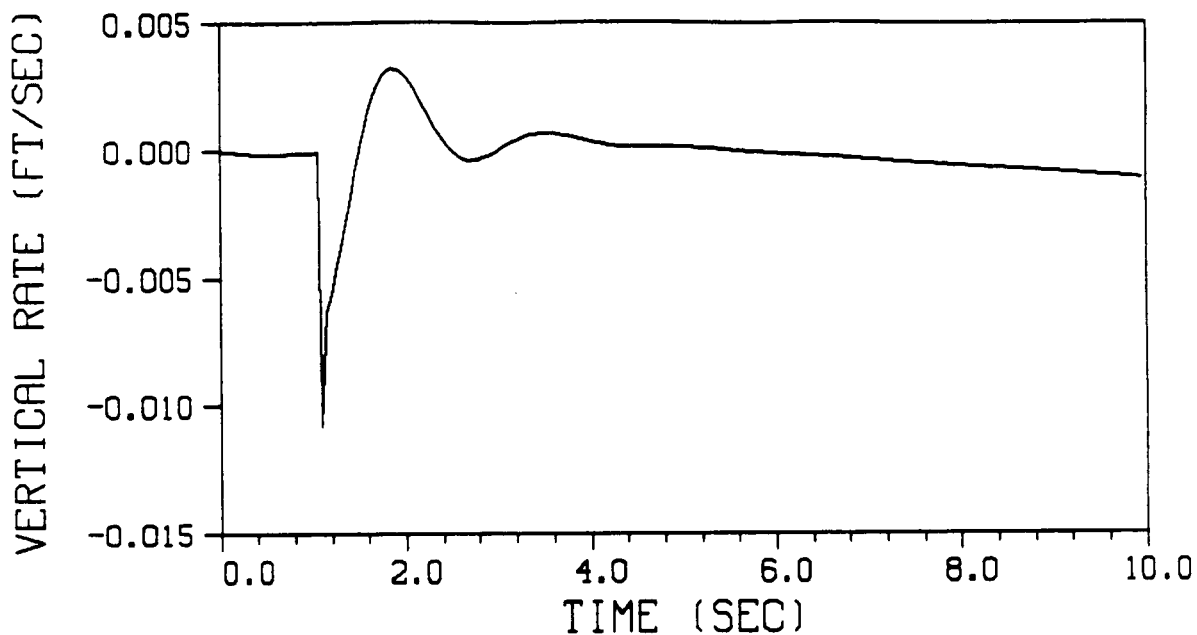
Plot B.1.-7. - Short period response of the Harrier AV-8B pitch rate due to an impulse of the lateral stick.



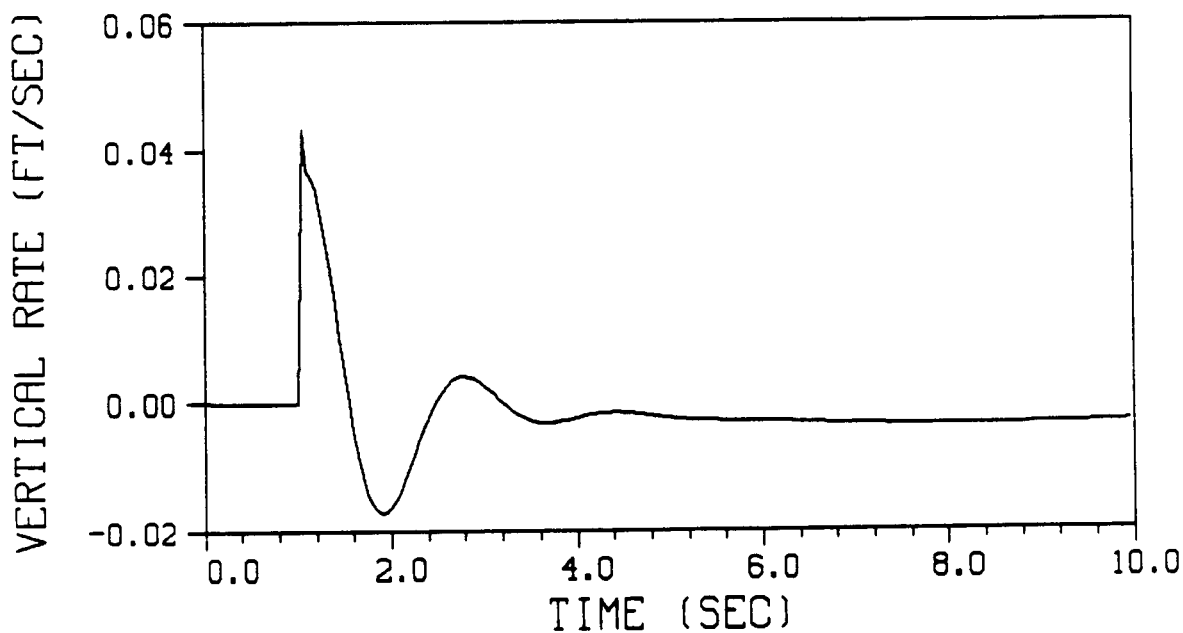
Plot B.1.-8. - Short period response of the Harrier AV-8B pitch rate due to an impulse of the rudder pedals.



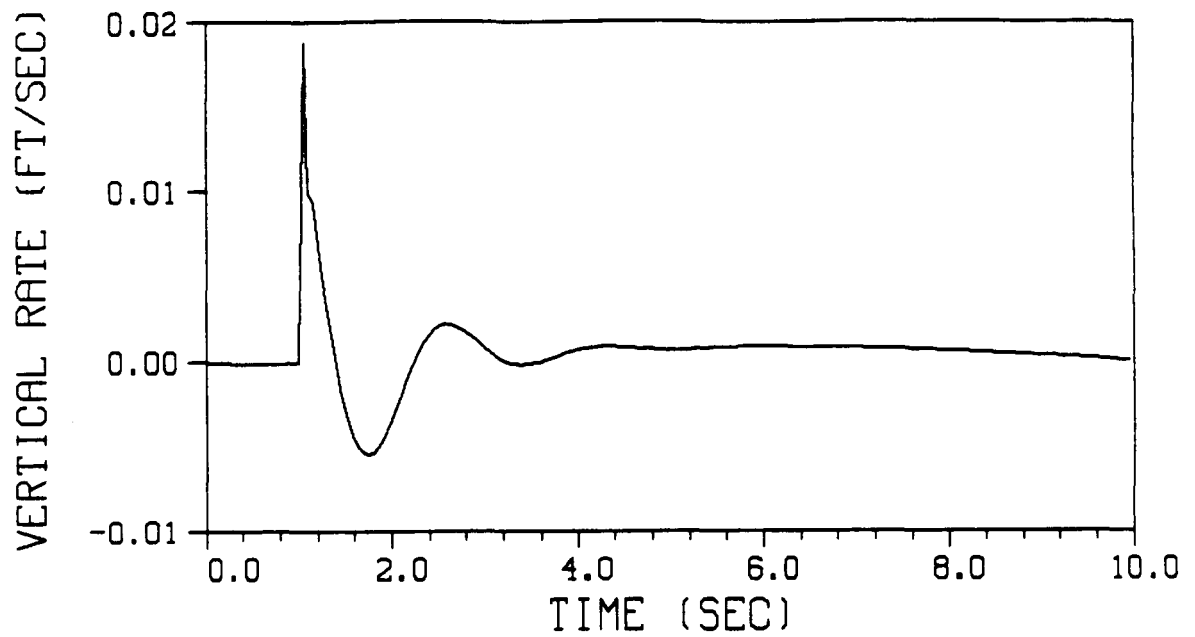
Plot B.1.-9. - Simulation model vertical rate response of the Harrier AV-8B due to a 1 inch impulse of the longitudinal stick.



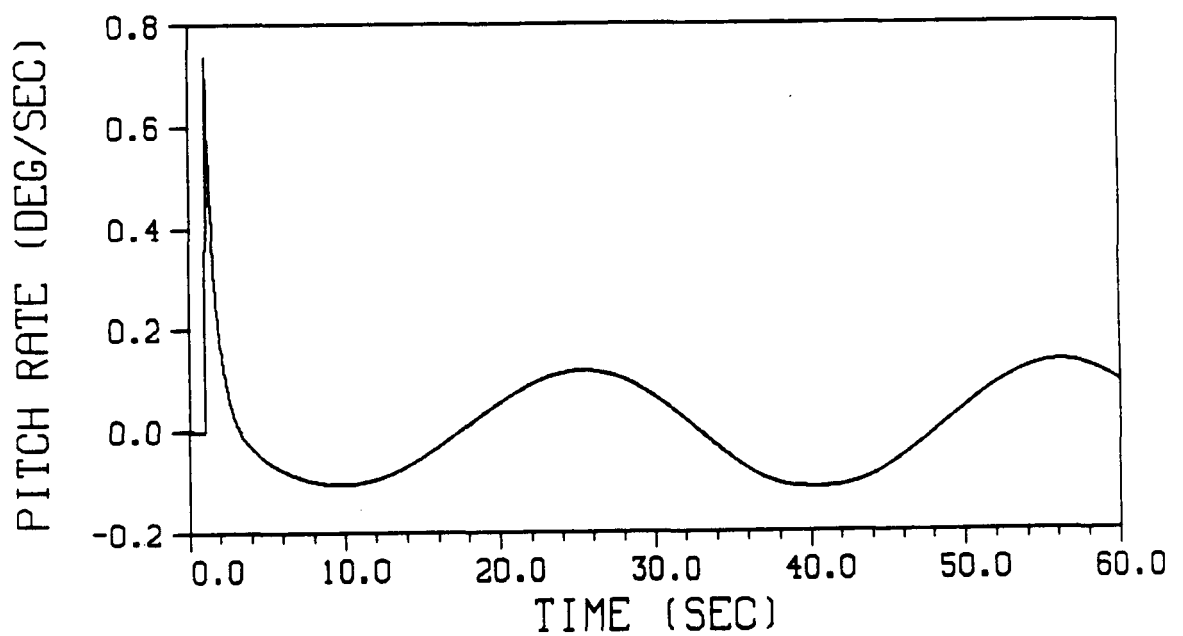
Plot B.1.-10. - Simulation model vertical rate response of the Harrier AV-8B due to a 5 degree impulse of the nozzle angle.



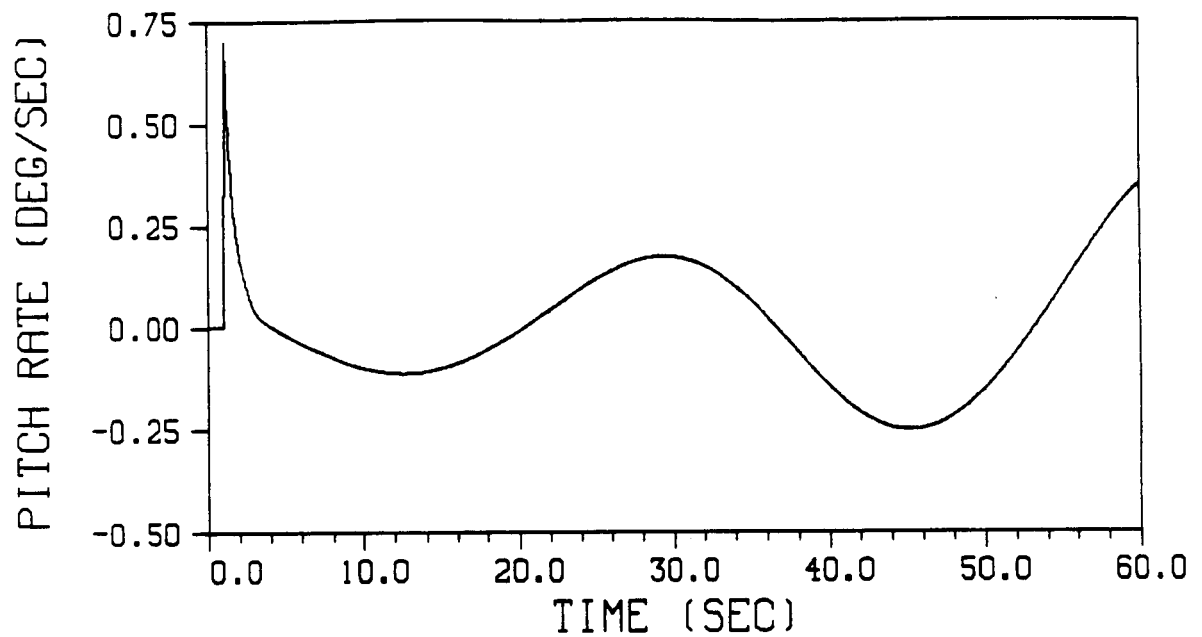
Plot B.1.-11. - Short period response of the Harrier AV-8B vertical rate due to an impulse of the lateral stick.



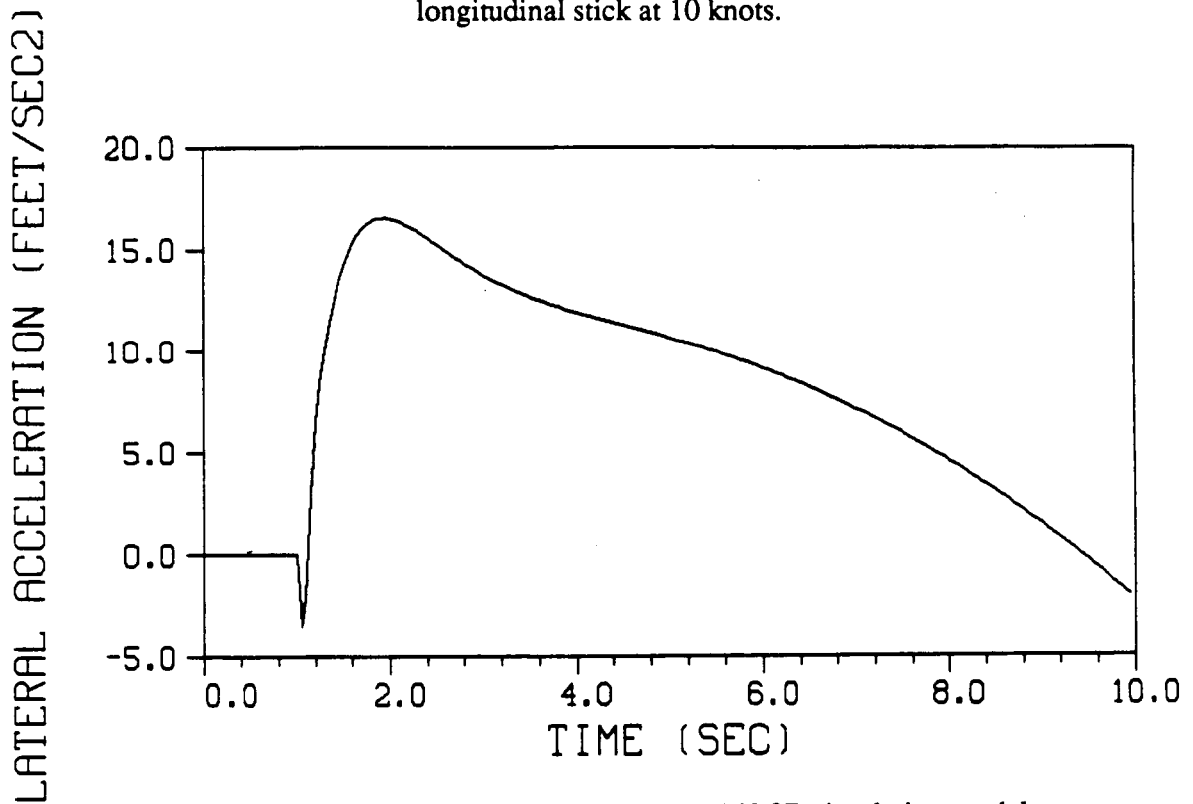
Plot B.1.-12. - Short period response of the Harrier AV-8B vertical rate due to an impulse of the rudder pedals.



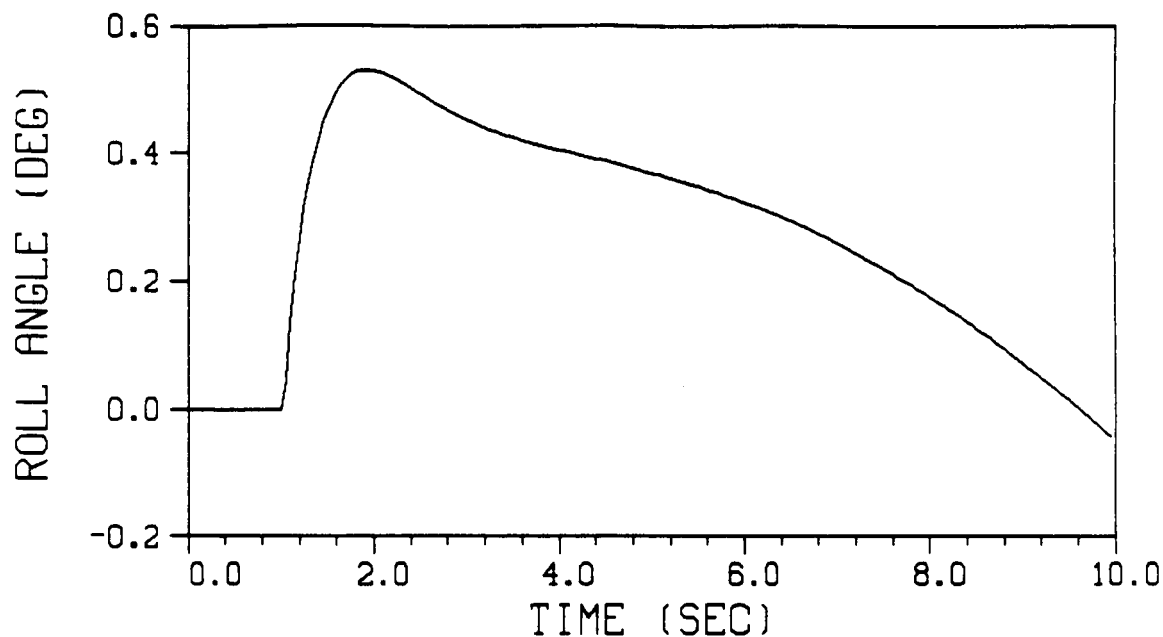
Plot B.1.-13. - Pitch rate response of the Harrier AV-8B due to an impulse of the longitudinal stick at a near hover.



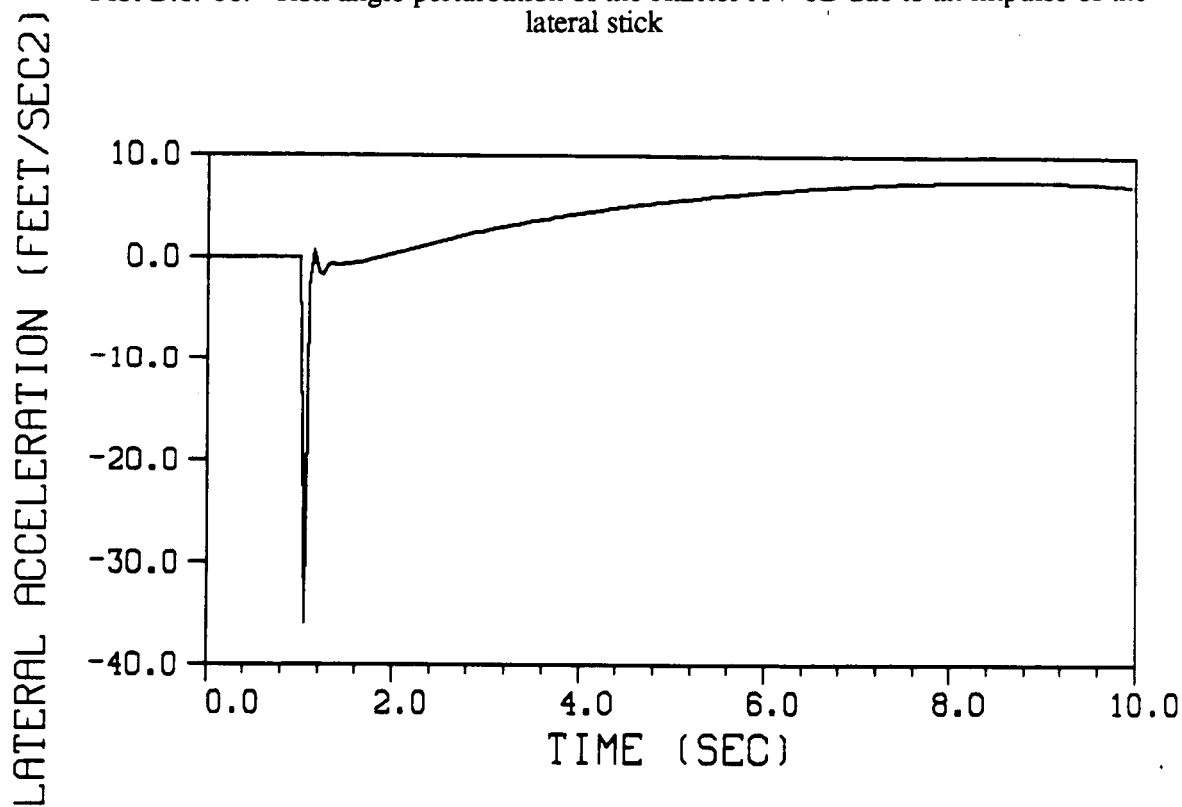
Plot B.1.-14. - Pitch rate response of the Harrier AV-8B due to an impulse of the longitudinal stick at 10 knots.



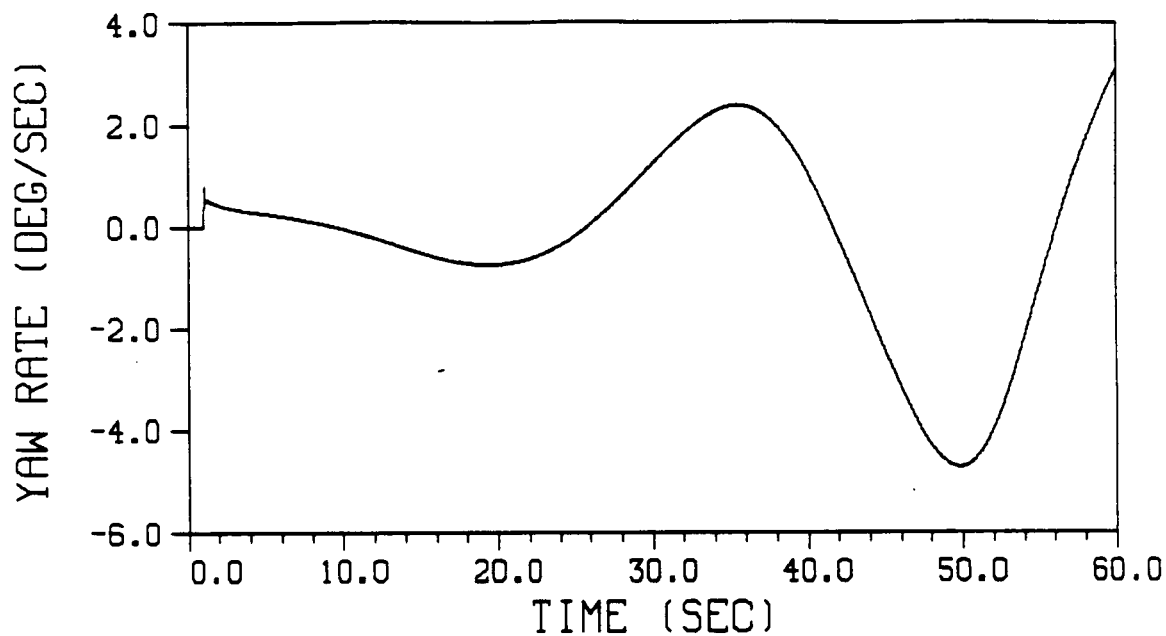
Plot B.1.-15. - Lateral acceleration of the Harrier AV-8B simulation model program due to the roll angle of Plot B.1.-16.



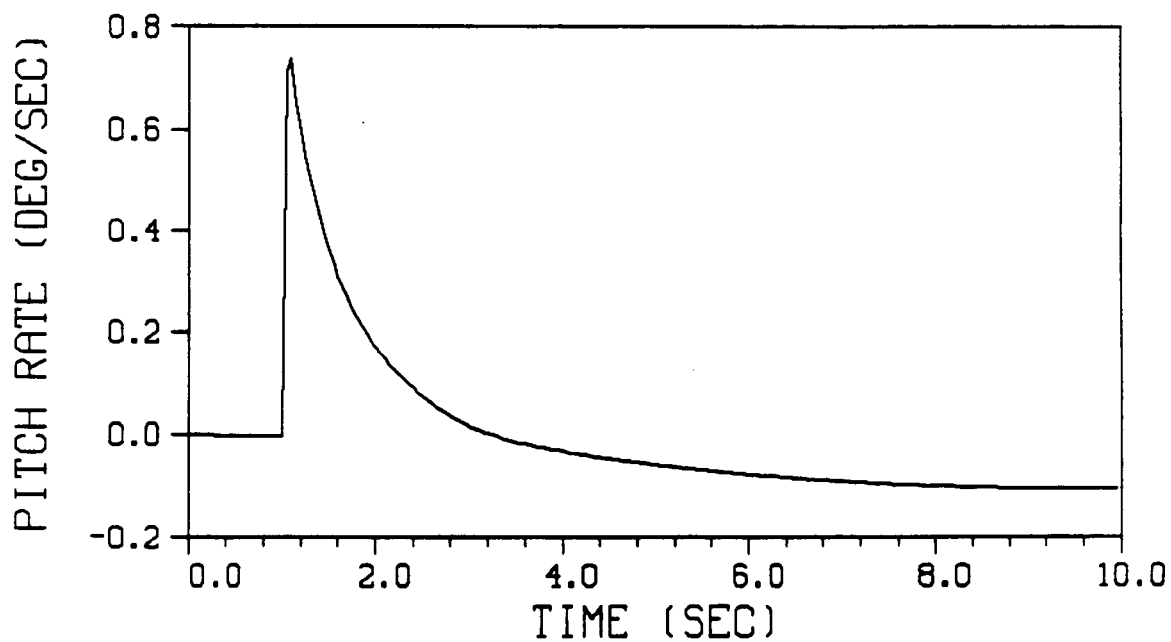
Plot B.1.-16. - Roll angle perturbation of the Harrier AV-8B due to an impulse of the lateral stick



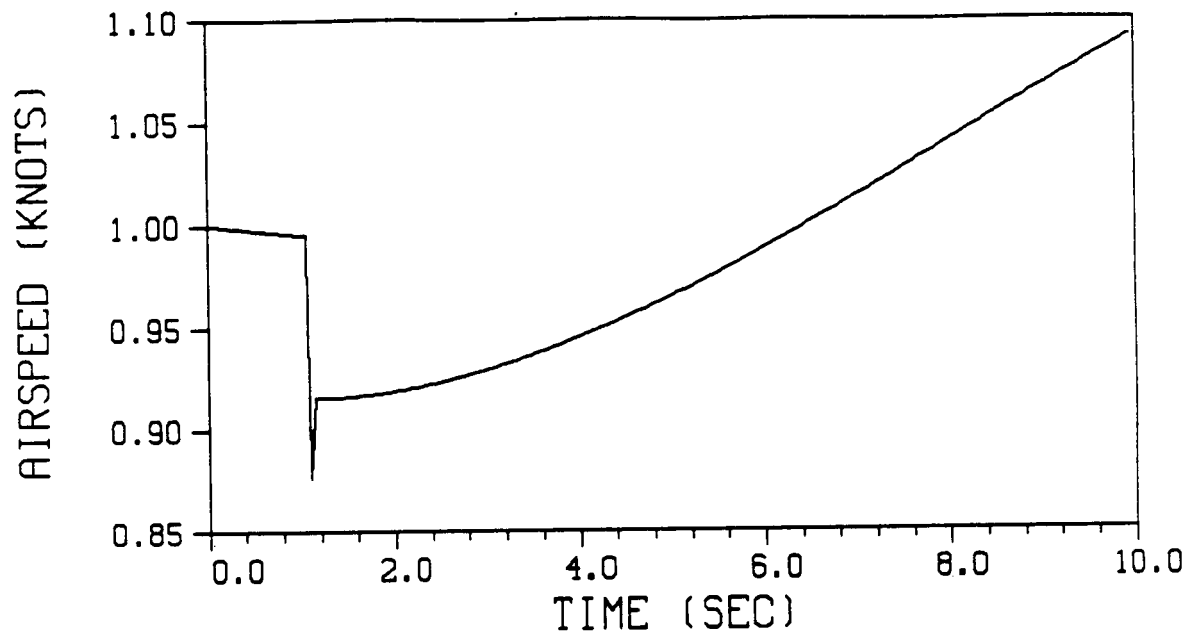
Plot B.1.-17. - Lateral acceleration of the Harrier AV-8B due to an impulse of the rudder pedals.



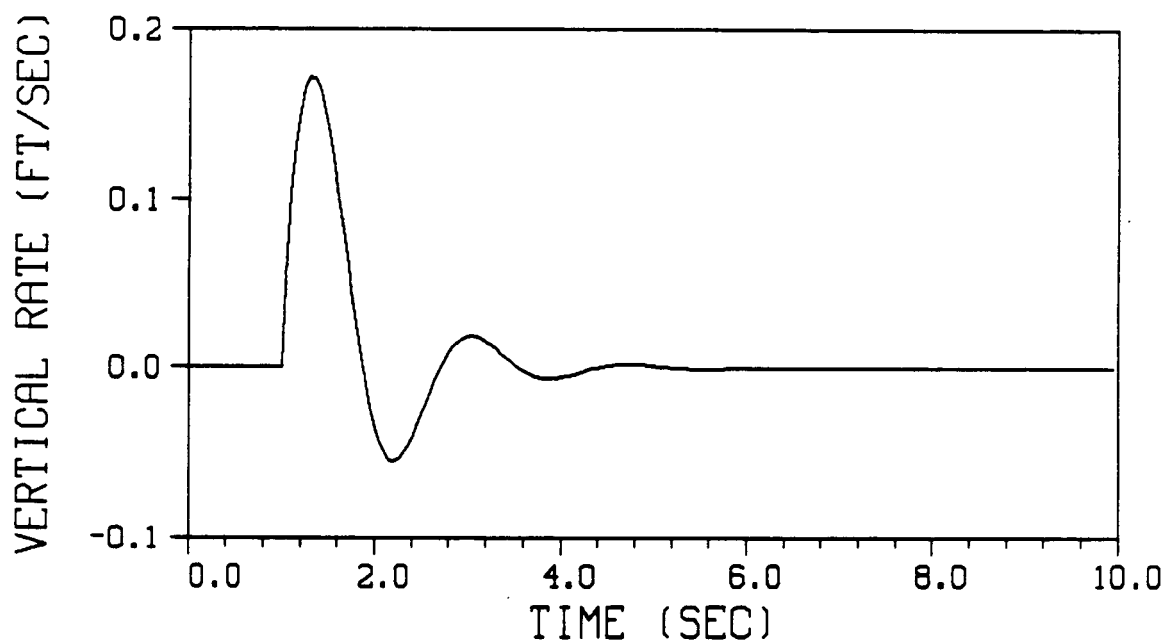
Plot B.1.-18. - Yaw rate response of the Harrier AV-8B due to an impulse of the rudder pedals in a near hover.



Plot B.2.-1. - Short period dynamics of the Harrier AV-8B pitch rate response due to an impulse of the longitudinal stick in a near hover.

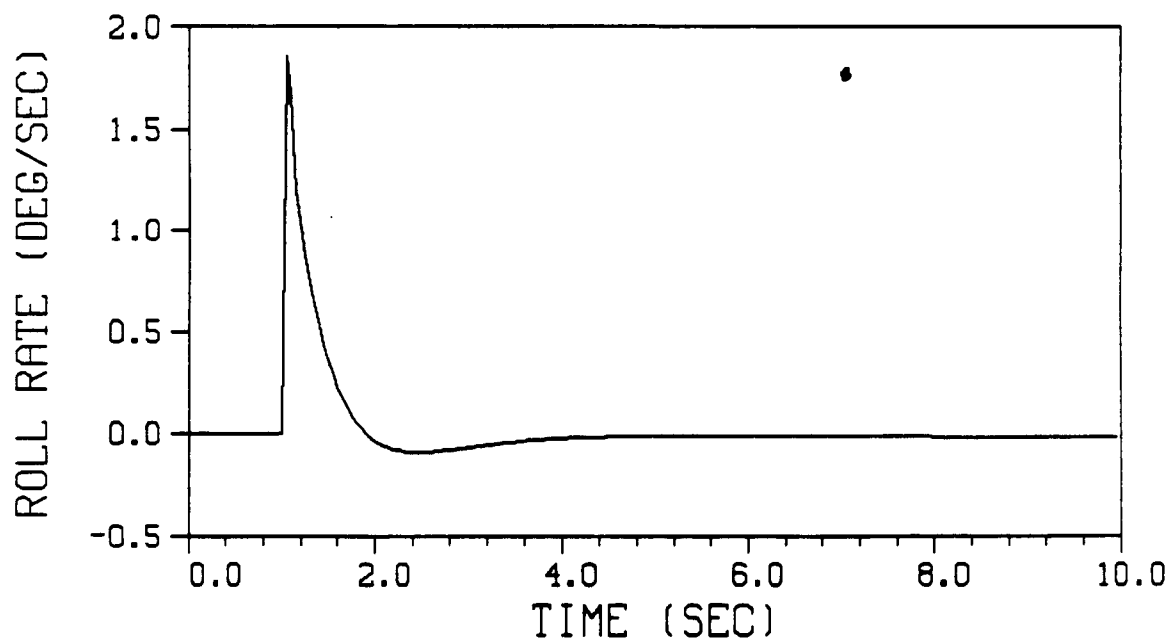


Plot B.2.-2. - Short period dynamics of the Harrier AV-8B forward velocity due to a 5 degree impulse of the nozzle angle at a near hover.

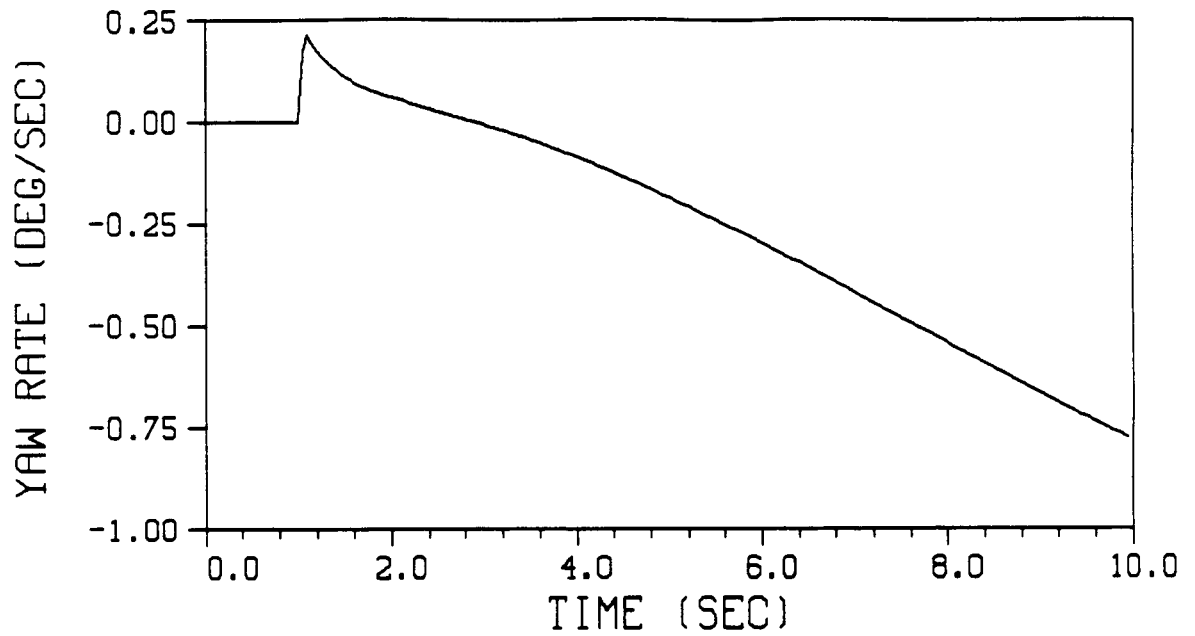


Plot B.2.-3. - Short period response of the Harrier AV-8B vertical rate due to an impulse of the throttle at a near hover.

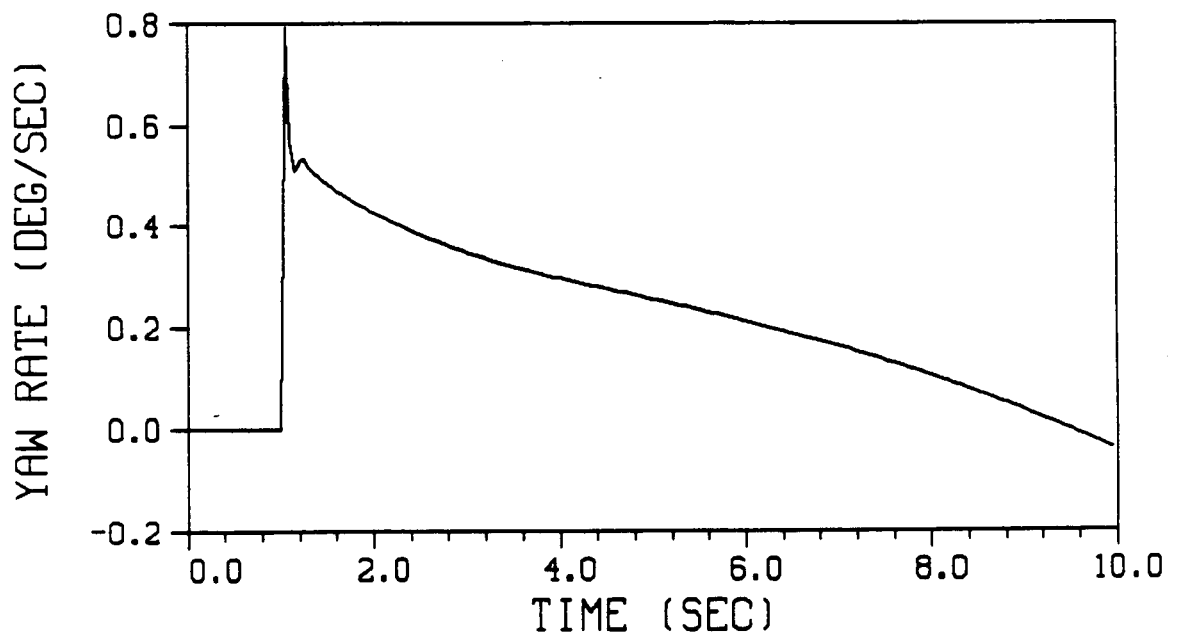
Plot B.2.-4. - Short period response of the Harrier AV-8B engine speed due to an impulse of the throttle.



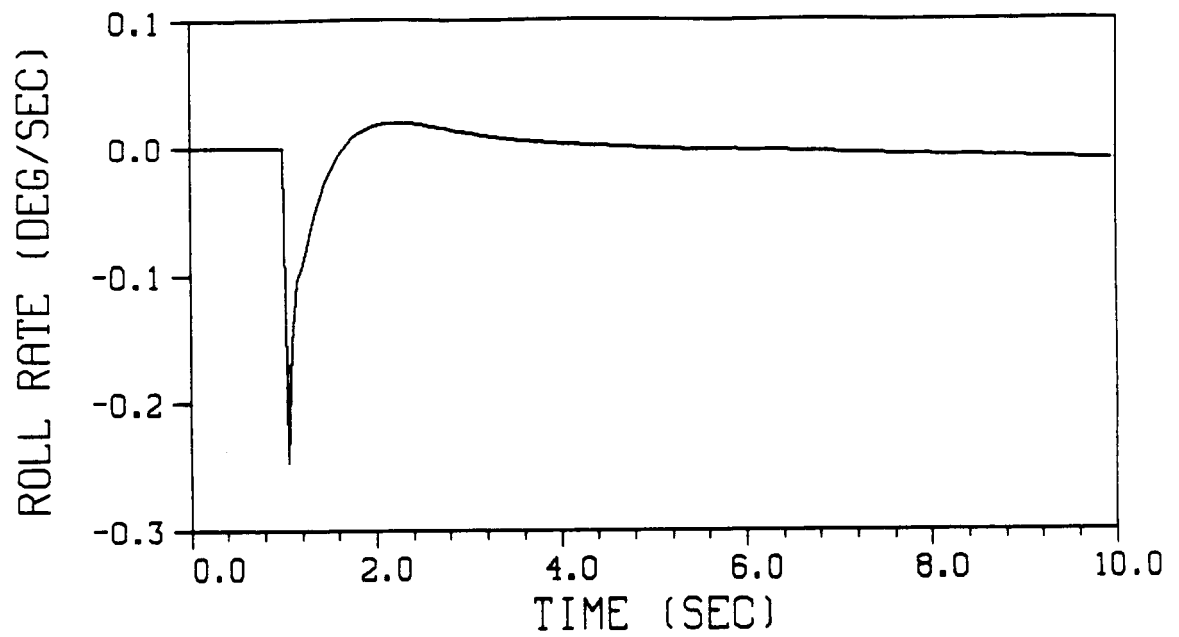
Plot B.2.-5. - Short period dynamics of the Harrier AV-8B roll rate due to an impulse of the lateral stick at a near hover.



Plot B.2.-6. - Short period dynamics of the Harrier AV-8B yaw rate due to an impulse of the lateral stick at a near hover.



Plot B.2.-7. - Short period response of the Harrier AV-8B yaw rate due to an impulse of the rudder pedals at a near hover.



Plot B.2.-8. - Short period response of the Harrier AV-8B pitch rate due to an impulse of the rudder pedals at a near hover.

APPENDIX III

The Adaptive Control Model of a Pilot in V/STOL Aircraft Control Loops

This is a version of the Thesis for a Master of Science Degree

by Senol Kucuk

AN ADAPTIVE HUMAN RESPONSE MECHANISM CONTROLLING THE V/STOL AIRCRAFT

Department of Electrical Engineering
University of Pittsburgh, 1988.

Final Report for NASA Grant NAG 3-729

Computer Simulation of a Pilot in V/STOL Aircraft Control Loops

Funded By:

**NASA Lewis Research Center
21000 Brookpark Road
Cleveland, OH 44135**

PRINCIPAL INVESTIGATORS:

William G. Vogt
Professor of Electrical Engineering
University of Pittsburgh
Pittsburgh, PA 15261
(412) 624-9686

Marlin H. Mickle
Professor of Electrical Engineering
University of Pittsburgh
Pittsburgh, PA 15261
(412) 624-9682

PARTICIPANTS:

Mark E. Zipf, Research Assistant
Department of Electrical Engineering
University of Pittsburgh
Pittsburgh, PA 15261

Senol Kucuk, Research Assistant
Department of Electrical Engineering
University of Pittsburgh
Pittsburgh, PA 15261

**AN ADAPTIVE HUMAN RESPONSE MECHANISM
CONTROLLING THE V/STOL AIRCRAFT**

by

Senol KUCUK

B.S. in E.E., Middle East Technical University, TURKEY, 1985

**Submitted to the Graduate Faculty
of the School of Engineering
in partial fulfillment of
the requirements for the degree of
Master of Science
in
Electrical Engineering**

University of Pittsburgh

1988

**The author grants permission
to reproduce single copies**

Signed _____

ACKNOWLEDGMENTS

I would like to thank my major advisors Dr. W. G. Vogt and Dr. M. H. Mickle for their support and guidance in the course of this project. I would also like to thank to the member of my thesis committee Dr. E. W. Kamen for his efforts on the behalf of my thesis.

This project was supported by NASA under NASA Research Grant No. NAG 3-729. I would also like to thank James R. Mihaloeuw from NASA-Lewis for his helpful assistance and encouragement in this research.

I wish to dedicate this thesis to my family for their unfailing concern, understanding and support throughout my graduate career in the U.S.A.

ABSTRACT

SIGNATURE _____

AN ADAPTIVE HUMAN RESPONSE MECHANISM CONTROLLING THE V/STOL AIRCRAFT

Senol KUCUK, M.S.

University of Pittsburgh

Importance of the role of human operator in control systems has lead to the particular area of manual control theory. Human describing functions have been developed to model human behavior for manual control studies to take advantage of the successful and safe human operations. Although adaptivity of the complex human mechanism is known to occur, no complete human response model can simulate this while actively participating in a manual control task. Single or multi-variable models, as well as optimal control models are available but require the knowledge of the controlled element dynamics. Here, we present a single variable approach that can be extended for multi-variable tasks where a low order human response model is used together with its rules, to adapt the model on-line, being capable of responding to the changes in the controlled element dynamics.

Basic control theory concepts are used to combine the model, constrained with the physical observations, particularly, for the case of aircraft control. Pilot experience is represented as the initial model parameters. An adaptive root-locus method is presented as the adaptation law of the model where the closed loop bandwidth of the system is to be preserved in a stable manner with the adjustments of the pilot model parameters. Pilot operating regions are taken from case studies of pilot handling qualities which relate the latter to the closed loop bandwidth and damping of the closed loop pilot-aircraft combination. Pilot limitations are characterized by the amount of force to be exerted on the controls by the pilot model. A Kalman filter parameter estimator is presented as the controlled element identifier of the adaptive model where any discrepancies of the open loop dynamics from the predicted one, are sensed to be compensated. The model is simulated in a non-linear aircraft simulation environment under different scenarios where it is subjected to perform simple maneuvers over a thrust vectored V/STOL aircraft.

DESCRIPTORS

Adaptive human model	Human describing function
Human pilot	Human response
Kalman filter	Man-machine systems
Manual control	Parameter estimation
Root locus	V/STOL

1.0 INTRODUCTION

Man-machine systems have been an important research area in recent years. Among these is the modelling of non-linear human behavior under different circumstances, especially in closing the loop of a control system. The latter is of great significance to control engineers and designers because it enables the possibility of digital or analog computer simulations of the complex human mechanism to perform certain tasks. Although it may not be possible or even not desirable to eliminate the human component in most control systems, it certainly is worth while to obtain mathematical models describing the relationship between man and machine where his presence can make a system self-optimizing. His ability to learn and adjust so as to adapt to the environment suggests that human study himself. In other words, it is "human modelling of human behavior". We will discuss the human pilot-aircraft combination, in that respect.

1.1 The Human Pilot

The mathematical analysis of two different aircraft may differ in general. For the pilot, however, aircraft and their control systems are deliberately designed so that there are only minor differences. After a short training period which involves trial-and-error, the human pilot can fly either of the aircraft. Both aircraft obey the same equations of motion, and since the pilot is the same, one analysis can be applicable to the other. Indeed, pilot opinion is an important issue in the design and testing of a new aircraft. This is because of the close relationship between what the pilot considers a "flyable" aircraft and the small perturbation analysis of the dynamics of the aircraft.

The pilot flies the airplane by the feedback method. He senses by sight or feels by "the seat of the pants" the motion of the aircraft, and moves the controls so as to minimize the error difference between the actual and some desired motion. In other words, the pilot responds to the motion of the aircraft, perceived by the sense organs, both directly and indirectly through the flight instruments such as the altimeter, speedometer, etc. He has other cues, the more the better, but they should all be in perfect harmony, and not contradictory.

The efficiency of the controls depends on the relation between the dynamic characteristics of the airframe and those of the control system, particularly on the length of any time lags. A certain interval of time elapses between the instant a disturbance appears and the instant the corresponding control movement or force becomes active as a result of the control applied. During this short interval, another signal can not take effect. This appears to be the basic non-continuity of the sensation response activity. This time delay plays an important role in the stability of the closed loop system since any stable system can be made unstable by introducing sufficient time delay into the loop. The pilot is then required to adjust his gain to produce the optimum response consistent with the stability within his human limitations. We can summarize the processes occurring in this interval in the following sequence: (see Figure (1))

1. Sensing of the disturbance or the controlled element by the pilot,
2. Response of the pilot which includes the computing element, selecting the variables that will be acted upon, choosing the controls considered to be the most efficient as well as the manner in which they will be acted upon, (the computing element consists in comparing the signal at the input with the known potentialities of the controls of the machine and the experience of the pilot)
3. The muscular movement of the pilot,
4. Further transmission of the controls through the respective control system

linkage to the output (aerodynamical control surfaces, engine throttle, etc.) and the transition process until a steady state is reached; at this stage mode switching of the pilot from dynamic operator to static takes place.

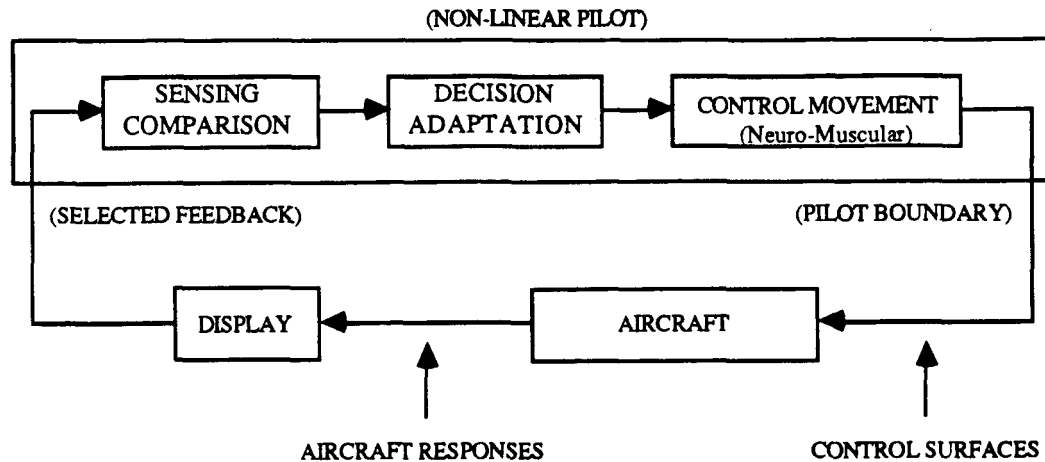


Figure 1. Processes occurring in the manual pilot control

This is a negative feedback control, where the controller (pilot), must close the loop according to some desired, overall behavior. Therefore, we will use the term, pilot "closes the loop", for this process. Furthermore, this behavior can be related to the bandwidth and damping ratio of the closed loop system. Kolk (1961) has studied the handling qualities and described a typical pilot in terms of the undamped natural frequency and the damping ratio, while rating them as "best", "good", "fair" and "poor" (see Figure (2)). Ashley (1972), reproduces Kolk's results in his small perturbation stability and response analysis. The ξ in the range, 0.5-0.8, and ω_n in the range, 3-4 rad/sec, retain considerable validity today as a basis for preliminary determination of what constitutes a good pilot or equivalently good-flying airplane. Etkin (1972), also has

a similar analysis. Thus, Kolk's chart will be our main design consideration. Judgements on simulating pilot model effectiveness will be done by comparison with the desired ranges.

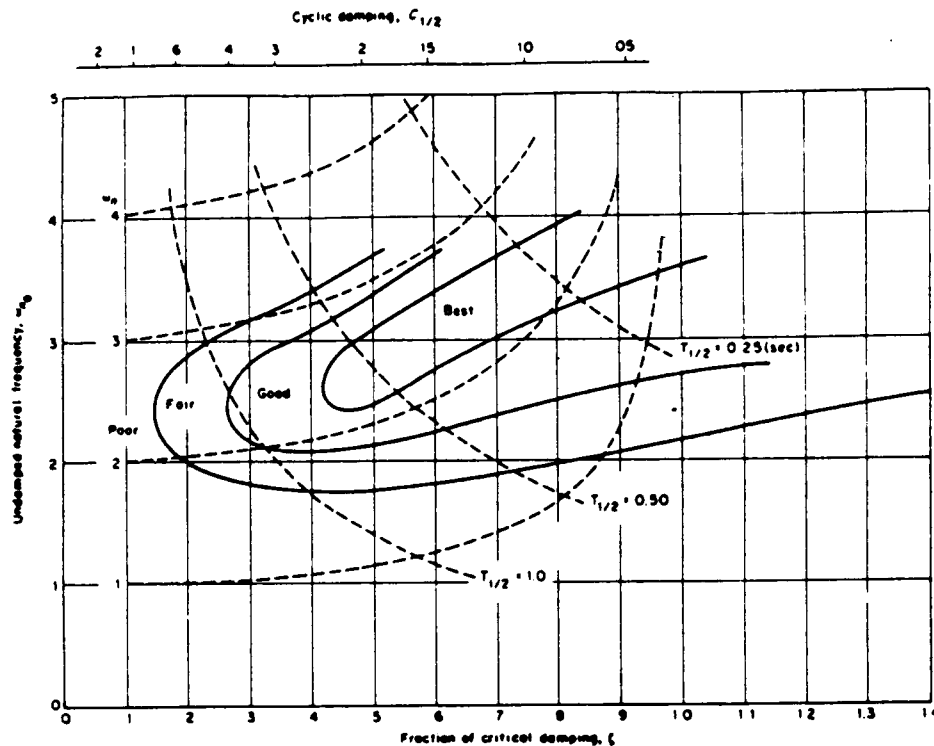


Figure 2. Kolk's chart on closed loop pilot characteristics

There is also an element of the control system, whose response characteristics vary not only from person to person, but also in the same individual according to his degree of fatigue, psychological and physiological condition which will later be referred to as the remnant. Unlike the automatic pilot, where the equations of motion for the control system are known with sufficient accuracy, it is not possible to permit the description of the control system by means of dynamic equations.

A human pilot reasons on the basis of the total information received but not necessarily simultaneously, about the controlled variable, relying on his flying experience. The processing of the information may not be instantaneous, moreover some information may not be used at all. In this respect, the possibilities of the computing element of the automatic pilot are inevitably more limited. In the case of the automatic pilot, by its detecting instruments (sensors, on-line computers, estimators, etc.) certain input signals, representing the well-defined components of the motion, should cause the autopilot to react. Under all circumstances, an automatic pilot watches only certain selected components of motion.

Many of the pilot's impression's of an airplane's flying qualities are related to the forces he must exert on the controls to hold them in the positions required to trim the airplane. If they are too large, he will be called upon to supply unreasonable exertion. If they are too small, the airplane may seem too sensitive or "touchy" or insufficient margin of stability may be indicated. In general, a pilot's flying qualities can be divided into two parts: static and dynamic responses. Static characteristics involve mainly the relationships between control deflection and force to trim the aircraft in steady equilibrium flight conditions of various sorts. This is the case of unaccelerated flight where a pilot responds mostly to disturbances. If these relations are regular and familiar, the control lever position and force provide the pilot with an immediate sense of the aircraft state, (angle of attack, sideslip, or speed). Proper static characteristics are prerequisite to good dynamic response.

Dynamic response, refers to the character of aircraft motions following disturbances from equilibrium. They may be atmospheric gusts, control movements to re-adjust the angular positioning, speed or the altitude of the vehicle, or any other events

producing unbalanced force or moments in general resulting in linear and angular acceleration. The airplane responds to these in characteristic ways, which define its dynamics, and which greatly affect a pilot's ability to fly easily and with precision.

The pilot is more or less concerned with the behavior of some of the many responses of the aircraft (pitch, roll, yaw, rates, speed, altitude, etc.), seeking to maintain them within certain limits or to cancel them by adequate control movements, which will be referred to as the controlled or the constrained variables. Hacker (1970) characterizes this relation by a system of partially controlled motion and discusses the stability in the case of a human pilot in parallel with constrained stability.

The remaining will be uncontrolled or free variables. However, the solution of the dynamic equations with some of the variables being constrained will also affect the free variables. Furthermore, the aircraft is to be controlled as a whole. Therefore, it is more appropriate to refer to the free variables as indirectly controlled variables.

The pilot's reflexes are selective with respect to the components of the motion. The control in this case is exerted over the sufficiently low modes of the motion induced by the disturbance, and in the rest of the flight, the stability is to be secured through the inherent properties of the machine.

Under standard flying conditions, like cruising along a straight path, (except when crossing a zone of intense atmospheric turbulence), the pilot usually achieves a correction through the controls that is even more efficient. In practice, he succeeds by achieving a satisfactory approximation of the controlled variables, induced by the disturbances and the deviations of those variables.

In order to secure the highest efficiency of control so as to determine in a given case, the optimum action to the deviation of a certain variable induced by the disturbance, the pilot generally resorts to several controls simultaneously. But one control also affects the quasi-totality of the equations of motion. The number of controls available, in general, is not equal to the number of the constrained variables, yet an experienced pilot is able to control all of the aircraft responses. Therefore limitation of the controllable variables, with the number of inputs seems artificial in the human pilot-aircraft combination case, due to the nature of partially and simultaneous control.

In summary,

- The pilot closes the loop in a stable manner,
- Closed loop bandwidth and damping are the measure of his flying qualities,
- There is a time delay between the sensed feedback element and the action,
- The pilot resorts to controls simultaneously,
- The pilot's decision process includes the estimation of the aircraft states and motion, and his opinion based on his flying experience,
- The pilot responses can be divided into static and dynamic; static response is the case of equilibrium flight where the pilot trims the aircraft to cancel the moments and balance the forces acting on the aircraft while dynamic response includes the control movements for maneuvering or changing the aircraft state,
- In general, the response of a human pilot will be different than the auto-pilot: it is not possible to relate human behavior to the equations of motion directly,
- There are stability considerations in the sense of delayed closed loop motion due to visual pilot feedback and partially controlled motion due to simultaneous control,
- There are bandwidth considerations since there is a limit of how rapidly and how strongly the pilot can move the controls.

Combining the above aspects, we come up with the general model shown in Figure

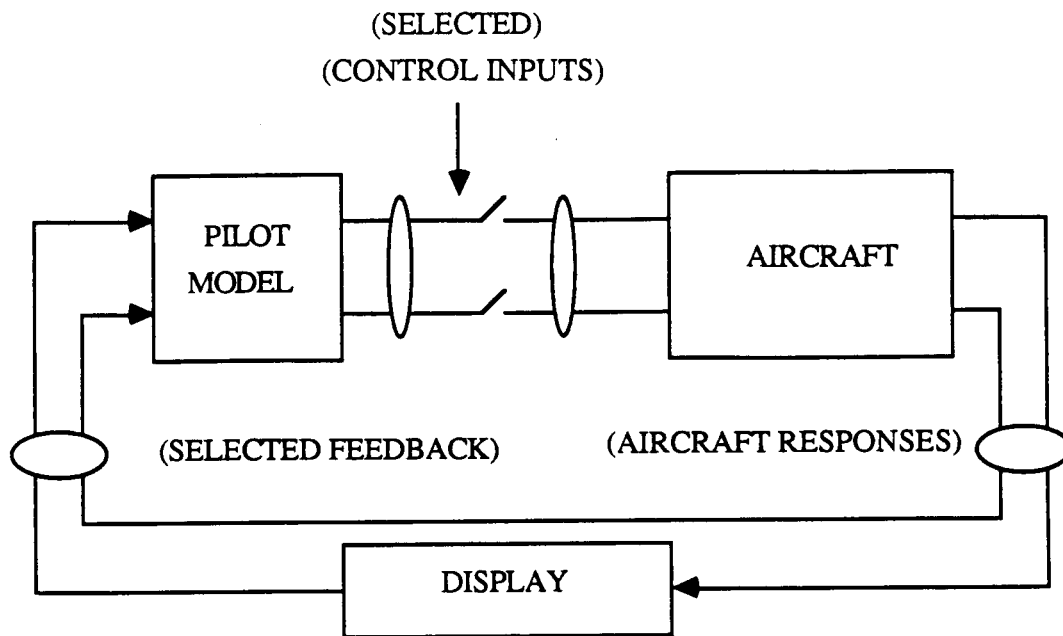


Figure 3. General Pilot Model

(3). Which set of controls are to be selected, or which set of aircraft responses are to be used for feedback, are the decisions of the pilot. In most of the cases, one of those inputs, the primary control input, is for the control of a specific response of the aircraft, while the other controls act as a regulating or a secondary control set, trying to stabilize the modes of the aircraft motion disturbed by the primary input. The primary control set will be characterized by a single variable compensatory loop as in Figure (4). The system is compensatory since the pilot acts depending on the error information only. The rate of error signal which is estimated by the pilot by differentiating the error signal is also available. This information is the measure of pilot's estimation and detection process of the adaptation to the changes in the aircraft dynamics.

For example, the lateral control is activated by the ailerons through the lateral stick,

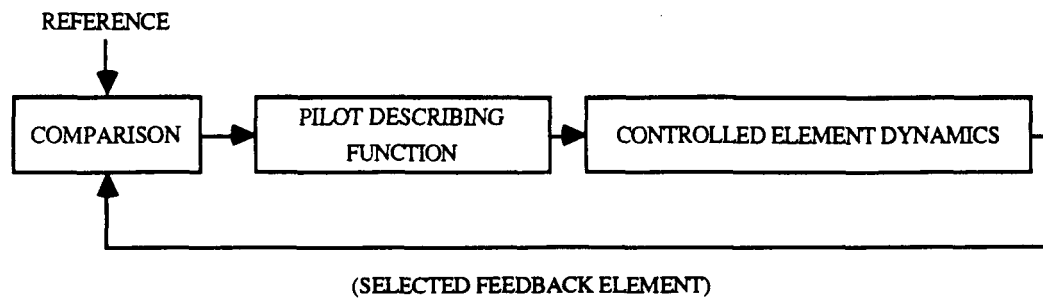


Figure 4. Single variable pilot model

but this causes a non-zero sideslip angle which is regulated by the rudder pedals. Also the pitch angle of the aircraft changes slightly, and that is regulated by the longitudinal stick changing the elevator angle. This is called a "coordinated-turn".

Further discussion of the human pilot for engineering analysis can be found in Kolk (1961), Seckel (1964), Hacker (1970) and Etkin (1972). These books discuss the aircraft dynamics and equations of motion while relating the theory to the human pilot. Seckel has more than five hundred references on handling qualities, human pilots, aircraft dynamics and theory.

1.2 The Aircraft

The aircraft is a rigid body consisting of a fuselage which carries the pilot and the wings to lift the aircraft. From the pilot's point of view, there is the cockpit with the provided instrumentations and the control units. Since we are discussing what the pilot observes in the aircraft, we will only mention the basic parts of the aircraft control mechanism.

Ailerons, elevators, rudders and tabs are typical parts of an aircraft that can move relative to the airframe. These are activated by the pilot for different purposes. The forces that would be required for the pilot to hold or displace them directly over some region of the flight envelope, far exceed the human capability. They are, therefore, provided by power boost in the form of hydraulic actuators. The pilot feels the artificial force of these actuators which define his boundary. These power boosted and manual controls, together with automatic gadgetry, assist the pilot, e.g., autopilots are employed to help maintain the direction, speed, and altitude of flight, while Stability Augmentation Systems (SAS) modify the apparent behavior so as to improve controllability of the aircraft and make the handling qualities more acceptable to the pilot.

Thrust is the reactive force applied to the vehicle, which may simply counterbalance drag (the aerodynamic force opposing the direction of the motion in the atmosphere), or may produce longitudinal acceleration or increased altitude. The thrust or engine throttle setting is the most common input for controlling the rate of climb or descent.

The propulsion system is often housed in a distinct element of vehicle such as a nacelle or jet-engine pod. Alternatively, it may be internal with only an air inlet or exhaust nozzle visible from the outside.

Weight is another force that dominates the performance of the vehicle. In level cruising flight, weight is counterbalanced by an aerodynamic force (lift) normal to the flight direction. Some lift is usually contributed by the fuselage, but a more efficient device for its production is the wing. A wing is a flattened, often cambered or twisted surface which intersects the fuselage, but usually has its longest dimension (span) normal to the airspeed vector. A well designed wing is an effective device for lift generation.

The most common arrangement, for lifting surfaces, known as a tail or empennage, has its location at the rear of the fuselage and consists of one portion (horizontal stabilizer) roughly parallel to the wing plane and a second (vertical stabilizer or fin) which is perpendicular to the wing plane, lying in the vehicle's central plane of symmetry.

The horizontal stabilizer applies pitching moments, which work to fix the inclination of the relative wind to the wing plane (angle of attack). It also assists in the trimming process of cancelling pitching moments about the center of mass due to the wing lift, fuselage, etc.

The wing lift depends on both angle of attack and airspeed so that this angle must be readily adjustable to ensure that the weight can be supported in various flight conditions. The most efficient way to make the required pitching moment adjustments has usually proved to be by controlling the tail lift with a trailing edge elevator.

Yawing control is supplied by the rudder, a flap acting at the trailing edge of the vertical stabilizer. The rudder has a trimming function in such situations as a steady turn or multi-engine flight when one engine is inoperable.

Rolling is accomplished by the ailerons and/or spoilers, placed near each wing tip and deflected in an anti-symmetrical manner. At high speeds, rolling moment may be exerted simply by the differential rotation of two all movable horizontal stabilizers.

The wing flaps resemble control surfaces but they are actuated slowly and only at low speeds where they augment wing lift to facilitate landing or take-off.

As mentioned earlier, trimming is one of the activities of the pilot. There are trimming devices, usually tabs, that help the pilot maintain the equilibrium so that controlled free flight can be set up at any speed by the appropriate settings.

For a conventional aircraft, the longitudinal control system consists of the engine throttle setting and the elevator angle through the longitudinal stick (forward and backward movements). The lateral control system is the ailerons (rightward and leftward movements of the lateral stick) and the rudder pedals operated by the feet. Although in mixed modes both of the control units affect each other, it is sometimes useful to separate the control mechanisms into longitudinal and lateral. The tabs are manually adjusted by the pilot for control free flight.

We will use a V/STOL (Vertical and Short Take-Off and Landing) aircraft in our simulations which is capable of adjusting the direction of the engine gross thrust vector as opposed to the conventional aircraft. Thrust vectoring is used to lift the aircraft for VTOL and STOL mode or to adjust the thrust vector to the optimum angle for a given flight condition.

1.3 The Simulation Program

The Harrier AV-8B model is a single seat transonic light attack V/STOL aircraft. Conventional aerodynamic controls are utilized for wingborne flight and engine bleed air reaction controls are used in jetborne flight with both systems operative during transition modes.

The Harrier AV-8B flight control system consists of conventional ailerons, rudder,

and stabilizer with a reaction control system (RCS) acting about all three axes during hover and transition. The stabilizer and ailerons are power operated while the rudder is connected directly to the rudder pedals. A single channel, limited authority Stability Augmentation System (SAS) is provided to facilitate control in hover and transition.

The engine provides lift thrust for take-off and landing, cruise thrust for conventional wingborne flight, deflected thrust for inflight maneuvering and compensator bleed air for the aircraft RCS. This is achieved by a nozzle system that can direct the engine thrust from zero degrees through vertical and even a reverse thrust position relative to the engine center line. The nozzle lever is the only additional cockpit instrument required for the V/STOL operation, and the only additional cockpit instrument is the gauge which displays the angular position of the nozzles. Engine operation in the conventional flight is similar to that of other engines.

The non-linear simulation program for Harrier AV-8B^{(1)*}, provided by NASA-Lewis, computes six degree of freedom aircraft motion⁽²⁾ and some of the aircraft performance parameters. The program is based on wind tunnel measurements and parameter identification methods⁽³⁾, and it will be our basic simulation environment for model testing and insertion of the pilot models. The simulation program provides all the cockpit controls (longitudinal stabilizer, ailerons, rudder, thrust and nozzle angle setting) and the switches (SAS, RCS, Gear, etc.) that are used by a human pilot⁽⁴⁾⁽⁵⁾.

* Parenthetical references placed superior to the line of text refer to the bibliography.

1.4 Equations of Motion

Although we will not discuss the equations of motion for the aircraft in detail, we suggest the book by Etkin (1959) and his revised (1972) texts. Like Ashley (1972), most of the recent text books refer to Etkin's work. There are other books by Moses (1945), Babister (1961) and Miele (1962), that are worthy of note.

As Ashley discusses in chapter two of his book, the six-degree of freedom aircraft motion can be characterized by nine states, (U, V, W) , (P, Q, R) , (Φ, Θ, h) (see Appendix A for the definition of aircraft parameters). One can also add Ψ , but since it has no influence on gravitational terms or the airloads, it can be dropped. Linearized analysis on the equations suggest that the longitudinal and lateral components of the motion can be de-coupled into two four state equations, even for the case when bank, turn and sideslip angles are small but non-zero. Although longitudinal components appear in lateral motion equations, and vice versa, in most of the practical cases coupling can be ignored.

If the aircraft is symmetrical, it is legitimate to consider pure longitudinal motions when the initial lateral rates are zero. These changes are basically in forward velocity, angle of attack and pitch attitude. The affected states are (U, W, Q, Θ) . This results in a fourth order characteristic equation whose roots are the modes of the longitudinal motion. In general, the longitudinal characteristic equation has two complex conjugate roots: one defining the short-period mode, and the other having very small damping defining the phugoid (see Ashley (1974), Etkin (1972), Kolk (1961), Hacker(1970)) mode. If the change in the rate of altitude, \dot{h} , is not negligible with respect to the other variables, then it should be added to the state equation, but for small perturbation analysis we can always neglect its effect.

Of the two modes, the short period is the most important one to the pilot, because these poles define how the aircraft will react shortly after he applies control movement to the longitudinal stick. It contains most of the angle of attack response to control deflection and the variation of the normal acceleration necessary for maneuvering. When the mode is of high frequency and well-damped, the airplane responds almost instantly, without overshoot to elevator movements. If the reaction of the aircraft is poor or there is a delay, it will be difficult for the pilot to handle efficiently for which he uses the term "sluggish". On the other hand, the phugoid mode does not have a significant effect on pilot's flying qualities. The phugoid poles are very close to the origin, even unstable in some of the cases. However, the mode is usually so long in period that it has very little influence on the pilot and is easily guided or altered. Consider a human guiding an automobile for example. Continuous adjustments must be made to correct the heading of the car depending on the road conditions, but these corrections are so small in magnitude that, they do not affect the quality of driving. The same situation applies for the aircraft case. In conditions, where continuous, active control is required anyway, the phugoid properties are probably not even perceptible to the pilot.

The corresponding lateral-directional modes can be characterized by the spiral mode, roll mode, and the oscillatory Dutch-Roll mode, which primarily affect the states (V, W, P, Φ) . The spiral mode is like the phugoid (except that rather than a complex conjugate pole pair, the spiral mode is characterized by a very large negative pole), the pilot counteracts any evidence of these motions long before they have time to build up or become unstable. The other modes are, however, primary determinants of the pilot's perception of aircraft handling qualities. While there is no simple way of analyzing these important lateral-directional modes, Seckel (1961) has an interesting discussion of a human pilot trying to control the bank attitude by positioning the ailerons in the right

direction and in proportion to the error between the actual and desired bank angle. By linearized equations of motion and root locus techniques (see Figure (5)), Seckel shows that the closed loop system can be unstable for specific values of the pilot gain. This is what is known as the Dutch-Roll excitation. The sideslip swings back and forth, accompanied by oscillations in pitch angle. The solution is, of course, introducing the rudders, for coordinating the roll. This becomes highly difficult especially at high speeds due to the limited abilities of the human pilot.

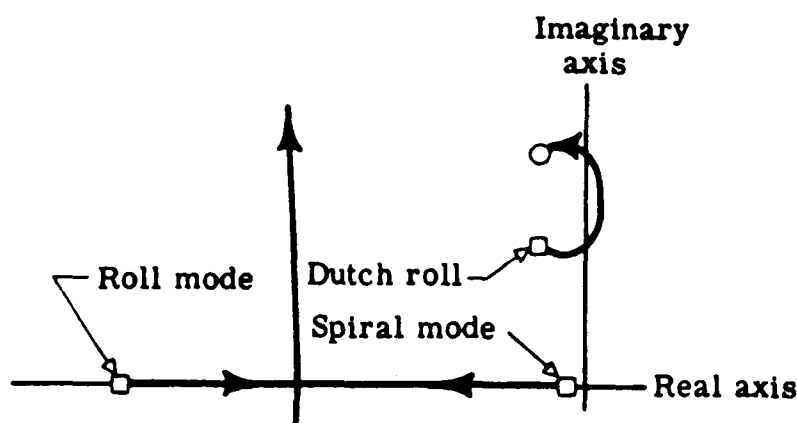


Figure 5. Root Locus of lateral control modes, from Seckel

1.5 Statement of the Problem

We wish to investigate the properties of models that can describe the human behavior in feedback type of systems by simulating these models in linear or non-linear environments. In other words, we want models that resemble human behavior or at least behavior a human can be capable of performing. In the presence of such models, the

analysis of the complex control tasks performed easily by humans, such as driving a car or flying an airplane, become available. It is the adaptive behavior of the human mechanism, without knowing the exact dynamic equations, capable of re-adjusting to different environments, that forces the search for mathematical describing functions. Unfortunately, the theory of adaptive control is not directly applicable for such an analysis. Such a model has been investigated at Wright Air Development Center in the late 1950's. Extensive amounts of experimental data have been studied and a fairly simple, yet effective model has been developed⁽⁶⁾. The details of the model can be found in the final version of the paper written by D.T.McRuer and E.S.Krendel⁽⁷⁾. One such application of the model is its performance while actively participating in the control of an aircraft, and being capable of responding to the changes in the aircraft model as well as to certain maneuvers.

One of the difficulties in utilizing the McRuer-Krendel human response model for different flight configurations is that parameters of the human model must be re-adjusted as parameters of the plant change. Consider an inexperienced human pilot being trained to control the aircraft for the first time. He will be provided with the control units and their purposes, but this alone is not sufficient enough to fly the aircraft without the actual training. As soon as he is given the full control of the aircraft, he will be in an action-reaction state, observing the responses corresponding to his commands while collecting and using this information for his next control attempt. As he begins to get used to the controls, he will be able to guess how the aircraft will respond depending on his command and if there are any discrepancies, he will correct them as in the case of guiding the automobile. The experience of the pilot reflects how well this estimation procedure is performed. In other words, the experience of a pilot is his knowledge of the open loop dynamic behavior of the aircraft. However, this knowledge can not be

expressed by a numerical dynamic set of equations. The pilot has an internal representation of the plant dynamics. Now consider the experienced pilot. It is clear that, even if the pilot is experienced, his action will differ depending on the aircraft configuration. This is partly due to the randomness of the human nature and partly to the changes of the dynamic relationship of the aircraft, especially to the speed and the angular rates. Therefore the adaptation process of the pilot continues even if he is an experienced pilot. In order to model this experience, we must have some knowledge of the open loop dynamics as the human pilot gets through training. As the human pilot selects the parameters best suited for the aircraft's configuration, we must obtain a set of human model parameters to be used at specific flight configurations. However, before a new pilot model is developed, a new set of transfer function estimates relating the behavior of the aircraft at the specified flight condition has to be obtained from the trimmed (unaccelerated) aircraft. These flight tests involve low order approximations of the primary responses through impulse, pulse or step inputs from the control mechanisms. This is exactly how the human pilot proceeds in controlling the aircraft, approximating the modes of the open loop dynamics that are perceptible to him and altering his parameters accordingly.

Once the estimate of the open loop transfer function is available, the loop is then closed using root locus techniques for the selection of the closed loop poles. The selection of the human pilot involves the proper assignment for a stable closed loop system with the desired bandwidth. So we will select our human model parameters that will satisfy the latter constraint used by the human pilot. As we will discuss in Chapter 2, the McRuer-Krendel human response model has a non-linear delay term, $e^{-T_D s}$ for the pure transmission delay of the visual lag. However, to be able to apply the root locus method, the non-linear delay element $e^{-T_D s}$ has to be handled before any analysis. One

way of proceeding is to approximate $e^{-T_D s}$ by a finite number of poles at a large distance from the origin, on the negative real axis⁽⁸⁾. Unfortunately, numerical problems are inevitable.

The most important drawback is that, all the following analysis must be done off-line: (1) trim the aircraft at the desired initial flight configuration; (2) record the impulse responses; (3) approximate low order transfer functions using time and frequency domain data; (4) choose primary response variables and control set; (5) calculate the human response parameters via root locus techniques; (6) insert the pilot model and (7) repeat this process until satisfactory responses are observed.

Our aim will be to simplify this process and close the loop on-line and adaptively, as the actual pilot does. We therefore need an on-line estimator scheme to monitor the changes in the open loop transfer function which the pilot is closing and use these estimates to adapt the pilot model. While the actual pilot just "does" the estimation, we need a parameter estimator for the simulation.

In Chapter 2, we develop a discrete time McRuer-Krendel human response model using the step invariant transformation. Although the transformation is trivial, the resulting model eliminates the non-linear delay element yielding a finite number of poles at the origin in the z -domain. Therefore we can use ordinary root locus analysis.

In order to close the loop with the desired bandwidth and damping, no way other than the root locus method is known and implementable. In Chapter 2, we separate the discrete time McRuer-Krendel model into two parts: one relating the time delay and the muscular element, the other being the adaptive or the compensating part which is our primary concern. Chapter three discusses the root locus method and a way to close the

loop adaptively. Applying the phase constraint of the root locus method in Chapter 3, we obtain a linear equation for the possible assignments of the adaptive pole-zero pair of the human response model which is suitable for on-line calculations. The adaptation acts as a phase equalizer and makes sure that the phase constraint is satisfied at the desired closed loop location, hence closing the loop. Unfortunately this procedure alone is not sufficient. The stability and error minimization arguments should be added for optimum values, and the adaptation must proceed accordingly. The adaptive pilot model is utilized in Chapter 5, and the extension for the multivariable control case is discussed.

Chapter 4, describes a time series parameter estimation technique using Kalman filters which can be easily modified to estimate transfer functions, parameters of the state and output equations. This chapter can be treated separately since it only deals with parameter estimation. Examples will be given to demonstrate the applications of the algorithm and computational aspects will be discussed.

Finally in Chapter 6, we combine the diagrams and equations for the adaptive pilot and discuss the resulting pilot insertions and compare with the static pilots⁽⁹⁾⁽¹⁰⁾⁽¹¹⁾ previously reported.

2.0 MATHEMATICAL MODELLING OF THE HUMAN RESPONSE

A human is intermittent in his operation, his bandwidth is limited by the time required for decisions and action, his senses are non-linear, and his awareness of output movement is of limited accuracy. However, he has the ability to detect signals in the presence of noise, and his presence can make a system adaptive and self-optimizing. Although his behavior is non-linear, it is not for a long time. There are periods when he acts in a non-linear manner, like the impulsive reactions in case of a sudden emergency, but most of his responses are observed to be linear. This aspect helps modelling the effect of a human in a closed loop system.

In the case of a control system, the basic human output is the control movement of skeletal muscles resulting in limb displacement or application of force. The knowledge of the limb position and force output is due not only to vision but to sense organs in muscles and joints known as the "proprioceptors". The sensory outputs of these organs provide feedback signals which make possible the regulation of skilled muscular movements. This feedback is transmitted by afferent nerve fibers from the muscles to the central nervous system, and after being processed, the control signal is sent to the limbs. Kelley (1968), discusses the neuro-muscular system for manual control purposes. However, very efficient approximate models for engineering analysis are utilized⁽¹²⁾.

If the human-control system combination was completely linear, the analysis could have been quite simple. In the case of the human pilot-aircraft, neither the aircraft nor the human pilot present any linear behavior. Although non-linear models can be developed, the analysis of such systems is highly complex, and the results are not much

better than linear models. Another approach is to approximate these non-linear relationships by linear or quasi-linear models.

Despite this non-linear, adaptive human pilot mechanism, many linear and low order models have been successfully developed. Of these models the low order model⁽¹³⁾ is the result of a servomechanism model approach of the human operator. This model demonstrated that human operator dynamics in single loop compensatory systems could be described by quasi-linear functions. A study on a variety of controlled element dynamics and random appearing input commands with different bandwidths confirmed the applicability of such a model⁽⁶⁾.

There are other complex models relating optimum control theory to the experienced pilot behavior⁽¹⁴⁾⁽¹⁵⁾, or discrete models⁽¹⁶⁾. The Optimal Control Model (OCM) has better results in the low and high frequencies, but the basic disadvantage of the model is its complexity. The model consists of a Kalman Filter estimator, a predictor, a simplified neuro-muscular equivalent and a linear state feedback capable of multivariable control tasks.

The McRuer-Krendel model⁽⁷⁾ has been simulated for the Black Hawk helicopter and for the Harrier AV-8B aircraft, for single and multiple cascaded pilot configurations⁽⁹⁾⁽¹⁰⁾⁽¹¹⁾, and the results confirm the model. Pilot parameters for the model are chosen after extensive aircraft testing for the flight configurations that are being considered in the simulations as an analogy to pilot training.

While the discrete domain model⁽¹⁶⁾ only gives the freedom of choosing the order of the transfer function, the McRuer-Krendel model has adjustable parameters for the adaptive nature of the human pilot. We will transfer this continuous domain model into

the discrete domain, for reasons that will become clear later, and use this model to simulate simple maneuvers in a non-linear aircraft simulation environment.

2.1 The McRuer-Krendel Human Response Model

The McRuer-Krendel model is a single-degree of freedom quasi-linear model based on best fit analysis of experimental pilot data⁽⁶⁾⁽⁷⁾. The general form is given by,

$$H_p(s) = K_p e^{-T_D s} \frac{(T_L s + 1)}{(T_P s + 1)} \left\{ \frac{(T_K s + 1)}{(T_K s + 1)(T_{N_1} s + 1)} \frac{1}{[(s/\omega_N)^2 + 2(\xi_N/\omega_N)s + 1]} \right\} \quad (2-1)$$

where $H_p(s)$ is the transfer function of the human response, often referred to as the describing function, s is the complex Laplace transform variable, the input is the error signal, while the output is the corresponding control displacement. McRuer and Krendel discuss typical values of the precision model⁽⁷⁾. In order to characterize the random component, a remnant is added to the control displacement as in Figure (6).

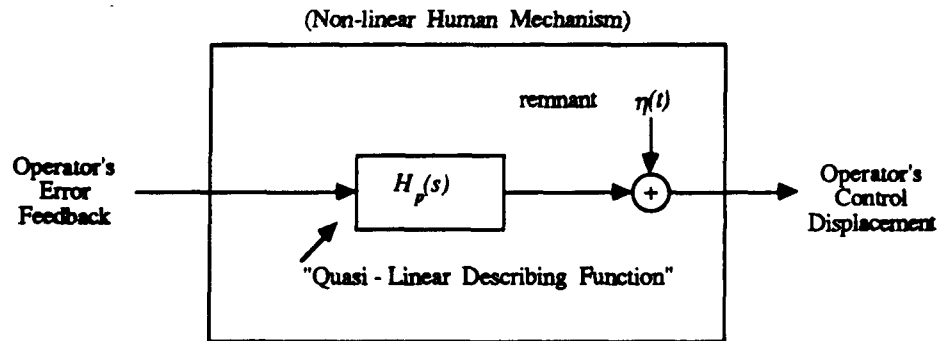


Figure 6. Human describing function model

Although there is no easy way of analyzing the remnant, the model in equation (2-1) can further be simplified to obtain the transfer function,

$$H_p(s) = \frac{K_p e^{-T_D s} (T_L s + 1)}{(T_N s + 1)(T_I s + 1)} \quad (2-2)$$

where very low and very high frequency accuracy is not necessary. This is a reasonable assumption for the human pilot since, as discussed before, the bandwidth of the closed loop is 3-4 rad/sec (or 0.48-0.64 Hz). In equation (2-2), $e^{-T_D s}$ is the pure transmission time delay within the nerve conduction and stimulation. Although the time delay parameter T_D changes are estimated to be between 0.13-0.23 seconds and even 0.30 for some of the cases, it is not known to exceed 0.30 seconds (see Kelley(1968)). The changes in the time delay can be significant depending on the particular control task but not for a specific control task⁽¹⁷⁾, e.g., the time delay of a driver will be different than that of a pilot, but pilots with similar experience and training will have similar lags. Therefore, we will assume that $T_D = 0.20$ and is constant for the rest of the discussion. The OCM model⁽¹⁴⁾ has a similar argument on the time delay. The term $1/(T_N s + 1)$ is an approximation of the neuro-muscular lag of the arm meaning that the pilot can not move his arm faster than the rate of this pole. The value of T_N is assumed to be constant and approximately 0.10. The remaining term, $K_p(T_L s + 1)/(T_I s + 1)$, is the adaptive part of the model (a time dependent variable gain and a lead-lag compensator) whose parameters are altered by the pilot to the particular flight configuration. The constraints on the model parameters are as follows:

$$0.0 \leq T_L \leq 2.50 \quad (T_L \neq T_N) \quad (2-3a)$$

$$0.0 \leq T_I \leq 20.0 \quad (2-3b)$$

$$T_N = 0.10 \quad (2-3c)$$

$$T_D = 0.20 \quad (2-3d)$$

The lead-lag compensator part is based on the assumption that the human is required to furnish at least one differentiation and one integration to obtain the desired performance, and the constraints on the parameters, T_L and T_I determine how efficient the integration and differentiation processes are performed by the human. This concept of a human capable of differentiation and integration is a common assumption. The complete model with the remnant added is given in Figure (7).

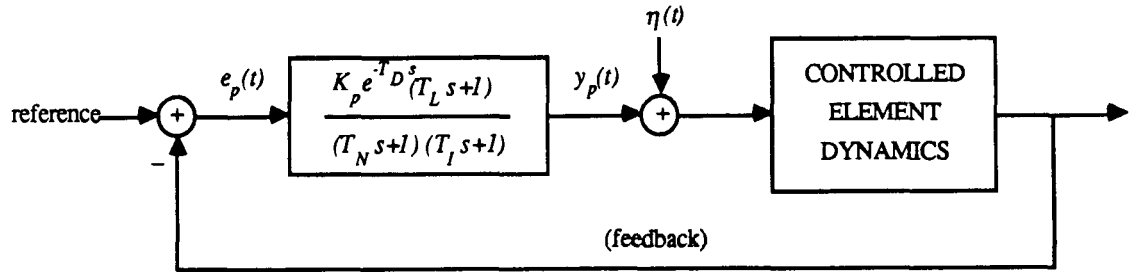


Figure 7. Complete single variable model

The resulting differential equation will be,

$$(T_N T_I) \ddot{y}_p(t) + (T_N + T_I) \dot{y}_p(t) + y_p(t) = K_p T_L \dot{e}_p(t - T_D) + K_p e_p(t - T_D) + \eta(t) \quad (2-4)$$

The quantity $y_p(t)$ is the pilot's control displacement, and the input is the feedback error signal $e_p(t)$. If $T_L \dot{e}_p(t) \gg e_p(t)$, then the output of the model is derived by the rate of the error signal, else if $T_L \dot{e}_p(t) \ll e_p(t)$, then the output is a function of the error signal itself. When they are in the same order, the effect is mixed.

The solution of equation (2-4) defines the modes of the pilot, and the resulting control displacement defines the modes of the closed loop system. Even though there are

a few parameters to be adjusted, the analysis is still not trivial because of the time delay, time-varying pilot parameters and time-varying aircraft dynamics.

Now recall that the external world is sampled for a brief period of time during which the sensing of the feedback component and comparison with respect to a desired motion takes place. It is clear that within this interval another signal can not be processed. The error signal is sensed and held until current information is processed. The total time delay of the decision depends on the pilot's abilities but also on the visual information lag. The compensator network parameters are then selected by the pilot and the location of the pole-zero pair is placed accordingly. Finally there is the input of the neuro-muscular element, and the desired control displacement is sent through the muscles. Unfortunately the desired and commanded controls may differ which greatly affects the pilot's control qualities. Thus the pilot is ready for another sample of the error, but we must note that he is responding to some error signal previous to the present error because of the delay.

The assumption of sampling leads to the model in Figure (8).

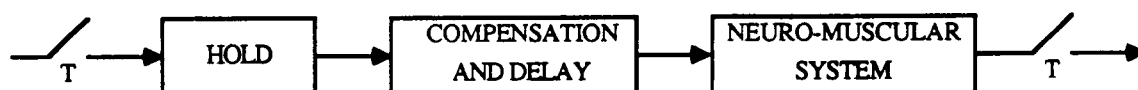


Figure 8. Sampled Human Response Model

Experiments show that it is impossible to deal correctly with every stimulus in a sequence when the stimuli are closer than some time interval from each other (about 0.5 second, Kelley (1968)). This in a way shows that sampling occurs in the human

mechanism because the latter phenomenon can be explained by the sampling theorem where a frequency aliasing occurs due to over-sampling. In other words the human can not respond faster than his bandwidth. Indeed a similar sampled data model has been suggested by McRuer⁽¹⁸⁾ himself, and others have already been studied. However the relative simplicity and the successful simulation results of the McRuer-Krendel model suggest a direct sample-and-hold equivalent of this model for discrete domain analysis. This is legitimate if the bandwidth of the human mechanism is preserved which means that the sampling theorem must be satisfied. Under these conditions, we obtain the discrete time McRuer-Krendel model given by (see Appendix B for derivation):

$$H_p(z^{-1}) = \frac{Kz^{-d}(z^{-1}-\gamma z^{-2})}{(1-\beta z^{-1})(1-\alpha z^{-1})} \quad (2-5)$$

It is not surprising that the structure of the model does not change by sampling. Now the pure transmission delay is represented by z^{-d} , the neuro-muscular component is $1/(1-\beta z^{-1})$ and the adaptive part is $K(1-\gamma z^{-1})/(1-\alpha z^{-1})$. The pole locations are easily found by the relation $z=e^{sT}$. For the zero at γ however, the derivation is not straightforward because sampling relocates the system zeros. We used Greek letters for the discrete model parameters in order not to mix them with the continuous model. The gain K is scaled because of the sampling but that does not have any significance in the design. The zero and the poles of the model are given by,

$$\alpha = e^{(-T/T_I)} \quad (2-6a)$$

$$\beta = e^{(-T/T_N)} \quad (2-6b)$$

$$\gamma = 1 - \frac{(1-\beta)}{1 + \frac{(T_L - T_N)(\alpha - \beta)}{(T_I - T_N)(1-\alpha)}} \quad (2-6c)$$

This is for the case when $T_I \neq T_N$. Otherwise, the partial fraction expansion changes, but we will always avoid the situation $T_I = T_N$ to make the analysis simpler.

Assume that T_p , and thus also α , is fixed, then γ is a function of T_L only. It is easily seen that in that case the local maximum and minimum of the γ is obtained at the limits of T_L , and also that γ is an increasing function of T_L yielding,

$$\gamma_{(T_L=0.0)} \leq \gamma(\alpha) \leq \gamma_{(T_L=2.50)} \quad (2-7)$$

The only drawback to this is that while T_p is changing the possible locations for choosing the zero is changing as well. This is different than the continuous model where pole/zero locations can be assigned independently. The resulting discrete time difference equation is given by,

$$y_p(k) = (\beta + \alpha)y_p(k-1) - (\beta\alpha)y_p(k-2) + Ke_p(k-d-1) - K\gamma e_p(k-d-2) \quad (2-8)$$

The quantity $e_p(k)$ here represents the error information, and $y_p(k)$ is the corresponding pilot control displacement calculated at the discrete times.

The simulation program discussed in Section (1.5) updates the parameters at 0.05 second periods allowing the control inputs to be inputted at these instants. That gives a sampling frequency of 20 Hz. If we recall that the closed-loop bandwidth is desired to be 0.48-0.64 Hz, and the maximum bandwidth of a human pilot is estimated to be 0.96, a sampling frequency of 20 Hz gives a fairly safe region to operate. Furthermore this program is being used by NASA for real time human piloted simulators implying that 20 Hz sampling does not degrade human performance.

Now that T is fixed at 0.05 second, with $T_N=0.10$ and $T_D=0.20$, our model becomes,

$$H_p(z^{-1}) = Kz^{-4} \frac{(z^{-1} - \gamma z^{-2})}{(1 - 0.6065z^{-1})(1 - \alpha z^{-1})} \quad (2-9)$$

For this choice Figure (9) shows the region of the model zeros while α is changing from

minimum to maximum defined by the inequality in equation (2-3b). It is seen that zero location lies inside the unit circle, and since the poles are stable as well, the resulting model is minimal phase. This is regarded to be an advantage because systems with non-minimal phase characteristics may have undesirable responses.

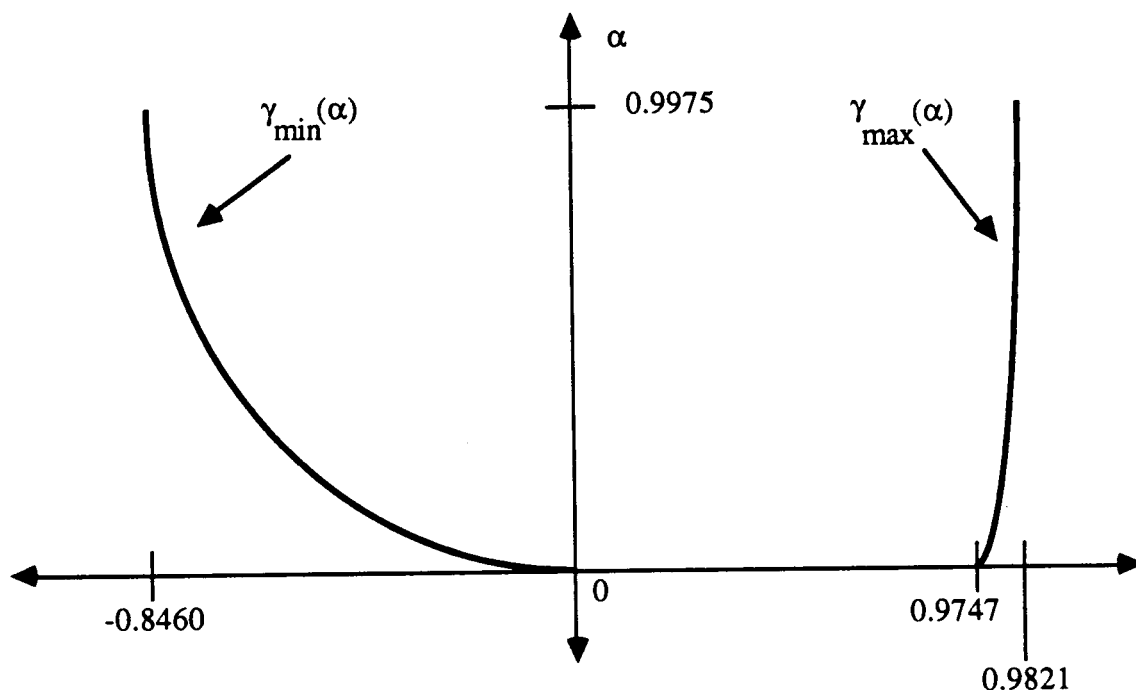


Figure 9. γ_{\min} and γ_{\max} versus α

The discrete model has some advantages. First of all, the non-linear pure time delay element $e^{-T_D s}$ is eliminated and replaced by poles at the origin so that the analysis of the root locus is simpler. The pilot is characterized by a difference equation instead of a differential equation which means that any discrete identification method as well as discrete optimization necessary for the adaptation process of the pilot model can be applied. The model turns out to be minimal phase, but one extra constraint is added on the adaptive portion of the model. The parameters of the lead-lag equalization network are to be selected more carefully as a result of the sample and hold equivalent where the

zeros are relocated. Once the pole α is fixed, there is a region where the zero γ can be chosen, but this does not introduce any significant difficulty in the analysis.

2.2 Adaptation Procedure

The adaptation procedure can be divided into four parts: detection, modification, identification and optimization. We will combine detection and identification in one group, and modification and optimization in another.

It is reasonable to assume that a well-trained pilot has an internal representation of the plant dynamics and will be able to identify any changes very rapidly. For a skilled pilot, the identification of the unexpected modes of the system can be in times of order of a reaction time from the time of detection. The detection-identification structure of our model will consist of a linear time-varying plant representation and a parameter estimator which will update the unknown potentialities of the model parameters to desired accuracy constrained by the uncertainties of pilot input with respect to the plant output. For simulation purposes, we will not include the effect of the remnant. We have argued that the system was a compensatory feedback type system, and that only the error signal was available to the pilot. However, the human pilot is capable of monitoring the rate of the error signal⁽¹²⁾, namely, $\dot{e}_p(t)$. If we approximate the first of the error signal in the following way,

$$\dot{e}_p(t) = \frac{e_p(t) - e_p(t-T)}{T} = \frac{r(t) - y(t) - (r(t-T) - y(t-T))}{T} \quad (2-10)$$

we can see that the rate of the error signal is proportional to the output. Therefore we argue that we can use the controlled element measurements and the pilot's control

displacement in a parameter estimation scheme which will be the one discussed in Chapter 4.

The second group, modification-optimization involves the proper selection of the lead-lag compensator that will result in a stable response and minimum mean square error. This will not work properly unless the estimate information of the detection-identification is responding to the changes in dynamics properly. If the estimate has some uncertainty in it, which often occurs in the pilot training where the inexperienced pilot over-estimates the next state of the aircraft and pushes the control stick too hard, then the system may become unstable. But this does not mean that the optimization is not working. Of the possible solutions for the lead-lag network parameters, the optimum pair must be found if such a solution exists over the flight envelope that is of question.

If we put together the basic parts of the adaptation, we end up with the model in Figure (10).

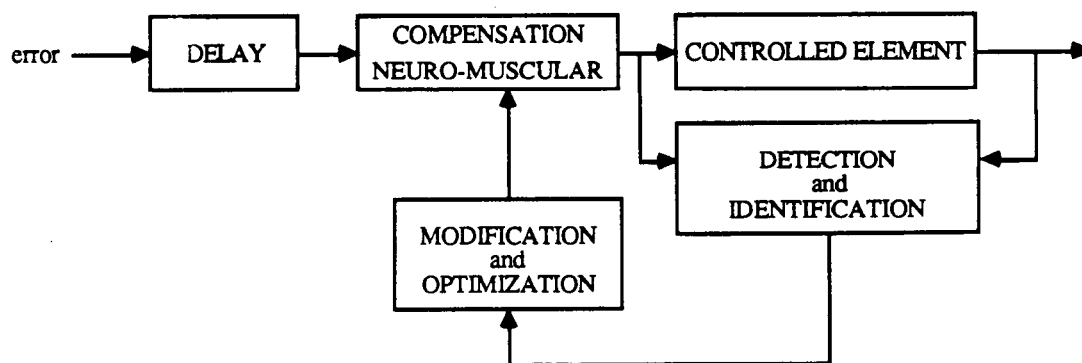


Figure 10. The Adaptation Procedure of the Pilot Model

3.0 CLOSING THE LOOP

In this chapter we will establish the equations for the closed loop pilot-aircraft system. Figure (11) shows the basic configuration of our pilot-in-the-loop model. Notice that this is a single variable closed loop compensatory system. The remaining responses other than the one being controlled are ignored at this point and later will be regarded as the disturbances. This is legitimate if the remaining variables are changing slowly with respect to the controlled element. This can be the case where the pilot is only provided by the pitch angle information and longitudinal stick input to control aircraft's pitch response.

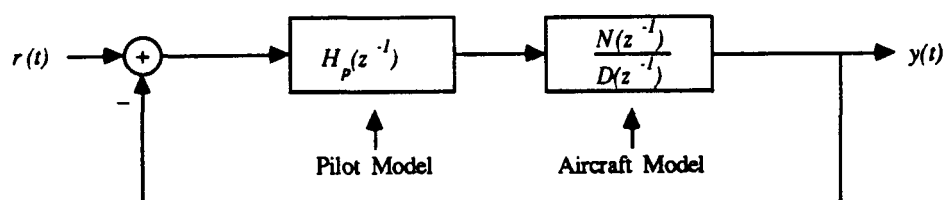


Figure 11. Compensatory single variable pilot control

Before further discussion some assumptions must be made. For the rest of the chapter we will assume the following. Assumptions (a) the controlled element dynamics can be decoupled from the rest of the aircraft responses, (b) there exists a describing function of the human response, and it can be approximated by quasi-linear models, (c) the remnant of the model is approximately zero, (d) the aircraft dynamics and the properties of the

controlled element are known to some accuracy. The rest of the analysis will be carried in the discrete domain.

3.1 Root-Locus

Given the pilot describing function $H_p(z^{-1})$ and assuming that the aircraft dynamics can be modelled by the ratio of two rational polynomials, namely $N(z^{-1})/D(z^{-1})$, the closed loop system transfer function $T(z^{-1})$ from the reference $r(t)$ to the output $y(t)$ can be given by, (refer to Figure (11))

$$T(z^{-1}) = \frac{Y(z^{-1})}{R(z^{-1})} = \frac{H_p(z^{-1}) \frac{N(z^{-1})}{D(z^{-1})}}{1 + H_p(z^{-1}) \frac{N(z^{-1})}{D(z^{-1})}} \quad (3-1)$$

or,

$$T(z^{-1}) = \frac{H_p(z^{-1})N(z^{-1})}{D(z^{-1}) + H_p(z^{-1})N(z^{-1})} \quad (3-2)$$

If the pilot describing function is the discrete model derived in Chapter 2, then $T(z^{-1})$ becomes,

$$T(z^{-1}) = K \frac{z^{-d}(z^{-1} - \gamma z^{-2})N(z^{-1})}{\Delta_{CL}(z^{-1})} \quad (3-3)$$

where $\Delta_{CL}(z^{-1})$ is the characteristic polynomial given by,

$$\Delta_{CL}(z^{-1}) = (1 - \beta z^{-1})(1 - \alpha z^{-1})D(z^{-1}) + K z^{-d}(z^{-1} - \gamma z^{-2})N(z^{-1}) \quad (3-4)$$

Now we can argue the stability of the system. This is a complicated procedure especially when the aircraft dynamics is changing where the polynomials $N(z^{-1})$ and $D(z^{-1})$ are functions of time. It is important to note that there is no constraint on the order of the open loop aircraft transfer function. It may be impossible for the pilot to identify all the modes of the controlled element except for the ones that lie inside his bandwidth. The pilot adaptation involves an internal representation of the open loop system but not highly sophisticated. The pilot is watching the modes that are perceptible to him which leads to the conclusion that the model of the open loop that is sensed by the pilot is a low order approximation of the system. The approximation should be valid for low frequency regions or approximately $0.1 < \omega < 20$ rad/sec⁽¹⁹⁾. The parameters of this pilot-decided model are updated, if any discrepancies occur, and if the pilot is experienced enough to sense these changes.

The closed loop system is stable if and only if the roots of $\Delta_{CL}(z^{-1})=0$ lie inside the unit circle. The method of root locus becomes useful for such an analysis where the closed loop poles are plotted as a function of the variable component of the equation. In the case of a linear system the loci are plotted as a function of the open loop gain. Unfortunately, there is more than one variable in equation (3-4). To proceed, we will investigate the properties of the closed loop system only when the pilot parameters are changing. For that purpose we re-write the loci equation in terms of the pilot gain. This is obtained by equating equation (3-4) to zero and solving for pilot gain K , which results,

$$K = K(z^{-1}) = -\frac{D(z^{-1})(1-\beta z^{-1})(1-\alpha z^{-1})}{N(z^{-1})z^{-d}(z^{-1}-\gamma z^{-2})} \quad (3-5)$$

All of the closed loop poles must satisfy equation (3-5). The order of the closed system is strictly determined by the order of the open loop transfer function. The constraints are on

the closed loop bandwidth and the corresponding phase margin. Then if z_{CL} is one of the closed loop poles, $K(z_{CL}^{-1})$ must be a real number since the gain can not be complex. But the z -transform variable z^{-1} is complex, so although the polynomials $N(z^{-1})$ and $D(z^{-1})$ have real coefficients. The result of equation (3-5) may not necessarily be a real number and those satisfying the latter argument define the root-locus of the closed loop system. Equivalently, we end up with the basic phase constraint of the root locus method which says that the gain in equation (3-5) must be real, or the complex argument of the gain must be zero, namely,

$$\angle K(z^{-1}) = \begin{cases} \pm (2n+1)180 & \text{for } K > 0 \\ \pm (2n)180 & \text{for } K < 0 \end{cases} \quad n=0,1,2,\dots \quad (3-6)$$

The case of K being negative is necessary as we will investigate later in Chapter 6 that the relative airspeed of the R is decreasing by the increasing nozzle angle. If the pilot is required to increase the speed of the aircraft, then he must provide a negative gain.

Now that we have characterized the closed loop poles both as a function of the pilot parameters and the dynamics of the controlled element, we will relate the root locus method to the adaptive portion or the lead-lag equalization network of the McRuer-Krendel human response model in the discrete domain.

Let us re-write equation (3-5) in the following way by separating the pilot determined part from the others which he can not influence, such as time delay, the neuro-muscular lag, and the controlled element dynamics,

$$K(z^{-1}) = \left\{ -\frac{D(z^{-1})(1-\beta z^{-1})}{N(z^{-1})z^{-(d+1)}} \right\} \frac{(1-\alpha z^{-1})}{(1-\gamma z^{-1})} \quad (3-7)$$

In equation (3-7), terms inside of the braces denote the non-reachable part for the pilot, and the remaining term which involves the discrete pole-zero pair α - γ is the equalization of the pilot which he alters for optimum flying conditions or equivalently optimum closed loop pole locations that are dominated by the non-reachable term or at least by the available amount of information on this term.

The adaptation is known to occur in the pilot mechanism, and we can explain such an adaptation by the phase requirement necessary to satisfy the phase constraint of the root locus defined in equation (3-7) at the desired closed loop pole location. In other words, the pilot changes the closed loop poles by the proper selection of his adaptive pole-zero pair and gain according to the variations of equation (3-7).

Assume that,

$$K_f(z^{-1}) = -\frac{D(z^{-1})(1-\beta z^{-1})}{N(z^{-1})z^{-(d+1)}} \quad (3-8)$$

which reduces equation (3-7) to,

$$K(z^{-1}) = K_f(z^{-1}) \frac{(1-\alpha z^{-1})}{(1-\gamma z^{-1})} \quad (3-9)$$

As is usually done in bode plot analysis, we treat the magnitude and phase of the equation (3-9) in two different equations because this simplifies the analysis. For phase analysis, the equation (3-9) reduces to,

$$\angle K(z^{-1}) = \angle K_f(z^{-1}) + \angle \left(\frac{1 - \alpha z^{-1}}{1 - \gamma z^{-1}} \right) \quad (3-10)$$

Let us examine the adaptive part $(1 - \alpha z^{-1}) / (1 - \gamma z^{-1})$ separately since we do not have any influence on the other terms. We can find the phase angle supplied by α and γ to the equation (3-10). We can write

$$\frac{1 - \alpha z^{-1}}{1 - \gamma z^{-1}} = \frac{z - \alpha}{z - \gamma} \quad (3-11)$$

Then the phase contribution of α and γ can be seen from the graphical representation of $(z - \alpha)$ and $(z - \gamma)$ in the complex plane as in Figure (12).

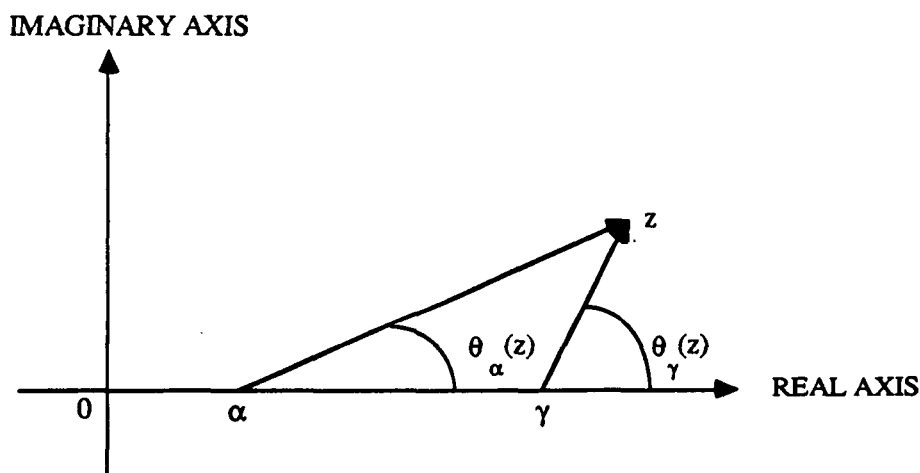


Figure 12. Graphical representation of the adaptive part

where, z is any desired pole location to be included in the loci. Then

$$\angle \left(\frac{1-\alpha z^{-1}}{1-\gamma z^{-1}} \right) = \theta_{\alpha}(z^{-1}) - \theta_{\gamma}(z^{-1}) \quad (3-12)$$

$\theta_{\alpha}(z^{-1}), \theta_{\gamma}(z^{-1})$ are as defined in Figure (12). By representing the closed loop behavior of the system with the root locus plot of the closed loop pole locations, the procedure of controlling the aircraft like the human pilot is now reduced to the appropriate assignment of α and γ that will satisfy equation (3-10). By the following definitions

$$\angle K(z^{-1}) = \theta_K(z^{-1}) \quad (3-13a)$$

$$\angle K_f(z^{-1}) = \theta_f(z^{-1}) \quad (3-13b)$$

equation (3-10) becomes,

$$\theta_K(z^{-1}) - \theta_f(z^{-1}) = \theta_{\alpha}(z^{-1}) - \theta_{\gamma}(z^{-1}) \quad (3-14)$$

Provided that $\angle K(z^{-1})$ and $\angle K_f(z^{-1})$ are known, the equation (3-14) can be solved. Although the equation looks like a linear equation, because of the possible set of assignments of α and γ , further analysis must be done. This can also be seen from Figure (12), α and γ can move right or left while still keeping a constant phase angle ($\theta_{\alpha}(z^{-1}) - \theta_{\gamma}(z^{-1})$).

If the quantity $\theta_{\alpha}(z^{-1}) - \theta_{\gamma}(z^{-1})$ is negative, then the pole lags the zero (Figure (13.a)). Conversely if $\theta_{\alpha}(z^{-1}) - \theta_{\gamma}(z^{-1})$ is positive then the pole leads the zero (Figure (13.b)). Once α and γ are fixed the corresponding gain is calculated from equation (3-9) by evaluating the right hand side at $z=z_{CL}$, z_{CL} , being the desired closed loop pole. Then, by taking the magnitude of each side of the equation (3-9),

$$|K(z_{CL}^{-1})| = |K_f(z_{CL}^{-1})| \frac{|(1-\alpha z_{CL}^{-1})|}{|(1-\gamma z_{CL}^{-1})|} \quad (3-15)$$

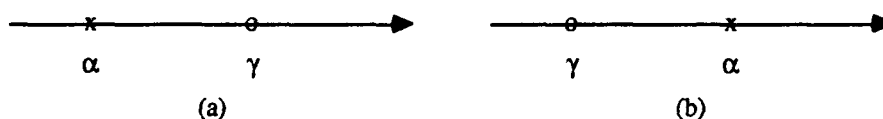


Figure 13. Possible pole/zero assignments

There may be more than one possible choice of the α - γ pair for the same task forcing other constraints for the assignment process. Just as the human pilot does, we must pick the pair that will result in the minimum error signal and a stable closed system. This is the optimization process. Unfortunately, the pilot-aircraft combination can not be guaranteed to be stable though an experienced pilot will try to maintain the opposite. But if instability occurs, this must be sensed, and the closed loop pole must be relocated. This is also necessary if the open loop transfer function has resonances at the pilot desired closed loop pole which makes the control very "touchy" so that the pilot must exert a considerable amount of force on the controls. Therefore the closed loop pole must be relocated within the allowable limits if possible. In the next section, we will define the limits of the desired closed loop system poles both in the continuous and the discrete domains to combine the Root Locus criterion with the closed loop poles.

3.2 Closed Loop Poles

In the introduction section, we indicated that the pilot's flying qualities can be determined by the closed loop bandwidth. We also related this bandwidth constraint into the undamped natural frequency and the damping ratio of the resulting closed loop transfer function. Now we will relate the region defined by

$$3.0 \leq \omega_n \leq 4.0 \text{ rad/sec} \quad (3-16a)$$

$$0.5 \leq \xi \leq 0.8 \quad (3-16b)$$

to the closed loop poles.

The second order, dominant complex conjugate poles are given by,

$$s = -\xi\omega_n \pm j\sqrt{1-\xi^2}\omega_n \quad (3-17)$$

applying the region defined in equation (3-16a) and (3-16b), we can plot the resulting s -domain poles as in Figure (14). The transformation $z=e^{sT}$, maps the poles in equation (3-17) to the z -domain poles as,

$$z = e^{-\xi\omega_n T} [\cos(\sqrt{1-\xi^2}\omega_n T) \pm j\sin(\sqrt{1-\xi^2}\omega_n T)] \quad (3-18)$$

The discrete poles change as the sampling time changes along with the resulting region of the desired closed loop poles. For $T=0.05$, the region of desired closed loop poles is given in Figure (15).

Therefore, we will assume that an experienced pilot adapts to the flight configuration in such a way that the dominant closed loop pole lies in these regions. And since it is the dominant pole, the bandwidth of the system is determined by this pole. For simulation purposes we will supply the desired closed loop pole to our model so that the

nominal value is used for most of the configurations, and the on-line adaptation scheme may change the precise location depending on the open loop transfer function, especially the behavior of the open loop transfer function at the pre-decided closed loop pole. If the system already has resonances at that pole, then the pilot must re-locate the closed loop pole within the regions of s -domain poles as in Figure (14) or equivalently z -domain poles as in Figure (15).

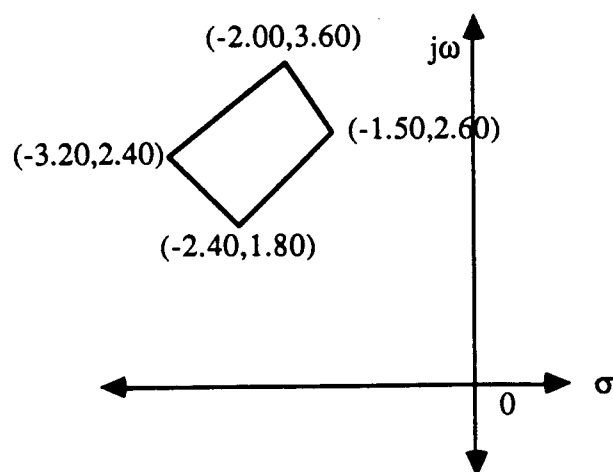


Figure 14. Closed loop poles in s -domain

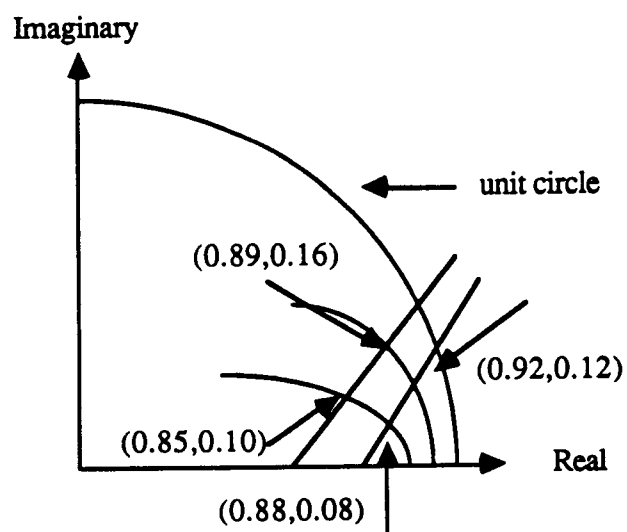


Figure 15. Closed loop poles in z -domain ($T=0.05$)

So far we have defined the behavior of the closed loop control system and related the Root Locus criterion to the adaptive part of our human response model. Although we have accomplished a desired result, it took a lot of assumptions to be able to get to this point. Unfortunately this is not sufficient. Now we will assume that the pilot's representation of the open loop aircraft dynamics can be modelled by a discrete difference equation based on the sampled available data of the input-output relation of the aircraft response. This is the identification part of the adaptive pilot model. We must also note that pilot does not know the aircraft dynamic equations nor the equations of motion exactly. He reasons on the information supplied and observed. For that purpose in the next chapter we will introduce a parameter estimation scheme based on discrete measurements.

4.0 ESTIMATION SCHEME

Kalman filter modelling is widely used in stochastic control. The idea is to model the system in question by a state and a measurement equation. The model can be fictitious but as long as it has the general form,

$$x_{k+1} = F_k x_k + G_k u_k + B_k w_k \quad (4-1a)$$

$$y_k = C_k^T x_k + J_k u_k + D_k v_k \quad (4-1b)$$

the theory can be applied. The unknown or unmeasurable states of the system are estimated with the information of input/output measurements and previous estimates. The basic assumptions on w_k and v_k are as follows: w_k and v_k are independent, zero mean, white-gaussian, random noises, and

$$E[w_k w_j^T] = Q_k \delta_{k-j} \quad (4-2a)$$

$$E[v_k v_j^T] = R_k \delta_{k-j} \quad (4-2b)$$

where $E[f]$ denotes the expected value of the variable f . If the noises are not white, the theory is still available by adding extra states to the state equation that characterize the spectrum of the noise by the innovations approach provided that the frequency spectrum of the noises are known⁽²⁰⁾.

Both Anderson⁽²¹⁾ and Goodwin-Sin⁽²²⁾ discussed a state model for the parameter estimation purposes where all the unknown plant parameters are put in the state equation in the following way,

$$\theta_{k+1} = \theta_k + w_k \quad (4-3)$$

and any measurement of the known plant characteristics are modelled by the measurement equation,

$$z_k = H_k^T \theta_k + v_k \quad (4-4)$$

We have found this model approach to be quite effective after extensive simulation on discrete and sampled data systems. The convergence rates are found to be faster than the Recursive Least Square (RLS) estimator schemes we tried, and the estimates agreed with the parameters of the simulated system. By appropriate selection of the noise covariances of this filter, the RLS filter can also be obtained. The basic assumptions on w_k and v_k apply. Once the estimation is put into the form of a Kalman filter, all the properties of the Kalman filter theory can be used such as the best linear estimator property of the Kalman filter and the convergence of the estimates.

If the unknown plant parameters and plant measurements can be put into the formulation,

$$\theta_{k+1} = \theta_k + w_k \quad (4-5a)$$

$$z_k = H_k^T \theta_k + v_k \quad (4-5b)$$

we can use the following Kalman filter equations for the estimation of the plant dynamics, given as,

$$K_k = P_k H_k [H_k^T P_k H_k + R_k]^{-1} \quad (4-6a)$$

$$\hat{\theta}_{k+1} = \hat{\theta}_k + K_k [z_k - H_k^T \hat{\theta}_k] \quad (4-6b)$$

$$P_{k+1} = P_k - K_k H_k^T P_k + Q_k \quad (4-6c)$$

No restrictions on the order of the state vector and the amount of measurements are required. The filter is started with the initial conditions on the covariance matrix and

estimates, namely with $P_0, \hat{\theta}_0$. The estimates are updated by the equations (4-6a), (4-6b) and (4-6c) at each measurement to be taken at discrete sampling frequencies.

The choice of R_k and Q_k are the preliminary determinations on how the filter will behave. The covariance of the measurement noise v_k determines the quality of the measurements. For example if $R_k=0$, then there is no measurement noise. The choice of $Q_k=0$ drops the state equation to

$$\theta_{k+1} = \theta_k \quad (4-7)$$

which means that the system is a Linear Time Invariant (LTI) system. This can also be observed from the covariance update in equation (4-6c). The value of Q_k is added to the covariance so that it does not vanish by converging to zero. If the covariance matrix is zero, then the estimate can not change an undesirable situation. By keeping Q_k non-zero, the filter can estimate the parameters of time-varying systems. P_0 and Q_k are usually assumed to be diagonal matrices, namely, $P_0=p_0I$ and $Q_k=\rho_kI$, p_0 is some big positive number while ρ_k is some small positive number.

We will now investigate different types of configurations for the estimation process.

4.1 Applications

4.1.1 SISO Case

Suppose the input and output relationship of a discrete system can be given by the following difference equation,

$$y_k = \sum_{i=1}^n a_i(k) y_{k-i} + \sum_{j=d}^{m+d} b_j(k) u_{k-j} \quad (4-8)$$

Then choose,

$$\theta_k = [a_1(k) \dots a_n(k) b_d(k) \dots b_{m+d}(k)]^T \quad (4-9a)$$

$$H_k = [y_{k-1} \dots y_{k-n} u_{k-d} \dots u_{k-m-d}]^T \quad (4-9b)$$

The resulting filter equations are given by,

$$K_k = P_k H_k [H_k^T P_k H_k + R_k]^{-1} \quad (4-10a)$$

$$\hat{\theta}_{k+1} = \hat{\theta}_k + K_k [y_k - H_k^T \hat{\theta}_k] \text{ with } \hat{\theta}_0 \quad (4-10b)$$

$$P_{k+1} = P_k - K_k H_k^T P_k + Q_k \text{ with } P_0 \quad (4-10c)$$

$$H_{k+1} = [y_k \dots y_{k-n+1} u_{k-d+1} \dots u_{k-m-d+1}]^T \quad (4-10d)$$

It is easily seen that if $R_k=1$ and $Q_k=0$, the above filter is exactly the RLS estimator. Unfortunately the estimator can not be run off-line because the vector H_k , or the regressor, is a function of the previous measurements of the system input and output.

4.1.2 MIMO Case

Assume that a MIMO discrete system can be characterized by the following difference equation,

$$y_k^p = \sum_{l=1}^L \sum_{i=1}^{n_l} \alpha_i^{pl}(k) y_{k-i}^l + \sum_{l=1}^M \sum_{j=d_l}^{m_l+d_l} b_j^{pl}(k) u_{k-j}^l \quad p=1 \dots L \quad (4-11)$$

where there are L outputs and M inputs, i^{th} output and j^{th} input are y_k^i , u_k^j , respectively. We have two choices to model this system: we can put all the unknown parameters in one big state equation, or we can separate the state equations into smaller parts of each representing the unknown parameters for one output equation. Although it looks hard to put into words, it is easier to see by the following definitions,

$$\Theta_k^p = [\alpha_1^{p1}(k) \dots \alpha_n^{p1}(k) \alpha_1^{p2}(k) \dots \alpha_n^{p2}(k) \dots \alpha_1^{pL}(k) \dots \alpha_n^{pL}(k) \\ b_d^{p1}(k) \dots b_{m+d}^{p1}(k) b_d^{p2}(k) \dots b_{m+d}^{p2}(k) \dots b_d^{pL}(k) \dots b_{m+d}^{pL}(k)]^T \quad (4-12a)$$

$p=1 \dots L$

$$H_k = [y_{k-1}^1 \dots y_{k-n}^1 \ y_{k-1}^2 \dots y_{k-n}^2 \dots y_{k-1}^L \dots y_{k-n}^L \\ u_{k-d}^1 \dots u_{k-m-d}^1 \ u_{k-d}^2 \dots u_{k-m-d}^2 \dots u_{k-d}^L \dots u_{k-m-d}^L]^T \quad (4-12b)$$

where $d=\min(d_1 \dots d_L)$, $n=\max(n_1 \dots n_L)$, $m=\max(m_1 \dots m_L)$. This suggests that there are L separate estimators, each having the same form but calculated independently. Now recall that the original Kalman gain equation and covariance update equation involve only H_k . So by appropriate assumptions, the gain and covariance update equations of these separate estimators can be calculated only once and used for the estimate updates, only if the initial covariances are the same for all of the estimators, but this value is re-definable and one can assume that all the initial uncertainties are the same. Goodwin and Sin (1984) discuss such a simplification.

The final form of the equations is as follows,

$$K_k = P_k H_k [H_k^T P_k H_k + R_k]^{-1} \quad (4-13a)$$

$$\hat{\theta}_{k+1}^l = \hat{\theta}_k^l + K_k [y_k^l - H_k^T \hat{\theta}_k^l] \quad \text{with } \hat{\theta}_0^l \quad l = 1 \dots L \quad (4-13b)$$

$$P_{k+1} = P_k - K_k H_k^T P_k + Q_k \quad \text{with } P_0 \quad (4-13c)$$

$$H_{k+1} = [y_k^1 \dots y_{k-n+1}^1 \quad y_k^2 \dots y_{k-n+1}^2 \dots y_k^L \dots y_{k-n+1}^L \\ u_{k-d+1}^1 \dots u_{k-m-d+1}^1 \quad u_{k-d+1}^2 \dots u_{k-m-d+1}^2 \dots u_{k-d+1}^L \dots u_{k-m-d+1}^L]^T \quad (4-13d)$$

4.1.3 Estimating the Parameters of STATE-OUTPUT Equations

It is sometimes necessary to have some information of the parameters of state and output matrices of a time-varying plant. Such an application may be the adaptive-optimal control. At each sample by the current values of the time-varying state and output equation parameters, the discrete Ricatti equation is solved, and the solution is used for the control of the system.

Assume that a time-varying discrete system can be modelled by the following n -state, m -input state equation:

$$x_{k+1} = F_k x_k + G_k u_k \quad (4-14)$$

Given the state and the input measurements, x and u we wish to estimate the parameters of the state and input matrices, F and G . Let us re-write the equation (4-14) in terms of x_k , as,

$$x_k = F_{k-1} x_{k-1} + G_{k-1} u_{k-1} \quad (4-15)$$

Then the l^{th} state equation will be,

$$x_k^l = \sum_{i=1}^n f_{li}(k-1)x_{k-1}^i + \sum_{j=1}^m g_{lj}(k-1)u_{k-1}^j \quad (4-16)$$

or if,

$$\theta_k^l = [f_{l1}(k-1) \dots f_{ln}(k-1) g_{l1}(k-1) \dots g_{lm}(k-1)]^T \quad (4-17a)$$

$$H_k = [x_{k-1}^1 \dots x_{k-1}^n u_{k-1}^1 \dots u_{k-1}^m]^T \quad (4-17b)$$

$$x_k^l = H_k^T \theta_k^l \quad l=1 \dots n \quad (4-17c)$$

Then we can use the same argument of MIMO case to have the following equations for the estimation of the unknown parameters:

$$K_k = P_k H_k [H_k^T P_k H_k + R_k]^{-1} \quad (4-18a)$$

$$\hat{\theta}_{k+1}^l = \hat{\theta}_k^l + K_k [x_k^l - H_k^T \hat{\theta}_k^l] \quad \text{with } \hat{\theta}_0^l \quad l=1 \dots n \quad (4-18b)$$

$$P_{k+1} = P_k - K_k H_k^T P_k + Q_k \quad \text{with } P_0 \quad (4-18c)$$

$$H_{k+1} = [x_k^1 \dots x_k^n u_k^1 \dots u_k^m]^T \quad (4-18d)$$

In the same way the p -output equation

$$y_k = C_k x_k + D_k u_k \quad (4-19)$$

can be put into a parameter estimation scheme structure by the following definitions,

$$\theta_k^i = [c_{i1}(k) \dots c_{in}(k) d_{i1}(k) \dots d_{im}(k)]^T \quad (4-20a)$$

$$H_k = [x_k^1 \dots x_k^n u_k^1 \dots u_k^m]^T \quad (4-20b)$$

$$y_k^i = H_k^T \theta_k^i \quad i=1 \dots p \quad (4-20c)$$

to have the filter equations,

$$H_k = [x_k^1 \dots x_k^n u_k^1 \dots u_k^m]^T \quad (4-21a)$$

$$K_k = P_k H_k [H_k^T P_k H_k + R_k]^{-1} \quad (4-21b)$$

$$\hat{\theta}_{k+1}^i = \hat{\theta}_k^i + K_k [y_k^i - H_k^T \hat{\theta}_k^i] \quad \text{with } \hat{\theta}_0^i \quad i=1 \dots p \quad (4-21c)$$

$$P_{k+1} = P_k - K_k H_k^T P_k + Q_k \quad \text{with } P_0 \quad (4-21d)$$

4.2 Computational Aspects

Let us examine the gain and covariance update equations and how to implement them since the parameter update is relatively easier to handle with respect to the others. Recall equations (4-6a) and (4-6c):

$$K_k = P_k H_k [H_k^T P_k H_k + R_k]^{-1} \quad (4-22a)$$

$$P_{k+1} = P_k - K_k H_k^T P_k + Q_k \quad (4-22b)$$

They have the common expression $P_k H_k$. If we rename this quantity with a temporary variable, T_k , then equations become,

$$T_k = P_k H_k \quad (4-23a)$$

$$K_k = T_k [H_k^T T_k + R_k]^{-1} \quad (4-23b)$$

$$P_{k+1} = P_k - K_k T_k^T + Q_k \quad (4-23c)$$

The efficiency of an algorithm is often judged by the number of operations necessary to carry one update of the parameters. Assume that the order of the state vector is N . Table (1) shows the required operations of each equation in the estimator.

To summarize, for each application of the Kalman filter parameter estimator scheme, Table (2) shows the total number of operations. The latter argument includes the

effect of a symmetric covariance matrix which obviously reduces the necessary operations.

Table 1. Number of operations for the Kalman Filter Parameter Estimator

Equation	(*,/)	(+,-)
$T_k = P_k H_k$	N^2	$N(N-1)$
$K_k = T_k [H_k^T T_k + R_k]^{-1}$	$2N$	N
$\hat{\theta}_{k+1} = \hat{\theta}_k + K_k [z_k - H_k^T \hat{\theta}_k]$	$2N$	$2N$
$P_{k+1} = P_k - K_k T_k^T + Q_k$	$N(N+1)/2$	$N + N(N+1)/2$
Total	$1.5N^2 + 4.5N$	$1.5N^2 + 3.5N$

Table 2. Total operations for the Kalman Filter Parameter Estimators

TYPE	N	(*,/)	(+,-)
SISO	$n+m$	$1.5N^2 + 4.5N$	$1.5N^2 + 3.5N$
MIMO	$Ln + Mm$	$1.5N^2 + (2.5 + 2L)N$	$1.5N^2 + (1.5 + 2L)N$
STATE	$n+m$	$3.5N^2 + 2.5N$	$3.5N^2 + 1.5N$
OUTPUT	$n+m$	$1.5N^2 + (2.5 + 2p)N$	$1.5 + (1.5 + 2p)N$

To demonstrate the algorithm, we will take the case of SISO and apply the filter (see Appendix C). Now we will simplify the above equations where P_k is replaced by a linear array of length $N(N+1)/2$ to take the advantage of its symmetry. Consider the following mapping,

$$P = \begin{bmatrix} p_{11} & & & & & \\ p_{21} & p_{22} & & & & \\ p_{31} & p_{32} & p_{33} & & & \\ \vdots & & & & & \end{bmatrix}$$

$$P_{LINEAR} = [p_{11} \quad p_{21} \quad p_{22} \quad p_{31} \quad p_{32} \quad p_{33} \quad \dots]$$

The location of the equivalent linear array is found from the symmetric array's indices by the following equation,

$$P(i, j) = \begin{cases} P_{LINEAR}(i \times (i-1)/2 + j) & \text{if } i \geq j \\ P_{LINEAR}(j \times (j-1)/2 + i) & \text{else} \end{cases} \quad (4-24)$$

Notice that although we are introducing extra arguments to be calculated, the necessary storage is reduced from N^2 to $N(N+1)/2$ for the covariance matrix P_k , and the remaining $N(N-1)/2$ storage can be used for the temporary variable T_k ($N(N-1)/2 \geq N$ for $N \geq 3$). Furthermore equation (4-24) requires only integer operations as opposed to the floating point calculations which are the most time consuming operations.

Let us examine the evaluation of T_k . The l^{th} component of T_k is given by,

$$t^l = \sum_{j=1}^N P[l, j] \times H[j].$$

So starting from the first element, the following sequences relate the referred indices of the covariance matrix to the index of the linear equivalent covariance array,

l	sequence
1	(1, 2, 4, 7, 11, 16, ...)
2	(2, 3, 5, 8, 12, 17, ...)
3	(4, 5, 6, 9, 10, 18, ...)
4	(7, 8, 9, 10, 14, 19, ...)
5	(11, 12, 13, 14, 15, 20, ...)
6	(16, 17, 18, 19, 20, 21, ...)
\vdots	

Then we can simplify this procedure by a recursive sequence formulation, $s(i,j)$, because when it comes to evaluate the covariance matrix one needs the exact locations of the matrix indices and that can be simplified.

The first column is given by,

$$s(l,1) = s(l-1,1) + l - 1, \quad s(0,1) = 1.$$

So $s(1,1)=1+1-1=1$, $s(2,1)=1+2-1=2$, $s(3,1)=2+3-1=4$, and so on. In the same formulation, the rows are given by,

$$s(l,k) = \begin{cases} s(l,k-1) + 1 & 1 \leq k \leq l \\ s(l,k-1) + k - 1 & k > l \end{cases}.$$

Thus for the third row, as an example, $s(3,1)=4$. Then $s(3,2)=4+1=5$, $s(3,3)=5+1=6$, $s(3,4)=6+4-1=9$, $s(3,5)=9+5-1=13$, etc..

If a similar argument is made on the evaluation of the covariance, which is rather simple after the recursive sequence is formulated, the algorithm can be simplified by taking the recursivity and the linear array formulation into account (see Appendix D).

Finally, we wish to consider the real time application of the above algorithms. It is certain that, as in every "current estimator", after the measurements are taken, a certain computation time must be taken into consideration. Only after the necessary calculations are made, a new estimate is available, and that might be a disadvantage where on-line adaptation is to be applied to the system.

Consider the SISO case of section (4.1.1). Suppose that the Kalman gain K_k was already calculated before the measurements are taken. Then the estimates can be updated just after the measurements with a small time delay for the necessary calculations. This is possible if the regressor H_k is not a function of the current values of the input and output, namely y_k and u_k , which implies that $d \geq 1$. In that case we have the following filter equations:

$$\hat{\theta}_{k+1} = \hat{\theta}_k + K_k [z_k - H_k^T \hat{\theta}_k] \quad (4-25a)$$

$$P_{k+1} = P_k - K_k H_k^T P_k + Q_k \quad (4-25b)$$

$$\text{update } H_{k+1} \quad (4-25c)$$

$$T_{k+1} = P_{k+1} H_{k+1} \quad (4-25d)$$

$$K_{k+1} = T_{k+1} [H_{k+1}^T T_{k+1} + R_{k+1}]^{-1} \quad (4-25e)$$

The time indices of the gain equation are increased and placed properly after the covariance update equation.

Now assume that H_k has terms involving the current values of input u_k , then partition the matrices in such a way that most of the calculations can be done before u_k is available.

The following are the equations emphasizing the latter argument:

$$T_k = T_k + P_k \begin{bmatrix} u_k \\ 0 \end{bmatrix}$$

$$\delta_k = \delta_k + \begin{bmatrix} u_k \\ 0 \end{bmatrix} T_k + R_k$$

$$K_k = T_k \delta_k^{-1}$$

$$\varepsilon_k = z_k - [u_k \ 0] \hat{\theta}_k - \varepsilon_k$$

$$\hat{\theta}_{k+1} = \hat{\theta}_k + K_k \varepsilon_k$$

$$P_{k+1} = P_k - K_k T_k^T + Q_k$$

$$H_{k+1} = [0 \ y_k \ \dots \ y_{k-n+1} \ u_k \ \dots \ u_{k-m+1}]^T$$

$$T_{k+1} = P_{k+1} H_{k+1}$$

$$\varepsilon_{k+1} = H_{k+1}^T \hat{\theta}_{k+1}$$

$$\delta_{k+1} = H_{k+1}^T T_{k+1}$$

In other words the above simplification ignores the effect of u_k in the equations until it becomes available.

4.3 Examples

Consider the second order sampled data system ($T=0.05$ sec) characterized by the difference equation,

$$y_k = a_1(k)y_{k-1} + a_2(k)y_{k-2} + b_1(k)u_{k-1}$$

where the parameters $a_1(k)$, $a_2(k)$ and $b_1(k)$ are to be estimated based on input-output measurements. Figures (16), (17) and (18) show the Kalman Filter (with $Q_k=10^{-20}I$, $P_0=10^3I$, $\hat{\theta}_0=0$), together with the RLS (with $P_0=10^3I$, $\hat{\theta}_0=0$) results for a Gaussian random sequence input (persistent excitation). No measurement noise is

assumed. The same system is simulated by a step input and the results are given in Figures (19), (20), (21).

It is observed that, for the persistent excitation case, the Kalman Filter follows the step changes in the parameters, and converges to the actual parameter values. However, for the case where the system is derived by a step input, the estimates have offset values, but the number of discrete frequencies in the input sequence strictly affect the number of identifiable parameters⁽²³⁾. Nevertheless, the Kalman Filter follows the changes in each case where the RLS estimator fails to respond to the parameter changes in both of the cases. Furthermore, a simple analysis shows that, the resulting transfer function given by the Kalman Filter estimates for the step input matches the actual transfer function for low frequency regions.

Consider the following system (ball-in-the-hoop) given by the state equation,

$$\begin{bmatrix} \theta(t) \\ \dot{\theta}(t) \\ \Psi(t) \\ \Psi'(t) \end{bmatrix} = F \begin{bmatrix} \theta(t) \\ \dot{\theta}(t) \\ \Psi(t) \\ \Psi'(t) \end{bmatrix} + G u(t)$$

where

$$F = \begin{bmatrix} 0.0 & 1.0 & 0.0 & 0.0 \\ 0.0 & -1.7518 & -3.936 & 0.0 \\ 0.0 & 0.0 & 0.0 & 1.0 \\ 0.0 & -0.6029 & -75.66 & 0.0 \end{bmatrix}$$

$$G = \begin{bmatrix} 0.0 \\ 29.094 \\ 0.0 \\ 100.14 \end{bmatrix}$$

The system is sampled at $T=0.10$ sec., and excited by a step input to identify the parameters of the state and input matrices. Five state measurements were taken (see Table (3)).

Table 3. State measurements of "ball-in-the-hoop" system

Time	$\theta(t)$	$\dot{\theta}(t)$	$\Psi(t)$	$\dot{\Psi}(t)$
0.00	0.000000	0.000000	-1.000000	0.000000
0.10	0.154597	2.978369	-0.601010	7.439874
0.20	0.570984	6.789393	0.302242	9.448706
0.30	1.176426	5.223810	1.055641	4.641170
0.40	1.915283	7.950068	1.115215	-3.537536
0.50	2.764527	9.048253	0.431920	-9.266817

The estimates of the state and input matrices are given in (Appendix E) where the Kalman Filter was used as a parameter estimator. The final estimates ($t=0.50$) match the parameters of the equivalent sampled data system. Also note that the order of the covariance matrix is $5(=4+1)$, not $20(=4^2+4)$.

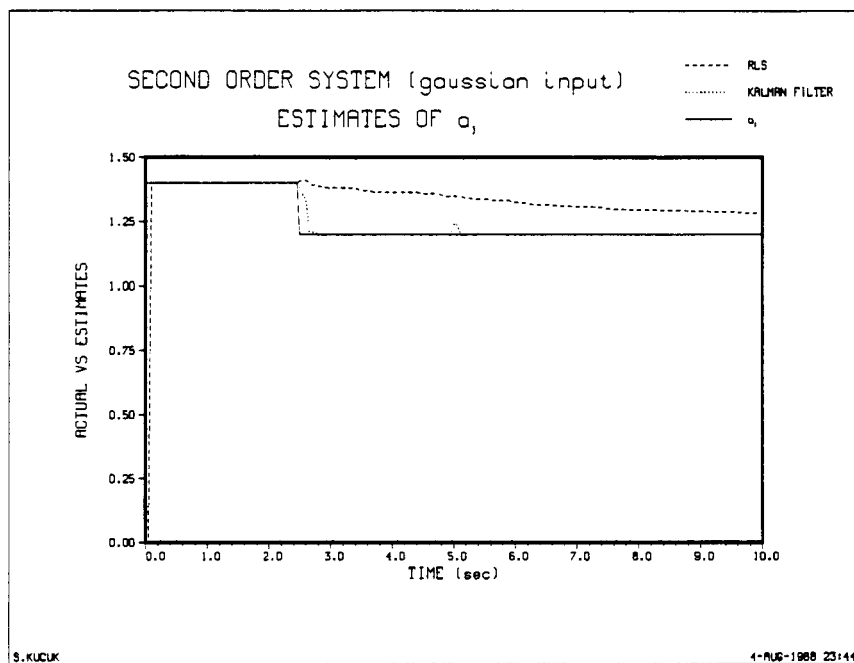


Figure 16. Kalman Filter vs RLS estimate of a_1 , (Gaussian input)

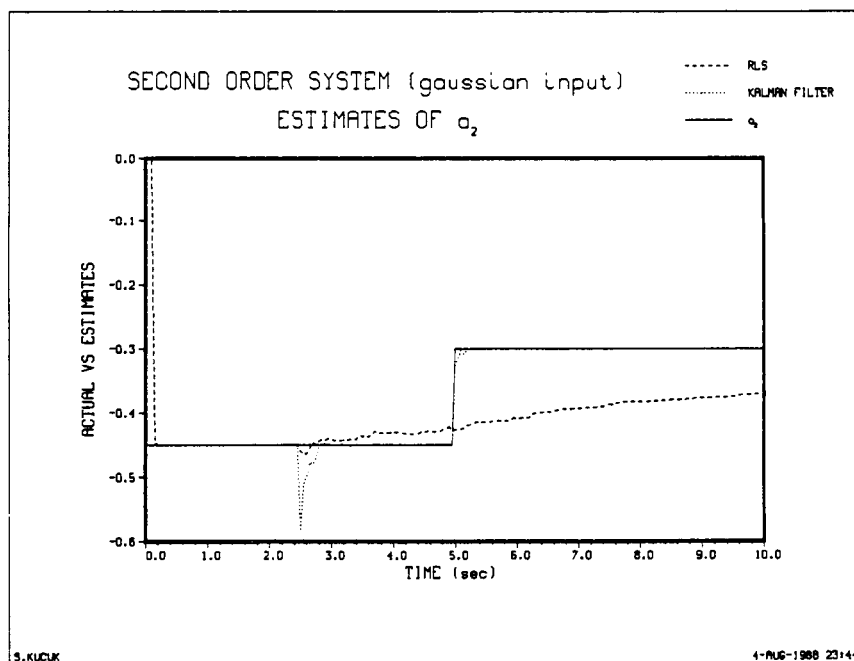


Figure 17. Kalman Filter vs RLS estimate of a_2 , (Gaussian input)

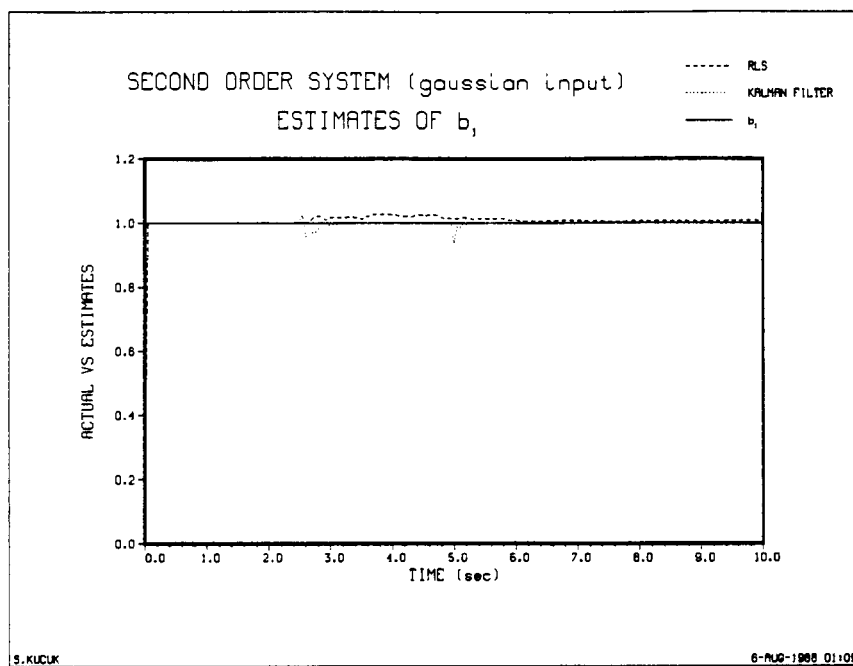


Figure 18. Kalman Filter vs RLS estimate of b_1 , (Gaussian input)

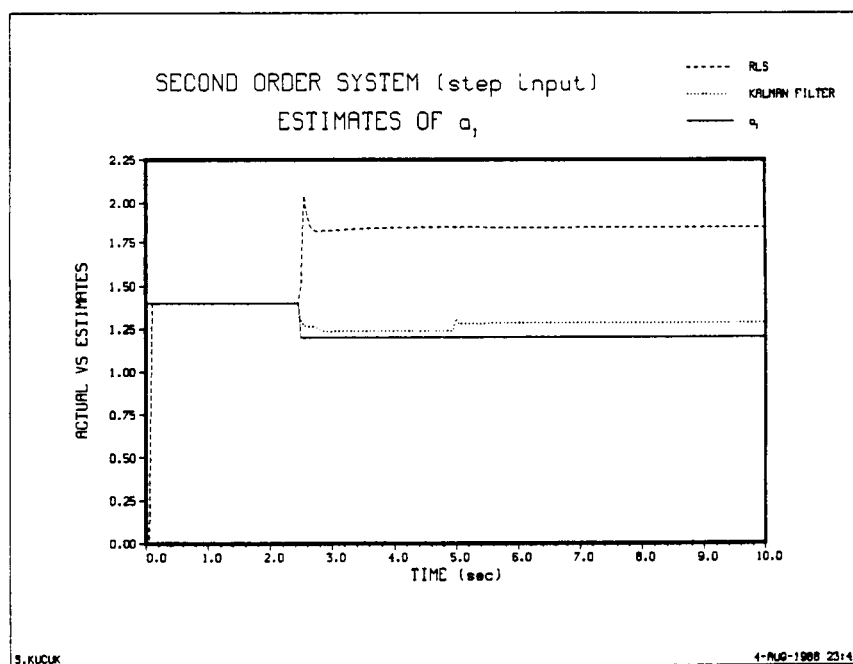


Figure 19. Kalman Filter vs RLS estimate of a_1 , (Step input)

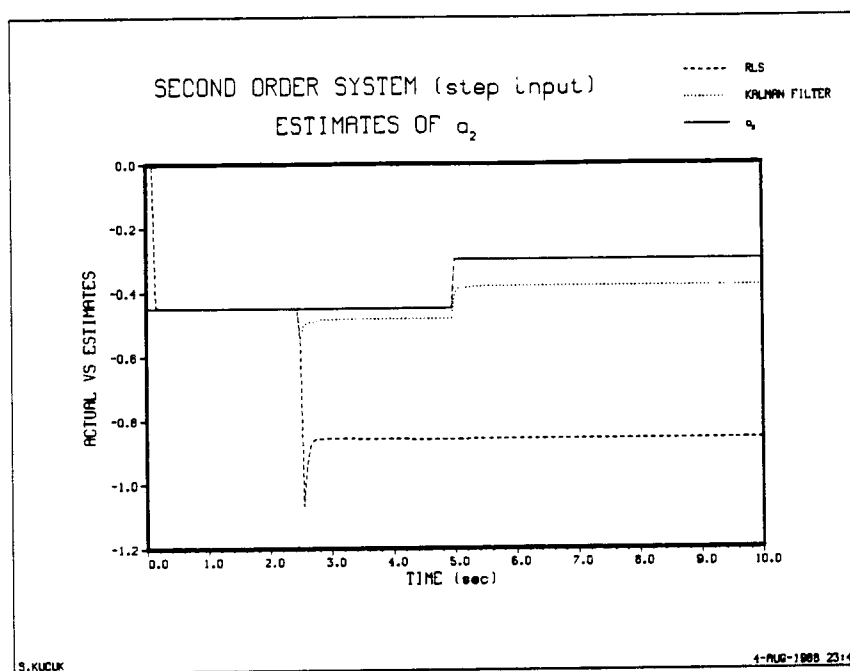


Figure 20. Kalman Filter vs RLS estimate of a_2 , (Step input)

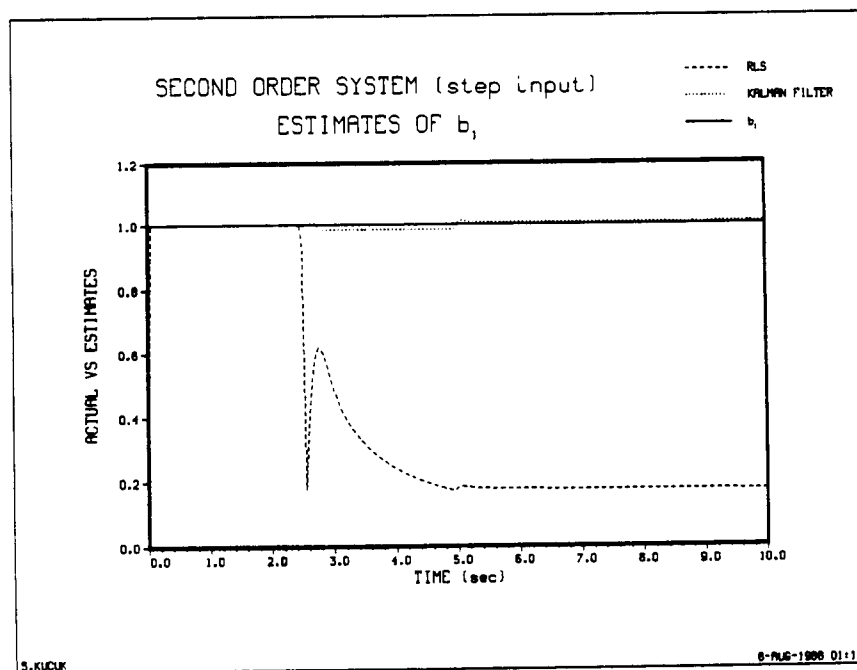


Figure 21. Kalman Filter vs RLS estimate of b_1 , (Step input)

5.0 THE ADAPTIVE PILOT MODEL

In this chapter we will combine the adaptive pilot model with the discrete McRuer-Krendel human describing model derived in Chapter 2, the Root Locus criterion and the closed loop operating regions defined in Chapter 3, and the estimation scheme discussed in Chapter 4.

In Section (2.3), the adaptation process was divided into two groups. The first was the detection and identification. The adaptive model that will be developed, will have a discrete time difference equation for the identification which is derived by the detector. The detector monitors the control displacement of the pilot and the rate of the error signal which is proportional to the controlled element's output value. This can be through the instrumentation or through the senses or a combination. If there is any uncertainty in the detection, like trying to observe visual feedback in the dark, the identification must be done accordingly to include the effect of measurement error.

The most important part of the adaptation procedure is the modification and optimization, although we can not separate any of the parts of the adaptation because any failure of one will directly affect the whole procedure. In Chapter 3, we related the closed loop human-aircraft modes to the adaptive pole-zero pair of the human response model as a function of the controlled element dynamics. The closed loop bandwidth has a nominal value which the pilot knows from his experience. He knows that if the controls are pushed faster than some value, which he must have estimated by that time, then the aircraft will be responding in a "sluggish" way or the responses will be too fast where there may be oscillations or the forces on the aircraft may be dangerous. If he fails to

react slower than some value, then the aircraft may fail to respond in time for the proper action. Thus the pilot knows what to do when it comes to maneuvering the aircraft. The responses can not be too slow or too fast but must be in the proper operating region. Any optimization must be within this region. If the aircraft denies any attempt to operate in that region, the pilot must decide to relocate the operating region as safely as possible.

Keeping these facts in mind, our modification procedure must do the appropriate selection of the closed loop bandwidth, equivalently the dominant closed loop poles. The key element will be the necessary pilot gain required to perform a certain maneuver. If the pilot gain is bigger than some value, then closed loop pole must be changed. This can be related to the gain equation (3-15) of Section (3.1). The pilot gain is proportional with the magnitude of the denominator dynamics and inversely proportional with the numerator dynamics of the controlled element. A big gain then indicates that the controlled element has some resonances at the desired closed loop frequencies. Relating the latter argument to the root locus is the case where the pole and the open loop system zero of the plant are very close to each other.

On the other hand, if the required pilot gain is too small, this indicates that the plant has already modes at the desired closed loop location. This might be dangerous because the pilot can not maintain control. The aircraft responds, but the pilot is not totally in charge.

Therefore in any of the above cases, the judgment must be made on the desired operating poles. Once the selection does not contradict the limits of the region, then the necessary phase required from the adaptive pole-zero pair is determined. The rest is the optimal solution for the pole and zero that will satisfy the phase constraint and minimize

the error signal. The corresponding procedure defining our adaptive pilot model is given in Figure (22).

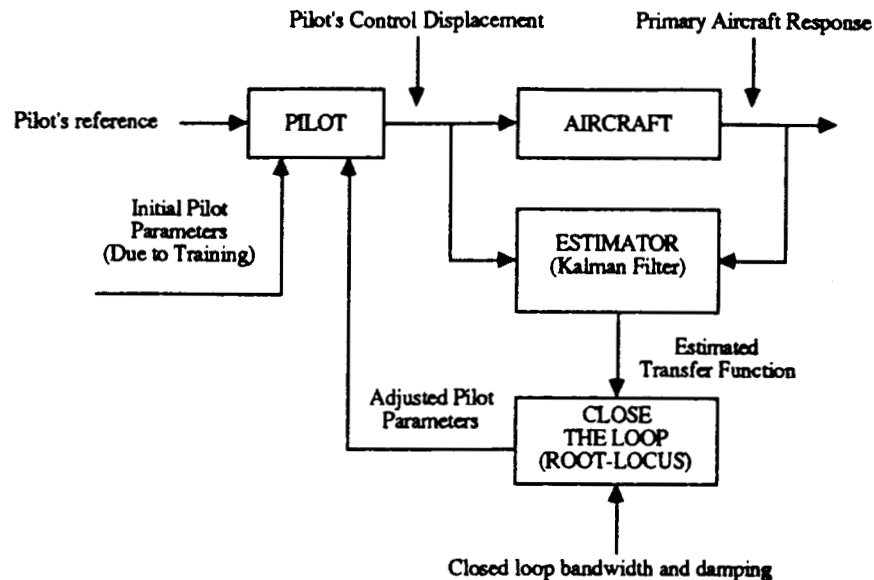


Figure 22. The Adaptive Pilot Model

Let us examine the processes in the adaptive model. As soon as the error signal is active, the adaptation begins. The error signal is held until the current information is processed and the control is applied. The error is then delayed because of the pilot's visual lags. The current estimate of the controlled element dynamics from the Kalman filter estimator is used to get information on the frequency content at the desired closed loop pole. This pole is the nominal operating value. Since we related the adaptation to the root locus criterion, the estimate of the open loop transfer function is used to evaluate the value of equation (3-8). This gives the part of the phase necessary which is not determined by the pilot in equation (3-9). Then the type of gain is selected depending on

the relative change of the primary response variable. The difference gives the phase that must be provided by the adaptive pole-zero of the human response mechanism, but first the absolute magnitude of the gain must be checked to make sure that pilot does not use the limits of the controls, or he does not have to provide extensive gain to move the controls. If the latter occurs, then this requires the pole-relocation procedure. Until the gain is in the allowable limits, the closed loop pole is moved in the operating region. Then the phase required by the pole and zero pair is fixed. The rest is the optimization problem. The values of the zero and pole are searched that will minimize the error signal and at the same time supplying the desired phase difference to close the loop at the desired closed loop pole. After the adaptive part of the human response is evaluated, the output is sent to the neuro-muscular equivalent of the model which sends the appropriate commands through the nerves to the muscles to perform the desired task. Finally the adaptive model is ready to process another error signal, and this goes on until the steady state is reached or the desired maneuvering is fulfilled.

The problem now is to give the model some initial knowledge to start the algorithm. This is the analogy to pilot training. The adaptive model needs some initial values of the model parameters so that they will be used until adaptation is necessary or the estimators converge to give reliable estimates of the controlled element dynamics. Nevertheless, this is a primitive attempt to describe pilot training. A real pilot, depending on the scenario, would not only adjust the initial values of parameters ($H_p(s; t=t_0)$), but also start the control sequence properly ($\{u_p(t); t_0 \leq t \leq T_f\}$). Unfortunately, we do not have the starting control sequence, but an expert system would.

The initial parameters are calculated, as we mentioned earlier, by aircraft testing at the desired flight envelope and using low order approximations to design the pilot

parameters via root locus techniques. These are used as the static part of the pilot model which are subject to change. This is actually what happens in real pilot control. The pilot has a pre-determined idea of how the aircraft will behave at that operating region. So he moves the controls depending on this information. But if he fails to succeed in the maneuvering, by monitoring the input-output relationship, he adjusts to the changing environment. The flowchart in Figure (23) demonstrates the adaptation algorithm.

To conclude this chapter we will mention the multivariable manual control case. The pilot actually resorts to controls depending on the configuration and he uses the best combination possible to maintain the controllability, stability and the performance. This means that he can, and will, use more than one control at a time; for example while in the coordinated turn he uses the longitudinal and lateral sticks by one hand, the rudder pedals by his feet, and the throttle or nozzle settings by the other hand whenever necessary. We will simulate this multivariable control case by having more than one single variable loop, each closing the loop from the primary response variable to the corresponding pilot input. The multivariable pilot loops are shown in Figure (24). This seems to be a good approximation where the pilot is required to fulfill simple maneuvers over the aircraft speed, altitude or the angular positioning. Although the single variable loops do not affect each other directly, one's output will change the other through the dynamic equations. Furthermore we will add constraints about the behavior of the aircraft state for the optimization problem of each one of the adaptive loops so that better results can be obtained. In the next chapter, we will give some examples on how to design the static pilots and simulate them in the Harrier AV-8B environment to perform simple tasks. The control loops will be multivariable loops. We will compare the static pilots by the adaptive pilots and discuss the results.

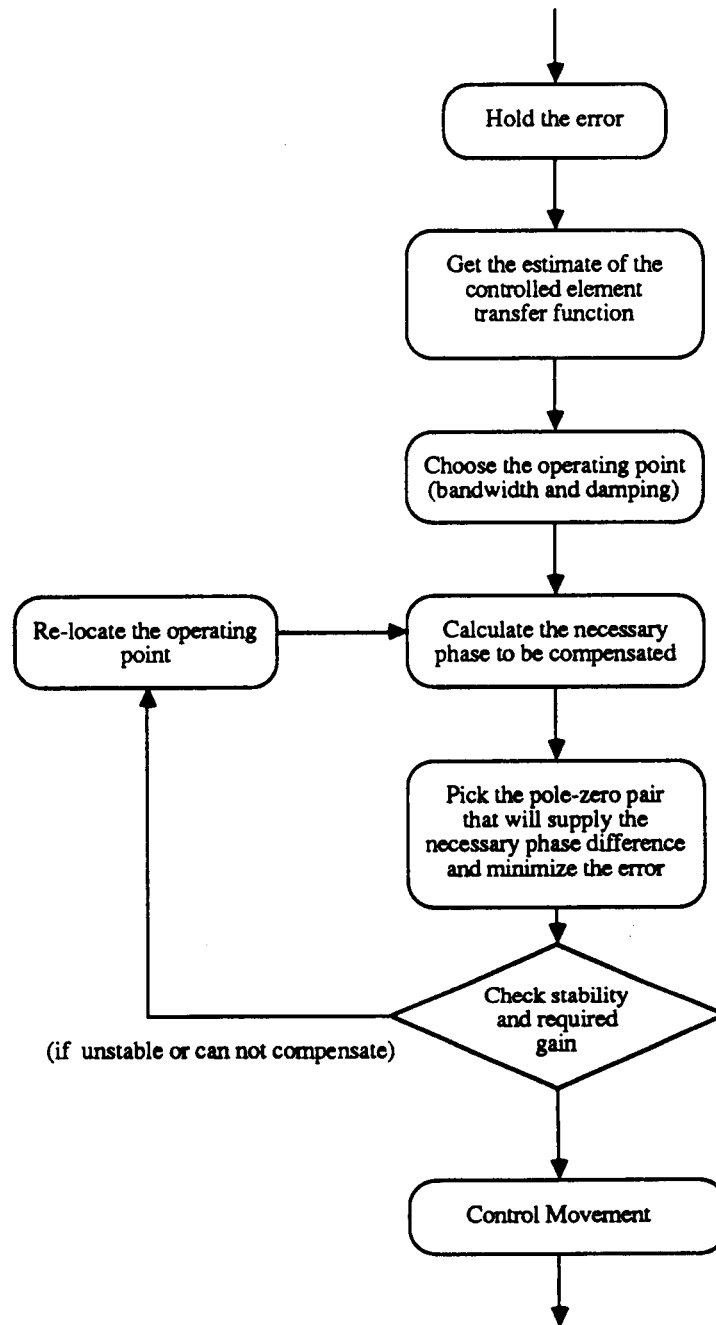


Figure 23. Flowchart of the adaptive pilot model

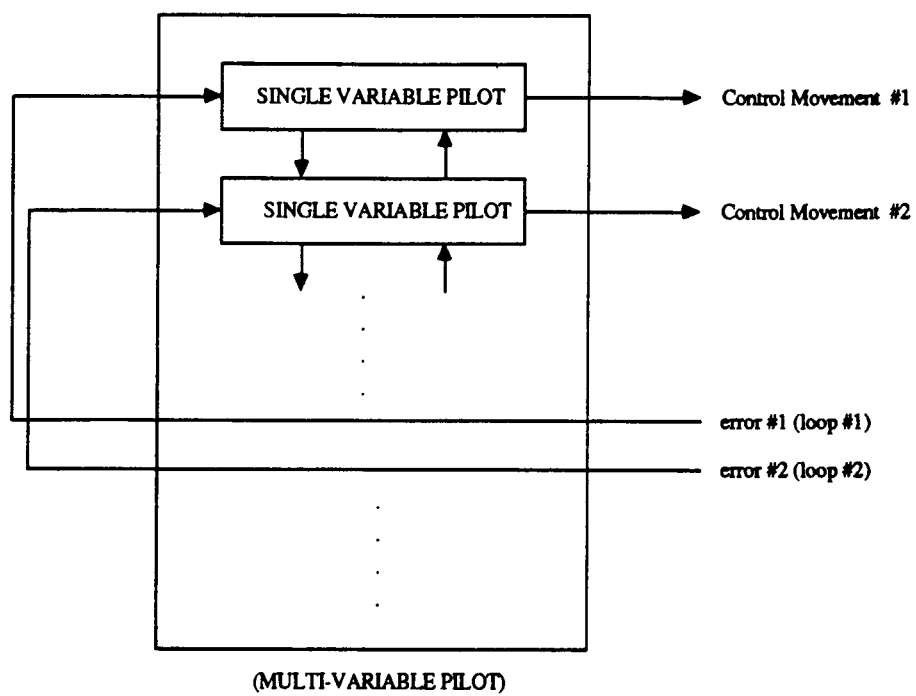


Figure 24. Multivariable pilot configurations

6.0 PILOT INSERTIONS

6.1 Selection of the control sets

An analysis of the Harrier AV-8B control system suggests the following: since the aircraft is symmetric, any movement of the longitudinal stick (to the elevator or stabilizer) creates longitudinal motions. Engine nozzle angle, which is the most important aspect of thrust vectoring, a unique feature of the Harrier AV-8B, is also symmetric. There are four nozzles, having two symmetric openings on each side of the aircraft, but not creating any lateral moments since only forward and downward components of the force changes in the equations of motion. Thrust, which affects the magnitude of the forces at the nozzles, must also have longitudinal effects since it is only adding force in the direction of the main thrust vector. Therefore the longitudinal pilot is characterized by controlling the stabilizer (longitudinal stick), engine throttle setting and nozzle angle setting. We will now investigate the primary variables of the longitudinal control set which means that by checking the responses of the aircraft, the primarily affected states from the control input are to be selected.

Let us examine the stabilizer first by testing the longitudinal stick through impulses. These tests will be taken from a trimmed flight condition which is very important. A trimmed aircraft is in equilibrium, and there are no accelerations (except the turbulances or changes in the relative wind) so that at this configuration small perturbation analysis can be performed. The length of the window is also important. As we mentioned earlier, the short period responses of the aircraft are perceptible to the

pilot. Furthermore since these tests are taken without a pilot in the loop, just the insertion of the required input sequence to the control units, the aircraft will go out of the trim conditions because of the disturbed motion unless new trim settings are determined. To summarize, we first trim the aircraft and then insert impulses to the controls one at a time and observe the aircraft responses within a small time window of three or may be four seconds length. This time interval will define the response of the aircraft shortly after the pilot has commanded. Also we will avoid numerator dynamics whenever possible in order to obtain simple all-pole transfer functions.

Consider the initial aircraft parameters, $(\Phi, \Theta, \Psi) = (0.0^\circ, 6.0^\circ, 0.0^\circ)$, at 20.0 knots, with nozzles directed at 81.77° , 100 ft. above sea level. This is a low speed configuration in the transition region to the high speed mode where nozzle angles are close to vertical, pointing downwards, which means that most of the thrust is used for the lifting of the aircraft. This is an advantage of the Harrier AV-8B aircraft. By directing the nozzle angles, it can fly at very low speeds without any difficulty.

Figures (25), (26), (27) and (28) show the pitch, pitch velocity, altitude and the airspeed responses of the Harrier AV-8B for the longitudinal stick impulse. The stick movement changes the elevator (stabilizer) angle. There is also the effect of front and aft RCS valves, but we will consider the combined effect since the pilot observes these total changes in the responses.

Altitude change is almost negligible. The speed drop is approximately 0.1 knots per second, but this is also a side effect of pitching up. The pitch angle of the aircraft increases the vertical lift component of the thrust at the same time decreasing the forward thrust vector which as a result drops the forward velocity. This causes the relative speed

of the aircraft to drop significantly. Similarly, if the aircraft was pitching down, with only the stabilizer, then the speed would tend to increase.

The primary response of the stabilizer, and the main purpose, is the control of the pitch angle. This seems trivial because by adjusting the elevator angle, equivalently by directioning the "nose" of the aircraft, pitching moments are applied thus changing the pitch angle. If the pilot needs to pitch-up, he must pull the longitudinal stick. Conversely he pushes the stick to pitch-down. So the primary response is the pitch angle, and the remaining changes in altitude, forward and downward velocities, angle of attack are disturbances to be regulated for the case of the longitudinal stabilizer input.

From the control point of view, the pitch velocity response can be approximated by a first order pole which reduces the transfer function from the longitudinal stick to the pitch rate to be,

$$\frac{\delta_e(s)}{\theta(s)} \propto \frac{1}{s + a\{\theta, \delta_e\}} \quad (6-1)$$

The pitch angle is then given by the pure integration of the pitch rate:

$$\frac{\delta_e(s)}{\theta(s)} \propto \frac{1}{s(s + a\{\theta, \delta_e\})} \quad (6-2)$$

Next we will analyze the nozzle angle setting. Figures (29), (30), (31) and (32) show the airspeed, altitude, pitch angle and the pitch rate responses for a positive impulse on the nozzle angles. Slowing of the aircraft is reasonable since increasing nozzle angle means more power for lifting as in the case of a pitch-up command. While the pitch angle and altitude do not change too much, we notice a step-like response in the airspeed. The primary response then is observed to be the airspeed and this assumption confirms with

the Harrier AV-8B pilots. In fact, it seems obvious that by changing the effective angle of the main thrust vector, all the body axis forces of the aircraft change, and it is the fastest way to change the speed. However, the nozzle setting can also be used to control the altitude since by changing the downward speed component, the altitude can be adjusted. Also changes in nozzle angle setting applies pitching moments to be regulated.

The speed response can be approximated by a step within the region of our interest, resulting,

$$\frac{\delta_{\theta_j}(s)}{v_{eq}(s)} \propto -\frac{1}{s} \quad (6-3)$$

Once again the other responses will be the regulating set. We must mention that the pilot may wish to control the aircraft, say the pitch angle, through the controls of the nozzle angles. That is possible, but we are only trying to model the most common configurations of the aircraft control mechanism. Of course the latter case can be modelled as a separate mode, and transfer functions can be obtained. However, it will not be a regular scheme.

In Section (1.2) we mentioned that the throttle setting is the most common input for altitude control. If the altitude is being controlled, then the feedback is from the altitude response. Otherwise, if the constraints are on the rate of the altitude, then the feedback is taken from the altitude rate response of the aircraft. Figures (33), (34), (35) and (36) show the rate of the altitude, altitude, pitch angle, and the airspeed results for a positive throttle impulse which controls the flow of the fuel to be combusted in the engine. Unlike the nozzle angle control, no noticeable effect can be seen in the pitch or the speed and that is the main reason for its use in altitude control. The approximated transfer functions are as follows:

$$\frac{\delta_{TH}(s)}{h(s)} \propto \frac{1}{s^2 + 2\xi\{\dot{h}, \delta_{TH}\}\omega_n\{\dot{h}, \delta_{TH}\}s + \omega_n^2\{\dot{h}, \delta_{TH}\}} \quad (6-4a)$$

$$\frac{\delta_{TH}(s)}{h(s)} \propto \frac{1}{s(s^2 + 2\xi\{\dot{h}, \delta_{TH}\}\omega_n\{\dot{h}, \delta_{TH}\}s + \omega_n^2\{\dot{h}, \delta_{TH}\})} \quad (6-4b)$$

A second order response is observed in the altitude rate, and altitude is the pure integral of this signal. Once again if the desired command is a change in the altitude, then altitude will be the feedback element. On the other hand, if the primary concern is on the rate of climb or descent, then the rate of the altitude is used in the feedback control.

The lateral control set is the lateral stick, which includes the effect of ailerons, and the RCS valves, and the rudder operated separately from the lateral stick through the pedals. The same aircraft with the initial rates is subjected to a positive impulse input at the ailerons, and Figures (37), (38), (39) and (40) show the corresponding roll angle, roll rate, yaw angle and the yaw rate responses. The primary response in this case is the roll angle. Transfer functions are estimated to be,

$$\frac{\delta_a(s)}{r(s)} \propto \frac{1}{s + a\{r, \delta_a\}} \quad (6-5a)$$

$$\frac{\delta_a(s)}{\Phi(s)} \propto \frac{1}{s(s + a\{r, \delta_a\})} \quad (6-5b)$$

The sideslip, yaw, yaw rate and roll angle changes are given in Figures (41), (42), (43) and (44) for a positive rudder pedal impulse. The sign of the rudder pedal input in this case implies the right or left pedal movements. Notice the change of the sideslip angle. Zero sideslip is very important, and it must be fulfilled whenever possible because it changes the aerodynamic behaviour of the aircraft. From outside of the aircraft the vehicle seems to slide in a direction not parallel to the fuselage. The wind then is exerted by an angle to the aircraft.

The primary response of the rudder is the sideslip angle for coordinating a turn and yaw angle for heading adjustments which can be approximated by the transfer functions given by:

$$\frac{\delta_r(s)}{\beta(s)} \approx \frac{1}{s(s+a\{\beta, \delta_r\})} \quad (6-6a)$$

$$\frac{\delta_r(s)}{\Psi(s)} \approx \frac{(s+b\{\Psi, \delta_r\})}{s^2(s+a\{\Psi, \delta_r\})} \quad (6-6b)$$

Thus we have examined all the controls supplied to the Harrier AV-8B pilot. However, there are also the assisting devices provided to the pilot like the SAS switch. The SAS unit adds a single pole to the mechanism and closes a feedback loop to the control unit before it is connected to the pilot stick input. This is a very limited control. In most of the cases the effect of the SAS control is within a 5% range so that it does not interfere with the pilot control so the pilot has full authority on the aircraft. But in cases where the pilot does not hold the stick continuously and incremental adjustments must be made to compensate the phugoid or the spiral mode, the SAS becomes quite useful. Although it can not hold the current configuration of the aircraft for a long period because of its limited authority, the SAS devices are used commonly at low speeds by the pilots. For that reason we will assume that the SAS is fully engaged in our simulations while using the Harrier AV-8B simulation program provided by NASA-Lewis. The above responses used for the approximate transfer function analysis were also taken with the SAS switch activated. Let us add that the SAS unit is inoperative at high speeds and high speed configuration is a very sensitive operating region. Therefore we will insert our pilot models to the simulation program at low speed operating conditions.

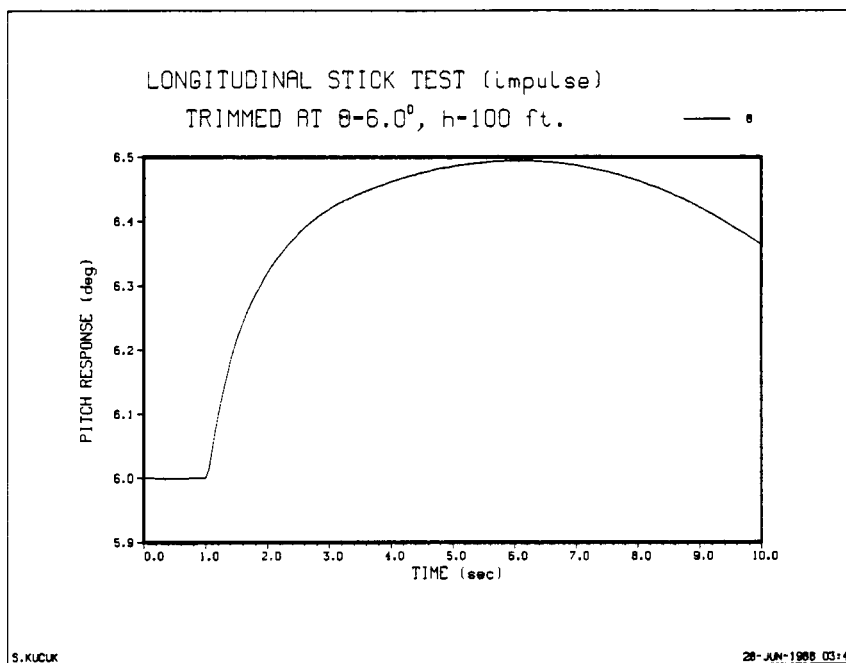


Figure 25. Pitch response to a longitudinal stick impulse

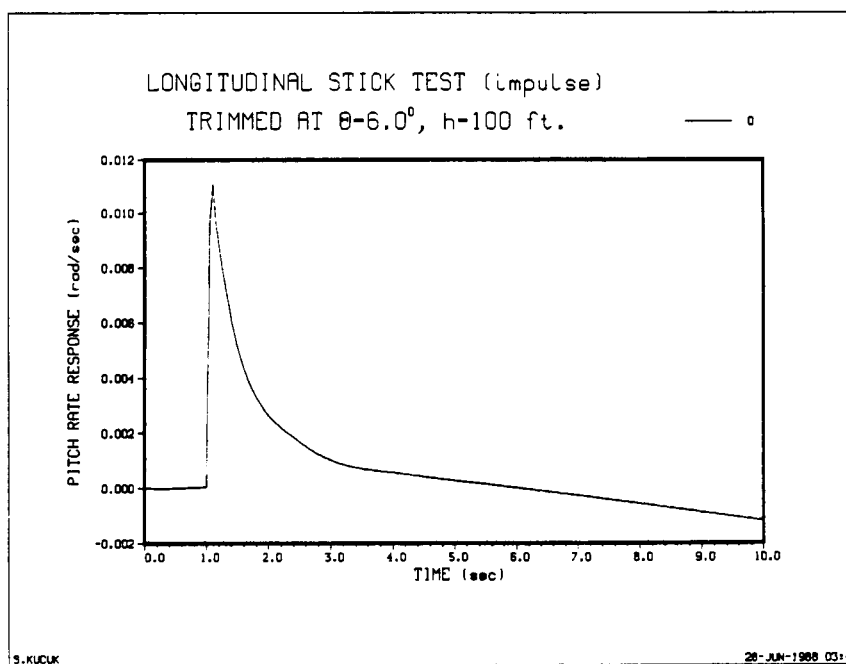


Figure 26. Pitch rate response to a longitudinal stick impulse

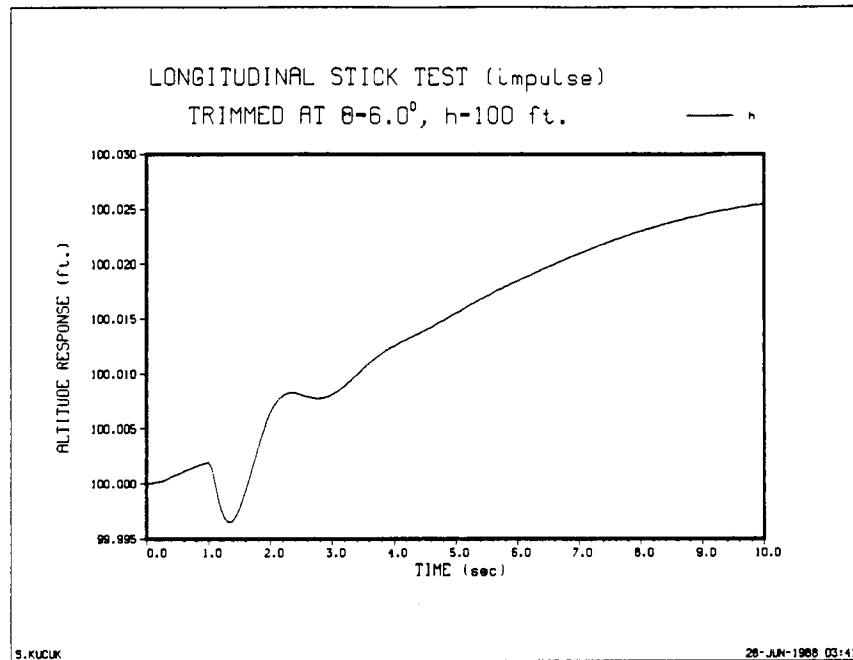


Figure 27. Altitude response to a longitudinal stick impulse

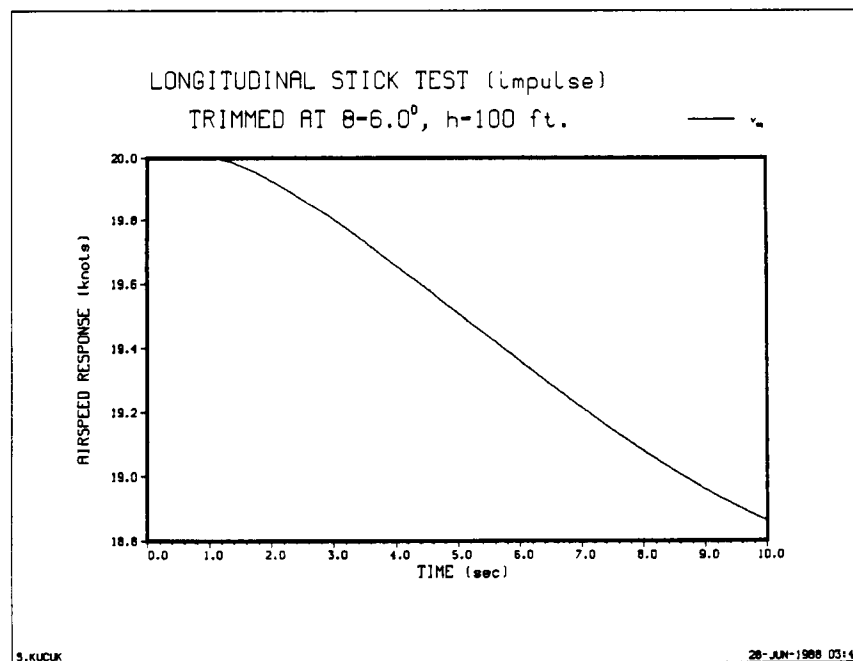


Figure 28. Airspeed response to a longitudinal stick impulse

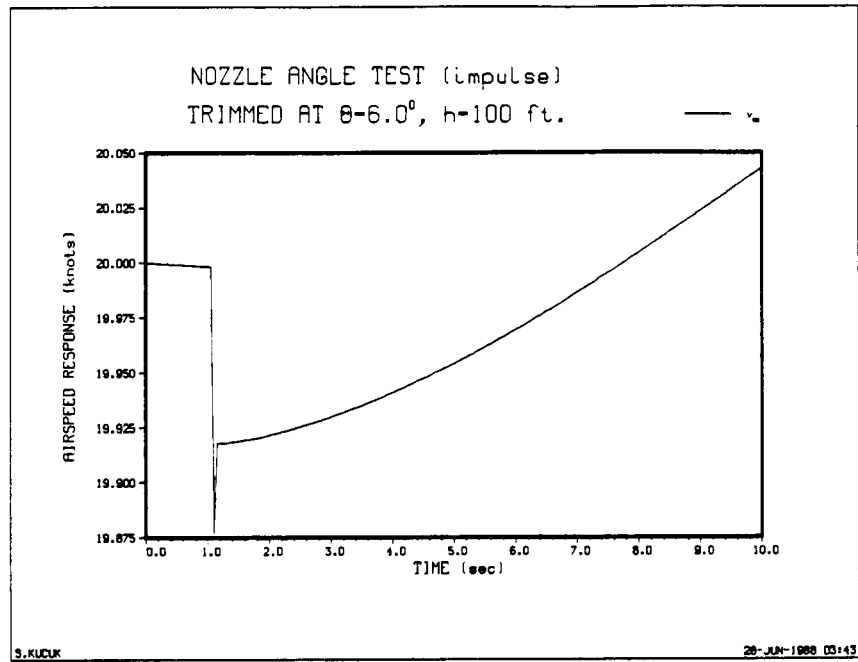


Figure 29. Airspeed response to a nozzle setting impulse

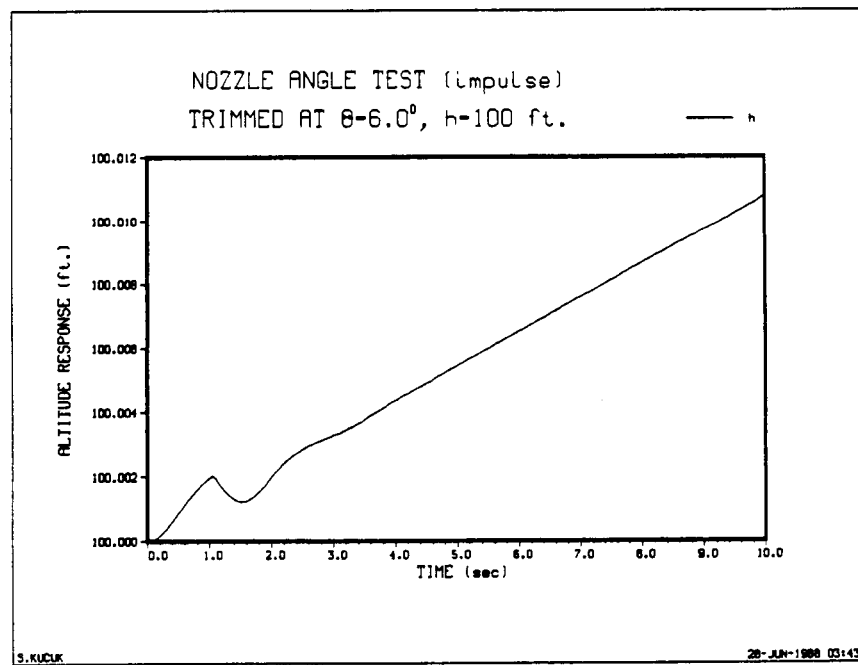


Figure 30. Altitude response to a nozzle setting impulse

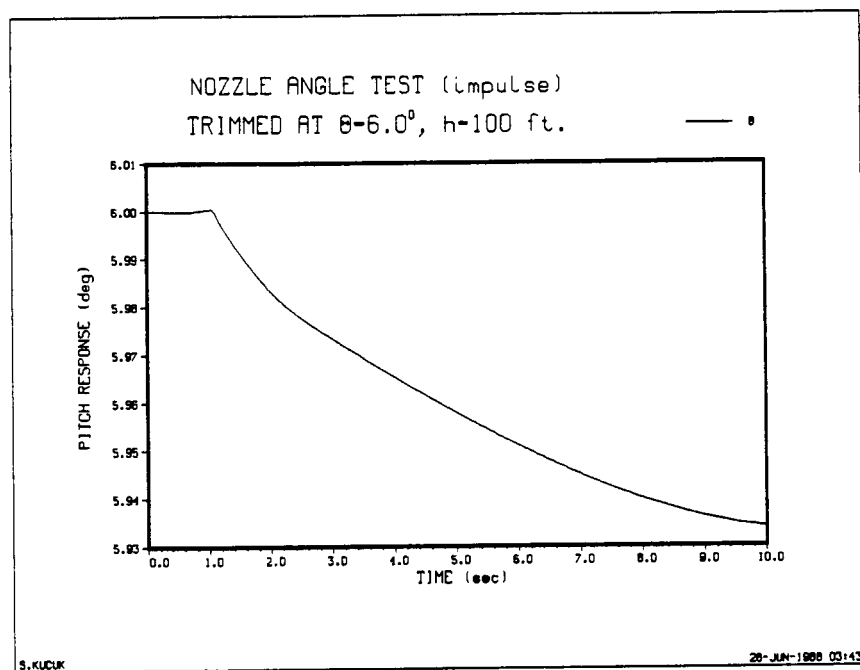


Figure 31. Pitch response to a nozzle setting impulse

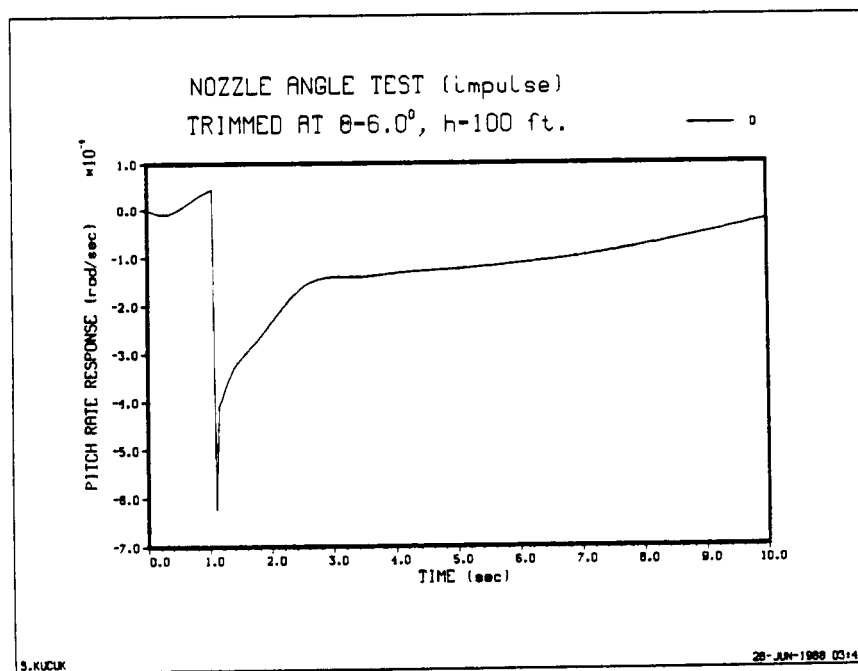


Figure 32. Pitch rate response to a nozzle setting impulse

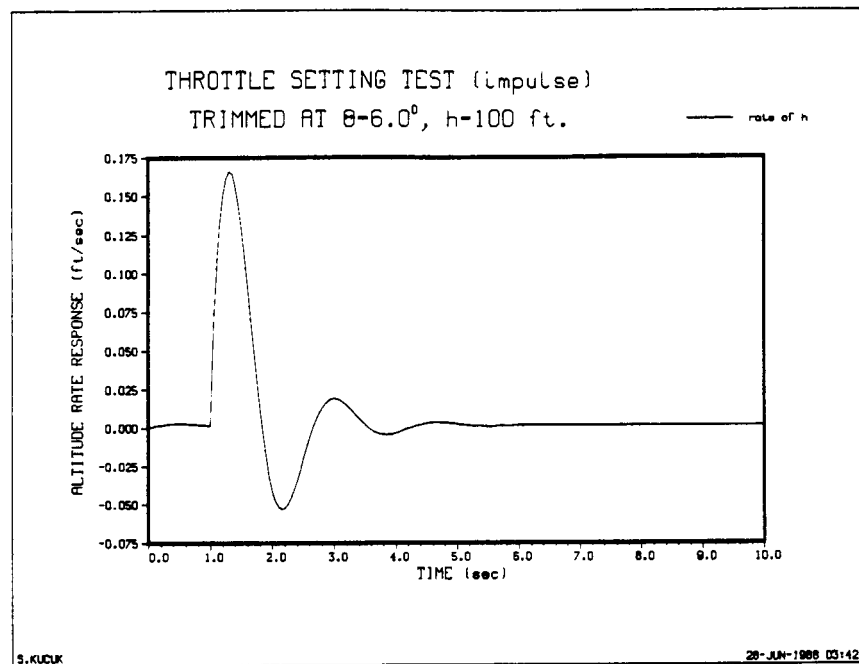


Figure 33. Altitude rate response to a throttle setting impulse

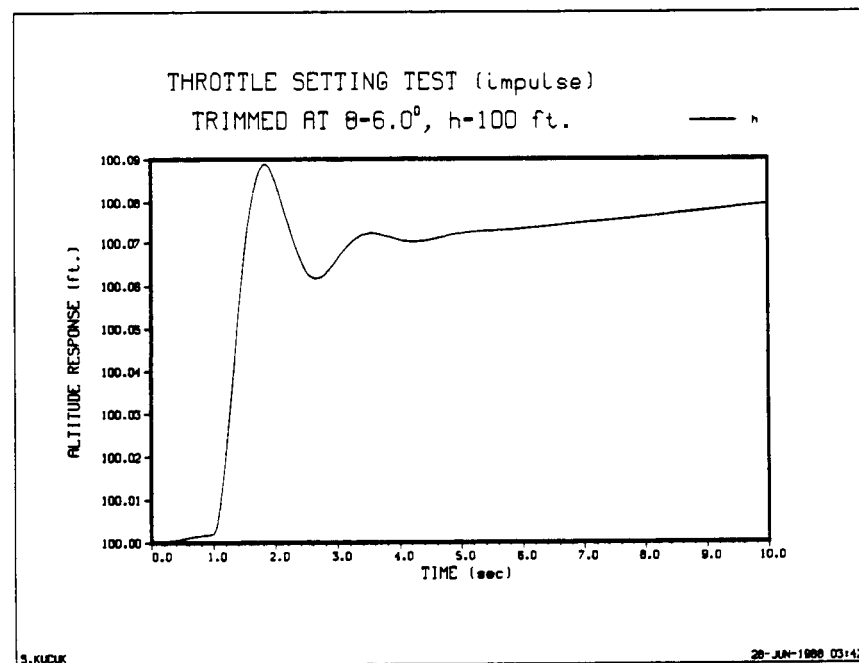


Figure 34. Altitude response to a throttle setting impulse

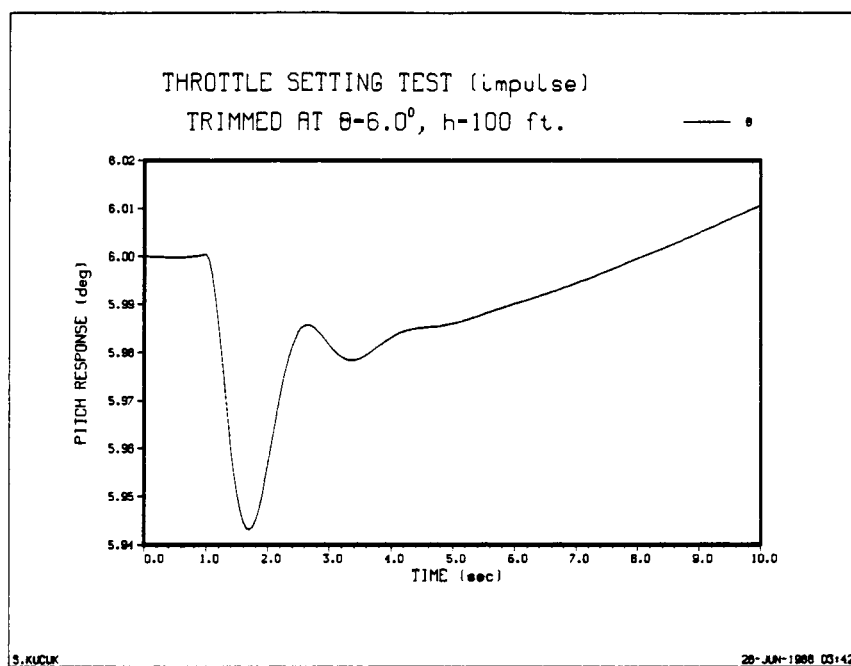


Figure 35. Pitch response to a throttle setting impulse

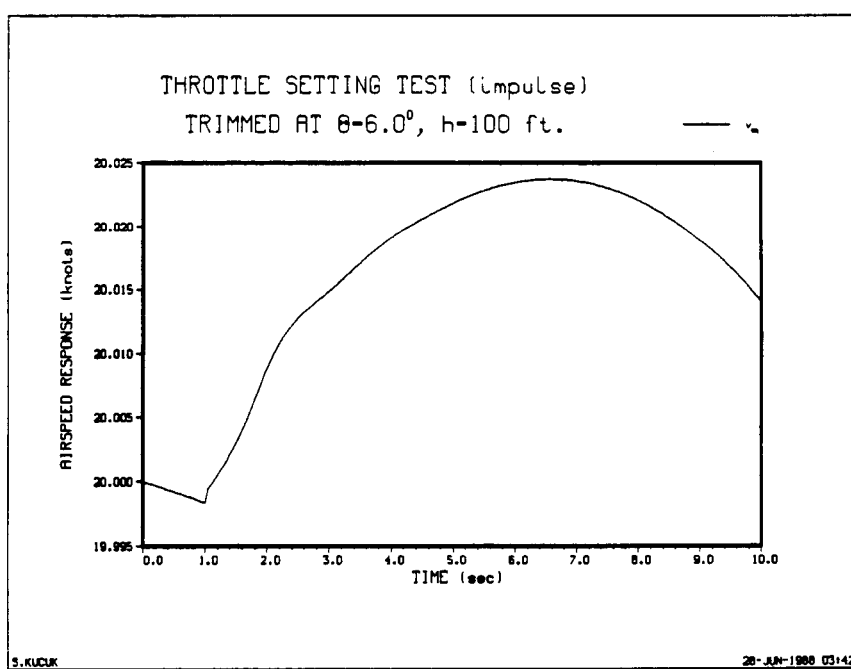


Figure 36. Airspeed response to a throttle setting impulse

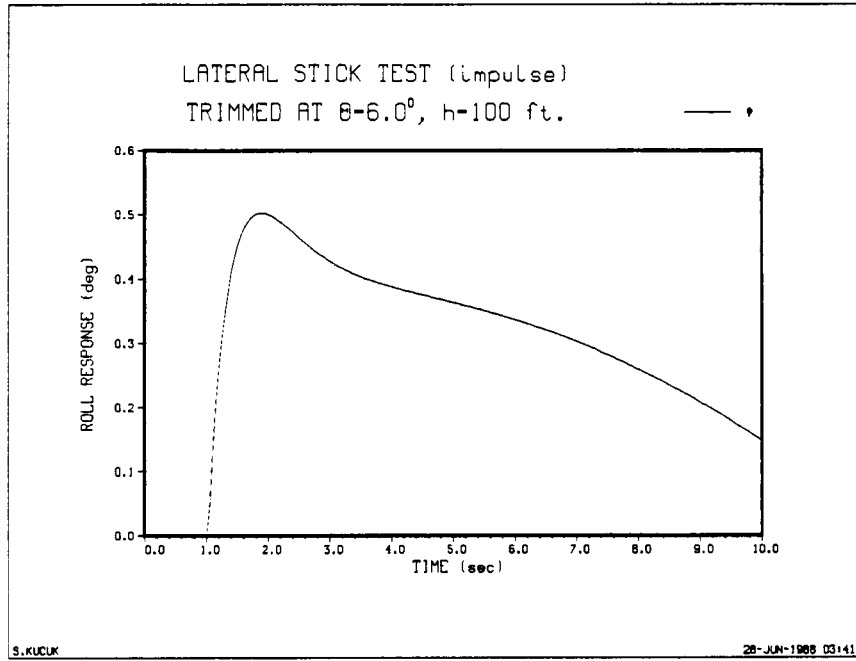


Figure 37. Roll response to a lateral stick impulse

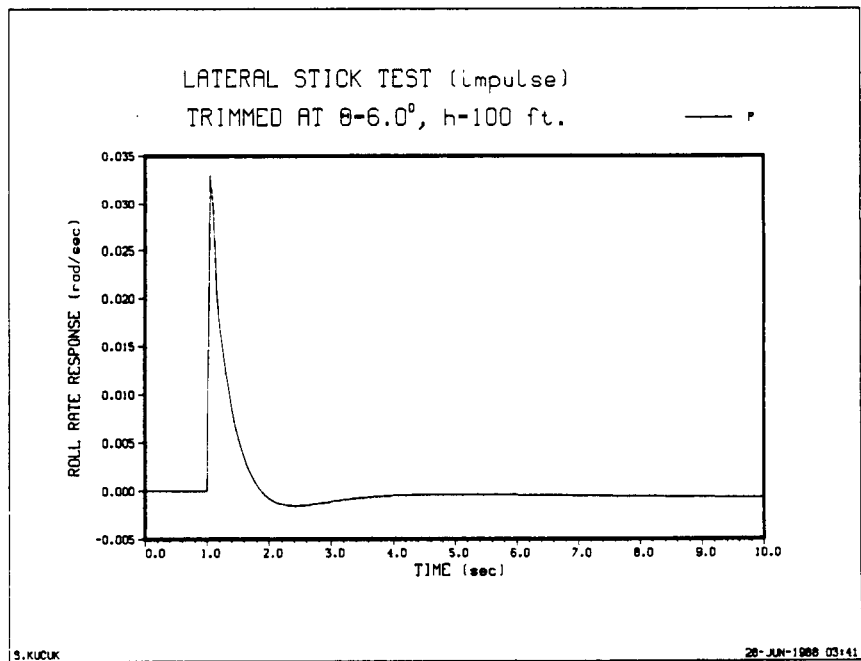


Figure 38. Roll rate response to a lateral stick impulse

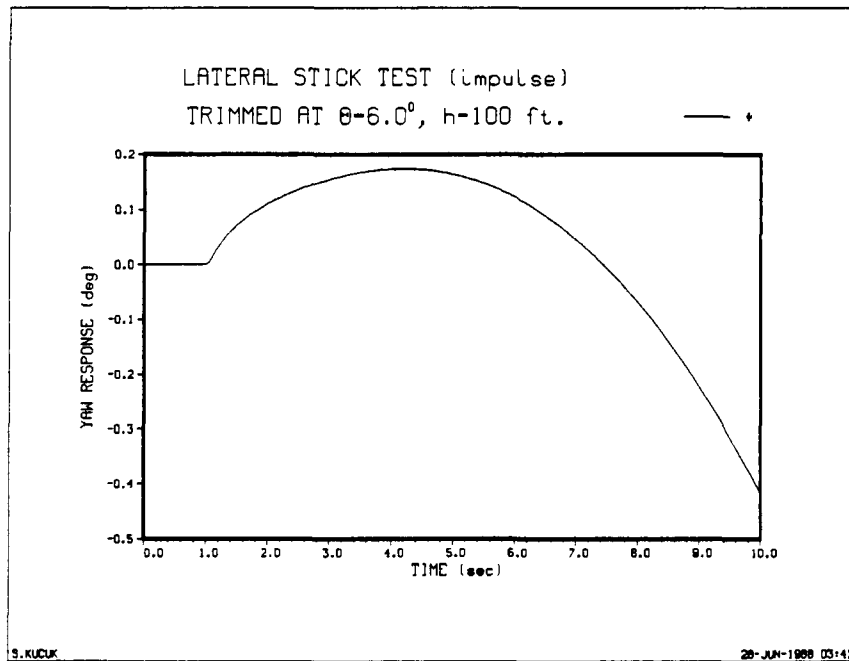


Figure 39. Yaw response to a lateral stick impulse

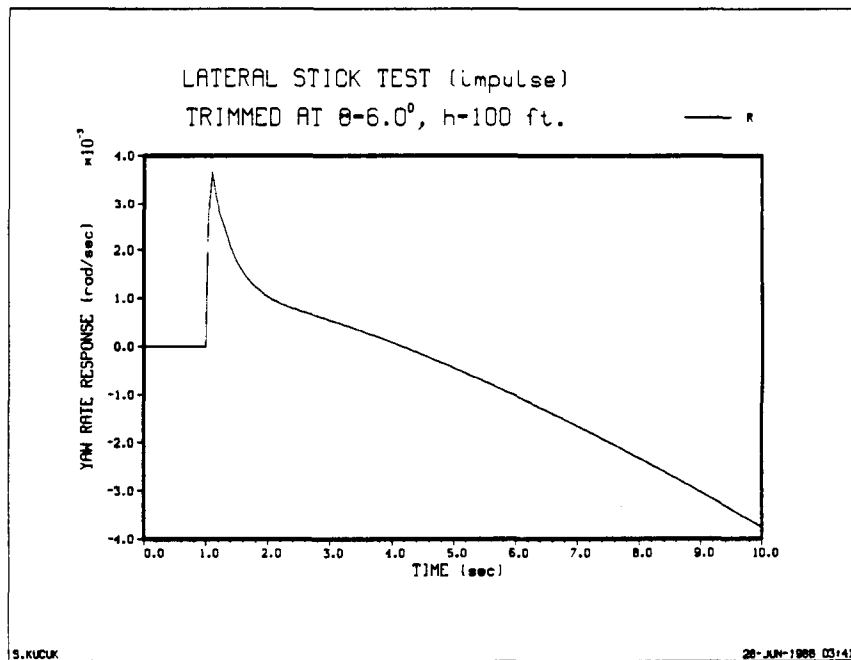


Figure 40. Yaw rate response to a lateral stick impulse

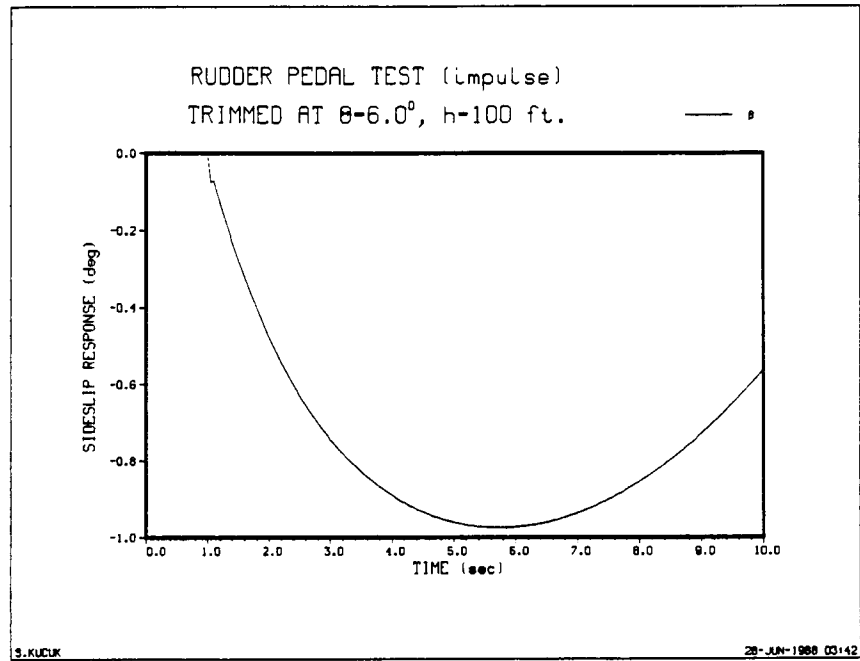


Figure 41. Sideslip response to a rudder impulse

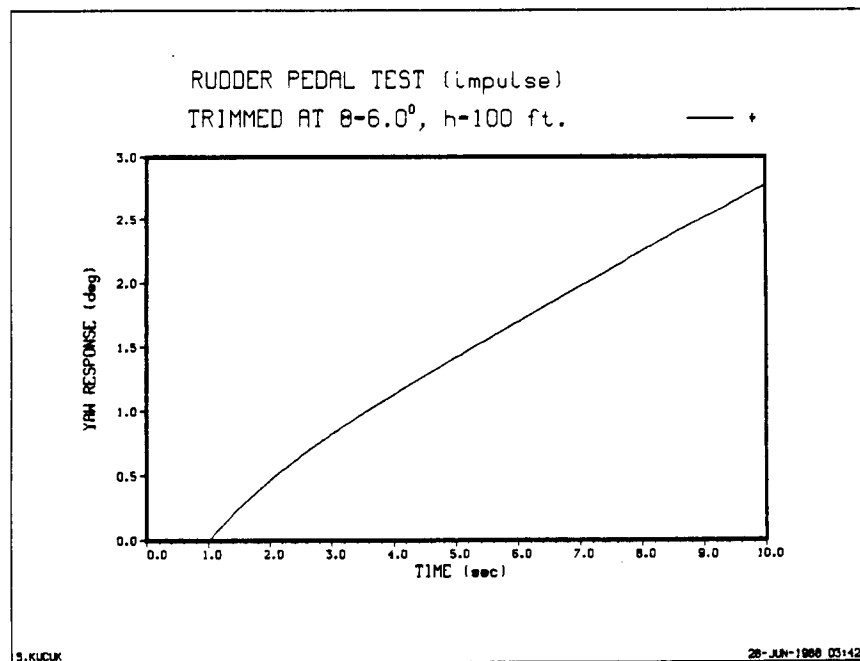


Figure 42. Yaw response to a rudder impulse

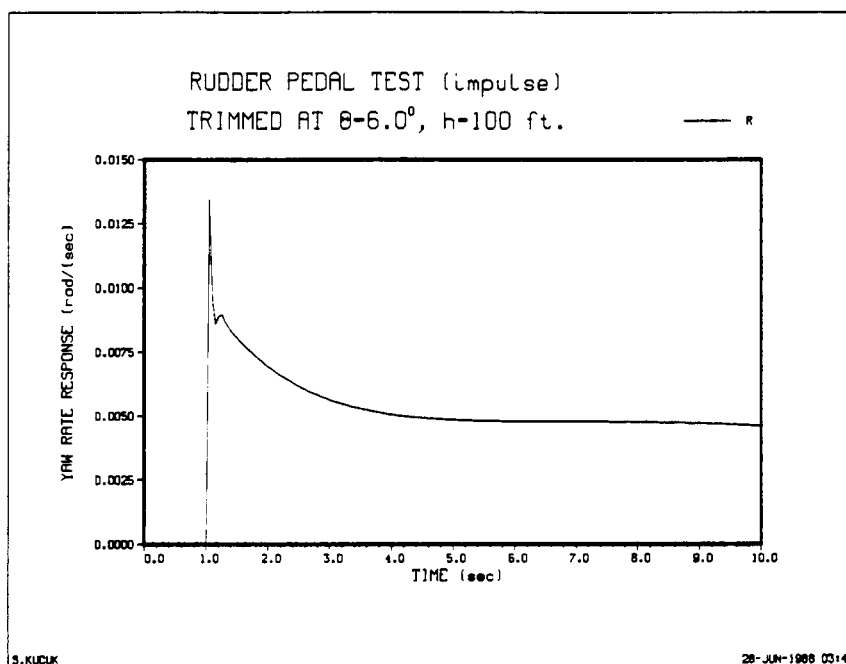


Figure 43. Yaw rate response to a rudder impulse

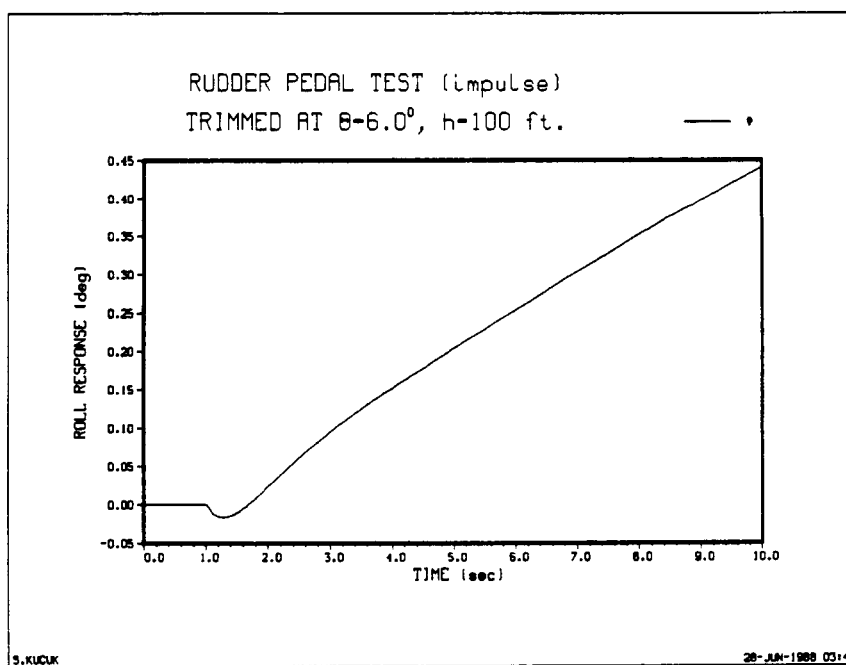


Figure 44. Roll response to a rudder impulse

6.2 Static Pilot Runs

As mentioned earlier, the static pilot parameters are calculated off-line using the time and frequency data of the trimmed aircraft at the desired initial flight conditions. The selection of the static pilot parameters will also affect the adaptive pilot since the experience of the adaptive pilot is provided by the static pilot. We will later illustrate this by varying the activation time of the adaptive pilot which is the adaptive pilot of Chapter 5.

The Harrier AV-8B is trimmed at 25 knots with the initial angular positioning $(\Phi, \Theta, \Psi) = (0.0^\circ, 6.50^\circ, 0.0^\circ)$ at 100 ft. above sea level. The same analysis of Section (6.1) is applied to the impulse response data, and the following discrete pilot parameters in equations (6-7a), (6-7b), (6-7c), (6-7d) and (6-7e) are calculated to close the longitudinal stick through the pitch angle, lateral stick through the roll angle, rudder pedals through the heading, nozzle angle setting through the airspeed and the throttle setting through the altitude, respectively. Equations (6-7a), (6-7d) and (6-7e) define the longitudinal directional pilot. Equations (6-7b) and (6-7c) define the lateral directional pilot.

$$H_{\Theta}^{\delta_e}(z^{-1}) = 0.2z^{-4} \frac{(z^{-1} - 0.94z^{-2})}{(1 - 0.6065z^{-1})(1 - 0.7778z^{-1})} \quad (6-7a)$$

$$H_{\Phi}^{\delta_a}(z^{-1}) = 0.69317z^{-4} \frac{(z^{-1} - 0.93z^{-2})}{(1 - 0.6065z^{-1})(1 - 0.22475z^{-1})} \quad (6-7b)$$

$$H_{\Psi}^{\delta_r}(z^{-1}) = 0.54017z^{-4} \frac{(z^{-1} - 0.94z^{-2})}{(1 - 0.6065z^{-1})(1 - 0.45535z^{-1})} \quad (6-7c)$$

$$H_{v_{eq}}^{\delta_{\theta_j}}(z^{-1}) = -0.4z^{-4} \frac{(z^{-1} - 0.605z^{-2})}{(1 - 0.6065z^{-1})(1 - 0.6z^{-1})} \quad (6-7d)$$

$$H_h^{\delta_{TH}}(z^{-1}) = 1.46997z^{-4} \frac{(z^{-1} - 0.965z^{-2})}{(1 - 0.6065z^{-1})(1 - 0.87952z^{-1})} \quad (6-7e)$$

First, the longitudinal pilot was commanded a $+10^\circ$ pitch response and required to hold the speed of the aircraft. Almost downward pointing nozzles will cause a significant loss in the speed by pitching-up so the constraint on the relative speed of the aircraft becomes essential. Figures (45) and (46) show the pitch angle and the airspeed responses of the aircraft. The loop associated with the pitch angle is type-1, so the steady state error is almost zero, but the speed loop is type-0. This is why there is approximately 10 knots drop in the speed even though the pilot was required to hold the speed at 25 knots. To overcome this situation, the pilot's adjustable pole can be shifted as close as to $z=1$, so that the error is minimal, but a type-1 loop in the speed causes a very sluggish response. Any oscillations in this loop must be avoided. For that reason, we will ignore this steady state error. A following argument is that, if the pilot senses the final value of the speed, he can always change his reference so that the gap can be compensated. The pilot's performance is shown in Figures (47) and (48). The latter are the corresponding control movements of the pilot models to obtain the responses of Figures (45) and (46).

In the next scenario, the altitude pilot is activated to achieve a +10 ft. altitude command after $t=5.0$ sec. The resulting pitch angle, speed, and the altitude responses of the aircraft for the three-variable pilot model are given in Figures (49), (50) and (51). The corresponding control movements are shown in Figures (52), (53) and (54). This example shows how efficient the single variable loops act as a complete multi-variable pilot model.

Let us examine this simulation. First the pitch pilot receives a command to adjust the pitch angle of the aircraft and acts on the longitudinal stick. The change in the aircraft state is sensed by the nozzle and altitude pilots and they act on the controls to regulate these changes caused by the pitch pilot. Then at $t=5.0$ sec., the altitude pilot receives an

increase in altitude command by 10 ft. and acts on the throttle as a primary control mechanism not to regulate. The changes in throttle affect the aircraft state once again, and the pitch pilot and nozzle pilot react to regulate the disturbed motion caused by the altitude pilot until the steady state is reached.

In addition to the pitch, altitude, and speed loops, we will add to the above case a coordinated heading change maneuver where the heading of the aircraft is to be adjusted with rudder movements while the longitudinal stick holds the pitch angle, the lateral stick minimizes the roll angle, and the throttle setting is used to maintain the altitude of the aircraft. Also the nozzle angle setting will be used to regulate the aircraft speed. Therefore, this maneuver requires all of the five main control mechanisms to be used.

The pilot is required to change his heading by $+5^\circ$ in approximately 5 seconds, after $t=10.0$ sec. Another constraint becomes effective for this case where the disturbed roll of the aircraft, due to the yaw-roll coupling, must be regulated although small in magnitude. The pitch, yaw, roll, speed and altitude responses for the above simulation are given in Figures (55), (56), (57), (58) and (59). The corresponding control movements of the pilots are given in Figures (60), (61), (62), (63) and (64).

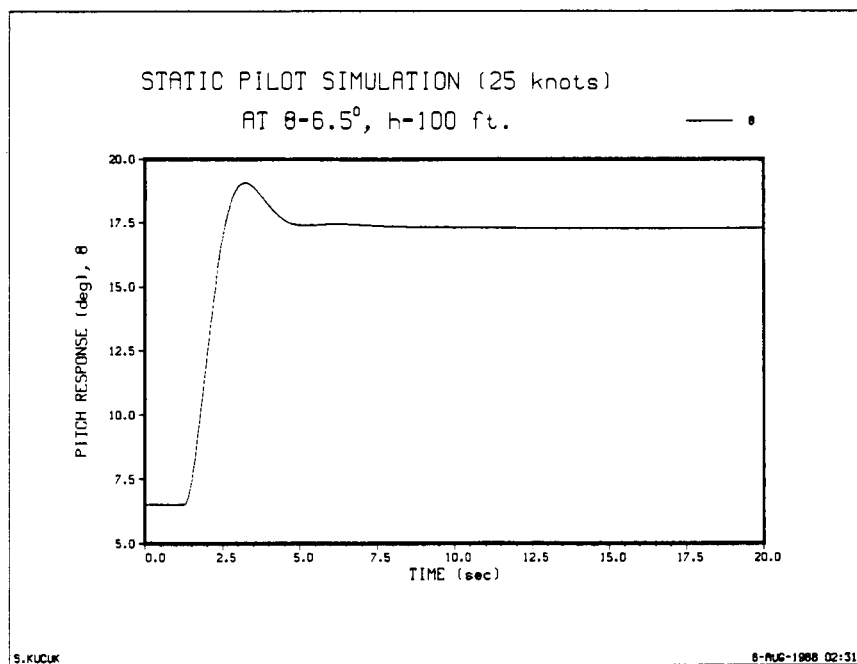


Figure 45. Pitch response, two-pilot configuration

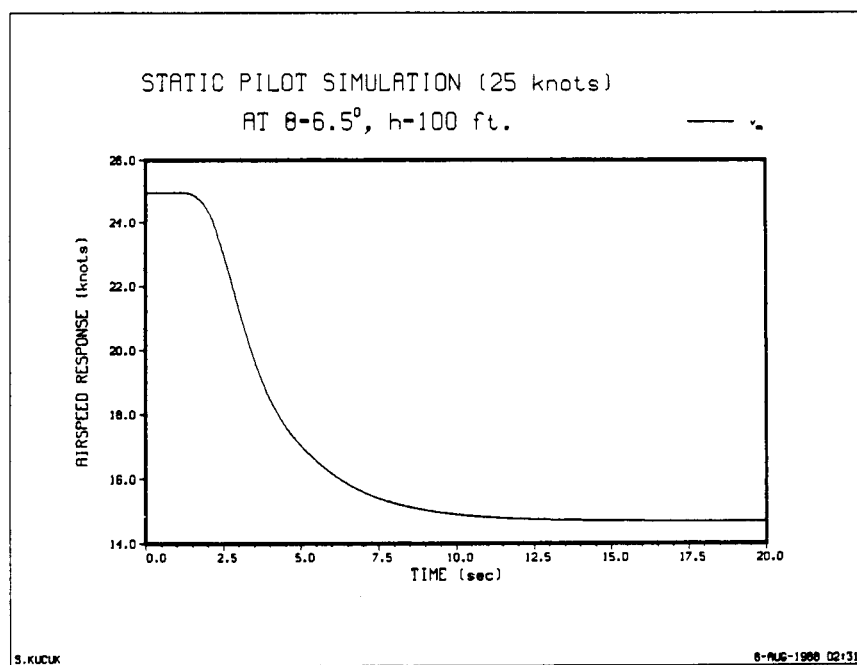


Figure 46. Airspeed response, two-pilot configuration

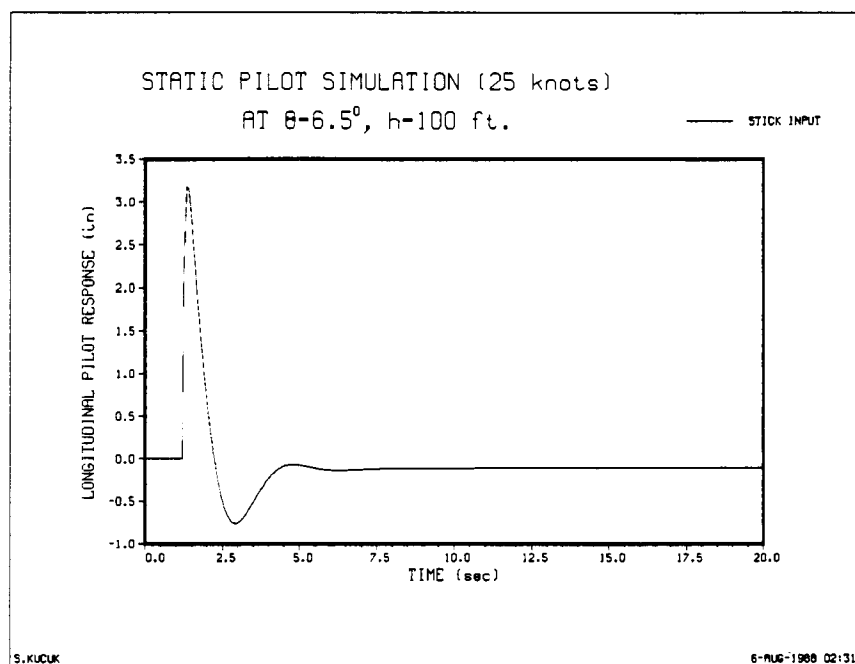


Figure 47. Longitudinal stick pilot response, two-pilot configuration

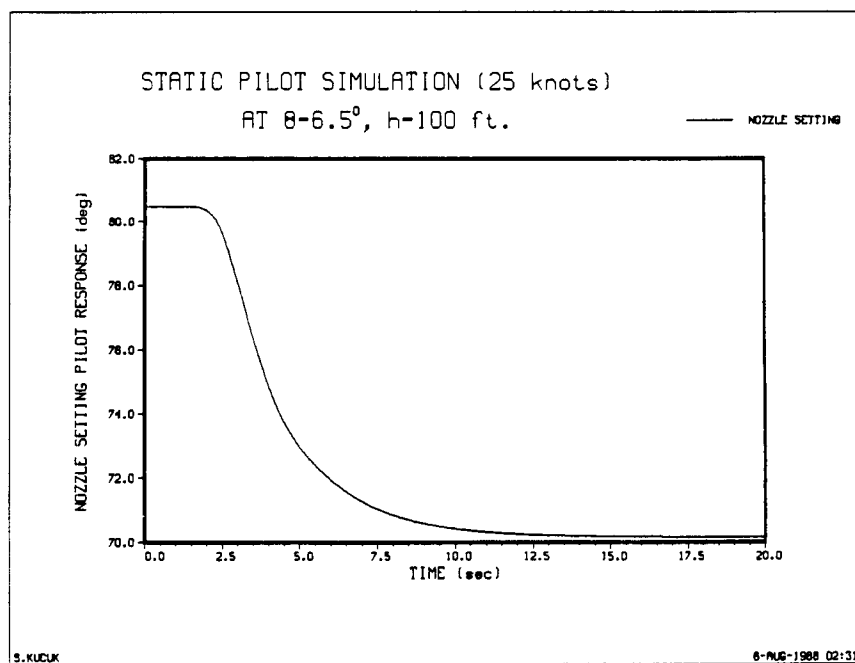


Figure 48. Nozzle setting pilot response, two-pilot configuration

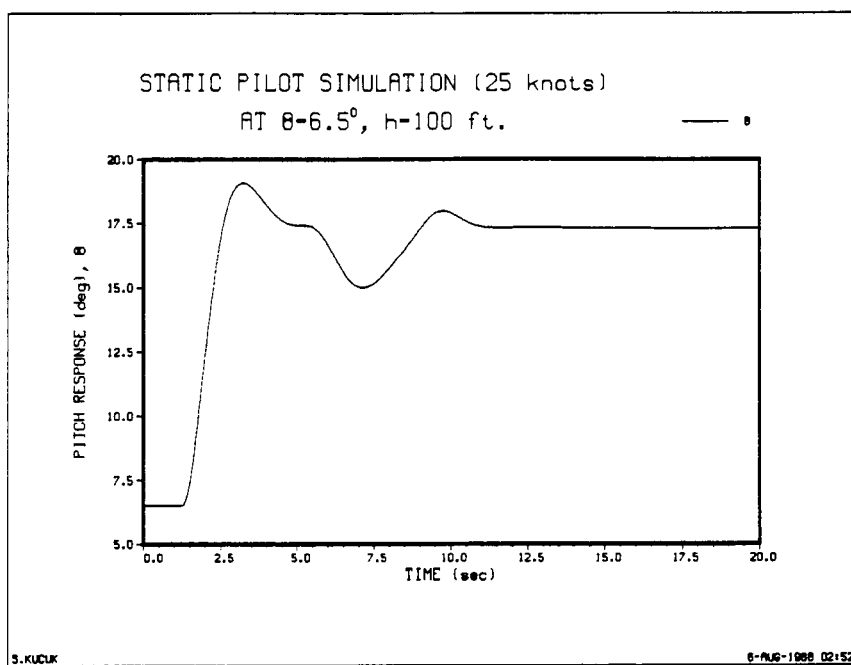


Figure 49. Pitch response, three-pilot configuration

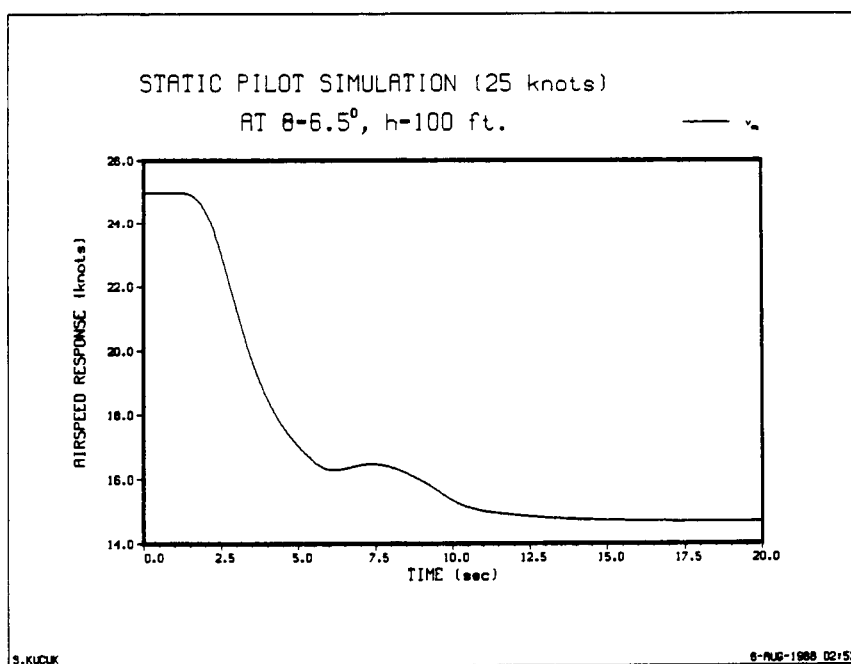


Figure 50. Airspeed response, three-pilot configuration

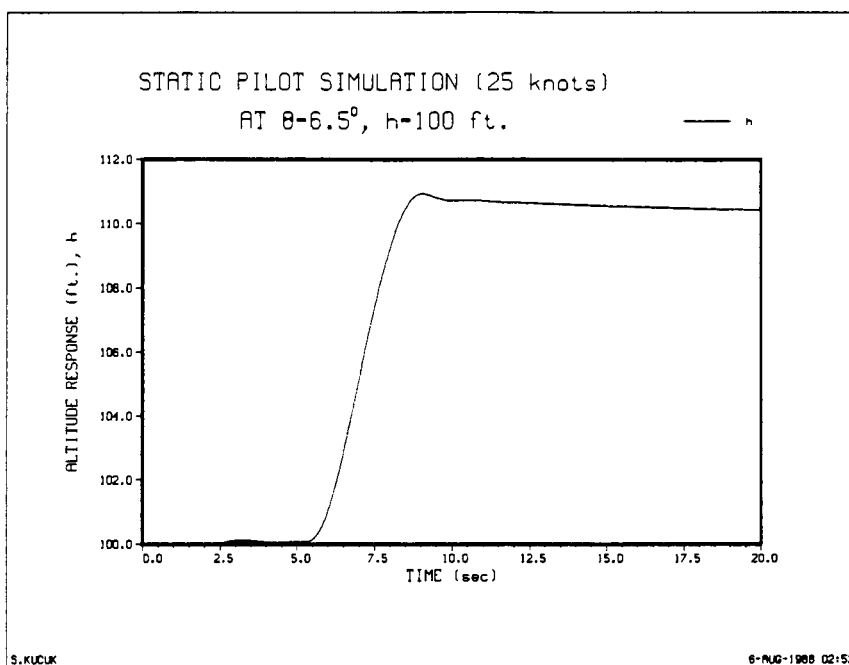


Figure 51. Altitude response, three-pilot configuration

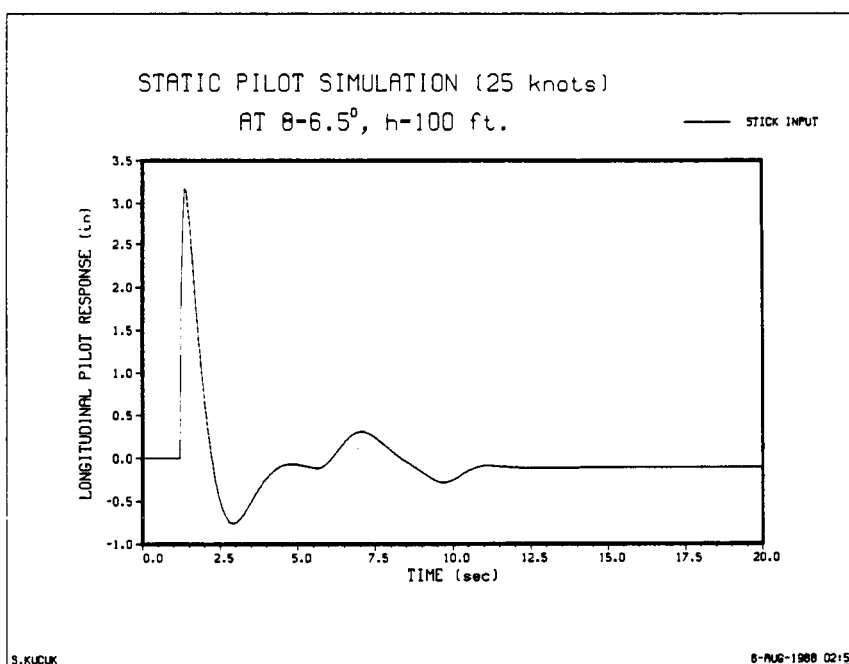


Figure 52. Longitudinal stick pilot response, three-pilot configuration

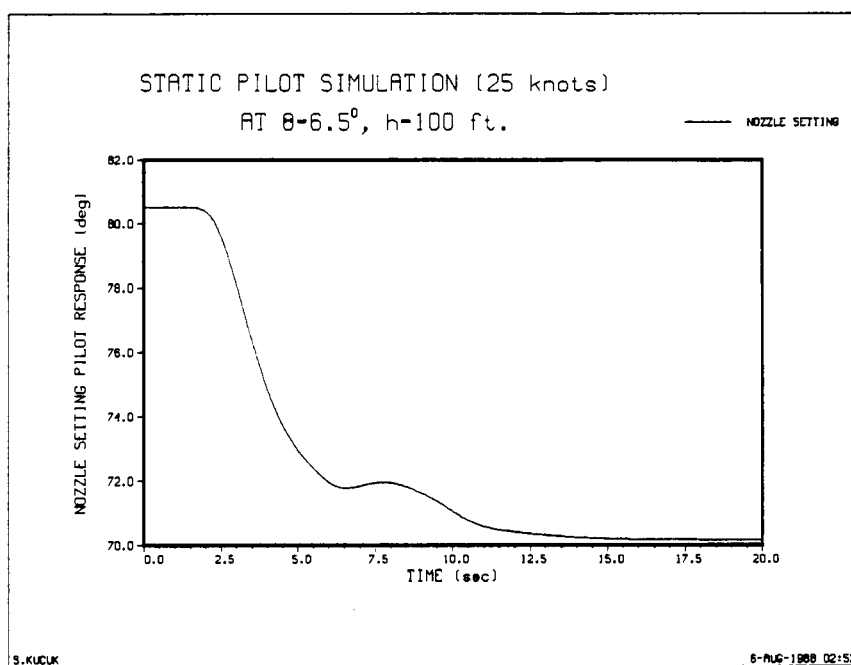


Figure 53. Nozzle setting pilot response, three-pilot configuration

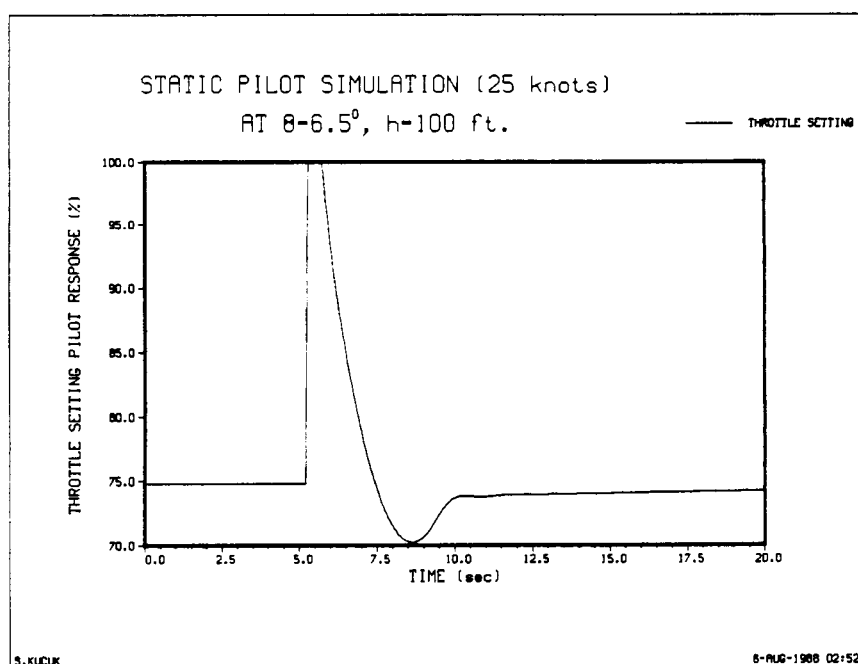


Figure 54. Throttle setting pilot response, three-pilot configuration

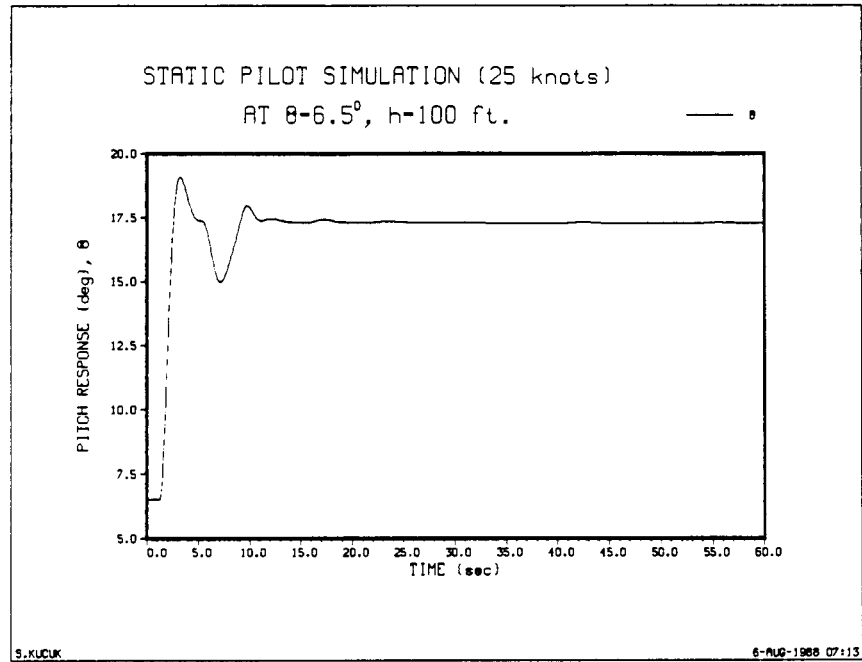


Figure 55. Pitch response, five-pilot configuration

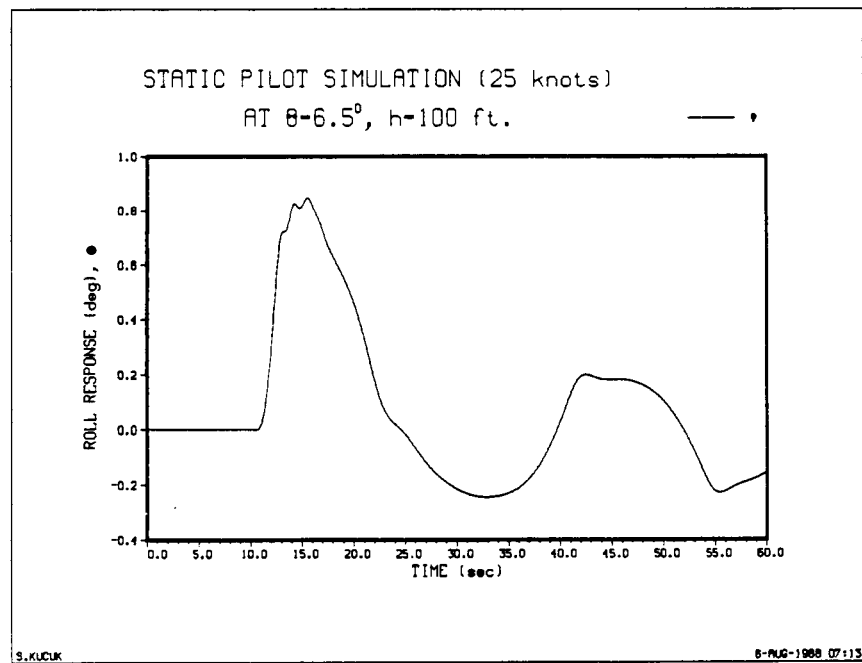


Figure 56. Roll response, five-pilot configuration

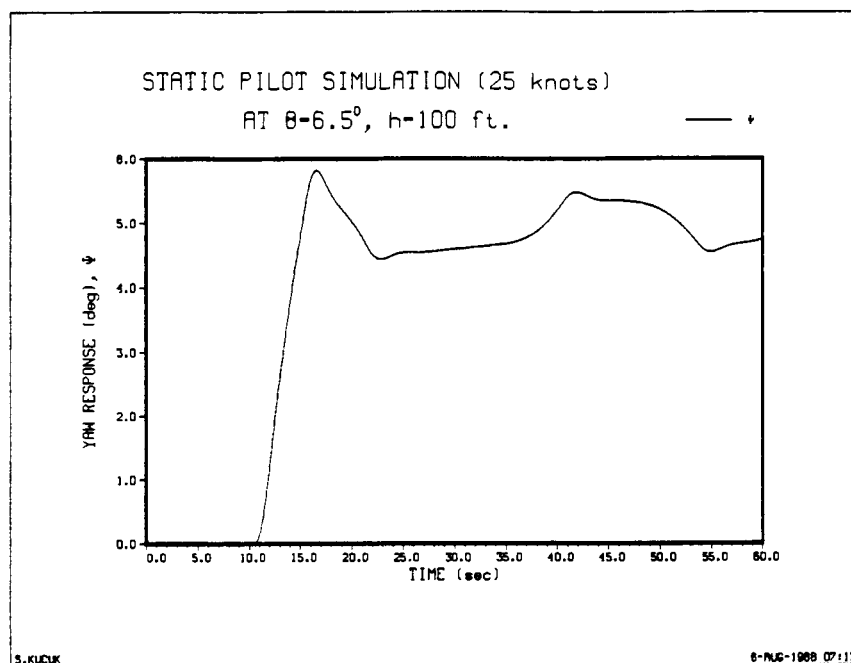


Figure 57. Yaw response, five-pilot configuration

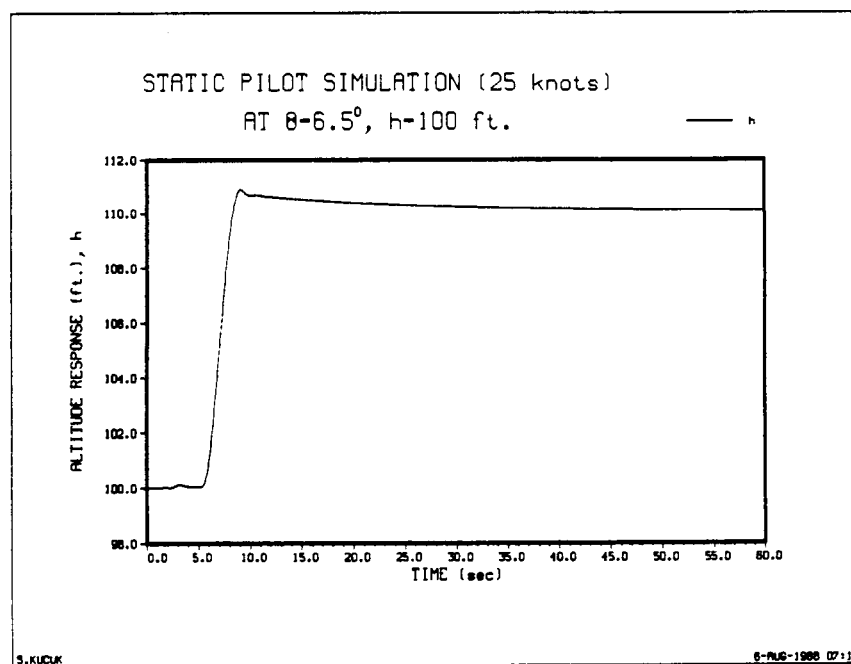


Figure 58. Altitude response, five-pilot configuration

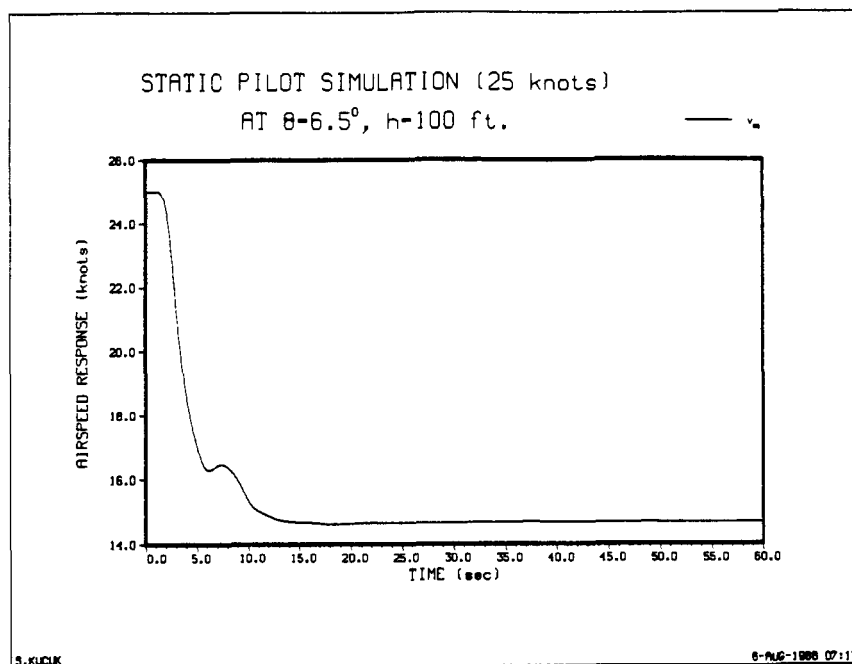


Figure 59. Airspeed response, five-pilot configuration

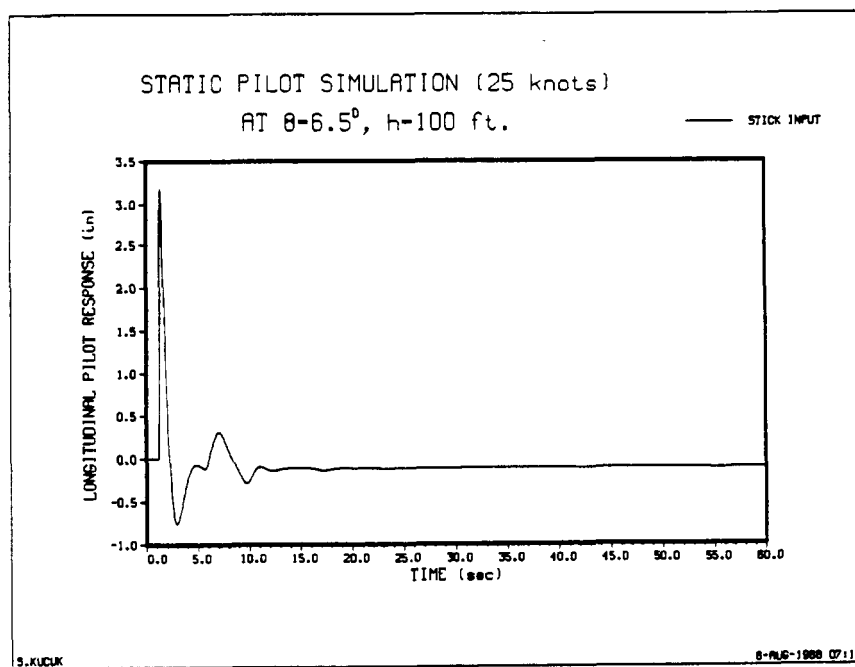


Figure 60. Longitudinal stick pilot response, five-pilot configuration

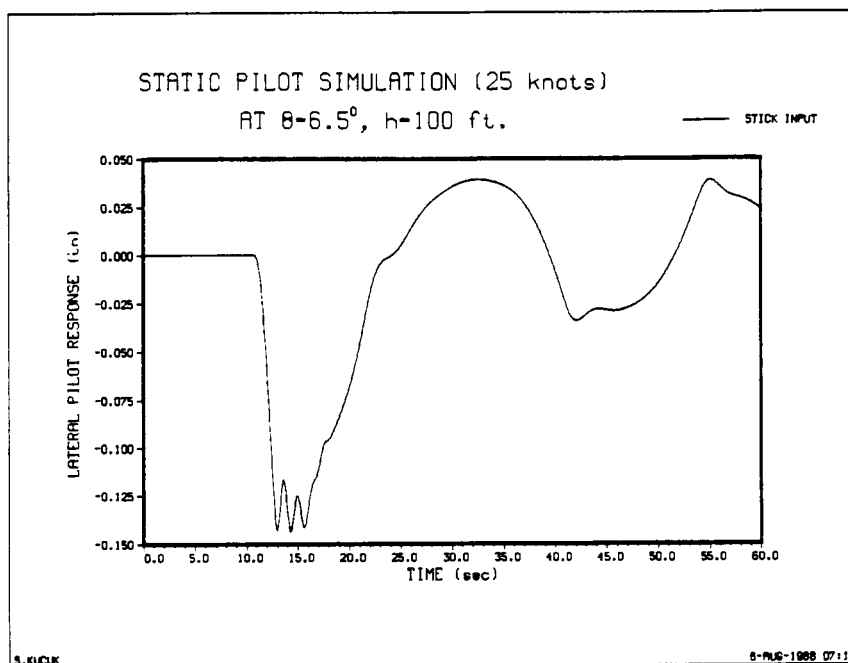


Figure 61. Lateral stick pilot response, five-pilot configuration

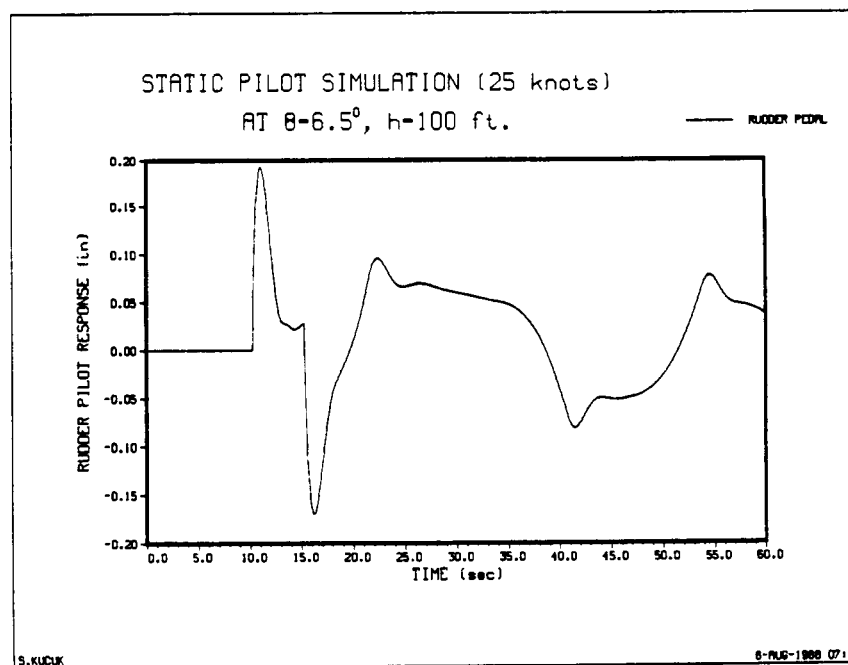


Figure 62. Rudder pedal pilot response, five-pilot configuration

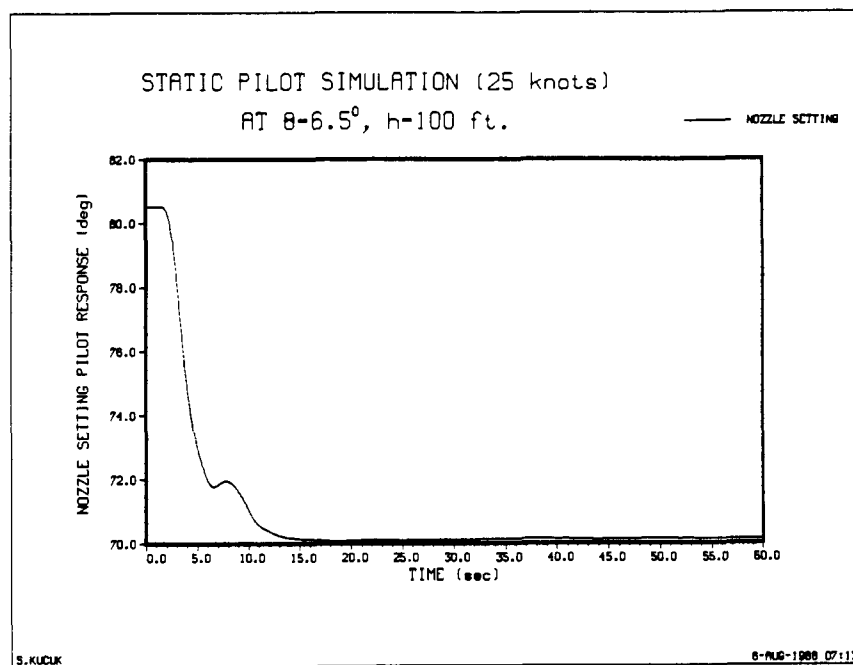


Figure 63. Nozzle setting pilot response, five-pilot configuration

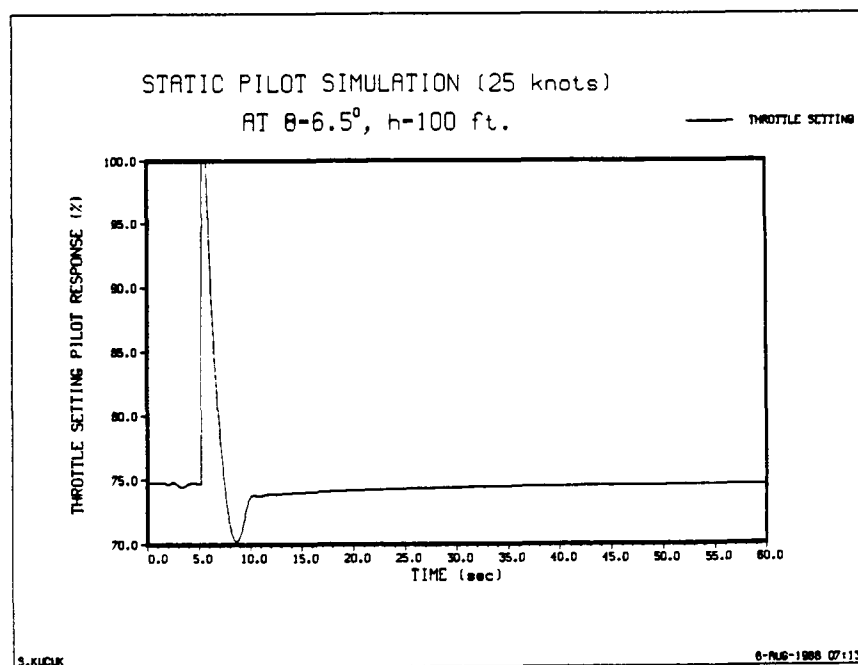


Figure 64. Throttle setting pilot response, five-pilot configuration

6.3 Adaptive Pilot Runs

Now that we have simulated and verified the static pilots, we will investigate the behavior of the adaptive pilot model. In order to simulate the adaptive pilot model, we chose $z_{CL}=0.90\pm j0.10$ to be the desired dominant close loop operating poles corresponding to a damping ratio of 0.6676 and an undamped natural frequency of 2.973 rad/sec which is in the middle of the "best" rated region of Figure (2). Recall that the adaptive pilot compensates the necessary phase to close the loop at $z_{CL}=0.90\pm j0.10$. For that reason, the model relocates the adjustable pole/zero pair of the discrete human response model of equation (2-5), in such a way that the phase contribution of the pole and zero gives the necessary compensation. We also mentioned that there is no unique solution to this problem. Therefore, our criterion was based on the location of the adjustable pole, α . The pole, α , is moved towards the origin $z=0$, as a function of the required phase. The zero, γ , is then chosen accordingly, and a table look-up was designed to store the values of the pole/zero values for specific conditions. Therefore, in the simulation, after the information of the phase to be compensated is available, the model searches the table to find the appropriate values of α and γ . Although there is no proof to the latter argument, we have mentioned that an experienced pilot is almost deterministic in his responses, knowing how to react and when to react at various configurations as is our model.

Figures (65), (66), (67) and (68) show the pitch angle and speed responses of the aircraft, longitudinal stick and nozzle setting movements of the adaptive pilot model where the adaptation starts at $t=5.0$ sec. The adjusted pole/zero and gains of the pilot model are given in Figures (69), (70), (71), and (72). Three numerator and three denominator coefficients are used in the identification process of the adaptive pilot model

where the controlled element dynamics is estimated. A rather interesting behavior is observed in the adaptive model's output. As soon as the adaptation starts, the model applies very rapid, approximately symmetric, push-and-pull type of movements to the controls until it can identify the information related with the controls. This is not an actual "learning" process, in the sense that the model acts deliberately on the controls to identify the system modes, but it is a result of the current information available to the model. Suppose that a human is given an adjustment stick that is attached to a spring-mass system where he is subjected to a control task to find the equilibrium value of the stick that will balance the mass. If he has no idea of what to do, the first response of the human will be to move the stick forward and backward, simultaneously, until the desired action is performed. The same situation applies to a human guiding a car, for example. For heading maneuvers, the human knows the boundaries of the steering wheel. To make a right turn, in his first attempt, he may push the wheel more than the optimum value, but if such a case happens he will pull the wheel back, rather in a panic, rapidly correcting his action. Although it is hard to prove such an argument, we find a close relationship between the learning process of a human and the output of the adaptive model. However, we must also note that this type of learning may be dangerous in some of the cases.

Also, when compared with the same static, two-pilot configuration in Figures (45), (46), (47) and (48) the adaptive pilots performed better. Especially, the nozzle setting pilot, has better steady state response where it is required to hold the speed of the aircraft due to pitch changes. The static pilot stabilized at approximately 15 knots while the adaptive pilot converged to a steady state value of approximately 23 knots.

Figures (73), (74), (75), (76), (77), (78), (79), and (80) show the results when the adaptive pilots are activated at $t=2.0$ sec. This case clearly shows the importance of the

static pilot performance. If the adaptive pilot is not given sufficient time to converge its parameters, the adaptation results are not better than the static pilots. In the absence of a decisionmaking, adaptive pilot will not perform efficiently.

However, once the adaptive pilot parameters converge, the pilot can respond to maneuvers, and his performance can be compared with the performance of the static pilot. Figures (81) through (118) compare the adaptive and the static pilot performances for five different scenarios.

Figures (81), (82), (83), and (84) show a pitch-up response followed by a speed-up and a pitch-down maneuver performed by the adaptive and the static pilots. Notice that in both pitch and the speed loops the adaptive pilot has better steady state errors. The longitudinal stick and the nozzle angle setting pilots are adaptive after $t=5$ sec.

Figures (85), (86), (87), (88), (89), (90), (91), (92), (93), and (94) show a $+10^\circ$ pitch-up followed by a coordinated $+5^\circ$ heading change with a $+10$ ft. altitude change maneuver and at the same time the speed of the aircraft is to be regulated by the nozzles. The aircraft is constrained to have a 0° roll angle to coordinate the heading change. The longitudinal stick and the rudder pedal pilots are adaptive after $t=5$ sec. and $t=15$ sec. respectively.

Figures (95), (96), (97), (98), (99), (100), (101), and (102) show a pitching, yawing, and a speed-up with 0° rolling maneuver where all the loops are closed with the adaptive pilots. The longitudinal stick and the nozzle angle pilots become adaptive after $t=5$ sec. while the rudder pedal and the lateral stick pilots are adaptive after $t=25$ sec. and $t=28$ sec. respectively.

Figures (103), (104), (105), (106), (107), (108), (109), and (110) show a rolling based maneuver with 0° heading constraint. Figures (111), (112), (113), (114), (115), (116), (117), and (118) show a similar scenario where the adaptation times are given by $t=5$ sec. for the longitudinal stick and the nozzle setting pilots, $t=40$ sec. and $t=43$ sec. for the rudder pedal and the lateral stick pilots, respectively.

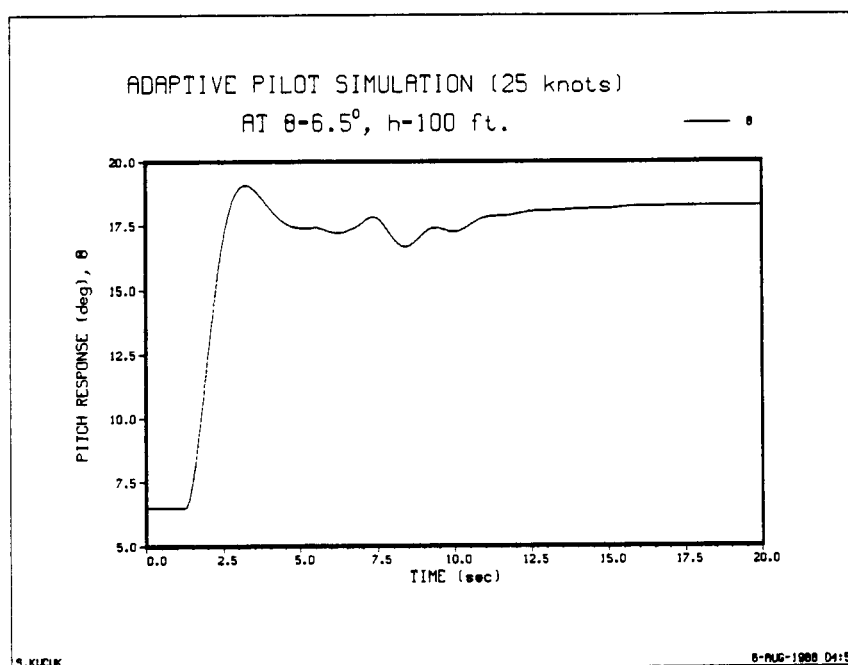


Figure 65. Pitch response, two-pilot configuration, adaptive after $t=5$ sec

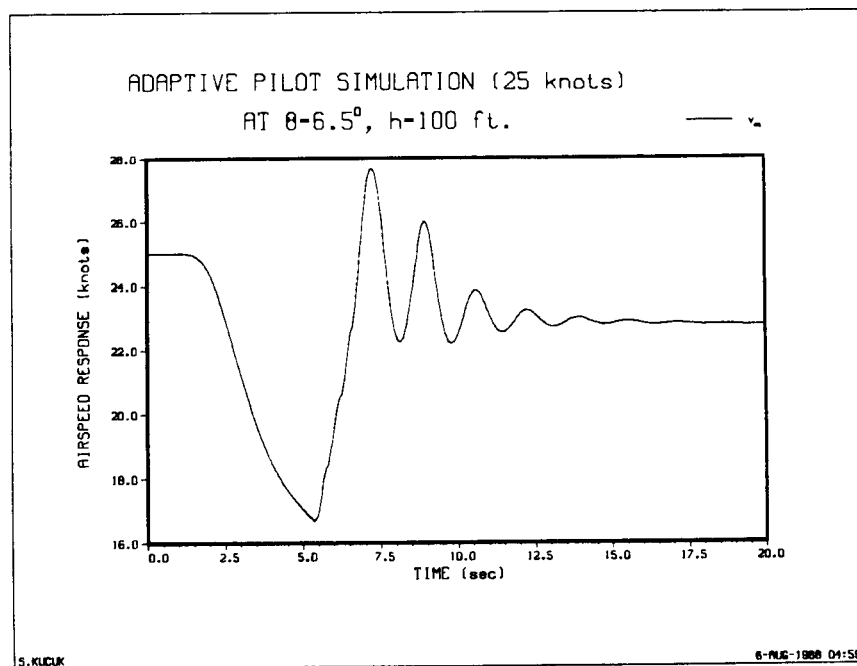


Figure 66. Airspeed response, two-pilot configuration, adaptive after $t=5$ sec

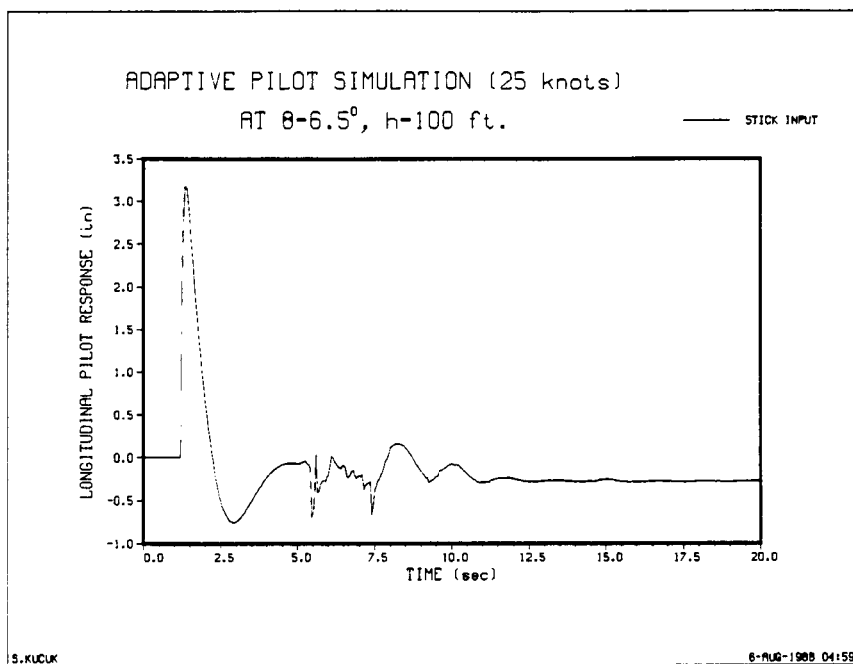


Figure 67. Longitudinal stick pilot response, two-pilot configuration, adaptive after $t=5$ sec

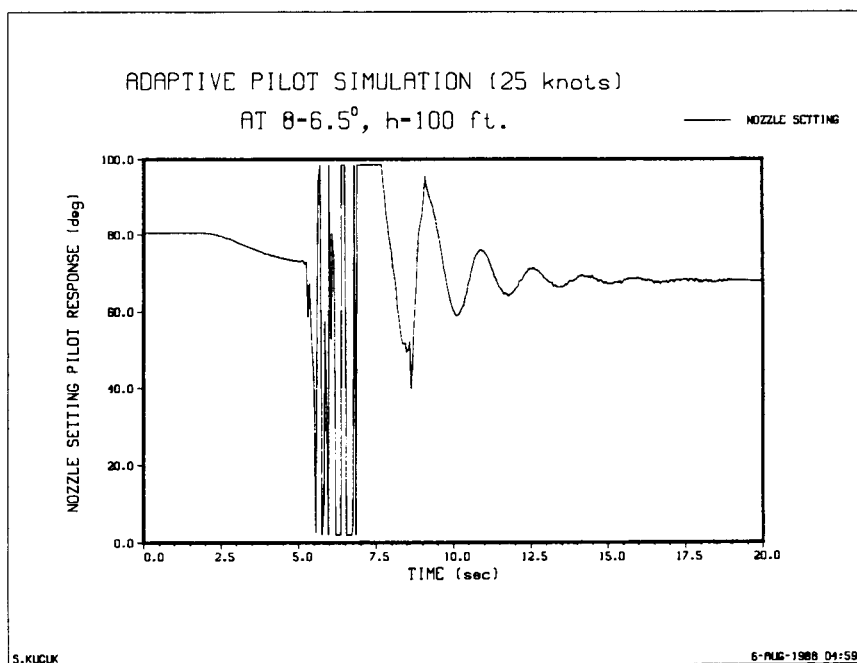


Figure 68. Nozzle setting pilot response, two-pilot configuration, adaptive after $t=5$ sec

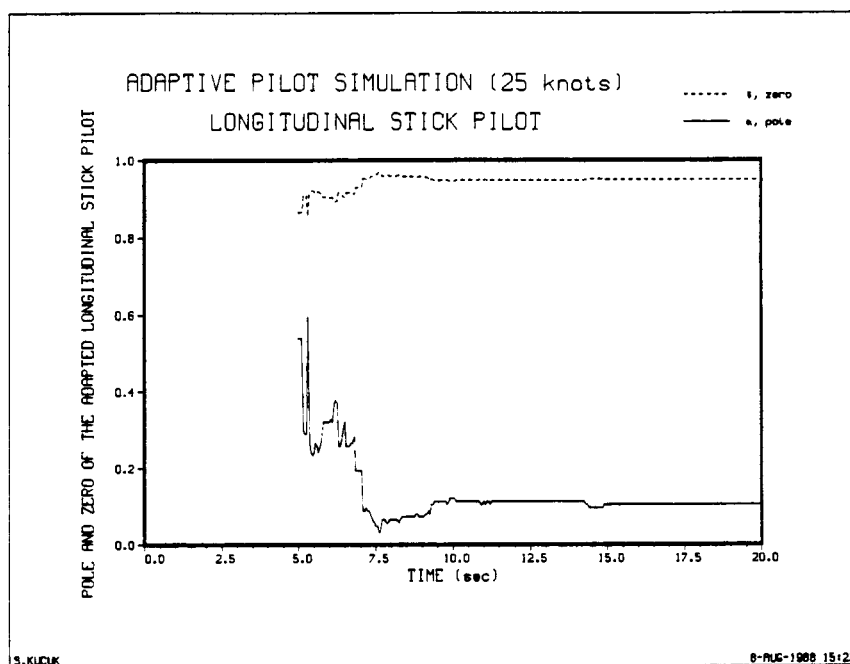


Figure 69. Longitudinal stick pilot, adapted pilot pole/zero, two-pilot configuration, adaptive after $t=5$ sec

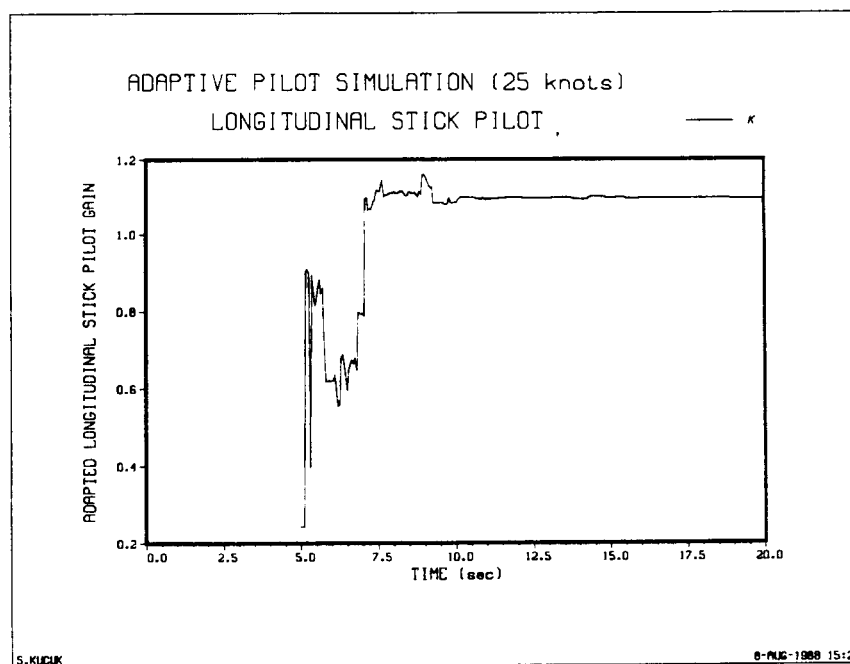


Figure 70. Longitudinal stick pilot, adapted pilot gain, two-pilot configuration, adaptive after $t=5$ sec

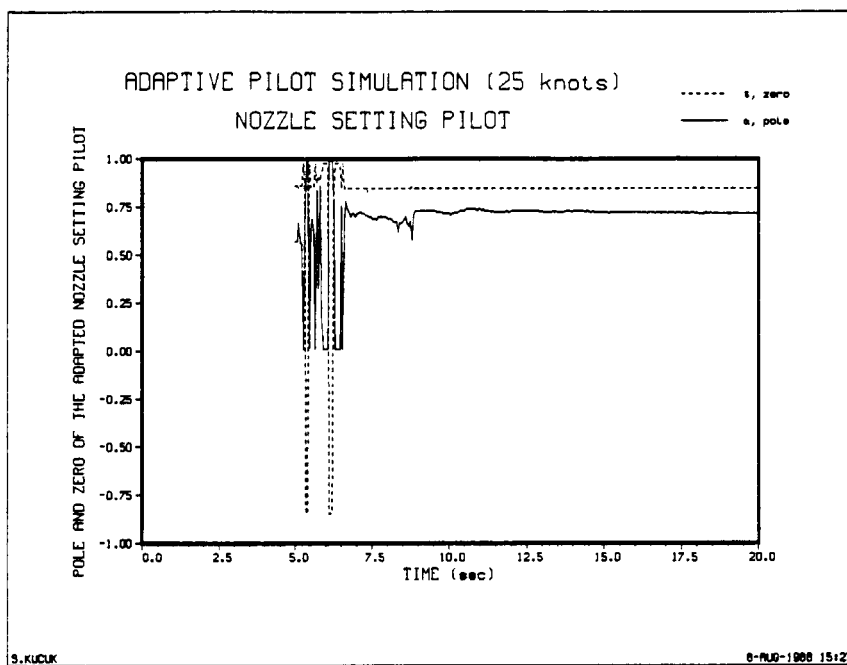


Figure 71. Nozzle setting pilot, adapted pilot pole/zero, two-pilot configuration, adaptive after $t=5$ sec

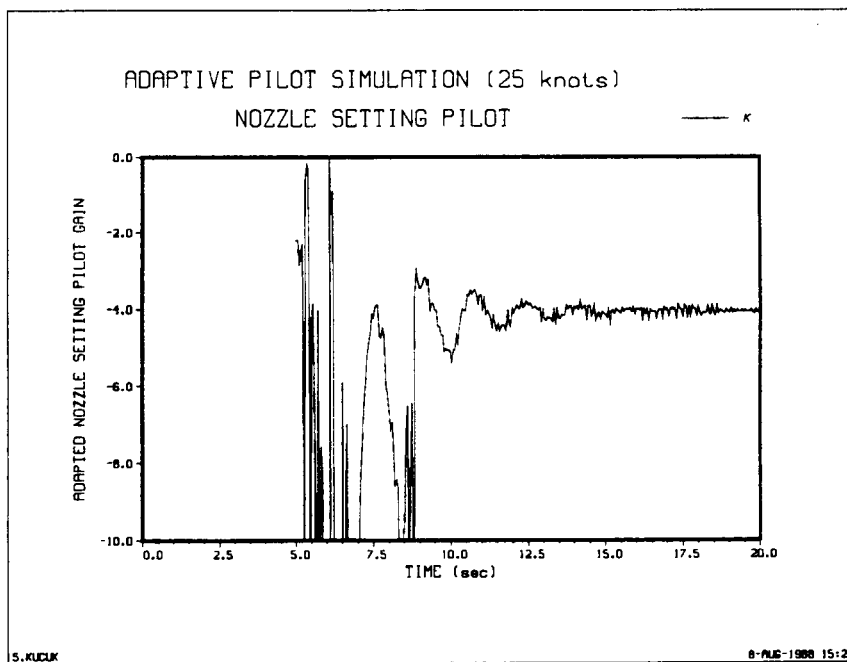


Figure 72. Nozzle setting pilot, adapted pilot gain, two-pilot configuration, adaptive after $t=5$ sec

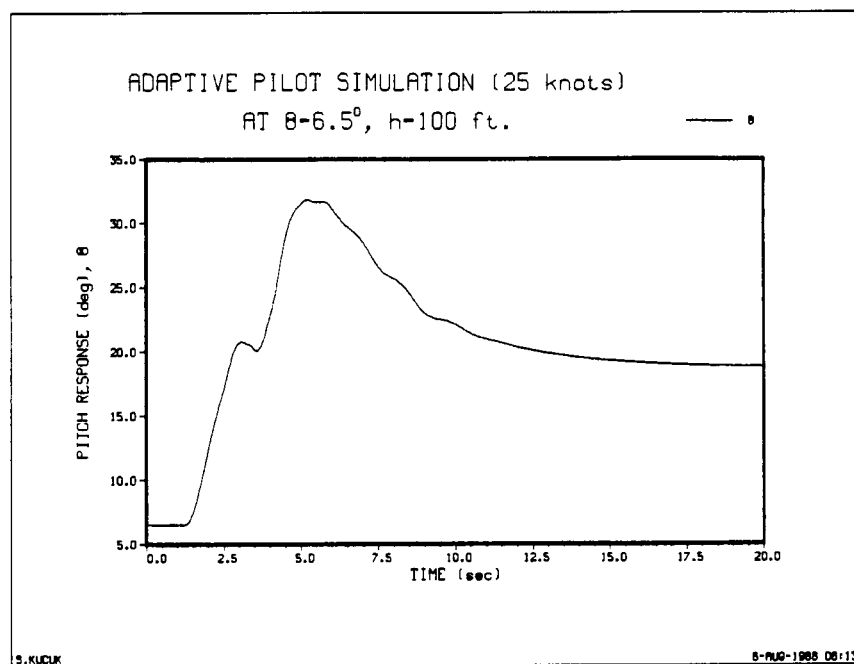


Figure 73. Pitch response, two-pilot configuration, adaptive after $t=2$ sec

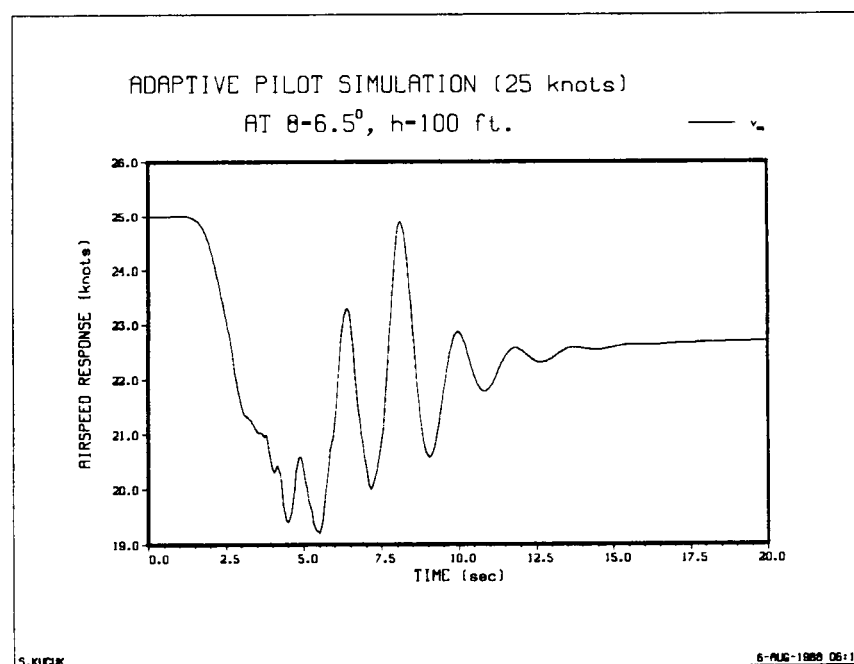


Figure 74. Airspeed response, two-pilot configuration, adaptive after $t=2$ sec

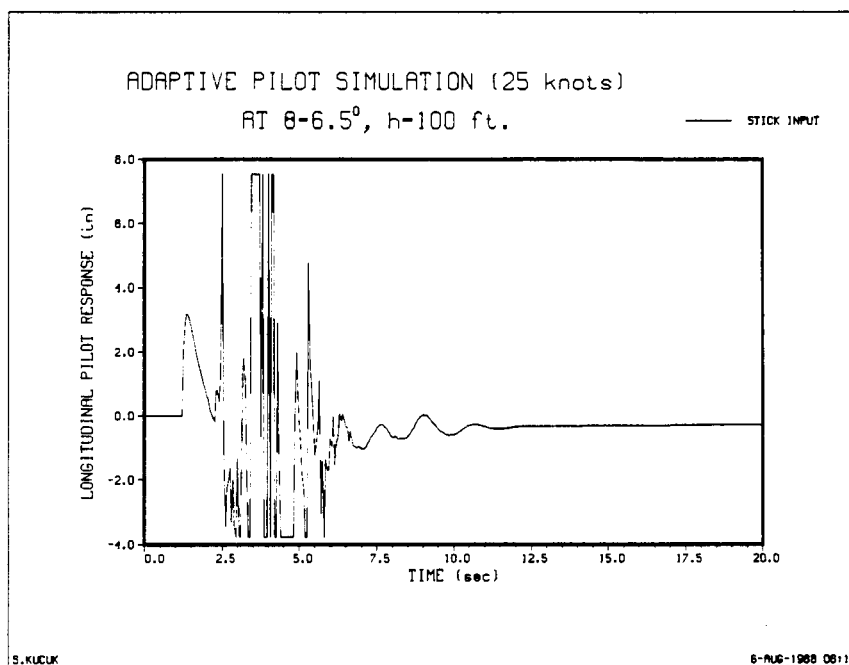


Figure 75. Longitudinal stick pilot response, two-pilot configuration, adaptive after $t=2$ sec

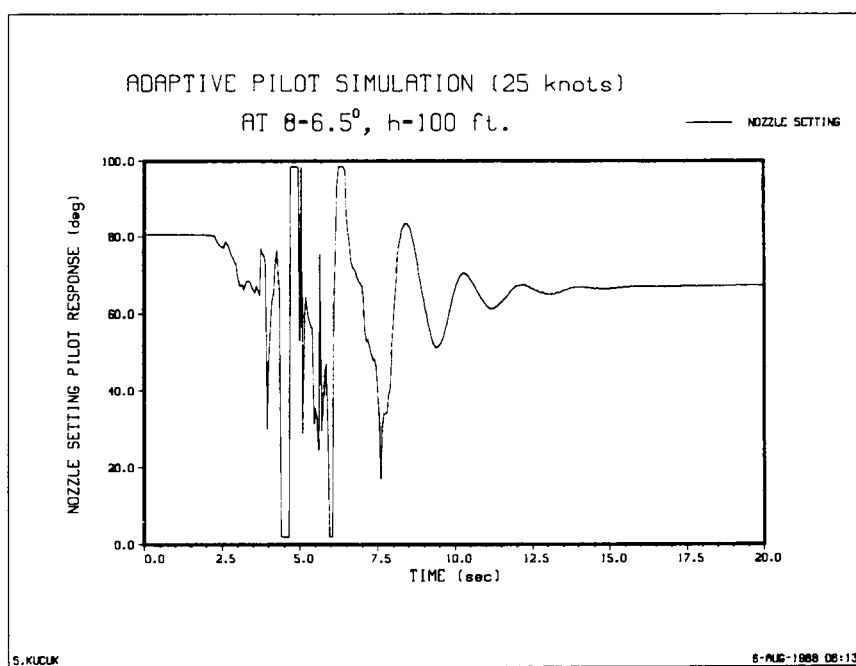


Figure 76. Nozzle setting pilot response, two-pilot configuration, adaptive after $t=2$ sec

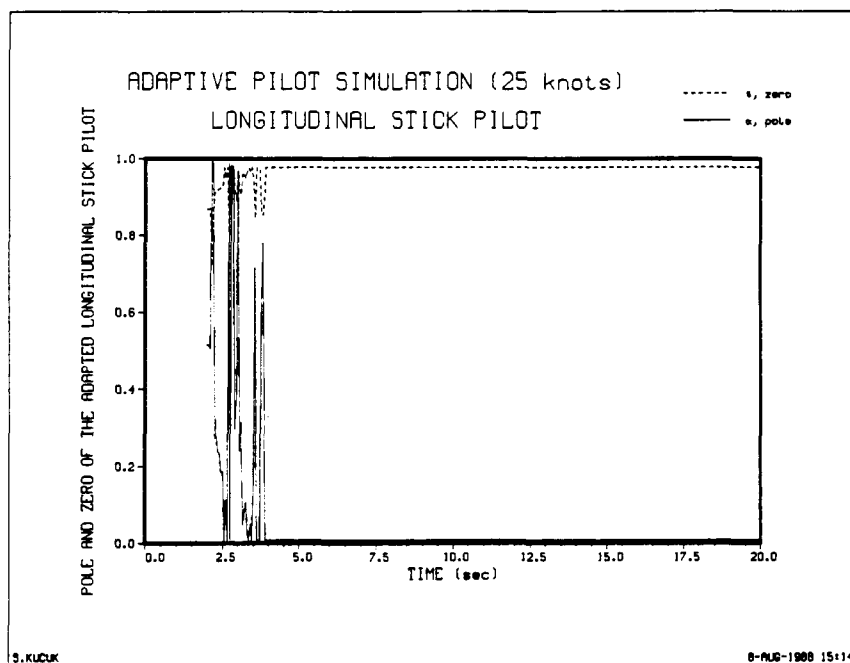


Figure 77. Longitudinal stick pilot, adapted pilot pole/zero, two-pilot configuration, adaptive after $t=2$ sec

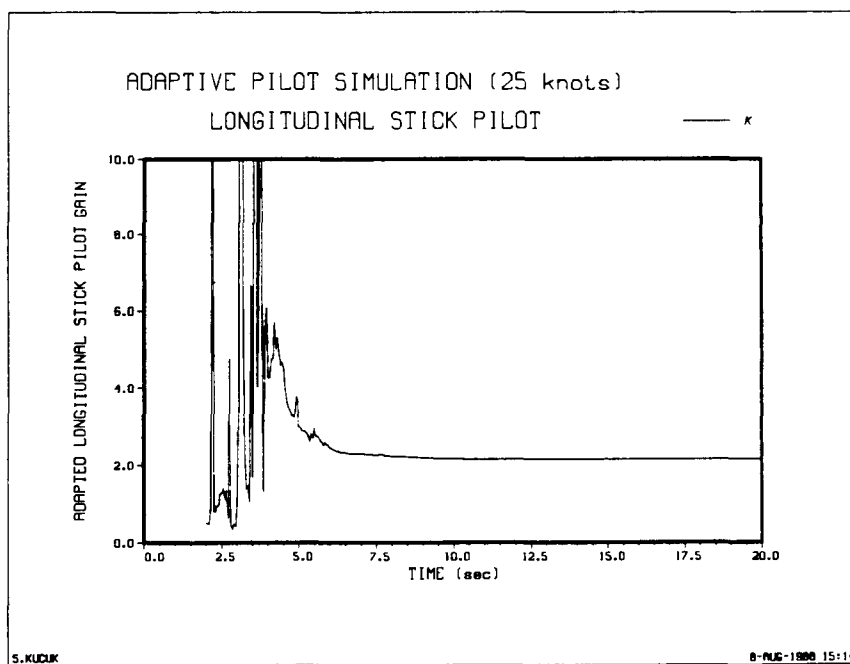


Figure 78. Longitudinal stick pilot, adapted pilot gain, two-pilot configuration, adaptive after $t=2$ sec

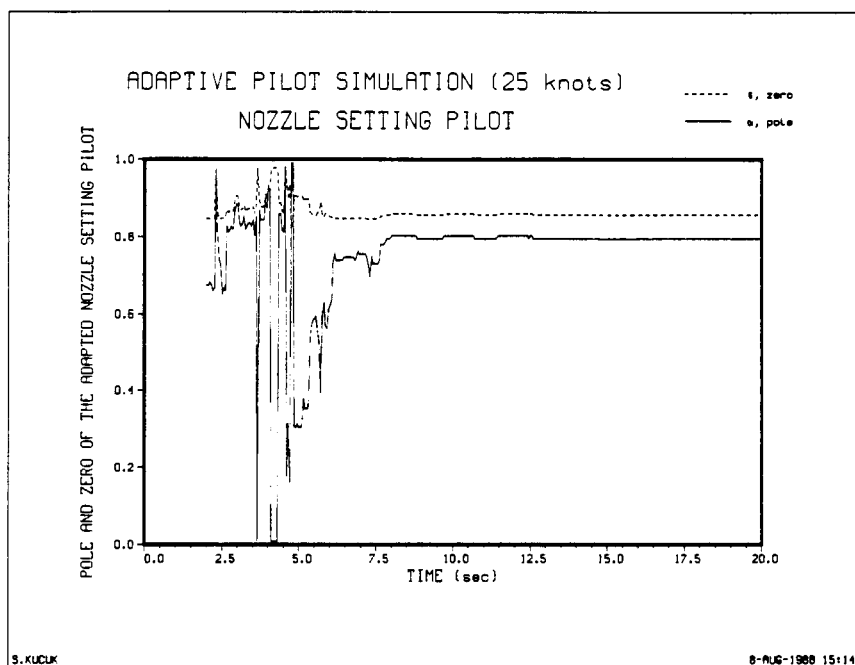


Figure 79. Nozzle setting pilot, adapted pilot pole/zero, two-pilot configuration, adaptive after $t=2$ sec

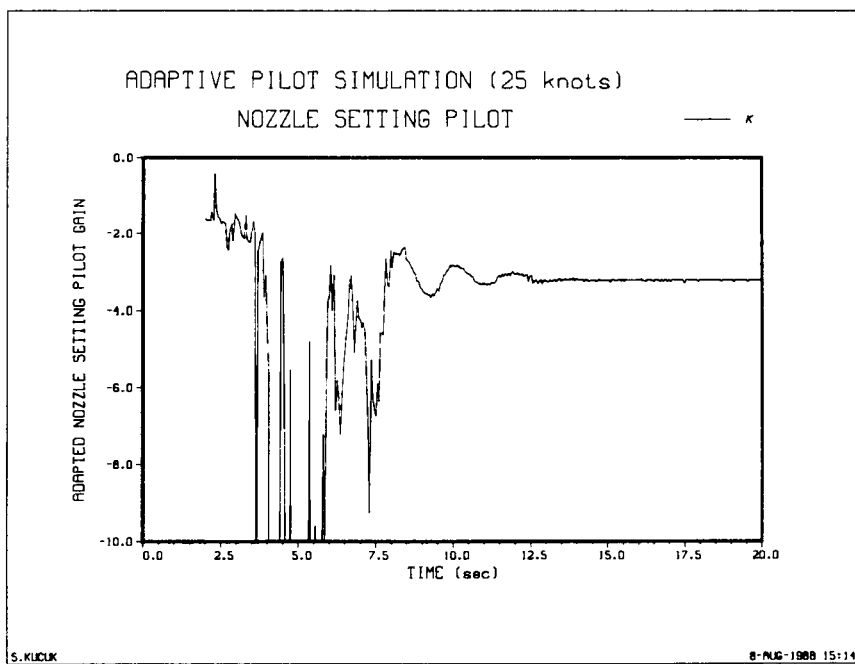


Figure 80. Nozzle setting pilot, adapted pilot gain, two-pilot configuration, adaptive after $t=2$ sec

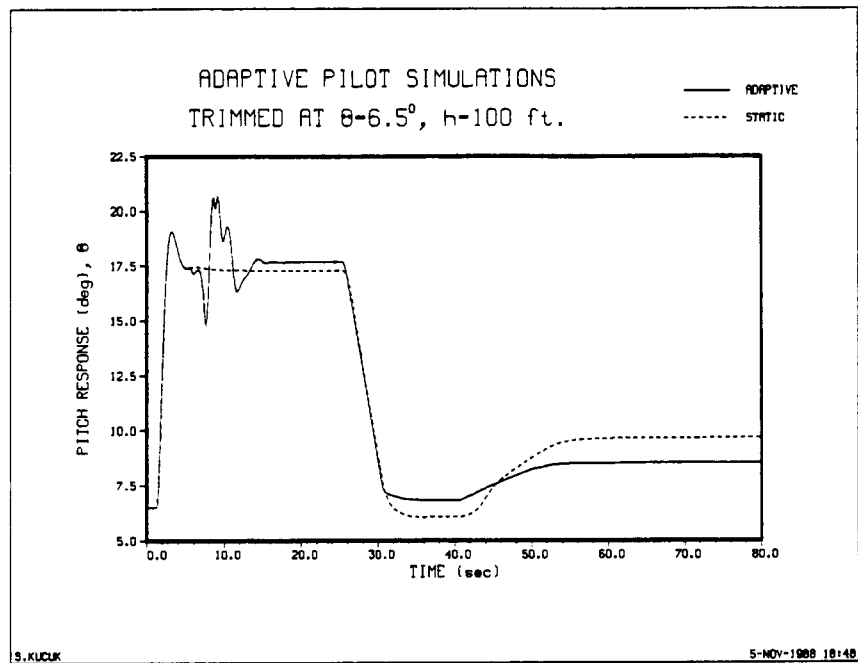


Figure 81. Pitch response, two-pilot configuration, adaptive after $t=5$ sec

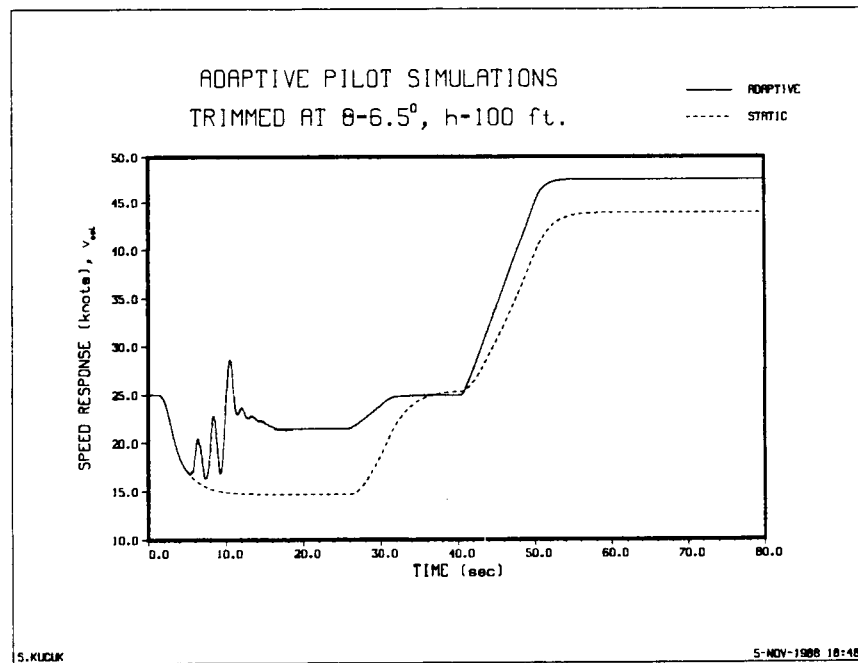


Figure 82. Airspeed response, two-pilot configuration, adaptive after $t=5$ sec

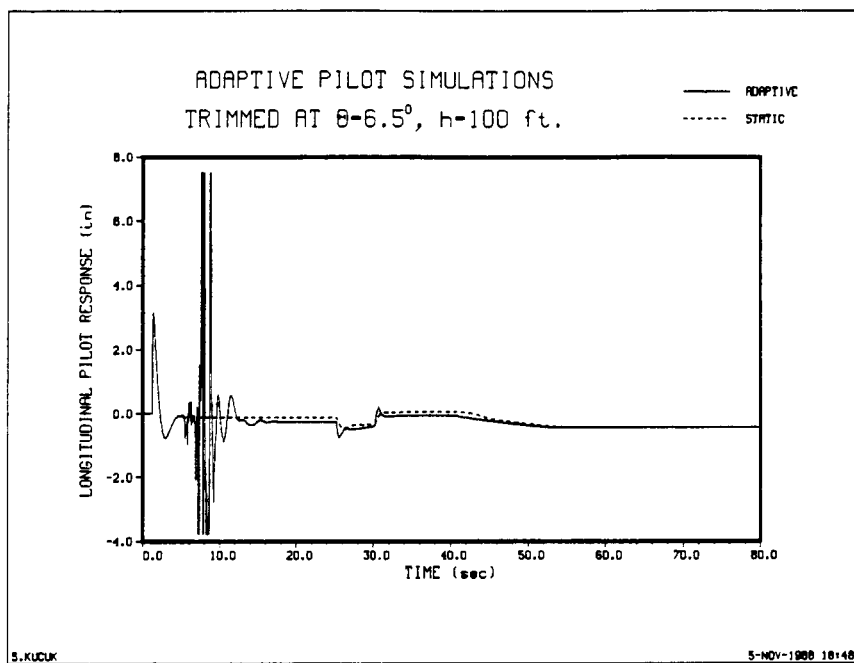


Figure 83. Longitudinal stick pilot response, two-pilot configuration, adaptive after $t=5$ sec

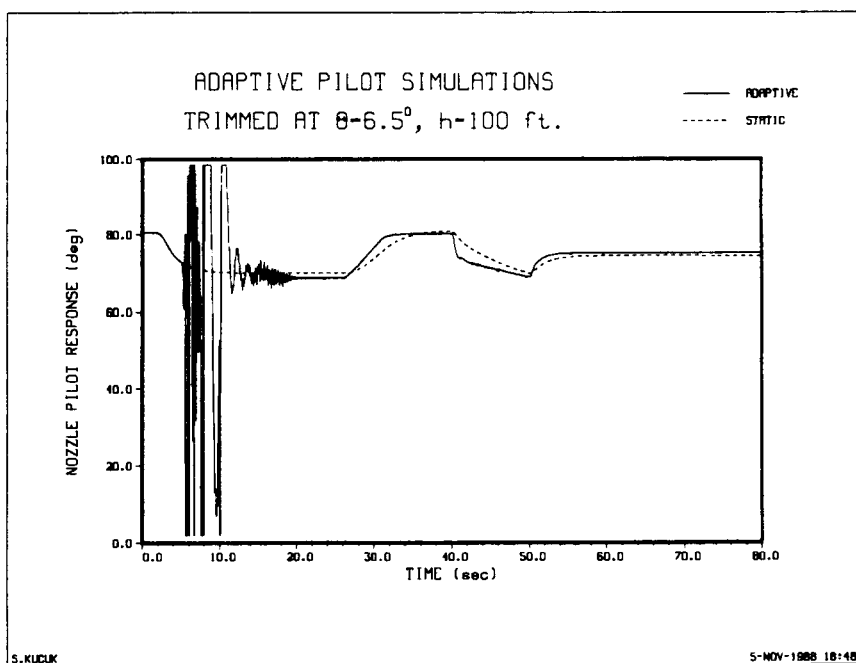


Figure 84. Nozzle setting pilot response, two-pilot configuration, adaptive after $t=5$ sec

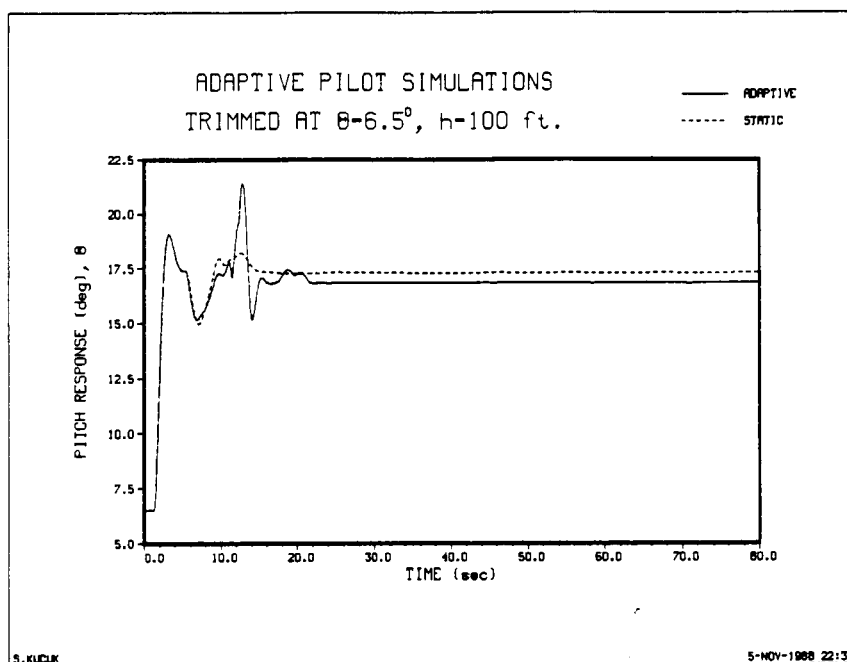


Figure 85. Pitch response, five-pilot configuration, adaptive after $t=5$ sec

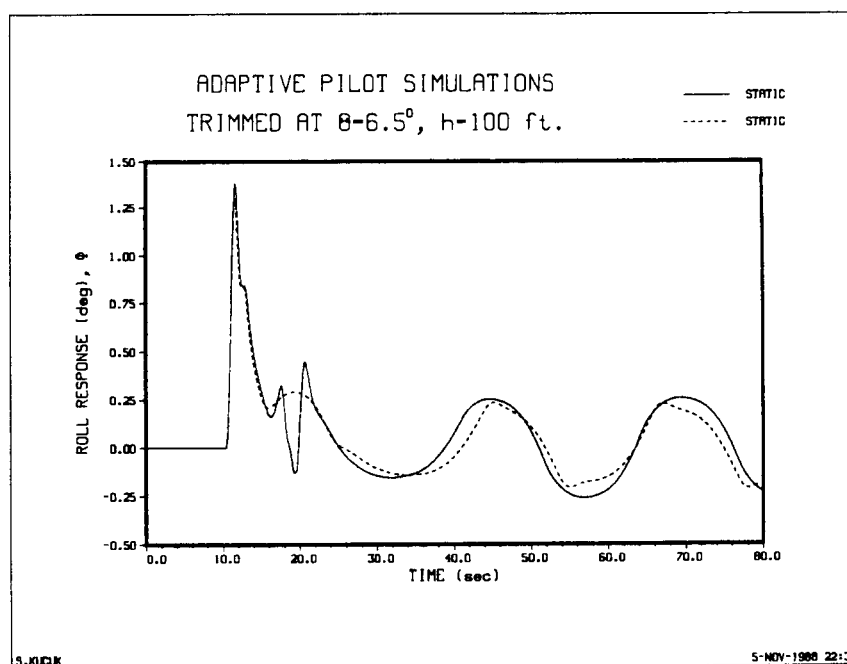


Figure 86. Roll response, five-pilot configuration

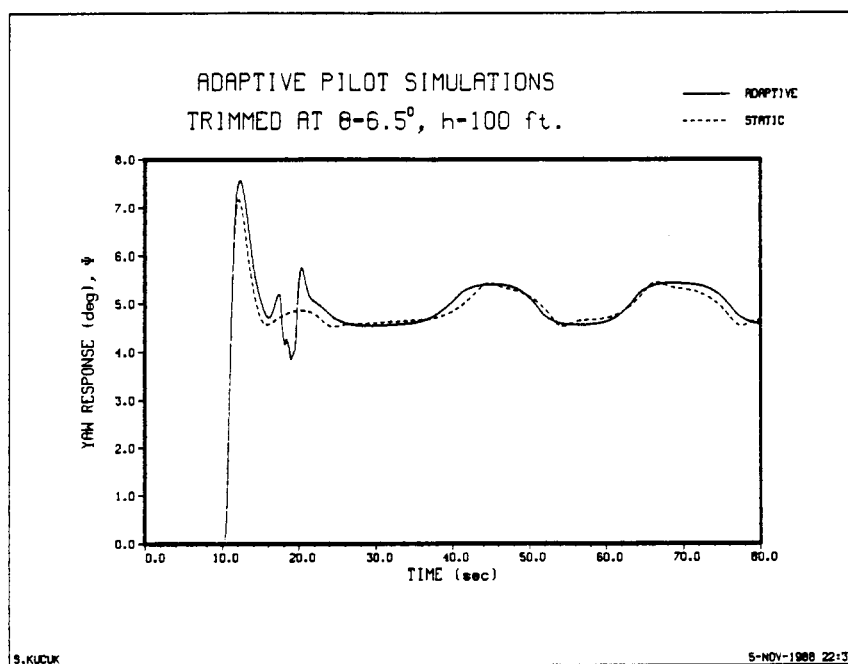


Figure 87. Yaw response, five-pilot configuration, adaptive after $t=15$ sec

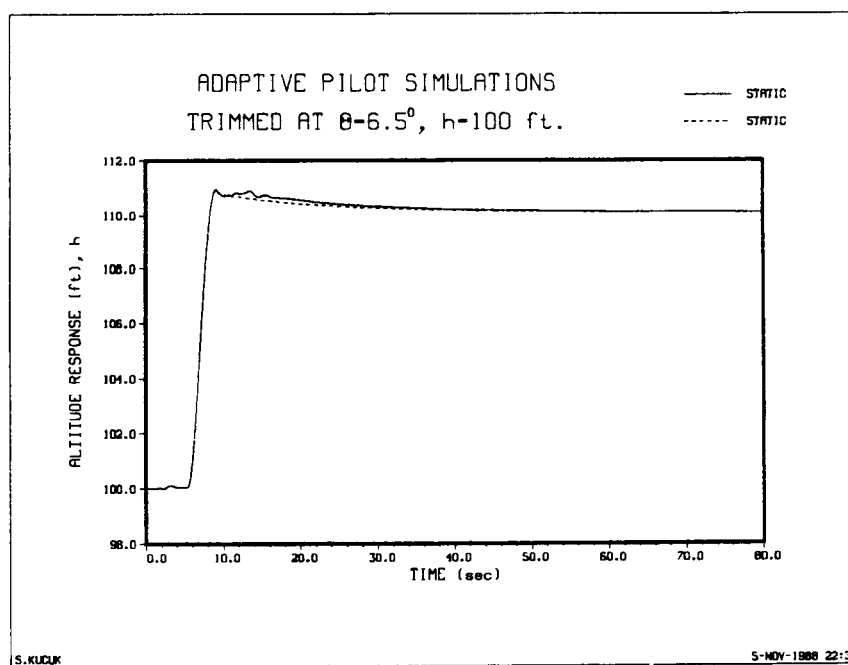


Figure 88. Altitude response, five-pilot configuration

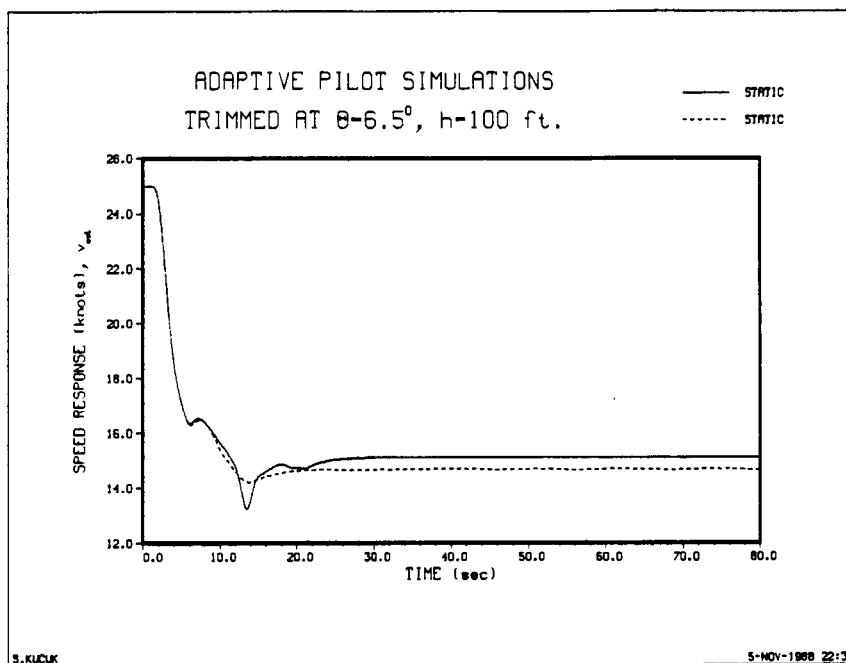


Figure 89. Airspeed response, five-pilot configuration

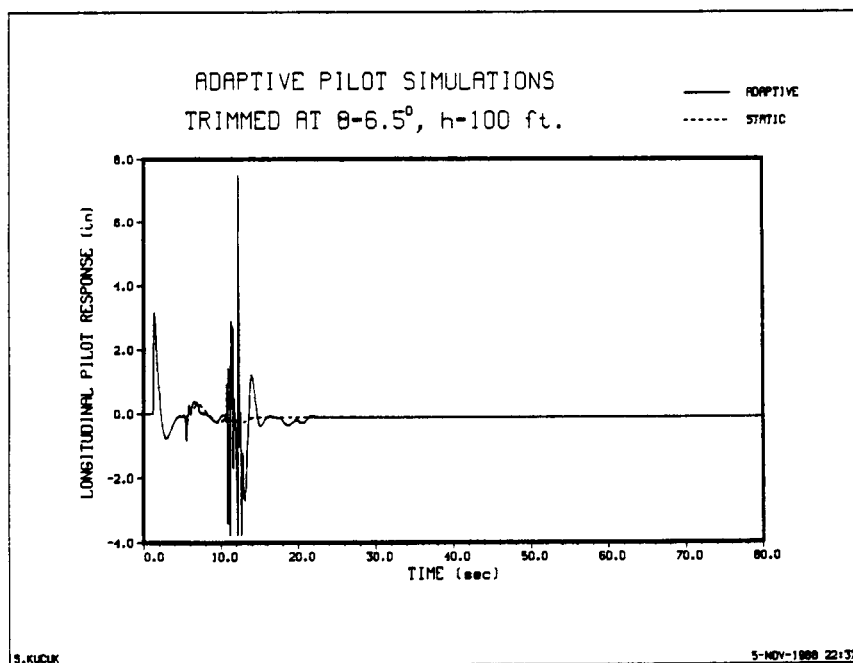


Figure 90. Longitudinal stick pilot response, five-pilot configuration, adaptive after $t=5$ sec

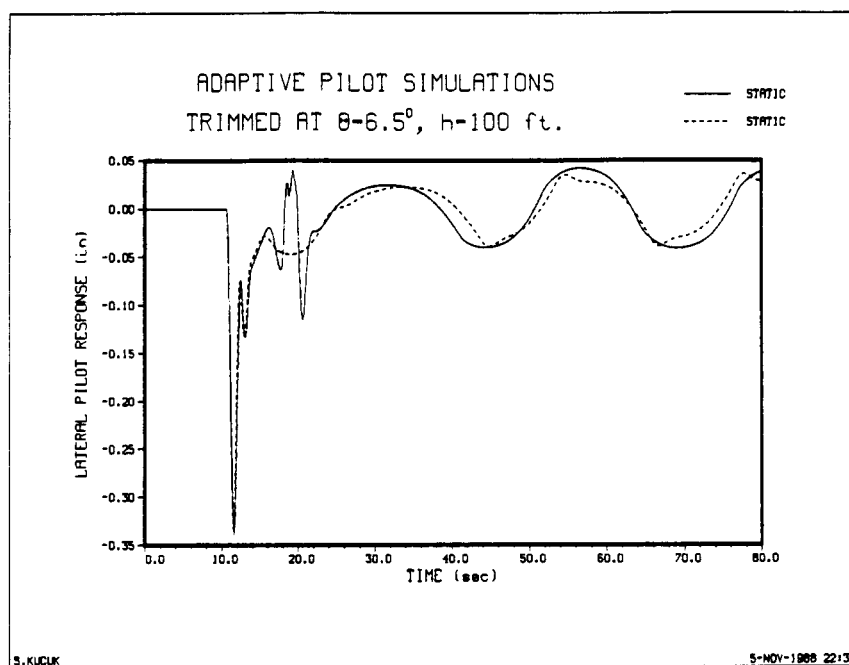


Figure 91. Lateral stick pilot response, five-pilot configuration

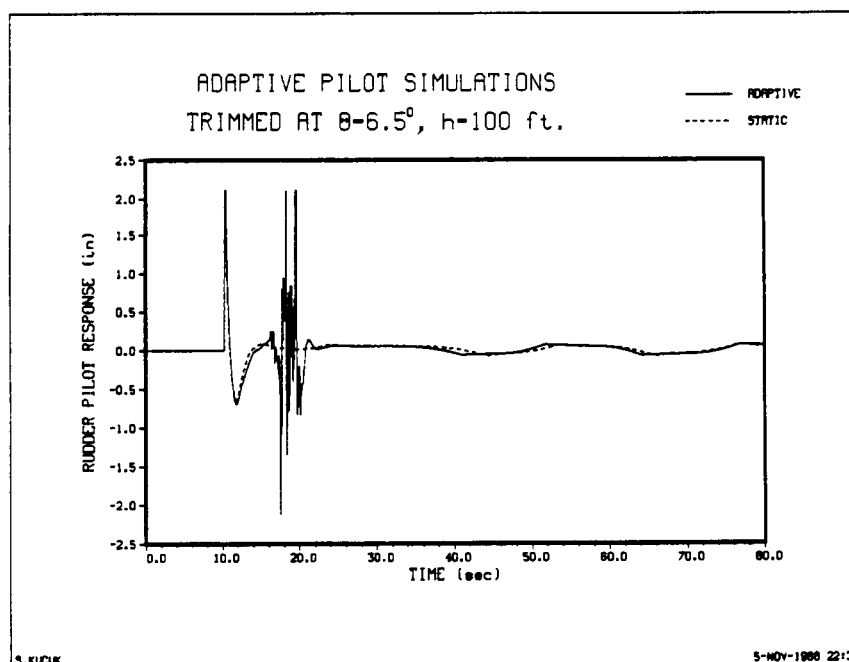


Figure 92. Rudder pedal pilot response, five-pilot configuration, adaptive after $t=15$ sec

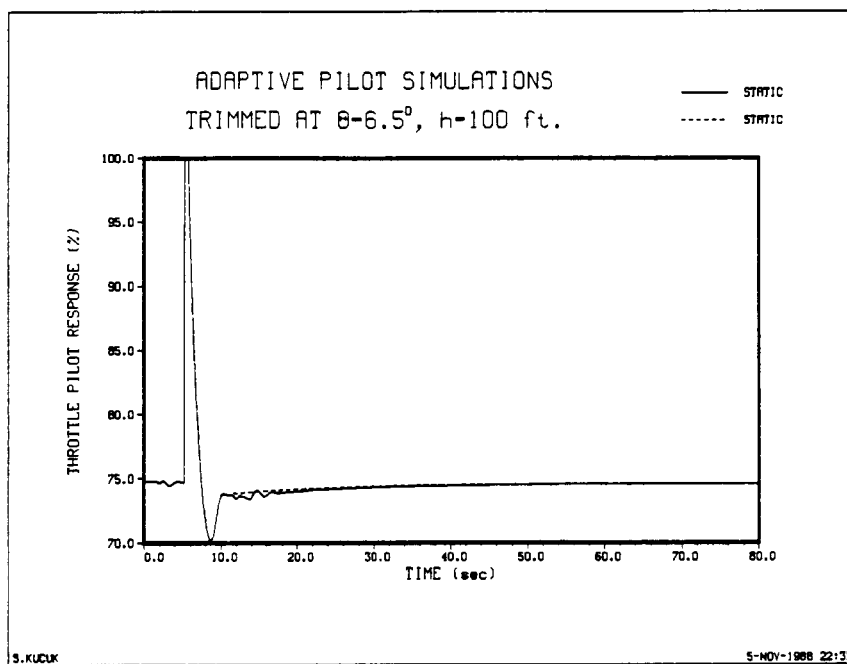


Figure 93. Throttle setting pilot response, five-pilot configuration

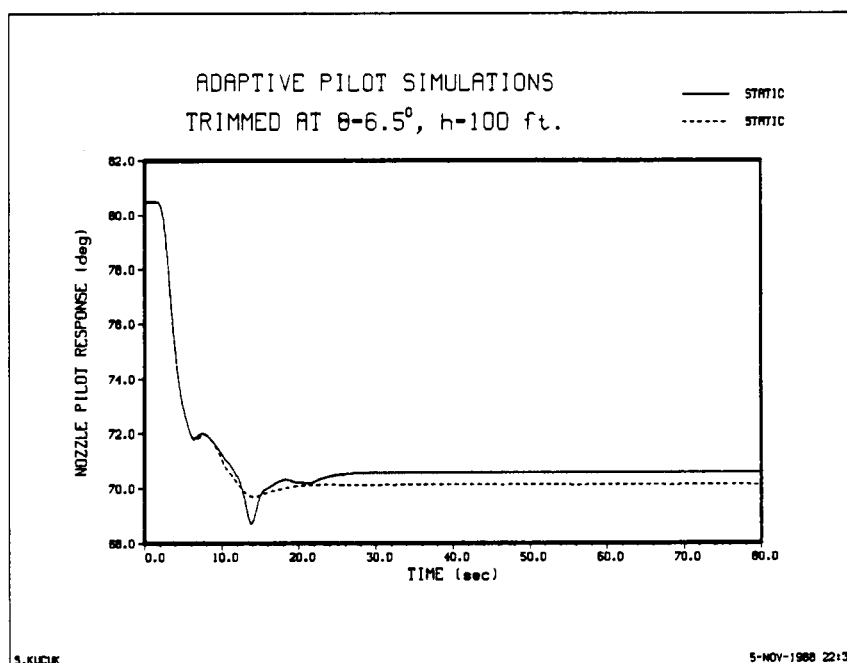


Figure 94. Nozzle setting pilot response, five-pilot configuration

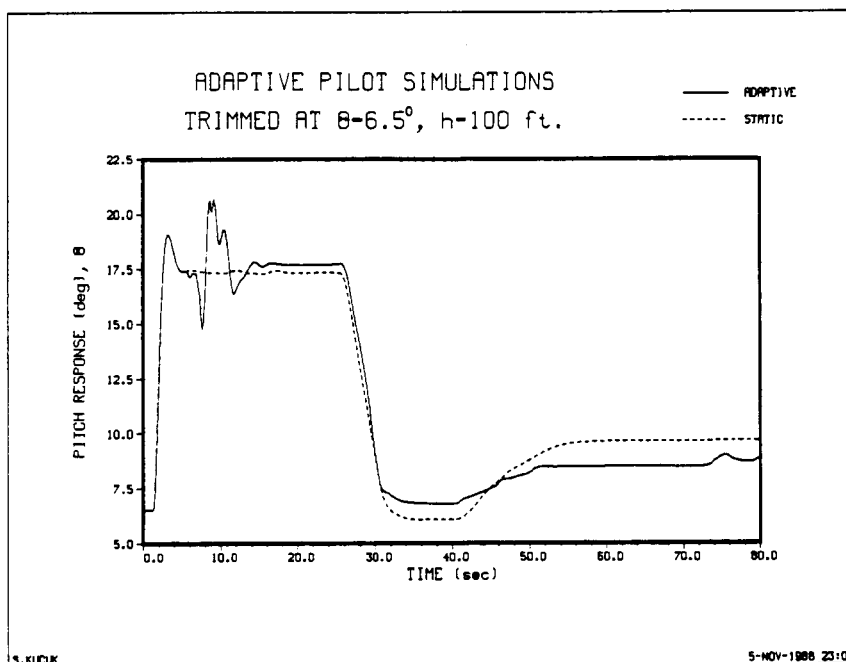


Figure 95. Pitch response, four-pilot configuration, adaptive after $t=5$ sec

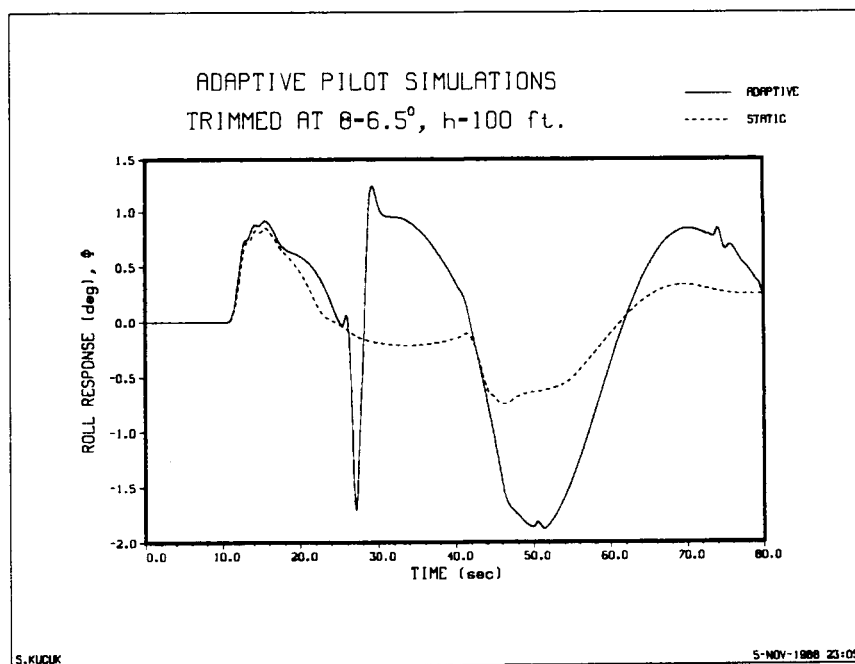


Figure 96. Roll response, four-pilot configuration, adaptive after $t=28$ sec

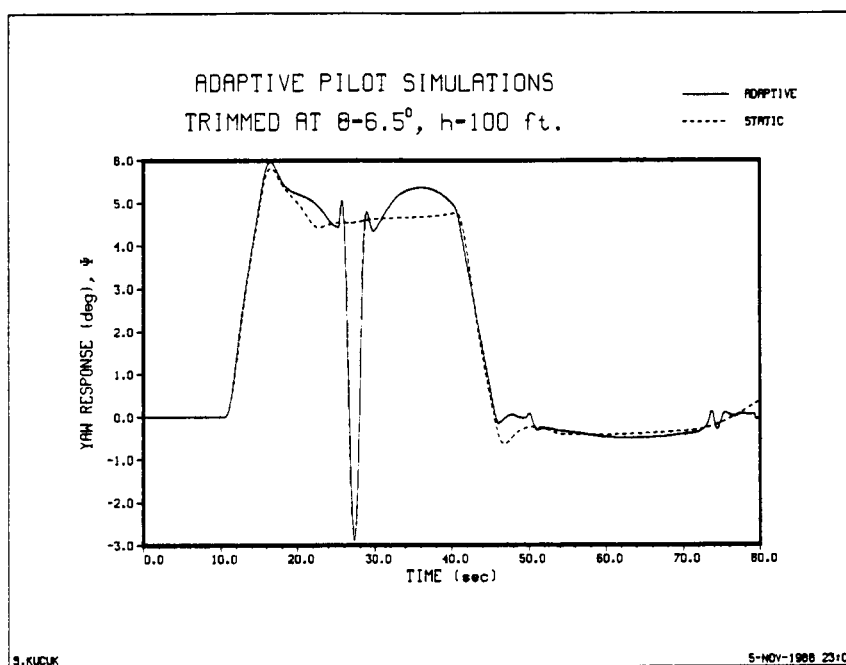


Figure 97. Yaw response, four-pilot configuration, adaptive after $t=25$ sec

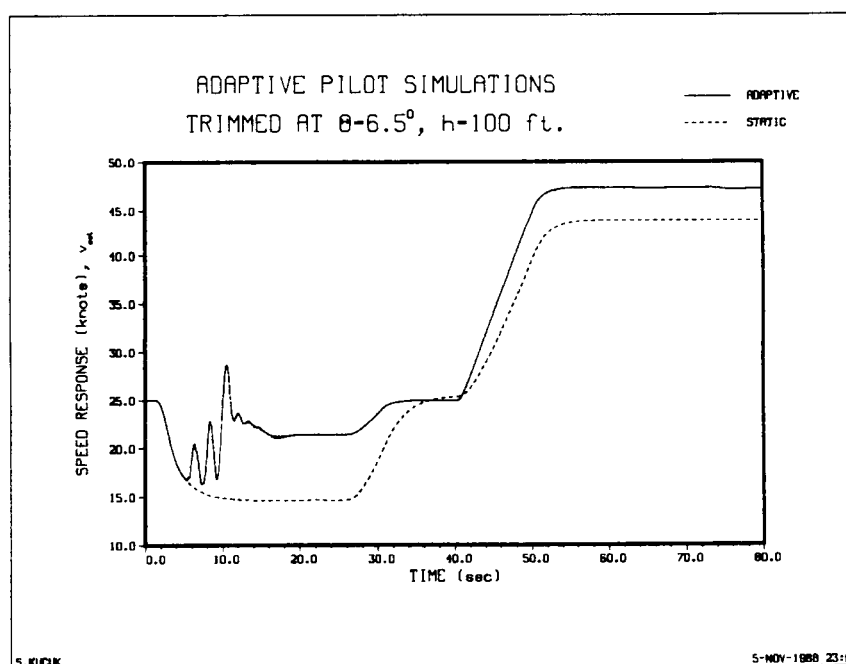


Figure 98. Airspeed response, four-pilot configuration, adaptive after $t=5$ sec

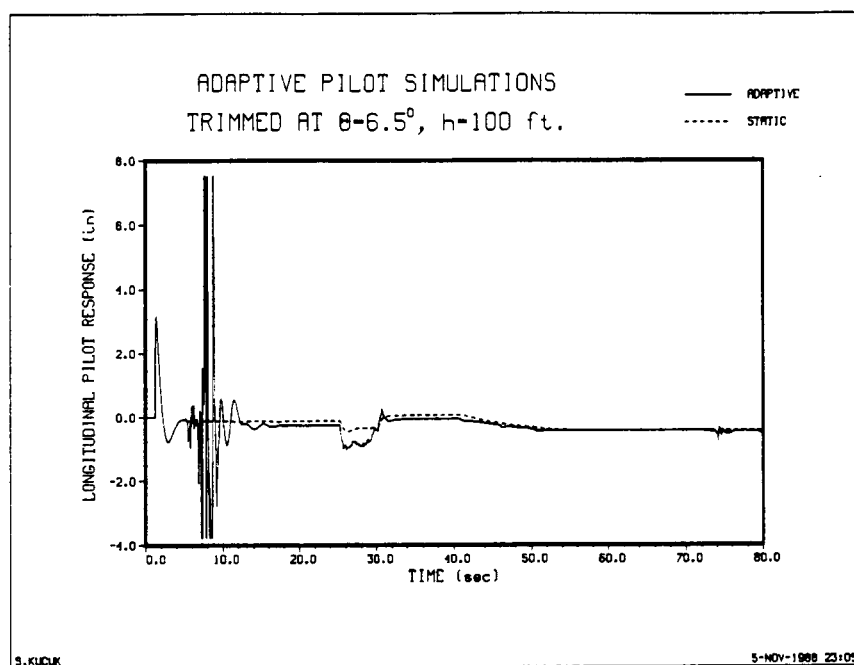


Figure 99. Longitudinal stick pilot response, four-pilot configuration, adaptive after $t=5$ sec

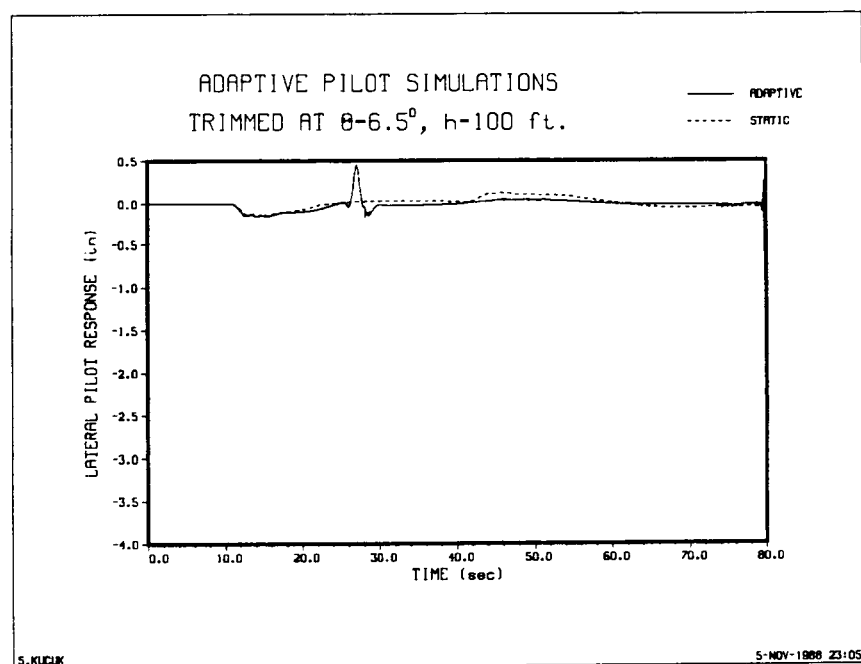


Figure 100. Lateral stick pilot response, four-pilot configuration, adaptive after $t=28$ sec

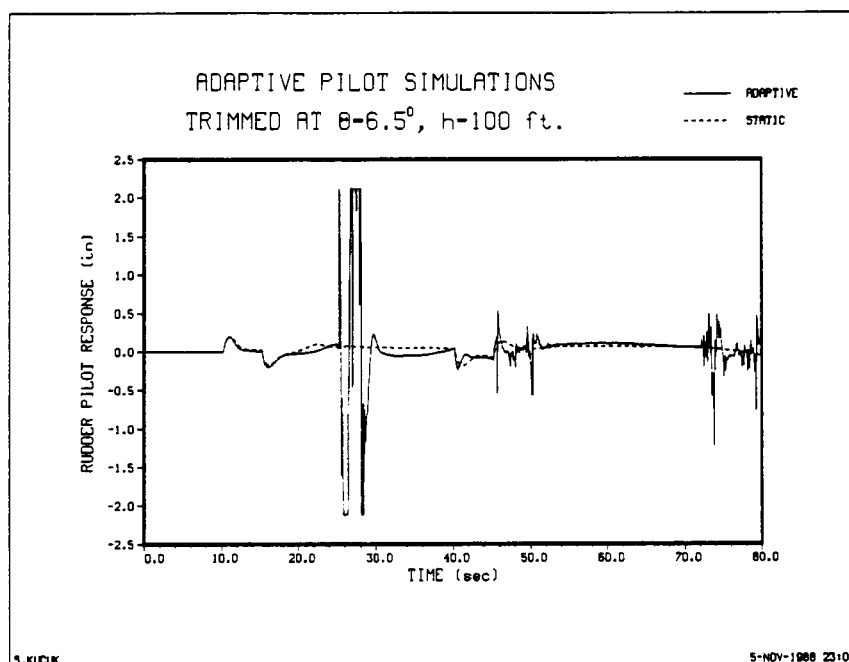


Figure 101. Rudder pedal pilot response, four-pilot configuration, adaptive after $t=25$ sec

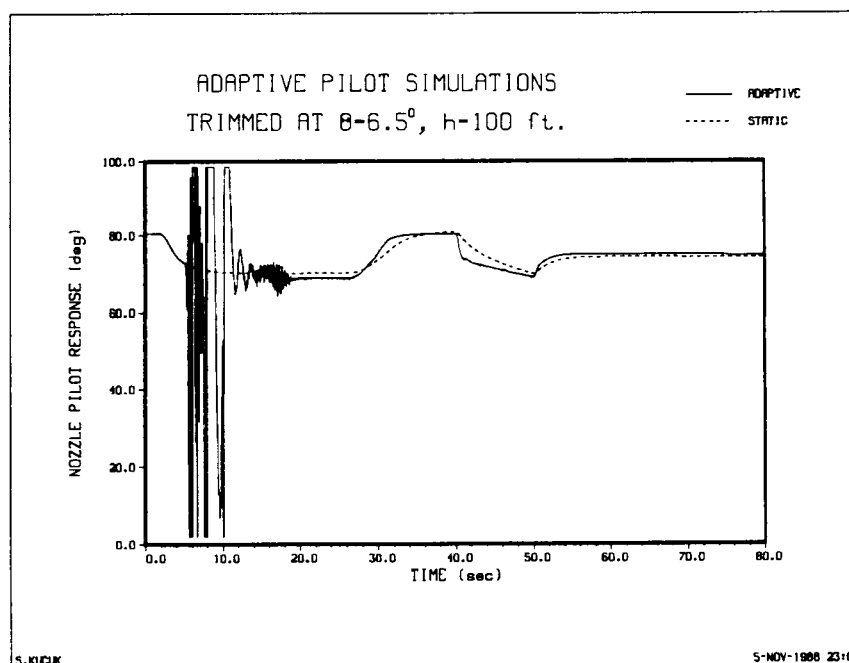


Figure 102. Nozzle setting pilot response, four-pilot configuration, adaptive after $t=5$ sec

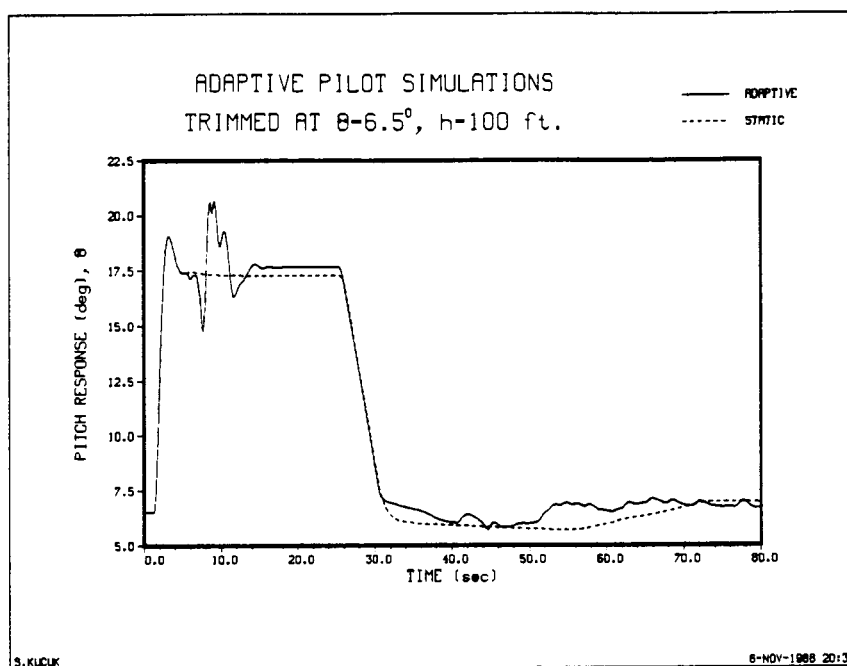


Figure 103. Pitch response, four-pilot configuration, adaptive after $t=5$ sec

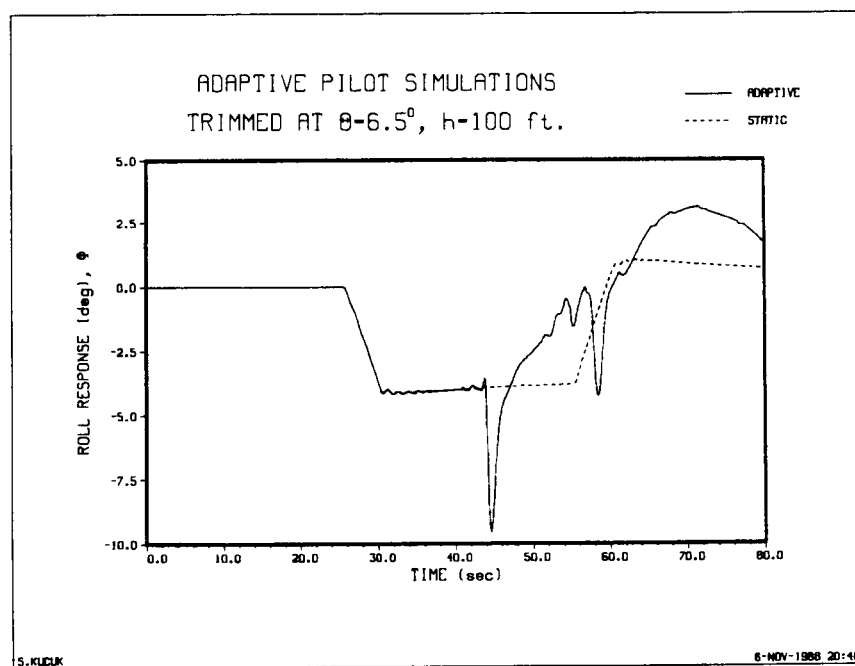


Figure 104. Roll response, four-pilot configuration, adaptive after $t=40$ sec

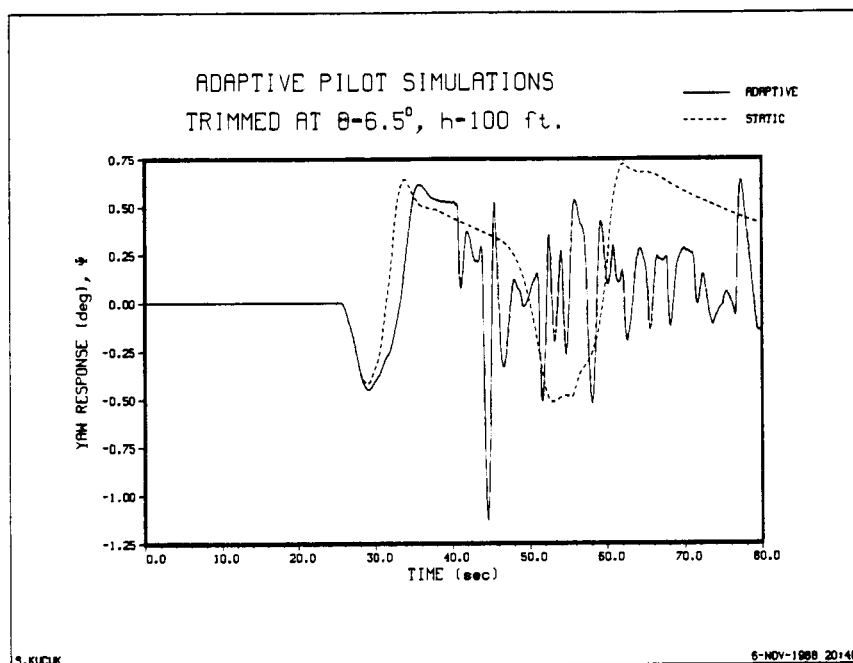


Figure 105. Yaw response, four-pilot configuration, adaptive after $t=43$ sec

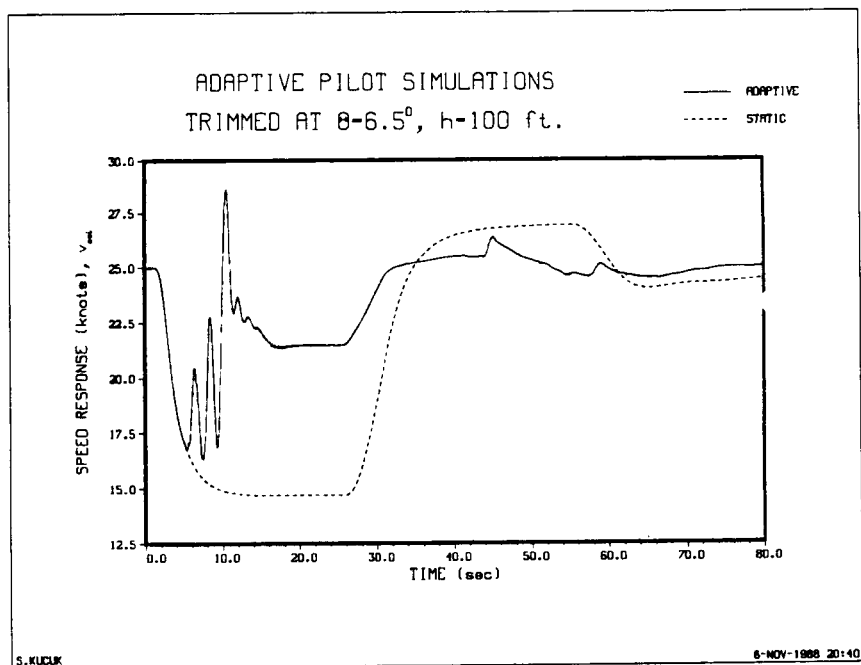


Figure 106. Airspeed response, four-pilot configuration, adaptive after $t=5$ sec

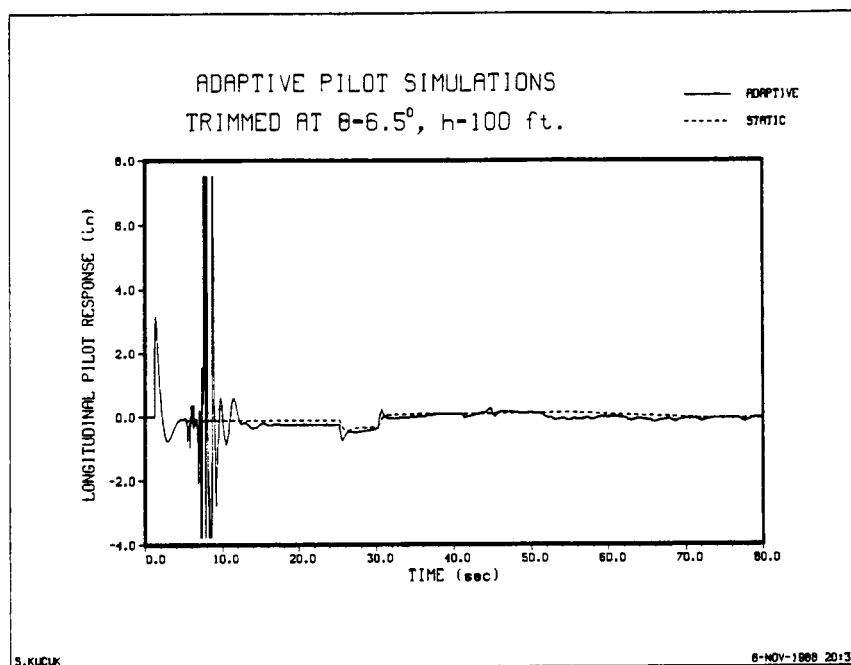


Figure 107. Longitudinal stick pilot response, four-pilot configuration, adaptive after $t=5$ sec

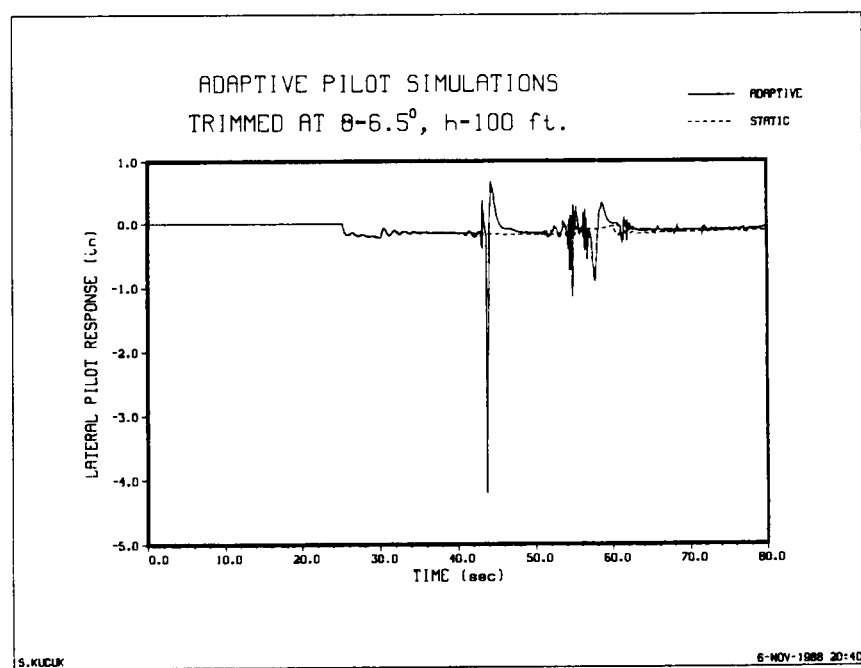


Figure 108. Lateral stick pilot response, four-pilot configuration, adaptive after $t=40$ sec

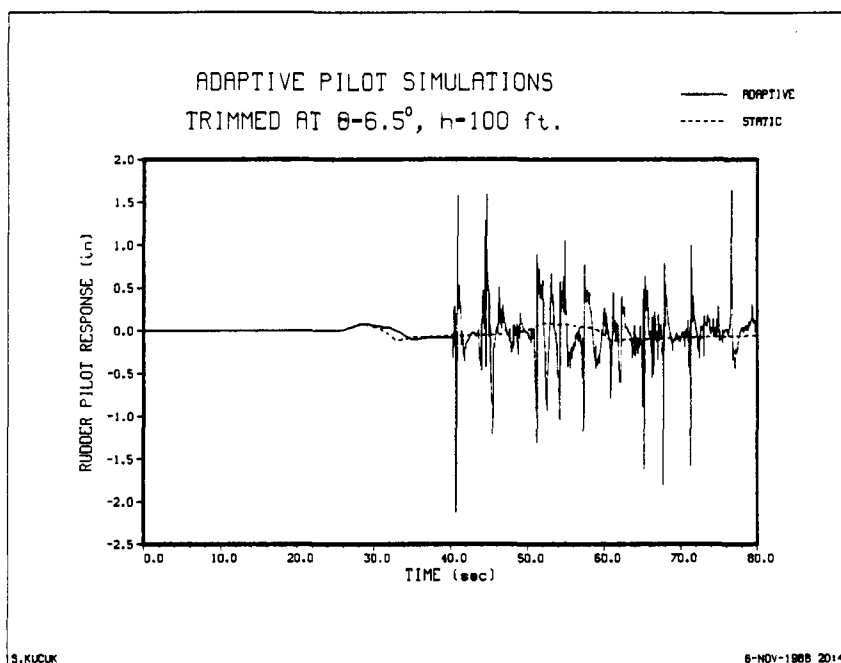


Figure 109. Rudder pedal pilot response, four-pilot configuration, adaptive after $t=43$ sec

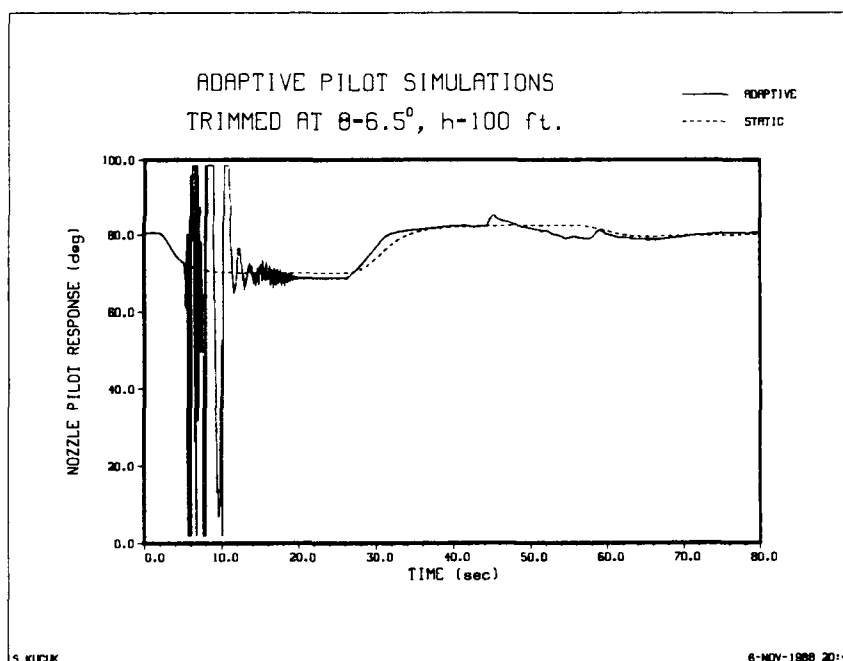


Figure 110. Nozzle setting pilot response, four-pilot configuration, adaptive after $t=5$ sec

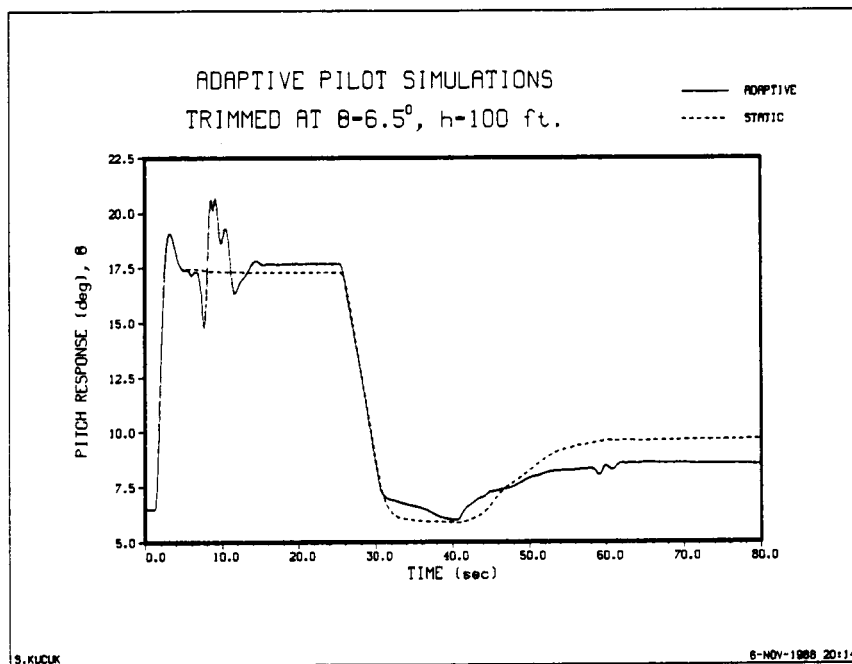


Figure 111. Pitch response, four-pilot configuration, adaptive after $t=5$ sec

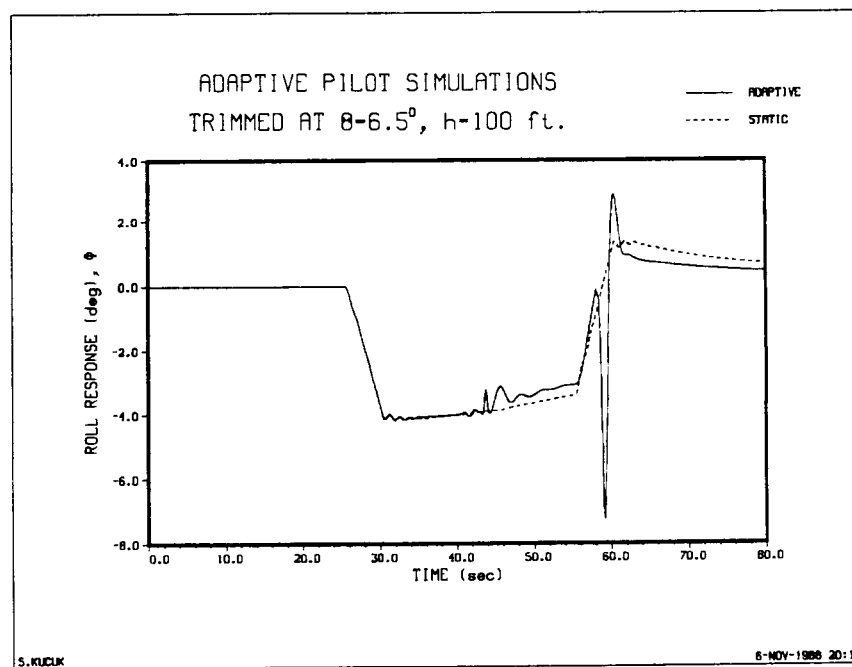


Figure 112. Roll response, four-pilot configuration, adaptive after $t=40$ sec

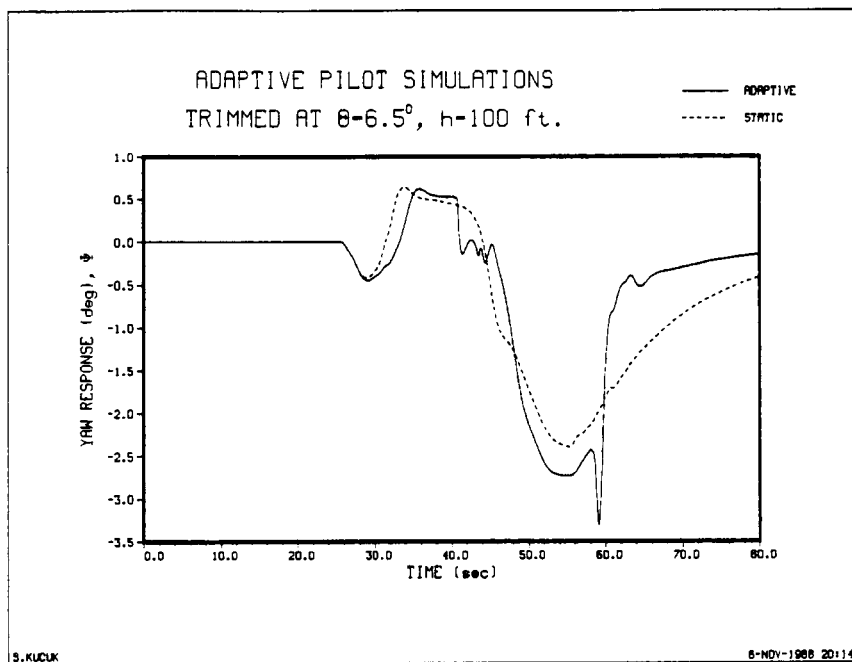


Figure 113. Yaw response, four-pilot configuration, adaptive after $t=43$ sec

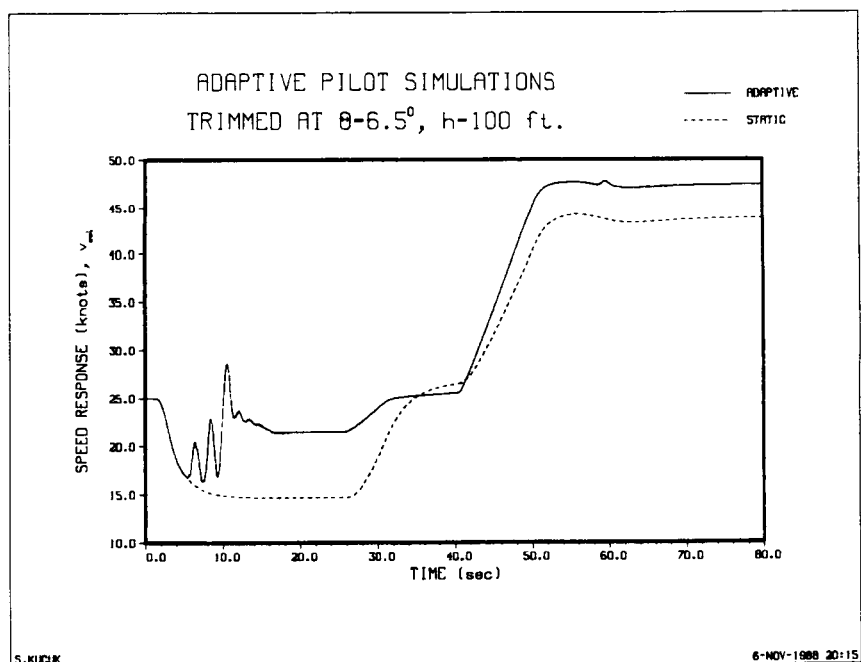


Figure 114. Airspeed response, four-pilot configuration, adaptive after $t=5$ sec

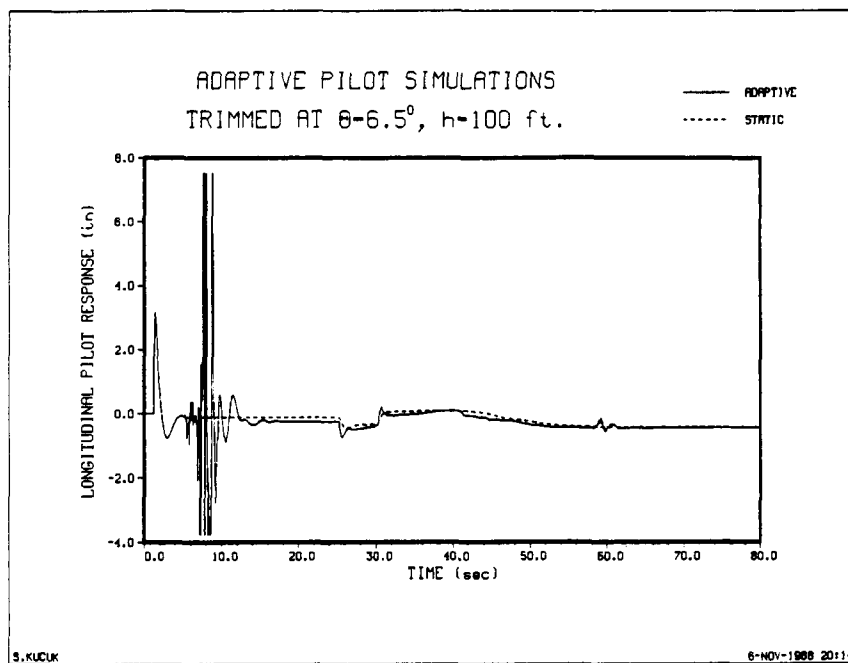


Figure 115. Longitudinal stick pilot response, four-pilot configuration, adaptive after $t=5$ sec

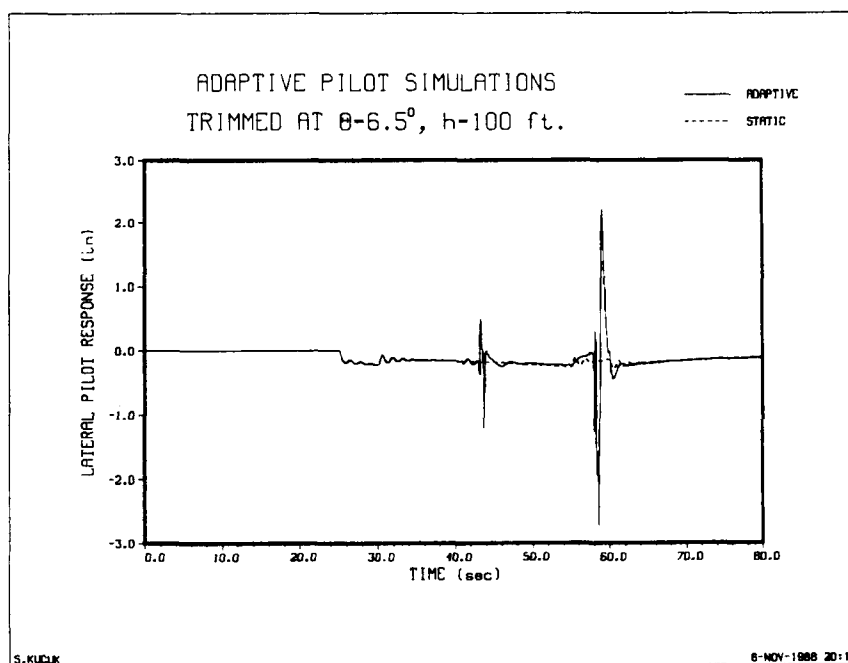


Figure 116. Lateral stick pilot response, four-pilot configuration, adaptive after $t=40$ sec

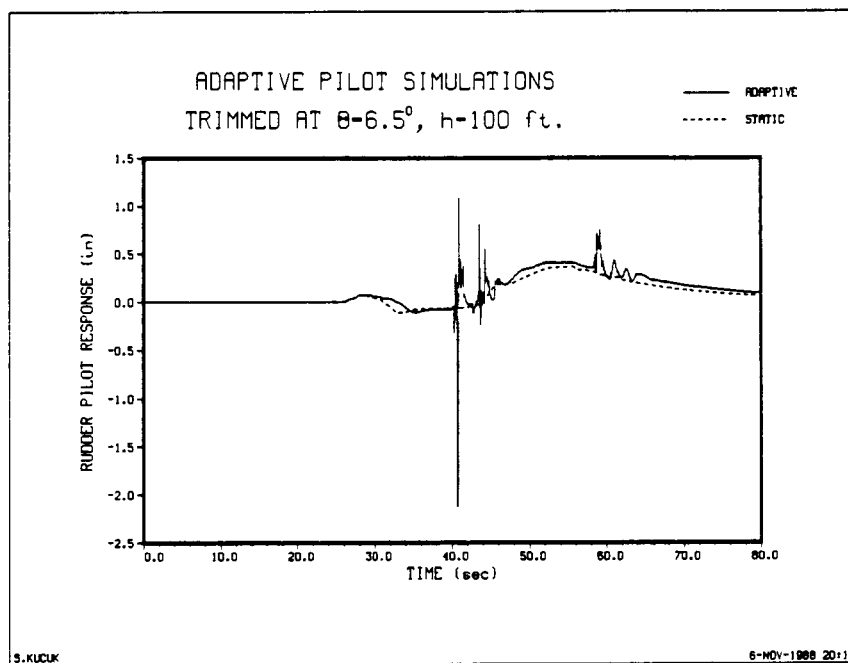


Figure 117. Rudder pedal pilot response, four-pilot configuration, adaptive after $t=43$ sec

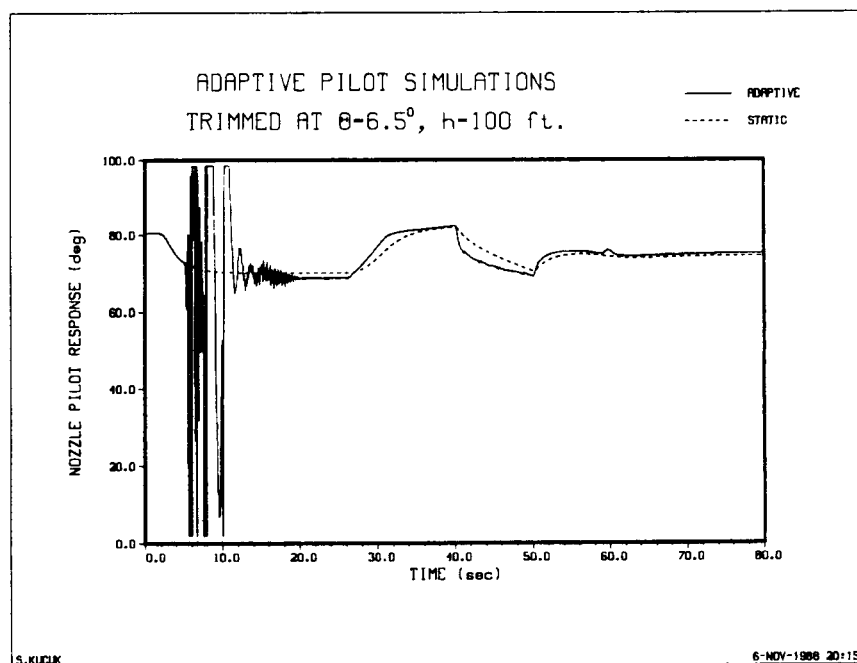


Figure 118. Nozzle setting pilot response, four-pilot configuration, adaptive after $t=5$ sec

6.4 Matching Actual Pilot Data

Some actual pilot data was provided by NASA-Lewis for the evaluation of the computer pilot simulations and comparisons. We chose the vertical tracking task where the actual trained pilots were subjected to vertical maneuvers over the aircraft. In order to simulate such a case, a careful reasoning of the actual pilot reaction must be undertaken. It is very important to be able to choose the primary responses of the aircraft to be consistent with the actual pilot commands. The concern becomes "why" and "when". After a careful analysis the altitude, and the heading (yaw) were found to be the primary response which the pilot is controlling. The others, like the pitch, roll, and speed were constrained to have magnitudes within an allowed region to be consistent with the actual data. The actual aircraft was sitting on the ground with no thrust. The pilot activated the throttle at $t=15$ sec. and continued to gain altitude until $h=80$ ft. He maintained his altitude until $t=75$ sec., when he started a descent to $h=40$ ft. and went back to $h=80$ ft. after $t=105$ sec. Meanwhile at $t=25$ sec. the rudder pedals were activated by the pilot to change the heading of the aircraft which started at 15° . The heading changed in a ramp-like behavior when the pilot finally decided to stop the heading of 70° at $t=55$ sec. All the time and relative aircraft parameter references are approximate. Due to some limitations of the simulation environment, our simulations had to be given approximate aircraft parameters like the initial speed, altitude and angular positions, but unlike the actual aircraft, without thrust the aircraft would have crashed if we did not trim the aircraft so that it will stay at approximately 5 ft. in the air. In the simulation, all aircraft parameters are calculated with respect to the center of gravity (CG), and 5 ft. corresponds to the altitude of the CG. Although the actual aircraft is on the ground with an CG altitude of 5 ft., the same situation applies to an aircraft at 5 ft. above the ground in the simulation. The actual pilot waited for 15 sec. before he activated the throttle

but since the aircraft was on the ground, neither the altitude nor the speed of the aircraft did change. On the other hand, in a similar scenario, the same aircraft being simulated in the simulation environment crashed due to the lack of the thrust. For that reason, our pilot will have an initial thrust corresponding to a throttle setting that will trim the aircraft.

We used the static pilot transfer functions of equations (6-7a), (6-7b), (6-7c), (6-7d), and (6-7e) to close the loops with the decoded references of each loop corresponding to the above observations of the actual data. We did not use the adaptive pilot algorithms because of the fact that the adaptive pilots may cause undesirable responses within the "adaptation" process and may carry-off the aircraft to a configuration other than the one being simulated. The decoded reference here means the appropriate selection of the reference signals of the single-variable loops. For example, the heading loop was given a ramp signal at $t=25$ sec. and a step input at $t=75$ sec., so the rudder pilot will try to follow these references and minimize the error just like the actual pilot. However, the rudder pilot had some difficulties in controlling the heading angle in the simulations. In order to examine the actual pilot parameters, we subjected the rudder pilot data of the actual pilot response to the discrete time McRuer-Krendel model where the pilot pole, zero and gain were estimated. The analysis revealed a discrete pole at approximately, $z=-0.45$. This was a surprising result, and explained the failing behavior of our rudder pilot model in this particular case. Throughout the analysis, we assumed that such a pole can not exist in the model since all the poles are expected to be positive and stable, resulting in the fact that the poles and zeros of our pilot model should be located between $z=0$ and $z=1$, inside the unit circle. Another observation is that this pole has almost the same magnitude with the rudder pilot model of equation (6-7c) but has an opposite sign. Therefore, by using the approximated rudder pilot parameters given in equation (6-8),

$$H_{\psi}^{\delta}(z^{-1}) = 0.288z^{-4} \frac{(z^{-1} - 0.96z^{-2})}{(1 - 0.6065z^{-1})(1 + 0.448z^{-1})} \quad (6-8)$$

we obtained results which were very close to the actual pilot data. Figures* (119), (120), (121), (122), (123), (124), (125), (126), (127), and (128) compare the actual and simulated aircraft responses and the control movements of the actual pilot and simulated pilot models. As we mentioned earlier, the pitch and roll loops were not primary responses of the aircraft for this case. For that reason, these responses of the actual and simulated aircraft do not match exactly, but in the average sense the responses follow each other. Furthermore, in actual pilot control case, any longitudinal movement of the stick may have non-zero effects on the lateral stick due to human limitations, and vice versa. The human pilot may want to move the stick only in the longitudinal direction, but this may cause the activation of small lateral movements. However, the simulated pilot will not have this kind of behavior unless it is told so. That is why, as soon as the human pilot activates the longitudinal stick, the lateral stick also has small movements which result in small changes in the roll angle of the aircraft. Figure (124) compare the longitudinal stick input of the pilots. Notice the very close behavior of the pilots. Since both pilots are giving full thrust to gain altitude (refer to Figure (127)), the aircraft will pitch-up. The pilot must then use the stick to regulate the pitch. Figure (124) shows that both pilots push the stick in the same manner to compensate the latter. The roll responses of the actual and simulated cases have same boundaries but due to the reasons explained before they are not exactly the same. However, the altitude and heading responses follow each other closely, being the primary responses of the simulated case. The throttle settings are also very close to each other. Both pilots require full thrust from the aircraft for fast altitude changes. Notice that the throttle setting of the actual pilot starts from 0%,

*The actual pilot control inputs had initial offsets and were shifted to origin for comparison purposes

while our pilot starts from approximately 75%, due to the startup conditions. The rudder pedal inputs are approximately same for a period, but as the configuration of the aircraft changes, the responses differ, although they both fulfill the heading requirements. Also, the nozzle setting of our simulated pilot had to be adjusted slightly to stabilize the speed changes, but once again in the average sense the actual pilot nozzle setting and the simulated nozzle setting follow each other. Finally, we should mention that it is not surprising to expect some differences from the actual pilot data. While the actual pilot is using all his training experience and skills, our model has only five, second-order transfer functions to simulate the human pilot. However, the responses are remarkably close to each other, and the pilot models can in fact control the aircraft, similar to the human pilot.

Figures (129), (130), (131), (132), (133), (134), (135), (136), (137), and (138) compare the static pilots with the actual pilot data for a lateral tracking task, and Figures (139), (140), (141), (142), (143), (144), (145), (146), (147), and (148) show the adaptive pilot performances for the same maneuver. As we mentioned before, after the adaptive pilots converge, the responses are similar.

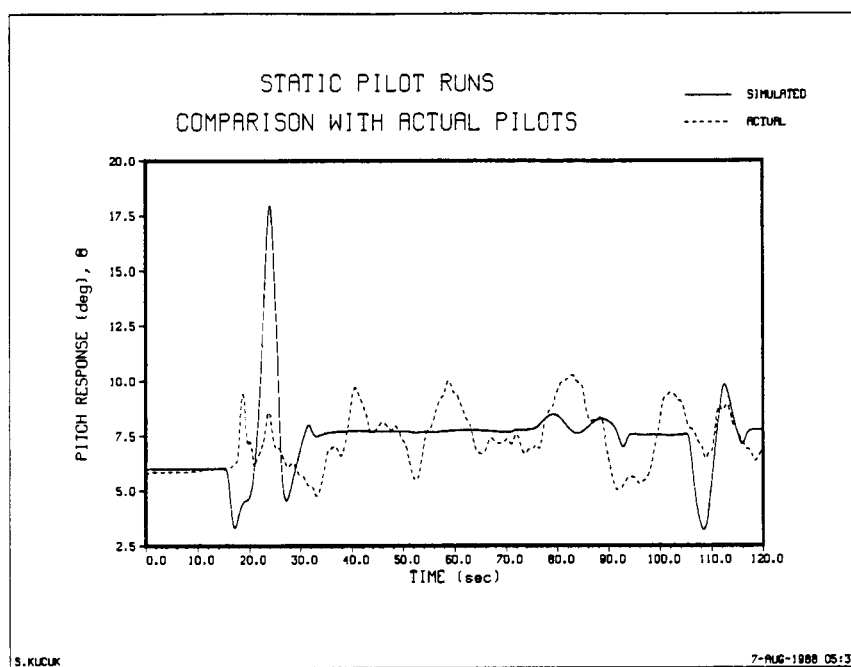


Figure 119. Actual vs simulated pitch response (from NASA data)

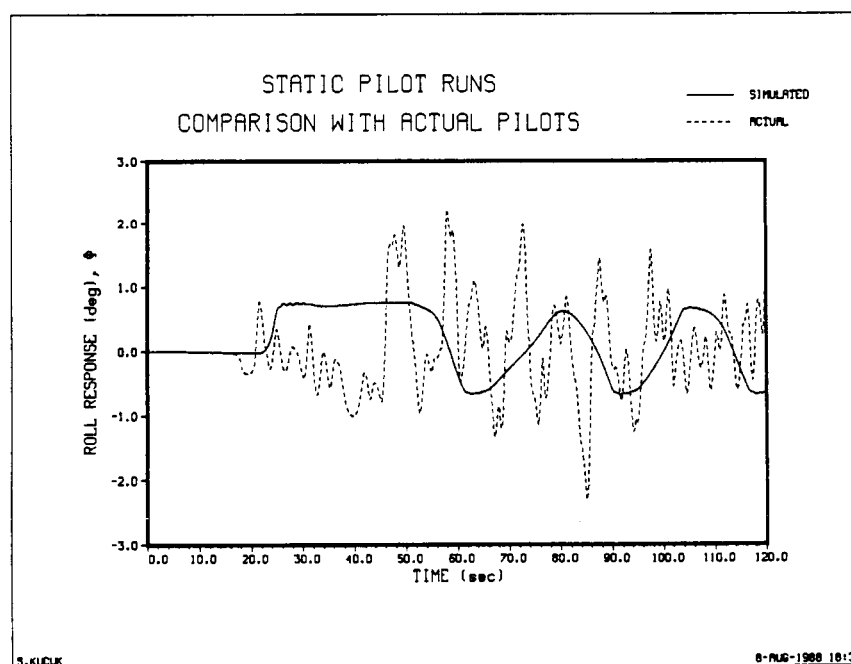


Figure 120. Actual vs simulated roll response (from NASA data)

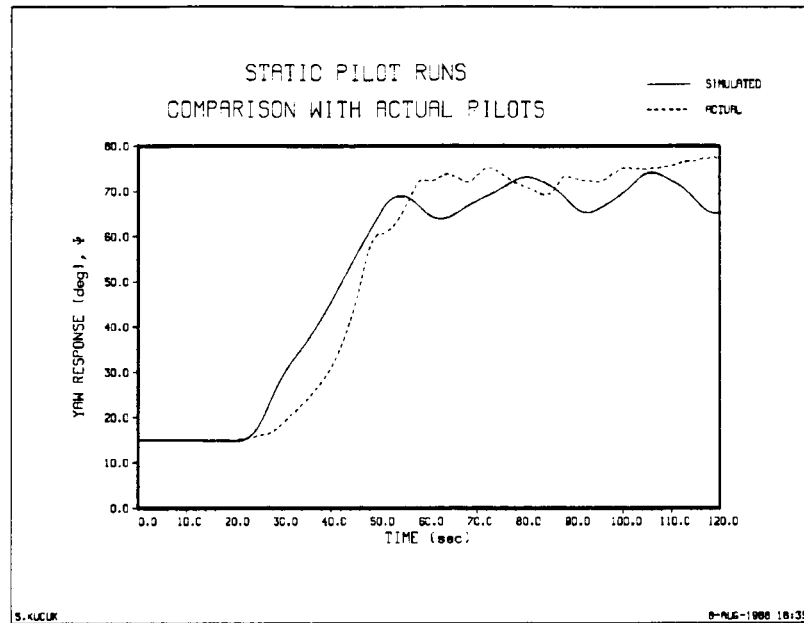


Figure 121. Actual vs simulated yaw response (from NASA data)

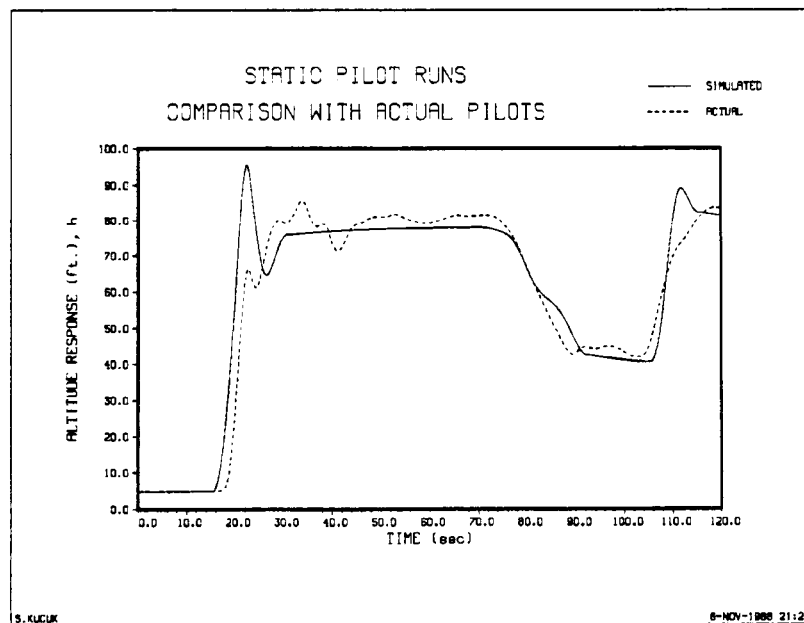


Figure 122. Actual vs simulated altitude response (from NASA data)

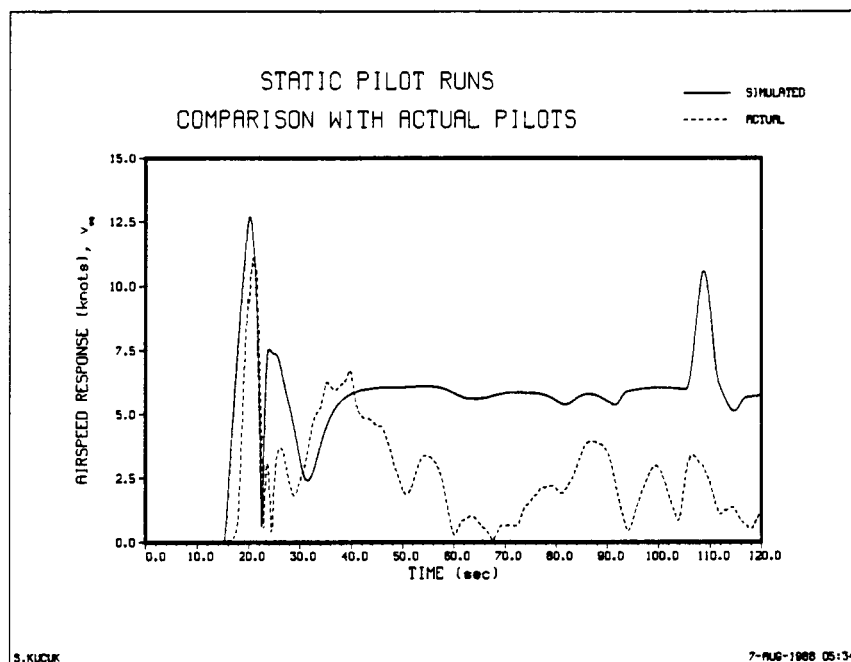


Figure 123. Actual vs simulated speed response (from NASA data)

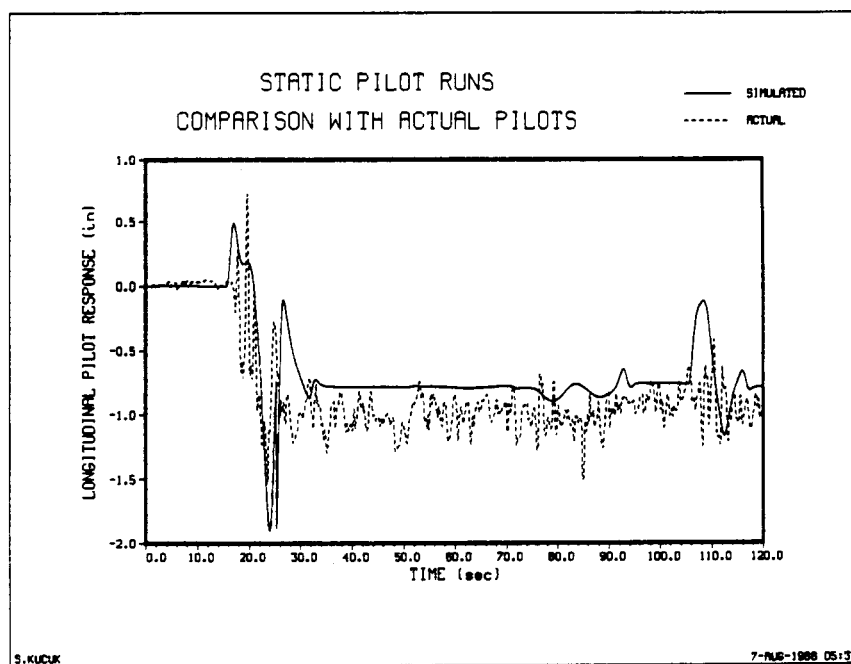


Figure 124. Actual vs simulated longitudinal stick input (from NASA data)

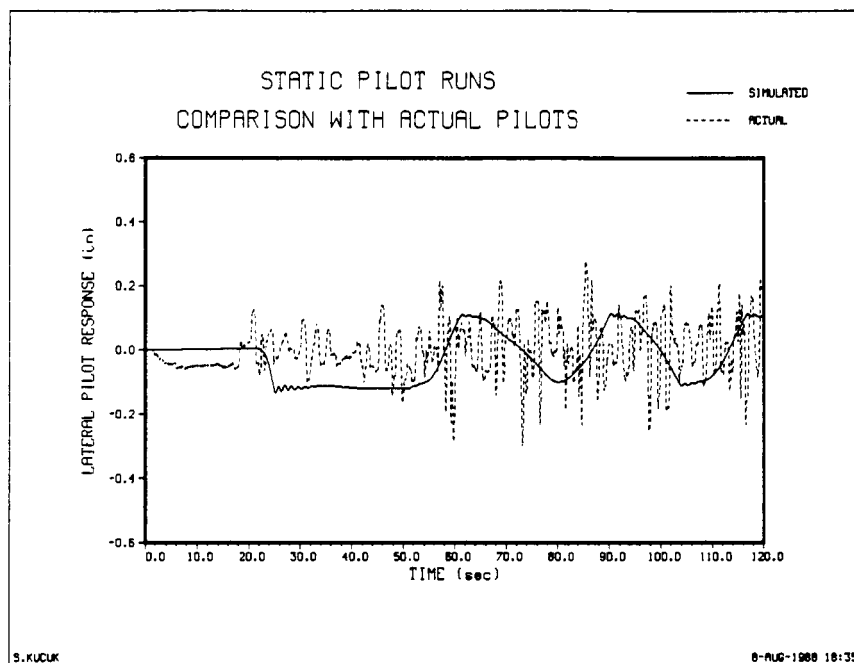


Figure 125. Actual vs simulated lateral stick input (from NASA data)

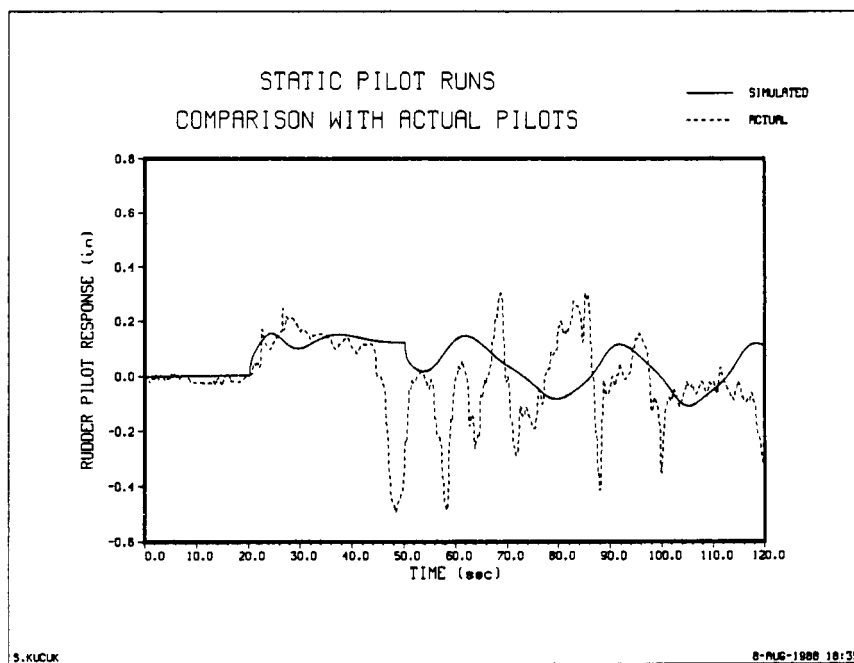


Figure 126. Actual vs simulated rudder pedal input (from NASA data)

ORIGINAL PAGE IS
OF POOR QUALITY

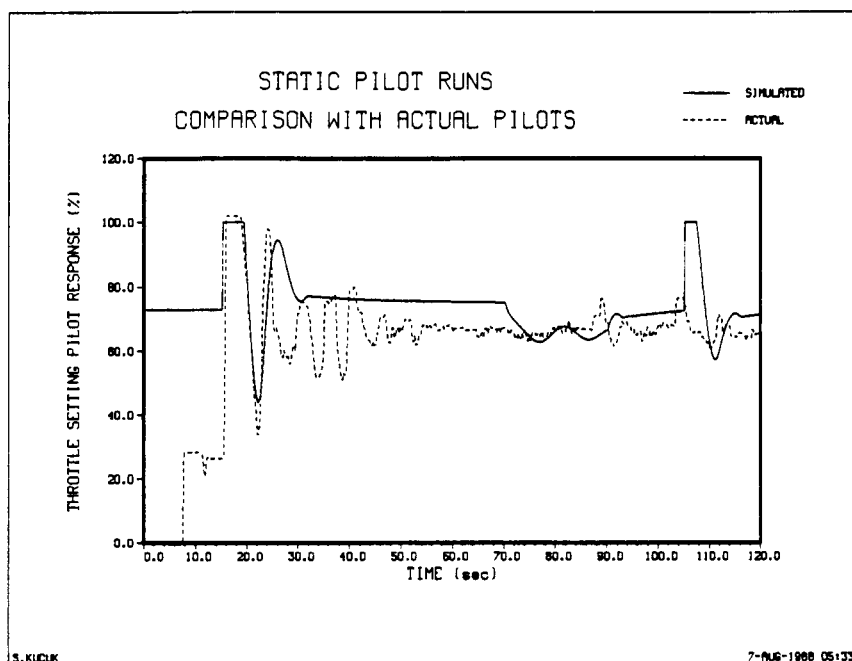


Figure 127. Actual vs simulated throttle setting input (from NASA data)

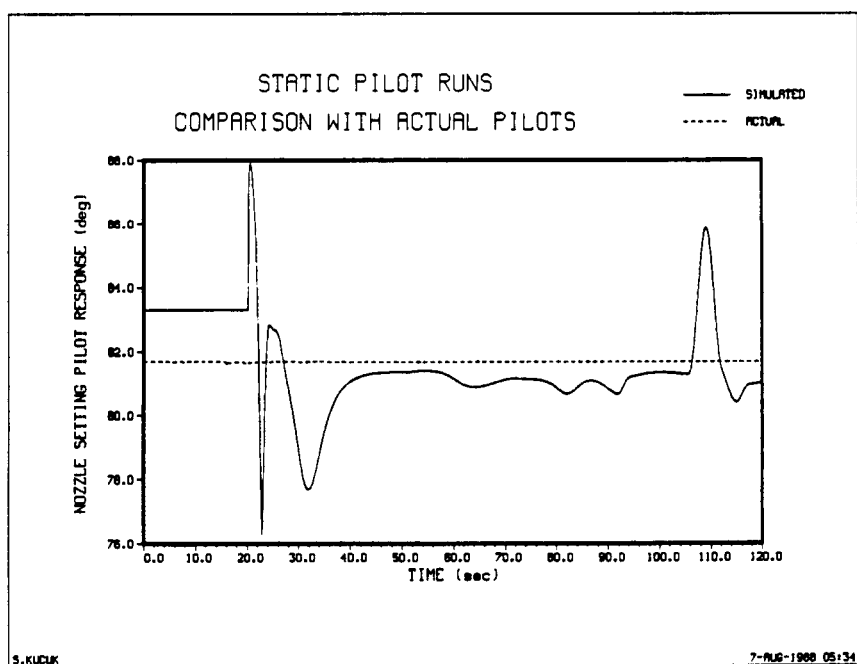


Figure 128. Actual vs simulated nozzle setting input (from NASA data)

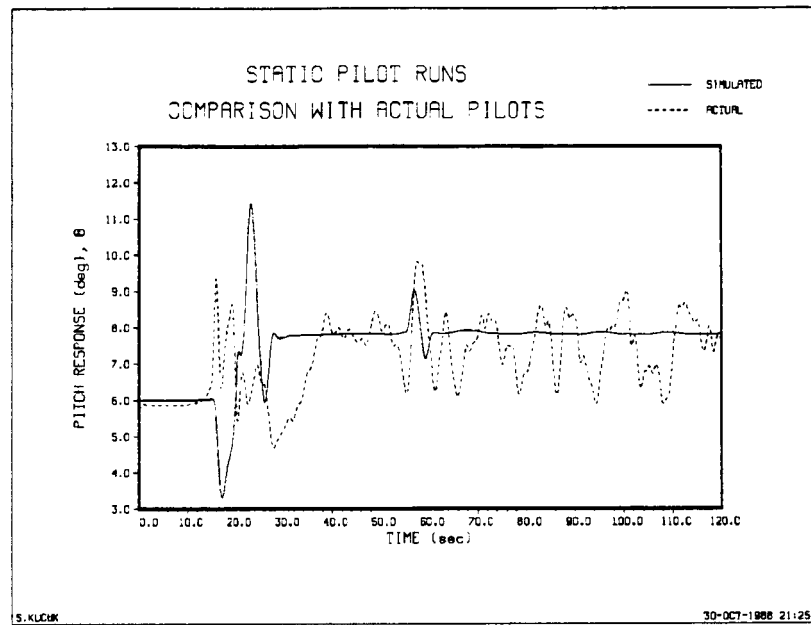


Figure 129. Actual vs simulated pitch response (from NASA data)

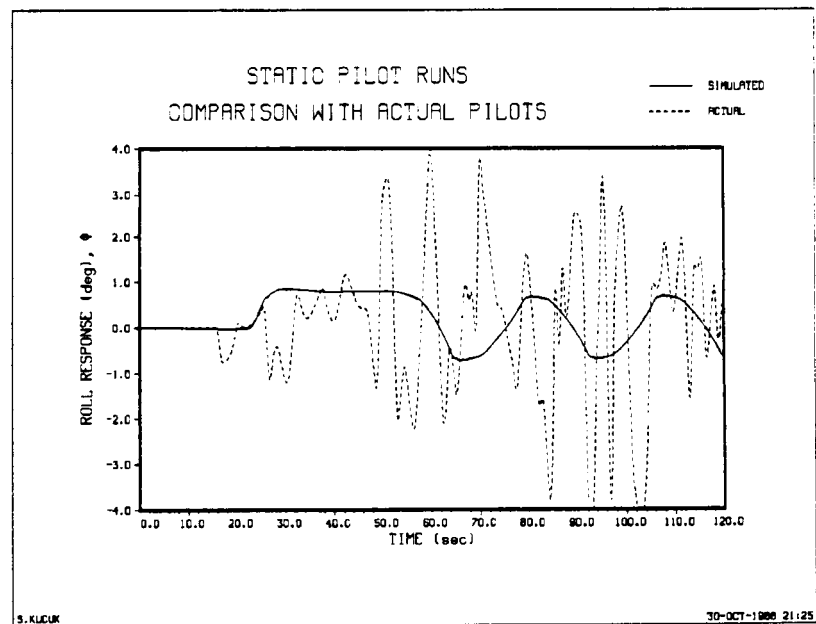


Figure 130. Actual vs simulated roll response (from NASA data)

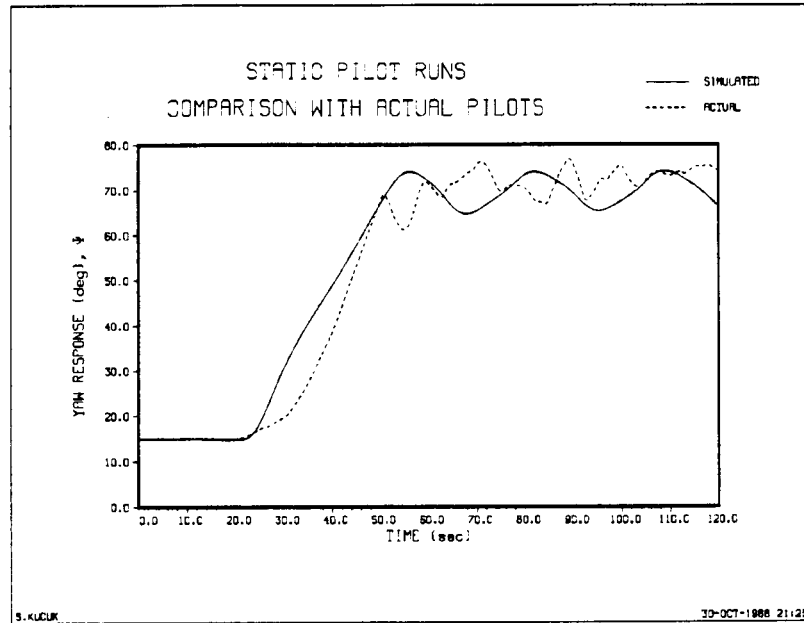


Figure 131. Actual vs simulated yaw response (from NASA data)

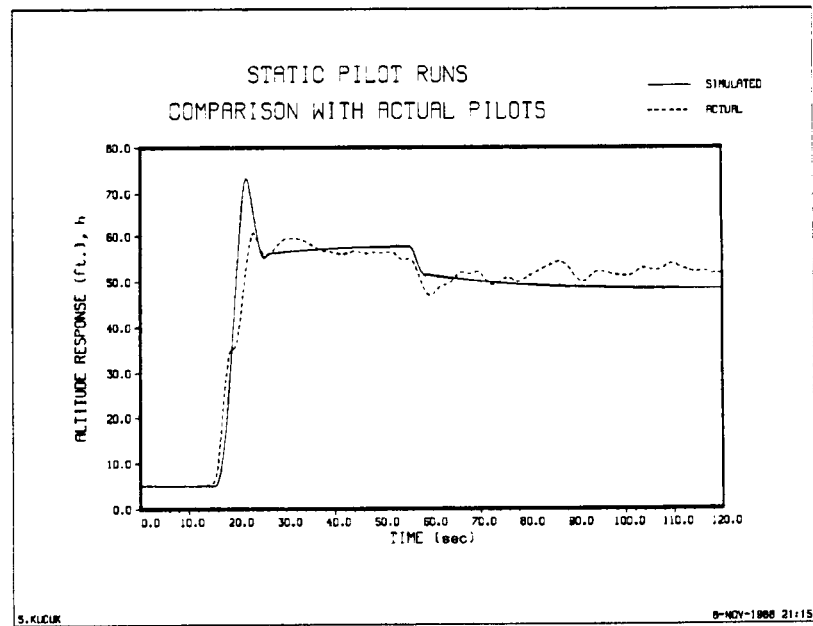


Figure 132. Actual vs simulated altitude response (from NASA data)

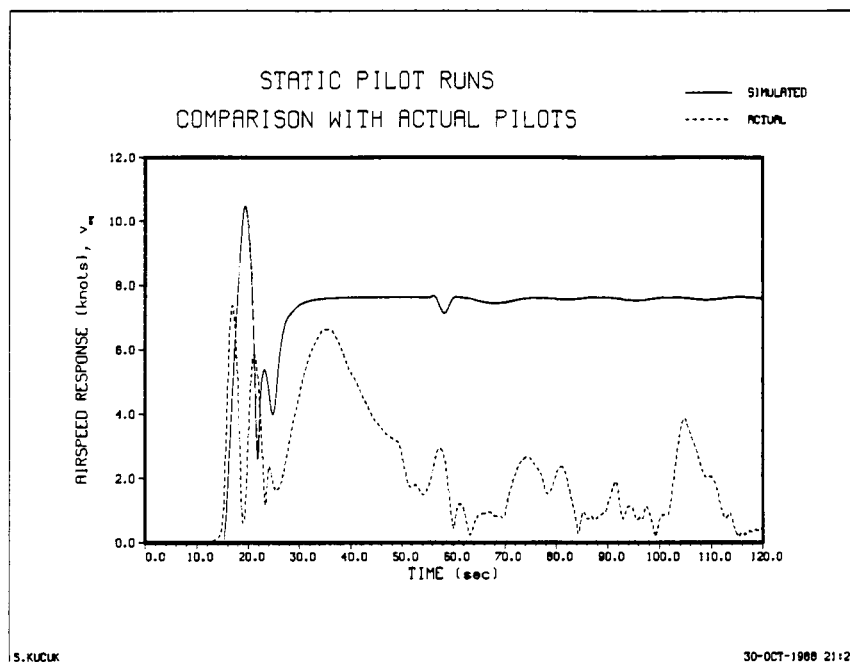


Figure 133. Actual vs simulated speed response (from NASA data)

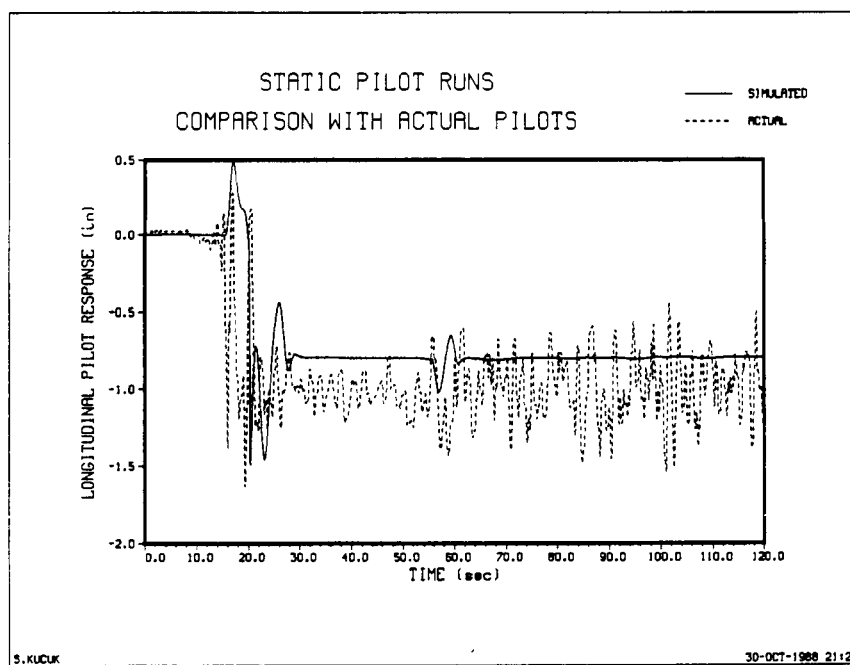


Figure 134. Actual vs simulated longitudinal stick input (from NASA data)

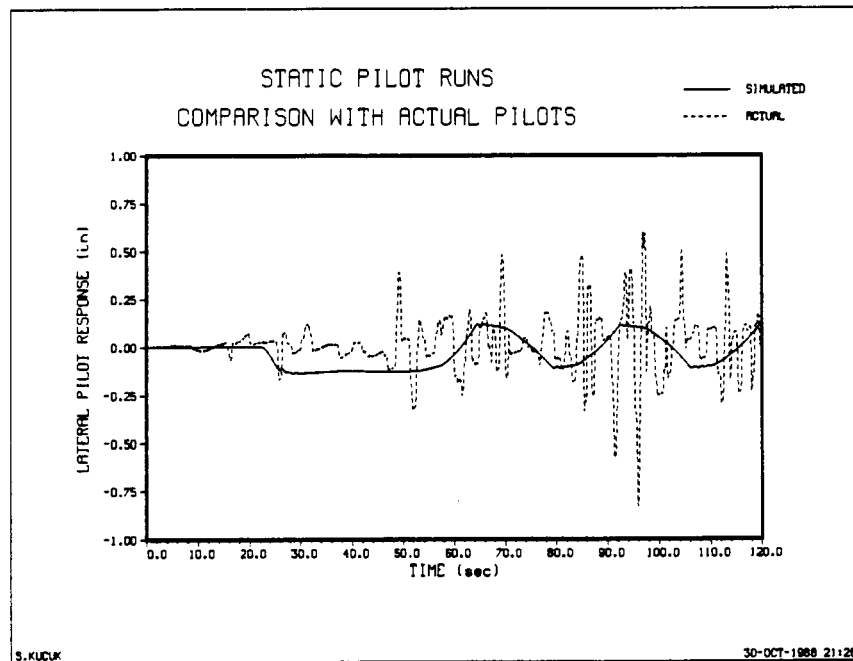


Figure 135. Actual vs simulated lateral stick input (from NASA data)

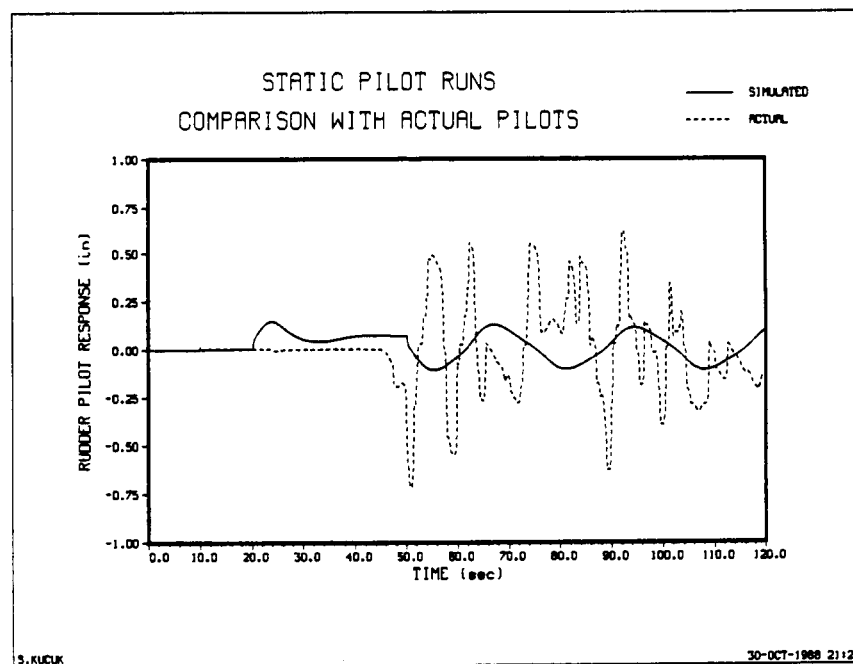


Figure 136. Actual vs simulated rudder pedal input (from NASA data)

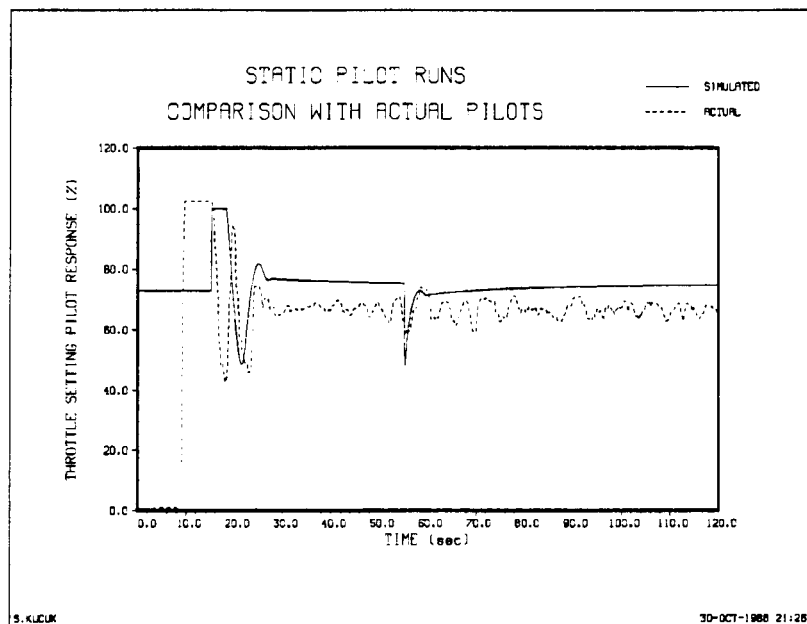


Figure 137. Actual vs simulated throttle setting input (from NASA data)

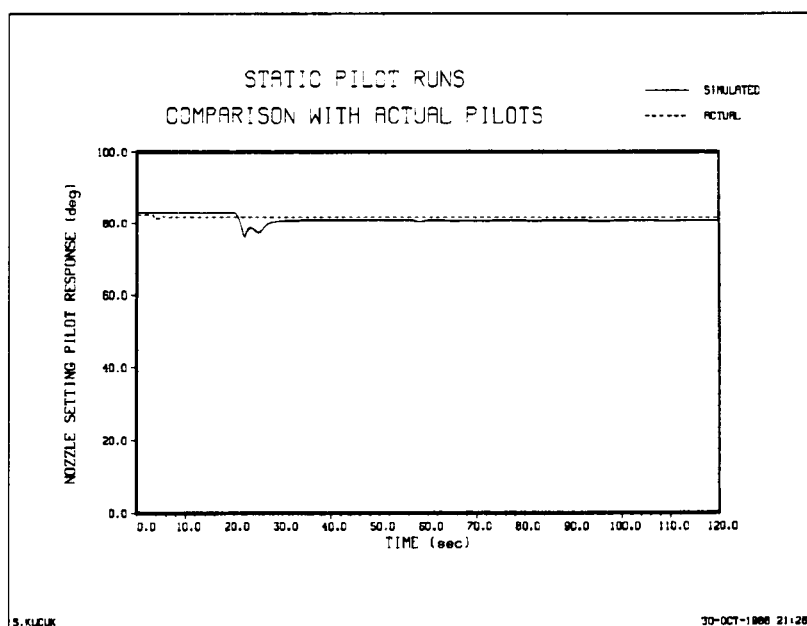


Figure 138. Actual vs simulated nozzle setting input (from NASA data)

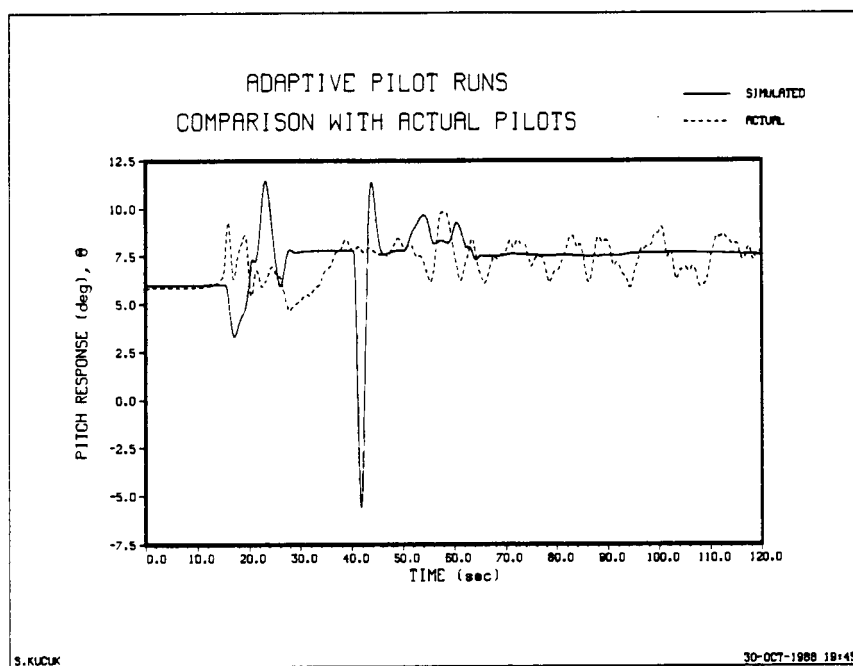


Figure 139. Actual vs simulated pitch response (from NASA data)

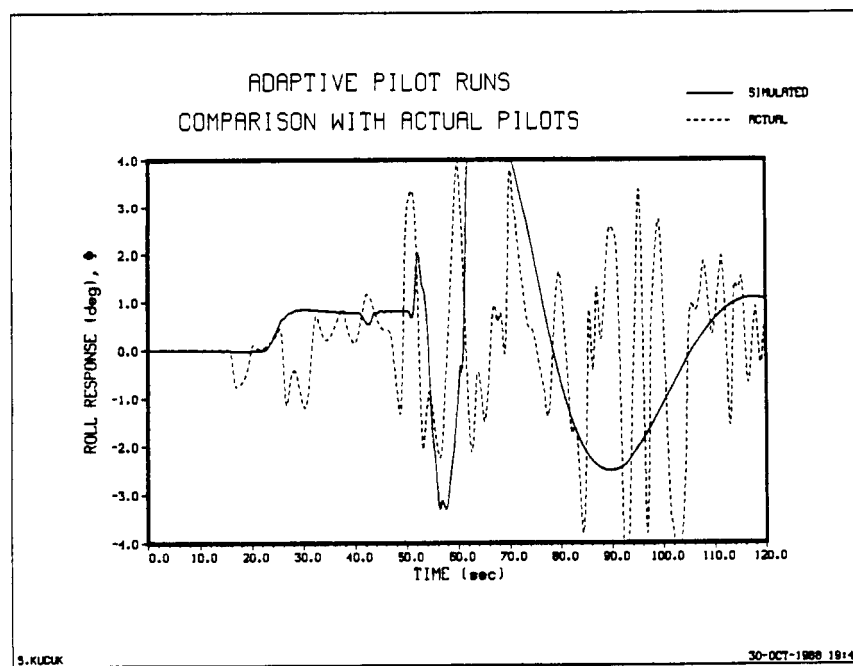


Figure 140. Actual vs simulated roll response (from NASA data)

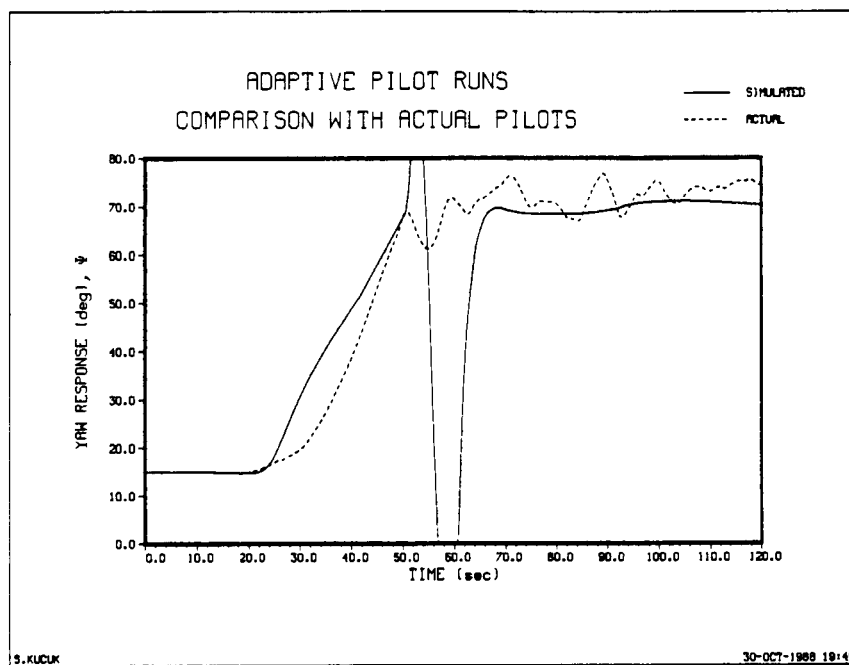


Figure 141. Actual vs simulated yaw response (from NASA data)

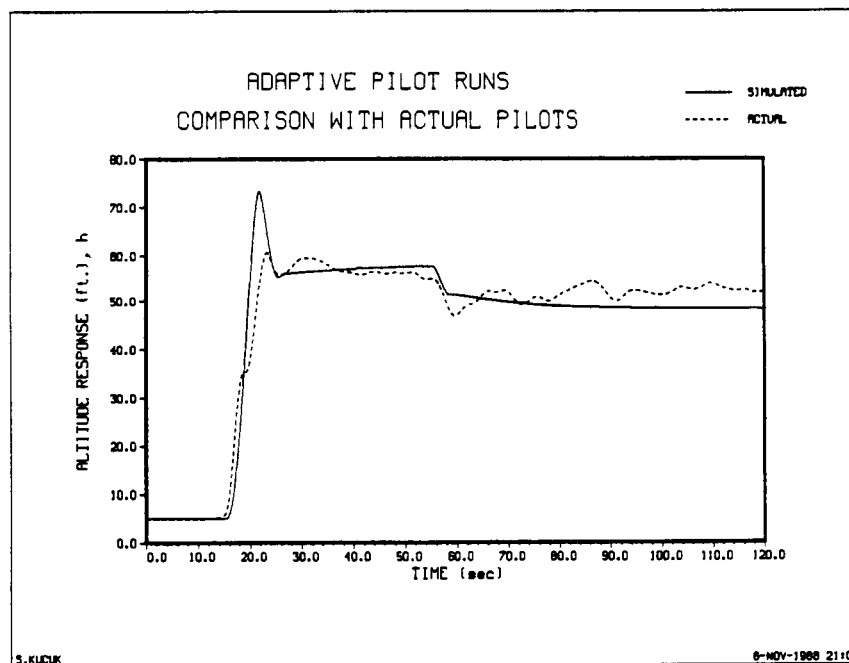


Figure 142. Actual vs simulated altitude response (from NASA data)

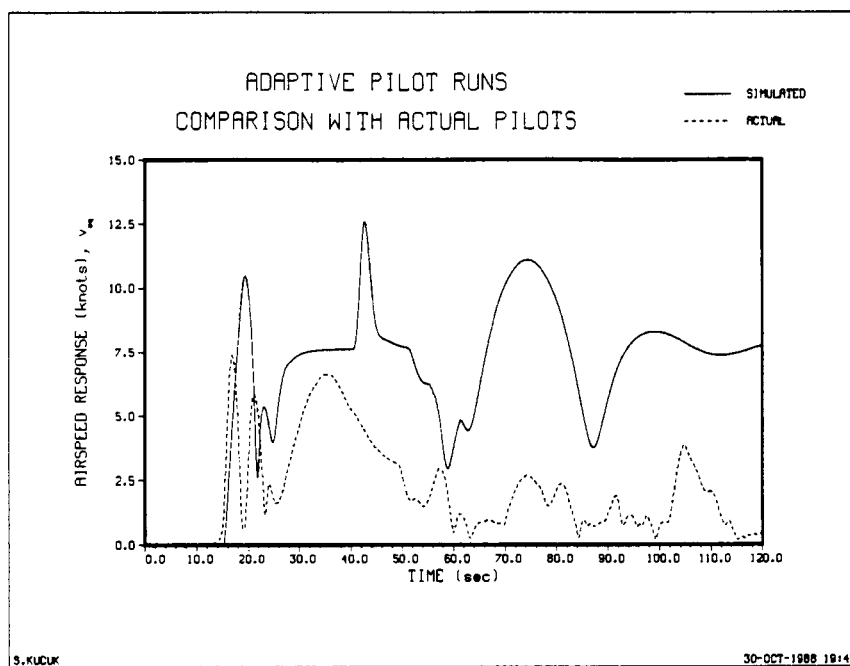


Figure 143. Actual vs simulated speed response (from NASA data)

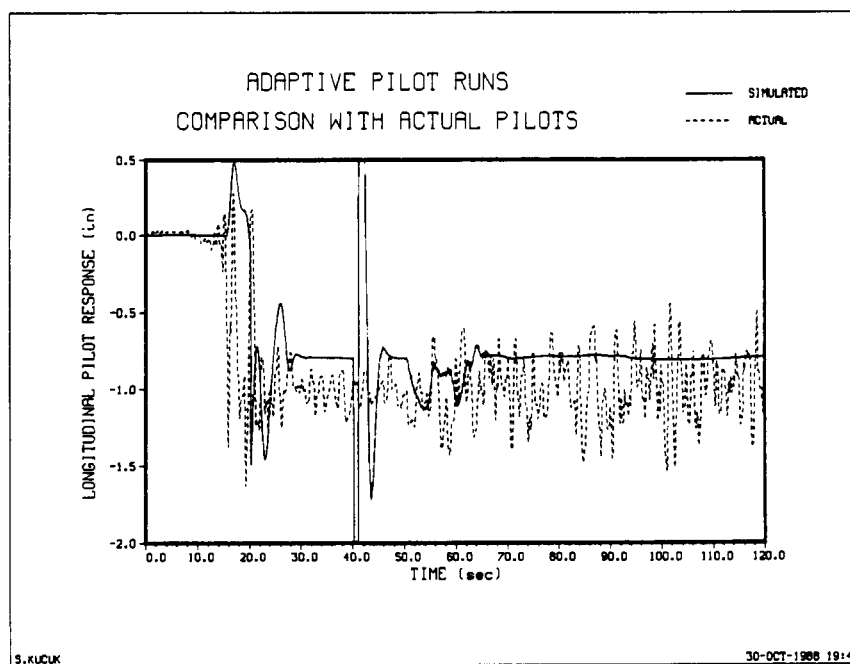


Figure 144. Actual vs simulated longitudinal stick input (from NASA data)

ORIGINAL PAGE IS
OF POOR QUALITY

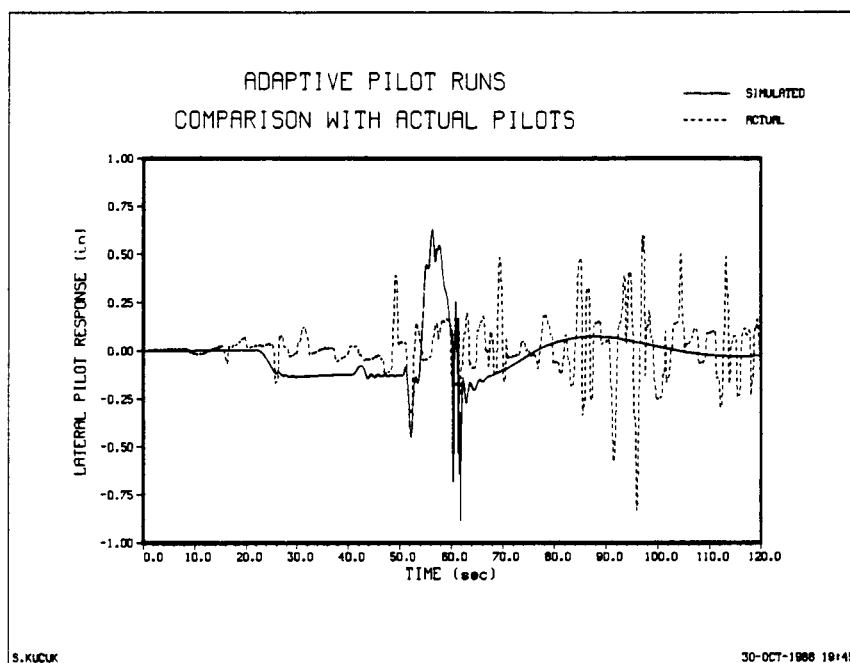


Figure 145. Actual vs simulated lateral stick input (from NASA data)

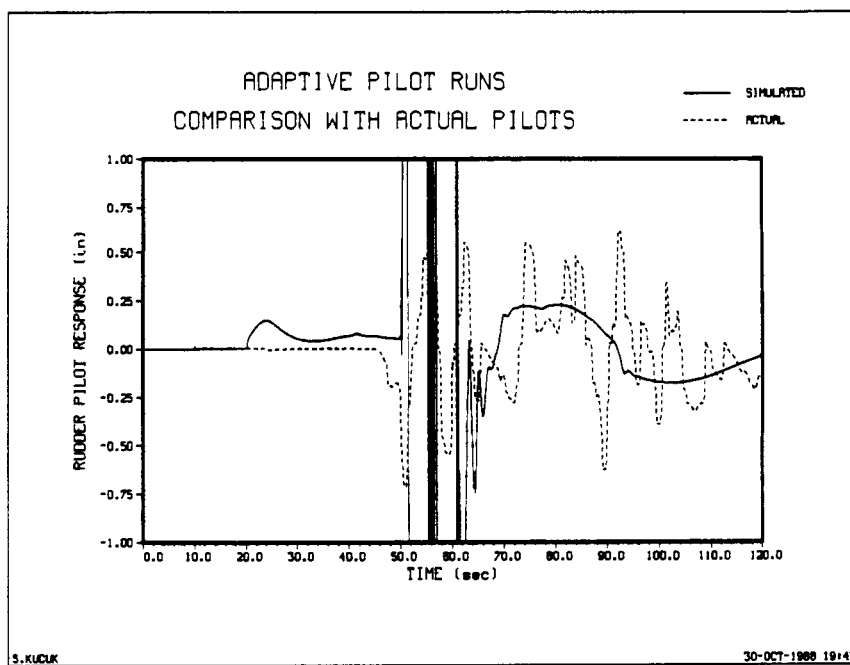


Figure 146. Actual vs simulated rudder pedal input (from NASA data)

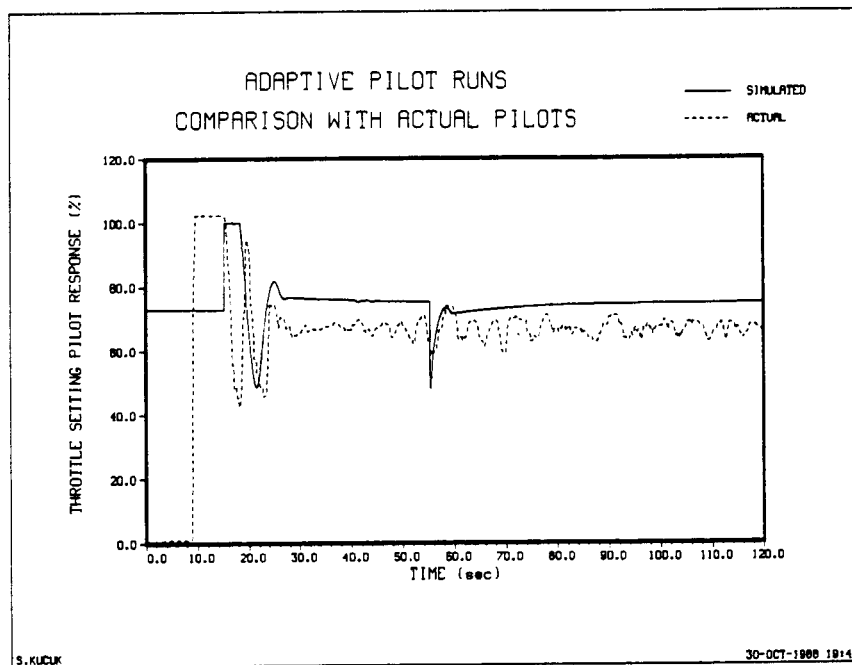


Figure 147. Actual vs simulated throttle setting input (from NASA data)

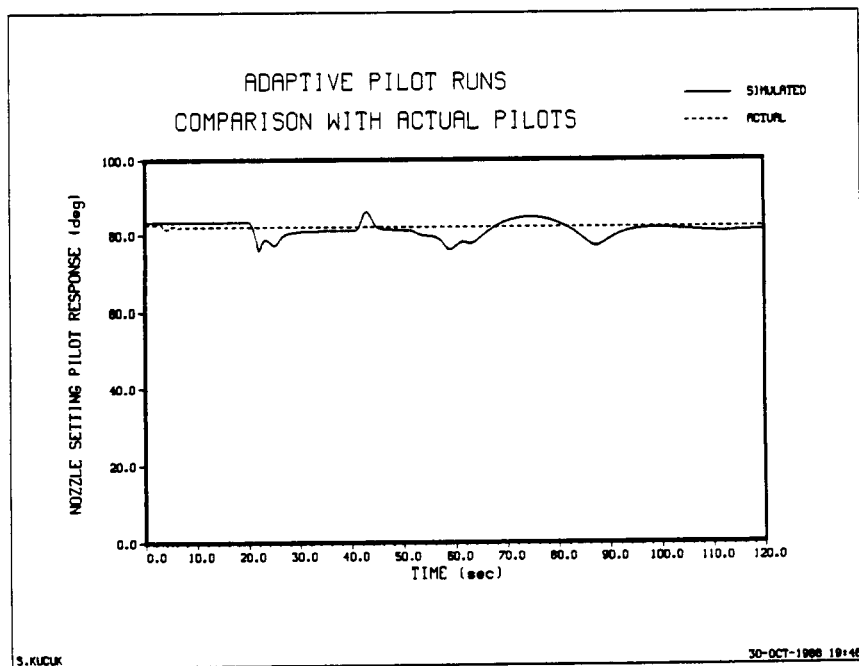


Figure 148. Actual vs simulated nozzle setting input (from NASA data)

7.0 CONCLUSION

7.1 Results and Discussions

We have developed an adaptive human response model for compensatory type feedback systems. Although the adaptation of a human will not necessarily be the adaptation of our model, the model is based on physical evidence. The model is verified in a non-linear aircraft simulation environment closing all the control loops generally closed by the Harrier AV-8B pilot. Though simple in approach, the de-coupled, multi-variable control structure consisting of single variable control loops fulfills the requirements. This can be related to the basic idea in the design of the aircraft control mechanisms. Each control unit is coupled to the quasi-totality of the aircraft dynamic equations, but each control unit has a "primary" response perceived by the human pilot. For example, rolling moments are created by the lateral stick and equivalently by the lateral movements of the main stick. But as the roll-yaw coupling is excited by increasing the roll angle, the heading as well as the sideslip, the pitch angle, and the altitude of the aircraft are disturbed. Then the rudders are used to suppress the roll-yaw coupling, the throttle setting is used to hold the altitude, and the longitudinal stick is activated for the pitch angle adjustments. It is clear that, the secondary controls are for the regulation of the disturbed modes of the aircraft. The other aspect is the "parallel processing" capability of the human structure. Each single variable control loop can be thought as one parallel processing unit related for one specific purpose but actively monitoring the other control loops.

The first step in the model development is the compilation of the physical data where the typical behavior of the human pilot is analyzed within the process of controlling the aircraft. The control mechanisms and their effects are carefully examined. The importance of this stage is inevitable because it is that particular behavior of the human pilot that we wish to be able to predict and to model the human pilot's appearance in the aircraft by means of mathematical equations.

The findings are that, the human pilot uses feedback, sensing and estimating all the information he could get through or without the instrumentation as well as deciding experiencing and remembering his performance. Not all the information is used for the control process. He also has constraints on the aircraft variables. His aim is to stabilize, re-position, and follow trajectories without risking the aircraft meaning that he should avoid dangerous maneuvers. The combat pilot may not be in this category.

These constraints lead to classical control concepts like the settling time, overshoot, rise time, closed loop bandwidth, and damping ratio. This is where we branch to the area of mathematics from physics. Fortunately, many successful studies have been done on the handling qualities of pilots throughout the years.

Then we assume the existence of a "human-describing function" in the sense that the model will generate outputs similar to that of the actual pilot in a similar environment. The response must be approximately the same in the frequency domain and preferably the same in the time domain.

The third step is the simulation where we place this model in a feedback type control loop. There, the open loop is described by the pilot model and the aircraft dynamics.

We chose a well-developed and documented, low order human response mechanism proposed in the late 1950's by D.T. McRuer and E.S. Krendel. This model was a result of a controls approach idea, to the human response, that began by Tustin. The human operator in the control loop of a feedback system is assumed to compensate the open loop transfer function, being capable of integrating and differentiating, while moving the closed loop to the desired operating regions.

The McRuer-Krendel model has variable parameters and ranges of the parameters to model the adaptivity of the human response. However, the selection of these parameters is rather complex and not trivial. In their studies, McRuer and Krendel showed that by appropriate selection of these parameters, within the frequency region assumed to be the bandwidth of the human mechanism, the model can fit a variety of experimental data.

As mentioned earlier, studies on the pilot handling qualities relate the closed loop bandwidth and damping to the pilot performances. This idea is used to apply the root locus technique to select the human response model parameters that will close the control loop of an aircraft control mechanism with the desired damping and bandwidth⁽⁹⁾⁽¹⁰⁾⁽¹¹⁾. As a part of this research, simulation programs were provided by NASA-Lewis, where they were used to get information of the aircraft control mechanisms, and the open loop aircraft transfer functions by injecting control sequences to the specific control surfaces of the aircraft. The resulting data is analyzed to approximate low order transfer function models of the aircraft dynamics both in time and frequency domains. The low order approximations were used in conjunction with the human response model in the root locus method to select the pilot parameters. However, once the model parameters are chosen, the model becomes static and capable of only operating at that specific flight configuration which the approximate transfer function was taken.

We studied the adaptation process of the human pilot and concluded that the typical adaptation involved detection, identification, optimization and modification processes. By appropriate assumptions, these four concepts led to an adaptive human response model. We related the detection to the pilot senses. The identification was a parameter estimator where the open loop aircraft dynamics were approximated by low order discrete transfer functions. The proper selection of the model parameters was related to the optimization where constraints like closed loop bandwidth and damping, as well as stability and minimum steady state error criteria were applied. Finally, the optimal model parameters were used to modify the human response model.

In order not to go back to the s -domain from the z -domain by approximate transformations, we transformed the human response model into the z -domain. There, concepts like the sampling theorem and step invariant transformation were effectively applied. The sampling theorem was used to make sure that the bandwidth of the human response model was preserved in s to z transformation by putting constraints on the sampling time consistent with human limitations. The step invariant transformation used the fact that the pilot's error information and corresponding control displacement were approximately constant for a brief period of time during which the decision and action of the pilot took place. Also, the discrete model had some advantages over the s -domain model. Thus, we had the basic modules of the adaptive model.

As in every adaptive control system, we needed a rule for the adaptation. The human response model has an adjustable pole-zero pair which corresponds to the lead-lag network compensator of the s -domain McRuer-Krendel model, a neuro-muscular pole constant, a gain, a delay and a remnant. We assumed a zero remnant based on the observation that an experienced pilot will behave almost deterministically. Moreover, the

time delay and the neuro-muscular pole were assumed to be constants based on the fact that pilots with similar experiences would have similar behaviors. Therefore, the adjustable pole-zero pair and most importantly the pilot's adjustable gain were to be subjected to the adaptation law.

The solution in selecting an effective adaptation law was to use the root locus criterion on-line for the modification of the model parameters. As in an off-line root locus design procedure, first the desired closed loop pole is selected. Then, the phase contribution of each open loop pole and zero are calculated leading to the amount of phase to be compensated to force the closed loop system's characteristic equation to have the desired closed loop poles, and that they are the dominant poles. Furthermore, the stability and phase margin requirements must be assured.

The pilot gain does not have a significant effect in the phase calculation, except that a positive or a negative pilot gain changes the phase constraint of the root locus criterion. The most important contributor is the pole-zero pair since neither the open loop dynamics nor the neuro-muscular bandwidth of the pilot model can be changed. They need to be re-located to give the necessary phase compensation.

Not all the values of the open loop transfer function are required in the calculation involving the effect of the aircraft dynamics. Once the pilot gain is characterized in terms of the open loop transfer function this becomes more clear. The only information required to continue with the adaptation is the value of the open loop aircraft transfer function evaluated at the desired closed loop pole. The magnitude and phase of this complex number will be used in the root locus criterion to adapt the model. Therefore, although we use a parameter estimator to approximate the aircraft dynamics in terms of

transfer functions, only a specific frequency information of the transfer function is used in calculating the phase to be compensated by the pilot model. Also, it is used to define the pilot boundaries where the resonances of the aircraft dynamics at the operating region are monitored.

We used a pre-calculated table look-up for the appropriate selection of the pole-zero pairs. Throughout the simulation, rather than calculating the necessary pole and zero that will fit the current requirements at each sample, the table is searched and the entries of that specific row are used for the adaptation.

Once the adaptive pole-zero pair is available, the pilot gain is calculated and checked to prevent any excess gain to be provided by the pilot to the control mechanisms. This process is repeated at each sampling time, thus providing an on-line adaptive human response mechanism. Adaptive, since the aircraft dynamics are continuously monitored to sense any model changes due to the non-linearities, and human response, since the adaptation is constrained on the values of the human describing function model which has a similar bandwidth and frequency response as the human pilot.

We needed initial pilot parameters to start the algorithm. For that reason, we assumed that these initial parameters will reflect pilot's experience and his knowledge of the aircraft. In general, the control process of the human pilot has two stages. First, the available information is used to activate the control. Any differences of the controlled element behavior than the predicted one are corrected in the next stage. That is more likely where the adaptation process occurs. However, it is essential that the initial knowledge is accurate since the adaptation will not be of much help if the aircraft becomes unstable as a result of the initial reaction of the pilot. In the case of the human

pilot, this is guaranteed by extensive training of the pilots where the pilot has enough initial knowledge of the aircraft dynamics. The predicted and commanded behavior of the aircraft will very likely be the same. Therefore, we supplied the static pilot parameters that were calculated off-line from the aircraft data as our initial model parameters. By inserting the static pilots to the aircraft control loops and testing their performances, we modelled the training process of the human pilots. As mentioned earlier, this is a primitive attempt to describe pilot training. Even though we supply the initial pilot parameters, we can not apply the proper starting control sequence. The static pilot activated the control and the adaptive pilot took the control after sufficient amount of time that will leave enough time for the transfer function estimators to converge.

Thus, we have analyzed and simulated an adaptive human response mechanism where the root locus method is used as the adaptation law. This approach is also applicable for other type of feedback systems where the controller is not necessarily a human pilot model.

For most of the simulated cases, the adaptive model performed better than the static models trying to minimize a possible non-zero steady-state error caused by the static pilot's performance. However, we concluded that the adaptation with the current constraints is more suitable to the longitudinal control set of the aircraft mechanism although it performed well for the lateral control sets. An analysis of some actual pilot data in a lateral tracking task, provided by NASA-Lewis, suggested that, for this particular scenario, the McRuer-Krendel model does not seem to be adequate.

Furthermore, the adaptive model should operate at a variety of flight configurations since any changes in the aircraft dynamics are sensed and compensated on-line as the human pilot will try to compensate.

We also showed for a specific case that the model is capable of performing the tasks that were carried by human pilots. Although a careful investigation of the actual scenario is necessary, the results were satisfactory.

We also concluded that, for the simulated cases, the single variable approach to a complete multi-variable control mechanism is very efficient as well as simple. However, the effects of the remnant and the time delay, the neuro-muscular approximation, and the performance of the adaptive model in other aircraft environments, remain to be studied. A variety of actual pilot data should be analyzed for better understanding of the actual pilot behavior towards the development of efficient describing functions of the human response with an expert system-like adaptive mechanism. The adaptive model will remain the same but it should have a database of extra rules to follow just like the human pilot. Fortunately, this will compensate for the absence of a "remembering" process of the pilot which our model does not have at this time. Only the current information is processed by the adaptive pilot model. For that reason, the models should be constrained with rules defined by the actual pilot behavior. Throughout the years, different models were investigated for those human behavior that would fit in one model but not another. Nevertheless, without any human reasoning, no such model will ever find any use.

7.2 Suggestions for Further Research

The key factor in modelling of the human mechanism is decisionmaking. Of all the possible choices the best reaction will be "selected" by the human operator. It is certain that there is no unique adaptation procedure performed by the human. Instead a set of rules define his reactions and boundaries. The more the rules, the more complicated the decision making process becomes. However, it is that decisionmaking that makes the

human operator's appearance safe and reliable. These aspects like decisionmaking, adapting, defining and updating the rules together with many others define his intelligence.

In that sense, the model proposed in this thesis is not "decisionmaking". Although adaptive, there is only a few rules satisfied by the model compared with the human pilot. The closed loop bandwidth of the pilot-aircraft combination resembles actual human pilot operating regions. Also the simulated control movements of the model are consistent with the human muscular limitations. As an adaptation law the root-locus performs well but within the process of adaptation the model generates somewhat undesirable outputs which may be dangerous.

This can partly be solved by supplying the model a set of transfer function estimates corresponding to different flight configurations. The detail of these transfer functions will directly depend on the pilot's knowledge of the aircraft. In this way, the model will not only have initial human describing function parameters but an initial information of specific flight configurations which the human pilot gets through training. Unfortunately, the training can not be efficiently modelled by this approach. Instead the assumption of a well-trained pilot simplifies the situation.

A well-trained, experienced human pilot will be almost deterministic in his reactions. Furthermore, his reactions will be optimal for that configuration. In that respect, selecting the pilot poles and zeros for specific configurations resembles the human pilot's deterministic reactions since the model will select the same poles and zeros every time it is subjected to that same flight configuration; hence, it will react the same. However, a human pilot in a type-1 loop will not add an integrator to the system⁽²⁴⁾. On

the other hand, when subjected to a type-0 system, the human operator will use his integrating ability to act as an integrator so that the "steady-state" error is minimized. For that reason, different sets of pole-zero selections for different aircraft control sets is more appropriate rather than having only one table look-up as in our adaptive simulations. For example, the longitudinal stick pilot and the nozzle setting pilot adaptations will be different because the former is a type-1 loop while the latter is almost type-0.

The "sampled human response" idea resulting from a "sampled external world" point of view fits the nature of the human mechanism. However, by starting from a continuous domain model and transferring into the discrete domain, as in our case, does not take the full advantage of the discrete domain. Left half plane poles and zeros are estimated by discrete models⁽¹⁶⁾. For that reason, better discrete human response models should be investigated by analyzing actual pilot data. In fact, we can record the typical responses of the human pilots and use them as a part of the adaptation procedure. It would be practically impossible to record all the time histories but the estimated pilot model poles and zeros can be used.

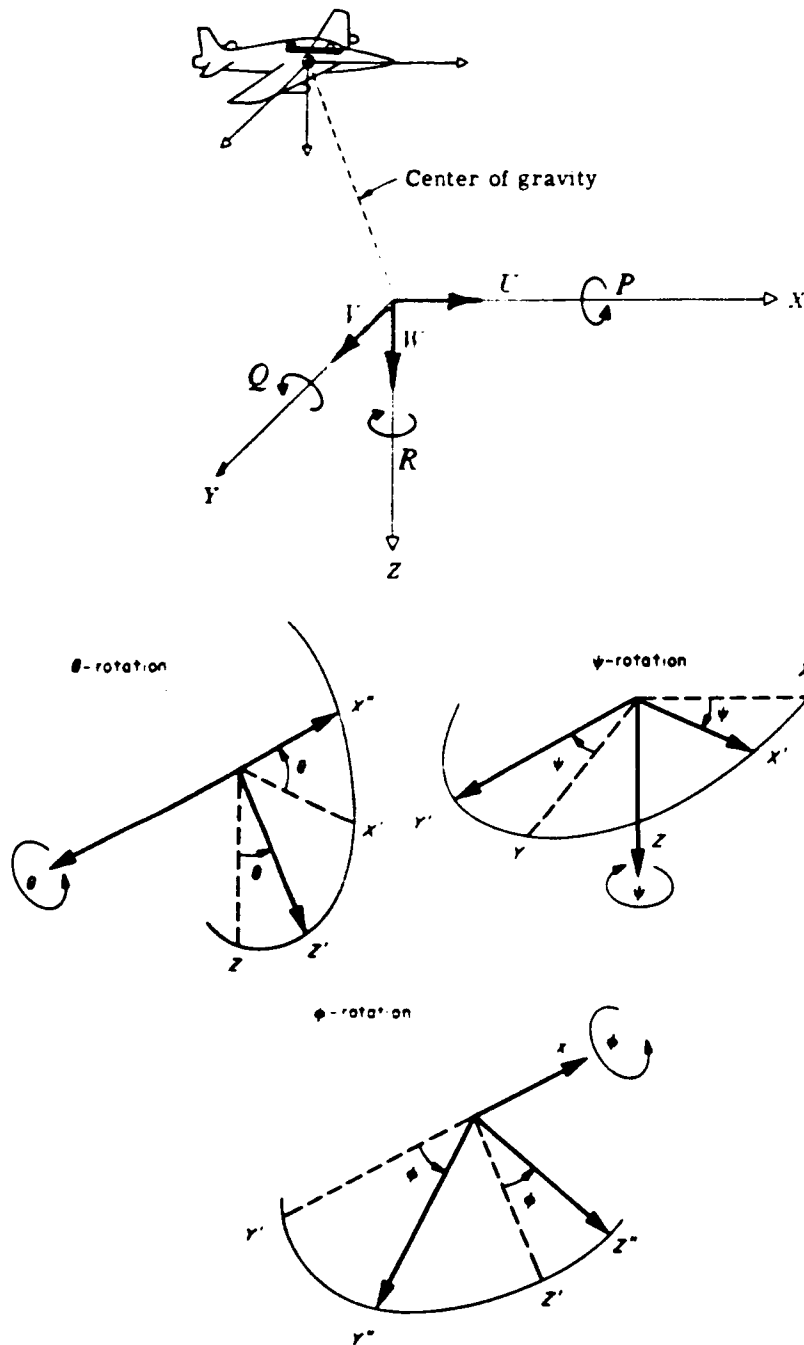
Considering the comparison of the actual and simulated pilot response of Section (6.4), the only problem in commanding the model is the selection of the primary reference variables and the application of the desired reference sequences. For example, if it is desired to gain altitude, then the command is an increment in the altitude loop reference. If a descent is required, then the altitude loop will be given a negative ramp as an input.

Starting the pilot model with no adaptation and then activating the adaptation process seems to be a good approach to model a human's reaction where he first uses the

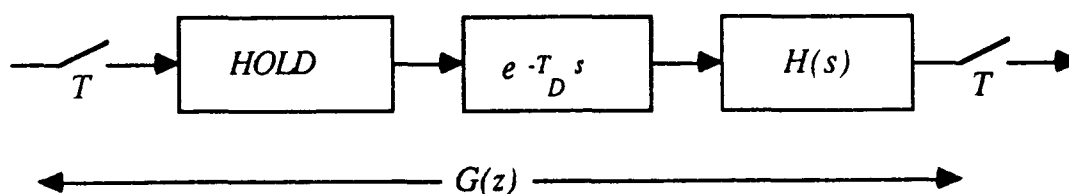
best knowledge about that situation. However, as is shown in the adaptive pilot simulations, the problem is how to start the adaptation "smoothly". The estimated pilot gains oscillates for a brief period of time during which the adaptation procedure converges. This should be solvable by adding artificial intelligence or decisionmaking to the model by adding extra rules to be followed. This is a very rich area for future research.

APPENDIX A.

APPENDIX A. **DEFINITION OF THE AIRCRAFT PARAMETERS**



APPENDIX B.
STEP-INVARIANT TRANSFORMATION OF THE HUMAN RESPONSE
MODEL



The step-invariant transformation is defined by:

$$G(z) = \frac{z-1}{z} \mathcal{Z} \left\{ \mathcal{F}^{-1} \left\{ \frac{e^{-T_D s} H(s)}{s} \right\} \right\} \Big|_{t=kT}$$

let

$$F(s) = \frac{H(s)}{s}$$

then, if

$$\begin{aligned} f(t) &\leftrightarrow F(s) \\ \therefore f(t-T_D) &\leftrightarrow e^{-T_D s} F(s) \end{aligned}$$

it follows that

$$\mathcal{F}^{-1} \left\{ e^{-T_D s} H(s) \right\} = f(t-T_D)$$

then, let

$$\begin{aligned} f(kT) &\leftrightarrow F(z) \\ \therefore f[(k-d)T] &\leftrightarrow z^{-d} F(z) \end{aligned}$$

by choosing, $T_D = dT$

$$\mathbf{Z}\left\{f(t-T_D) \Big|_{t=kT}\right\} \leftrightarrow z^{-d}F(z)$$

$$\therefore G(z) = \frac{z-1}{z} z^{-d} F(z)$$

where

$$F(z) = \mathbf{Z}\left\{\mathcal{L}^{-1}\left\{\frac{H(s)}{s}\right\} \Big|_{t=kT}\right\}$$

for the McRuer-Krendel human response model

$$H(s) = K_p \frac{(T_L s + 1)}{(T_N s + 1)(T_I s + 1)}$$

Case. I ($T_N \neq T_I$)

$$\frac{H(s)}{s} = K_p \left\{ \frac{1}{s} + \frac{T_L - T_N}{T_N - T_I} \frac{1}{T_N s + 1} + \frac{T_L - T_I}{T_I - T_N} \frac{1}{T_I s + 1} \right\}$$

then

$$F(z) = K_p \frac{z(b_1 z + b_2)}{(z-1)(z-e^{-T/T_I})(z-e^{-T/T_N})}$$

where

$$b_1 = 1 - \beta \frac{T_L - T_N}{T_I - T_N} + \alpha \frac{T_L - T_I}{T_I - T_N}$$

$$b_2 = \beta \alpha - \alpha \frac{T_L - T_N}{T_I - T_N} + \beta \frac{T_L - T_I}{T_I - T_N}$$

then

$$G(z) = K z^{-d} \frac{(z^{-1} - \gamma z^{-2})}{(1 - \alpha z^{-1})(1 - \beta z^{-1})}$$

with

$$\alpha = e^{-T/T_I}$$

$$\beta = e^{-T/T_N}$$

$$K = K_p b_1$$

$$\gamma = -\frac{b_2}{b_1} = 1 - \frac{(1-\beta)}{1 + \frac{(T_L - T_N)(\alpha - \beta)}{(T_I - T_N)(1-\alpha)}}$$

Case. II ($T_N = T_I$)

In the same way

$$G(z) = Kz^{-d} \frac{(z^{-1} - \gamma z^{-2})}{(1 - \beta z^{-1})^2}$$

with

$$\beta = e^{-T/T_N}$$

$$K = K_p [\beta T(T_L - T_N) + 1 - \beta]$$

$$\gamma = 1 - \frac{(1-\beta)^2}{1 - \beta[T(T_L - T_N) - 1]}$$

APPENDIX C.

APPENDIX C.
KALMAN FILTER PARAMETER ESTIMATION ALGORITHM (PSEUDO
CODE)

```

/* SISO case, input is  $u_{k-d}$ , output is  $y_k$  */
/* Given  $n, m$  and  $d$  */
/* Gain update */
sum_1 := 0;
for i := 1 to N do begin
    sum_2 := 0;
    for j := 1 to N do begin
        sum_2 := sum_2 +  $P[i, j]$  *  $H[j]$ ;
    end;
     $T[i]$  := sum_2;
    sum_1 := sum_1 +  $H[i]$  *  $T[i]$ ;
end;
sum_1 := sum_1 +  $R_k$ ;
for i := 1 to N do begin
     $K[i]$  :=  $T[i]$  / sum_1;
end;
/* Parameter update */
sum_3 := 0;
for i := 1 to N do begin
    sum_3 := sum_3 +  $H[i]$  *  $\hat{\theta}[i]$ ;
end;
 $\epsilon_k$  :=  $z_k$  - sum_3;
for i := 1 to N do begin
     $\hat{\theta}[i]$  :=  $\hat{\theta}[i]$  +  $K[i]$  *  $\epsilon_k$ ;
end;
/* Covariance update */
for i := 1 to N do begin
    for j := 1 to i do begin
         $P[j, i]$  :=  $P[j, i]$  -  $K[i]$  *  $T[j]$ ;
         $P[i, j]$  :=  $P[j, i]$ ;
    end;
     $P[i, i]$  :=  $P[i, i]$  +  $\rho_k$ ;
end;
/* Regressor update */
for i := 0 to  $n - 2$  do begin
     $H[n - i]$  :=  $H[n - i - 1]$ ;

```

```
end;  
H[1] :=  $z_k$ ;  
for i := 0 to  $m - 2$  do begin  
     $H[n + m - i] := H[n + m - i - 1]$ ;  
end;  
 $H[n + 1] := u_{k-d+1}$ ;  
/* End of one update */
```

APPENDIX D.

APPENDIX D.
SIMPLIFIED KALMAN FILTER PARAMETER ESTIMATION ALGORITHM
(PSEUDO CODE)

```

/* SISO case, input is  $u_{k-d}$ , output is  $y_k$  */
/* Given  $n, m$  and  $d$  */
/* Gain update */
sum_1 := 0;
pointer_1 := 1;
for i := 1 to N do begin
    sum_2 := 0;
    pointer_2 := pointer_1 + i - 2;
    for j := 1 to N do begin
        if (j ≤ i) then (pointer_2 := pointer_2 + 1);
        else (pointer_2 := pointer_2 + j - 1);
        sum_2 := sum_2 +  $P_{LINEAR}$ [pointer_2] *  $\bar{H}[j]$ ;
    end;
    T[i] := sum_2;
    sum_1 := sum_1 +  $H[i]$  * T[i];
    pointer_1 := pointer_1 + i - 1;
end;
sum_1 := sum_1 +  $R_k$ ;
for i := 1 to N do begin
    K[i] := T[i] / sum_1;
end;
/* Parameter update */
sum_3 := 0;
for i := 1 to N do begin
    sum_3 := sum_3 +  $H[i]$  *  $\hat{\theta}[i]$ ;
end;
 $\epsilon_k := z_k - \text{sum\_3}$ ;
for i := 1 to N do begin
     $\hat{\theta}[i] := \hat{\theta}[i] + K[i] * \epsilon_k$ ;
end;
/* Covariance update */
pointer_1 := 1;
for i := 1 to N do begin
    pointer_2 := pointer_1 + i - 2;
    for j := 1 to i do begin
        pointer_2 := pointer_2 + 1;
    end;
end;

```

```

         $P_{LINEAR}[\text{pointer\_2}] := P_{LINEAR}[\text{pointer\_2}] - K[i] * T[j];$ 
    end;
     $P_{LINEAR}[\text{pointer\_2}] := P_{LINEAR}[\text{pointer\_2}] + \rho_k;$ 
     $\text{pointer\_1} := \text{pointer\_1} + i - 1;$ 
end;
/* Regressor update */
for i := 0 to  $n - 2$  do begin
     $H[n - i] := H[n - i - 1];$ 
end;
 $H[1] := z_k;$ 
for i := 0 to  $m - 2$  do begin
     $H[n + m - i] := H[n + m - i - 1];$ 
end;
 $H[n + 1] := u_{k-d+1};$ 
/* End of one update */

```

APPENDIX E.

APPENDIX E.

KALMAN FILTER ESTIMATES OF THE "BALL-IN-THE-HOOP" PROBLEM

$$\hat{\Phi}_{t=0.10} = \begin{bmatrix} 0.00000000 & 0.00000000 & -0.07729860 & 0.00000000 \\ 0.00000000 & 0.00000000 & -1.48918450 & 0.00000000 \\ 0.00000000 & 0.00000000 & 0.30050501 & 0.00000000 \\ 0.00000000 & 0.00000000 & -3.71993697 & 0.00000000 \end{bmatrix}$$

$$\hat{\Phi}_{t=0.20} = \begin{bmatrix} 0.00107484 & 0.02070723 & -0.07591160 & 0.05172603 \\ 0.00682456 & 0.13147752 & -1.48037796 & 0.32842678 \\ 0.00188267 & 0.03627024 & 0.30293443 & 0.09060195 \\ 0.00839500 & 0.16173255 & -3.70910391 & 0.40400292 \end{bmatrix}$$

$$\hat{\Phi}_{t=0.30} = \begin{bmatrix} 0.08688898 & 0.31142050 & 0.01461274 & -0.07129169 \\ 0.32585235 & 1.21225070 & -1.14383923 & -0.12891131 \\ 0.03723846 & 0.15604535 & 0.34023085 & 0.03991812 \\ -0.42391242 & -1.30279900 & -4.16514002 & 1.02373153 \end{bmatrix}$$

$$\hat{\Phi}_{r=0.40} = \begin{bmatrix} 0.14098586 & 0.21043570 & 0.17209159 & -0.04043441 \\ 0.56745262 & 0.76124586 & -0.44052820 & 0.00889937 \\ 0.13203274 & -0.02091092 & 0.61618198 & 0.09398952 \\ -1.18354381 & 0.11523515 & -6.37646677 & 0.59043187 \end{bmatrix}$$

$$\hat{\Phi}_{r=0.50} = \begin{bmatrix} 1.00000000 & 0.09173982 & -0.01741165 & -0.00060458 \\ 0.00000000 & 0.83965469 & -0.31534503 & -0.01741165 \\ 0.00000000 & -0.00266704 & 0.64530913 & 0.08786757 \\ 0.00000000 & -0.04830323 & -6.63756304 & 0.64530913 \end{bmatrix}$$

$$\hat{\Gamma}_{r=0.10} = \begin{bmatrix} 0.07729860 \\ 1.48918450 \\ -0.30050501 \\ 3.71993697 \end{bmatrix}$$

$$\hat{\Gamma}_{r=0.20} = \begin{bmatrix} 0.07868559 \\ 1.49799103 \\ -0.29807558 \\ 3.73077002 \end{bmatrix}$$

$$\hat{\Gamma}_{t=0.30} = \begin{bmatrix} 0.16920993 \\ 1.83452976 \\ -0.26077916 \\ 3.27473392 \end{bmatrix}$$

$$\hat{\Gamma}_{t=0.40} = \begin{bmatrix} 0.32668878 \\ 2.53784079 \\ 0.01517197 \\ 1.06340716 \end{bmatrix}$$

$$\hat{\Gamma}_{t=0.50} = \begin{bmatrix} 0.13718554 \\ 2.66302396 \\ 0.04429912 \\ 0.80231090 \end{bmatrix}$$

BIBLIOGRAPHY

BIBLIOGRAPHY

1. Anderson, L. C. and J. W. Bunnell, AV-8B Simulation Model (Palo Alto, California: Systems Control Technology, Inc., November 1985).
2. MacFarland, Richard E., A Standard Linematic Model for Flight Simulation at NASA-Ames, NASA CR-2497, (Mountain View, California: Computer Sciences Corporation, January, 1975).
3. Anderson, L. C., AV-8B System Identification Results: Low and High Speed Longitudinal Model (Palo Alto, California: Systems Control Technology, Inc., April 1984).
4. Anderson, L. C. and J. C. Bunnell, AV-8B Simulation Software User's Guide (Palo Alto, California: Systems Control Technology, Inc., May 1985).
5. Anderson, L. C., and J. C. Bunnell, AV-8B Simulation Model, Engineering Specification (Palo Alto, California: Systems Control Technology, Inc., January 1985).
6. McRuer, D. T., D. Graham, E. Krendel, and W. Reisner, Jr., "Human Dynamics in Compensatory Systems", Air Force Flight Dynamics Laboratory", AFFDL-TR-65-15, 1965.
7. McRuer, D. T. and E. S. Krendel, Dynamic Response of Human Operators, (Wright Air Development Center, TR-56-524, October, 1957).
8. Kuo, B. C., Automatic Control Systems (4th edition; Englewood Cliffs, New Jersey: Prentice Hall, 1982), pp. 454-455.
9. Proceedings of the Eighteenth Modeling and Simulation Conference, University of Pittsburgh, April 23-24, 1987, "Computer Simulation of Multiple Pilots Flying a Modern High Performance Helicopter, by Mark E. Zipf, William G. Vogt, Marlin H. Mickle, Ronald G. Hoelzeman, Fei Kai, James R. Mihaleow", pp. 1295-1314.
10. Proceedings of the Eighteenth Modeling and Simulation Conference, University of Pittsburgh, April 23-24, 1987, "Computer Simulation of a Single Pilot Flying a Modern High Performance Helicopter, by Mark E. Zipf, William G. Vogt, Marlin H. Mickle, Ronald G. Hoelzeman, Fei Kai, James R. Mihaleow", pp. 1279-1294.

11. Proceedings of the Nineteenth Modeling and Simulation Conference, University of Pittsburgh, May 5-6, 1988, "A Computer Simulation of Low Order Pilot Models Flying a Thrust Vected V/STOL Research Aircraft, by Mark E. Zipf, William G. Vogt, Marlin H. Mickle, Senol Kucuk, James R. Mihaleow", (Preprint), 44p.
12. Second Annual NASA-University Conference on Manual Control, February 28-March 2, 1966, pp.39-43.
13. McRuer, D. T. and E. S. Krendel, "Human Operator as a Servo System Element", Journal of the Franklin Institute, Vol. 267, (May, 1959), pp. 381-403.
14. Kleinman D. L., S. Baron, and W. H. Levison, "An Optimal Control Model of Human Response, Part I: Theory and Validation", Automatica, Vol. 6, (1970), pp.357-369.
15. Kleinman D. L., S. Baron, and W. H. Levison, "An Optimal Control Model of Human Response, Part II: Prediction of Human Performance in a Complex Task", Automatica, Vol. 6, (1970), pp.371-383.
16. Gloeckner, M., "Identification of a Parametric Model of the Human Operator in Closed Loop Control Tasks", Identification and System Parameter Estimation, Vol.2, IFAC, pp. 809-816.
17. Landyshev, Alexander, N. "Human Poles and Zeros", ISA Transactions, Vol.8, No.4, (1969), pp. 322-328.
18. Bekey, G., "Mathematical Models of the Human Operator", Instruments and Control Systems, Vol.33, (July, 1960), pp. 1121-1125.
19. Salvendy, Gavriel, (ed.), "Handbook of Human Factors", (New York: John Wiley & Sons, 1987), pp. 1216.
20. Anderson, Brian D. O. and John B. Moore, Optimal Filtering, (Englewood Cliffs: New Jersey, Prentice Hall, 1979), pp. 223-254.
21. Anderson, Brian D. O. and John B. Moore, Optimal Filtering, (Englewood Cliffs: New Jersey, Prentice Hall, 1979), pp. 50-52.
22. Goodwin, Graham C. and Kwai Sang Sin, Adaptive Filtering Prediction and Control, (Englewood Cliffs: New Jersey, Prentice Hall, 1984), pp. 67.
23. Johnson, Richard, C. Jr., "Lectures on Adaptive Parameter Estimation", (Englewood Cliffs: New Jersey, Prentice Hall, 1988), Thomas, Kailath, (ed.), pp. 42-45.
24. McRuer, D. T., "Human Dynamics in Man-Machine Systems", Automatica, Vol. 16(3), (1980), pp. 237-253

REFERENCES NOT CITED

REFERENCES NOT CITED

- Ashley, Holt, Engineering Analysis of Flight Vehicles (Reading, Massachusetts: Addison-Wesley, 1974)
- Babister, A. W., Aircraft Stability and Control (New York: MacMillan Company, 1961)
- Etkin, Bernard, Dynamics of Flight (New York: John Wiley & Sons, 1959)
- Etkin, Bernard, Dynamics of Atmospheric Flight (New York: John Wiley & Sons, 1972)
- Goodwin, Graham C. and Kwai Sang Sin, Adaptive Filtering Prediction and Control (Englewood Cliffs, New Jersey: Prentice-Hall, 1984)
- Hacker, T., Flight Stability and Control (New York: American Elsevier, 1970), Bellmann, Richard (ed.)
- Kelley, C. R., Manual and Automatic Control (New York: John Wiley & Sons, 1968)
- Kolk, W. R., Modern Flight Dynamics (Englewood Cliffs, New Jersey: Prentice-Hall, 1961)
- Miele, Angelo, Flight Mechanics (Reading Mass.: Addison-Wesley, 1962)
- Mises, Richard Von, Theory of Flight (New York: Dover, 1959)
- Seckel, Edward, Stability and Control of Airplanes and Helicopters (New York: Academic Press, 1964)